Quantifying the influence of sexual reproduction on the spatial eco-evo dynamics of species characterized by complex traits: asymptotic methods.

Léonard Dekens

THÈSE de DOCTORAT DE L'UNIVERSITÉ DE LYON

Opérée au sein de :

l'Université Claude Bernard Lyon 1

École Doctorale N°512

École Doctorale en Informatique et Mathématiques de Lyon

Spécialité de doctorat : Mathématiques

Soutenue publiquement le 07/07/2022, par :

Léonard DEKENS

Quantifying the influence of sexual reproduction on the spatial eco-evo dynamics of species characterized by complex traits: asymptotic methods.

Devant le jury composé de :

VÉBER Amandine	DR CNRS	Université Paris Cité	**Rapporteuse**
LOU Yuan	Professeur	Shanghai Jiao Tong University	**Rapporteur**
DÉBARRE Florence	CR CNRS	Sorbonne Université	**Examinatrice**
DESVILLETTES Laurent	Professeur	Université Paris Cité	**Examinateur**
SANTAMBROGIO Filippo	Professeur	Université Claude Bernard Lyon 1	**Examinateur**
CALVEZ Vincent	DR CNRS	Université Claude Bernard Lyon 1	**Directeur de thèse**
MIRRAHIMI Sepideh	DR CNRS	Université de Montpellier	**Directrice de thèse**
OTTO Sarah	Professeure	University of British Columbia	**Invitée**

Remerciements/Acknowledgments

Comme beaucoup de travaux académiques, ma thèse s'appuie sur de nombreux autres contributions scientifiques, au croisement de différents domaines et d'institutions académiques. Son déroulement et les résultats présentés dans ce manuscrit ont fortement bénéficié de l'influence de certaines personnes en particulier, que cette section se dédie à expliciter et remercier.

En premier lieu, je voudrais faire part de ma gratitude sans bornes envers mes direct.rice.eur.s de thèse, Vincent Calvez et Sepideh Mirrahimi. Cette gratitude prend sa source dans la confiance que vous m'avez accordée au tout début alors que je revenais de deux années passées loin de toute institution académique. Elle s'est nourrie à la fois de tous vos encouragements et vos actes de valorisations de mes tentatives et esquisses d'idées et de la bienveillance émotionnelle et du soutien matériel qui ont permis à ma curiosité scientifique de s'épanouir. Elle est également inspirée par tous les conseils avisés, mathématiques et non-mathématiques, et les corrections minutieuses qui ont guidé, amélioré et clarifié mes projets, ainsi que leur présentation dans cette forme finale. Le cas échéant, j'espère pouvoir un jour faire preuve de ce même équilibre d'encadrement délicat qui a contribué à créer les circonstances et l'atmosphère essentielles sans lesquelles ce travail n'aurait jamais été. Cela a été crucial en particulier depuis mars 2020 et la période pandémique, qui a constitué la majeure partie de mon temps de thèse. Je suis enfin conscient de l'insuffisance de ces quelques lignes. Merci pour tout.

My following thoughts of gratitude are for Sally Otto, who I am deeply honored to be calling a research supervisor and mentor in the field of evolutionary biology. As I once said, the extent of these thoughts is only matched by the distance between France and British Columbia. It has been a humbling privilege to be welcomed as I was in your lab at UBC. I particularly remember the generous and thoughtful support that you gave to the (at first) lost French student in mathematics visiting the BRC. I still feel this generosity after all my visits, which took place before and during the first year of my PhD. Your patient and clear explanations of evolutionary phenomena, to which I was getting acquainted with the difficulties that are inherent to the introduction to a new field, have profoundly shaped my scientific trajectory and guided me to aspire to stand at the interface between two disciplines with the best of my developing abilities. The opportunities provided by the visits at your lab in the BRC broadened my research perspectives, as you encouraged my enthusiasm to attend numerous discussion groups and seminars, and brought me to strengthen my oral presentations, especially towards non-mathematicians. I would also like to take the opportunity to thank the Otto lab members who made me feel as if I was one of theirs: Linnea Sandell, Ailene Macpherson, Seth Watt, Nikkie Love, Alireza Ghaseminejad and Anna Bazzicalupo. Finally, I acknowledge that, for this part of my PhD, I lived and worked on the ancestral, unceded and occupied lands of the Musqueam, Squamish and Tlseil-Waututh peoples.

I immensely thank Amandine Véber and Yuan Lou for accepting to act as referees for my PhD thesis, for I am conscious that it is a great and generous favour, and for their helpful comments. I hope that the efforts towards clarity that I put towards writing my manuscript compensated somehow for its length.

Je remercie profondément Florence Débarre, Laurent Desvillettes et Filippo Santambrogio pour avoir accepté le rôle d'examinat.eur.rice de ma thèse et de dédier de leur temps pour participer à ma soutenance.

Merci également à Amandine Véber et Anne-Laure Fougères pour avoir accepté de constituer mon comité de suivi de thèse et m'avoir offert des avis précieux pour la deuxième moitié de ma thèse.

Ma thèse, dont j'ai essayé d'orienter la trajectoire à l'interface de l'analyse d'équations aux dérivées partielles et la biologie évolutive, a par conséquent beaucoup bénéficié de mes interactions avec de nombreu.x.ses chercheu.r.se.s de ces deux domaines, que j'aimerais remercier sincèrement pour la bienveillance avec laquelle ielles ont partagé leur expertise: Ophélie Ronce, Florence Débarre, Denis Roze, Sébastien Lions, Jeannette Whitton, Jennifer Williams, John Welch, Gael Raoul, Alison Etheridge, Amandine Véber, Raphaël Forien, Jimmy Garnier, Quentin Griette, Léo Girardin et bien d'autres. Un grand merci particulièrement à Florian Patout, qui a toujours été disponible pour répondre à mes questions avant et pendant ma thèse et dont la connaissance pointue de l'analyse asymptotique du modèle infinitésimal a été précieuse.

Merci à Mete Demircigil, qui a égayé de nombreuses expériences de thèse que j'ai partagées avec lui: un sprint de modélisation du COVID à Mayotte, ma première conférence (virtuelle), une charge d'enseignement et des discussions sur des documentaires ARTE d'histoire des religions ou du colonialisme. Merci à Marion Jeannin pour m'avoir si bien accueilli dans le bureau au début de ma thèse et m'avoir aidé à naviguer la première année de l'ICJ entre TDs et missions à Vancouver. Merci également à Kyriaki Dariva et David Wahiche pour avoir été de très sympathiques co-bureaux et d'avoir rendu mon temps à l'ICJ toujours plaisant.

Mes missions ont joué un rôle central dans ma thèse, que ce soit en visite académique à UBC (Vancouver), Toulouse et Montpellier ou en conférences, workshops ou école de recherche. C'est pourquoi je ressens particulièrement un sentiment immense de gratitude envers Céline Laurent, qui a organisé toutes mes missions de visite à Vancouver ou de conférence, a collecté un nombre impressionnant de reçus de ma part à mes retours et a toujours essayé et réussi à faciliter mes trajets. Ma thèse lui doit beaucoup et je me sens privilégié d'avoir pu me reposer autant sur sa disponibilité et sa bienveillance. Je remercie également grandement toute l'équipe administrative de l'ICJ, notamment Christine Le Sueur pour avoir toujours été à mon écoute et m'a aguillé sur nombre démarches administratives.

Ma thèse a bien entendu été ponctuée d'étapes administratives en relation avec l'école doctorale et l'université. Merci à la direction de l'École Doctorale Infomaths (Hamamache Kheddouci, Dragos Iftimie et Renée El Melhem) et à Fabienne Macro du pôle Doctorat de l'UCBL pour m'avoir accompagné à les surmonter.

En tout ce qui concerne les aspects informatiques, d'autant plus essentiels à une thèse que celle-ci se déroule pendant une pandémie, je remercie Vincent Farget pour avoir configuré mon ordinateur et répondu à mes questions lors de bugs informatiques stressants, et Benoît Fabrèges pour ses nombreux conseils éclairants en matière algorithmique et pour m'avoir appris à utiliser le cluster de l'ICJ, ce qui a crucialement accéléré mon planning de simulations.

Une nouvelle aventure s'annonce pour moi au MAP5, dont j'ai pu avoir un aperçu dans mes derniers mois de thèse: merci à Anne Estrade et Amandine Véber pour m'avoir accueilli dans le labo depuis janvier, et à Apolline Louvet pour des discussions stimulantes.

These acknowledgments are also an opportunity to reflect on the time which led to this adventure that now comes to an end. Eco-Reality and Kexmin Field Station on Salt Spring Island have played a major part in bringing me to consider doing a PhD in maths applied to the natural world. I would like to convey my warmest thoughts to Cleome and Jan for welcoming me over and over again at their farm, Brent for taking me on hikes to educate me about the traditional knowledge of the ecology of Mount Maxwell and Ruckle Provincial Park (and Banff!), and Kate for all the greenhouse and garden work done side by side.

Finally, from even before its start, and ongoing throughout my PhD, I have been so grateful to be calling Gil Henriques and Linnea Sandell my friends, and to have been their roommates for almost a year in Vancouver, in particular during the first months of the COVID-19 pan-

demic. Thank you for creating a work atmosphere in our living room when the BRC was closed, and also for sharing the monthly brunches on the patio with us. The influence on my PhD work from all our conversations: about evolutionary biology, how to communicate science and maths, decolonizing science or the mysteries of the lifecycle of yeasts is greater than you think. Of course, there is one person still missing in this paragraph, even though her spirit runs through this whole work. Barbara, I feel so fortunate to be your partner, and I thank you so much for everything, for sharing my life throughout this PhD, from Vancouver to Europe, as an essential part of my support system and so much more. I hope I can be the same for you during your own PhD, and well beyond.

Enfin, à mes parents, à qui je dois presque tout, à mon frère et ma soeur, qui me connaissent si bien : merci pour votre soutien indéfectible et pour vos conseils toujours pertinents donnés autour de la table à manger. どうもありがとう.

Abstract

My thesis focuses on the asymptotic analysis of integro-differential models quantifying the influence of certain features of sexual reproduction on the eco-evolutionary dynamics of spatially distributed species characterized by quantitative traits with complex genetic architecture. It extends the analytical toolkit to study the dynamics of singular distributions arising in a regime where diversity introduced by reproduction is small. In the first chapter, I use separation of times scales techniques and completely characterize the equilibria of a population living in a discrete heterogeneous environment connected by migration, whose local adaptation is quantified by the action of selection on a quantitative trait resulting from a large number of small diallelic effects. In the second chapter, I explicit the biological framework underlying the previous chapter thanks to individual-based simulations with an explicit genetic description. In a third chapter, I propose a new hybrid model allowing to include the effect of a major gene onto the trait characterizing local adaptation in the previous context, whose analysis sheds some lights on an undocumented evolutionary phenomenon. In the fourth chapter, I present an explicit long-time approximation of the solution of a reaction-diffusion equation modelling the phenomenon of evolution of dispersion along range expansions, where the diffusion coefficient is the trait under evolution. In the fifth chapter, I analyse a new integro-differential model which describes the dynamics of quantitative alleles under general allelic interaction and selection function. In an annex, I present my contribution to a modelling project of the COVID-19 epidemic in Mayotte.

Keywords – *Integro-differential models, eco-evolutionary dynamics, sexual reproduction, spatial structure, quantitative traits, asymptotic analysis.*

Résumé

Ma thèse porte sur l'étude asymptotique de modèles intégro-différentiels quantifiant l'influence de certains aspects de la reproduction sexuée sur la dynamique éco-évolutive d'espèces spatialement distribuées caractérisées par des traits quantitatifs à architecture génétique complexe. Elle étend la gamme d'outils analytiques pour l'étude de la dynamique de distributions singulières dans un régime de faible variance introduite par reproduction. Dans le chapitre 1, j'utilise des techniques de séparation d'échelles de temps et caractérise complètement les états stationnaires du cas d'une population vivant dans un environnement hétérogène discret, connecté par migration, et dont l'adaptation locale est quantifiée par l'effet de la sélection sur un trait résultant de nombreuses contributions dialléliques à petits effets. Dans le chapitre 2, j'explicite le cadre biologique sous-tendant le chapitre précédent grâce à des simulations individus-centrées à description génétique explicite. Dans le chapitre 3, je propose un nouveau modèle hybride permettant d'inclure l'effet d'un gène fort sur le trait polygénique d'adaptation locale précédent, dont l'analyse met en lumière un phénomène biologique inédit. Dans le chapitre 4, je présente une approximation explicite en temps long de la solution d'une équation de réaction-diffusion modélisant le phénomène d'évolution de la dispersion lors d'invasions spatiales, où le coefficient de diffusion est le trait sous évolution. Dans le chapitre 5, j'analyse un nouveau modèle intégro-différentiel qui décrit la dynamique d'allèles quantitatifs sous des formes générales d'interaction allélique et de sélection. Dans une annexe, je présente ma contribution à un projet de modélisation de l'épidemie du COVID-19 à Mayotte.

Mots clés – *Modèles intégro-différentiels, dynamiques éco-évolutives, reproduction sexuée, structure spatiale, traits quantitatifs, analyse asymptotique.*

Résumé substantiel en francais

Étudier conjointement les dynamiques écologiques et évolutives d'espèces spatialement distributées est particulièrement crucial aujourd'hui, alors que le dérèglement climatique fragmente les écosystèmes, perturbe les transitions entre habitats et précipite le déclin d'espèces qui ne s'adaptent pas assez rapidement. Ces conditions sont également propices aux phénomènes d'évolution de la résistance (voir Resistance project 2018), qui commencent déjà à peser sur les systèmes alimentaire (résistance aux pesticides) et de santé (résistance aux antibiotiques/vaccins) de nos sociétés (cela revêt un sens particulier lors de la rédaction d'une thèse de doctorat en 2022). De plus, la mondialisation de notre réseau de transport a redéfini la répartition spatiale des espèces à un rythme sans précédent, ce qui résulte dans l'introduction massive d'espèces dans de nouveaux territoires et dans des invasions où l'adaption est primordiale. Cela a des conséquences sérieuses pour la conservation d'écosystèmes et d'espèces natives (Liu et al. 2020), dont la préservation soustend la résilience de ces mêmes systèmes alimentaire et de santé.

Prédir comment ces phénomènes complexes mêlant écologie et évolution se déroulent est ardu, car ils font intervenir a minima plusieurs forces dont les actions s'entrecroisent: la génération de diversité par reproduction, la variation de pressions locales de sélection naturelle, la distribution hétérogène de ressources à travers l'espace, et la capacité à se mouvoir par dispersion/migration. Y arriver requiert à la fois de quantifier l'importance relative de ces forces sur la dynamique évolutive des espèces et de rationaliser leur interaction. Les modèles mathématiques sont des outils appropriés dans cette optique. Cependant, ils deviennent particulièrement intriqués lorsqu'ils considèrent l'interconnexion des changements démographiques locaux et de l'évolution de traits distribués spatialement dans la population. Cela est exacerbé lorsqu'on considère des traits quantitatifs qui proviennent d'une structure génétique complexe et transmis par reproduction sexuée, qui fait intervenir de façon inhérente des processus non-linéaires (deux parents sont nécessaires) et non-locaux (le trait d'un descendant peut être distant de ceux de ses deux parents).

Tout le long de ma thèse, j'ai eu pour but de construire et d'analyser des modèles intégro-différentiels afin de quantifier l'influence de la reproduction sexuée sur les dynamiques spatiales éco-évolutives qui façonnent l'adaptation d'espèces. En particulier, j'ai développé des outils pour étudier ces dynamiques lorsque l'adaptation des individus dépend de traits quantitatifs résultant d'architectures génétiques intriquées.

Dans un premier chapitre introductif, j'introduis les processus évolutifs majeurs qui dictent l'adaptation d'espèces, particulièrement en rapport avec l'espace et le mode de reproduction: la sélection naturelle, la dérive génétique (élément stochastique particulièrement important dans les dynamiques de petites populations), le flux de gènes dans l'espace du aux mouvements migratoires ou dispersifs des individus et la génération de nouveaux traits par reproduction (par exemple, via mutations pour la reproduction asexuée/clonale, mais également la recombinaison et ségrégation allélique pour la reproduction sexuée). Puis, je présente l'état de l'art constitué d'études basées sur des modèles intégro-différentiels qui décrivent les dynamiques éco-évolutives de grandes populations via leur distributions en traits. D'abord, je discute du cas d'espèces se reproduisant asexuellement, ou clonalement (tout individu descend d'un seul parent), où les opérateurs de reproduction les plus fréquents sont linéaires et modélisent l'occurrence de mutations, soit non-localement via une convolution avec un noyau de mutation, soit localement via un opérateur laplacien de diffusion. Je décris particulièrement les travaux qui développent la méthodologie asymptotique de petite variance de mutation introduite par [Diekmann, Jabin, et al. 2005], qui permet de déduire des informations quantitatives sur

les distributions en trait n_ε lorsque celles-ci se concentrent vers des mesures n, comme des sommes de masses de Dirac, sous l'action de la sélection naturelle et de mutations de petite variance $\sqrt{\varepsilon}$ (voir Perthame and Barles 2008; Barles, Mirrahimi, and Perthame 2009; Lorz, Mirrahimi, and Perthame 2011 par exemple). Pour ce faire, cette méthodologie introduit un ansatz WKB suivant une transformation logarithmique d'Hopf-Cole: $u_\varepsilon := \varepsilon \log(\varepsilon n_\varepsilon)$, dont l'objet résultant u_ε converge (au moins formellement) vers une limite u plus régulière que la mesure limite n. Dans ces études avec des populations asexuées, cette limite u est souvent une solution de viscosité d'une équation de Hamilton-Jacoi sous contrainte (la contrainte étant liée à la taille de population qui doit rester bornée). Je distingue les études avec un espace homogène, de celles considérant un espace hétérogène discret (par exemple Mirrahimi 2017) et enfin un espace continu. Dans cette dernière catégorie est utilisée une méthodologie similaire (introduite antérieurement par Evans and Souganidis 1989) pour dériver analytiquement la vitesse de fronts de propagation solution d'équations de réaction-diffusion non-locales grâce aux niveaux de solutions d'équations d'Hamilton-Jacobi auxiliaires (voir Bouin and Mirrahimi 2015 par exemple). Une attention particulière est portée sur les études portant sur le phénomène de tri spatial résultant de l'évolution d'un trait de dispersion, modélisée par le fait que le coefficent de diffusion des équations de réaction-diffusion correspondantes est le trait sous évolution, ce qui produit des fronts accélérants (voir Bouin, Henderson, and Ryzhik 2017a; Berestycki, Mouhot, and Raoul n.d.; Calvez, Henderson, et al. 2022). Dans un deuxième temps, je me tourne vers les modèles intégro-différentiels avec des populations sexuées caractérisées par un trait quantitatif, où l'effet stochastique de la ségrégation des chromosomes est souvent traduit par le modèle infinitésimal de Fisher (Fisher 1919). Celui-ci, supposant que le trait résulte de nombreuses contributions additives de petits effets dialléliques, caractérise la déviation du trait d'un individu par rapport à la moyenne des traits de ses parents via une gaussienne à variance constante, appelée la variance de ségrégation (le cadre de validité de ce modèle est précisé dans Barton, Etheridge, and Véber 2017). Plusieurs études emploient les propriétés de contraction que possède l'opérateur non-local et non-linéaire qui découle du modèle infinitésimal, afin de décrire analytiquement les trajectoires évolutives de populations dans un environnement homogène (Calvez, Garnier, and Patout 2019; Patout 2020; Raoul 2021). Certaines d'entre elles adaptent la méthodologie de petite variance développée pour la reproduction asexuée, avec une différence notable: la variance dans leur cas est contrainte par la variance de ségrégation supposée petite ε^2, ce qui à son tour contraint formellement la distribution en trait n_ε à être proche d'une gaussienne (ou de façon équivalente, à ce que le terme principal de l'ansatz $u_\varepsilon = \varepsilon^2 \log(\varepsilon n_\varepsilon)$ soit quadratique). L'objectif principal de l'analyse perturbative présentée dans [Calvez, Garnier, and Patout 2019] est donc de caractériser le correcteur à ce profil gaussien, solution d'un problème faisant intervenir un terme de différence fini qui tranche avec la structure Hamilton-Jacobi asexuée. Il n'existe pas d'études similaires incluant une dimension spatiale hétérogène discrète et peu avec un espace continu. Mes projets de thèse avaient donc pour but de combler ce vide relatif.

Dans un deuxième chapitre, je présente un travail publié seul en 2022 dans "Journal of Mathematical Biology" (Dekens 2022). Dans celui-ci, j'étudie l'adaptation d'une espèce sexuée à un environnement hétérogène constitué de deux habitats symétriques caractérisés par des traits optimaux différents et reliés par migration, question classique de génétique quantitative. L'article de référence [Ronce and Kirkpatrick 2001] utilise une hypothèse gaussienne à variance fixe ad-hoc sur les distributions locales en trait afin de clore le système ODE décrivant la dynamique macroscopique des moments de ces distributions. Les auteures intuitent numériquement l'existence d'équilibres asymétriques bistables non triviaux, selon

lesquels la population occupe principalement un des habitats qui acte comme une source pour les autres. Dans mon travail, je résous ces deux limitations en utilisant la méthodologie de petite variance de ségrégation décrite précédemment pour compléter l'analyse des états stationnaires du système intégro-différentiel qui fait intervenir l'opérateur de reproduction du modèle infinitésimal. Pour ce faire, j'apporte des éléments de justifications à l'approximation gaussienne utilisée dans [Ronce and Kirkpatrick 2001], et je combine ensuite une analyse lente-rapide avec une propriété de polynômes symétriques (reflétant la symétrie de l'environnement) pour réduire la complexité algébrique du système. En particulier, je décris exhaustivement les équilibres asymétriques bistables mis en valeur dans [Ronce and Kirkpatrick 2001].

Le chapitre suivant présente un court travail numérique qui se base sur des simulations individus-centrées, avec description explicite des informations génétiques. Il a pour but de préciser le cadre biologique sous-tendant l'étude précédente, notamment d'examiner à quoi correspondent les hypothèses sous-jacentes du modèle infinitésimal tel que je l'ai utilisé dans un environnement hétérogène, à savoir que la variance de ségrégation peut être considérée comme constante par rapport au temps, à l'espace et aux familles, tout en étant petite par rapport aux autres paramètres. En comparant les trajectoires numériques du modèle intégro-différentiel déterministe avec celles des simulations individus-centrées stochastique et grâce à une étude systématique des variances de ségrégations, je montre que ces hypothèses sont valides lorsque l'intervalle des traits s'étend bien au-delà des traits optimaux locaux, soit que la sélection est stabilisante.

Le quatrième chapitre décrit un projet que j'ai initié en collaboration avec Sarah Otto (UBC, Vancouver) lors de ma dernière longue visite académique dans son équipe et dont les résultats sont actuellement sous révision post-soumission (Dekens, Otto, and Calvez 2021). Les hétérogénéités spatiales sont connues pour promouvoir un panorama de réponses génétiques, combinant des gènes à effets majeurs à une pléiade de gènes à petits effets (Orr 2001; Walsh and Lynch 2018). Cependant, les modèles de génétiques de populations sont souvent limités dans leur possibilité analytique et restreints aux environnements homogènes à cause de la grande complexité de l'espace des paramètres. Ma motivation originelle était de prendre une nouvelle approche et de construire un modèle hybride liant génétique quantitative et génétique des populations qui est adapté à des développements théoriques. Le problème de trop grande complexité est contourné en considérant une composante quantitative qui modélise un arrière-plan génétique d'une multitude de petits effets, et qui est héritée selon le modèle infinitésimal. Le trait sous sélection est somme de cette composante quantitative et d'un effet fort discret provenant de deux allèles A/a qui ségrègent au même gène. Il en résulte un nouvel opérateur de reproduction, dont l'effet de contrainte asymptotique dans le régime de petite variance de ségrégation nécessite des résultats d'analyse convexe nouveaux pour être identifié. Ceux-ci me permettent de prédire un phénomène contre-intuitif et non documenté de perte d'un des allèles majeurs sous forte sélection, confirmé par simulations individus-centrées. Ce travail inclut également une description schématique de la méthode en vue d'aider à l'appliquer à des modèles plus complexes de génétiques des populations.

Le cinquième chapitre présente un travail en collaboration avec Florian Lavigne publié en 2021 dans "SIAM Journal of Applied Mathematics" (Dekens and Lavigne 2021). Il s'intéresse au phénomène d'évolution des capacités de dispersion d'individus lors d'invasions spatiales, comme celle des crapauds-buffles en Australie (Phillips, Brown, Webb, et al. 2006), dont le front est composé d'individus avec des pattes plus longues et plus endurantes (tri spatial).

La dynamique de l'invasion spatiale structurée en trait est modélisée par une équation de réaction-diffusion dont le coefficient de diffusion est le trait sous évolution. Plusieurs études pour populations asexuées dérivent analytiquement le taux d'accélération de fronts solutions $\propto \boldsymbol{t}^{3/2}$, où la variable $\boldsymbol{t}$ est le temps (Bouin, Henderson, and Ryzhik 2017a; Berestycki, Mouhot, and Raoul n.d.; Calvez, Henderson, et al. 2022), en utilisant l'opérateur diffusif de mutations. En remplaçant ce dernier par l'opérateur de reproduction sexuée du modèle infinitésimal, le taux d'accélération a numériquement été montré être inférieur pour les populations sexuées : ($\propto \boldsymbol{t}^{\frac{5}{4}}$ - Calvez, Crevat, et al. 2020). Dans le travail avec Florian Lavigne, nous obtenons une approximation explicite de la distribution en trait spatiale en temps long, qui résout un problème limite dérivé formellement. Notamment, le trait moyen est explicitement décrit, à l'arrière et à l'avant du front, et l'approximation (numériquement confirmée) montre que la distribution à l'arrière du front est stationnaire et localement gaussienne, à variance contrainte par la variance de ségrégation, ce qui est qualitativement très différent du cas asexué.

Le sixième chapitre présente un travail en révision post-soumission effectué avec Sepideh Mirrahimi (Dekens and Mirrahimi 2021). Si la régulation d'expression génétique est désormais acceptée comme un mécanisme majeur des dynamiques d'adaptation (Romero, Ruvinsky, and Gilad 2012; Lenormand, Fyon, et al. 2020), les modèles de continuum d'allèles, qui proviennent de [Kimura 1965], sont restreints par des hypothèses sur la nature de la sélection et sur les interactions entre gènes qui ne sont pas nécessairement adaptées à étudier l'influence de la régulation d'expression génétique. Pour passer outre ces limitations, nous introduisons un nouveau modèle intégro-différentiel qui décrit les dynamiques éco-évolutives d'une espèce sexuée soumise à la compétition pour les ressources et la sélection naturelle dans un espace homogène. Il fait intervenir un opérateur de reproduction sexuée non-linéaire et non-local différent du modèle infinitésimal, car il décrit la transmission d'allèles quantitatifs à deux gènes (x, y) selon les lois Mendéliennes. L'interaction entre ces allèles peut être très générale, et est soumise à l'effet létal d'une fonction de sélection naturelle également générale. Dans un régime où la variance est faible au sein de la population, je montre la convergence forte (le long de sous-suites) de l'ansatz WKB $u_\varepsilon = \varepsilon \log(\varepsilon n_\varepsilon)$ (n_ε est la distribution des allèles) vers une limite u qui décorrèle les allèles x et y. Bien que les équations limites présentent des difficultés analytiques nouvelles en terme de régularité, leur étude permet d'illustrer quantitativement la richesse du modèle en terme de diversité des trajectoires qui peuvent être obtenues et décrites, selon la fonction de sélection et l'interaction entre gènes choisies.

Enfin, dans un chapitre annexe, je présente ma contribution (supervisée par Vincent Calvez) à un projet de modélisation de l'épidémie du COVID-19 à Mayotte, commencé en Mai 2020 en collaboration avec l'ARS de Mayotte, le Centre Universitaire de Mayotte et la plate-forme MODCOV19. En particulier, je décris le modèle épidémiologique structuré en âge sur lequel j'ai travaillé. Celui-ci avait pour but d'évaluer l'influence de la démographie particulière de Mayotte (plus de la moitié de la populations a moins de 20 ans) et son implémentation a nécessité une exploration bibliographique fouillée et intense. Les résultats de simulations numériques concernant la réouverture des écoles en mai 2020 sont également montrés.

Contents

Chapter 1

Introduction

Studying the joint dynamics of the ecology and evolution of spatially distributed species is especially crucial now, as climate deregulation fragments ecosystems and disrupts the dynamics which connect habitats, precipitating the decline of species that cannot adapt fast enough. These dynamics can also harbour the potentiality for the evolution of resistance (see Resistance project 2018), which already heavily pressurizes our societies' food (e.g. pesticides) and health (e.g. pathogens/viruses) systems (the latter conveys a particular resonance when writing a PhD thesis in 2022). Moreover, as a result of our globalized transport networks, species ranges have also been redefined at a pace never seen before, resulting in mass introduction of species to new territories and subsequent invasions where adaptation is key. This has serious consequences for the conservation of native species and ecosystems (Liu et al. 2020), which underlies the resilience of the same health and food systems.

Predicting how these complex phenomena unfold is challenging, as they involve at least several intertwined forces: the generation of diversity by reproduction, varying pressures of natural selection, heterogeneous distribution of resources across space, and the capacity for dispersal and migration. Doing so requires both quantifying the relative importance of these components on the evolutionary dynamics of species and rationalizing how they interact. Mathematical models are thus powerful tools for these purposes. However, they become particularly intricate when considering the interplay between local demographic changes and the evolution of traits distributed in the population. This is exacerbated when considering the transmission of quantitative traits with complex genetic architectures according to sexual reproduction, which inherently involves non-linear and non-local processes.

Throughout my PhD, I aimed to build and analyse integro-differential models to quantify the influence of certain features of sexual reproduction on the spatial eco-evolutionary dynamics shaping species adaptation. In particular, I developed tools for studying such dynamics when adaptation is characterized by quantitative traits resulting from complex genetic architectures.

1.1 Biological motivations

1.1.1 A brief overview of evolutionary theory and models

If one has the privilege to take a quick naturalist look around, it is often sufficient to be astonished at the sheer diversity of patterns that constitute the surrounding ecosystems. If ecology (the study of these ecosystems and their constituents) explains how this wide array of living organizations interact in the present, evolutionary theory completes it by describing the interplay of the processes that shape(d) it.

The most iconic of these processes (but not the only participating one) is *natural selection*, first theorized by [Darwin and Wallace 1858] following their separate peregrinations in South America and South-East Asia, and more extensively in the famous seminal book "On the Origin of Species" (Darwin, 1859). Natural selection describes the following: in a given environment and in a given population, individuals which have certain *traits* (for example, leaf shape, number of teeth or flowering time) survive better and produce on average more offsprings (which inherit these traits) than individuals with other traits. According to this view, natural selection requires some diversity for it to act upon and favour certain traits under given environmental pressures. Upon the biased transmission of these traits by descent, patterns emerge at the population trait distribution level as signs of the adaptation of species to their environment. The conceptual power of natural selection resides thus in its ability to articulate these two seemingly opposing concepts of variation and adaptation.

However, if it highlights the interaction between two constitutive elements (environment and varying traits in a population), Darwin and Wallace's theory lacked the exact description of the support of trait inheritance across generations which closes the loop (it is even more remarkable that they elaborated this theory without). The rediscovery of Mendel's work on peas' hybridization in the turn of the 20th century brought upon the notion of *genes* or *loci*, which can be seen as the discrete microscopic bricks of heritable information underlying the expression of macroscopic traits at the individual level. Within a population, different versions of each gene segregate, called *alleles*, which can translate in different traits. Over time, evolutionary processes change the frequencies of alleles in a population and therefore its trait distribution.

To quantify these changes and rationalize the influence of evolutionary processes, mathematical models have flourished, first underlying the Evolutionary Synthesis in the first half of the 20th century, under the impulsion of several protagonists: the most well-known are Fisher, Wright and Haldane. Their separate contributions provided a unified view of evolution, resolving the paradox of discrete Mendelian alleles resulting in apparently gradually changing continuous trait under (in particular) natural selection, and founded the framework of population genetics. Population genetic models aim at predicting how changes in allelic frequencies within a population occur through time under various contexts. Because explicitly modelling the joint dynamics of a large number of alleles is mathematically challenging due to the high complexity in variables that arises, population genetic models tend to consider the dynamics of adaption through a few major effect alleles (like eye's color - see Bürger 2020 for a review on multi-loci theory). One recurring question is how variation is maintained in view of *genetic drift* in finite populations. The latter designs the chance component that resides in the dynamics of alleles, even neutral ones w.r.t natural selection, which inevitably leads to allele *loss/fixation* events in the whole population, and therefore the reduction of genetic variation

(especially in small populations, where individuals carrying rare alleles might die by chance before reproducing).

On the other end of the spectrum, quantitative genetic models aim at modelling directly the dynamics of continuous quantitative traits within a population (like leaf shape, fur patterns or flowering time), resulting from the combined effects of a large number of small effects genes (Fisher 1919). Their study has been of sustained interest for animal and plant breeding companies. Since such polygenic traits often have complex genetic architectures, which are nowadays increasingly identified by Genome Wide Associations Studies (GWAS), the precise description of their inheritance is often hidden in quantitative genetic models, which rather focus on the focal trait's transmission. Moreover, because the natural mathematical objects of these models are trait distributions, whose temporal dynamics are described by Partial Differential Equations (PDE), such models often assume ad-hoc hypotheses on the trait distribution in order to reduce the analysis to a moment-based approach describing the temporal dynamics of macroscopic variables thanks to Ordinary Differential Equations (ODE) (see Burger 2000 for such methods).

1.1.2 The influence of spatial structure in evolutionary theory

(For a more detailed review, I recommend the interested reader to consult the introduction of Débarre 2010). Spatial heterogeneities and structures are ubiquitous, and thus most species do not live in homogeneous spaces, meaning that individuals live, mate and die depending on local environmental and demographic pressures. Therefore, models based on assumptions of well-mixed populations under homogeneous conditions, which cannot capture the local effects of spatial heterogeneities, might not reflect accurately the dynamics of spatially distributed species. In the scope of my PhD, I am interested in the influence of two particular types of spatial structure on species evolution: *discrete heterogeneous* (or patchy) environments and *continuous* environments.

Discrete heterogeneous (patchy) environments. According to this modelling of space, the considered environments are constituted by several patches in which local conditions are homogeneous, but potentially different between patches. A reasonable representation would be small islands separated by large stretches of sea. If they are not connected by *migration*, the local subpopulations are in *reproductive isolation* and the local adaptation to their patch can be described by models assuming well-mixed populations. However, as soon as migration connects the patches, the transfer of population that ensues between patches can translate on the genetic viewpoint into *gene flow*, as different alleles that have potentially been favored under the local conditions of each patch reach new habitats. Whether or not this disrupts the *local adaptation* of subpopulations is a central question in models quantifying *migration load* (as reviewed in Ronce 2007), and is linked to the notion of the maintenance or loss of *polymorphism* (at the gene of trait level) in face of *gene swamping* (describing the undermining of local selection due to strong gene flow). At the species level, it relates to the maintenance of its range through the qualifications of *generalist species*, (a species which thrives under a wide range of conditions) or *specialist species* (a species which thrives under a restricted range of conditions). At the clade's level (above the species level), this can also relate to the notions of *hybridization* (offsprings that are produced due to crosses between species) or *speciation* (the separation of a species into two distinct species, classified as *allopatric* in

the case of separate patches).

Quantifying the conditions under which these patterns of adaptation to a heterogeneous environment occur, a minima under migration and natural selection, has been explored by population genetics since the early years of the field. As reviewed in [Felsenstein 1976], the first population genetic models with spatial structure are due to Wright (Wright 1931) and Haldane (Haldane 1932), which introduce separately a one-locus *continent-island model* (a framework which considers that one patch's population is much larger than the other's and is therefore not influenced by the latter). Two alleles segregate at the focal locus and one is favored in the island, the other deleterious and the aim of the studies is to describe the maintenance of the favoured allele in the island. These studies paved the way to others accounting for more loci [Bürger and Akerman 2011] (two-locus continent-island model), [Akerman and Bürger 2014] (two-locus two-patch model), or more alleles per locus [Nagylaki and Lou 2001], [Nagylaki and Lou 2007] (one multi-allelic locus), [Bürger 2009a] and [Bürger 2009b]. Because the systems become quickly too involved to derive conditions in the most general case, the previous studies often use perturbative theory to analyse the equilibria of the focal system in various asymptotic regimes (weak/strong local selection, low/high migration - see also Karlin and McGregor 1972 for the methods). However, as the genetic architecture of traits related to local adaptation might not be restricted to major effect genes and can be polygenic (Orr 2001), similar questions have also been tackled by quantitative genetics models (Ronce and Kirkpatrick 2001; Hendry, Day, and Taylor 2001; Débarre, Ronce, and Gandon 2013; Débarre and Gandon 2011; Débarre, Yeaman, and Guillaume 2015). They highlight in particular the need for modelling jointly the trait and demographic dynamics, as their interplay can greatly influence the outcomes of the system in case of great discrepancy between local population sizes (Ronce and Kirkpatrick 2001). This emphasizes in turn the need to understand the underlying assumptions of how regulation and natural selection are modelled, and their consequences, as these matter in a context of discrete spatial structure (Débarre and Gandon 2011).

Continuous environments When the space available to a species is considered very large and with a low granularity, the species can be considered as evolving in a continuous environment, using the framework of reaction-diffusion equations. The first models study the dynamics of invasion by a homogeneously beneficial allele (Kolmogorov, Petrovsky, and Piskunov 1937, Fisher 1937), and quantify the speed of the invasion. Later, the adaptation of species to a *cline* (defined as "a gradient of continuous variation though space for a genetic or phenotypic character" in Donoghue et al. 2014, IV.3) focused modelling efforts from population genetics to understand the interplay between gene flow and local adaptation in a continuous environment separated in two (continuous) habitats (Haldane 1948, Fisher 1950), Slatkin 1973, Nagylaki 1975, Nagylaki 1978, see Débarre and Gandon 2010 for a recent study). Later, the adaptation of species range to a linear trait cline raised interest: a landmark paper [Kirkpatrick and Barton 1997] proposed a moment-based model that tracks both the demographic and trait changes through time and space. Its analysis highlights the possibility for limited range adaptation to a linear cline, an equilibrium that differs from the traditional dichotomy of invasion/extinction.

Species expansion in continuous environment has sustained an increasing interest, as they can be subsequent for example to the introduction of invasive species into new territories, which can threaten the conservation of native species (Liu et al. 2020). In the last two decades, field studies have highlighted a phenomenon of *spatial sorting* of traits related to dispersal abilities, where individuals at the front of an expansion present *dispersal trait* advantages: wingspan or strength in butterflies (Saastamoinen 2008), crickets (Thomas et al. 2001), birds (Berthouly-

Salazar et al. 2012); seed and stems characteristics in plants (Monty and Mahy 2010; Williams, Kendall, and Levine 2016); legs stamina and length in the infamous cane-toads invasion in Australia since the 1930's (Phillips, Brown, Webb, et al. 2006, Shine, Alford, et al. 2021). Spatial sorting of dispersal trait poses new challenge for the conservation of native ecosystems, as evidences have been mounting that it can lead to the acceleration of the invasion front (Phillips, Brown, Webb, et al. 2006; Shine, Alford, et al. 2021). This sparked a modelling effort for the evolution of dispersal in continuous environment, which often involves to study the spatial evolution of polygenic morphological traits (Ronce 2007). (Note that the evolution of dispersal in patchy environment has also been a subject of population genetic studies since the 1970's with for example [Balkau and Feldman 1973], [Hamilton and May 1977], [Hastings 1983], and of invasion analysis in bounded continuous environment [Dockery et al. 1998]).

1.1.3 Mode of reproduction: sexual vs. asexual

As evolution relies on modification by descent when genes are passed across generations, how these genes are transmitted, and subsequently the traits that they encode, is an essential component of evolutionary dynamics. Indeed, part of the variation, which is required for natural selection to act upon, is generated during the inheritance process. Throughout my PhD, I have been exploring the influence on eco-evolutionary dynamics of some features specific to sexual reproduction.

Brief overview of asexual and sexual reproduction In the history of life, *asexual reproduction* or clonal reproduction, according to which a single parent transmit all its genetic information to its offspring, was the first process of genetic transmission. No variation would be generated, if it was not for the alterations occurring during the replication of genetic information, the *mutations*. This mode of reproduction is still quite widespread in *prokaryotes* (single-celled organism that does not have a nucleus), for example in bacteria, and can be extended to include virus replication.

However, there exists a different mode of reproduction that fungi, plant and animal species (including humans), which constitute the "visible part" of our ecosystems, employ. Indeed, many of the latter use, at least facultatively, *sexual reproduction*, which is defined broadly as the "production of offspring that are a mixture between two different parental genotypes" (Donoghue et al. 2014, IV, 4 - note that this includes processes affecting prokaryotes, like horizontal-gene transfer between bacteria, which is, very roughly, a physical exchange of DNA from one individual to another). Sex is ubiquitous and evidences indicate that it has in fact evolved multiple times in parallel until now (as suggested by the different sex chromosomes Z/W in birds, compared to X/Y in mammals), but keeping similar features between these parallel apparitions, that are strikingly different from asexual reproduction. Despite these observations, the evolution of sex has long been (and continue being) a mystery for evolutionary biologists (Otto 2009). Indeed, engaging in the sexual reproduction act is often more costly, and each parent transmits only half of its genetic information to each offspring (versus all of it under asexual reproduction), which has been coined *the cost of sex*. One might interject that sexual reproduction does maintain intrinsically more variation in a population than asexual reproduction, even without any mutation occurring, due to the genetic shuffling or *segregation of parental alleles during meiosis* according to Mendelian laws. Consequently, it might increase the efficiency of the weeding action of natural selection (at least, it was how sex was presented in my high school biology class). However, the relationship between sex and variation is more intricate than this, and the review [Otto 2009] provides with an illuminating analogy with

poker, that works well for haploid individuals (only one copy of each gene), to illustrate why. Consider that one has a particularly good hand of cards. Then would that person be on average more successful if half of their cards were chosen randomly and exchanged for an equal number of cards from another successful hand, but potentially with a different combination?

This analogy highlights the role of *recombination* in sexual reproduction, which breaks *linkage* between alleles. One however has to recall that linkage has a high spatial component, as genes that are close on the chromosome tend (mostly) to be inherited together, except when there exists a *hot-spot* for recombination between them (a slightly more faithful version of the analogy might be that closest cards in the hand have a higher probability to be kept or exchanged together). Moreover, recombination includes the chromosome segregation during meiosis, but also the *crossing-over* phenomenon that happens at the molecular level when breaks in the DNA strands get repaired. Conceptually, both recombination and linkage are double-edge swords, as recombination can dissociate deleterious alleles' transmission from beneficial ones or allow the association of beneficial ones (previously linked by genetic drift) while linkage can favor certain combinations to be inherited together.

Recombination in population genetic models. As recombination is a central mechanism in sexual reproduction, its role in various contexts has been under scrutiny in the field of population genetics. [Hill and Robertson 1966] identified an effect due to the interplay between genetic drift, recombination and selection, coined the *Hill-Robertson effect*, which suggests that recombination leads to a faster fixation of a combination of two beneficial alleles. This effect was quantified in a mathematical framework by [Felsenstein 1974] (see also Otto and Barton 1997, Roze and Barton 2006 for further theoretical investigations and developments, and Otto and Barton 2001 for numerical ones). Furthermore, the key concept of *modifier genes*, which change the occurrence of crossing-over events and thus recombination rates (introduced by theoretical models of the 1970's (Feldman 1972) has allowed the role of recombination in spatially structure environment and with genetic drift to be investigated in [Lenormand and Otto 2000] (haploid populations in a two-patch model, n viability loci and one modifier locus, with epistasis), [Martin, Otto, and Lenormand 2006] (n patches, two-locus two-alleles model, genetic drift and selection, no epistasis), [Roze 2009] (diploid individuals, three-locus with dominance and epistasis) (see Otto and Lenormand 2002 for a review). They highlight in particular the role of *epistasis* (the non-additive effects of the interactions between several alleles at different loci) in favouring or not favouring recombination.

Limited range of sexual reproduction From a quantitative genetic view, the intricate genetic architecture underlying the focal complex evolving trait prevents to model precisely subtle changes in recombination rates between precise loci and derive analytical conclusions. Even modelling the effect of segregation of large number of alleles during meiosis on the transmission of the trait from two parents to an offspring required a conceptual step in the early days of evolutionary theory, and resulted in the *infinitesimal model* (Fisher 1919; Bulmer 1971; Lange 1978; Bulmer 1980; Barton, Etheridge, and Véber 2017, see also Section 1.2.3 for a lot more details). The latter is parsimonious in terms of parameters and has therefore been used in several theoretical studies (Slatkin 1970; Roughgarden 1972; Turelli and Barton 1990; Turelli and Barton 1994 for example). One of them, [Roughgarden 1972], explores the difference between asexual and sexual populations related to the evolution of their niche width (the variety of resources that they can exploit). It shows that, even by solely considering segregation through the infinitesimal model, sexual populations evolve more narrow niches under the shuffling action of segregation, in comparison to asexual ones, that can evolve to an

optimal niche width (from a large initial variance in trait). A driving question of this PhD is the following: to what extent does this feature of constrained variation induced by segregation of alleles with sexual reproduction intertwine with spatial structure, and compare to asexual populations?

This relates to the field of *geographic parthenogenesis* (Tilquin and Kokko 2016 for a review), which investigates the differences of spatial distributions between closely related asexual and sexual populations, for example, in *facultative* asexual plant species (species where individuals can reproduce through sex by pollination from another plant, but also self-mate). Differences can be latitudinal (see simulations in Peck, Yearsley, and Waxman 1998), but some field studies have also suggested the influence of historical glaciation events on the spatial distribution patterns of asexual/sexual Townsendia daisies (Thompson and Whitton 2006). This species has a much more limited spatial range for sexual populations than for the asexual ones, despite sexual individuals being as successful as asexual ones when planted outside their range during reciprocal transplant experiments (Hersh 2020).

1.2 State of the art

1.2.1 Delimitation of the scope

Species' ecological and evolutionary fates are both driven by biological phenomena occurring at individual and populations level. On one hand, the success or failure of each microscopic individual within a given environment, in terms of survival and offspring generation, depends both on their own genetic information, determining their own particular heritable traits, and on non-local ecological interactions with the whole neighboring ecosystem, like competition for resources, and might present a high stochasticity. On the other hand, the macroscopic population dynamics are driven by all the individuals' life successes or failures upon which it constantly feedbacks. In some cases, for example in relatively large populations, the stochasticity of individual trajectories might be thought to be averaging itself to produce rather deterministic population dynamics. Additionally to this scaling relative to population size, ecological phenomena and evolutionary consequences might also occur on different time scales, according to the seminal intuition of Darwin regarding gradual evolution of complex (continuous) traits (which is the focal interest of my PhD, rather than discrete ones). However, rigorously quantifying this kind of intuition requires a careful examination of the various scaling limits that appear in *individual-based models*, that follow the stochastic ecological trajectories of all individuals constituents of an evolving population. This has been done for example in a landmark paper [Champagnat, Ferrière, and Méléard 2006] that uses a birth-death stochastic individual-based model for asexually reproducing populations that accounts for various biological phenomena that drive individual's life, such as natural selection, non-local interactions like competition for resources, and non-faithful genes transmissions involving mutations. They show that, in the limit of large populations, their re-normalized stochastic process converges to a deterministic *partial differential equation* (PDE) describing the dynamics of a trait distribution n. A generic example of such a PDE is the following (it should be emphasized that [Champagnat, Ferrière, and Méléard 2006] derived more detailed PDEs, which will be presented more in depth in the next section)

$$\partial_t n(t,z) = \mathcal{B}[n](t,z) - \mathcal{D}[n](t,z). \tag{1.1}$$

In (1.1), $\mathcal{B}[n](t,z)$ (resp. $\mathcal{D}[n](t,z)$) represents a birth (resp. death) term of individuals with continuous trait $z \in \mathbb{R}^d$ at time $t > 0$, which can also depend non-locally on the whole

distribution trait n (see details in the next section).

As a more concrete and very basic example of what kind of PDE can be obtained (although the scope of [Champagnat, Ferrière, and Méléard 2006] is much more in depth), I will specify an example of birth and death terms as follows: $\mathcal{B}[n] : (t,z) \mapsto r\, n(t,z)$, where $r > 0$ is the reproductive/growth rate, and $\mathcal{D}[n] : (t,z) \mapsto [s(z) + \kappa \int_{\mathbb{R}^d} n(z')dz']\, n(t,z)$, where $s : \mathbb{R}^d \to \mathbb{R}_+$ is the function quantifying the mortality provoked by natural trait-dependent selection, and $\kappa > 0$ measure the intensity of the uniform competition for resources. The PDE (1.1) then reads

$$\partial_t n(t,z) = n(t,z)\left[r - s(z) - \kappa \int_{\mathbb{R}^d} n(t,z')dz'\right]. \tag{1.2}$$

Note that if we ignore the effect of natural selection (setting $s \equiv 0$) and integrate over all the trait space $\mathbb{R}^d$, (1.2) reduces to the famous logistic growth equation, that can be classified as the archetypal ecological model:

$$\frac{d}{dt}N(t) = (r - \kappa N(t))N(t), \tag{1.3}$$

where $N(t)$ denotes the population size at time t. A population whose dynamics are governed by this logistic equation grows exponentially when small and then saturates when its size reaches $\frac{r}{\kappa}$, as its derivative in time becomes negative. The exponential growth at small density comes from the birth operator considered in (1.2), which is linear, and can describe for example a situation with asexual populations and completely faithful trait transmission. In the population dynamics models combining ecology and evolution that will be described and studied henceforth, the birth term will be of special focus, because we consider that the events that introduce the diversity necessary for natural selection to act upon occur during reproduction and birth (mutations/segregation/recombination).

A straight-forward extension of (1.1) that will be of interest in the next sections integrates a heterogeneous spatial structure. Suppose the species occupies two habitats, which are connected by migration. Then, indexing the parameters and variables by habitat, one can consider the following system

$$\begin{cases} \partial_t n_1(t,z) = \mathcal{B}_1[n_1](t,z) - \mathcal{D}_1[n_1](t,z) + \mathcal{M}_{2\to1}[n_1,n_2](t,z) - \mathcal{M}_{1\to2}[n_1,n_2](t,z), \\ \partial_t n_2(t,z) = \mathcal{B}_2[n_2](t,z) - \mathcal{D}_2[n_2](t,z) + \mathcal{M}_{1\to2}[n_1,n_2](t,z) - \mathcal{M}_{2\to1}[n_1,n_2](t,z). \end{cases} \tag{1.4}$$

Here, the operators $\mathcal{M}_{i\to j}, (i,j = 1,2)$ represent the instantaneous transfer of individuals by migration from the habitat i to the habitat j. A case that will be specifically shown below is the one of constant migration rate $m > 0$ from one habitat to the other, which translates into: $\mathcal{M}_{1\to2}[n_1,n_2] = m\, n_1$ and $\mathcal{M}_{2\to1}[n_1,n_2] = m\, n_2$. Note that (1.4) is easily generalized for situations involving $H \geq 2$ different habitats.

In a later work [Champagnat and Méléard 2007], the authors derive, similarly as in their previous work, the limit objects obtained when considering spatially distributed species whose individuals diffuse at a trait-dependent and space-dependent rate in a continuum according to various renormalizations limits. In the large population asymptotics, it is a reaction-diffusion PDE acting on a spatial trait distribution $n(t,x,z)$, where x denotes the spatial variable, of general form given by

$$\partial_t n(t,x,z) = \mathcal{B}[n](t,x,z) - \mathcal{D}[n](t,x,z) + \mathcal{M}[n](t,x,z). \tag{1.5}$$

Here, $\mathcal{M}[n](t,x,z)$ represents the instantaneous spatial movement of individuals with trait z at location x. Setting it to be the diffusion operator of the heat equation $\mathcal{M}[n](t,x,z) =$

$\Delta_x n(t,x,z)$ and adding it to the logistic growth equation (1.3) yields the famous and widely studied local FKPP equation (from the names of the people that studied its properties first)

$$\partial_t N(t,x) = N(t,x)(r - \kappa N(t,x)) + \Delta_x N(t,x). \tag{1.6}$$

Note that, without integrating over all the traits, it would have yielded a non-local version of the FKPP equation.

In my PhD thesis, I will focus on such large populations deterministic limits, and thus on PDE/integro-differential equations (like the generic ones (1.1),(1.4),(1.5)) that describe how the adaptation of species characterized by continuous traits/phenotypes is shaped by the interplay between space-dependent ecological mechanisms (birth, death, migration/dispersal) and reproduction-dependent evolutionary mechanisms (mutations, segregation/recombination), particularly for sexually reproducing populations.

Remark: Adaptive dynamics. [Champagnat, Ferrière, and Méléard 2006] obtained another mathematical limit object, when simultaneously taking large population and rare mutations limits: a jump process model. This kind of model translates the heuristics that the occurrences of mutations are so sparse that, after a mutation appears, the ecological dynamics of the historic strain and the variant with the mutation are deterministic and reach a steady state before another mutation occurs. This trait substitution process, modelled by the so-called *canonical equation*, is the fundamental object of study of *adaptive dynamics*, originating from *evolutionary game theory* (see Metz et al. 1996; Dieckmann and Law 1996; Geritz et al. 1997 for seminal works, and Champagnat, Ferrière, and Ben Arous 2002 for more details on the derivation of the canonical equation from stochastic processes). As this approach relies on the (ecological) competition of a resident and a mutant population that are not structured according to a continuum of traits (between the occurrence of two consecutive mutations), I will consider it outside of the scope of my PhD work. I would like to mention however that this formalism has yielded numerous works studying the effect of spatial structure on the adaptive dynamics of asexual species, especially on the evolution of dispersal. I will present a quick overview of them at the end of the next section centered on works for asexual populations, for they introduce interesting concepts, like the ideal free distributions. Furthermore, I anticipate on the next section, which will highlight, among other approaches, one relying on small mutational variance (but where mutations are not rare, and most of the time, even frequent), which borrow adaptive dynamics nomenclature to describe similar concepts (although, once again, the underlying biological framework is undoubtedly distinct).

I will next present and discuss anterior works fitting within the scope of my PhD thesis, of which I have tried to roughly draw the boundaries above. I will contrast studies for asexually reproducing populations from those for sexually reproducing populations, and within each section, distinguish works for well-mixed populations (homogeneous space), next, populations structured in discrete heterogeneous environments and finally in continuous environments.

1.2.2 Asexually reproducing populations

In asexually reproducing populations, as every offspring is a genetic clone of its sole parent, the main source of genetic/trait diversity that can support evolution of a species are the mutations that occasionally arise during the transmission of genetic information. Despite the variety of how exactly the mutational molecular process occurs, their effects on a quantitative trait have

been modelled essentially through two types of reproduction operators. These were formally introduced in the seminal work of [Kimura 1965], which promoted the idea of a *continuum-of-alleles*. He considered that there is a low probability that two mutations arising independently in a population and affecting the same gene have the same exact effect. Consequently, parallel repeated mutations at a focal locus in a population would result in infinitely many alleles segregating at this locus. Therefore, he thought that a continuous view of alleles' effects was more adequate than a discrete one in certain situations. He formally derived two operators to model the effect of mutation on a single focal locus in a haploid population. The first is a non-local integral operator

$$\begin{aligned}\mathcal{B}^{\text{mut}}_{\text{non-local}}[n](t,z) &= (1-\mu(z))n(t,z) + \int_{\mathbb{R}} \mu(z')K(z-z')n(t,z')dz' \\ &= (1-\mu(z))n(t,z) + (K * \mu n(t,\cdot))(z).\end{aligned} \tag{1.7}$$

In (1.7), the parameter $\mu \geq 0$ is the mutation rate (here supposed to be constant but trait-dependent) and K is the mutation kernel, which quantifies the probability that an offspring of a parent with trait z' displays a trait z, deviated by mutations. Typical assumptions on K is that it is the density of an unbiased probability measure with finite variance, which translates into $\int_{\mathbb{R}^d} K(z)dz = 1$, $\int_{\mathbb{R}^d} zK(z)dz = 0$ and $\int_{\mathbb{R}^d} z^2K(z)dz = \sigma_M^2$, where σ_M^2 is the mutational variance. Next, considering a Taylor expansion and neglecting higher moments of K under the intuition of small mutational steps, he formally derived his famous localized *diffusion approximation* operator

$$\mathcal{B}^{\text{mut}}_{\text{local}}[n](t,z) = (1-\mu(z))n(t,z) + \frac{\sigma_M^2}{2}\Delta_z(\mu n)(t,z). \tag{1.8}$$

Note that originally, Kimura intended for (1.7) and (1.8) to be applied to a single focal locus in haploid (sexual) populations. However, as reviewed in the classical population genetic models textbook [Burger 2000], it has since been increasingly transposed to the study of quantitative traits in asexual populations, as the transmission processes in these particular cases are quite similar.

These two operators (1.7) and (1.8) were indeed rigorously obtained in [Champagnat, Ferrière, and Méléard 2006] at the limit of renormalizations of stochastic processes (in even more general forms). The first non-local operator (1.7) is derived in the limit of large populations, whereas the second one requires additional rescaling, considering that birth and death are accelerated, while the mutational variance is small (small effects mutations).

As will be described in the next subsections, the mutational operators (1.7) and (1.8) have been widely used in models studying the adaptation of asexually reproducing populations through mutations in various contexts. One reason for this success relies on the fact that both $\mathcal{B}^{\text{mut}}_{\text{local}}$ and $\mathcal{B}^{\text{mut}}_{\text{non-local}}$ are linear operators. Moreover, the presence of the Laplacian operator in (1.8) opens the potential to use classical analytical tools for the study of linear elliptic or parabolic PDEs. Note that, due to the properties of the mutational kernel K, these operators also preserve the mass and the center of mass of the trait distribution n considered:

$$\int_{\mathbb{R}^d} \mathcal{B}^{\text{mut}}_{\text{non-local}}[n](z)dz = \int_{\mathbb{R}^d} n(z)dz, \qquad \int_{\mathbb{R}^d} z\mathcal{B}^{\text{mut}}_{\text{non-local}}[n](z)dz = \int_{\mathbb{R}^d} zn(z)dz.$$

Finally, one can also see that any distribution with finite second-moment that is fixed under the action of $\mathcal{B}^{\text{mut}}_{\text{non-local}}$ leads satisfies $(\hat{\mu n})(\xi) = 0$ wherever $\hat{K}(\xi) \neq 1$ for all $\xi \in \mathbb{R}^d$, where $\hat{\cdot}$ denotes the Fourier transform. For example, for a typical choice of Gaussian mutational kernel K, the last condition is almost always satisfied. Hence n must be 0 almost everywhere.

Furthermore, any non-negative distribution n fixed under the action of $\mathcal{B}^{\text{mut}}_{\text{local}}$ is solution of the elliptic equation $\Delta_z(\mu n) = \mu n$. Then the elliptic maximum principle implies that there cannot exist compactly supported or even thin-tailed fixed points of $\mathcal{B}^{\text{mut}}_{\text{local}}$. This translates the fact that introducing mutations without any other forces (natural selection) only increases the phenotypic range of a distribution, either through a convolution or a diffusion operator.

In the rest of this section, I will present a view of the different works and PDE approaches that have been produced to improve the understanding of the mechanisms of eco-evo adaptation of asexual species in homogeneous, discrete heterogeneous and continuous space. Although my central interest lies within the study of sexual populations, I will detail in some lengths the following studies, to illustrate the richness of techniques and results that have been used and obtained, and draw a contrast w.r.t. analogous sexual populations studies.

1.2.2.1 Homogeneous space

In this subsection, I will mainly present works that illustrate a particular prolific approach that was developed significantly for asexual quantitative genetic models in the last two decades, which is the *small variance methodology*, for it has strong ties with most, if not all, of my PhD works. I will also nonetheless give a brief overview of other approaches used to study asexual reproducing populations in homogeneous environment.

Small mutational variance methodology. The small variance methodology was introduced for quantitative genetics models by [Diekmann, Jabin, et al. 2005], in a model studying the possibility for *evolutionary branching* in response to trait-dependent access to two resources, modelling mutations thanks to a non-local operator (1.7). Assuming that the mutations variance ε^2 was small, and expecting therefore the trait distribution n_ε to concentrate, they used the so-called Hopf-Cole transform on the latter

$$n_\varepsilon = e^{\frac{u_\varepsilon}{\varepsilon}}. \tag{HC}$$

The intuition behind this transform and the subsequent shift in the main analysis that is carried on the ansatz u_ε rather than on n_ε are detailed in Box 1.2.2.1. The authors of [Diekmann, Jabin, et al. 2005] showed that the differential equation obtained on the ansatz u_ε was formally converging toward a *constrained Hamilton-Jacobi equation*, characterizing the limit u as a *viscosity solution* of the latter. By doing so, they transposed the analysis from a singular problem to a more regular and better known type of equation, to which there exists a rich variety of results (see Barles 2013). The constrained nature of the limit equation comes from the fact that asymptotically, coupling (HC) with a bounded population size $I_\varepsilon := \int_{\mathbb{R}^d} n_\varepsilon(z)dz < +\infty$ implies (at least formally), that u is non-positive and reaches 0 somewhere (see also Box 1.2.2.1 for the details).

The use of transform like (HC) was not new in the theory of PDE at the time, for this formalism from geometric optics was popularized in particular in the study of large-time behaviour of reaction-diffusion equations, where the limit object u is a viscosity solution of a *Hamilton-Jacobi equation*, whose levels sets characterize the front propagation's dynamics (see Evans and Souganidis 1989 for a PDE point of view using methods from the optimal control theory). However, the novelty in the context of quantitative genetics comes from the feedback from the non-local bounded population size which *constrains* the non-positive limit u to reach 0 somewhere.

To my knowledge, the first study that rigorously established the link between the PDE on the trait density of a quantitative genetic model for asexual populations and viscos-

ity solutions of a constrained Hamilton-Jacobi equation in the regime of small mutational variance is [Perthame and Barles 2008]. The authors consider that the population is subject to the environmental pressure $R(z, I_\varepsilon(t))$, combining for example the effect of trait-dependent natural selection and decreasing w.r.t. a non-local term of competition for resources $I_\varepsilon(t) = \int_{\mathbb{R}^d} \psi(z) n_\varepsilon(z) dz$, with ψ positive, bounded away from 0, and smooth. One might want to keep in mind, for an easy interpretation of the non-local term I_ε, that $\psi \equiv 1$ (uniform competition) leads to I_ε reducing to the population size: $I_\varepsilon = \rho_\varepsilon := \int_{\mathbb{R}^d} n_\varepsilon(z) dz$. Further, the authors model the effect of mutations thanks to the local operator (1.8) in the following non-linear equation

$$\varepsilon \partial_t n_\varepsilon(t,z) = \varepsilon^2 \Delta_z n_\varepsilon(t,z) + R(z, I_\varepsilon(t)) n_\varepsilon(t,z), \qquad z \in \mathbb{R}^d, \quad t > 0. \tag{1.9}$$

Notice that the time is rescaled by the small parameter ε, as the effect of the small mutations requires such long time scales to have an influence on the dynamics. Once again, we emphasize the non-locality of the parabolic equation (1.9) through the non-local population feedback due to the decreasing dependence of R on I_ε (the latter translating the increase of competition with higher population sizes). The main results of [Perthame and Barles 2008] set the stepping stones for future studies: they first obtain preliminary uniform BV estimates on the non-local competition term I_ε, which shows the convergence of I_ε toward a limit I in L^1, and therefore the weak convergence of n_ε towards a limit measure n. The challenge is to understand where the singular measure n concentrates (ie. its support). The BV control of the non-local term I_ε is next instrumental to prove the convergence along subsequences of the Hopf-Cole ansatz $u_\varepsilon = \varepsilon \log(\varepsilon n_\varepsilon)$ (see also (HC)) toward a viscosity solution of the following constrained Hamilton-Jacobi equation:

$$\begin{cases} \partial_t u(t,z) = |\nabla u(t,z)|^2 + R(z, I(t)), \qquad z \in \mathbb{R}^d, \quad t > 0, \\ \max(u(t,\cdot)) = 0. \end{cases} \tag{1.10}$$

I refer to the Box 1.2.2.1 for heuristics about the derivation of (1.10). The actual proof involves obtaining *Lipschitz estimates and uniform bounds on* u_ε when ε is small, so that the *Arzela-Ascoli theorem* applies. The link between the limit measure n (obtained by weak convergence of n_ε following a priori estimates) and the limit function u is that the support of n is a subset of the zeros of u (see the third paragraph of the Box 1.2.2.1 for heuristics). In particular, the authors show that when the trait is unidimensional ($z \in \mathbb{R}$) and the environmental pressure term $R(z, I)$ is monotonic w.r.t. the trait z, the population remains *monomorphic* at the dominant trait $\bar{z}(t)$ ($n(t,\cdot) = \delta_{\bar{z}(t)}$) all along its evolutionary trajectory. In this case, they also derive a *canonical equation* that describes explicitly the dynamics of the dominant trait $\bar{z}(t)$. Moreover, the convergence $u_\varepsilon \to u$ along subsequences highlights the fact that uniqueness of the limit solution u among viscosity solutions of (1.10) is not a priori guaranteed (see much below the later developments on that question by [Mirrahimi and Roquejoffre 2016] and [Calvez and Lam 2022]). [Perthame and Barles 2008] highlights one particular case where it can nonetheless be obtained. This occurs when assuming a specific form of the environmental reaction term $R(z, I) = \mathcal{B}(z) - Q(I)\mathcal{D}(z)$, which decouples trait-dependent birth and death terms, and where the non-local environmental feedback term I only affects one of them as a factor.

Box 1.2.2.1: Small variance methodology for studying concentration phenomena: heuristics

Singular limit n. In the context we are interested in, as the size of population $I_\varepsilon := \int_{\mathbb{R}^d} n_\varepsilon(z)dz$ is constrained to remain bounded, and even positive for persisting populations, the population trait density is expected to concentrate under the balanced influence of the reduction of diversity induced by the trait-dependent selection-competition and the introduction of diversity from mutations with small variance ε^2. From a priori uniform estimates on I_ε dependent on the specific problem, one might obtain, at the limit of vanishing variance, that the population density n_ε converges weakly to a *singular* Dirac (or sum of Dirac, both) measure n concentrated on the fittest traits. One interesting features would be to determine the support of that measure, which would indicate the fittest dominant traits on which the population density concentrates.

A quadratic/Gaussian example. The value of considering the Hopf-Cole transform (HC) can be illustrated with the example of the convergence of Gaussian densities to Dirac measures, setting $u_\varepsilon : z \mapsto -\frac{|z-\bar{z}_\varepsilon|^2}{2} - \frac{\varepsilon \log(2\pi\varepsilon)}{2}$, and assuming that $\bar{z}_\varepsilon$ converges to a limit $\bar{z}$ when ε vanishes. Together with (HC), the latter yields that (n_ε) are Gaussian with vanishing variance, thus converging in the sense of measures to $n = \delta_{\bar{z}}$. However, (u_ε), that are close to quadratic functions, converges strongly toward a smooth function $u = -\frac{|z-\bar{z}|^2}{2}$. The idea is that studying the asymptotic properties of u (for example its zero set, which contains the support of n) is much more accessible than for n, and that this might lead to derive quantitative fundamental information on the evolutionary trajectories of the population retained by u in the limit.

Formal derivation of a constrained Hamilton-Jacobi equation. For a specific example, let us consider the equation (1.9). Performing the transform $n_\varepsilon = e^{\frac{u_\varepsilon}{\varepsilon}}$ and plugging the latter in (1.9) divided by n_ε reads

$$\partial_t u_\varepsilon(t,z) = \varepsilon \Delta u_\varepsilon(t,z) + |\nabla u_\varepsilon(t,z)|^2 + R(z, I_\varepsilon(t)). \tag{1.11}$$

Upon appropriate convergence estimates of I_ε toward I and appropriate estimates on u_ε, the equation (1.11) yields the first line of (1.10). The constraint $\max(u) = 0$ is obtained by noticing that

$$\int_{\mathbb{R}^d} \psi(z') e^{\frac{u_\varepsilon(t,z')}{\varepsilon}} dz' = I_\varepsilon(t).$$

Formally, the integral term diverges asymptotically if there exists z_0 such that $u_\varepsilon(z_0) > \delta > 0$ uniformly w.r.t. ε and vanishes, if u_ε is uniformly bounded by above by a negative constant. It also formally hints that the support of the limit measure n is a subset of the zero set of u.

Some remarks. This formal derivation reveals several key points of interest. First, it justifies a posteriori the time scaling of (1.9), and highlights the discrepancy between the variance in trait of the population (of order ε), much larger than the contributing mutational variance (of order ε^2). Second, passing from the second order parabolic equation (1.9) to the first order (although genuinely non-linear) equation (1.10) opens the analysis to use tools like the method of characteristics. Third, the constraint $\max(u(t,\cdot)) = 0$ for all $t > 0$ adjusts the non-local term I in order to be verified. Fourth, the term $H(z, I(t), \nabla u(t,z)) = -|\nabla u(t,z)|^2 - R(z, I(t))$ is the *Hamiltonian*, which is concave and is associated to the *Lagrangian* $L(q) = \sup_{p \in \mathbb{R}^d} [pq - H(p)] = -\frac{|q|^2}{4} + R(z, I(t))$. The viscosity theory of Hamilton-Jacobi equations, which is beyond the scope of my PhD, links the viscosity solutions to the trajectories that minimize the action of the Lagrangian (see Evans and Souganidis 1989 for an example on a non-constrained Hamilton-Jacobi equation arising from reaction-diffusion equation). If one replaces the local mutation operator (1.8) by the non-local integral version (1.7) in (1.9) (like in [Barles, Mirrahimi, and Perthame 2009]), one obtains another Hamiltonian in the analogous constrained Hamilton-Jacobi limit equation: $H(p) = -\int_{\mathbb{R}^d} K(z') e^{p \cdot z'} dz' + R(z, I(t))$ (the Laplace transform of the mutational kernel K).

Next, in [Barles, Mirrahimi, and Perthame 2009], results were derived for a similar framework as in [Perthame and Barles 2008], but with a non-local reproduction/mutations opera-

tor (1.7) including a trait and population size-dependent birth rate (bounded and Lipschitz continuous)

$$\begin{cases} \varepsilon \partial_t n_\varepsilon(t,z) = \displaystyle\int_{R^d} \frac{1}{\varepsilon^d} K\left(\frac{z-z'}{\varepsilon}\right) b(z', I_\varepsilon(t)) n_\varepsilon(t,z') dz' + R(z, I_\varepsilon(t)) n_\varepsilon(t,z), \\ I_\varepsilon(t) = \displaystyle\int_{\mathbb{R}^d} \psi(z') n_\varepsilon(t,z') dz', \qquad z \in \mathbb{R}^d, \quad t \geq 0. \end{cases} \tag{1.12}$$

In the same asymptotics of vanishing mutational variance ε^2, they show the convergence of the Hopf-Cole transform ansatz u_ε (see (HC)) toward a viscosity solution of a constrained Hamilton-Jacobi equation, but with a different Hamiltonian than in [Perthame and Barles 2008] (see the last paragraph of Box 1.2.2.1).

In [Lorz, Mirrahimi, and Perthame 2011], the authors show that, when considering the action of the local operator (1.8) to model the mutations on a multi-dimensional trait $z \in \mathbb{R}^d$, the assumptions of concavity of the inital state and of the reaction term $R(z, I)$ w.r.t its dependence on the trait were propagating forward in time along solutions u of the constrained Hamilton-Jacobi equation (1.10). This implies new regularity of the trajectories, as it ensures *monomorphism* of the trait distribution at all time, with the dynamics of the regular dominant trait encoded in a canonical equation. Furthermore, the long-term stability of a steady state is ensured thanks to a Lyapunov-type argument. Further regularity on the non-local term I ($W^{1,\infty}$ instead of L^1) is obtained (as no jump occurs due to the monomorphism).

Despite the achievements of these initial studies, how uniqueness of the limit object u could be guaranteed beyond the specific case mentioned in [Perthame and Barles 2008] was still quite an open question. However, the propagation in time of [Lorz, Mirrahimi, and Perthame 2011] paved way for the first significant uniqueness result in [Mirrahimi and Roquejoffre 2016] (see also [Mirrahimi and Roquejoffre 2015] for a succinct summary). This study focuses on the constrained Hamilton-Jacobi equation (1.10), assuming concavity on the initial state and the reaction term similarly as in [Lorz, Mirrahimi, and Perthame 2011]. Inspired by the fact that monomorphism arises under these conditions, they transformed the constrained equation (1.10) into a system constituted of the *unconstrained Hamilton-Jacobi equation* (first line of (1.10)) coupled with the *canonical equation* that describes the dynamics of the dominant trait $\bar{z}(t)$ (which exists and is regular according to Lorz, Mirrahimi, and Perthame 2011). Furthermore, the non-local term $I(t)$ is implicitly defined by the constraint in the monomorphic population:

$$\begin{cases} \partial_t u(t,z) = |\nabla u(t,z)|^2 + R(z, I(t)), \quad z \in \mathbb{R}^d, \quad t \in [0,T], \\ \frac{d\bar{z}}{dt} = \left(D^2 u(t, \bar{z}(t))\right)^{-1} \nabla_z R(I(t), \bar{z}(t)), \quad t \in [0,T], \\ R(\bar{z}(t), I(t)) = 0, \quad t \in [0,T]. \end{cases} \tag{1.13}$$

The authors use dynamic programming to work with the variational representation of solutions of the unconstrained Hamilton-Jacobi equation (first line of (1.13)) as minimization of the Lagrangian action along paths. Thanks to the latter, they proved that there exists a unique viscosity, bounded from above solution to the unconstrained equation (first line of (1.13)), which is actually a classical regular solution. Using the uniqueness of the unconstrained equation for fixed I and its regularity, they deduced the uniqueness of the solution to the system (1.13), thanks to a Banach fixed-point argument, and therefore the uniqueness of the (classical) solution to the original Hamilton-Jacobi equation (1.10).

More recently, an even more general uniqueness result was established in [Calvez and Lam 2022], that goes beyond the concavity of the initial data and reaction term framework considered in [Mirrahimi and Roquejoffre 2016]. This new result applies to general convex and super-linear Hamiltonian $p \mapsto H(z, I, p)$ (encompassing hamiltonians obtained with the

small variance methodology from both the local and non-local reproduction operators (1.7) and (1.8)), that are also decreasing w.r.t. the non-local term I. They consider therefore the following constrained equation

$$\begin{cases} \partial_t u(t,z) + H(z, I(t), \nabla_z u(t,z)) = 0, \quad z \in \mathbb{R}^d, \quad t \in [0,T[, \\ \max(u(t,\cdot)) = 0, \quad \forall t \in [0,T[. \end{cases} \tag{1.14}$$

The uniqueness of the solution (u, I) to the constrained Hamilton-Jacobi equation is obtained among the pairs of viscosity solution and BV functions, and therefore encompasses situations of jumps of the population size. This constitutes a uniqueness result in a larger class of solutions as in [Mirrahimi and Roquejoffre 2016], where it was obtained among classical solutions u and regular non-local term I (due to the smoothness of monomorphic trajectories). The proof uses the duality Hamilton/Lagrangian to work almost exclusively on variational formulation of minimization of the Lagrangian action along paths. The constraint of non-positivity is reflected by the role of the non-local term $I(t)$ which has to adjust the minimal Lagrangian action along optimal paths (wherever they might end) to stay zero at each time. A first preliminary result is the BV regularity of $\dot{\gamma}$ for such optimal paths γ that minimize the Lagrangian action. The main result is proved by contradiction, considering (u_1, I_1) and (u_2, I_2) two solutions of (1.14) with I_1, I_2 BV functions and using that crossed terms in the variational formulation have a sign by minimization and the constraint.

Finally, [Lam 2019] obtains a series of results within the small mutational variance framework/Hopf-Cole transform/constrained Hamilton-Jacobi equation. The author studies the steady states of an equation which is similar to the one considered in [Perthame and Barles 2008] and [Lorz, Mirrahimi, and Perthame 2011], but with two differences. First, the reaction term decouples a trait-dependent selection on fecundity term and a non-local mortality by trait-dependent competition through a kernel $K(z, z')$ (intensity of competition between individuals with trait z and z'). Second, and this is a significant difference, the trait considered is unidimensional and bounded in an interval. This allows to go further in the steady states analysis asymptotically w.r.t the vanishing mutational variance, which the author characterizes as threefold according to a ratio between competition and selection representing the *capacity of one trait to invade another*. This quantity is commonly used in adaptive dynamics studies. If this invasion ratio is uniformly convex and minimal along one direction in one point in the interior of the trait interval, then the population will concentrate asymptotically on this interior point as a Dirac mass. If this invasion ratio is uniformly concave and maximal along one direction, then the population will concentrate asymptotically as a sum of two Dirac masses at the edge of the trait interval. If the invasion ratios against the extremal traits are both monotonic (with opposing signs), then there exists at least two asymptotic steady states which are Dirac masses at each edge. Interestingly, it links patterns of evolution to the type of selection: stabilizing, disruptive and directional (in the order of the results).

Let me finally mention that a similar small mutational variance framework led to several results in *time-fluctuating environments*. In [Mirrahimi, Perthame, and Souganidis 2015], the authors show that, simultaneously accelerating the time and making the mutational variance vanish, concavity in a setting similar as in Lorz, Mirrahimi, and Perthame 2011 propagates along solutions straining when ε vanishes to the dynamics of a single time-fluctuating Dirac mass. Later, in [Figueroa Iglesias and Mirrahimi 2018], the authors first prove the existence and uniqueness of a long time solution to the time-periodic equation (with positive mutational variance) that has a fluctuating population size. They next describe the asymptotic behaviour when the mutational variance vanishes, solving the constrained Hamilton-Jacobi equation

that arises as monomorphism occurs (following the uniqueness of the maximum for the average birth rate over a time period), ensuring uniqueness and regularity of a classical solution u. Furthermore, adaption of asexual population to a space homogeneous, time-fluctuating environment has also been studied with other methods that do not place themselves in small mutational variance (see [Carrère and Nadin 2020], which highlights the potential beneficial effect of mutations that are not small on the mean population size).

Finally, a related approach using the Hopf-Cole transform on the trait density of an asexual population was employed to study its long time adaptive behaviour subject to natural selection on the fecundity, general competitive interactions, and faithful trait transmission (no mutations are considered). Traits are assumed to be compactly supported. Due to the absence of mutations, there is no asymptotic Hamilton-Jacobi equation, but a constraint still holds to avoid the population either to blow up or to go extinct. [Desvillettes et al. 2008] obtains results on the well-posedness and the weak convergence of the trait distribution towards a measure, supported at maximal points of the reaction term. They further study the stability of Dirac masses that can arise and developed numerical methods to capture accurately such phenomena. In a later work [Jabin and Raoul 2011], the authors found a Lyapunov functional for the previous equation (which follows an assumption that the competitive interactions are positive-definite) and thus ensuring the global stability of some steady states.

Other PDE approaches. In this paragraph, I will try to give a quick overview on other PDE approaches that aim at deriving quantitative information about the evolutionary dynamics of asexually reproducing populations under mutation-selection balance affecting the *relative fitness of individuals*, so without considering any demographical changes in the population size. One class of models that is built according to this approach is based on the non-linear, non-local *replicator-mutator equation*, introduced by [Kimura 1965]

$$\partial_t n(t,z) = \sigma_M^2 \Delta_z n(t,z) + \left[s(z) - \int_{\mathbb{R}} s(z') n(t,z') dz' \right] n(t,z), \quad t \geq 0, \quad z \in \mathbb{R}. \tag{1.15}$$

The relative fitness is characterized by the trait dependent selection function s and the mutations are modelled with the localized reproduction operator (1.8), with a mutational variance σ_M^2. One can verify that the population size, initially normalized at 1, remains constant after integration of (1.15) over all the trait space. This constitutes a first difference with the Hamilton-Jacobi approach, which allows to account for demographical changes. The second difference is that the relative fitness function s is often quite specifically chosen to derive analytical quantitative information on the fitness distribution, as illustrated below.

A first set of papers study the case where $\boxed{s(z) = z}$, which means that mutations directly affect the fitness (Alfaro and Carles 2014; Martin and Roques 2016; Gil et al. 2017; Gil et al. 2019; Alfaro and Veruete 2020). In the case where the mutations are modelled in (1.15) thanks to the *local diffusive operator*, [Alfaro and Carles 2014] finds explicit solutions, which allow to derive quantitative information on the relative fitness distribution, and qualitative asymptotic behaviour (extinction/persistence), while [Alfaro and Veruete 2020] later use *cumulants generating functions (CGF)* on a slightly different replicator-mutator equation to derive quantitative asymptotic behavior on the first two moments of the fitness distribution. In the case where the mutations are modelled in (1.15) thanks to the *non-local diffusive operator*, the use of *CGF* leads similarly to derive quantitative information on the trajectories of the first two moments of the fitness distribution (Martin and Roques 2016; Gil et al. 2017), or inform on the concentration behaviour of the stationary fitness distribution when the mutation kernel is fitness-dependent (Gil et al. 2019).

A second set of studies focuses on the case where the selection function is confining $\boxed{s(z) \underset{|x|\to\infty}{\longrightarrow} = -\infty}$ (Alfaro and Veruete 2019; Hamel, Lavigne, Martin, et al. 2020; Alfaro, Gabriel, and Kavian 2021). In the multi-dimensional case where the fitness function is specifically taken as quadratic $\boxed{s(z) = -||z||^2}$ and mutations are modelled by a local diffusive operator extending (1.8) to account for different mutations variances w.r.t different coordinates of the trait z, the authors of [Hamel, Lavigne, Martin, et al. 2020] use *CGF* and obtain explicit formula which provide quantitative information of the trajectory of the mean trait. With more general confing selection function, [Alfaro and Veruete 2020] (local mutation operator (1.8)) and [Alfaro, Gabriel, and Kavian 2021] (non-local mutation operator (1.7)) take advantage of the properties of the solutions n of (1.15), which can be directly deduced from the properties of the solutions $\tilde{n}$ to the *analogous linearized and localized equation*, through a straight-forward transformation $n := \frac{\tilde{n}}{\int_{\mathbb{R}} \tilde{n}(z')dz'}$. The latter allows to use linear spectral analysis tools and the semi-group of contraction theory to derive qualitative asymptotic behaviour (extinction/persistence) which can be transposed on the solutions of the non-local, non-linear replicator-mutator model (1.15).

1.2.2.2 Discrete heterogeneous environments

In the dynamics of local adaptation to a discrete heterogeneous environment where different values of a quantitative traits are optimal in different habitats that are connected by density-dependent migration, demography plays a central role as it underlies the intensity of *gene/trait flow* between habitats.

A Hamilton-Jacobi approach on eco-evo dynamics. In [Mirrahimi 2017], the author studies the distributions at equilibrium in asexual populations through a model that allows to track demographical changes through birth, death and migration events (see (1.4)) as well as trait evolution, thanks to the introduction of mutations with vanishing variance via a local operator (1.8). Namely, the aim is to analytically describe the steady states of the following non-linear, non-local elliptic system (for all $z \in \mathbb{R}$)

$$\begin{cases} \varepsilon^2 \begin{pmatrix} \Delta n_1^\varepsilon(z) \\ \Delta n_2^\varepsilon(z) \end{pmatrix} = \begin{pmatrix} R_1(z, N_1^\varepsilon) - m_1 & m_2 \\ m_1 & R_2(z, N_2^\varepsilon) - m_2 \end{pmatrix} \begin{pmatrix} n_1^\varepsilon(z) \\ n_2^\varepsilon(z) \end{pmatrix} =: \mathcal{A}(z, N_1^\varepsilon, N_2^\varepsilon) \begin{pmatrix} n_1^\varepsilon(z) \\ n_2^\varepsilon(z) \end{pmatrix}, \\ \\ N_1^\varepsilon = \int_{\mathbb{R}} n_1^\varepsilon(z')dz', \quad N_2^\varepsilon = \int_{\mathbb{R}} n_2^\varepsilon(z')dz'. \end{cases} \tag{1.16}$$

The author chose to focus on a specific reaction term $R(z, N_i^\varepsilon) = (r_i - g_i(z - \theta_i)^2 - \kappa_i N_i^\varepsilon)$, which involves a quadratic stabilizing selection term and a non-local uniform competition for resources term. The latter is common in in quantitative genetics models (see Ronce and Kirkpatrick 2001; Hendry, Day, and Taylor 2001; Débarre, Ronce, and Gandon 2013 for example) and allows the analysis to be pushed further and highlights its value, for it leads to characterize explicitly the equilibrium variables. Besides, the basis of the asymptotic analysis of vanishing mutational variance remains robust to general reaction terms. Moreover, one can notice that the habitats are asymmetrical as they can differ in their growth rate r_i, strength of selection g_i towards a local optimal trait θ_i, intensity of uniform local competition for resources κ_i and outward migration rate m_i.

A first part of the study introduces concepts borrowed from adaptive dynamics, by first defining $W(z, N_1^\varepsilon, N_2^\varepsilon)$ the leading eigenvalue of the reaction-migration matrix $\mathcal{A}(z, N_1^\varepsilon, N_2^\varepsilon)$

as the *effective fitness* of the population (the growth rate of individuals of trait z in the demographic state $N_1^\varepsilon, N_2^\varepsilon$). The latter in turn defines the notion of *Evolutionary Stable Strategy (ESS)* (states of the system that cannot be invaded by a mutant) by any discrete set of traits Ω^* that verifies that $W(\cdot, N_1^*, N_2^*)$ is always non-negative and cancels at least for all $z^* \in \Omega^*$, where (N_1^*, N_2^*) are the *demographic equilibrium* associated to Ω^*, defined through the eigenvectors associated to each $W(z^*, N_1^*, N_2^*)$ with $z^* \in \Omega^*$. The first main result of the paper is to prove that there exist a unique ESS, and algebraically characterize it, which requires to explicitly compute $W(z, N_1, N_2)$ and identify the conditions to find the trait(s) that composed the ESS, which is possible with specific choice of the quadratic selection. The author shows that, when migration is below a certain threshold defined by selection, the unique ESS is composed of two diametrically opposed dominant traits $(-z_D^*, z_D^*)$ defining a dimorphic population, whereas it is composed of a unique trait defining a monomorphic population when migration is beyond this threshold. I emphasize on the fact that the dimorphic ESS and its demographic equilibrium (N_1^*, N_2^*) are explicitly known in the case of quadractic selection. This allows to show that $W(\cdot, N_1^*, N_2^*)$ cancels exactly at the ESS Ω^* (might it be dimorphic or monomorphic), which is instrumental to conclude the next part.

The other part of the analysis focuses on the study of the ansatz $u_i^\varepsilon = \varepsilon \log(\sqrt{\varepsilon} n_i^\varepsilon)$, according to the methodology of small mutational variance (see also the Box 1.2.2.1). From (1.16), the ansatz satisfy the following

$$\left[\varepsilon \begin{pmatrix} \Delta u_1^\varepsilon(z) \\ \Delta u_2^\varepsilon(z) \end{pmatrix} + \begin{pmatrix} -|u_1^\varepsilon(z)'|^2 \\ -|u_2^\varepsilon(z)'|^2 \end{pmatrix}\right] \cdot \begin{pmatrix} 1 \\ e^{\frac{u_1^\varepsilon(z) - u_2^\varepsilon(z)}{\varepsilon}} \end{pmatrix} = \mathcal{A}(z, N_1^\varepsilon, N_2^\varepsilon) \begin{pmatrix} 1 \\ e^{\frac{u_1^\varepsilon(z) - u_2^\varepsilon(z)}{\varepsilon}} \end{pmatrix}, \quad z \in \mathbb{R}. \tag{1.17}$$

The originality compared to the homogeneous space studies comes from the term $e^{\frac{u_1^\varepsilon - u_2^\varepsilon}{\varepsilon}}$ which appears from the migration that mixes n_1^ε and n_2^ε in both equations in (1.16). One can notice that (1.17) hints, at least formally, that, in the limit of vanishing variance, u_1^ε and u_2^ε, if they converge, should converge to the same limit u, so that $z \mapsto e^{\frac{u_1^\varepsilon(z) - u_2^\varepsilon(z)}{\varepsilon}}$ remains well balanced within (1.17). This implies formally that when $\varepsilon \to 0$, $-|u'(z)|^2$ is the leading eigenvalue of $\mathcal{A}(z, N_1, N_2)$, which is by definition $W(z, N_1, N_2)$, associated with an eigenvector with positive entries (N_1^ε and N_2^ε are preliminary shown to converge along subsequences towards N_1 and N_2 thanks to a priori classical bounds in the limit of vanishing variance).

In agreement with the previous presented heuristics, the first main result of this part is the convergence along subsequences of u_1^ε and u_2^ε towards the same limit u, solution of the following constrained Hamilton Jacobi equation

$$\begin{cases} -u'(z)^2 = W(z, N_1, N_2), & z \in \mathbb{R}, \\ \max(u) = 0. \end{cases} \tag{1.18}$$

The latter relies on the application of the *Arzela-Ascoli theorem* following Lipschitz estimates and uniform bounds on u_i^ε. The uniform bounds are obtained from a localized *Harnack inequality between local trait densities* n_1^ε *and* n_2^ε, and a L_1 control of the masses far from the origin. The arguments for the Lipschitz bounds are technically intricate. The convergence result toward a viscosity solution of (1.18) is robust w.r.t. general reaction terms in each habitat $R_i(z, N_i)$. Recall that, in the homogeneous space studies, since the convergence is obtained along subsequences only, the uniqueness is not guaranteed and, in the case where it is proved, requires various additional conditions and remains quite challenging.

However, in [Mirrahimi 2017], the results of the first part on the ESS obtained with the specific choice of quadratic growth functions $R(z, N_i) = r_i - g_i(z - \theta_i)^2 - \kappa_i N_i$ allows to prove

the uniqueness of the limit u. To understand why, recall that typically, in the limit of small variance, the support of the limit measures n_1 and n_2 (obtained by weak convergence of n_1^ε and n_2^ε) is contained in the zero set of the limit function u. From (1.18), the latter is itself contained in the zero set of $W(\cdot, N_1, N_2)$, where (N_1, N_2) is the demographical equilibrium. However, the support of n is the (unique) ESS of the system, which has been shown in this particular case to be exactly the zeros of $W(\cdot, N_1, N_2)$ (end of the first part). This leads to identify exactly the zero set of u with the zero set of $W(\cdot, N_1, N_2)$. Thanks to a property of identifiability of a viscosity solution u to the Hamilton-Jacobi equation (1.18) by the values it takes on the maxima of $W(\cdot, N_1, N_2)$, which are all 0, the author finally shows the uniqueness of the limit u, solution of the contrained Hamilton-Jacobi equation (1.18) in the case of quadratic growth functions. This allows the derivation of an explicit variational formula for u, as the demographic equilibrium associated to the unique ESS and the leading eigenvalue Hamiltonian function W determines completely the optimal path involved. The explicit formula for $W(\cdot, N_1^*, N_2^*)$ and its non-linear and non-trivial dependence with the demographical equilibrium (N_1^*, N_2^*) highlights the fact that the demographical equilibrium is strongly involved in the dynamics of local adaptation and justifies a posteriori the modelling choice to include its influence on the quantitative trait dynamics. Finally, the author also derives results form the *source-sink case* under *one-way migration*.

The follow-up work [Mirrahimi and Gandon 2020] is targeted at presenting and illustrating the quantitative results that can be obtained from this Hamilton-Jacobi approach and how they translate in terms of adaptation patterns under migration-mutation-selection balance, in symmetrical/asymmetrical discrete heterogeneous environments. Among the results from [Mirrahimi 2017] that they expose, I would like to highlight two in particular, as they are relevant to illustrate the structural differences between asexual and sexual populations' adaptation. The first one is that, in symmetrical environments (meaning that the growth rate r, the outward migration rate m, the selection strength g and the competition's intensity do not depend on the habitat), the only equilibrium of the system is symmetrical, either dimorphic when migration is below a certain level of selection, or monomorphic when it is above it. Note also that in the dimorphic equilibrium, the local subpopulation trait densitites are bimodal, and therefore, are not well approximated by Gaussian densities, as it is commonly assumed in quantitative genetic models. The second one comes from the derivations of approximations of the macroscopic moments of the trait densities n_1^ε and n_2^ε when the mutational variance is small but not 0, as these can be useful and informative for biologists. Even in the case of monomorphic equilibrium, it highlights the fact that the variance in trait of the asexual population depends on the combined effects of migration, selection and mutation.

Link with a quantitative genetics/adaptive dynamics study. The two articles [Mirrahimi 2017] and [Mirrahimi and Gandon 2020] improve the understanding of the underlying conditions of the results obtained in a previous study [Débarre, Ronce, and Gandon 2013]. In this work, the authors focus on the quantitative and qualitative description of the steady states of a similar quantitative genetics PDE model, on which they use tools from adaptive dynamics in a regime of small mutational variance. Thanks to these, they formally derive, in a symmetrical environment setting, macroscopic description of the local trait densities, and conditions for symmetrical dimorphism and symmetrical monomorphism to arise, that are very close from the approximations obtained in [Mirrahimi 2017] and [Mirrahimi and Gandon 2020]. However, they also found that a locally stable *asymmetrical* monomorphic equilibrium existed, which is not in agreement with the analysis done in [Mirrahimi 2017]. I will commentate more on this discrepancy in results in light on my own work on the adaptation of sexual populations

to a symmetrical discrete heterogeneous environment (see Section 1.3.1).

Other PDE approaches. I would like to mention that other PDE approaches that I described in the last paragraph of the last section presenting homogeneous space studies have also been used to analyse the evolutionary dynamics modelling specific qualitative evolutionary questions arising in discrete heterogeneous environments. Replicator-mutator models have been useful in that regard, on situations that are not too influenced by the dynamics of the demography, which these models are not suited to account for: probability of establishment in a new habitat with one-way migration from source to sink using cumulant generating functions in [Lavigne et al. 2020] (there is no demographic feedback on the source, and the saturation in the sink can be neglected), or conditions of extinction or persistence through an eigenvalue problem (Hamel, Lavigne, and Roques 2021).

1.2.2.3 Continuous space

Overview of the FKPP equation. Since the first half of the last century, reaction-diffusion equations have been used to model the adaptation of populations in a structured and continuous space. The archetypal and seminal example is the spatial propagation of an advantageous allele A, replacing a resident allele a, a phenomenon modelled simultaneously and independently, on the one hand, in [Kolmogorov, Petrovsky, and Piskunov 1937], and on the other hand, in [Fisher 1937], through the non-linear FKPP equation (1.6) that we recall here

$$\begin{cases} \partial_t N(t,x) = rN(t,x)(1-N(t,x)) + D\Delta_x N(t,x), \quad t>0, \quad x\in\mathbb{R}, \\ N(0,x) = \mathbf{1}_{\mathbb{R}_-}(z), \quad x\in\mathbb{R}. \end{cases} \tag{1.19}$$

The latter models the spatial dynamics of a population whose individuals diffuse spatially randomly according to the heat operator with coefficent D, and constitutes a population under local logistic growth, with a saturating effect when $N \equiv 1$, and with initial growth at small populations r. The reaction term $N \mapsto rN(1-N)$ has two equilibria, an unstable one at $N=0$ and a stable one at $N=1$. Consequently, the authors cited above show that there exist travelling waves with constant speed c connecting the stable state 1 at $-\infty$ to the unstable equilibrium 0 at $+\infty$, provided that the speed c is above a certain threshold c^* depending on the diffusion coefficient and the initial growth rate of small populations (for (1.19) $c^* = 2\sqrt{rD}$). Although [Kolmogorov, Petrovsky, and Piskunov 1937] use a phase plane analysis to deduce the minimal propagation speed, the latter can be identified formally by solving the dispersion relation obtained when searching the travelling waves solutions $e^{\lambda(x-ct)}$ of the following linearized version of (1.19)

$$\begin{cases} \partial_t N(t,x) = rN(t,x) + D\Delta_x N(t,x), \quad t>0, \quad x\in\mathbb{R}. \end{cases} \tag{1.20}$$

Indeed, the parabolic equation (1.19), despite being non-linear, respects the maximum principle, so the propagation speed obtained from (1.20) provides an upper bound for the analogous quantity for (1.19) (which is shown to be the actual speed).

The importance of these results and their influence since their publications cannot be understated, especially on models of ecological invasions. Since then, the constant minimal speed result of the reaction-diffusion equation (1.19) has been derived for various reaction terms, in arbitrary high dimension (see the landmark population genetic work Aronson and Weinberger 1978, which includes among others the analysis of the case of bistable reaction terms, in which case the propagation speed is uniquely determined). Further correcting terms

have been derived to improve the fine understanding of the influence of the non-linearity on the propagation speed (Bramson 1978; Bramson 1983) and obtaining new estimates are still a current challenge.

A geometric optics Hamilton-Jacobi approach for local reaction-diffusion equations. Around the turn of the century, a new approach from geometric optics has been introduced to study large time asymptotics of reaction-diffusion equations related to (1.19), in [Freidlin 1986] from a probabilistic point of view and in [Evans and Souganidis 1989] with a PDE framework. I will illustrate heuristic about their method on a multidimensional version of the FKPP equation example. First they consider a rescaling of the time and space variables $\hat{N}(t,x) = N\left(\frac{t}{\varepsilon}, \frac{x}{\varepsilon}\right)$, where ε is a small positive parameter that allows to follow large-time dynamics on the propagation front. $\hat{N}$ is solution of:

$$\begin{cases} \varepsilon \partial_t \hat{N}(t,x) = \varepsilon^2 \Delta_x \hat{N}(t,x) + \hat{N}(t,x)(1-\hat{N}(t,x)), \quad t \geq 0, \quad x \in \mathbb{R}^d, \\ \hat{N}(0,x) = g(x), \quad x \in \mathbb{R}^d. \end{cases} \tag{1.21}$$

Assumptions on g is that it is nonegative, smooth, bounded, Lipschitz, and its suppport G_0 is bounded and smooth. Next, following the observation that the steady states of (1.19) are 0 and 1, they aim at characterizing the asymptotic set G that will characterize the support of the limit of $\hat{N}$ when ε vanishes. To that effect, they introduced the WKB ansatz according to a Hopf-Cole transform $U_\varepsilon = \varepsilon \log\left(\hat{N}\right)$. The ansatz U_ε is solution of the following equation:

$$\begin{cases} \partial_t U_\varepsilon(t,x) = |\nabla_x U_\varepsilon(t,x)|^2 + \varepsilon \Delta_x U_\varepsilon(t,x) + 1 - e^{\frac{U_\varepsilon(t,x)}{\varepsilon}}, \quad t > 0, \quad x \in \mathbb{R}^d, \\ U_\varepsilon(0,x) = \varepsilon \log(g(x)), \quad x \in \mathrm{int}(G_0), \\ U_\varepsilon(0,x) = -\infty, \quad x \notin G_0. \end{cases} \tag{1.22}$$

They show, by establishing uniform and Lipschitz bounds on U_ε thanks to comparison principles, that, according to the Arzela-Ascoli theorem, U_ε converges toward the unique viscosity solution U (expressed with a variational formula minimizing the action of the Lagrangian $L : q \mapsto \frac{|q|^2}{4}$ along paths with stopping times) of the Hamilton-Jacobi inequality that reads:

$$\begin{cases} \max\left[\partial_t U(t,x) - |\nabla_x U(t,x)|^2 - 1,\ U(t,x)\right] = 0, \quad t > 0, \quad x \in \mathbb{R}^d, \\ U(0,x) = 0, \quad x \in \mathrm{int}(G_0), \\ U(0,x) = -\infty, \quad x \notin G_0. \end{cases} \tag{1.23}$$

Doing so, they describe the large time dynamics of the propagation front as zero level set of U.

This approach has been adapted for the study of the propagation dynamics of asexual populations structured according to a quantitative trait z (taken as uni-dimensional henceforth to simplify), dispersing in a continuous space. This leads to consider non-local reaction-diffusion equations, like the non-local FKPP equation on the population trait density n (characterized by the variables $(t,x,z) \in \mathbb{R}_+^* \times \Omega \times I$)

$$\begin{cases} \partial_t n(t,x,z) = \mathcal{B}[n](t,x,z) + D(z)\Delta_x n(t,x,z) + n(t,x,z)\left(1 - \rho(t,x)\right), \\ \rho(t,x) = \int_I n(t,x,z')dz', \quad t \geq 0, \quad x \in \Omega, \\ n(0,x,z) = n_0(x,z), \quad x \in \Omega, \quad z \in I. \end{cases} \tag{1.24}$$

The saturation term modelling uniform competition for resources locally in space, non-locally in trait leads to some failures of comparison principles, as non-monotonic waves can propagate (Berestycki, Nadin, et al. 2009). This brings analytical challenges to quantify the speed of the expansion of such populations.

In what follows, the reproduction operator $\mathcal{B}$ considered will be the localized mutation Laplacian operator (1.8). I will present some non-local reaction-diffusion works that study the interplay between ecology and evolution on the propagation of asexual populations structured by a quantitative trait. I will first discuss the constant space diffusion case ($D(z) = 1$), and next focus on the phenomenon of evolution of dispersal, where the space diffusion coefficient is a function of the trait under evolution (typically, $D(z) = z$).

Constant diffusion The first eco-evolutionary framework that I will present is the study of the *local adaptation of populations to a spatially continuous environment*.

[Bouin and Mirrahimi 2015] studies the *long-time behaviour* of a propagating population under *small spatial diffusion*, characterized by a bounded quantitative trait $z \in I$ and subject to a general spatial selection $r(x, z)$ (upper bounded by a constant and lower bounded by $x \mapsto -|x|^2 + A$). I will detail heuristically their approach inspired by [Evans and Souganidis 1989], as it is found also in other studies on evolution of dispersal. They consider the following rescaled equation (for $(t, x, z) \in \mathbb{R}_+^* \times \mathbb{R}^d \times I$)

$$\varepsilon \partial_t n_\varepsilon(t, x, z) = \varepsilon^2 \Delta_x n_\varepsilon(t, x, z) + \sigma_M^2 \Delta_z n_\varepsilon(t, x, z) + n_\varepsilon(t, x, z) \left[r(x, z) - \rho_\varepsilon(t, x) \right],$$

with homogeneous Neumann boundary conditions on ∂I. Notice that the mutational variance is not considered small. Consequently, the trait variable is expected to be a fast variable and the space variable a slow one. This *separation of time scales* is highlighted by what follows. Aligning with the approach employed in [Evans and Souganidis 1989], the authors introduce the WKB ansatz $u_\varepsilon = \varepsilon \log(n_\varepsilon)$, which solves:

$$\partial_t u_\varepsilon(t, x, z) = \varepsilon \Delta_x u_\varepsilon + |\nabla_x u_\varepsilon|^2 + \frac{\sigma_M^2 \Delta_z u_\varepsilon}{\varepsilon} + \frac{\sigma_M^2 |\nabla_z u_\varepsilon|^2}{\varepsilon^2} + r(x, z) - \rho_\varepsilon. \tag{1.25}$$

The influence of the successive orders in ε involved in (1.25) of u_ε can be formally untangled by considering a (formal) Taylor expansion

$$u_\varepsilon(t, x, z) = u_0(t, x, z) + \varepsilon u_1(t, x, z) + o(\varepsilon).$$

Indeed, using this expansion in (1.25) asymptotically leads first to $\sigma_M^2 |\nabla_z u_0(t, x, z)|^2 = 0$, hence the main term u_0 does not depend on the trait variable z, $u_0(\cdot, \cdot, z) = u_0(\cdot, \cdot)$. Next, considering the terms of order ε^0, regrouping by dependence on variables and denoting ρ_0 the formal limit of ρ_ε reads

$$\left[\partial_t u_0 - |\nabla_x u_0|^2 + \rho_0 \right](t, x) = \left[\sigma_M^2 \left(\Delta_z u_1(t, x, \cdot) + |\nabla_z u_1(t, x, \cdot)|^2 \right) + r(x, \cdot) \right](z) \tag{1.26}$$

The latter can be interpreted as the asymptotic link between the slow spatial propagation (l.h.s of (1.26)), which reminds of the limit equation (1.23) in [Evans and Souganidis 1989], and the effects of trait-dependent effects of mutation and local adaptation (r.h.s of (1.26)), which has an elliptic form characterizing a fast-reached steady state w.r.t. z. Note indeed that the time variable t in the r.h.s. of (1.26) is uncorrelated from the trait variable z due to the differentials w.r.t z, which implies that u_1 separates variables: $u_1(t, x, z) = \mu(t, x) + \log(Q_x(z))$ (the log ensures the simplification $\Delta_z \log(Q_x) + |\nabla_z \log(Q_x)|^2 = \frac{\Delta_z Q_x}{Q_x}$). In turn, the Hopf-Cole transform implies that n_ε also separates fast and slow variables

$$n_\varepsilon(t,x,z) \approx Q_x(z)\, e^{\frac{u_0(t,x)}{\varepsilon}+\mu(t,x)}. \tag{1.27}$$

The latter suggests the following *two-step reformulation of* (1.25). First, one should solve the space-dependent elliptic eigenvalue problem (with homogeneous Neumann boundary condition) given by the r.h.s. of (1.26)

$$\sigma_M^2 \Delta_z Q_x(\cdot) + r(x,\cdot)Q_x(\cdot) = \sigma_M^2 H(x) Q_x(\cdot). \tag{1.28}$$

The authors show that there exists a unique smooth eigenpair (H,Q) solving (1.28). The eigenvalue H (which is linked to the local population size ρ_0 through (1.26), depending on if $u_0 = 0$ or is negative) next identifies the limit *Hamilton-Jacobi problem* encoding the dynamics of the front (notice the resemblance with (1.23), up to the sign)

$$\max\left[u(t,x), \partial_t u(t,x) - |\nabla_x u(t,x)|^2 - H(x)\right] = 0. \tag{1.29}$$

The main result of [Bouin and Mirrahimi 2015] is the convergence of u_ε to the unique viscosity solution u of (1.29), which defines the invaded region depending on it being zero or negative. I also would like to emphasize on the neat fast-slow structure of the problem, which will also be found again in studies on the evolution of dispersal with a different asymptotics at large times and with small mutations. Finally, the effective Hamiltonian solving the eigenvalue problem encoding the fast reached equilibrium of the trait-dependent elliptic part, is also a mild remainder of the analogous Hamiltonian structure deduced from an eigenvalue problem in [Mirrahimi 2017] (steady states in discrete heterogeneous environments).

In [Alfaro, Coville, and Raoul 2013], the authors consider a more specific biological question, which is the local adaptation to a *spatial environmental gradient/cline*. Precisely, the study (1.24) with $D \equiv 1$, and a more complex reaction term:

$$n(t,x,z)\left[r(z-Bx) - \int_{\mathbb{R}} k(z'-Bx, z-Bx) n(t,x,z')dz'\right];$$

which includes a selection term deriving *local adaptation along a linear spatial cline* and a local in space, non-local in trait term of trait-dependent competitive interactions. The main result of their work is showing the existence of travelling waves of constant speed above a minimial speed c^* when the principal eigenvalue of the problem is negative or the extinction of the population when it is positive. The main challenge is in the first case. They construct the waves by approximating the problem by considering the space to be bounded slabs, of increasing radius. In the compact slabs, they reduce the travelling wave problem to an elliptic problem, on which they employ a *Leray-Schauder fixed point argument*, using a *Harnack inequality* to control the non-local competition term. A later study [Alfaro, Berestycki, and Raoul 2017] studies a similar framework, but where the local adaptation depends on a *constant climate shift*, thus carried on the variable $x - c_{\text{climate}}t$. They show that different behaviours regarding extinction/persistence can occur depending on the shifting growth rate, either the population should keep pace with the climate to persist in case of a stringent local selection, or it can persist behind while lagging at a lower speed where selection is more permissible.

Moreover, I will mention that there are also works on non-linear and non-local reaction-diffusion equation in [Alfaro and Ducrot 2018], [Alfaro, Girardin, et al. 2021] considering a particular effect of the trait on the growth rate, namely considering that the trait under mutation is the strength of an *Allee effect*. The *Allee effect* is a phenomenon that translates the potential reduction of growth rate at low density (for example, modelling an increased effect of density-dependent of predation on small populations). When its strength is large

enough, it even leads to a negative growth rate at low density, which translates into a typically bistable reaction term, which was showed to change qualitatively the *pushed/pulled* nature of propagation fronts with constant diffusion, on the maintenance of neutral genetic diversity at the front (Roques et al. 2012). [Alfaro and Ducrot 2018] shows that, in a model where ecology and evolution are described in separate equations, the evolution of the Allee effect in very small initial populations can eventually lead to persistence (hair-trigger effect) and *evolutionary rescue*, whereas such populations would go extinct with a fixed Allee effect. Moreover, [Alfaro, Girardin, et al. 2021] study the interplay of the evolution of the Allee effect through mutations and the reaction-diffusion dynamics in a single equation. Their main result is a thorough characterization of the qualitative outcomes on persistence/extinction, which is established thanks to eigenvalue problems, point-wise comparison principles and integral estimates.

Finally, an evolutionary reaction-advection-diffusion problem that has sparked growing recent interest, following the rapid progress in *gene editing* (thanks to the technology CRISPR-9), is the study of propagation of *gene drives* (humanly manufactured heritable alleles that lowers the fitness of its vessel) for controlling ecological populations, like mosquitoes, and of their impact for conservation (Rode et al. 2019). The main aims of such PDE studies is to understand the conditions of spread and long time control of these drives (Girardin, Calvez, and Débarre 2019, Girardin and Débarre 2021).

Evolution of dispersal The evolution of dispersal has been attracting sustained interest, both for the complexity of the dispersal patterns that it can occasion in spatially distributed species (Ronce 2007) and for the original and intricate mathematical challenges that it poses in the reaction-diffusion field. The models that arise are motivated by deriving qualitative (Is evolution selecting for low or high dispersal rates?) and quantitative features of the influence of evolving dispersal on the propagation of a species (How fast can a species evolving its morphological dispersal means -wings/legs/weight- expand and invade new regions? How does the interplay between spatial propagation and dispersal trait structure the population?) through the generic equation for asexual reproduction:

$$\begin{cases} \partial_t n(t,x,z) = \sigma_M^2 \Delta_z n(t,x,z) + z\Delta_x n(t,x,z) + n(t,x,z)\left(1-\rho(t,x)\right), \\ \rho(t,x) = \int_I n(t,x,z')dz', \quad t \geq 0, \quad x \in \Omega, \\ n(0,x,z) = n_0(x,z), \quad x \in \Omega, \quad z \in I. \end{cases} \tag{1.30}$$

(In all that follows, the necessary boundary conditions are considered as Neumann homogeneous). Notice that the spatial diffusion coefficient is the quantitative trait z which can mutate according to the localized reproduction operator derived from (1.8), involving a trait diffusion term. This trait dependence on the spatial diffusion radically changes the behaviour of (1.30) in comparison to the constant diffusion case (1.24) ($D \equiv 1$), where travelling waves are shown to be spreading at constant speed. I will structure the rest of this subsection by distinguishing studies interested in the case of a bounded trait interval $I \subset \mathbb{R}_+^*$ and unbounded spatial environment $\Omega = \mathbb{R}$, from in a bounded spatial environment Ω and finally present the ones modelling unbounded trait and space $I =]1, +\infty[$, $\Omega = \mathbb{R}$, for the qualitative conclusions diverge significantly between these cases.

1) Bounded trait interval I, unbounded spatial environment $\mathbb{R}$. In this case, one would expect that, as the competition for resources, which is local in space but non-local in trait, advantages individuals in low densities regions in an unbounded space, the highest possible dispersal rate would be selected for in order to be able to reach inhabited regions. This

would lead to a constant speed propagation corresponding to the highest dispersal trait. This simple intuition is somewhat confirmed by the following studies, although the actual rate of propagation is more involved, as formally presented in [Bouin, Calvez, et al. 2012] and shown in [Bouin and Calvez 2014] and [Turanova 2015]. These last two studies adopt radically different approaches, but deduce consistent results. The earlier [Bouin and Calvez 2014] focuses on establishing the existence of travelling waves combining a smooth monotonic profile $Q_\lambda(z)$ increasing w.r.t. the trait z and an exponential spatial decay $e^{-\lambda(x-ct)}$, propagating at constant minimal speed identified through an elliptic eigenvalue problem. The increasing profile $Q_\lambda(z)$ at the front illustrates the spatial sorting effect, according to which higher values of the dispersal trait are selected for, consistently with the above verbal intuition. Furthermore, the authors use a *Leray-Schauder fixed point argument* on approximated travelling wave problems $Q_\lambda(z)e^{-\lambda(x-ct)}$ in a spatial slab, combined with Harnack inequalities to control the non-local term (similarly in spirit as in [Alfaro, Coville, and Raoul 2013]). One interesting feature is that the elliptic eigenvalue problem (1.31) bears some resemblances with the one that I described earlier from [Bouin and Mirrahimi 2015] (1.28)

$$\sigma_M^2 \Delta_z Q_\lambda(z) + (1 + z\lambda^2 - \lambda c(\lambda)) Q_\lambda(z) = 0. \tag{1.31}$$

However, the eigenvalue $H_\lambda(z) = 1 + z\lambda^2 - \lambda c(\lambda)$ is different and determines the critical speed $c^* = \min c(\lambda)$. The link is made clearer in [Turanova 2015], in which the author adopts a Hamilton-Jacobi approach coupled with the eigenvalue problem (1.31) to study the asymptotic behaviour of solutions at large times and in the limit of small spatial diffusion. The equation reads

$$\varepsilon \partial_t n(t,x,z) = \varepsilon^2 \, z \, \Delta_x n(t,x,z) + \sigma_M^2 \Delta_z n(t,x,z) + n(t,x,z) \left[r(x,z) - \rho(t,x) \right].$$

Notice the resemblance in the time and space scaling with [Bouin and Mirrahimi 2015]. The heuristics are also similar, with z being a fast variable and x a slow one (consistent with the monotonic trait profile form in Bouin and Calvez 2014). Therefore, the Hamiltonian H_λ involved in the limit Hamilton-Jacobi equation derived in [Turanova 2015] (whose solution characterizes the movement of the propagation front) is obtained from the elliptic eigenvalue problem (1.31) describing the fast equilibrium on the dispersal trait distribution for any given spatial decay. The asymptotic definition of invaded/empty regions linked to the limit Hamilton-Jacobi equation is one of the two main results of [Turanova 2015], the other one, that is crucial to prove the convergence result, being a uniform upper bound to the trait distribution, which is a remarkable result. It is a key argument in a later work [Bouin, Henderson, and Ryzhik 2017b], in which the authors derive the next term in the travelling waves propagation after the constant speed from [Bouin and Calvez 2014]. They prove and use in particular an improved Harnack inequality for their non-local parabolic framework, which allows to shift the analysis to an equation with a localized reaction, where the comparison principle holds.

2) Bounded space. The studies of this case [Dockery et al. 1998], [Perthame and Souganidis 2016], [Lam and Lou 2017] reveal a sharp behaviour of dispersal trait distributions, contrasting with the previous case where space was unbounded. Indeed, the common qualitative conclusion here is that *the slowest dispersal rate is favoured and becomes eventually predominant in the whole population*, which was obtained with adaptive dynamics tools when considering a finite and discrete trait space in [Dockery et al. 1998]. It is opposite to the phenomenon discussed in the last paragraph and shown by [Bouin and Calvez 2014] and [Turanova 2015] when the space is unbounded, namely that higher dispersal traits are favored at the front. I mention also that the first results on (1.30) with both bounded trait interval I and bounded

space Ω that I know of are derived in [Arnold, Desvillettes, and Prévost 2012], which shows the existence of non-trivial steady states to a weak formulation of (1.30), thanks to a fixed point argument on regularized equations.

The concentration phenomenon that is intuited is studied for continuously distributed dispersal traits simultaneously and independently using a *Hamilton-Jacobi approach in a small mutational variance asymptotics* in two slightly different studies [Lam and Lou 2017] (bounded traits and non-constant growth rate) and [Perthame and Souganidis 2016] (unbounded traits, but 1-periodic diffusion coefficient minimised at $z_m \in [0, 1[$). The scaling is different from [Bouin and Mirrahimi 2015] and [Turanova 2015], since the variance of mutation is rescaled, and not the space variable x:

$$\begin{cases} \varepsilon^2 \Delta_z n(t,x,z) + z\Delta_x n(t,x,z) + n(t,x,z)\left(1-\rho(t,x)\right) = 0, \\ \rho(t,x) = \int_I n(t,x,z')dz', \quad t \geq 0, \quad x \in \Omega, \\ n(0,x,z) = n_0(x,z), \quad x \in \Omega, \quad z \in I. \end{cases} \tag{1.32}$$

Consequently, the fast variable is here the space variable x and the slow one that will concentrate according to a constrained Hamilton Jacobi equation is the dispersal trait variable z, as the main term u_0 of the WKB ansatz $u_\varepsilon = \varepsilon \log(n_\varepsilon)$ does not see the space dependency. The structure of the analysis is thus presenting a similar two-step limit problem with some (mirrored) similarities with [Bouin and Mirrahimi 2015] and [Turanova 2015]. The first step is an elliptic eigenvalue problem which characterizes the fast equilibria in space for a given dispersal trait value. The eigenvalue defines the Hamiltonian involved in the limit Hamilton-Jacobi equation, constrained because of the boundedness of the domains considered. The main result of [Perthame and Souganidis 2016] is the weak convergence of n_ε toward the Dirac mass centered in the slowest dispersal trait z_m with a prefactor given by a local FKPP equation (with constant diffusion with coefficient z_m). [Lam and Lou 2017] provides additionally some L^∞ estimates on the convergence of n_ε.

I will mention also the later work of [Hao, Lam, and Lou 2019], which tackles a similar problem, but with an additional advection term that is also influenced by the trait under evolution alongside the diffusion coefficient. This models therefore the evolution of conditional dispersal (in contrast to that of random dispersal, when only diffusion is considered). They study the concentration phenomena that arise in the limit of small mutational variance thanks to a Hamilton-Jacobi approach on a WKB ansatz obtained thanks to a Hopf-Cole transform. One particularity is that they study *the steady states in a small neighborhood of points that satisfy particular convexity/monotony properties of the invasion fitness.* They define here this concept borrowed from adaptive dynamics by an elliptic eigenvalue problem between two specific traits. This invasion fitness is linked to the Hamiltonian (principal eigenvalue of a related problem) that is involved in the limit constrained Hamilton-Jacobi equation. Their main result, following the convergence of the ansatz to the viscosity solution of the limit constrained Hamilton-Jacobi equation, is analogous in spirit to the main result of [Lam 2019], linking the qualitative features of steady states (concentration at the lower edge of the small neighborhood, at an intermediate point, or at both edges of the small neighborhood) to features of the local invasion fitness (increasing, convex, concave).

3) Unbounded space $[1, +\infty[$, unbounded trait. In the case of both unbounded traits and space, [Bouin, Calvez, et al. 2012] predicts using formal derivations on a Hamilton-Jacobi approach that the average trait at the long-time propagation front increases at an asymptotic rate linear in time (for long-time asymptotics), whereas the spatial position of the front accelerates at a rate proportional to $t^{\frac{3}{2}}$. This phenomenon of structure of dispersal

trait by spatial position has been coined as *spatial sorting*, as fastest individuals (or their descendants) get to the edge of the invasion quicker than slower ones. [Bouin, Henderson, and Ryzhik 2017a] and [Berestycki, Mouhot, and Raoul n.d.] study two equations related to the evolution of dispersal. The first is with a local reaction term $n(t,x,z)(1-n(t,x,z))$, modelling the competition for resources among individuals both at the same location and sharing the same dispersal trait, and the second one is with the non-local reaction term as in (1.30) (the competition is local in space, non-local in trait). The authors of [Bouin, Henderson, and Ryzhik 2017a] derive two results, one for each equation. In the local case, they show a precise estimation of the long-time position of the front $X(t) = \frac{4}{3}t^{\frac{3}{2}}$. To do so, they focus on the linearized equation and make a suitable *self-similar change in variables* (reminiscent of the one in Evans and Souganidis 1989) by defining

$$n_\varepsilon(t,x,z) = n\left(\frac{t}{\varepsilon}, \frac{x}{\varepsilon^{\frac{3}{2}}}, \frac{z}{\varepsilon}\right). \tag{1.33}$$

Next, they perform a Hopf-Cole transform $u_\varepsilon = \varepsilon \log(n_\varepsilon)$. under the change of variable (1.33), the WKB ansatz is solution of the following equation obtained from the *linearized* equation

$$\partial_t u_\varepsilon(t,x,z) = \varepsilon\left(z\Delta_x u_\varepsilon(t,x,z) + \Delta_z u_\varepsilon(t,x,z)\right) + z|\nabla_x u_\varepsilon|^2 + |\nabla_z u_\varepsilon|^2. \tag{1.34}$$

Since the Hamiltonian here is quite simple, they can compute explicitly the optimal paths of the variational formula minimizing the Lagrangian action, and thus define sup-solutions to the non-linear equation to get an upper bound. They also build sub-solutions by locally following the optimal paths for the linearized equation trailing just behind the front, and obtain a matching lower bound, hence the sharp result of $X(t) = \frac{4}{3}t^{\frac{3}{2}}$. With the non-local reaction term however, the lack of comparison principle prevents them from using optimal paths from the linearized equation as for the local case, as these meet the region where the population size saturates (contradicting the fact that they are established assuming non-saturation). Therefore, for the non-local equation, they obtain an upper bound for the prefactor of $\frac{4}{3}$ and a non-matching lower bound in a weak sense. I will mention that, in the additional case of a non-local competition between traits that are in a uniform bounded range (parametrized by A>0) modelled by the reaction term $n(t,x,z)\left(1 - \int_{\min(1,z-A)}^{z+A} n(t,x,z')dz'\right)$, [Berestycki, Mouhot, and Raoul n.d.] found the same acceleration rate $\frac{4}{3}t^{\frac{3}{2}}$ as for the local reaction term $n(1-n)$, thanks to probabilistic arguments.

The last chapter in date on the accurate estimation of the rate of acceleration for asexual population that can evolve their dispersal trait and subject to a competition for resources, locally in space, non-local in trait, has been written recently in [Calvez, Henderson, et al. 2022]. The main result is that the prefactor to the spatial rate of acceleration for the non-local competition is strictly lower than $\frac{4}{3}$, which is the analogous quantity for the localized competition (see Bouin, Henderson, and Ryzhik 2017a). This is quite surprising, since there was no discrepancy between the local equation and the slightly less local one from [Berestycki, Mouhot, and Raoul n.d.]. To prove their result, the authors also employ a *geometric optics/Hamilton-Jacobi approach*, similarly as in [Evans and Souganidis 1989] and [Bouin, Henderson, and Ryzhik 2017a], with the *self-similar rescaling of variables* (1.33). The limit Hamilton-Jacobi equation that they consider is similar to the formal limit of (1.34), although with an additional term for the non-local population size ρ, which they roughly approximate in their analysis with an indicator function $\mu \mathbf{1}_{x \leq \alpha t^{3/2}}$ (with a prefactor parameter α and a level μ). They do not prove the convergence of the WKB ansatz $u_\varepsilon = \varepsilon \log(n_\varepsilon)$ towards a viscosity solution of the limit Hamilton-Jacobi problem. Rather, they use the variational formulation of minimization of the

Lagrangian action on optimal paths to argue by contradiction. One of the key results is that the *variational quantity does not depend on μ if it the latter is greater than $\frac{1}{2}$*. The Figure 3 of [Calvez, Henderson, et al. 2022] offers a great illustration of the difference between the optimal paths corresponding to the Lagrangian obtained from the linearized equation in the local/non-local case in [Bouin, Henderson, and Ryzhik 2017a] and those used in [Calvez, Henderson, et al. 2022], which bend when approaching the saturating region due to the discontinuity of the indicator function used to approximate the non-local term ρ.

Appendix: Evolution of dispersal in adaptive dynamics The evolution of dispersal has also been extensively studied with the viewpoint of *adaptive dynamics* applied to reaction-diffusion-advection systems (see for example Cantrell, Cosner, and Lou 2010; Lam and Lou 2014b; Lam and Lou 2014a; Lou and Lutscher 2014; Lam, Lou, and Lutscher 2015; Cantrell, Cosner, Lewis, et al. 2020; Hao, Lam, and Lou 2021). These can for example model ecological populations in streams, where the flow of the water is modelled by an advection term. The typical approach is to consider two species in competition that are differing from one (or more) parameter, like the advection term (Cantrell, Cosner, and Lou 2010), the advection coefficent (Lam and Lou 2014b), the diffusion coefficient (Lou and Lutscher 2014), Lam and Lou 2014a, Lam, Lou, and Lutscher 2015, Hao, Lam, and Lou 2021), or both (Cantrell, Cosner, Lewis, et al. 2020), and analyse the existence and uniqueness of stable invasion strategies. These models rely on a separation of time scales between the ecological dynamics and the mutations' occurrences. The models built in that framework offer a robust way to give analytical insights on the influence of subtle parameters on the success of a given strategy, like the boundary conditions of the spatial domain (Lou and Lutscher 2014; Lam, Lou, and Lutscher 2015; Hao, Lam, and Lou 2021) or the spatial environmental variation (Lam and Lou 2014b; Lam and Lou 2014a). One strategy in particular is highlighted as often, but not always, being evolutionary stable upon existence: the so-called *ideal free dispersal strategy resulting in an ideal free distribution of species*, describing an equilibrium under which all individuals have the same fitness independent of their spatial position and therefore without any net movement of individuals. Determining the evolutionary stability of such equilibria is of sustained interest (Cantrell, Cosner, and Lou 2010; Lam and Lou 2014b; Cantrell, Cosner, Lewis, et al. 2020). A concluding thought is on the scope of models that assume different levels of timescales (diffusion of individuals, population growth, evolution by mutation), and on the links that they entertain with more intricate models, whose analysis they could simplify while still recovering close results (Cantrell, Cosner, Lewis, et al. 2020).

1.2.2.4 Conclusion on asexual populations

The study of the adaptation of large asexually reproducing populations characterized by quantitative traits, under the combined effects of mutations, natural selection, population regulation by competition and migration/dispersal in structured environments, has driven PDE models to flourish in the aim of obtaining rigorous qualitative and quantitative insights. This success is partly due to the linearity of the reproduction operators involved, especially if it is combined with localness, that allows a variety of techniques to be deployed to analyse evolutionary dynamics. One line of method, the small variance methodology, stems from the introduction of geometric optics tools to the study of reaction-diffusion equations. It has been adapted to analyse concentration phenomena in non-local models in various contexts that arise when diversity introduced by reproduction is low compared to the pressure of natural selection toward the fittest traits. This method, which relies on a logarithmic transform and the study

of limit constrained Hamilton-Jacobi equations, has proved to be particularly suited to derive analytical predictions of the combined dynamics of ecology/demography and evolution of traits. It highlights and quantifies, among other features, how asexual populations can evolve their within-population trait variance, which underlies their adaptation capacity, under the interplay of selection, migration/dispersal and mutations.

1.2.3 Sexual populations

On the contrary to asexual reproduction, according to which a single individual passes down all its genetic information to its offsprings (up to mutations), sexual reproduction requires the mating of two individuals to produce offsprings, each bearing a mix of their parents information due to segregation during meiosis. As such, whereas modelling the inheritance of continuous traits in asexual populations involves linear operators (non-local (1.7), or local (1.8)), the transmission of continuous traits in sexual populations relies on non-linear (often quadratic, for the two parents), non-local (the offspring trait can be far from both parents') and non-monotone operators. Mathematical analysis of differential equations involving such collisional operators is therefore quite recent and challenging, for a lot of classical tools that intervene in the study of asexual populations (as presented in the previous section) are not suited to handle these inherent properties of sexual reproduction operators.

Among those, this thesis limits itself to kernel-based operators, which describes the distribution of offspring traits conditional to the parental traits z_1 and z_2 through a kernel $K(\cdot, z_1, z_2)$. Under the assumption of a *well-mixed* population (also called *panmictic*) where individuals mate randomly, the latter yields that the density $\mathcal{B}[n](z)$ of offsprings of trait $z \in \mathbb{R}^d$ generated in the whole population (described by the population trait distribution n) reads

$$\mathcal{B}_{\text{sex}}[n](z) = \iint_{\mathbb{R}^d \times \mathbb{R}^d} K(z, z_1, z_2) \frac{n(z_1)\, n(z_2)}{\int_{\mathbb{R}^d} n(z')dz'} dz_1\, dz_2. \tag{1.35}$$

Throughout my PhD, to model how diversity introduced by segregation influence the spatial eco-evo dynamics of sexually reproducing populations, I used mainly the so-called *infinitesimal model*, where the kernel is a Gaussian density of fixed variance, and that I detail below. However, I also got interested in other biological frameworks that require other kernels, like the following which characterizes the faithful transmission of two quantitative alleles in sexually reproducing haploid populations

$$K : \mathbb{R}^6 \to \mathbb{R}, ((x,y),(x_1,y_1),(x_2,y_2)) \mapsto \frac{1}{4}\left[\delta_{x=x_1,y=y_1} + \delta_{x=x_1,y=y_2} + \delta_{x=x_2,y=y_1} + \delta_{x=x_2,y=y_2}\right]. \tag{1.36}$$

In all what follows, I do not consider cases of sex-differentiating selection, and therefore that the dynamics of mating types of the system are similar, and do not need to be separately modelled.

The infinitesimal model. The infinitesimal model is a founding cornerstone of both population and quantitative genetics, as it was built more than a century ago to conciliate the Mendelian view of evolution (where adaptation comes from changes in allelic frequencies at certain genes with discrete effects) and the Biometricians view of evolution, for which complex continuous traits evolve gradually through time. In [Fisher 1919], Fisher considered complex quantitative traits resulting from a very large number L of infinitesimally small additive diallelic mendelian contributions (for example, $\pm\frac{1}{\sqrt{L}}$). He proposed that the stochastic inheritance

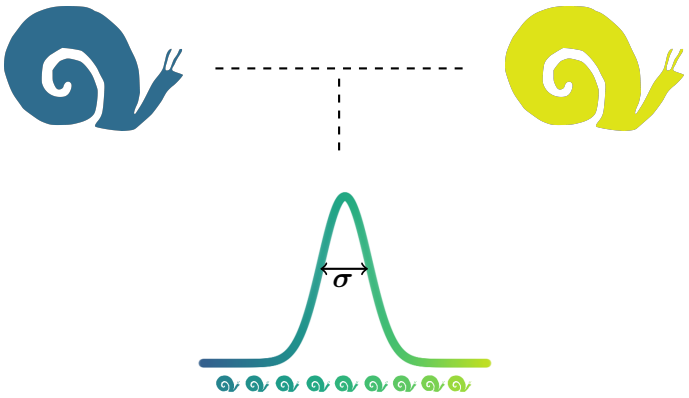

Figure 1.1: Illustration of the trait inheritance process according to the infinitesimal model.

of such traits occurs with a within-family variance that can asymptotically ($L \to \infty$) be considered as constant across time and families. Half a century later, in the spirit of a central limit theorem, first Bulmer (Bulmer 1971) and next Lange (Lange 1978) proposed that the within-family distribution of a complex polygenic traits whose genetic architecture is as described above is Gaussian centered on the mean parental trait, which is what I consider as the classical form of the infinitesimal model (for a more complete, detailed, and accurate historical view, see the review Turelli 2017 or the first section of Barton, Etheridge, and Véber 2017). Reformulated, it states that an offspring trait's variable $\mathcal{Z}$ deviates from the mean parental trait according to a Gaussian law, quantifying the stochasticity of the segregation through the parameter σ^2, called the *segregational variance* (see Fig. 1.1 for an illustration)

$$\mathcal{Z}|\{\mathcal{Z}_1 = z_1, \mathcal{Z}_2 = z_2\} \sim \frac{z_1 + z_2}{2} + \mathcal{N}\left(0, \sigma^2\right). \tag{1.37}$$

Rigorous derivation of the infinitesimal model: [Barton, Etheridge, and Véber 2017]

The statement of a segregational variance that is constant across time and families might seem surprising at first glance. Indeed, in the simplest case where all the alleles are *unlinked* (meaning their inheritance is independent of other alleles's) in a *haploid* population (only one copy of each gene per individual), the passing down of genotypes from two parents to their offspring introduces stochasticity, as each offspring's locus can receive either of its parents' allele at the same locus with an equal probability of $\frac{1}{2}$ during *segregation*. The within-family *segregational variance* of this process is therefore directly linked to the number of differences between the genotypes of the two parents and the variance at each locus (in the example above, the variance at each locus is $\left(\frac{1}{\sqrt{L}}\right)^2 = \frac{1}{L}$). In turn, the number of differences between the parents' genotypes, or equivalently, the number of identical alleles they share, which is averaged as the *identity by descent*, depends on the genealogical lineages that led to them. In a finite population, this within-family segregational variance is therefore inevitably eroded by *inbreeding*. However, in a large well-mixed population, one might think that this erosion by inbreeding is greatly reduced (even negligible in a certain asymptotic), hence this idea of segregational variance constant across time and families. Nevertheless, to precise in which asymptotic this statement might hold, one has to effectively track the building of inbreeding through time, or equivalently the *pedigree*.

This has recently been done in the landmark paper [Barton, Etheridge, and Véber 2017] which presents a rigorous derivation of the infinitesimal model. Thanks to a recently established sophisticated version of the central limit theorem, the authors show that the error between the within-family distribution, conditioned to knowing only the history of the parents (not their precise traits), and the Gaussian distribution centered on the mean parental traits and with a segregational variance eroded by inbreeding from the ancestral segregational variance V_0, is at most of order $\frac{t}{\sqrt{L}}$ after a generation time t (L being the number of genes that add to build the trait). The paper also indicates that this estimation is robust to its application in various biological settings, for example, with natural selection, or migration in a discrete heterogeneous environment. It also seems to justify (1.37) in the asymptotic where $L \to \infty$ (so that the segregational variance reduces to $V_0(1-F_j)$, where F_j is the probability of identity between the parents of the $j-th$ individual), and then in the limit of large population (that leads formally to $F_j \to 0$).

Box 1.2.3: Link between variance at linkage equilibrium, segregational variance and allelic effects

In [Barton, Etheridge, and Véber 2017], the ancestral segregational variance V_0 is linked to the concept of the ancestral *variance at linkage equilibrium* and denoted σ^2_{LE} (also denoted V_{LE}, see Turelli and Barton 1994; Tufto 2000; Tufto 2001). The latter is the variance in the ancestral population considering alleles are distributed independently between different loci (more precisely, that the frequency of any couple of alleles in the population is the product of the allelic frequencies); as we consider an ancestral population where alleles are randomly distributed, the frequency of each allele at each locus is furthermore of $\frac{1}{2}$. Note that the variance at linkage equilibrium in general at a given time is the sum of the variances at each locus at that given time, so depends on the frequency of the alleles at each locus.
In this configuration, σ^2_{LE} is then linked to the diallelic effects as the latter read $\pm\frac{\sigma_{LE}}{\sqrt{L}}$. Indeed, if the loci are assumed unlinked, the alleles distributed at each loci according to a Bernoulli law of parameter $\frac{1}{2}$, and that each individual is independent of all others, then the each individual's trait is distributed according to a binomial law of parameter $\left(L, \frac{1}{2}\right)$ taking values in $\left\{-\frac{\sigma_{LE}}{\sqrt{L}}, \frac{\sigma_{LE}}{\sqrt{L}}\right\}$. Its variance is therefore equal to $L \times \frac{1}{2}\left[\left(-\frac{\sigma_{LE}}{\sqrt{L}}\right)^2 + \left(\frac{\sigma_{LE}}{\sqrt{L}}\right)^2\right] = \sigma^2_{LE}$, which equals the variance in the population, as individuals are independent.
Moreover, to show that $V_0 = \frac{\sigma^2_{LE}}{2}$ (Turelli and Barton 1994, Barton, Etheridge, and Véber 2017), consider the i-th and j-th individuals, and let us denote X^l_i (resp. X^l_j) the random variable of their allele at locus l. Let us introduce Y^l the random variable which equals X^l_i or X^l_j with equal probability $\frac{1}{2}$ (the allele inherited by their offspring). Then, as all alleles are unlinked, we obtain for the segregational variance within the (i,j) family:

$$\begin{aligned} V_{0,i,j} &= \sum_{l=1}^{L} \mathbb{E}\left[\left(Y^l - \frac{X^l_i + X^l_j}{2}\right)^2\right] = \sum_{l=1}^{L} \mathbb{E}\left[\left(Y^l - \frac{X^l_i + X^l_j}{2}\right)^2 \mathbf{1}_{X^l_i \neq X^l_j}\right] \\ &= \sum_{l=1}^{L} \mathbb{E}[(Y^l)^2 \mathbf{1}_{X^l_i \neq X^l_j}] = \frac{\sigma^2_{LE}}{L} \sum_{l=1}^{L} \mathbb{P}[X^l_i \neq X^l_j] = \frac{\sigma^2_{LE}}{L} \sum_{l=1}^{L} \frac{1}{2} = \frac{\sigma^2_{LE}}{2}, \end{aligned}$$

where we use the fact that if $X^l_j = X^i_j$, then $Y^l = \frac{X^l_i + X^l_j}{2}$ and that $(Y^l)^2 = \frac{\sigma^2_{LE}}{L}$ (as the allelic effects sum to 0). Therefore, as all pairs are independent, we conclude that $V_0 = \frac{\sigma^2_{LE}}{2}$.

The latter (1.37) yields the following infinitesimal model $\mathcal{B}^{\mathrm{IM}}_\sigma$ integral operator deduced from (1.35) with a Gaussian kernel of variance σ^2

$$\mathcal{B}^{\mathrm{IM}}_\sigma[n](z) = \frac{1}{\sqrt{2\pi}\sigma} \iint_{\mathbb{R}\times\mathbb{R}} \exp\left[\frac{z - \frac{z_1+z_2}{2}}{2\sigma^2}\right]^2 \frac{n(z_1)\, n(z_2)}{\int_{\mathbb{R}^d} n(z')dz'} dz_1\, dz_2. \tag{1.38}$$

(For simplicity, I consider henceforth real-valued traits, but $\mathcal{B}^{\mathrm{IM}}_\sigma$ can also be defined for multi-dimensional traits in $\mathbb{R}^d$.) This integral operator can be seen as a collisional operator, and is of great mathematical interest in its own right. I highlight here the main properties that it had been shown to verify

1. the operator $\mathcal{B}^{\mathrm{IM}}_\sigma$ conserves the mass (population size) and the center of mass (mean trait)

$$N := \int_{\mathbb{R}} n(z')dz' = \int_{\mathbb{R}} \mathcal{B}^{\mathrm{IM}}_\sigma[n](z')dz', \qquad \bar{z} = \frac{1}{N}\int_{\mathbb{R}} z' n(z')dz' = \frac{1}{N}\int_{\mathbb{R}} \mathcal{B}^{\mathrm{IM}}_\sigma[n](z')dz'.$$

2. any Gaussian distribution of variance $2\sigma^2$ (twice the segregational variance) is a fixed

point of $\mathcal{B}_\sigma^{\mathrm{IM}}$ (Bulmer 1980). A reformulation is that such distribution are steady states of a constant size population under random mating according to the infinitesimal model

$$\partial_t n(t,z) = \mathcal{B}_\sigma^{\mathrm{IM}}[n](t,z) - n(t,z). \tag{1.39}$$

This is in sharp contrast with the asexual reproduction operators (1.7) and (1.8).

3. similarly as for the Boltzmann operator modelling particles' collision, which is nonexpansive by Tanaka's inequality (see Villani 2008), the operator (1.39) contracts for the quadratic Wasserstein distance W_2; for two probability distributions n_1 and n_2 with the same center of mass,

$$W_2\left(\mathcal{B}_\sigma^{\mathrm{IM}}[n_1], \mathcal{B}_\sigma^{\mathrm{IM}}[n_2]\right)^2 \leq \frac{1}{2} W_2\left(n_1, n_2\right)^2. \tag{1.40}$$

A proof of that fact can be consulted in [Raoul 2017], and a counter-example where the centers of mass differ is presented in [Calvez, Lepoutre, and Poyato 2022]. We recall that the quadratic Wasserstein distance W_2 is defined on the set of probability distributions with finite variances as

$$W_2(n_1,n_2)^2 = \inf_{\mu \in \Pi[n_1,n_2]} \iint_{\mathbb{R}^d \times \mathbb{R}^d} |x-y|^2 d\mu(x,y), \tag{1.41}$$

where $\Pi[n_1,n_2]$ is the subset of probability distributions with finite variance on $\mathbb{R}^d \times \mathbb{R}^d$ which have marginals n_1 and n_2. This metric is the optimal transport metric for the cost of the Euclidian distance (see Villani 2008 for reference), which can be illustrated by its application on two Dirac distributions : $W_2(\delta_a, \delta_b)^2 = |a-b|^2$ (the cost of moving a Dirac mass between two locations is equal to the Euclidian distance between them).

4. the integral operator (1.38) can be rewritten as a double convolution

$$\mathcal{B}_\sigma^{\mathrm{IM}}[n] = G_{0,\sigma^2} * \tilde{n} * \frac{\tilde{n}}{N}, \tag{1.42}$$

where $\tilde{n} : z \mapsto n(2z)$. This property (which implies the Gaussian fixed point one) is practical from a numerical viewpoint, as Fast Fourier Transform algorithms can be used instead of double sums to speed up simulations (for applications, see for example Turelli and Barton 1994, Tufto 2000, Tufto 2001).

Because the infinitesimal model allows to reduce a priori high-dimensional genetic questions to a one-parameter ones (the segregational variance) when studying adaptation in populations characterized by *polygenic* traits, the infinitesimal model has been used in some population genetic models to answer evolutionary questions.

These studies point to the fact that the variance in trait in a well-mixed population where reproduction is modelled by the infinitesimal model is highly constrained by the segregational variance, even under natural selection. [Slatkin 1970] shows that under *stabilizing selection*, the variance in the population is bounded below by the segregational variance σ^2 and by above by twice the segregational variance $2\sigma^2$, bounds that both do not depend on the strength of selection. This result aligns with the fundamental findings of [Roughgarden 1972] which shows in an analysis using Fourier transforms that the variance in trait in sexual populations subject to selection and competition for resources will not have the same response to selection as asexual populations, as it is heavily influenced by the segregational variance (close to $2\sigma^2$, see

fig. 9 of Roughgarden 1972), whereas asexual population with large initial variance can evolve their variance to an optimal one (without mutations).

Later, other population genetic studies examine the link between multi-loci models and the infinitesimal model, and the validity to the Gaussian approximation of breeding values (heritable part of the trait) in the whole population, assuming constant population size (no demographic dynamics). At this point, it must be stressed that the infinitesimal model does not assume a within-population Gaussian distribution of trait or breeding values (rather a within-family one), and does not lead in all generality to such distributions. However, [Turelli and Barton 1990] shows by computing Taylor expansions that, in a homogeneous space, weak quadratic selection on many loci of small effects leads to distributions that are approximately Gaussian. This fact essentially translates a *Quasi-Linkage-Equilibrium (QLE)* state, meaning that selection does not bias (or very little) the occurrence of any particular pair of alleles (*linkage disequilibrium*). A few years later, in a homogeneous space, constant population size multi-loci model, the same authors approximate in [Turelli and Barton 1994] the dynamics of the mean trait and variance in trait under strong truncation selection and recombination thanks to cumulants of the trait distribution, and indicate that they stay close to those obtained when assuming Gaussian trait distributions, even if the skewness is away from 0.

Finally, I will mention that the infinitesimal model is also known in the field of animal breeding as the *animal model* and has been widely used both on wild and domesticated animal and plant populations in the last two decades as a base of a lot of statistical studies to separate heritable and environmental effects (see Kruuk 2004, Hill 2014, Bernardo 2020 for reviews).

I will next detail more lengthily works in homogeneous, heterogeneous and continuous space that study the adaptation of large sexually reproducing populations while combining the dynamics of demography/ecology and evolution, in the aim of further delimit the scope of my PhD.

1.2.3.1 Homogeneous space

Recently, there has been an increasing interest in analytically describing the eco-evo dynamics of large sexual panmictic populations subject to natural selection acting on a quantitative trait in a homogeneous space, using integro-differential equations and modelling trait inheritance through kernels (1.35) (Calvez, Garnier, and Patout 2019, Patout 2020, Raoul 2021, Garnier et al. 2022, Calvez, Lepoutre, and Poyato 2022, Perthame, Strugarek, and Taing 2021). The majority focuses on modelling the influence of segregation with the infinitesimal model operator (1.39). [Calvez, Garnier, and Patout 2019], [Patout 2020], [Raoul 2021], take advantage of the properties of contraction and of Gaussian fixed point of the infinitesimal model operator shown in the previous subsection. However, they developed different analytical methods aimed at different asymptotics. [Calvez, Lepoutre, and Poyato 2022] employs another approach to highlight an ergodic property of (1.39) without any restricting asymptotic regime. Finally [Perthame, Strugarek, and Taing 2021] focuses on the influence of small mutations on asymmetrical kernels of trait transmission.

Small segregational variance asymptotics. In [Calvez, Garnier, and Patout 2019] and [Patout 2020], the authors study the following equation:

$$\varepsilon^2 \partial_t \tilde{n}_\varepsilon(t,z) = \mathcal{B}_{\frac{\varepsilon}{\sqrt{2}}}[\tilde{n}_\varepsilon](t,z) - m(z)\tilde{n}_\varepsilon(t,z), \qquad z \in \mathbb{R}^d, \quad t > 0. \tag{1.43}$$

The equation (1.43) models the evolutionary dynamics of a sexual population under natural selection affecting its mortality m, according to a quantitative trait $z \in \mathbb{R}^d$ inherited according

to the infinitesimal model operator (1.39). They adopt a methodology of small variance close to the one developed for asexual models (see Box Section 1.2.2.1) as they consider that the segregational variance $\frac{\varepsilon^2}{2}$ is small. Consequently, as diversity introduced by reproduction is small, the time is rescaled to see the effect of selection on evolution (hence the ε^2 factor in front of the time derivative). I will recall in some details their approach and results, as it shares strong links with some of my works.

Steady states of (1.43). The authors of [Calvez, Garnier, and Patout 2019] study the solutions of (1.43) of the form $e^{\lambda_\varepsilon t} n_\varepsilon(z)$. The variable n_ε is a distribution profile and $\lambda_\varepsilon \in \mathbb{R}$ represents a population growth rate which gives a demographic dimension to the problem (it therefore considers (1.43) as the linearized equation of a model with a non-local competition/saturation term). They are searched as solutions of

$$\frac{\mathcal{B}_{\frac{\varepsilon}{\sqrt{2}}}[n_\varepsilon](z)}{n_\varepsilon(z)} = \lambda_\varepsilon + m(z), \qquad z \in \mathbb{R}^d. \tag{1.44}$$

Note that the equation (1.44) highlights the fact that the reproduction term $\frac{\mathcal{B}_{\frac{\varepsilon}{\sqrt{2}}}[n_\varepsilon](z)}{n_\varepsilon(z)}$ must formally remain bounded when ε vanishes, in order to balance the r.h.s of (1.44). They adapt the small variance methodology used in asexual studies (Section 1.2.2.1) by introducing the following ansatz $u_\varepsilon = u_0 + \varepsilon^2 v_\varepsilon$:

$$n_\varepsilon(z) = \frac{1}{\sqrt{2\pi}\varepsilon} e^{-\frac{u_\varepsilon}{\varepsilon^2}} = \frac{1}{\sqrt{2\pi}\varepsilon} e^{-\frac{u_0}{\varepsilon^2} - v_\varepsilon}. \tag{1.45}$$

A formal analysis of the term $\frac{\mathcal{B}_{\frac{\varepsilon}{\sqrt{2}}}[n_\varepsilon](z)}{n_\varepsilon(z)}$ with the ansatz (1.45) in [Garnier et al. 2022] reveals that, when ε vanishes, for the latter to remain bounded, u_0 must formally satisfy the following constraint:

$$\forall z \in \mathbb{R}, \max_{(z_1,z_2)} \left[-\left(z - \frac{z_1+z_2}{2} \right)^2 + u_0(z) - u_0(z_1) - u_0(z_2) + \min u_0 \right] = 0. \tag{1.46}$$

A quick look at (1.46) shows that the main term u_0 is asymptotically characterized independently of natural selection, as the small segregational variance formally isolates the reproduction term. As a matter of fact, it is shown that, up to additive constant, (1.46) determines completely u_0 as the quadratic function $\frac{(z-z^*)^2}{2}$, where z^* is unknown at this stage (see Garnier et al. 2022, which formally compares the adaptation of asexual and sexual populations to a linearly changing environment in the regimes of small variance, for the convex analysis arguments that lead to this characterization). It must be emphasized that this is a crucial difference with comparable asexual studies with the small mutational variance asymptotics (Section 1.2.2.1), for whom the limit object u_0 is viscosity solution of a constrained Hamilton-Jacobi which depends directly on selection. The concentration phenomenon in sexual populations under the infinitesimal model and the regime of small variance is highly influenced by segregation, and not selection as for asexual models in a comparable regime. Another way to state this is to observe that here, the variance in trait of the population is of the same order as the segregational variance (ε^2) whereas, in asexual models of mutation-selection balance, the variance in trait of the population (ε) is much larger than the mutational variance (ε^2), and requires selection to be stabilized (see Box 1.2.2.1). This is qualitatively consistent with the findings of [Roughgarden 1972] on the evolution of niche width presented earlier (see Section 1.2.3). This implies several points:

1. In virtue of the latter and (1.45), the profile that is under investigation in the small variance regime is a small perturbation of a Gaussian profile.

2. The unknowns on which selection acts and upon which the analysis of [Calvez, Garnier, and Patout 2019] is carried, are the asymptotic dominant trait z^* and the deviation to the limit Gaussian profile v_ε (the asymptotic dominant trait z^* can be fixed to 0 up to a translation of the selection m), which has to be controlled to confirm the main Gaussian profile.

3. The analysis for sexual reproduction with the infinitesimal model in a regime of small variance focuses on a higher degree of approximation than for analogous asexual models.

Following (1.45) with the identification of $u_0(z) = \frac{(z-z^*)^2}{2}$ leads to a reformulation problem involving a finite-difference term instead of a Hamiltonian characteristic of asexual models in small variance regime

$$\exp\left[v_\varepsilon(z) + v_\varepsilon(z^*) - 2v_\varepsilon\left(\frac{z+z^*}{2}\right)\right] I_\varepsilon(v_\varepsilon)(z) = \lambda_\varepsilon + m(z), \quad z \in \mathbb{R}^d, \tag{1.47}$$

where $I_\varepsilon(v_\varepsilon)(z)$ is an integral term that is shown to converge uniformly toward 1 thanks to suitable Lipschitz estimates. Consequently, the following limit problem can be derived from (1.47) upon convergence of $v_\varepsilon \to v$ and $\lambda_\varepsilon \to \lambda$:

$$\exp\left[v(z) + v(z^*) - 2v\left(\frac{z+z^*}{2}\right)\right] = \lambda + m(z), \quad z \in \mathbb{R}^d. \tag{1.48}$$

Interestingly, (1.48) identifies λ and z^*, the former as $\lambda = 1 - m(z^*)$ by evaluating (1.47) in z^* and the latter as a critical point of m by differentiating (1.47) and evaluating in z^*. Furthermore, it shows that the limit object $v = \lim_{\varepsilon \to 0} v_\varepsilon$ can be expressed explicitly as an infinite series by inverting the finite difference operator involved in (1.48), up to its linear part. As linear functions are in the kernel of the finite-difference operator involved in (1.48), the linear part of v cannot be determined from (1.48).

The main result of [Calvez, Garnier, and Patout 2019] is therefore the local existence and uniqueness of v_ε solution of (1.47) (and therefore n_ε solution of (1.43)) thanks to a contraction-mapping fixed point theorem in a subspace of $\mathcal{C}^3(\mathbb{R}^d)$ (using the contractive properties of the infinitesimal model operator on the first three derivatives of v_ε) and its convergence to the limit objects previously identified (the linear part is treated separately as a by-product of the main analysis thanks to an implicit function theorem). The local uniqueness aspect of the result is important, as their analysis indicates that the trait distribution can concentrate at local minima of m (provided that their level under m are not too high compared to the global minima).

Cauchy problem of (1.43). The aim of [Patout 2020] is to study the time-marching problem (1.43) by searching for solution of the form $\tilde{n}_\varepsilon(t,z) = e^{\frac{\lambda_\varepsilon t}{\varepsilon}} n_\varepsilon(t,z)$. It relies on the same small segregational variance framework as in [Calvez, Garnier, and Patout 2019] using the WKB ansatz

$$n_\varepsilon(t,z) = \frac{1}{\sqrt{2\pi}\varepsilon} \exp\left[-\frac{(z - z^*(t))^2}{2\varepsilon^2} - v(t,z) - \varepsilon^2 r_\varepsilon(t,z)\right], \qquad t > 0, \quad z \in \mathbb{R}^d, \tag{1.49}$$

The main result is the uniform control of order ε^2 of the dynamics of the perturbation $r_\varepsilon(t,z)$ when the initial state at $\varepsilon > 0$ is sufficiently close to the limit solution. This requires another

perturbative approach rather than the contraction-mapping fixed point argument which cannot apply due to the time derivative.

The preliminary stages consists, as in [Calvez, Garnier, and Patout 2019], in identifying the dynamics of the limit objects $\lambda(t), z^*(t), v(t,z)$ defined analogously as in [Calvez, Garnier, and Patout 2019]. Unsurprisingly, the limit equation involves a similar finite difference term as in (1.47)

$$\exp\left[v(t,z)+v(t,z^*(t))-2v\left(t,\frac{z+z^*(t)}{2}\right)\right]=\lambda'(t)+z^{*\prime}(t)(z-z^*(t))+m(z),\quad z\in\mathbb{R}^d,\quad t>0. \tag{1.50}$$

The dynamics $\lambda'(t)+m(z^*(t))=1$ and $z^{*\prime}(t)+m'(z^*(t))=0$ are obtained by evaluating (1.50) in $z^*(t)$ and differentiating (1.50) and evaluating in $z^*(t)$, and the non-linear part of $v(t,z)$ is identified as an explicit infinite serie obtained by inverting the finite difference operator as for the stationary problem above. Notice that the equation on $z^*(t)$ is similar to the canonical equation obtained in asexual models, as it descends the selection gradient, but here with a constant variance. This limit analysis allows to deduce the equation verified by $r_\varepsilon(t,z)$, which is non-linear and quite involved (as the exponentiated finite difference term still appears). Nevertheless, its linearization is informative and is at the core of the strategy to prove that r_ε is bounded through a stability result:

$$\varepsilon^2\partial_t\hat{r}_\varepsilon(t,z)=M(t,z)\left[2\hat{r}_\varepsilon\left(t,\frac{z+z^*(t)}{2}\right)-\hat{r}_\varepsilon(t,z)-\hat{r}_\varepsilon(t,z^*(t))\right], \tag{1.51}$$

where M is a function independent of $\hat{r}_\varepsilon$. Therefore, the stability of the dynamics of $\hat{r}_\varepsilon(t,z)$ can be inferred from the spectrum of the linear operator T defined as

$$T(f)(t,z)=2f\left(t,\frac{z+z^*(t)}{2}\right)-f(t,z)-f(t,z^*(t)).$$

The first eigenvalue is 0 with multiplicity 2, associated to the dual eigenvector δ_{z^*} (evaluation in z^*) and δ'_{z^*} (differentiating and evaluating in z^*), and therefore affecting the stability of the affine part of r_ε. The affine part of r_ε is thus driven by slow dynamics (solution of ODE in a comparable time scale as the macroscopic variable $\lambda(t)$ and $z^*(t)$) compared to its non-linear counterpart, associated to negative eigenvalues and therefore converging quickly to a bounded value.

Wasserstein estimates under weak and compactly supported selection. In [Raoul 2021], the author proposes a methodology different from the perturbative approach used in [Calvez, Garnier, and Patout 2019] and [Patout 2020] to study the adaptation of well-mixed sexually reproducing populations over time, subject to uniform competition for resources through a non-local term and weak natural selection affecting their fecundity (and not their mortality as in the two previously presented studies) according to a quantitative trait $z\in\mathbb{R}$. The inheritance of the trait is according to the infinitesimal model, but, here, the trait transmission kernel incorporates the slight increase or decrease $z\mapsto 1+\alpha a(z)$ due to selection on fecundity (α, the selection strength, is a small parameter) and thus differs slightly from the Gaussian kernel (1.39):

$$\mathcal{B}^{\tilde{\mathrm{IM}}}_\sigma[n](z)=\frac{1}{\sqrt{2\pi}\sigma}\iint_{\mathbb{R}\times\mathbb{R}}\exp\left[\frac{z-\frac{z_1+z_2}{2}}{2\sigma^2}\right]^2\frac{(1+\alpha a(z_1))n(z_1)\,(1+\alpha a(z_2))n(z_2)}{\int_{\mathbb{R}^d}n(z')dz'}dz_1\,dz_2. \tag{1.52}$$

The non-linear non-local equation describing the eco-evo dynamics of the population reads

$$\partial_t n(t,z) = \mathcal{B}_\sigma^{\tilde{\mathrm{IM}}}[n](t,z) - \frac{\left[\int_{\mathbb{R}}(1+\alpha a(z'))n(t,z')dz'\right]^2}{\int_{\mathbb{R}} n(t,z')dz'} n(t,z). \tag{1.53}$$

The main result of [Raoul 2021] is the existence and local uniqueness of a stable steady state (1.53), which is close to Gaussian distributions of variance $2\sigma^2$, with exponential convergence toward this steady state under some conditions. The integro-differential equation (1.53) can asymptotically be summarized by the dynamics of the mean trait and the population size.

This result relies heavily on an extension of the Wasserstein contractive property of the infinitesimal model operator (equivalent to (1.52) with $\alpha = 0$) to when the selection strength α is small. Recall that the contraction does not hold necessarily if the center of mass changes, which is likely to occur with selection. The idea here is therefore to dominate the selection by the contraction, hence the weak selection regime. More precisely, the approach used is inspired from [Bolley, Gentil, and Guillin 2012] and provides some Wasserstein control even in the presence of weak multiplicative selection when the distributions are uniformly bounded away from 0. For that reason, a crucial additional assumption in [Raoul 2021] is that the selection function a is compactly supported. Tail estimates are also derived to complete the analysis.

Ergodic property of the infinitesimal model operator under quadratic selection Let us also mention that an ergodic property of the infinitesimal model operator (1.39) was proved in a discrete-time model under quadratic stabilizing selection in [Calvez, Lepoutre, and Poyato 2022], without restriction to an asymptotic regime (nor small segregational variance, nor weak selection). A thorough study of the propagation of information along the pedigree shows that the influence of the initial state is lost rapidly, which entails exponential convergence toward a unique steady state thanks to non-expansiveness estimates (different from the Wasserstein metric one).

Asymmetrical sexual reproduction kernels: small mutational variance. Finally, let us mention the work of [Perthame, Strugarek, and Taing 2021] in which is analysed the influence of asymmetrical sexual reproduction kernels on a competition-selection-mutation model, thanks to a small variance approach. Asymmetry in sexual reproduction can for example arise as a trade-off of evolving resistance at the expense of a loss of fertility in female mosquitoes. Specifically, the authors consider two sorts of kernels: asymmetrical fecundity kernels K_ε^{AF} and asymmetrical heredity kernels K_ε^{AH} that include non-local mutations kernels with small variance ε (similarly as introduced by Kimura 1965 and used in asexual models presented in Section 1.2.2.1)

$$\begin{aligned} &K_\varepsilon^{AF}(z,z_1,z_2) = B(z_1)\frac{\alpha\left(\frac{z-z_2}{\varepsilon},z_1\right)}{\varepsilon}, \qquad K_\varepsilon^{AH}(z,z_1,z_2) = K_0(z-z_1)\frac{G\left(\frac{z-z_2}{\varepsilon}\right)}{\varepsilon}, \\ &\forall z_1 \in \mathbb{R}, \int_{\mathbb{R}} \alpha(x,z_1)\,dx = 1, \qquad \int_{\mathbb{R}} G(x)dx = 1, \qquad B \geq 0, \qquad K_0 \geq 0. \end{aligned} \tag{1.54}$$

Unlike the infinitesimal model operator (1.39), the asymmetrical kernels (1.54) focus on modelling mutations on the trait to introduce diversity rather than segregation. Two types of results are derived. The first is the existence of uniform BV-bounds on the population sizes with both types of asymmetrical kernels (even more general ones for the asymmetrical fecundity), but only when the selection-competition term is not trait-dependent (although

non-local). The second one concerns the WKB ansatz obtained through the Hopf-Cole transform $u_\varepsilon = \varepsilon \ln(n_\varepsilon)$. It states locally uniform Lipschitz bounds in space and time for both class of kernels (1.54) and therefore the strong convergence of u_ε toward a Lipschitz limit u along subsequences. However, the time-dependency and the lack of regularity of some of the terms prevent to identify this limit as a viscosity solution of constrained Hamilton-Jacobi equations, which they derive formally.

To conclude on the studies of the adaptation of large sexually reproducing populations through integro-differential equations: different asymptotics have yielded qualitative and quantitative result when segregation is modelled according to the infinitesimal model operator. However, beyond the limitations of the asymptotic regime considered, they each have their own technical limitations. On the one hand, the perturbative approach in the small segregational variance regime is highly technical, despite the limit problem being quite easy to describe. Extensions of this method of proof to a spatial structure might thus be even more technical, as/and the limit problem might be more intricate, despite its a priori robustness. On the other hand, the approach using Wasserstein estimates in weak selection regime does not look the best to handle losses of mass by selection, which would be even more non-local with spatial structure. Finally, the study with asymmetrical kernels is inspirational to carry analyses in homogeneous space with rather different kernels than the Gaussian one involved in the classical version of the infinitesimal model, for example corresponding to a different genetic architecture. This motivates a joint work with Sepideh Mirrahimi presented in Section 1.3.4.

1.2.3.2 Discrete heterogeneous space

Back-and-forth migration models. Two decades ago, a landmark paper [Ronce and Kirkpatrick 2001] used a quantitative genetic models to describe the eco-evo adaptation of a population in a two-patch symmetrical environment connected by constant migration, subject to local population regulation and stabilizing selection toward local different optima. Assuming that the two local trait distributions remain Gaussian with a constant variance, independent of the patch, they reduced the analysis to a non-linear ODE system with four macroscopic variables (local sizes of population and local mean traits). Even though the reproduction mode is left unspecified, it is assumed to be sexual populations (from personal communication with one of the authors), which is a priori consistent with fixed variance result in homogeneous space studies (see Section 1.2.3.1). Despite the symmetry of the environment, they found that both symmetrical and asymmetrical steady states (the latter only numerically observed) could exist, and even co-exist, contrasting with the analytical finding of [Mirrahimi 2017] for asexual populations. Asymmetrical situations correspond to specialist species that are mainly adapted to one patch and does not occupy fully all the available range (when selection is strong enough compared to migration, especially with asymmetrical initial population sizes), while symmetrical ones correspond to generalist species which occupy the whole range of habitats by being equally (mal)adapted to all (when selection is weak compared to migration). Their study highlights the need to take into account the demographic feedback on evolutionary dynamics in discrete heterogeneous environment, as the coupled effects can result into non-trivial dynamics, including hysteresis phenomena (coined as "*migrational meltdown*").

A very recent population genetic work also tracking demographic changes [Szép, Sachdeva, and Barton 2021] shows some interesting influences of the interplay between migration, selection and genetic drift on the patterns of local adaptation to a discrete heterogeneous environment, where local populations are also subject to regulation (competition for resources). The

discrete heterogeneous environment is constituted by infinitely many patches all connected by migration, each patch either belonging to a frequent first type of habitat or a rare second type of habitat. The authors use a stochastic multi-loci model modelling the joint dynamics of demography and alleles frequencies. More precisely, at each locus, two alleles (0 or 1) segregate under local *directional selection*, so that individuals with alleles 1 at all loci are optimally adapted to one habitat, whereas individual with alleles 0 are optimally adapted to the other, and any mix is less adapted everywhere. Moreover, selection is decoupled per loci (multiplicative for discrete-time model, and additive for continuous time model) and acts linearly on the vector of allele frequencies, which simplifies the dynamics of the joint distribution. Migration between infinitely many demes allows to average its effect, instead of tracking every exchange between every particular pairs of demes. In complement of the stochastic model, a formal deterministic diffusion approximation is also derived. The study highlights two qualitative phenomena. The first occurs when selection is weak compared to the stochastic drift, which promotes *gene swamping* (replacement of alleles from one habitat to another) from the common habitat onto the rare habitat. When selection is strong compared to the stochastic drift, there exists a threshold on the migration rate above which local adaptation to the rare habitat fails. Note that this biological framework exhibits two main differences from the one studied in [Ronce and Kirkpatrick 2001]. Indeed, in the latter, *stabilizing selection* (which means it is locally concave around optimal traits, as the optimum is reached at an intermediate trait in the full trait range) is considered instead of *directional selection* (the selection is monotonic around the optimal trait, as the optimum is reached on a boundary on the full trait range). Moreover, the trait in [Ronce and Kirkpatrick 2001], which can be thought to be additive w.r.t small effects loci, is nonetheless under quadratic selection, which would include non-linear cross terms if it were to be expressed as sum of small effects loci, which is different from the framework studided in [Szép, Sachdeva, and Barton 2021] (additive effects of selection w.r.t all loci, see above).

There exists other quantitative genetic models which rather keep the local subpopulations sizes constant for analytical purposes. For instance, [Débarre, Yeaman, and Guillaume 2015] presents a study in two parts to illustrate how patterns of local adaptation in a two-patch environment can skew local distributions of a quantitative trait. The first part introduces a discrete-time model with constant population sizes which highlights the role of the local skews in trait on the differentiation between locally adapted subpopulations, in contrast with the analogous quantity derived in [Hendry, Day, and Taylor 2001] by assuming Gaussian local trait distributions. In the second part of their article, the authors use individual-based simulations to investigate the influence of a major effect locus combined with 19 small effects loci to drive the local trait distributions away from Gaussian profiles (all effects are fixed at first, and next results from IBS with evolvable effects are shown). On the one hand, they indicate that when all the 20 loci have small effect, local trait distributions are close to being Gaussian (when the standard deviation at linkage equilibrium is $\sigma_{LE} = 0.4$ and the local optima $\pm\theta = \pm 1$) and on the other hand, they show that if one locus has a much larger effect, then the local distributions are more highly skewed.

One-way migration models. Other works in quantitative genetics examined the relationship between the infinitesimal model with both moment-based approaches (Tufto 2001, Barton and Etheridge 2018) and multi-loci models (Tufto 2000, Huisman and Tufto 2012) in *one-way migration*-selection in two-patches model (also called *source-sink*, as one patch - the sink - only receives incomers from the other patch - the source - which is not affected by any migrational feedback, which results in less involved systems).

In [Tufto 2001], the author describes the equilibria of a deterministic moments-based reduction that results from a Gaussian approximation of the local trait distribution in the sink to study establishment despite maladaptation from a polygenic trait, inspired by the work of Turelli and Barton 1994 (homogeneous space) on the link between infinitesimal model and Gaussian approximation of trait distribution. He found that multiple equilibria can coexist when migration is small and selection strong enough, including ones with small populations sizes (sign of maldaptation). Population size can also drop under strong migration and weak selection if the genetic deviation of the individuals that migrate is too far from the sink optimum.

More recently, the work of [Barton and Etheridge 2018] focuses on a similar biological framework (establishment in a sink of locally maladapted newcomers from a source in a one-way migration-selection model, where adaptation comes from a polygenic trait). However, their main approach is stochastic, so it incorporates the influence of both random drift and inbreeding to account for the erosion of the segregational variance of the infinitesimal model in the estimation of the probability of establishment under *directional selection* (the selection function is monotonic on the considered trait space). They show that the quantity of interest is mainly influenced by the mean trait and the genetic variation in the source population (how far a newcomer will be and how fast can it adapts). They also highlight a non-monotonic convex type of behaviour w.r.t. increasing migration regarding the mean time to establishment (fig. 4 of their article). The latter decreases when migration is below a certain threshold as (relatively) strong enough selections favor quickly the rare fit migrants to found a successful lineage. Conversely, the time to establishment increases on average when migration is above a threshold, as migration holds back local adaptation by increased gene flow from the source. They also derive a diffusion deterministic approximation ODE system on macroscopic elements (population size, mean traits), assuming constant variance and Gaussian approximation of trait values to study the deterministic steady states (with extensions to study how to incorporate inbreeding, density-dependent regulation and stabilizing selection).

One can turn next to multi-loci simulations models with a one-way migration between two patches and local stabilizing selection in each patch. [Tufto 2000] presents a discrete-time numerical study to understand the influence of several types of Gaussian approximation of the trait distribution in a sink (with fixed variance like at linkage equilibrium, or updated variance) versus the infinitesimal model, with reference to a multi-loci model. The author found that, if selection and migration are not too strong, or if the immigrants can compensate their initial maladaptation with a large enough genetic variance σ^2_{LE}, the model assuming normality with fixed variance (ignoring linkage disequilibrium) and the infinitesimal model are in good agreement on the predicted mean traits and variance in trait. Relative to a multi-loci model (1, 2 or 5 loci), the numerical recursions under the infinitesimal model show the same pattern of agreement with the multi-loci model, except when the genetic variance is too small to bridge the maladaptation of newcomers, or if selection and migration are both too strong builds linkage disequilibrium in both cases. One can notice that the order of the chosen life cycle (reproduction, migration followed by selection) might exaggerate the effect of strong selection, as newcomers do not have chance to breed with the local population before getting culled.

In [Huisman and Tufto 2012], a different numerical study is performed, to quantify the consistence of the infinitesimal model with multi-loci individual-based models with unequal allelic effects (the effective allele number indicated in the simulations are between 5 and 20) when modelling the effects of *truncation selection* (all individuals with traits above a certain threshold die) and migration from a "donor farm" to a focal wild population under stabilizing

selection. At the beginning of the simulation, the donor farm is created as a copy of the adapted wild population and then subjected to repeated truncation selection until the divergence between the wild and farm populations reach a certain level. Then, 50 generations of the following life cycle: migration (from the donor farm to the wild population) - reproduction/selection (fitness impacts the selection of parents) is repeated for 50 generations. The study shows that the infinitesimal model is in very good agreement with the multi-loci ones on the dynamics of the mean trait of the wild population. However, the variance in trait might be overestimated with the infinitesimal model, the largest difference being when selection is strong and migration is small, as the frequencies of alleles change and therefore the variance at linkage equilibrium. This discrepancy decreases as the number of (effective) alleles increases.

To conclude, it seems like there is great interest on modelling the adaptation of sexual populations characterized by a polygenic trait to a patchy environment. The one-way migration case has produced a lot of studies, which employ formal Gaussian approximations of trait distributions in deterministic settings, while its validity w.r.t. the deterministic infinitesimal model (with constant segregational variance) and multi-loci simulations has been numerically investigated. However, in a two-patch setting with back and forth migration and stabilizing selection, some analytical questions are still to be answered. [Ronce and Kirkpatrick 2001] shows that, in this context, the dynamics of demography coupled with evolution gives way to non-trivial adaptation patterns, that are yet to be analytically derived. The validity of the Gaussian approximation of local trait distributions needs to be clarified in this two-patch setting with back and forth migration, as other numerical multi-loci studies indicate that asymmetry in the trait distributions might be important to estimate (Yeaman and Guillaume 2009), while [Mirrahimi 2017] found that bimodal equilibria exist in asexual populations, which violate this assumption. Moreover, the limits of the infinitesimal model w.r.t. multi-loci models in this heterogeneous environment context should be studied. All these three goals are addressed in the two works presented in Section 1.3.1. Finally, most of the presented multi-loci models (except Huisman and Tufto 2012) assume equal allelic effects. However, it is noted in [Turelli 2017] that incorporating major allele in this polygenic trait, infinitesimal model framework is of great interest, as it is hinted numerically that large effect responses can evolve to promote local adaptation (Yeaman and Whitlock 2011). This motivates the study presented in Section 1.3.2, conducted in collaboration with Sarah Otto and Vincent Calvez.

1.2.3.3 Continuous space

In this section, I will try to illustrate how the study of large sexual populations structured in trait and (continuous) space is not as widely tackled as for asexual populations, while yielding qualitatively and quantitatively different dynamics. It is in part due to the new challenges that arise with a space and trait dependent genuine non-linearity and non-localness of the generic reproduction operator (1.35) (except for the simplest segregation kernels) compared to its asexual diffusion approximations counterparts (linear local (1.8) and non-local (1.8)). In particular, the wide array of tools developed for reaction-diffusion equations (comparison/-monotony principles, linearization, spectral problem, geometric optics approximations, to cite a few) might either not apply or need to be adapted. As for asexual populations, I will distinguish constant space diffusion studies from those focusing on accelerating invasions due to the evolution of dispersal.

Constant diffusion The theoretical study of spatially distributed species' range in a continuous environment has been attracting sustained interest from population genetic models. In 1997, the highly influential article [Kirkpatrick and Barton 1997] focused on populations characterized by a quantitative trait underlying local adaptation to a *spatial environmental gradient* through stabilizing selection around an optimum Bx depending linearly on the space variable (the parameter B represents the slope of the environmental gradient). Without specifying explicitly whether sexual or asexual populations were considered, they derive a system of coupled PDE of the local population size N and the mean trait $\bar{z}$ of the population, assuming that the genetic variance is fixed and that the quantitative trait is normally distributed (which closes the following system)

$$\begin{cases} \partial_t N(t,x) = \Delta_x N(t,x) + N(t,x)(1 - N(t,x)) - \frac{(\bar{z}-Bx)^2}{2} N(t,x), \\ \partial_t \bar{z}(t,x) = \Delta_x \bar{z}(t,x) + 2\partial_x \bar{z}(t,x)\partial_x \log(N(t,x)) + A(Bx - \bar{z}(t,x))\bar{z}(t,x). \end{cases} \tag{1.55}$$

Additionally to the Laplacian operator for the space diffusion, the first equation presents a logistic growth term and a quadratic mortality term from stabilizing selection centered on the optimal trait Bx. The second one presents the classical selection gradient with intensity A and an additional term provoked by the gene flow following the transfer of population from regions from high to low density $2\partial_x \bar{z}(t,x)\partial_x \log(N(t,x))$. The popularity of this article also comes from the qualitative behaviours whose conditions were obtained via numerical simulations (fig. 2). There are three types of evolutionary fates: if the slope of the environment gradient B is small enough, the population invades the whole space, if it increases past a certain threshold depending on A, the population stabilizes at limited range, and if the slope B is too large, it goes extinct. The limited range scenario is somewhat reminiscent of the limited niche width for sexual populations in [Roughgarden 1972], especially with regard to [Alfaro, Coville, and Raoul 2013], which shows that this phenomenon does not appear in their study of asexual populations. Finally, let us mention some extensions to this model in population genetics, like [Polechová, Barton, and Marion 2009] that include a time-dependency in the spatial optimal trait (modelling climate change). More than a decade later, [Mirrahimi and Raoul 2013] aimed at deriving the macroscopic differential system studied in the very renowned paper [Kirkpatrick and Barton 1997], that studies the spatial adaptation of species to an *environmental gradient*, from a mesoscopic integro-differential equation involving a spatial version of the infinitesimal model operator (1.39)

$$\begin{aligned} \partial_t n(t,x,z) = C \left[\iint_{\mathbb{R}\times\mathbb{R}} \frac{\exp\left[\frac{z-\frac{z_1+z_2}{2}}{2\sigma^2}\right]^2}{\sqrt{2\pi}\sigma} \frac{n(t,x,z_1)\, n(t,x,z_2)}{\int_{\mathbb{R}^d} n(t,x,z')dz'} dz_1\, dz_2 - n(t,x,v) \right] \\ + \Delta_x n(t,x,z) + \left[1 + A - (z-Bx)^2 n(t,x,z) - \int_{\mathbb{R}^d} n(t,x,z')dz' \right] n(t,x,z) \end{aligned} \tag{1.56}$$

This model introduces the parameter $C \geq 1$, which is the ratio between reproduction rate and growth rate. A and B share the same meaning as in (1.55). Indeed, [Mirrahimi and Raoul 2013] formally derives (1.55) in an asymptotic regime where the reproduction rate C is large (the segregation dominates the selection), which allows them to close the moment-based system. They also noticed that then, the trait variance is constant and equal to the twice the segregational variance at linkage equilibrium. Furthermore, in an additional weak selection asymptotic (A and B small), they reduce (1.56) to a single PDE on $\bar{z}(t,x)$, which presents singularities at constant trait distance from the local optimum trait. However, they show

by extraction that there exists (non-unique) viscosity solutions to this simplified model, that quantitatively approximates well the limited range and invasion scenario.

Moreover, notice that there is no existence or uniqueness result on solutions of (1.55), mainly due to the gene flow term. This is in contrast with the integro-differential equation (1.56), at least when the trait and spatial domains are compact. Indeed, the first results regarding trait and space structured integro-differential equations modelling the interplay between dispersal by laplacian diffusion, selection/non-local competition and sexual reproduction, where the effect of segregation involves general (smooth) kernels K in (1.35), are derived in [Prevost 2004]. Under compactness and regularity assumptions, well-posedness of strong solutions is shown, where in particular a uniform lower bound on the initial local population is essential for the uniqueness (unlike for asexual populations). A few years later, [Raoul 2017] shows a rigorous asymptotic derivation of the Kirkpatrick-Barton equations (1.55) from (1.56) in the same asymptotic of large reproduction rate as was used formally in [Mirrahimi and Raoul 2013]. The proof involves Wasserstein estimates following the contraction (1.40) and the maximum principle on the macroscopic parabolic system (1.55). Moreover, the author also proves the existence and uniqueness of a solution to a macroscopic differential system which is asymptotically close to (1.55).

I will also mention the work of [Miller and Zeng 2014], which also formally derived the Kirkpatrick-Barton system (1.55), only with diploid asexual populations, with several assumptions: the quantitative trait is sum of l unlinked loci, and at each locus is assumed a continuous distribution of alleles that is symmetrical with constant genetic variance (it extends a little a previous assumption used for the same aim in [Barton 2001] of normal distribution at each locus), which they link to the infinitesimal model for sexual populations. The analysis is also placed in a weak selection, slow environmental change asymptotic (which is close to the large reproduction rate asymptotic of [Mirrahimi and Raoul 2013] and [Raoul 2017]). Moreover, they performed a perturbation analysis around steady states of a simplified model that only involved the local mean trait $\bar{z}(t,x)$, assuming a Gaussian profile for the local distribution (this simplified model was also shown in Kirkpatrick and Barton 1997), and obtained some stability result. Coming back to the validity of the Kirkpatrick-Barton model for asexual populations, it seems that it really comes down to the validity of the assumption on the allelic distribution at each loci. I emphasize also that the limited range equilibrium is not shared by [Alfaro, Coville, and Raoul 2013], which studies asexual populations characterized by a quantitative trait in the same context.

Evolution of dispersal To my knowledge, contrasting with the numerous studies presented in Section 1.2.2.3, the only deterministic study that models the influence of specifically sexual reproduction on the phenomenon of spatial sorting of dispersal trait during invasions is the recent one [Calvez, Crevat, et al. 2020], using the infinitesimal model to model the dispersal trait inheritance process. Formal arguments, backed by numerical simulations, are given that indicate that the large-time acceleration of sexual populations is significantly slower, at a rate of order $t^{\frac{5}{4}}$ whereas I recall that asexual populations accelerate at a rate of order $t^{\frac{3}{2}}$ (see Bouin, Henderson, and Ryzhik 2017a; Calvez, Henderson, et al. 2022). The joint work with Florian Lavigne, presented in Section 1.3.3, aims at giving a solution to the formally derived limit problem that provides an explicit approximation of the spatial density at large times.

1.2.3.4 Conclusion on sexual populations.

The study of the adaptation of large sexually reproducing populations characterized by a quantitative trait and subject to natural selection, population regulation and migration/dispersal is mathematically challenging. This stems from inherent features of the trait inheritance process, which is non-linear, non-local and non-monotone, and therefore less suited to existing analytical tools for integro/partial differential equations.

When considering a well-mixed population in a homogeneous space, several methods have been developed, using almost exclusively the infinitesimal model to describe the process of segregation of parental alleles. One in particular aims at studying concentration phenomena when diversity introduced by the segregation process is low compared to the pressure of natural selection toward the fittest traits, inspired by an analogous method developed for asexual populations. However, it requires here highly technical controls on even finer approximations to account for the influence of natural selection, as the latter is dominated by the mixing segregation process in this asymptotic. This is highlighted by the fact that the within-population variance in large sexual populations, which is the support of the action of selection, is highly strained by the segregation process under the infinitesimal model. One of the aims of my PhD is to diversify the models for sexual population in homogeneous environment beyond the infinitesimal model to account for the influence of other genetic background to quantitative traits.

Moreover, for the study of sexual populations in spatially structured environments, existing quantitative genetic models often rely on ad-hoc reduction to moment-based models using a Gaussian approximation of trait distributions. One of my goals is to clarify the range of validity of such an assumption, in particular in certain asymptotics, and derive robust quantitative insights on the influence of sexual reproduction over the adaptation of spatially distributed sexual populations, in heterogeneous and continuous environments.

1.3 Presentation of PhD results

1.3.1 Adaptation of sexual populations characterized by a quantitative polygenic trait to a patchy environment

1.3.1.1 Main theoretical study

This project, which I published in the Journal of Mathematical Biology as sole author (Dekens 2022), has two aims relating to the adaptation of sexually reproducing populations in a discrete heterogeneous environment. The first is to precise the range of validity of the Gaussian assumption classically made in reference quantitative genetic models. The second is to complete the analysis of the steady states encoding the local adaptation patterns of such populations.

Motivation If heterogeneous environments are ubiquitous, and therefore parts of most ecosystems, the evolutionary patterns of local adaptation and maladaptation are not fully understood yet. Two decades ago, a landmark quantitative genetic study [Ronce and Kirkpatrick 2001] coined the term *migrational meltdown* to describe the surprising dynamics of the checkerspot butterfly, which after a particularly harsh winter, switched their previously main host

plant for a formerly pseudo-sink one, after which the population never recovered completely. [Ronce and Kirkpatrick 2001] aims at describing these dynamics in a symmetrical two-patch model. They specifically make a Gaussian assumption on the local trait distributions with fixed variance to reduce the analysis to the macroscopic moment-based system, a classical assumption in quantitative genetic models (Hendry, Day, and Taylor 2001; Tufto 2001), but whose validity, especially in the context of heterogeneous environments, is not clear. Thanks to this hypothesis, they analytically found a symmetrical equilibrium describing a population that is equally adapted (or maladapted) to both habitats, characterizing a generalist species (a species that occupies the whole available range). Moreover, bistable monomorphic asymmetrical equilibria corresponding to the non-trivial source-sink scenario that contribute to explain the migrational meltdown for a specialist species (a species that occupies only part of the available range) were highlighted by means of numerical simulations, but remained analytically elusive. Later, these asymmetrical equilibria were also found numerically in the two-patch quantitative genetic model for asexual populations [Débarre, Ronce, and Gandon 2013] that uses adaptive dynamics tools in a limit of vanishing mutational variance. The authors formally characterized these monomorphic asymmetrical equilibria as locally stable singular strategies, that co-existed with a symmetrical polymorphic one. Recently, [Mirrahimi 2017] and [Mirrahimi and Gandon 2020] showed rigorously that, in asexual populations and in the limit of vanishing mutational variance, only symmetrical equilibria, either dimorphic or monomorphic, are stable, and do not need to be Gaussian. Note that the variances in trait of the local subpopulations are fixed in [Ronce and Kirkpatrick 2001], but not in [Débarre, Ronce, and Gandon 2013], [Mirrahimi 2017] and [Mirrahimi and Gandon 2020].

The first goal of this project is therefore to clarify the range of validity of the Gaussian approximation used in [Ronce and Kirkpatrick 2001] with a two-patch model for sexually reproducing populations explicitly encoding the effect of the segregation on the inheritance of the quantitative trait. The second goal is to complete the analytical description of the steady states, in the hope that it can explain the discrepancies between the aforementioned studies.

Model We study the adaptation of a sexual population in a symmetrical heterogeneous environment where two patches are connected by back-and-forth migration at rate m, thanks to the following integro-differential system

$$\begin{cases} \varepsilon^2 \frac{\partial n_{\varepsilon,1}}{\partial t}(t,z) = \mathcal{B}_\varepsilon(n_{\varepsilon,1})(t,z) - g(z+1)^2 n_{\varepsilon,1}(t,z) - N_{\varepsilon,1}(t) n_{\varepsilon,1}(t,z) + m\left(n_{\varepsilon,2}(t,z) - n_{\varepsilon_1}(t,z)\right), \\ \varepsilon^2 \frac{\partial n_{\varepsilon,2}}{\partial t}(t,z) = \mathcal{B}_\varepsilon(n_{\varepsilon,2})(t,z) - g(z-1)^2 n_{\varepsilon,2}(t,z) - N_{\varepsilon,2}(t) n_{\varepsilon,2}(t,z) + m\left(n_{\varepsilon,1}(t,z) - n_{\varepsilon,2}(t,z)\right). \end{cases} \tag{1.57}$$

Aligning with [Ronce and Kirkpatrick 2001], the system (1.57) models the action of quadratic stabilizing selection toward local optima 1 and -1, with strength g, and local uniform population regulation by a non-local term of competition proportional to the size of the local subpopulation $N_{\varepsilon,i}$. We furthermore explicit the action of sexual reproduction on the local trait distributions $n_{\varepsilon,1}$ and $n_{\varepsilon,2}$ thanks to the infinitesimal model operator (1.39). The latter is expressed with a small rescaled segregational variance $\varepsilon^2 := \frac{\boldsymbol{\sigma}^2}{\boldsymbol{\theta}^2}$, as we place our analysis in the small segregational variance regime $\boldsymbol{\sigma}^2 \ll \boldsymbol{\theta}^2$ where the segregational variance prior to scaling $\boldsymbol{\sigma}^2$ is small compared to the heterogeneity of the environment (the difference between the local optima) prior to scaling, measured by $\boldsymbol{\theta}^2$. The time variable is rescaled accordingly, as we expect diversity to be slow to be generated by segregation.

Previous works (I recommend the interested reader to refer to Section 1.2.3, Section 1.2.3.1 and Section 1.2.3.2 for further details on this paragraph.) We recall that the infinitesimal model (Fisher 1919; Bulmer 1971; Lange 1978) relies on a *Gaussian assumption of the within-family trait distribution*, which does not automatically imply a Gaussian *within-population* trait distribution. However, in the context of the adaptation of sexual populations to natural selection in homogeneous environment (Turelli and Barton 1990), it is formally accepted that the Gaussian assumption on the trait distribution is valid under *weak quadratic selection regime*. Several studies formally extrapolated this assumption to *one-way migration studies*, where there is no demographic feedback from the sink, that only receives migrants, to the source, that only sends migrants. In one of them, [Tufto 2001] determines that multi-stability can arise between several co-existing equilibria. In another one, after their main stochastic analysis, the authors of [Barton and Etheridge 2018] formally derive deterministic approximations in the limit of large populations and examine the agreement between stochastic models and deterministic models with a Gaussian assumption on the trait distribution under directional and stabilizing selections.

Later studies have rigorously linked the validity of the Gaussian assumption for the within-population trait distribution to another regime than the weak selection one: a *small segregational variance regime* (Calvez, Garnier, and Patout 2019, Patout 2020), using a *perturbative approach close to a main Gaussian profile* to study a limit finite-difference type of equations. Their approach is related to high-frequencies techniques from geometric optics, first adapted for the study of reaction-diffusion equations (Freidlin 1986, Evans and Souganidis 1989), and then to integro-differential models for quantitative genetics, mainly for asexually reproducing populations in a limit of vanishing mutational variance (Diekmann, Jabin, et al. 2005; Perthame and Barles 2008; Barles, Mirrahimi, and Perthame 2009; Lorz, Mirrahimi, and Perthame 2011 for the first studies). The asymptotic limit derived in the analysis for asexual populations in homogeneous space, a constrained Hamilton-Jacobi equation, was also found and analysed in a model for asexual populations in patchy environment in [Mirrahimi 2017], where the author derives (among other results) all the possible steady states of the system.

Structure of the results

1. Quantifying the Gaussian assumption in the regime of small variance. I transposed formally the framework [Calvez, Garnier, and Patout 2019] and [Patout 2020] to the heterogeneous environment model (1.57), introducing the WKB ansatz U_i^ε and its series expansion $U_i^\varepsilon = u_0^i + \varepsilon^2 v_i^\varepsilon$. This constrains the local trait distributions to be Gaussian at the leading order, assuming that the arguments to control the error term v_i^ε of [Calvez, Garnier, and Patout 2019] hold in the present context. This allows me to quantify the approximation made by the Gaussian assumption and close the macroscopic moment-based system on the local population sizes $(N_{\varepsilon,1}, N_{\varepsilon,2})$ and the local mean traits $(\bar{z}_{\varepsilon,1}, \bar{z}_{\varepsilon,2})$. The ODE system obtained is equivalent under a change of variables to the one considered in [Ronce and Kirkpatrick 2001].

2. Separation of ecological and evolutionary time scales This result relates to the convergence, when ε vanishes, of the solutions of the moment-based ODE system

$$(P_\varepsilon) \quad \begin{cases} \varepsilon^2 \frac{d\bar{Y}_\varepsilon}{dt} = G(z_\varepsilon, \bar{Y}_\varepsilon) + \varepsilon^2 \nu_{N,\varepsilon}(t), \\ \frac{dz_\varepsilon}{dt} = -2g z_\varepsilon + F(\bar{Y}_\varepsilon) + \varepsilon^2 \nu_{z,\varepsilon}(t). \end{cases} \tag{1.58}$$

In the latter, I denote $\Omega = (\mathbb{R}_+^*)^2 \times \mathbb{R}$ and the functions $F : \Omega \to \mathbb{R}$ and $G : \mathbb{R} \times \Omega \to \mathbb{R}^3$. Moreover, $\bar{Y}_\varepsilon = \left(N_{1,\varepsilon}, N_{2,\varepsilon}, \frac{\bar{z}_{2,\varepsilon} - \bar{z}_{1,\varepsilon}}{2\varepsilon^2}\right)$ is the slow variable in Ω and $z_\varepsilon = \frac{\bar{z}_{2,\varepsilon} + \bar{z}_{1,\varepsilon}}{2}$. I prove the

following slow-fast theorem.

Theorem. *Consider the limit system*

$$(P_0) \quad \begin{cases} G(z(t), \bar{Y}(t)) = 0, \\ \frac{dz}{dt} = -2gz + F(\bar{Y}). \end{cases} \tag{1.59}$$

Then, for ε small enough, and for close enough initial conditions, the solutions of the perturbed system (1.58) $(\bar{Y}_\varepsilon, z_\varepsilon)$ converge locally in time toward the solutions $(\bar{Y}, z)$ of the limit system (1.3.1.1).

3. Complete analysis of the steady states of (1.59) in the regime of small variance. Additionally to the symmetrical equilibrium $(N_1, N_2, z^*) = (1-g, 1-g, 0)$ found in [Ronce and Kirkpatrick 2001] when selection pressure g is below the threshold 1, I show the following result

Proposition. *Under an explicit condition on the migration rate m and the selection strength g, there exists two mirrored asymmetrical equilibria (z^*, N_1^*, N_2^*) and $(-z^*, N_2^*, N_1^*)$ with $0 < N_1^* < N_2^*$, given by:*

$$\begin{cases} N_1^* = (1-m) + m\rho - 4g\frac{\rho^{*4}}{(\rho^{*2}+1)^2}, \\ N_2^* = (1-m) + \frac{m}{\rho^*} - 4g\frac{1}{(\rho^{*2}+1)^2}, \\ z^* = \frac{\rho^{*2}-1}{\rho^{*2}+1} \neq 0, \end{cases} \tag{1.60}$$

where $\rho^* = \frac{y^* + \sqrt{y^{*2}-4}}{2}$ and $y^* \left(= \rho^* + \frac{1}{\rho^*}\right)$ is the only root greater than 2 of the polynomial:

$$S(Y) = Y^3 + \frac{(1-4g)}{m}Y^2 - \frac{4g}{m}Y + \frac{4g}{m}.$$

Conversely, if the condition is not verified, there can be no asymmetrical equilibria.

Moreover, I show that such mirrored asymmetrical equilibria are always bistable upon existence, resulting in the loss of stability of the symmetrical equilibrium that separates them when the latter occurs.

Comments on the results and the framework

1. Heuristics behind the quantification of the Gaussian assumption In each equation of (1.57), the small variance regime $\varepsilon^2 \ll 1$ isolates the effect of the reproduction term, which should remain well-balanced with the others quantities involved. This constrains heavily the local trait distributions, an effect that can be better assessed when considering the WKB ansatz $U_i^\varepsilon = -\varepsilon^2 \log(\varepsilon n_{\varepsilon,i})$ (notice the different scaling with asexual studies) and its series expansion $U_i^\varepsilon = u_0^i + \varepsilon^2 v_i^\varepsilon$ (u_0^i is a non-negative function that cancels somewhere for the population size to remain bounded, see the third paragraph of Box 1.2.2.1. Assuming that the framework of [Calvez, Garnier, and Patout 2019] and [Patout 2020] which controls the error terms v_i^ε can be transposed here, the reproduction terms read

$$\frac{\mathcal{B}_\varepsilon(n_{\varepsilon,i})}{n_\varepsilon}(z) = \frac{1}{\sqrt{\pi}\varepsilon} \iint_{\mathbb{R}^2} \exp\left[\frac{1}{\varepsilon^2}\left[-\left[z - \frac{z_1+z_2}{2}\right]^2 + u_i^0(z) - u_i^0(z_1) - u_i^0(z_2)\right] + \mathcal{O}(1)\right] dz_1\, dz_2.$$

As ε vanishes, the last double integral term diverges or vanishes unless the following constraint is satisfied

$$\forall z \in \mathbb{R}, \max_{(z_1,z_2)} \left[-\left(z - \frac{z_1+z_2}{2} \right)^2 + u_i^0(z) - u_i^0(z_1) - u_i^0(z_2) \right] = 0. \tag{1.61}$$

The latter has been shown in [Garnier et al. 2022] to determine u_i^0 as a quadratic function $\frac{(z-z_i^*)^2}{2}$, which determines $n_{\varepsilon,i}$ to be Gaussian of predetermined variance at the leading order, but of undetermined mean z_i^*, which is the asymptotic dominant trait in the subpopulation i. The latter shifts due to selection, which occurs on a slower time scale, which is why it remains unknown at this stage where only the reproduction term is involved in the computation.

2. Behind the slow-fast analysis The slow-fast theorem relies mainly on the local stability of the slow manifold, defined by the first line of (1.59): $G(\bar{Y}, Z) = 0$, w.r.t. the fast variable $\bar{Y}$. The slow manifold can also be interpreted as the instantaneous ecological equilibria on the population sizes, due to the effects of migration, mortality and growth. Its linear stability analysis only involves the population size variables N_1 and N_2 and the migration rate m, whose action on demography explicitly ensures the local stability. However, the description of the slow manifold (solving a tangled system of two algebraic equations) is much more involved, with potential multi-branches (although we show that such multi-branches are not viable). I would also like to mention that this property of separation of time scales is robust with regard to its application in non-symmetrical environments with more habitats and more general selection functions.

3. Migration strains to monomorphism in the limit of small variance The symbolic representation of the perturbed system (1.58) and the limit one (1.59) hides the crucial reduction of complexity due to the separation of time scales. Indeed, if the former has four differential equations, the latter only has two algebraic ones (the slow manifold of the instantaneous ecological equilibria, on the limit population sizes) and the differential equation of the evolutionary dynamics of the dominant trait z^*, driven by the balance between the slow shift by selection and the fast demographic (ecological) equilibrium at the level z^*. The reason why only one dominant trait z^* appears in the limit system is because of the rapid blending effect of the migration between patches, which can be seen by the following ODE on the difference between the local mean traits that can be obtained from the perturbed system, before the reduction to (1.58) and the convergence to (1.59)

$$\varepsilon^2 \frac{d\left[\frac{\bar{z}_2^\varepsilon - \bar{z}_1^\varepsilon}{2}\right]}{dt} = -m \left[\frac{N_1^\varepsilon}{N_2^\varepsilon} + \frac{N_2^\varepsilon}{N_1^\varepsilon} \right] (\bar{z}_2^\varepsilon - \bar{z}_1^\varepsilon) + \mathcal{O}(\varepsilon^2).$$

Consequently, the two local mean traits relax rapidly toward the single asymptotic dominant trait z^* of the monomorphic population, as the demographic blending effect of the migration is bounded by below away from 0: $2m \leq m \left[\frac{N_1^\varepsilon}{N_2^\varepsilon} + \frac{N_2^\varepsilon}{N_1^\varepsilon} \right]$ (and minimal when the local subpopulations sizes coincide).

4. The symmetrical algebraic property of the steady states of the limit system To obtain the steady states of the limit system, one has to solve a *sixth order polynomial* $Q \in \mathbb{R}_6[X]$ closed on the variable $\frac{N_2^*}{N_1^*}$. However, the limit system (1.59) is symmetrical, which reflects the symmetry of the environments (not to be confused with the symmetry of equilibria:

asymmetrical equilibria can arise in symmetrical environments): it remains invariant under the transformation $(N_1^*, N_2^*, z^*) \mapsto (N_2^*, N_1^*, -z^*)$:

$$\begin{cases} \left[1 - N_1^* - g(z^*+1)^2 - m\right] N_1^* + mN_2^* = 0, \\ \left[1 - N_2^* - g(z^*-1)^2 - m\right] N_2^* + mN_1^* = 0, \\ \frac{dz^*}{dt} = 2g \left(\frac{\frac{N_2^*}{N_1^*} - \frac{N_1^*}{N_2^*}}{\frac{N_2^*}{N_1^*} + \frac{N_1^*}{N_2^*}} - z^* \right). \end{cases}$$

This is crucial, because it allows to define the *third-order polynomial* $S \in \mathbb{R}_3[X]$ defined in the proposition above such that

$$S\left(\frac{N_2^*}{N_1^*} + \frac{N_1^*}{N_2^*}\right) = Q\left(\frac{N_2^*}{N_1^*}\right).$$

The study of the positive roots of S that are larger than 2 is still quite involved, but is handled thanks to a *monotony property*.

5. Comparison with the asexual study [Mirrahimi 2017] The forced monomorphism in this study on sexual populations is a striking structural difference with the possibility of dimorphism shown in [Mirrahimi 2017], established in a similar small variance approach. It can be understood at several layers:

1. The more general one is that mutations have a spreading effect on distributions (see the operators (1.7) and (1.8)) whereas segregation described by the infinitesimal model is concentrating (see Section 1.2.3), adding a within-patch blending effect to the between-patch blending effect of migration.

2. This underlies most of the results of limited range of sexual populations with the infinitesimal model compared to asexual ones, from the limited niche width in [Roughgarden 1972], to the limited range equilibrium in the adaptation of sexual populations to changing continuous environment in [Kirkpatrick and Barton 1997], [Mirrahimi and Raoul 2013] and [Raoul 2017], which does not occur in asexual one (Alfaro, Coville, and Raoul 2013). In the present case, the analysis shows that specialist species (which only occupies a part of the total range accessible in the environment, corresponding to the asymmetrical equilibria) evolve in sexual populations under the approximate same conditions that would lead to generalist species by local adaptation (dimorphism) in asexual populations (see Fig. 1.2).

3. The last layer of comparison is more technical, and relates to the relationship between the support of trait distributions and the zeros of the WKB ansatz in the methodology of small variance. If we assume that we do not know yet that the sexual population is monomorphic in the limit of small variance, but that each local population is Gaussian at the leading order, centered in z_i^*, the steady states of (1.57) can be written under matrix form considering the series expansions of the WKB ansatz $U_i^\varepsilon = \frac{(z-z_i^*)^2}{2} + \varepsilon^2 v_\varepsilon^i$

$$\begin{aligned} \mathcal{A}(z, N_1^\varepsilon, N_2^\varepsilon) \begin{pmatrix} 1 \\ e^{\frac{(z-z_1^*)^2-(z-z_2^*)^2}{2\varepsilon^2}} \end{pmatrix} &= \begin{pmatrix} 1 \\ e^{\frac{(z-z_1^*)^2-(z-z_2^*)^2}{2\varepsilon^2}} \end{pmatrix} \cdot \begin{pmatrix} 1 - \frac{\mathcal{B}_\varepsilon(n_{\varepsilon,1})}{n_{\varepsilon,1}}(z) \\ 1 - \frac{\mathcal{B}_\varepsilon(n_{\varepsilon,2})}{n_{\varepsilon,2}}(z) \end{pmatrix} \\ &\underset{\varepsilon\to 0}{\approx} \begin{pmatrix} 1 \\ e^{\frac{(z-z_1^*)^2-(z-z_2^*)^2}{2\varepsilon^2}} \end{pmatrix} \cdot \begin{pmatrix} 1 - \exp\left[v_1^\varepsilon(z) + v_1^\varepsilon(z_1^*) - 2v_1^\varepsilon\left(\frac{z+z_1^*}{2}\right)\right] \\ 1 - \exp\left[v_2^\varepsilon(z) + v_2^\varepsilon(z_2^*) - 2v_2^\varepsilon\left(\frac{z+z_2^*}{2}\right)\right], \end{pmatrix} \end{aligned} \tag{1.62}$$

where $\mathcal{A}(z, N_1^\varepsilon, N_2^\varepsilon)$ is defined similarly as in (1.17) in [Mirrahimi 2017]. Notice the similar structure of (1.62) before the approximation, with (1.17) in [Mirrahimi 2017]. The mixed term $e^{\frac{(z-z_1^*)^2-(z-z_2^*)^2}{2\varepsilon^2}}$ on the leading terms in the expansion is analogous to the term $e^{\frac{u_1^\varepsilon(z)-u_2^\varepsilon(z)}{\varepsilon}}$ in (1.17). Both yield asymptotically that the leading terms are the same ($z_1^* = z_2^*$ and $u_1(z) = u_2(z)$), which implies that that the local trait distributions are asymptotically supported at the same points. In the sexual case, they can only be each supported at one point (because of the mixing effect of segregation by the infinitesimal model), which must be the same, hence the monomorphism, whereas in the asexual case, the limit object $u_1 = u_2 = u$ is not constrained to cancel only once, and can actually cancel twice under some conditions, hence the possibility of dimorphism. The fact that it cancels once or twice is not fixed a priori, for the analogous object in [Mirrahimi 2017] to the finite difference terms (1.62) is at the limit the Hamiltonian term $\begin{pmatrix} -|u_1(z)'|^2 \\ -|u_2(z)'|^2 \end{pmatrix} = \begin{pmatrix} -|u(z)'|^2 \\ -|u(z)'|^2 \end{pmatrix}$ in [Mirrahimi 2017] (see (1.17)). Therefore, it is determined by solving the constrained Hamilton-Jacobi equation on the limit u of the main terms u_1^ε and u_2^ε, on which the selection acts. This is very different than in (1.62), where the limit problem, on which the selection acts, does not see the leading terms (except for the unknown dominant trait z^*) and rather focuses on the next order terms, the correctors v_1^ε and v_2^ε, involved in the finite difference terms, as in [Calvez, Garnier, and Patout 2019]. As the correctors have no reason to be equal here, the asymptotic characterization of the Hamiltonian as the principal eigenvalue of $\mathcal{A}(z, N_1, N_2)$ in [Mirrahimi 2017] is lost here. This structural discrepancy between possible dimorphic equilibria in asexual populations and forced monomorphism can thus be read at the light of the respective influence of the asexual reproduction operators and the infinitesimal model one on the different orders of the series expansion of the WKB ansatz.

4. Note finally that monomorphism is only shown to be forced in the regime of small variance (for example, the relaxation of the local mean traits to the same value shown above is really due to ε being much smaller than the migration rate m). Actually, numerical simulations indicate that for small migration rates, dimorphism arise in sexual populations too, as this violates the small variance regime.

6. Link with the results of [Débarre, Ronce, and Gandon 2013]. I recall that in [Débarre, Ronce, and Gandon 2013], the authors study the steady states of a system similar to (1.57), only for asexual populations with the diffusion operator (1.8) for modelling mutations. They distinguish the study of monomorphic equilibria and dimorphic equilibria. The singular monomorphic strategies z_M are identified as the *singular points of the selection gradient* when the mutational variance vanishes, which is thus the leading eigenvalue $z \mapsto W(z, N_1, N_2)$ of the same matrix $\mathcal{A}(z, N_1, N_2)$ involved in (1.17) and (1.62). This means that they search for z_M which satisfies $W(z_M, N_1, N_2) = \partial_z W(z_M, N_1, N_2) = 0$. The interesting link with my model, is that the dominant trait z^* is also a singular point of the finite difference terms $1 - \exp\left[v_i^\varepsilon(z) + v_i^\varepsilon(z_2^*) - 2v_i^\varepsilon\left(\frac{z+z_2^*}{2}\right)\right]$ involved in (1.62) (it relates to the kernel of the finite difference operator, that is generated by δ_{z^*} and δ'_{z^*}, as explained in [Patout 2020], see in Section 1.2.3.1). The latter is the analogous to the selection gradient (but not an eigenvalue, see the previous comment on the link with Mirrahimi 2017). Therefore, the asymmetrical singular strategy whose existence is hinted mostly numerically in [Débarre, Ronce, and Gandon 2013] (they obtain an approximation for small migrations) is the asymmetrical equilibria identified

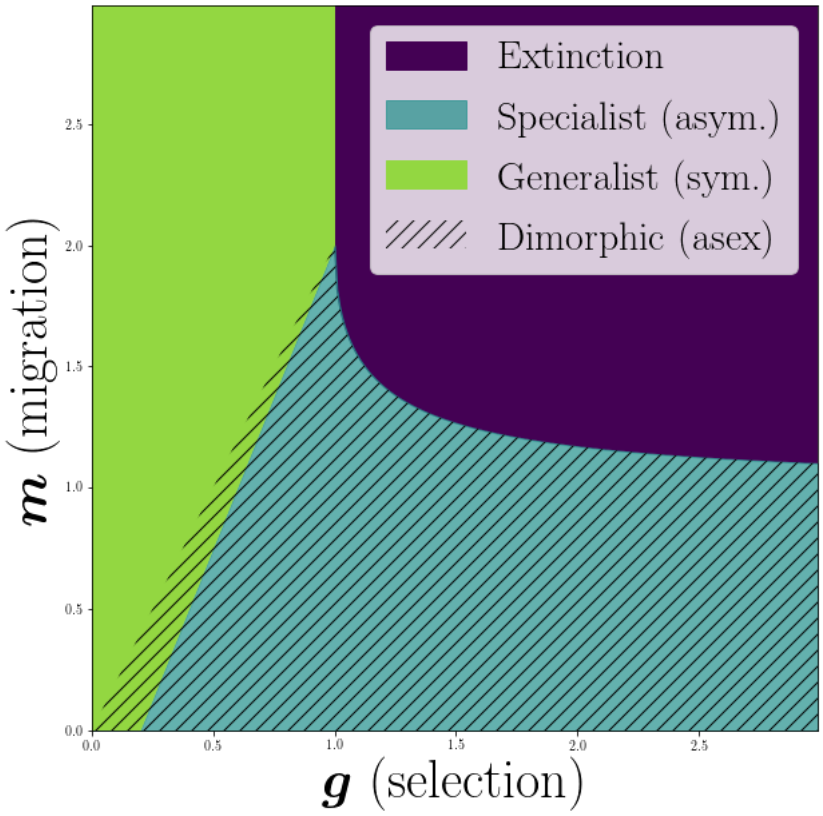

Figure 1.2: **Comparison between the monomorphic outcomes of sexual populations (Dekens 2022, blue and green) and the dimorphic ones in asexual populations (Mirrahimi 2017) in the limit of small variance.** Notice that the blue region at the bottom left, corresponding to the monomorphic asymmetrical equilibria (specialist species outcomes) in the present work, almost overlaps with the parameter region where dimorphism is the globally stable equilibrium for asexually reproducing populations (Mirrahimi 2017).

in my work (this is made obvious from the similarities between Fig. 1.2 and the figure 4 of Débarre, Ronce, and Gandon 2013). However, it is a priori different from the global ESS, which we recall are defined in [Mirrahimi 2017] as a specific type of singular strategy: a global maximum of $z \mapsto W(z, N_1, N_2)$. In particular, the analysis in [Mirrahimi 2017] shows that this asymmetrical equilibrium is not a global ESS, and is therefore not obtainable. Nevertheless, it is shown in the figure 2 of [Débarre, Ronce, and Gandon 2013]. This is because this figure was computed numerically with a cut-off for small densities, and therefore does not correspond to the asymptotic large population size. I must admit that in my explanation of this link in the discussion section of the published paper [Dekens 2022], I misunderstood [Débarre, Ronce, and Gandon 2013] by misreading the fact that they do not use a Gaussian assumption and I claimed the contrary. The link with their analysis is actually more profound than that, as shown in this comment.

7. Links with the analysis of [Calvez, Garnier, and Patout 2019], [Patout 2020]. The aforementioned studies are very technical, even though limit objects are easily determined (see Section 1.2.3.1). Actually controlling the error terms in the present work and thus justifying rigorously the heuristics presented in the first comment is likely to get even more technical, because of the additional coupling of the local demographic dynamics, which results in quite non-trivial steady states, but could probably be adapted. Instead, I rely on the formal assumption that suitable estimates can be performed, and this allows a more tractable framework to emerge on which to base the slow-fast analysis, which is reminiscent of the different time scales involved in the analysis in [Patout 2020].

8. Link between the small segregational variance and the weak selection regime. As Gaussian profiles arise at the leading order both in the small segregational variance regime used here ($\boldsymbol{\sigma}^2 \ll \boldsymbol{\theta}^2$), and in homogeneous environment in the weak quadratic selection regime (see Turelli and Barton 1990), it is natural to question whether this two regimes intersect or are the same. I address this question in the published paper [Dekens 2022], and find that it is different. I bring here new elements, that comfort this conclusion. The definition of weak selection in [Turelli and Barton 1990] found in formula 3.26, page 17, translates in our parameters as $\boldsymbol{g\sigma}^2 \ll 1$ and $\frac{\bar{z}-\boldsymbol{\theta}}{\boldsymbol{\sigma}} \approx \frac{\boldsymbol{\theta}}{\boldsymbol{\sigma}}$ of order 1. However, the last condition is precisely in contradiction with our small segregational variance regime $\boldsymbol{\sigma}^2 \ll \boldsymbol{\theta}^2$.

1.3.1.2 Supplementary numerical comparison with individual-based simulations

Motivation This short numerical project was conducted using multi-loci individual-based simulations (IBS) in order to assess to what extent the hypotheses underlying the classical version of the infinitesimal model, i.e. a constant segregational variance across time, space and families, are reasonably valid in a two-patch environment for large sexual populations, with respect to the number of loci involved and the ancestral variance at linkage equilibrium. A particular focus is put on the case where the latter is small, as this corresponds to the asymptotic regime according to which the analysis in [Dekens 2022] was conducted.

Model This study compares simulations from two models: a discrete-time deterministic model and a discrete-time multi-loci individual-based model.

The discrete-time deterministic model is described by the following equations (where $\Delta t = t_{l+1} - t_l = 0.1$ is small)

$$\begin{cases} n_1(t_{l+1},z) &= (1-m\Delta t)\ \exp\left[-\Delta t\left(q_1(z)+(1+r\Delta t)N_1(t_l)\right)\right]\ \left(n_1(t_l,z)+r\Delta t\mathcal{B}_\sigma[n_1(t_l,\cdot)](z)\right) \\ &\quad +m\Delta t\ \exp\left[-\Delta t\left(q_2(z)+(1+r\Delta t)N_2(t_l)\right)\right]\ \left(n_2(t_l,z)+r\Delta t\mathcal{B}_\sigma[n_2(t_l,\cdot)](z)\right), \\ n_2(t_{l+1},z) &= (1-m\Delta t)\ \exp\left[-\Delta t\left(q_2(z)+(1+r\Delta t)N_2(t_l)\right)\right]\ \left(n_2(t_l,z)+r\Delta t\mathcal{B}_\sigma[n_2(t_l,\cdot)](z)\right) \\ &\quad +m\Delta t\ \exp\left[-\Delta t\left(q_1(z)+(1+r\Delta t)N_1(t_l)\right)\right]\ \left(n_1(t_l,z)+r\Delta t\mathcal{B}_\sigma[n_1(t_l,\cdot)](z)\right). \end{cases} \tag{1.63}$$

It corresponds to the following life cycle , implemented via a *splitting scheme*: *reproduction* involving the infinitesimal model operator (1.39) at a rate r, followed by *selection/competition* ($q_i(z) = g(z-\theta_i)^2$ denotes the quadratic selection in habitat i with pressure g, and where the population size in the competition term is obtained after reproduction), and finally *migration* at a rate m. The segregational variance σ^2 is estimated thanks to the initial segregational variance in the IBS.

The IBS consider two local subpopulations of sexual diploid individuals characterized by a quantitative trait with an explicit multi-loci genetic architecture. It is obtained by adding di-allelic effects $\pm\frac{\sigma_{LE}}{2\sqrt{L}}$ from $L \in \{10, 100, 500\}$ unlinked loci (recall that the individuals are diploid), with the standard deviation at linkage equilibrium σ_{LE} either small ($\sigma_{LE} = 0.1$) or large ($\sigma_{LE} = 1$). The IBS follow the same life cycle as the deterministic model for 10^3 generations (of effective length Δt). They start with two locally adapted sexual diploid populations, one of which has a reduced initial populations size modelling a catastrophic event and resulting in an *asymmetrical initial state*. At the reproduction stage, all individuals find randomly a mate in their habitat and their union produce a viable offspring with probability $r\Delta t$. The *segregational variance* of each of these pairs is estimated at this stage. At the selection/competition stage, all individuals survive with a *probability dependent on their trait and the local population size* $\exp\left(-\Delta t q_i(z)\right)\ \exp\left(-\Delta t\frac{N_i}{K}\right)$, where K is the carrying capacity of each patch ($K = 10^4$ is large). At the migration stage, a number of migrants is drawn in each patch according to a *Poisson law of parameter* $m\Delta t$. For each of parameters, 20 replicates simulations are run.

Previous works (I recommend the interested reader to refer to Section 1.2.3.2 for further details on the content of this paragraph.)

The relationship between multi-loci IBS and discrete-time deterministic models has been studied in a context of *one-way migration*, where a source population sends migrants in a sink population under stabilizing selection around an optimum that differs from the source' mean trait, without migration in the other direction (Tufto 2000; Huisman and Tufto 2012).

In [Tufto 2000], the author compares (among others) a discrete-time deterministic model where the reproduction stage involves the infinitesimal model, with multi-loci models, with relatively few loci (1, 2 or 5). He found that the two are in good agreement when selection and migration are not too strong, or if the immigrants can compensate their initial maladaptation with a large enough variance at linkage equilibrium σ^2_{LE}. He also performed numerical simulations comparing the infinitesimal model based recursions with a model assuming normality of the population trait distribution with fixed variance, and drew similar conclusions. Moreover, he considered, among other values, a small variance at linkage equilibrium $\sigma^2_{LE} = 0.01$, and showed (fig. 2 of the article) that the trait variance in the population at equilibrium with the infinitesimal model can be very different for σ^2_{LE}, when migration is small, and selection very

strong ($g \in \{4, 20, 100\}$. Finally, one notable difference between our studies is the life cycle order (migration followed by selection in his case) and the generations' time length Δt (1 in his case).

In [Huisman and Tufto 2012], the IBS also include unequal effects between loci (5 or 20). Their results highlight that the dynamics of the mean traits are well approximated between the IBS and the deterministic model where segregation is modelled with the infinitesimal model. However, they indicate that the variance in trait might be overestimated, but less so as the number of loci increases (with fixed σ^2_{LE}).

Results Our study focuses on three types of outcomes

1. *small segregational variance*, computed from the IBS
2. *transient dynamics*, compared between the IBS and the deterministic model (1.63).
3. *qualitative final states*, compared between the IBS and the deterministic model (1.63).

   The study reveals that the trait range in the IBS, defined as $[-\sigma_{LE}\sqrt{L}, \sigma_{LE}\sqrt{L}]$, and thus depending on the number of loci $L \in \{10, 100, 500\}$ and standard deviations at linkage equilibrium $\sigma_{LE} \in \{0.1, 1\}$, is a crucial determinant. If the trait range extends beyond the local optima, the IBS indicate that the mean segregational variance is approximately constant across time, space and families, and remains small over the course of the simulations. These properties do not need to hold true if, conversely, the local optima are beyond the trait range. Moreover, if the trait range extends beyond the local optima, the comparison of both transient dynamics and qualitative outcomes between the IBS and the deterministic model are in excellent agreement, and deteriorates when it is not the case. When the local optima are just at the edge of the trait range, the transient dynamics produced by the IBS and the deterministic model are not always in agreement, but sufficiently so for the qualitative outcomes to be similar. When the local optima are well beyond the trait range and particularly when selection is strong, the IBS might lead to extinction whereas the deterministic model does not.

Comments

1. Link between the discrete-time deterministic model (1.63) and the continuous-time model in [Dekens 2022] The discrete-time deterministic model (1.63) is a discretization of the continuous-time model used in [Dekens 2022] (of which a rescaled version is (1.57)); Precisely, it uses a *splitting* scheme to handle the migration events, and a *Duhamel's integral formula* for the local events on small time intervals of length Δt. The two commute when Δt is small.

2. Proximity of transient dynamics : the comparison between the transient dynamics of the deterministic model and the IBS is quantified thanks to the *first Wasserstein distance*. For μ, ν two probability measures with finite means, the first Wasserstein distance between them is defined as $W_1(\mu, \nu) = \|F_\mu - F_\nu\|_{L_1}$, where F_μ and F_ν are the respective cumulative distribution functions. This distance is preferred to the L^1 norm, because it handles better distances between measures with disjoint support (which can occur due to concentrations around slightly different means) than the L^1 norm (the distance would always be equal to 2 with disjoint support).

3. The time length of the IBS as compared to [Barton, Etheridge, and Véber 2017] The IBS run for 10^3 generations of time length $\Delta t = 0.1$, so for 100 time units. In [Barton, Etheridge, and Véber 2017], the indicated typical time below which the approximation underlying the infinitesimal model is shown to hold is of order $\sqrt{L}$. Here, the 100 time units of the IBS are well beyond this typical time for $L = 10$ or $L = 100$, in which cases significant variations in the segregational variance across time are indeed observed in the simulations. However, I think that here, there might be an added effect of creation of Linkage Disequilibrium because the selection is directional in both cases, and the higher variations across time are for high selection levels.

4. The role of stabilizing selection This criterion on the relationship between the trait range and the local optima can be translated as the difference between directional (the local optima are beyond the trait range) and stabilizing selection (the trait range extends beyond the local optima). The reason for the failure of the infinitesimal model's hypotheses of constant segregational variance across time, space and families in large populations under directional selection comes from the building of *Linkage Disequilibrium*, as individual in each habitat have to accumulate the same alleles (either all +, or all -) to be adapted. On the contrary, under stabilizing selection, many allelic combinations can lead to adapted individuals in each habitat, which translates formally a state of *Quasi Linkage Equilibrium*.

5. Link with the approximation computed in [Sachdeva and Barton 2017] under the hypergeometric model. In [Sachdeva and Barton 2017], the authors study the eco-evolutionary dynamics of a haploid sexual population in a two-patch model, where the polygenic trait which determines the degree of local adaptation also quantifies mates' assortment. This polygenic trait results from the combined additive small diallelic effects $\pm\gamma$ at L loci. Even though the added assortative mating effect differs from the framework of this present work, one of the results presented in the equation (6) of the Appendix S1 of [Sachdeva and Barton 2017] connects to the result presented above. Indeed, under the hypergeometric model assumption that all allelic combinations with a given number of + alleles are equally represented in the population and when L is assumed large, they derive an approximation of the segregational variance $V(Y, Z)$ between two parents with traits Y and Z:

$$V(Y, Z) \approx \frac{\gamma^2 L}{2} - \frac{YZ}{2L}.$$

Therefore, the segregational variance can be considered as independent of the family if $\theta^2 \ll \gamma^2 L^2$, where $\pm\theta$ are the local trait optima. This exactly means that the phenotypic range $[-\gamma L, \gamma L]$ extends well beyond the local optima. In [Sachdeva and Barton 2017], the allelic effect γ is set at $\sqrt{\frac{2}{L}}$, but I checked that this approximation holds under a more general form for the allelic effect $\gamma = \sqrt{\frac{\sigma_{LE}}{L}}$.

5. Link with previous one-way migration works. Despite the framework presented here being different from the ones in [Tufto 2000] and [Huisman and Tufto 2012], for it allows migration to go back and forth, the fact that the initial populations is asymmetrical and thus the metapopulation displays pseudo source-sink dynamics under strong selection (asymmetrical equilibria of [Ronce and Kirkpatrick 2001] and [Dekens 2022]) makes the comparison relevant. The results are overall relatively consistent with these studies, conditioned on the differences in terms of number of loci (here a lot higher) and the commutativity of the different stages as a consequence of small generation length $\Delta t = 0.1$.

In [Tufto 2000], the latter has a significant importance, because of the succession of the migration and selection stages, which at high selection culls automatically all the migrants before allowing them to mate with the local population. However, the conclusion that the infinitesimal model and the Gaussian approximation are consistent with multi-loci IBS when the immigrants can compensate their initial maladaptation with a large enough σ^2_{LE} (at fixed distance between the sink's optimum and the source' mean trait) goes in the same direction as my conclusion on the trait range $[-\sigma_{LE}\sqrt{L}, \sigma_{LE}\sqrt{L}]$ extending beyond the local optima. Besides, I would also like to address the findings of [Tufto 2000] that the variance in trait at equilibrium is largely over σ^2_{LE} when the latter is small (0.01), as it is not observed here. My explanation for the discrepancy is the very strong selection levels considered (4, 20, and 100) and the life cycle order, as described above.

As for the observation that the recursions with the infinitesimal model in [Huisman and Tufto 2012] might overestimate the variance in trait when the difference between the subpopulations increases (fig. 5 of their article, with 5 loci), with this discrepancy in variance decreasing when the number of loci passes from 5 to 20 (fig. 6 of their article) aligns with our findings. Indeed, the first effect relates directly with the trait range including or not the local optima and the second relates to the fact that the trait range increases with the number of loci (at fixed σ_{LE}).

1.3.2 Combining population and quantitative genetic models: modelling the evolution of a hybrid genetic architecture in heterogeneous environments

This joint project with Sally Otto and Vincent Calvez, currently under peer-review (Dekens, Otto, and Calvez 2021), introduces a new mathematical framework that bridges population genetic and quantitative genetic models to study the influence of a polygenic quantitative background on a major effect polymorphism that underlies local adaptation of sexual populations to a heterogeneous environment.

Motivation The debate on the genetic architecture of adaptation has been animating most of the development of evolutionary biology. Since half a century ago, rapid progress and popularization of genetic sequencing have been alimenting it, through for instance Genome Wide Association Studies (GWAS), without clear-cut conclusions in whether most adaptive responses are due to major effect genes or arise from a polygenic background, especially when considering spatial structure (Orr 2001; Slate 2005). For example, the evolution of resistance to pesticide BT toxin have reached different conclusions between field (major genes) and lab experiment (polygenic, see McKenzie and Batterham 1994 and Groeters and Tabashnik 2000). In long-term experiments, polygenic responses have been shown to evolved under directional opposing selection (Laurie et al. 2004; Dudley et al. 2007), which conditions could arise in patchy environments. From a theoretical viewpoint, this is reflected by the dichotomy between population genetics and quantitative genetics. On the one hand, the adaptation of populations to local conditions under migration due to major effect polymorphism has been investigated in one-locus multi-allelic models (Nagylaki and Lou 2001, Nagylaki and Lou 2007) or two-locus models (Bürger and Akerman 2011, Akerman and Bürger 2014, Geroldinger and Bürger 2014). As increasing the number of loci yields rapidly a high cost in analytical complexity,

multi-locus models are usually restricted to consider either equal allelic effects (Lythgoe 1997, Szép, Sachdeva, and Barton 2021) or to asymptotic regimes of migration and selection (Bürger 2009a). On the other end of the spectrum, migration-selection quantitative genetic models do not include additional major effect locus to the focal quantitative trait (Ronce and Kirkpatrick 2001, Hendry, Day, and Taylor 2001, Débarre, Ronce, and Gandon 2013, Débarre and Otto 2016, Dekens 2022). However, a multi-loci simulation study by [Yeaman and Whitlock 2011] has shown that local adaptation could be underlined by tightly linked clusters of major loci at intermediate migration rates, a genetic pattern that arises from an ancestral architecture with only small effects thanks to mutations. Moreover, in [Débarre, Yeaman, and Guillaume 2015], the authors indicate that the presence of a major effect locus alongside 19 other smaller effect loci can skew the local trait distributions away from Gaussian profiles, and increase differentiation between subpopulations.

Model We consider that the focal trait $\boldsymbol{\zeta} \in \mathbb{R}$, which determines the adaptation of a sexually reproducing haploid population, is sum of two contributions $\boldsymbol{z} \in \mathbb{R}$ and $\pm\boldsymbol{\eta}$. The variable $\boldsymbol{z}$ represents the quantitative polygenic contribution resulting from the combined additive small allelic effects of a large number of loci, which is inherited according to the classical version of the infinitesimal model (with constant segregational variance $\boldsymbol{\sigma}^2$). The diallelic effects $\pm\boldsymbol{\eta}$ represents the contribution of two alleles A/a which segregate at a focal major effect locus, which is inherited according to Mendelian laws. Given a population with trait density $\boldsymbol{n}$ of total population size $\boldsymbol{N}$, we denote by $\boldsymbol{n}^A$ and $\boldsymbol{n}^a$ the trait distributions of the subpoplations carrying respectively A and a at the major effect locus. The combined inheritance process for offsprings born in this population with the major allele A and the quantitative trait $\boldsymbol{z}$ is described by the following reproduction operator extending the infinitesimal model one (1.39) (see Fig. 1.3 for an illustration)

$$\begin{aligned}\boldsymbol{\mathcal{B}}^{\boldsymbol{A}}_{\boldsymbol{\sigma}}[\boldsymbol{n}^{\boldsymbol{A}}_i, \boldsymbol{n}^{\boldsymbol{a}}_i](\boldsymbol{z}) &= \int_{\mathbb{R}^2} \frac{1}{\sqrt{\pi}\boldsymbol{\sigma}} \exp\left[-\frac{\left(\boldsymbol{z} - \frac{\boldsymbol{z_1}+\boldsymbol{z_2}}{2}\right)^2}{\boldsymbol{\sigma}^2}\right] \times \\ &\qquad \frac{1}{N_i}\left[\boldsymbol{n}^{\boldsymbol{A}}_i(\boldsymbol{z_1})\,\boldsymbol{n}^{\boldsymbol{A}}_i(\boldsymbol{z_2}) + \frac{1}{2}\left[\boldsymbol{n}^{\boldsymbol{A}}_i(\boldsymbol{z_1})\,\boldsymbol{n}^{\boldsymbol{a}}_i(\boldsymbol{z_2}) + \boldsymbol{n}^{\boldsymbol{a}}_i(\boldsymbol{z_1})\boldsymbol{n}^{\boldsymbol{A}}_i(\boldsymbol{z_2})\right]\right] d\boldsymbol{z_1}\, d\boldsymbol{z_2} \\ &= \int_{\mathbb{R}^2} \frac{1}{\sqrt{\pi}\boldsymbol{\sigma}} \exp\left[-\frac{\left(\boldsymbol{z} - \frac{\boldsymbol{z_1}+\boldsymbol{z_2}}{2}\right)^2}{\boldsymbol{\sigma}^2}\right] \boldsymbol{n}^{\boldsymbol{A}}_i(\boldsymbol{z_1})\,\frac{\boldsymbol{n}^{\boldsymbol{A}}_i(\boldsymbol{z_2}) + \boldsymbol{n}^{\boldsymbol{a}}_i(\boldsymbol{z_2})}{\boldsymbol{N_i}}\, d\boldsymbol{z_1}\, d\boldsymbol{z_2}.\end{aligned} \tag{1.64}$$

(The inheritance process for offspring born with a pair $(a, \boldsymbol{z})$ is encoded similarly). We aim at studying the eco-evo dynamics of a population that lives in a symmetrical heterogeneous environment that can be described similarly as in Section 1.3.1, in the regime where the segregational variance $\boldsymbol{\sigma^2}$ is small compared to $\boldsymbol{\theta}^2$ the parameter measuring the difference between the local optimal traits (or equivalently, $\boldsymbol{\eta}^2$, as we consider that the major alleles effects are of the same order than the local optima). Denoting $\varepsilon = \frac{\boldsymbol{\sigma}}{\boldsymbol{\theta}} \ll 1$ and rescaling the system (and dropping the bold font for the rescaled variables and parameters), we therefore study the following integro-differential system

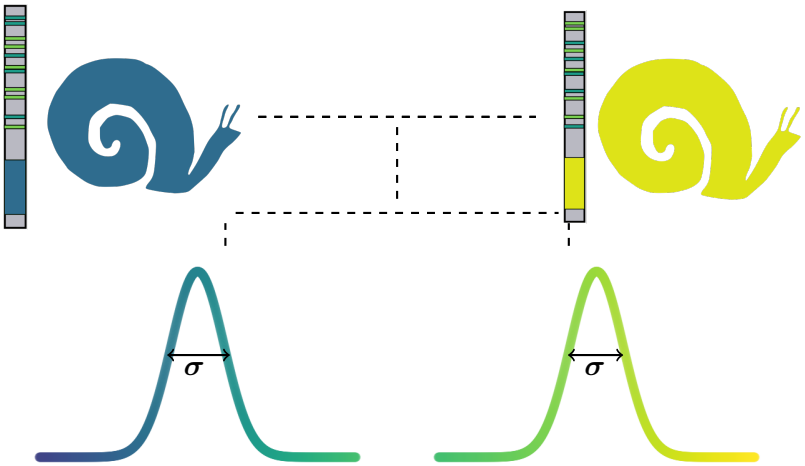

Figure 1.3: Illustration of the combined inheritance of the major effect locus and a quantitative background. The latter is inherited according to the infinitesimal model.

$$\begin{cases} \varepsilon^2 \frac{\partial n^A_{\varepsilon,1}}{\partial t}(t,z) = \mathcal{B}^A_\varepsilon[n^A_{\varepsilon,1}, n^a_{\varepsilon,1}](t,z) - g(z+\eta+1)^2\, n^A_{\varepsilon,1}(t,z) - N_{\varepsilon,1}(t)\, n^A_{\varepsilon,1}(t,z) \\ \qquad\qquad +m(n^A_{\varepsilon,2}(t,z) - n^A_{\varepsilon_1}(t,z)), \\ \varepsilon^2 \frac{\partial n^a_{\varepsilon,1}}{\partial t}(t,z) = \mathcal{B}^a_\varepsilon[n^a_{\varepsilon,1}, n^A_{\varepsilon,1}](t,z) - g(z-\eta+1)^2\, n^a_{\varepsilon,1}(t,z) - N_{\varepsilon,1}(t)\, n^a_{\varepsilon,1}(t,z) \\ \qquad\qquad +m(n^a_{\varepsilon,2}(t,z) - n^a_{\varepsilon_1}(t,z)), \\ \varepsilon^2 \frac{\partial n^A_{\varepsilon,2}}{\partial t}(t,z) = \mathcal{B}^A_\varepsilon[n^A_{\varepsilon,2}, n^a_{\varepsilon,2}](t,z) - g(z+\eta-1)^2\, n^A_{\varepsilon,2}(t,z) - N_{\varepsilon,2}(t)\, n^A_{\varepsilon,2}(t,z) \\ \qquad\qquad +m(n^A_{\varepsilon,1}(t,z) - n^A_{\varepsilon_2}(t,z)), \\ \varepsilon^2 \frac{\partial n^a_{\varepsilon,2}}{\partial t}(t,z) = \mathcal{B}^a_\varepsilon[n^a_{\varepsilon,2}, n^A_{\varepsilon,2}](t,z) - g(z-\eta-1)^2\, n^a_{\varepsilon,2}(t,z) - N_{\varepsilon,2}(t)\, n^a_{\varepsilon,2}(t,z) \\ \qquad\qquad +m(n^a_{\varepsilon,1}(t,z) - n^a_{\varepsilon_2}(t,z)), \end{cases} \tag{1.65}$$

Previous works. There exists quantitative genetic models or multi diallelic loci population genetic models, which study the evolution of the genetic architecture in response to an abrupt change of optimum (directional selection) in a homogeneous environment (Lande 1983; Chevin and Hospital 2008; Vladar and Barton 2014; Jain and Stephan 2017; Höllinger, Pennings, and Hermisson 2019), either by a *genetic sweep* (a major response from a single gene) or by a *shift in allelic frequencies* from a polygenic background. The quantitative genetics models assume that the polygenic contribution results in a Gaussian noise centered in the major effects (Lande 1983; Chevin and Hospital 2008). The population genetic models are interested in the short-term *mutation-selection balance* and show that there can exist a sharp threshold on the allelic effect sizes at each locus, over which fixation occurs, and below which polymorphism at this locus is maintained (Vladar and Barton 2014; Jain and Stephan 2017). This approach has been extended to include the influence of *genetic drift* (Höllinger, Pennings, and Hermisson 2019). However, up to our knowledge, no such framework or study exists on the effect of local stabilizing selection in a heterogeneous environment.

The small variance asymptotics approach has primarily been developed for the evolution of quantitative traits in asexual populations due to mutations (see Section 1.2.2, Diekmann, Jabin, et al. 2005; Perthame and Barles 2008; Barles, Mirrahimi, and Perthame 2009; Lorz, Mirrahimi, and Perthame 2011 in homogeneous environments, Mirrahimi 2017 in heterogeneous environments). It has recently been adapted to study the asymptotic influence of segregation in sexual populations according to the infinitesimal model operator (1.39)(see Section 1.2.3, Calvez, Garnier, and Patout 2019; Patout 2020 for rigorous approaches in homogeneous environments, Dekens 2022 in heterogeneous environments and Garnier et al. 2022 in changing environments). Moreover, one can notice that, upon fixation of a major allele and loss of the other, our system (1.65) reduces to the one (1.57) whose steady states have been determined in [Dekens 2022]. Therefore, as the outcomes of the system are known upon the loss of polymorphism at the major effect locus, its maintenance is the main goal here.

Structure and results The main objective is to determine the influence of the polygenic background on the major effect polymorphism, as the latter alone (with no polygenic background) is maintained whenever the population persists.

1. Determining the main asymptotic profiles. We consider the WKB ansatz $U^A_{\varepsilon,i} = -\varepsilon^2 \log(\varepsilon\, n^A_{\varepsilon,i})$ and the formal Taylor expansion $U^A_{\varepsilon,i} = u^A_{0,i} + \varepsilon^2 u^A_{\varepsilon,i}$. As in Section 1.3.1, the small variance regime asymptotically isolates the reproduction terms like $\frac{\mathcal{B}^A_\varepsilon[n^A_{\varepsilon,1}, n^a_{\varepsilon,1}]}{n^A_\varepsilon}$ in each equation of (1.65). For their contribution to remain bounded in (1.65), the main terms $u^A_{0,i}$ and $u^A_{0,i}$ must formally verify the following *constraint*

$$\begin{cases} \forall z \in \mathbb{R}, \quad \max\Big[\sup\limits_{z_1,z_2} u^A_{0,i}(z) - \big(z - \frac{z_1+z_2}{2}\big)^2 - u^A_{0,i}(z_1) - u^A_{0,i}(z_2), \\ \qquad\qquad \sup\limits_{z_1,z_2} u^A_{0,i}(z) - \big(z - \frac{z_1+z_2}{2}\big)^2 - u^A_{0,i}(z_1) - u^a_{0,i}(z_2)\Big] = 0, \\ \forall z \in \mathbb{R}, \quad \max\Big[\sup\limits_{z_1,z_2} u^a_{0,i}(z) - \big(z - \frac{z_1+z_2}{2}\big)^2 - u^a_{0,i}(z_1) - u^a_{0,i}(z_2), \\ \qquad\qquad \sup\limits_{z_1,z_2} u^a_{0,i}(z) - \big(z - \frac{z_1+z_2}{2}\big)^2 - u^A_{0,i}(z_1) - u^a_{0,i}(z_2)\Big] = 0. \end{cases} \tag{C}$$

Our first result relates to how (C) determines $u^A_{0,i}$ and $u^a_{0,i}$.

Proposition. *Let u^A_0 and u^a_0 satisfying Eq. (C), positive almost everywhere and cancelling somewhere. Then, there exists $z^* \in \mathbb{R}$ such that:*

$$\forall z \in \mathbb{R}, \quad u^A_0(z) = u^a_0(z) = \frac{(z-z^*)^2}{2}. \tag{1.66}$$

The allelic trait distributions $n^A_{\varepsilon,i}$ and $n^a_{\varepsilon,i}$ are therefore Gaussian at the main order, centered at the same habitat-dependent trait z^*_i.

2. Slow-fast analysis. Denoting $\Omega = (\mathbb{R}^*_+)^4 \times \mathbb{R}^3$, there exists $G \in C^\infty(\Omega \times \mathbb{R})$ and $F \in C^\infty(\Omega)$ such that the moment-based system deduced from (1.65) and closed thanks to the last proposition is equivalent to the following

$$\begin{cases} \varepsilon^2 \frac{d\bar{Y}_\varepsilon}{dt} = G(\bar{Y}_\varepsilon, Z_\varepsilon) + \mathcal{O}(\varepsilon^2), \\ \frac{dZ_\varepsilon}{dt} = -2g\, Z_\varepsilon + F(\bar{Y}_\varepsilon) + \mathcal{O}(\varepsilon^2), \end{cases} \tag{P_ε}$$

In the latter, $\bar{Y}_\varepsilon$ denotes the elements of Ω and is the *fast variable*. Its first four coordinates are the local allelic subpopulations sizes $N^a_{1,\varepsilon}, N^a_{1,\varepsilon}, N^A_{1,\varepsilon}, N^A_{2,\varepsilon}$ and the last three coordinates $\delta^A_\varepsilon, \delta^a_\varepsilon, \delta_\varepsilon$ are difference terms between the local allelic mean traits ($\delta^A_\varepsilon := \frac{z^A_{2,\varepsilon} - z^A_{1,\varepsilon}}{2\varepsilon^2}, \delta^a_\varepsilon := \frac{z^a_{2,\varepsilon} - z^a_{1,\varepsilon}}{2\varepsilon^2}, \delta_\varepsilon := \frac{z^A_{2,\varepsilon} + z^A_{1,\varepsilon} - z^a_{2,\varepsilon} - z^a_{1,\varepsilon}}{4\varepsilon^2}$). Furthermore, the variable Z_ε is the mean quantitative contribution in the meta-population and is the slow variable ($Z_\varepsilon := \frac{z^A_{2,\varepsilon} + z^A_{1,\varepsilon} + z^a_{2,\varepsilon} + z^a_{1,\varepsilon}}{4}$). We show the following asymptotic *separation of time scale*

Theorem. *Let* $(\bar{Y}, Z) \in \Omega \times]-1, 1[$ *be a solution of the limit system*

$$\begin{cases} G(\bar{Y}, Z) = 0, \\ \frac{dZ}{dt} = -2g\, Z + F(\bar{Y}), \end{cases} \tag{P_0}$$

Then, for ε *small enough and for close enough initial conditions, the solutions* $(\bar{Y}_\varepsilon, Z_\varepsilon)$ *of* (P_ε) *converge locally in time to the solutions* $(\bar{Y}, Z)$ *of* (P_ε) .

In particular, as δ^A_ε, δ^a_ε and δ_ε converge to finite limits, the average quantitative contributions in both patches are asymptotically equal (to Z). This is due to both migration mixing the quantitative contributions between patches, and segregation with small variance in the infinitesimal model mixing them within patches.

3. Stability of the symmetrical polymorphic equilibrium in the limit system. There exists a migration threshold $m^*(\eta)$, such that for $m \leq m^*(\eta)$, the symmetrical polymorphic equilibrium is unstable at weak selection, stable at intermediate selection and unstable at strong selection, due to the quantitative background (illustrated in Fig. 1.4). The maintenance of the major polymorphism exhibits a non-monotonic behaviour w.r.t. increasing selection, which is confirmed by individual-based simulations.

Comments on the results

1. Asymptotic regime The asymptotic regime $\boldsymbol{\sigma} \ll \boldsymbol{\theta}$ that is considered here is equivalent to $\boldsymbol{\sigma} \ll \boldsymbol{\eta}$, since the major effects are assumed to be of the same order as the local optima. The last regime can be interpreted as when the standard deviation at linkage equilibrium, which is linked to the small effects constituting the polygenic background (see Box 1.2.3), is small compared to the major locus effects.

2. Convex analysis to identify the main Gaussian profiles. The constraint (C) relies on the control of the error terms $u^A_{\varepsilon,i}$ and $u^a_{\varepsilon,i}$ in the series expansion, for which [Calvez, Garnier, and Patout 2019] provides an analytical framework. It arises as the asymptotic regime isolates the reproduction terms in each equation of (1.65), which should remain bounded and can be expressed thanks to the ansatz as follows

$$\begin{aligned} \frac{\mathcal{B}^{\mathcal{A}}_\varepsilon(n^A_\varepsilon, n^a_\varepsilon)(t,z)}{n^A_\varepsilon(z)} \propto \Bigg[&\int_{\mathbb{R}^2} \exp\left(\frac{1}{\varepsilon^2}\left[u^A_0(z) - \left(z - \frac{z_1+z_2}{2}\right)^2 - u^A_0(z_1) - u^A_0(z_2)\right]\right) \exp\left(\mathcal{O}(1)\right) dz_1 dz_2 \\ &+ \int_{\mathbb{R}^2} \exp\left(\frac{1}{\varepsilon^2}\left[u^A_0(z) - \left(z - \frac{z_1+z_2}{2}\right)^2 - u^A_0(z_1) - u^a_0(z_2)\right]\right) \exp\left(\mathcal{O}(1)\right) dz_1 dz_2 \Bigg]. \end{aligned} \tag{1.67}$$

The constraint (C) obtained from the latter is more involved than the analogous one when considering only the infinitesimal model operator (1.39) (like in Garnier et al. 2022, Calvez, Garnier, and Patout 2019, Patout 2020 or Dekens 2022), which would be obtained from (C)

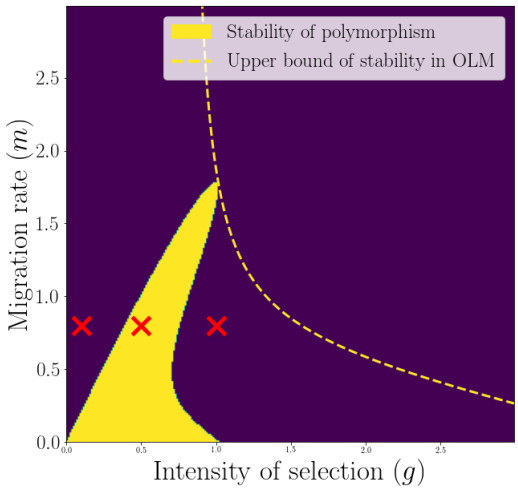

Figure 1.4: **Stability region of the symmetrical polymorphic equilibrium (in yellow), for the major effect locus $\eta = \frac{1}{2}$**, when migration (y-axis) and selection (x-axis) vary. The dashed curve represents the limit of the analogous stability region in the one-locus model (OLM, so without the quantitative background). The red crosses indicate the parameters used for the individual-based simulations whose results are shown in Fig. 1.5.

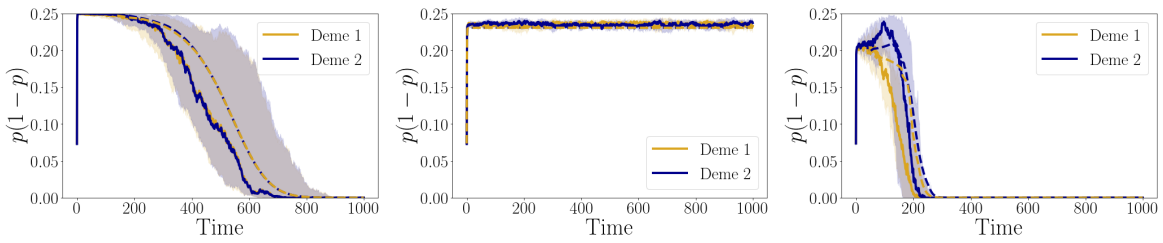

(a) Weak selection (b) Intermediate selection (c) Strong selection

Figure 1.5: **Dynamics of the local variances $p(1-p)$ at the major effect locus w.r.t. increasing selection.** The variable p is the local frequency of the allele A. In all three subfigures, the two colors correspond to the two local subpopulations, the solid curves display the average trajectory resulting from the IBS over 20 replicate simulations, the shaded regions indicate the confidence interval w.r.t. the quantiles 0.2 and 0.8, and the dashed lines are the average trajectories obtained from numerical recursions of the deterministic PDE model (1.65). The migration and selection parameters correspond to the red crosses in Fig. 1.4. Polymorphism at the major effect locus is lost if the variance at this locus reaches 0 (fixation of one allele in the metapopulation, loss of the other). Fig. 1.5a, Fig. 1.5b and Fig. 1.5c confirm the theoretical finding shown in Fig. 1.4, namely that at a fixed intermediate migration level, the major locus polymorphism is gained when increasing selection and subseqeuntly lost when selection increases past a certain threshold.

assuming that $u^A_{0,i} = u^a_{0,i}$ (and result then in the same Gaussian profile as proven in Garnier et al. 2022). The latter would be implied if all the suprema involved in (C) were zero. However, only the maximum of the suprema is zero here (due to the sum of the two integrals in (1.67)), which is a priori a lot weaker. Nevertheless, we proved than in this context it is equivalent, thanks to a monotony property of the convex conjugates of $u^A_{0,i}$ and $u^a_{0,i}$ when passing to the half arguments: $\left[u^A_{0,i}(z) \geq u^a_{0,i}(z)\right] \implies \left[u^A_{0,i}\left(\frac{z}{2}\right) \geq u^a_{0,i}\left(\frac{z}{2}\right)\right]$. We actually proved that the result holds true when considering an arbitrary finite number of different (geno)types, under a condition of graph connectivity (where a vertex connects two types if there is a positive probability that an offspring generated from parents of these types belongs to either of these types). I emphasize on the importance of this result, as it underlies the whole subsequent analysis, by allowing to close the moment-based system. This also justifies the Gaussian assumption of the quantitative background around the major alleles effects made in [Lande 1983]. Furthermore, the generalization could be used for studying the maintenance of major polymorphic responses in more complex population genetic frameworks, and we include a toolbox in our paper (Appendix A of Dekens, Otto, and Calvez 2021) to indicate how to apply it for such purposes.

3. Behind the separation of time scales Classically, the main argument for the separation of time scales is the stability of the slow manifold, defined by $G(\bar{Y}, Z) = 0$ (see (P_0)). I recall that G takes values in a space of dimension seven. However, G presents a *particular diagonal block structure*. The four first non-linear algebraic equations only involve the four populations sizes and the last three form a linear system in the rest of the variables, that can always be inverted, and therefore is not an issue. We moreover show that the first block of four non-linear algebraic equations has always *a unique explicit solution, which contrasts surprisingly* with the analogous system of only two equations in [Dekens 2022], that could have either one or three non-explicit solutions. Furthermore, to prove that the spectrum of the Jacobian associated to G is in the open left half-plane, we use the *Routh-Hurwitz criterion*, on the two blocks separately. Despite the still high dimensions involved (four and three), the signs conditions are shown to be verified (via a symbolic computation software). Furthermore, the separation of time scales is robust. It holds when the environment is assumed to be asymmetrical, and under non-quadratic selections functions. It essentially relies on the blending of the quantitative contributions due to segregation with small variance within patches and due to migration between patches.

4. Loss of polymorphism at strong selection. The result that the fast established polymorphism is slowly disrupted by the quantitative background under strong selection pressure for local adaptation is quite surprising, and to our knowledge, undocumented. Indeed, the intuition is that it would be most favored in this range of parameters, as the two alleles are the "largest assistants" for the trait to reach the local optima. This phenomenon does not occur when the major effect locus is considered alone (which is actually proven by the stability of the slow manifold property at the level $Z = 0$), which means that it is due to the quantitative background. My interpretation is that under strong selection, the quantitative background tries locally to diverge to push the local mean traits toward the optima, while being constrained by the concentration property of the infinitesimal model to stay similar between the two habitats, which causes the instability. Moreover, upon loss of the polymorphism at the major effect locus, the dynamics are described by the system involved in [Dekens 2022] (1.57), whose outcomes are determined.

5. Individual-based simulations (IBS). Because this phenomenon is surprising and undocumented, we conducted multi-loci individual-based simulations to confirm it. This allows to determine if this phenomenon of loss of polymorphism at strong selection actually occurs, in particular before genetic drift provokes the fixation. The IBS are performed thanks to the software SLiM (Haller and Messer 2019). The parameters for migration and selection are indicated by the red crosses in Fig. 1.4. The simulations are in discrete time, with short generations to approximate reasonably the continuous-time deterministic model. We show that the IBS and the continuous-time deterministic model (1.65) are in good agreement (see Fig. 1.5, which is obtained with 200 loci and an ancestral variance at linkage equilibrium of 0.01). The discrepancy between the IBS results and the findings of those performed in [Yeaman and Whitlock 2011] (tightly linked loci of major effects arise under intermediate migration, with no change in increasing selection) can have several sources. First, no mutation is considered here, whereas all alleles in [Yeaman and Whitlock 2011] can mutate at the same rate and with the same variance. Our framework also does not allow for recombination between alleles, which might favor linked divergent clusters under strong selection. Moreover, this phenomenon is not indicated in the results of IBS conducted in [Débarre, Yeaman, and Guillaume 2015], even with a fixed major effect locus. This has two explanations. First, the value of the standard deviation at linkage equilibrium $\sigma_{LE} \approx 0.44$ which they consider (corresponding to 19 loci with effects ± 0.1) is not indeed particularly small compared to the considered large effects (0.6) nor compared to the local optima (± 1). Moreover, the magnitude of the migration rate (<0.1) or the selection strength (0.04) are quite smaller. Therefore, the IBS conducted for the present work explore a different parameter range than in [Débarre, Yeaman, and Guillaume 2015].

1.3.3 A large-time analysis of the evolution of dispersal during invasions with sexual reproduction

This joint project with Florian Lavigne, published in SIAM Journal of Applied Mathematics (Dekens and Lavigne 2021), focuses on *quantifying the main features of the spatial trait distribution* in sexually reproducing populations produced by the evolution of dispersal along unbounded range expansions. By doing so, it aims at proving *insights on the influence of sexual reproduction on the phenomenon of spatial sorting* of the dispersal trait that arises in this situation.

Motivation Our globalized transport and exchange network has shifted species range at a pace and a magnitude that hardly have any historical comparison. The subsequent introduction of invasive species into new territories poses a rapidly growing threat for conservation of native species, which makes even more important to correctly assess invasions' speed. A number of studies have shown that range expansions, while being at first glance an ecological issue, is also influenced by species evolution (Travis and Dytham 2002, Ronce 2007, Phillips, Brown, and Shine 2010), through the evolution of dispersal traits, in plants (Monty and Mahy 2010; Williams, Kendall, and Levine 2016), butterflies (Saastamoinen 2008), crickets (Thomas et al. 2001), birds (Berthouly-Salazar et al. 2012) or infamously in cane-toads (Phillips, Brown, Webb, et al. 2006, Shine, Alford, et al. 2021). This phenomenon is coupled to the *spatial sorting* of the dispersal trait, as individuals at the leading edge of the invasion both present stronger, more enduring, larger wings/legs, and have a higher chance at surviving to reproduction due

to the low intensity of competition, therefore transmitting this high dispersal trait to their offspring. Spatial sorting of dispersal trait have been seen to result in an accelerating front (Phillips, Brown, Webb, et al. 2006; Shine, Alford, et al. 2021). Quantifying this phenomenon is highlighted in Ronce 2007 as a challenge for evolutionary models, since most traits that are shown to influence significantly the dispersal ability are morphological polygenic quantitative trait and that the reproduction mode (sexual, asexual) is also a factor that influences the invasion speed (Ochocki and Miller 2017; Williams, Hufbauer, and Miller 2019).

Model We study the evolution of dispersal in a large sexually reproducing population characterized by an unbounded by above quantitative dispersal trait $z \in [1, +\infty[$, in an unbounded continuous uni-dimensional space, through the following non-local, non-linear reaction-diffusion PDE

$$\begin{cases} \partial_t n(t,x,z) = \mathcal{B}_\sigma^{\mathrm{IM}}[n](t,x,z) - \rho(t,x) n(t,x,z) + z\Delta_x n(t,x,z), \quad t \geq 0,\, x \in \mathbb{R},\, z \in [1,+\infty[, \\ \rho(t,x) = \int_1^{+\infty} n(t,x,z')dz', \\ n(0,x,z) = n_0(x,z), \quad x \in \mathbb{R}, \quad z \in [1,+\infty[. \end{cases} \tag{1.68}$$

The sexual population is subject to uniform competition for local resources among all individuals at the same spatial position x, independently of their traits, which results in the non-local and non-linear term $-\rho(t,x)\, n(t,x,z)$. Furthermore, individuals disperse randomly in space according to their own quantitative trait z as diffusion coefficient. The final feature of the model that remains to be specified is the reproduction operator $\mathcal{B}_\sigma^{\mathrm{IM}}$, which is the infinitesimal reproduction operator (1.39), which I recall the spatial version here:

$$\mathcal{B}_\sigma^{\mathrm{IM}}[n](t,x,z) = \frac{1}{\sqrt{2\pi}\sigma} \iint_{\mathbb{R}\times\mathbb{R}} \exp\left[\frac{\left(z - \frac{z_1+z_2}{2}\right)^2}{2\sigma^2}\right] \frac{n(t,x,z_1)\, n(t,x,z_2)}{\int_{\mathbb{R}^d} n(t,x,z')dz'} dz_1\, dz_2. \tag{1.69}$$

It depends on the parameter σ^2, which is the within-family segregational variance, supposed here to be constant across time, space and families. The non-linear, non-local infinitesimal model operator encodes the transmission of the dispersal trait from one generation to the next under local in space and time random mating, considering that an offspring's trait typically deviate from the mean parental trait according to a Gaussian distribution whose (segregational) variance summarizes the stochasticity of the parental allelic segregation during meiosis (I invite the interested reader to refer to the section Section 1.2.3 for further details on the biological assumptions of the infinitesimal model and the main properties of the operator).

Previous works. (I recommend the interested reader to refer to Section 1.2.2.3 and Section 1.2.3.3 for a more in-depth view of the content of this paragraph). The dependence of the diffusion coefficient on the trait under evolution z constitutes a major difference with the archetypal reaction-diffusion of FKPP (Kolmogorov, Petrovsky, and Piskunov 1937, Fisher 1937), where there is no trait dependence (the population is a Dirac mass $n = \rho\delta_{z=z_0}$ for constant diffusion z_0) and $\mathcal{B}_\sigma^{\mathrm{IM}}[n]$ is replaced by ρ. In this model, the constant diffusion results in the existence of travelling waves propagating at constant speed (see for example Aronson and Weinberger 1978; Evans and Souganidis 1989 for the local reaction version (1.6), and Hamel and Ryzhik 2014 for the non-local reaction version (1.24)). This constant speed propagation feature following constant diffusion has been proved to be robust when the reaction term includes a trait and space-dependent local adaptation term (replacing $\mathcal{B}_\sigma^{\mathrm{IM}}[n](t,x,z)$ by $\sigma_M^2\Delta_z n(t,x,z) + a(x,z)n(t,x,z)$ for asexual populations (Alfaro, Coville, and Raoul 2013;

Bouin and Mirrahimi 2015). For sexual populations, with the same reproduction operator (1.69), there is an additional equilibrium describing a limited range expansion that can arise when local adaptation along a spatial cline is considered (Mirrahimi and Raoul 2013; Raoul 2017), when the dispersal trait's inheritance is modelled by the infinitesimal model reproduction operator (1.39).

In the last decade, the phenomenon of evolution of dispersal along range expansions, modelled by a trait-dependent diffusion as in (1.68) has sparked a growing interest from the quantitative genetics/PDE community. Note that the evolution of dispersal has also raised a great interest in adaptive dynamics (see for example Hastings 1983; Dockery et al. 1998; Cantrell, Cosner, and Lou 2010; Lam and Lou 2014b; Lam and Lou 2014a; Lou and Lutscher 2014; Lam, Lou, and Lutscher 2015; Cantrell, Cosner, Lewis, et al. 2020; Hao, Lam, and Lou 2021). However, existing models are almost exclusively for asexual populations, for which the non-linear, non-local operator $\mathcal{B}_\sigma^{\mathrm{IM}}[n]$ is replaced in (1.68) by the linear and local operator $n + \sigma_M^2 \Delta_z n$ modelling mutations on the trait with variance σ_M^2. Formal computations in [Bouin, Calvez, et al. 2012] suggested that the front of such an invasion accelerates at large times at an asymptotic rate proportional to $t^{\frac{3}{2}}$ to be at a spatial position $X(t) \approx \alpha t^{\frac{3}{2}}$. This intuition was later rigorously confirmed in [Bouin, Henderson, and Ryzhik 2017a], [Berestycki, Mouhot, and Raoul n.d.] and [Calvez, Henderson, et al. 2022], highlighting a surprising phenomenon of quantitative difference on the factor α with regard to the nature of the competition term (local: $\alpha = \frac{4}{3}$/non-local: $\alpha < \frac{4}{3}$). While [Berestycki, Mouhot, and Raoul n.d.] use a probabilistic approach to derive their result, [Bouin, Henderson, and Ryzhik 2017a] and [Calvez, Henderson, et al. 2022] employ a PDE approach inspired from geometric optics (Freidlin 1986, Evans and Souganidis 1989), introducing an self-similar change of variables and a WKB ansatz to describe the motion of the front thanks to the level-set of a Hamilton-Jacobi equation. This approach has also been used in [Bouin and Mirrahimi 2015] in the case of constant diffusion and with a local adaptation term, in [Bouin and Calvez 2014] and [Turanova 2015] to study the evolution of dispersal when the trait is bounded, or when the spatial domain is bounded (Perthame and Souganidis 2016, Lam and Lou 2017), where very different qualitative behaviours of the trait distribution arise in both cases (see the paragraph on evolution of dispersal in Section 1.2.2.3 for more details).

In the case of sexually reproducing populations under evolution of dispersal, numerical simulations have been conducted in [Calvez, Crevat, et al. 2020] that highlight the discrepancy between the acceleration rate of asexual and sexual populations during range expansions, using the infinitesimal model reproduction operator (1.39) to model the dispersal trait's inheritance. In the large time asymptotics, we expect the dispersal trait values at the front to become large and therefore the effective segregational variance compared to these trait values to be small. Consequently, this work has strong ties with [Calvez, Garnier, and Patout 2019] and [Patout 2020] that consider a similar small variance regime along with the infinitesimal model reproduction operator to derive their result on the adaptation of sexual populations to homogeneous space.

Main result. (Some notations of the article have been changed here for the sake of clarity and uniformity throughout the introduction.)

The spatial trait distribution n solution of (1.68) is conjectured to be approximated for large-time asymptotics as follows:

Conjecture. *Define the front position constant*

$$y_c = 4\left(\frac{\sigma}{3}\right)^{1/2}. \tag{1.70}$$

There exists $\delta_0 > 0$, such that, for all $0 < \delta \leq \delta_0$, the density n at time $t \geq T$ (where T is large) can be approximated by:

$$n(t,x,z) \approx \begin{cases} \frac{1}{2\sqrt{\pi}\sigma} \exp\left[-\frac{1}{4\sigma^2} \left[z - \bar{z}^{behind}(x) \right]^2 + \underset{\delta \to 0}{\mathcal{O}}(\delta) + \underset{t \to \infty}{\mathcal{O}}(\frac{1}{t}) \right], \\ \qquad\qquad \text{for } x \leq y_c\, t^{5/4}, \quad |z - \bar{z}^{behind}(x)| \leq \delta \bar{z}^{behind}(x), \\ \exp\left[\left(1 - \left(\frac{x}{y_c\, t^{5/4}} \right)^{4/3} \right) t \right] \\ \qquad \times \frac{1}{2\sqrt{\pi}\sigma} \exp\left[-\frac{1}{4\sigma^2} \left[z - \bar{z}^{ahead}(t,x) \right]^2 + \underset{\delta \to 0}{\mathcal{O}}\left(\delta + \delta^2 \left[\frac{x}{t^{5/4}} \right]^{8/3} \right) + \underset{t \to \infty}{\mathcal{O}}(\frac{1}{t}) \right], \\ \qquad\qquad \text{for } x \geq y_c\, t^{5/4}, \quad |z - \bar{z}^{ahead}(x)| \leq \delta \bar{z}^{ahead}(x). \end{cases} \tag{1.71}$$

The approximated mean dispersal trait behind and ahead of the front are given by:

$$\begin{cases} \bar{z}^{behind}(x) = \sigma^{4/5} (6x^2)^{1/5}, & x \leq y_c t^{5/4}, \\ \bar{z}^{ahead}(t,x) = \left(3\sigma^2 \frac{x^2}{2t} \right)^{1/3}, & x \geq y_c t^{5/4}. \end{cases} \tag{1.72}$$

As the approximation (1.71) is only a conjecture, results from a numerical resolution of (1.68) are also provided. It indicates that the conjectured approximation predicts reasonably well the position of the front $X(t) \approx y_c t^{\frac{5}{4}}$, the position of the mean trait $\bar{z}^{behind}$ behind the front and the local constant variance behind the front.

Comments on the result. The conjectured approximation (1.71) above suggests several *qualitative* and *quantitative* features of the spatial trait distributions. The first important one is the spatial position of the front, which is located at $X(t) \approx 4\left(\frac{\sigma}{3}\right)^{1/2} t^{\frac{5}{4}}$. Behind the front, the spatial distribution is approximately Gaussian, of constant variance $2\sigma^2$ (twice the segregational variance), and stationary, as the local mean trait $\bar{z}^{behind}$ only depends on the space variable x. Ahead of the front, the formula in (1.71) presents two multiplicative terms. The first is the prefactor of the trait distribution which quantifies the rapid exponential decay of the population ahead of the front. The second indicates that the spatial trait density ahead of the front is also approximately Gaussian, of same variance as behind the front, but with a different mean $\bar{z}^{ahead}$ (notice though that the mean trait is continuous at the interface, meaning that $\bar{z}^{behind}(y_c t^{5/4}) = \bar{z}^{ahead}(y_c t^{5/4})$). I draw the attention on the trait intervals on which the approximation holds, which are asymptotically large at large times and thus at large spatial position x. Moreover, the error term ahead of the front is close to $\underset{t \to +\infty}{\mathcal{O}}(\delta)$ near the front, as $\frac{x}{t^{5/4}} = y_c = \mathcal{O}(1)$ there, and the exponential decay rapidly shrinks the population size just ahead of the front.

A striking feature of the spatial trait distribution as approximated in (1.71) and seen in Fig. 1.6a, is the narrowness of the spatial trait distribution for sexual populations, compared to the one for asexual reproductions Fig. 1.6b. It seems to relate to the different accounts of the concentration properties inherent to the infinitesimal model operator, which can limit its spatial range (which is reminiscent of the limited range equilibrium specific to the propagation of sexual populations along a spatial cline Kirkpatrick and Barton 1997; Mirrahimi and Raoul 2013; Raoul 2017). Here, as a reminder of the same phenomenon in other contexts in [Roughgarden 1972], [Bulmer 1980], the local within-population variance in trait is approximated by twice the segregational variance, behind and ahead of the front. This constrained variance in

the dispersal trait is the structural reason of why sexual populations are significantly slower than asexual to invade with a pure spatial sorting effect under the rule of inheritance following the infinitesimal model.

Some heuristics.

1. WKB ansatz for large time asymptotics. Our formal analysis relies first on an self-similar change of variable, which is wired to be able to follow the accelerating front at large times (following [Calvez, Crevat, et al. 2020], combined with a WKB ansatz (like in Evans and Souganidis 1989; Bouin and Mirrahimi 2015; Turanova 2015; Perthame and Souganidis 2016; Bouin, Henderson, and Ryzhik 2017a; Calvez, Henderson, et al. 2022)

$$n(t,x,z) = \exp\left[-t\,u\left(\log(t), \frac{x}{t^{5/4}}, \frac{z}{t^{1/2}}\right)\right] =: \exp\left[-e^s\,u\left(s,y,\eta\right)\right]. \tag{1.73}$$

The WKB ansatz u is solution of the following equation, obtained from (1.73) and (1.68)

$$\begin{aligned} -u(s,y,\eta) - \partial_s u(s,y,\eta) + \frac{5}{4} y \partial_y u(s,y,\eta) + \frac{\eta}{2}\partial_\eta u(s,y,\eta) \\ = \eta\left[(\partial_y u(s,y,\eta))^2 - e^{-s}\Delta_y u(s,y,\eta)\right] + \left(I[u](s,y,\eta) - \varrho_u(s,y)\right), \end{aligned} \tag{1.74}$$

where the term $I[u](s,y,\eta)$ is the integral term that arises from the infinitesimal model operator, analogous as in [Calvez, Garnier, and Patout 2019], [Patout 2020]

$$\begin{aligned} I[u](s,y,\eta) = \frac{e^s}{\sqrt{2\pi\sigma^2}\varrho_u(s,y)} \\ \iint_{(e^{-s/2},\infty)^2} \exp\left[e^s\left(-\frac{\left(\eta - \frac{\eta_1+\eta_2}{2}\right)^2}{2\sigma^2} + \left[u(s,y,\eta) - u(s,y,\eta_1) - u(s,y,\eta_2)\right]\right)\right] d\eta_1\, d\eta_2. \end{aligned}$$

We are interested in the large time asymptotics, when $s \to +\infty$. Notice that the diffusion in space yields the same term $(\partial_y u(s,y,\eta))^2$ in (1.74) as in asexual studies, but that the corresponding derivative w.r.t. the trait variable (coming from the diffusion in trait modelling mutations in asexual populations) is replaced by the integral term $I[u]$, which comes from (1.69). Hence, the limit equation of (1.74) is not a Hamilton-Jacobi equation, and it is required to understand the asymptotic limit of $I[u]$ to derive it.

2. Decomposition of the main term u_0 and derivation of the limit equation. Following the heuristics given by [Garnier et al. 2022], [Calvez, Garnier, and Patout 2019] and [Patout 2020], we first consider the following series expansion of

$$u(s,y,\eta) = u_0(y,\eta) + e^{-s}u_1(y,\eta) + \underset{s\to+\infty}{\mathcal{O}}(e^{-2s}). \tag{1.75}$$

Notice that here, the segregational variance σ^2 is not assumed to be small per say, but the rescaling of the trait variable $\eta = \frac{z}{\sqrt{t}}$ implies that it becomes small compared to the trait values as t (or s) becomes large (as the effective segregational variance for η is $\sigma^2 e^{-\frac{s}{2}}$). This is why the arguments of the above references are likely to apply.

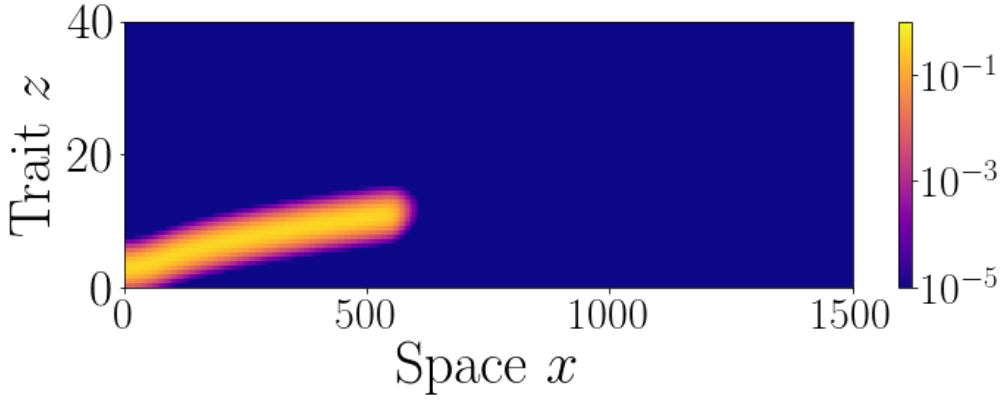

(a) Spatial distribution of a **sexual** population under evolution of dispersal at time $t = 100$, (numerical resolution of (1.68), with $\sigma^2 = \frac{1}{2}$).

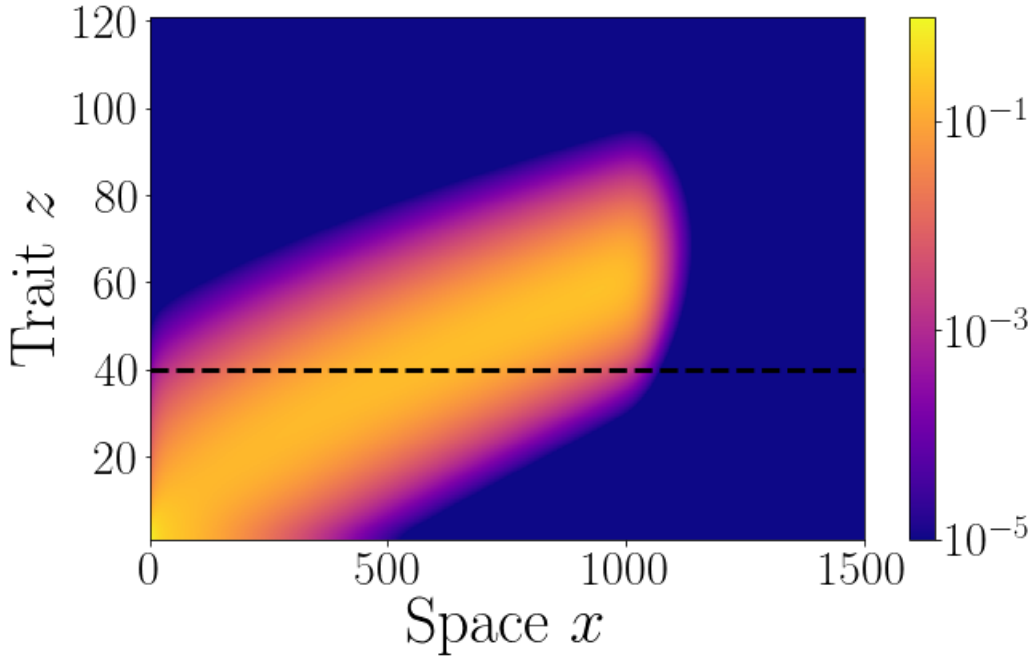

(b) Spatial distribution of an **asexual** population under evolution of dispersal at time $t = 100$, (numerical resolution of (1.30), with $\sigma_M^2 = \frac{1}{2}$). The black dashed line represents the upper trait value in Fig. 1.6a.

Figure 1.6: **Comparison of the spatial distributions of sexual (top panel) and asexual (bottom panel) under evolution of dispersal.** Both figures results from numerical resolutions of respectively (1.68) and (1.30), at the same time $t = 100$, and starting from the same initial conditions. Notice the difference of y-axis values for the dispersal trait between both figures (the black dashed line in the lower figure represents the upper trait value for the upper figure). Apart from the different spatial speed of invasions, and the difference in the trait values, one striking difference is the *variance* of the local trait distributions, quite narrow around the mean for the sexual population, and large for the asexual population.

They yield that u_0 must formally verify a constraint which determines its form as a quadratic function in the trait variable

$$u_0(y,\eta) = \lambda(y) + \frac{(\eta - \bar\eta(y))^2}{4\sigma^2}. \tag{1.76}$$

The space-dependent coefficients $\lambda(y)$ and $\bar\eta(y)$ are unknown at this stage (like in Patout 2020) and will be determined as solutions of the limit problem. Their significance is highlighted when used in (1.73): $\lambda(y)$ is the local spatial decay coefficient and $\bar\eta(y)$ is the local mean trait at the position y. The quadratic form (1.76) yields in turn a formal limit equation with a finite-difference term as in [Calvez, Garnier, and Patout 2019], [Patout 2020]. The limit equation of the steady states at large times is given by

$$\begin{aligned} -\lambda(y) - \frac{(\eta-\bar\eta(y))^2}{4\sigma^2} + \frac{1}{2}y\left[\lambda'(y) - \bar\eta'(y)\,\frac{\eta-\bar\eta(y)}{2\sigma^2}\right] + \frac{5}{4}\eta\frac{\eta-\bar\eta(y)}{2\sigma^2} - \eta\left[\lambda'(y) - \bar\eta'(y)\,\frac{\eta-\bar\eta(y)}{2\sigma^2}\right]^2 \\ + \mathbf{1}_{\{y\le y_c\}} = \exp\left[u_1(y,\eta) + u_1(y,\bar\eta(y)) - 2u_1\left(y, \frac{\eta+\bar\eta(y)}{2}\right)\right]. \end{aligned} \tag{1.77}$$

The l.h.s of (1.77) is much more involved than the analogous l.h.s. of the limit equation in [Patout 2020], and represents the interplay between the spatial sorting effect, the competition and segregation (r.h.s). One can notice that the competition is roughly approximated at the limit by an indicator function of the invaded region and therefore ignores the non-linear transition (similar to Calvez, Henderson, et al. 2022). The quantitative features of the spatial trait distribution ahead of the front should therefore be read with caution.

3. Solving the limit equation (1.77) The unknown of (1.77) are the functions $\lambda, \bar\eta, u_1$ and the constant y_c. The strategy is to first eliminate u_1, thanks to the kernel of finite-difference operator appearing on the r.h.s of (1.77). The latter is known from [Patout 2020] to be of dimension two, generated by the evaluation at the local mean trait $\delta_{\bar\eta}(y)$ and its derivative $\delta'_{\bar\eta}(y)$. Therefore, thanks to the latter, the following closed ODE system on $(\lambda, \bar\eta, y_c)$ is obtained

$$\forall y \neq y_c, \quad \begin{cases} -\lambda(y) + \frac{1}{2}y\lambda'(y) - \bar\eta(y)(\lambda'(y))^2 + \mathbf{1}_{\{y<y_c\}} = 1, \\ -\frac{1}{2}y\bar\eta'(y) + \frac{5}{4}\bar\eta(y) - 2\sigma^2(\lambda'(y))^2 + 2\bar\eta(y)\lambda'(y)\bar\eta'(y) = 0. \end{cases} \tag{1.78}$$

One of our results is the derivation of a solution of the latter (its uniqueness, though, is yet to be proved), which underlies the main terms of (1.71):

Proposition. *Let us define:*

$$y_c = 4\sqrt{\frac{\sigma}{3}}, \qquad \bar\eta : y \mapsto \begin{cases} \sigma^{4/5}\,6^{1/5}\,y^{2/5}, & \text{if } y \le y_c, \\ \left(\frac{3\sigma^2}{2}\right)^{1/3} y^{2/3}, & \text{if } y > y_c, \end{cases}$$

and:

$$\lambda : y \mapsto \begin{cases} 0, & \text{if } y \le y_c, \\ \left(\frac{3}{\sigma^4}\right)^{2/3} y^{4/3} - 1, & \text{if } y > y_c. \end{cases}$$

Then $\lambda, \bar\eta \in C^0(\mathbb{R}) \cap C^1(\mathbb{R}\backslash\{y_c\})$ and y_c, λ and $\bar\eta$ are solutions of (1.78).

Finally, the determination of $\lambda, \bar{\eta}, y_c$ allows to locally invert the finite-difference operator of the r.h.s of (1.77) to obtain the corrector u_1 as an infinite series ahead and behind the front, like in [Calvez, Garnier, and Patout 2019] and [Patout 2020], up to its affine part:

$$u_1(y,\eta) = \sum_{k\geq 0} 2^k \log\left[g\left(y, \bar{\eta}(y) + \frac{\eta - \bar{\eta}(y)}{2^k}\right)\right] + u(y,\bar{\eta}(y)) + \gamma(y)\left(\eta - \bar{\eta}(y)\right), \quad y \neq y_c, \ \left|\frac{\eta}{\bar{\eta}(y)} - 1\right| \leq \delta. \tag{1.79}$$

In (1.79), $g(y,\eta)$ denotes the l.h.s of (1.77) (notice that the closed ODE system (1.78) is equivalent to $g(y,\bar{\eta}(y)) = 1, \partial_\eta g(y,\bar{\eta}(y)) = 0$). The control of the infinite series involved in (1.79) on this interval leads to respective error terms $\mathcal{O}(\delta^2)$ and $\mathcal{O}\left(\delta^2\left[\frac{x}{t^{5/4}}\right]^{8/3}\right)$ behind and ahead of the front.

The affine part $\eta \mapsto u(y,\bar{\eta}(y)) + \gamma(y)\left(\eta - \bar{\eta}(y)\right)$ is in the kernel of the finite-difference operator (r.h.s of (1.77)), and thus has to be determined separately, both behind and ahead of the front. The constant part $u(y,\bar{\eta}(y))$ is set to $-\log(2\sqrt{\pi}\sigma)$ so that the limit local population size is normalized. Furthermore, the linear coefficient γ is identified by formally following analogous computations from [Calvez, Garnier, and Patout 2019] (see equations (1.10) and (3.2) of the latter):

$$\gamma(y) = \frac{3}{4}\frac{\partial_\eta^3 u_1(y,\bar{\eta}(y))}{\partial_\eta^2 u_1(y,\bar{\eta}(y))} = \frac{1}{2}\frac{\partial_\eta^3 g(y,\bar{\eta}(y))}{\partial_\eta^2 g(y,\bar{\eta}(y))} = \begin{cases} \frac{3}{2\bar{\eta}(y)} & \text{for } y < y_c, \\ \frac{-3}{2\bar{\eta}(y)} & \text{for } y > y_c. \end{cases} \tag{1.80}$$

I have to admit that the linear part, which increases the error terms by an additional $\mathcal{O}(\delta)$, has been overlooked in the published article.

4. Conclusion of the formal analysis The proposition presented in the last paragraph defines the rescaled front position y_c, the spatial decay coefficient λ and the local mean dispersal trait $\bar{\eta}$ which together identify completely the main quadratic term u_0 (see (1.76)) of the WKB ansatz (1.75). The equations (1.79) and (1.80) in turn identify completely the corrector term u_1 and its magnitude has been controlled. Finally, recasting all these information in the self-similar change of variable (1.73) yields the conjectured approximation (1.71).

1.3.4 Dirac dynamics of quantitative alleles under general genes interactions and selection in a sexual population

This joint project with Sepideh Mirrahimi, currently under peer-review (Dekens and Mirrahimi 2021), aims at proposing a PDE framework to analyse quantitatively the large-time *evolutionary trajectories of faithfully transmitted quantitative alleles* in a sexually reproducing population under general natural selection pressures.

Motivation. In the last two decades, evidences that *gene expression regulation* plays a significant role in the adaptation of species have been mounting, confirming intuition of the second half of the last century (see Romero, Ruvinsky, and Gilad 2012; Signor and Nuzhdin 2018; Anderson, Vilgalys, and Tung 2020; El Taher et al. 2021), even proposing new paradigms (see the alternative explanation for the degeneration of the Y chromosome by regulatory evolution in Lenormand, Fyon, et al. 2020). This calls for models that can analytically predict

how gene regulation systems can evolve, which requires the possibility to model a *broad range of genes interactions*. In particular, it requires doing so in the *continuum-of-alleles* framework, as slight differences in the regulation of a gene will translate for example into a slight change in the protein production that it controls.

The concept of *continuum-of-alleles* can be traced back to the seminal work of [Kimura 1965], which thought that such a situation could arise from random mutations (see also the beginning of Section 1.2.2). In this work, he derived some approximations by assuming a haploid population (or asexual), that all loci were unlinked, had additive effects on the trait and that the allelic values distributions at each locus was Gaussian. An extension to diploid sexual populations under similar assumptions of additivity between loci, and normality on the distribution of allelic values at each locus was presented later in [Lande 1975]. Our goal is to propose an analytical framework that bypasses these assumptions, to be able to model evolutionary dynamics involving gene expression regulation.

Model. We study the following non-local, non-linear integro-differential equation modelling the eco-evo dynamics of a sexually reproducing haploid population, characterized by two compactly supported quantitative alleles $(x, y) \in I \times J$ segregating at two different unlinked loci

$$\begin{cases} \varepsilon\, \partial_t n_\varepsilon(t,x,y) = \frac{r}{2}\left[\frac{\rho_\varepsilon^Y(t,x)\,\rho_\varepsilon^X(t,y)}{\rho_\varepsilon(t)} + n_\varepsilon(t,x,y)\right] - (m(x,y) + \kappa\,\rho_\varepsilon)\; n_\varepsilon(t,x,y), \\ \rho_\varepsilon^X(t,y) = \displaystyle\int_I n_\varepsilon(t,x',y)\,dx',\;\; \rho_\varepsilon^Y(t,x) = \int_J n_\varepsilon(t,x,y')\,dy',\;\; \rho_\varepsilon(t) = \iint_{I\times J} n_\varepsilon(t,x',y')\,dx'\,dy', \\ n_\varepsilon(0,x,y) = n_\varepsilon^0(x,y). \end{cases} \tag{$P\,(n_\varepsilon)$}$$

The population is subject to a smooth, bounded lethal natural selection at a rate $m(x, y) \geq 0$, which depends on the alleles carried by each individual, and to a uniform competition for resources with intensity proportional to the population size ρ_ε at a rate $\kappa > 0$. Notice that the natural selection term allows general interactions between the alleles values x and y. One idea for a specific example that we have in mind is to model *multiplicative interactions* between alleles under stabilizing selection $m(x, y) = (1 - xy)^2$ (with $I = J = [-2, 2]$).

The inheritance of a given pair of unlinked alleles (x, y) by an offspring is modelled thanks to the kernel (1.36), which results in the following reproduction operator $\mathcal{B}[n_\varepsilon] = \frac{1}{2}\left[\frac{\rho_\varepsilon^Y(x)\,\rho_\varepsilon^X(y)}{\rho_\varepsilon} + n_\varepsilon(t,x,y)\right]$. Under the assumption of random mating for haploid individuals, an offspring receives either both its alleles from one of its parents, or one from each parent, with equal probability (we assume that no mutation occur, see Fig. 1.7 for an illustration). Consequently, the marginals ρ_ε^X and ρ_ε^Y of the trait distribution n_ε w.r.t. both loci appear in the expression of $\mathcal{B}$. The reproduction rate is denoted by $r > 0$.

The initial population density n_ε^0 is assumed to have a *small initial variance* of order $\varepsilon > 0$, which would happen for example if some mutations had occured initially. This also anticipates on a future work that will include mutations. The time is thus rescaled accordingly, as the changes in the allelic distribution are expected to be perceived on a long time scale set by the small parameter ε. As no mutation is considered here, we expect the population trait density n_ε to keep its variance of order ε. Consequently, we introduce the WKB ansatz $u_\varepsilon = \varepsilon \log(\varepsilon\, n_\varepsilon)$

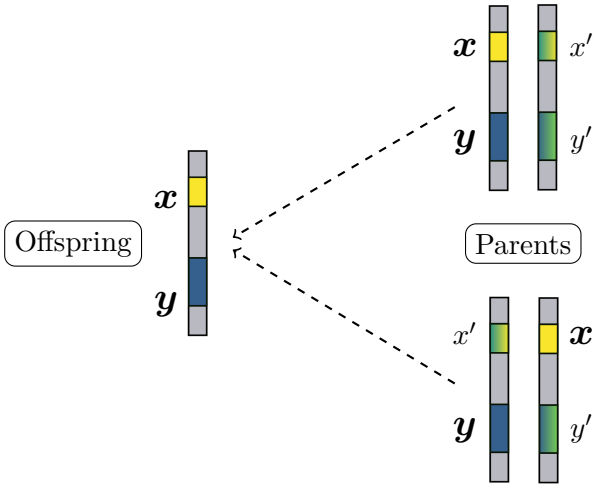

Figure 1.7: Faithful transmission of quantitative alleles at two locus in sexual haploid populations

and the corresponding equation, on which the main analysis is carried

$$\begin{cases} \partial_t\, u_\varepsilon(t,x,y) = \frac{r}{2\rho_\varepsilon(t)} \iint_{I\times J} \frac{1}{\varepsilon} \exp\left[\dfrac{u_\varepsilon(t,x,y') + u_\varepsilon(t,x',y) - u_\varepsilon(t,x,y)}{\varepsilon}\right] dx'\, dy' \\ \qquad\qquad\qquad\qquad\qquad\qquad\qquad\qquad - \left(m(x,y) + \kappa\,\rho_\varepsilon(t) - \frac{r}{2}\right), \\ u_\varepsilon(0,\cdot,\cdot) = \varepsilon \log(\varepsilon n_\varepsilon^0), \\ \rho_\varepsilon = \iint_{I\times J} \frac{1}{\varepsilon} \exp\left[\dfrac{u_\varepsilon(x',y')}{\varepsilon}\right] dx'\, dy'. \end{cases} \tag{P_{u_ε}}$$

Previous works. (I recommend to refer to Section 1.2.2.1 and Section 1.2.3.1 for more details on the content of this paragraph.)

As mentioned above, the model we consider here ($P\,(n_\varepsilon)$) is related to the continuum-of-alleles framework, to which it aims at extending the classical models (Kimura 1965; Lande 1975, see also Burger 2000 for a review). As such, it belongs to another framework than population genetic models, which also consider the evolution of a few loci, but with discrete effects (see Bürger 2020 for a review of multi-loci population genetic models). However, it is notable that a very similar equation was derived from an individual-based model in [Collet, Méléard, and Metz 2013] in the limit of large population, but for diploid populations characterized by a continuum-of-allele segregating at one locus. Their model also involves two variables (x, y), which denote the two copies of diploid individuals. In fact, their equation can be obtained under a change of variable $\tilde{m} = m - \frac{r}{2}$ as a particular case of ($P\,(n_\varepsilon)$), by assuming additionally that both the selection and the initial state are symmetrical. Indeed, a diploid offspring receives one allele from each of its parents, which is modelled by the non-linear reproduction term involving the marginals of the trait distribution. The symmetry condition is imposed by biological reasons, as the order of the alleles should not influence the dynamics. One can notice that under this symmetry condition, the solution of ($P\,(n_\varepsilon)$) is also symmetrical at all times.

The methodology using the WKB ansatz $u_\varepsilon = \varepsilon \log(\varepsilon\, n_\varepsilon)$ following the assumption of small variance in the initial population is similar in principle to the small mutational variance developed primarily for asexual studies (Diekmann, Jabin, et al. 2005; Perthame and Barles

2008; Barles, Mirrahimi, and Perthame 2009; Lorz, Mirrahimi, and Perthame 2011). However, the non-linear sexual reproduction operator yields different regularity estimates compared to the linear reproduction operator (1.8) or (1.7) (note also that no mutations is considered in our model, which leads to a limit problem which is not the typical constrained Hamilton-Jacobi equation obtained in the previously mentioned asexual studies).

A related small variance asymptotics is also considered in some studies on the evolution of a quantitative trait in sexual populations (Calvez, Garnier, and Patout 2019; Patout 2020; Perthame, Strugarek, and Taing 2021). Although the latter also models the transmission of trait across generations with a kernel-based integral operator, the genetic architectures underlying the quantitative trait are very different. [Calvez, Garnier, and Patout 2019] and [Patout 2020] uses the infinitesimal model, which assumes classically that the trait results from a large number of small discrete additive allelic effects, whereas in our case, the two allelic effects are considered nor small nor discrete nor additive (note that other asymptotics have also been considered with the infinitesimal model Mirrahimi and Raoul 2013; Raoul 2017; Raoul 2021, but are not comparable to ours either). Moreover, [Perthame, Strugarek, and Taing 2021] considers asymmetrical kernel on a single focal trait variable, whereas here, two variables (the allelic values x and y) are mixed between individuals by reproduction.

Main result The main result relates to the dynamics of u_ε in the limit when ε vanishes. It requires some typical hypothesis of regularity and boundedness on the initial distribution, that I will not detail here. However, I will state the following fundamental hypothesis that is both highly specific to our problem and informative on the asymptotic allelic distribution before stating the theorem

$$\exists\, 0 < \nu_m < \nu_M,\ \forall \varepsilon,\ \forall (x,y) \in I \times J, \quad \nu_m \leq \nu_\varepsilon^0(x,y) := \frac{\rho_\varepsilon^{X,0}(y)\,\rho_\varepsilon^{Y,0}(x)}{n_\varepsilon^0(x,y)\,\rho_\varepsilon^0} \leq \nu_M. \quad (H_{\text{multiplicative}})$$

Theorem. *Under some assumptions of regularity and boundedness on the initial distribution, along with $H_{multiplicative}$, for all $T > 0$, $u_\varepsilon \underset{\varepsilon \to 0}{\longrightarrow} u$ in $C^0([0,T] \times I \times J)$ (along subsequences). Additionally, u satisfies the following properties:*

(i) u is Lipschitz continuous,

(ii) u is non-positive and satisfies an additive separation of variables property:

$$\forall (t,x,y) \in [0,T] \times I \times J, \quad u(t,x,y) = u^Y(t,x) + u^X(t,y) := \max u(t,x,\cdot) + \max u(t,\cdot,y). \tag{1.81}$$

Furthermore, we have at all time t: $\max u^Y(t,\cdot) = \max u^X(t,\cdot) = 0$.

(iii) Link with the support of n. The limit measure $n(t,\cdot,\cdot)$ is supported at the zeros of $u(t,\cdot,\cdot)$ for a.e. t:

$$\begin{aligned} \operatorname{supp}(n(t,\cdot,\cdot)) &\subset \{(x,y)\,|\,u(t,x,y) = 0\} \\ &= \{x\,|\,u^Y(t,x) = 0\} \times \{y\,|\,u^X(t,y) = 0\}. \end{aligned}$$

(iv) u^X (resp. u^Y) satisfies the following limit equation for a.e. y:

$$\forall t \in [0,T] \quad u^X(t,y) = u^X(0,y) + r\,t - \kappa \int_0^t \rho(s)\,ds - \int_0^t \left\langle \phi^X(t,\cdot,y), m(\cdot,y) \right\rangle ds, \tag{1.82}$$

where ϕ^X *is the limit of* $\frac{n_\varepsilon}{\rho_\varepsilon^X}$ *in* $L^\infty\left(w^* - [0,T]\times I, M^1(I)\right)$*. Moreover, for a.e.* (t,y)

$$\operatorname{supp}\left(\phi^X(t,\cdot,y)\right) = \{x \,|\, u^Y(t,x) = 0\}.$$

Comments on the result

1. Preliminary results: well-posedness and convergence of ρ_ε. A preliminary result to Section 1.3.4 is the well-posedness of $(P(n_\varepsilon))$ thanks to a *contraction-mapping fixed point argument* and the weak convergence of n_ε toward a limit measure n (following the a priori uniform bounds on the population size ρ_ε). This preliminary result is however not sufficient to describe the support of the limit measure n (i.e. the dominant alleles in the population), which is why we study the dynamics of the ansatz u_ε and its convergence, which eventually informs on that support. Moreover, the regularity of the weakly defined limit population size ρ can be improved to be a BV function under an additional hypothesis on the selection m, namely that is separates variables additively ($m(x,y) = m^X(y) + m^Y(x)$.) This BV regularity is reminiscent of typical regularity of the analogous term in asexual studies, like [Perthame and Barles 2008], [Barles, Mirrahimi, and Perthame 2009] or [Lorz, Mirrahimi, and Perthame 2011].

2. Strong convergence of u_ε. The strong convergence of u_ε toward u (along subsequences) relies on the *Arzéla-Ascoli* theorem, which is frequently used in asexual studies in the regime of small mutational variance to show the convergence of the analogous ansatz u_ε towards its limit. The derivation of uniform bounds for u_ε follows classical arguments using the fact that the population size ρ_ε is uniformly bounded from above and below at all times (see Desvillettes et al. 2008; Perthame and Barles 2008; Barles, Mirrahimi, and Perthame 2009 for example, or also the third paragraph in Box for some details 1.2.2.1), while the uniform Lipschitz bounds in space result from a maximum principle respected by the equation on ∇u_ε. However, the derivation of uniform Lispchitz bounds in time is original, as it requires to bound uniformly the integral reproduction term in (P_{u_ε}), which is $\nu_\varepsilon := \frac{\rho_\varepsilon^X \rho_\varepsilon^Y}{n_\varepsilon \rho_\varepsilon}$. The uniform bound on ν_ε is a key result of our analysis and uses a comparison principle. Additionally to being instrumental in the derivation of Lipschitz bounds in time, it justifies $H_{\text{multiplicative}}$ and underlies the *additivity of the limit* u w.r.t. both variables. Another way to look at this is to state that, for a.e. (t,y), the limit measure $\phi^X(t,\cdot,y) \in M^1($ (weak limit of $\frac{n_\varepsilon}{\phi_\varepsilon^X}$) is *equivalent* to $\rho^Y(t,\cdot) \in M^1(I)$ (weak limit of ρ_ε^Y), and its support is therefore independent of y (last statement of Section 1.3.4). Finally, the fact that the support of the limit measure n is a subset of the zeros of the non-positive limit u is quite classical and obtained in the aforementioned asexual studies. However, here the specific additivity property of u makes it more specific, as the product of a subspace of I and a subspace of J.

3. Limit equations One can notice that the limit equations (1.82) on u^X and u^Y are quite different from the problem on u_ε (P_{u_ε}) for $\varepsilon > 0$. This is because, on the contrary to the convergence property of u_ε, the limit equations are instead obtained from the equations on the marginals ρ_ε^X and ρ_ε^Y

$$\begin{cases} \varepsilon\,\partial_t \rho_\varepsilon^X = (r - \kappa\,\rho_\varepsilon)\,\rho_\varepsilon^X - \int_I m(x,y)\,n_\varepsilon(t,x,y)\,dx, \\ \varepsilon\,\partial_t \rho_\varepsilon^Y = (r - \kappa\,\rho_\varepsilon)\,\rho_\varepsilon^Y - \int_J m(x,y)\,n_\varepsilon(t,x,y)\,dy, \end{cases} \tag{1.83}$$

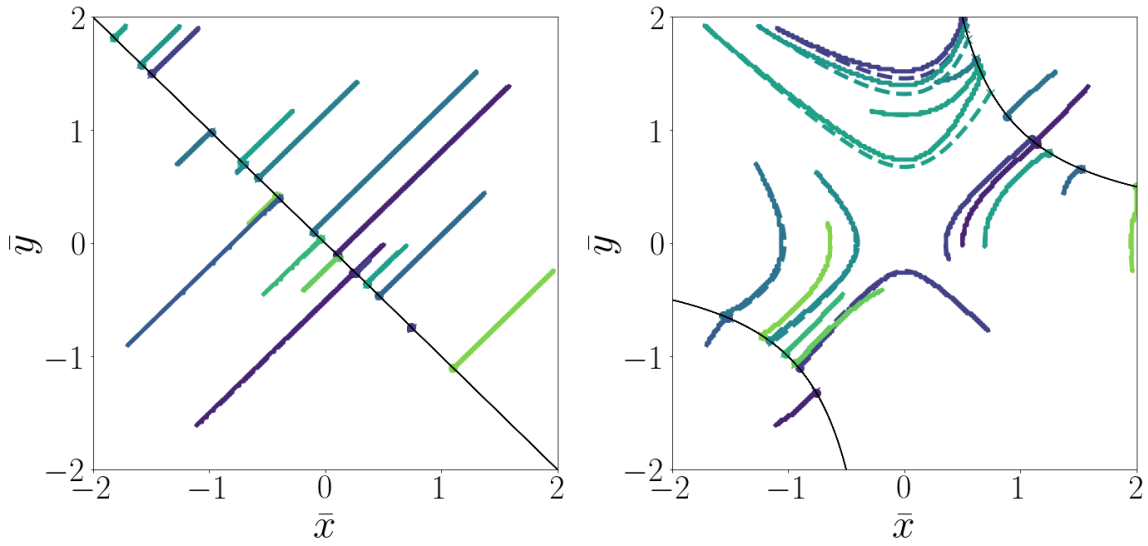

(a) $m(x,y) = (x+y)^2$.

(b) $m(x,y) = (1-xy)^2$.

Figure 1.8: **Comparison between the trajectories of the dominant alleles $(\bar{x}(t), \bar{y}(t))$ in a monomorphic population obtained from numerical recursions of $(P(n_\varepsilon))$ (full lines) and the canonical equations (dashed lines), with two different selection functions.** In each subfigure, each colored line corresponds to a trajectory departing from a uniformly randomly chosen monomorphic initial state (the set of initial states is the same between both figures). The black curve shows the region of steady states for each selection function: the diagonal $x + y = 0$ for Fig. 1.8a and the hyperbola $xy = 1$ for Fig. 1.8b. These two figures highlight the importance of a model and an analysis that can apply for various selection functions, as trajectories and steady states can be radically different from one particular to another.

Indeed, we dispose of the strong convergence $\varepsilon \log\left(\rho_\varepsilon^X\right) \to u_\varepsilon^X$ (subsequent to knowing that u^X and u^Y exist, from the first points of Section 1.3.4). The advantage of considering (1.83) reports the difficulty that the reproduction integral term in (P_{u_ε}) represents on the selection terms instead. However, the limit equations (1.82) is nonetheless suffering from a lack of regularity w.r.t the time t to be able to be differentiated into a PDE, due to the weakly defined measures ϕ^X and ϕ^Y, which are additional limit objects that are typically not present in asexual studies mentioned above. The lack of regularity is quite handicapping to pursue further analysis without assuming some additional regularity assumptions.

4. Monomorphic trajectories Consequently, under additional regularity assumptions, other results related to monomorphic trajectories in the population can be derived (the support of $n(t,\cdot,\cdot)$ is limited to only one pair $(\bar{x}(t), \bar{y}(t))$). If the selection is monotonic on the allelic space (directional selection), then the limit measure is a (moving) Dirac mass at all times (akin to [Perthame and Barles 2008]). Furthermore, when monomorphism is guaranteed, we derive the canonical equations describing the motion of the dominant alleles $(\bar{x}(t), \bar{y}(t))$. We illustrate the value of these equations by explicitly deriving those trajectories for various selection functions (in agreement with numerical resolutions), which indicates the variety of trajectories that can be obtained depending on the selection function and the initial state (see Fig. 1.8).

1.3.5 Annex: Short volunteer modelling project of the COVID-19 epidemic in Mayotte (early May 2020)

Context and motivation of the project. On the 11th of March 2020, the World Health Organization (WHO) assessed that the COVID-19 epidemic spreading around the globe had reached the pandemic stage. As public policies were considering extremely stringent measures to contain the first wave of the epidemic, modelling efforts sparked worldwide to try to provide some guiding elements. The academic platform of MODCOV19 was created to coordinate and support this effort in France. Through the intermediary of Amandine Véber (a member of MODCOV19), Vincent Calvez was put in contact with Julien Balicchi of the Regional Health Agency of Mayotte (ARS) in mid-April 2020.

The aim was to extend a first epidemiological model built in collaboration with a mathematician from the Centre Universitaire de Mayotte to account for the influence of the particular age structure of Mayotte's population on the trajectory of the COVID-19 epidemic wave that was unfolding there since mid-March 2020 (according to the reports at the time). Indeed, Mayotte is one of the French departments with the highest fecundity (over 4) and with over half of its total population under 20 (UN 2019 - per comparison, the same age class in the whole French population represents under 25 percent of the total French population). As studies were starting to be published showing large discrepancies of susceptibility to infection by COVID-19 with regard to age (Davies et al. 2020), it seemed relevant to include the demographic structure of Mayotte in the existing epidemiological model, in order to assess in particular how the reopening of school, forecasted to be on the 18th of May 2020, would impact the course of the epidemic and translate into severe cases, as requested by the ARS. The head of the ARS of Mayotte was forecasted to speak about the potential impact of this measure at the French Parliament during the week of the 11th of May 2020. Mete Demircigil and myself joined this short volunteer modelling project on the 5th of May 2020.

Description of my contribution to the project The annex at the end of my thesis presents the part of this short project to which I dedicated myself from the 5th of May to the 11th of May 2020, under the supervision of V. Calvez and in collaboration with the ARS of Mayotte. My first task was to dive into the scientific literature on the COVID-19 epidemic to reduce the number of parameter values of the age-structured model to be estimated, and next to implement this model into a Python code in order to give some quantitative predictions about the effect of school's reopening on the incidence level. The complementary part of the project, conducted by M. Demircigil and V. Calvez, was to analyse the hospitalizations and ICU data provided by the ARS of Mayotte and translate the dynamics of the age-specific incidence output of the Python code into age-specific dynamics of hospitalizations and ICU cases.

The numerical work that I did is based on a classical age-structured epidemiological model (Diekmann, Heesterbeek, and Britton 2013) which takes into account the particular age structure of Mayotte's population (UN 2019), with age-specific epidemiological parameters taken from studies done in well-known epidemiological groups (Davies et al. 2020; Nishiura, Linton, and Akhmetzhanov 2020; Li et al. 2020) and an age-structured contact matrix specific to Mayotte inspired by [Prem, Cook, and Jit 2017], stratified into different locations (school, home, work, others) which allows to investigate the effects of different public policies (confinement, school closing/reopening, remote working).

Outcomes The report and the figures obtained by simulations presented in the annex at the end of my PhD were provided to the ARS of Mayotte on the 11th of May 2020, as well as projections of hospitalizations and ICU cases estimated from the incidence output from the simulations described in this report. The head of the ARS of Mayotte communicated part of this report to the French Parliament and the presidential office. The schools reopening in Mayotte got delayed by a week, to the 25th of May 2020.

Conclusion I want to address a number of caveats surrounding this project, mainly due to the short time available (a week) to develop it from scratch to results and the relative inexperience of epidemiological models that I personally had at the start (I knew of age-structured epidemiological models without any real experience of working with them). Moreover, in May 2020, the epidemiological characteristics of the COVID-19 were not as well understood as nowadays (two years after) and were still under intense investigation, which produced a fast-growing vast literature that I had to navigate quickly, without prior knowledge of it. More in-depth sensitivity analyses and a better tuned statistical inference of some parameters w.r.t the incidence data were in particular lacking (although I investigated numerically a scenario assuming that the incidence data provided by the ARS were only reflecting a fraction of the total cases during the first month).

After this intense period in early May 2020, my involvement in the more global project decreased progressively as I focused on my main PhD projects, especially after I transferred the Python codes to Benoît Fabrèges (research engineer at the ICJ). B. Fabrèges joined the project in June 2020 and implemented a more robust statistical inference scheme of the initial parameters, in particular the date of the first imported case (the best estimation indicates that it occurred in February 2020, three weeks earlier compared to the date indicated to us by the ARS and used in this whole report). The global modelling project of the COVID-19 epidemic in Mayotte continued and was aiming at expand the model to explore among other features the effect of spatial heterogeneity, new variants and recontaminations in collaboration with the ARS of Mayotte. It motivated a serology study conducted by the ARS in Mayotte during the summer of 2021. I also punctually worked again for the global project of epidemic modelling in Mayotte in February 2021, to extend the age-structured model and the Python code to account for the variant Beta.

1.4 Perspectives

1. Emergence of major gene responses to local maladaptation. More fundamentally than the maintenance of major alleles responses to maladaptation in heterogeneous environments studied in [Dekens, Otto, and Calvez 2021], what are the biological conditions for such strong effects to emerge in the first place? Being able to analytically predict their rise is crucial, for example in the struggle against the evolution of resistance. In [Yeaman and Whitlock 2011], the authors explore the emergence of tightly linked alleles with strong effects as a consequence of an increase of migration between two habitats selecting toward different optima, through numerical simulations. However, this phenomenon is analytically challenging to study from the point of view of population genetic models (without strong limiting assumptions). Extending the framework of [Dekens, Otto, and Calvez 2021], I plan to build an integro-differential quantitative genetic model which enables to analytically capture and quantify this phenomenon. This requires to study an intricate inheritance process, which allows mutations to accumulate at a major locus with effect denoted $\eta \in \mathbb{R}$ while also encoding

the inheritance of an unlinked quantitative component $z \in \mathbb{R}$ (additive contribution of a large number of small effect loci), which reads on the offspring's variables $(\mathcal{Z}, \mathcal{E})$

$$\begin{aligned}(\mathcal{Z}, \mathcal{E}))|\left\{(\mathcal{Z}_1, \mathcal{E}_1) = (z_1, \eta_1), (\mathcal{Z}_2, \mathcal{E}_2) = (z_2, \eta_2)\right\} \\ \sim \left(\mathcal{N}\left(\frac{z_1 + z_2}{2}, \sigma_S^2\right), \mathcal{X}\mathcal{M}(\eta_1, V_M) + (1 - \mathcal{X})\mathcal{M}(\eta_2, V_M)\right),\end{aligned} \tag{1.84}$$

where $\mathcal{N}\left(\frac{z_1+z_2}{2}, \sigma_S^2\right)$ is a normal law of center the mean parental quantitative component and of variance σ_S^2, $\mathcal{X}$ is a Bernoulli law of parameter $\frac{1}{2}$ and $\mathcal{M}(\eta_i, V_M)$ is a mutation law with kernel K centered on the parental major allele η_i and of variance V_M. Note that if $\mathcal{M}(\eta_i, V_M)$ is replaced by a Dirac mass centered in η_i, then (1.84) reduces to the inheritance process where the major effect alleles are fixed (underlying the hybrid reproduction operator (1.64) of Dekens, Otto, and Calvez 2021). The inheritance process described in (1.84) translates into a collision-convolution reproduction operator $\tilde{\mathcal{B}}$ which extends the hybrid reproduction operator (1.64) to also include the non-local mutation operator (1.7)

$$\tilde{\mathcal{B}}(f)(z, \eta) = \frac{1}{\sqrt{\pi}\sigma} \int_{\mathbb{R}^3} \exp\left[\frac{-(z - \frac{z_1+z_2}{2})^2}{\sigma^2}\right] f(z_1, \eta_1) \frac{\int_{\mathbb{R}} K\left(\frac{\eta - \eta_2}{V_M}\right) f(z_2, \eta_2) d\eta_2}{\int_{\mathbb{R}^2} f(z', \eta') dz' d\eta'} dz_1 dz_2 d\eta_1. \tag{1.85}$$

Moreover, for each individual, the quantitative component z and the major effect allele η contribute additively to the trait under selection $\zeta = z + \eta$.

On the one hand, one can expect that if the mutational variance V_M of the focal major effect locus is small in a certain sense compared to the σ^2 the accumulation of mutations at the particular locus might not be significant on the timescale of adaptation. At the limit, the mutation law would be a Dirac mass (no mutations) and (1.85) would reduce to (1.64). On the other hand, if V_M is large in a certain sense compared to σ^2, then one would expect the major alleles to quickly adapt to match the local optima before the quantitative component can provoke the loss of one major allele.

Preliminary calculus suggests that, between solely major effects responses or solely polygenic responses to local adaptation, non-trivial hybrid dynamics can arise from a balance between the mutational variance of the major effect and the segregational variance of the polygenic background.

2. Evolutionary tipping points (ETP). Under climate deregulation, many ecosystems are expected to see their environmental conditions shift. Recent studies have shown that this environmental change can interact with existing feedback loop between the ecology and the evolution of a species and result in its abrupt extinction (Osmond and Klausmeier 2017, Cotto et al. 2019). Increasing our knowledge about the conditions that facilitate these sudden extinctions and the signs to detect them is urgent and necessary in face of further climate deregulation of ecosystems. For example, can ETP result from the fragmentation of environments? Answering analytically this question is challenging because, as pointed in [Osmond and Klausmeier 2017] and [Cotto et al. 2019], it requires a fine understanding of the different of stability of co-existing equilibria in the focal system. In the context of patchy environment, the stability analysis has been performed in [Dekens 2022] explicitly, and hints that under an environmental shift, spatially heterogeneous environments can indeed create conditions for ETP to occur. My goal is to derive quantitative results that will deepen the understanding of the theoretical conditions under which ETP arise.

3. Mutation-selection models for quantitative alleles under sexual reproduction. What are the conditions under which evolution of gene regulation leads to silencing a gene? The complex evolutionary dynamics displayed in the numerical simulations of [Lenormand, Fyon, et al. 2020] to investigate this phenomenon highlight the need for proposing mutation-selection models for quantitative alleles to isolate the separate influence of different mechanisms. For example, when considering two loci controlling the level expression of a gene under stabilizing selection, a two-step phenomenon can arise when the mutational variances at both loci differ. First, the dominant couple of allelic effect $(\bar{x}, \bar{y})$ converges toward a point of the manifold of optimal fitness. Next, due to asymmetrical mutations between the two loci, it can slide along this manifold. I aim to provide quantitative predictions on this phenomenon, through the study of a quantitative alleles model that extends the one introduced in Section 1.3.4 to allow for mutations to accumulate, first at one of the two loci, at rate p. Using the non-local mutational operator (1.7), with the mutational kernel K_ε^x with small variance ε, the corresponding reproduction operator reads

$$\mathcal{B}_\varepsilon^{\mathrm{Mut},x}(n_\varepsilon)(x,y) = \frac{p}{2}\left[\frac{\rho^X(y)(K_\varepsilon^x * \rho_\varepsilon^Y)(x)}{\rho_\varepsilon} + K_\varepsilon^x * [n_\varepsilon(\cdot, y)](x)\right] + \frac{1-p}{2}\left[\frac{\rho_\varepsilon^Y(x)\,\rho_\varepsilon^X(y)}{\rho_\varepsilon} + n_\varepsilon(x,y)\right].$$

Preliminary calculus indicate that the WKB ansatz converges toward the viscosity solution of a constrained Hamilton-Jacobi equation and that further regularity challenges arise.

4. Interplay between inbreeding, genetic drift and expansion load in range expansions. How does expansion load (the accumulation of deleterious mutations along the expansion) affect the speed of range expansions and what is its interplay with reproduction modes? According to numerical studies, the long-term effects of expansion load can be dramatic for invasions (Peischl, Kirkpatrick, and Excoffier 2015). A recent stochastic study by [Foutel-Rodier and Etheridge 2020] highlights the role of Mueller's ratchet and genetic drift to enhance expansion load in asexually reproducing populations. However, a quantitative understanding of the phenomena for sexual populations is lacking and challenging, because inbreeding, eroding the segregational variance, is likely to also influence how strong the expansion load might be. To quantitatively investigate this, I plan to build an agent-based model combining the stochastic IM (Barton, Etheridge, and Véber 2017) with the stepping-stone model. I will start by conducting simulations to apprehend the correlation between probability of identity and space for a neutral trait. Later, extensions to the spatial λ-Fleming Viot process (Barton, Etheridge, and Véber 2013) will be considered.

5. Assortative mating and speciation. I am interested in adding an effect of assortative mating to the infinitesimal model, to explore the dynamics of sympatric speciation due to mate's choice (Jiang, Bolnick, and Kirkpatrick 2013). Several quantitative genetic models have been studied to improve the analytical understanding of parapatric speciation w.r.t. mates' choice (Sachdeva and Barton 2017), and of the benefit that assortative mating w.r.t flowering time confers to help keeping pace with climate change (Godineau, Ronce, and Devaux 2021). The assortment of mates I propose here takes a different form corresponding to *postzygotic isolation*, modelled by a loss of fecundity that is function of the distance between the mates' traits encoded by a Gaussian kernel of variance σ_{AM}^2

$$\mathcal{B}^{AM}[n](z) = \iint_{\mathbb{R}^2} G_{0,\sigma_{AM}^2}(z_1 - z_2)\, G_{0,\sigma_S^2}\left(z - \frac{z_1+z_2}{2}\right) n(z_1)\, \frac{n(z_2)}{\int_{\mathbb{R}} n(z')dz'}\, dz_1\, dz_2.$$

The last operator combines collision (IM with segregational variance σ_S^2) and attraction effects (assortative mating). In the regime of small variance and under the balancing condition $\sigma_{AM}^2 = 4\sigma_S^2$, I could characterize the leading order term in the Hopf-Cole ansatz by means of convexity analysis, which is a promising first step. In contrast with previous studies reported in this manuscript, the leading order term is not a simple quadratic function (as in Calvez, Garnier, and Patout 2019; Patout 2020; Dekens 2022; Dekens, Otto, and Calvez 2021), but the minimum of several quadratic functions, allowing for co-existence of multiple dominant traits in the population. My goal is to derive the analytical conditions under which speciation occurs.

Last epistemological thought on the potential influence of eugenics on current mathematical modelling of evolution. Throughout the 20th century, the theory of evolution has been instrumentalized worldwide to justify multiple genocides including, but not restricted to, the well-documented practices of the Nazi regime in Germany before and during World War II, partly inspired by compulsory sterilization programs carried out in several states of the United States of America from the beginning of the 20th century (see p. 69 of Zuberi 2001), targeting (at least) African-American and Latina women at that time (see p. 90 of Solinger 2005). However, this horrendous weaponization of evolutionary theory did not appear out of thin air. It took roots, directly and indirectly, in the development of the *eugenics* school of thought. This was initiated by Francis Galton in the last decades of the 19th century, and later sustained by contributions of eminent academics, such as Karl Pearson and Ronald Fisher.

Francis Galton, Ronald Fisher and Karl Pearson all hold in common their pioneering contributions to a rich array of statistical tools which are widely used today, in the field of evolutionary biology and many others. Moreover, Fisher is considered as a founding father of modern evolutionary biology, due to the advances in the mathematical understanding of evolution that his work provided. Because of the vast scope of their research, we must also be aware of their role as founders and strong promoters of modern *eugenics*, the belief that it should be aimed to improve the genetic background of the human species

> "*[...] the science of improving stock, which is by no means confined to questions of judicious mating, but which, especially in the case of man, takes cognisance of all influences that tend in however remote a degree to give to the more suitable races or strains of blood a better chance of prevailing speedily over the less suitable than they otherwise would have had.*" (p. 24 of Galton 1883).

Francis Galton in particular was convinced that mental and intellectual abilities were inherited genetically, and included so-called characteristics as "feeblemindness" and "criminal nature"

> "*The perpetuation of the criminal class by heredity is a question difficult to grapple with on many accounts. Their vagrant habits, their illegitimate unions, and extreme untruthfulness, are among the difficulties of the investigation. It is, however, easy to show that the criminal nature tends to be inherited* " (p. 82 of Galton 1883).

Pearson, Galton's protégé, founded the Galton Laboratory of Eugenics in 1904, which edited the Annals of Eugenics from 1924 onward. In the two first issues, Pearson is co-author of a repulsing study (personal opinion) titled "*The Problem of Alien Immigration into Great Britain, illustrated by an examination of Russian and Polish Jewish Children*", whose conclusion after many varied physical measurements and intellectual tests is that "*Taken on the average, and regarding both sexes, this alien Jewish population is somewhat inferior physically and mentally to the*

native population" (Part II of this study). There is some argument over the extent of these individual's roles in promoting eugenics and it's influence on their scientific contributions. Ronald Fisher was the successor of Karl Pearson as head of the Galton Laboratory of Eugenics from 1933 to 1943. He opposed the 1952 Unesco statement about "The Race Question" (this topic was prompted by the weaponization of such notion to justify a genocidal agenda, particularly in the aftermath of the Nazi regime), because "*he believes that human groups differ profoundly "in their innate capacity for intellectual and emotional development"*" (p. 27 of the 1952 Unesco Statement). Conceding that it does not appear favorable in light of knowing that Fisher had "*previously viewed human value in terms of capacity for intellectual development*", the authors of [Bodmer et al. 2021] (all indicated as trustes of the Fisher Memorial Trust) seem to claim that this comment and more broadly the view of Fisher on eugenics should be read as reflections of societal paradigm of the time and are merely anecdotal in comparison to his enormous contribution to modern evolutionary biology and statistics.

However, one would argue precisely that Fisher's eugenics beliefs should be considered in concert with his lasting founding contributions to evolutionary theory, in particular to its mathematical modelling. This is because, while it is unreasonable to think that eugenics beliefs have tainted the mathematical quality of Fisher's reasoning, one still have to entertain the possibility that they have oriented the choices made when building his mathematical models. For example, Marcus Feldman explains in a 2017 interview with Quanta Magazine (*Finding the Actions That Alter Evolution*, by E. Svoboda)

> *"The modern synthesis developed in the 1930s and 1940s and basically had finished by the 1950s. At that time, little was known about the molecular biology of development — how what's going on in the development process itself influences what can happen to the evolutionary trajectory of cells and organisms. Although some of its originators were interested in behavior, many were steeped in the eugenics tradition. They would have thought that the majority of behaviors were determined by genes. The inclusion of other forms of inheritance totally changes evolutionary dynamics."*

This belief that "*the majority of behaviours were determined by genes*" is neither innocent, nor inconsequential on subsequent models. Indeed, all mathematical models require some initial choices of idealized framework and hypotheses if one is to hope to highlight a precise phenomenon related to the considered *research question*, which in turn can be influenced by personal beliefs or aims. One concrete example is the modelling of adaptation to (i) an optimal trait in a well-mixed population characterized by (ii) an entirely heritable quantitative trait, a very classical model of quantitative genetics. The range of analytical results that can be found is constrained by this initial modelling choice of considering a single optimum to which the population can or cannot adapt, and the assumption that inheritance of the quantitative trait underlying adaptation does not depend on, for instance, environmental factors.

These two modelling choices are not anecdotal, as they are quite frequent in mathematical models of evolution: throughout my PhD, I used both of them to some extent. From a mathematical viewpoint, there is an obvious reason for the recurrence of these modelling choices: complexifying these initial modelling hypothesis a priori decreases the prospect of conducting a full analysis. However, another reason exists in the background: the inertia of the academic paradigm, which is influenced to some degree by its foundation, which traces back, among a few others, to Fisher. Being aware of Fisher's eugenics beliefs, I want to question the following: What is the influence of eugenics on the current modelling choices made in mathematical studies of evolution of species, and how limiting is it (first and foremost, in my own work)? To assess this, I will first extend my knowledge about already existing

established theories , like cultural inheritance of phenotypes (Cavalli-Sforza and Feldman 1973) or niche construction (Laland, Odling-Smee, and Feldman 2003). I also plan to work even closer with biologists and with biological data providing actual new insights on the different influencing forces shaping the eco-evolutionary patterns of real-world species to ground my future research. Note that even nowadays, the question of whether the current theory of evolution allows to accurately model other forms of inheritance than genetic is debated among prominent evolutionary biologists (Laland, Uller, et al. 2014). Finally this question about the influence of eugenics on current mathematical modelling of evolution also connects with a recent work which deciphers how eugenic foundations have narrowed the lenses on key concepts of the theory of evolution (Branch et al. 2022).

It is of concern to me first because of the historical role of eugenics in weaponizing evolutionary theory toward systemic oppression (as discussed above). Moreover, the later is not precluded to the past and did not disappear with the Nuremberg trials and the end of WWII. Despite post-war institutions and academic journals changing names, which reflects a shift in paradigm (for instance, the Annals of Eugenics founded by Pearson became the Annals of Human Genetics in 1954), Angela Saini highlights in her excellent book (personal opinion) *Superior: the Return of Race Science* the current comeback/persistence of eugenics ideas in some science and institutions niches promoting white supremacy, as for instance the Pioneer fund and the academic journal "Mankind Quaterly" (Saini 2019).

Chapter 2

Evolutionary dynamics of complex traits in sexual populations in a heterogeneous environment: how normal?

2.1 Introduction

Most species occupy heterogeneous environments, in which the spatial structure is expected to play a significant role in the evolution of the diversity of a species. As a result of the balance between the mixing effect of migration connecting the different habitats of a species and the selective pressure reducing diversity within each habitat, several equilibrium states encoding the local adaptation of a species can be reached. Will the species succeed to persist in a wide range of habitat available and thus thrive as a generalist species? Will it become adapted to specific sets of conditions as what we call a specialist species? Evolutionary biology fields have taken a sustained interest in these questions, in population genetics (Lythgoe 1997; Nagylaki and Lou 2001; Bürger and Akerman 2011; Akerman and Bürger 2014), adaptive dynamics (Meszéna, Czibula, and Geritz 1997; Day 2000) or quantitative genetics (Tufto 2000; Ronce and Kirkpatrick 2001; Hendry, Day, and Taylor 2001; Yeaman and Guillaume 2009; Débarre, Ronce, and Gandon 2013; Débarre, Yeaman, and Guillaume 2015; Mirrahimi 2017; Lavigne et al. 2020; Mirrahimi and Gandon 2020). Here we adopt the framework of quantitative genetics, which models the adaptation of a continuous trait without giving explicitly its underlying genetic architecture. Additionally, we specifically choose to analyse the influence of sexual reproduction as mating system.

Model. We build our model within a biological framework shared with classical studies (Ronce and Kirkpatrick 2001; Hendry, Day, and Taylor 2001; Débarre, Ronce, and Gandon 2013). We consider a sexual population whose individuals are characterized by a quantitative phenotypic trait $\boldsymbol{z} \in \mathbb{R}$ and evolving in a heterogeneous environment constituted by two habitats that we will assume to be symmetric (i.e, sharing the same ecological parameters except for their optimal traits), as illustrated in Fig. 2.1.

The density of population at a given time $\boldsymbol{t}$ with respect to a phenotype $\boldsymbol{z}$ in habitat $i \in \{1, 2\}$ is denoted $\boldsymbol{n_i(t, z)} \in L^1(\mathbb{R}_+ \times \mathbb{R})$, for which we further assume that $\boldsymbol{z}^k \boldsymbol{n_i(t, z)} \in L^1(\mathbb{R}_+ \times \mathbb{R})$ for $k < 4$.

Local maladaptation is the source of mortality in our model: stabilizing selection acts

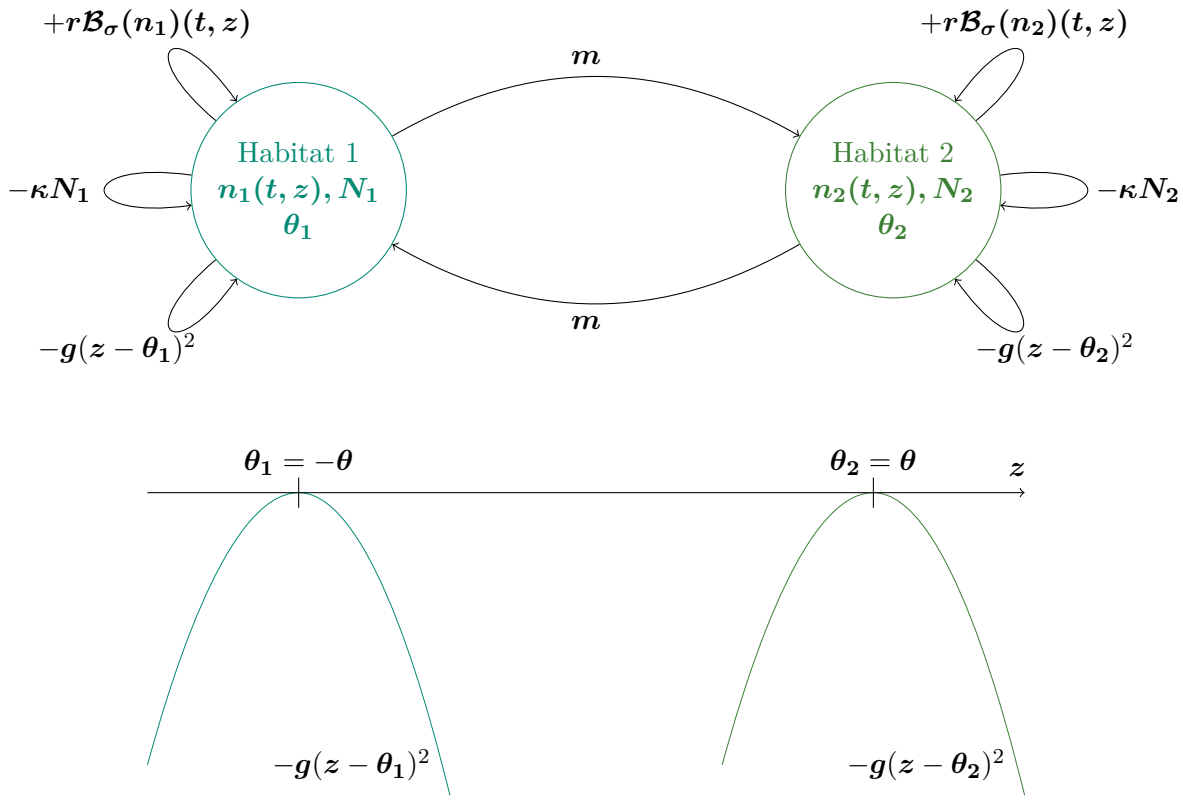

Figure 2.1: **Heterogeneous symmetrical environment framework for a quantitative trait z.** The upper part of the figure illustrates the different biological forces acting in each habitat (reproduction, competition for resources, selection) and between them (migration). The lower part of the figure draws the local quadratic selection functions considered, where θ_1 and θ_2 are the local optimal traits. The parameters are the same in both habitats, except for the local optimal traits.

quadratically in each patch toward an optimal phenotype $\theta_i \in \mathbb{R}$ with an intensity $g > 0$. Define θ as half the distance between the two local optima: $\theta := \frac{|\theta_2 - \theta_1|}{2}$. Up to a translation in the phenotypic space, we can consider without loss of generality that $0 < \theta_2 = -\theta_1 = \theta$. Additionally, competition for resources regulates the total size of the subpopulation $N_i(t) = \int_{\mathbb{R}} n_i(t, z')\, dz'$ in each patch with an intensity $\kappa > 0$. The mortality rate of an individual with phenotypic trait $z \in \mathbb{R}$ is thus given by:

$$M[n_i(t,z)] = -g(z-\theta_i)^2 - \kappa N_i.$$

Migration between the two patches occurs symmetrically at a rate $m > 0$. The exchange of individuals from patch i to patch j of a given phenotype $z \in \mathbb{R}$ at time $t \geq 0$ is thereby:

$$m\left(n_j(t,z) - n_i(t,z)\right).$$

Finally, we denote by $\mathcal{B}_\sigma(n_i)(t,z)$ the number of new individuals that are born at time $t \geq 0$ in patch i with a phenotype $z \in \mathbb{R}$ due to sexual reproduction. That phenomenon is occurring at a rate $r > 0$, and the parameter σ is a measure of the segregational variance linked to the trait inheritance process. The sexual reproduction operator is at this point still

unspecified and will be defined below. However, we will consider that it respects the following conservative properties :

$$\forall t \in \mathbb{R}_+, \int_{\mathbb{R}} \mathcal{B}_{\sigma}(n_i)(t,z)\,dz = \int_{\mathbb{R}} n_i(t,z)\,dz, \quad \int_{\mathbb{R}} z\mathcal{B}_{\sigma}(n_i)(t,z)\,dz = \int_{\mathbb{R}} z\,n_i(t,z)\,dz.$$

The dynamics of the local trait distributions are therefore given by:

$$\begin{cases} \frac{\partial n_1}{\partial t}(t,z) = r\mathcal{B}_{\sigma}(n_1)(t,z) - g(z-\theta_1)^2 n_1(t,z) - \kappa N_1(t) n_1(t,z) + m\left(n_2(t,z) - n_1(t,z)\right), \\ \frac{\partial n_2}{\partial t}(t,z) = r\mathcal{B}_{\sigma}(n_2)(t,z) - g(z-\theta_2)^2 n_2(t,z) - \kappa N_2(t) n_2(t,z) + m\left(n_1(t,z) - n_2(t,z)\right). \end{cases} \tag{2.1}$$

System of moments and gaussian assumption. Quantitative genetics studies often model the dynamics of the sizes of the subpopulations $N_1 > 0$ and $N_2 > 0$ and their mean traits $\overline{z}_1$ and $\overline{z}_2$ (where $N_i := \int_{\mathbb{R}} n_i(t,z)\,dz$ and $\overline{z}_i := \frac{1}{N_i}\int_{\mathbb{R}} z\,n_i(t,z)\,dz$). Although we intend to follow the dynamics of the whole trait distributions, for the sake of comparison, we derive ordinary differential equations for the first moments of the trait distributions by integrating (2.1) with regard to z:

$$\begin{cases} \frac{dN_i}{dt} = \left[r - \kappa N_i(t) - g(\overline{z}_i(t) - \theta_i)^2 - g{\sigma_i}^2\right] N_i(t) + m(N_j(t) - N_i(t)), \\ \frac{d\overline{z}_i}{dt} = 2{\sigma_i}^2 g(\theta_i - \overline{z}_i(t)) - g\psi_i^3 + m\frac{N_j(t)}{N_i(t}(\overline{z}_j(t) - \overline{z}_i(t)). \end{cases} \tag{2.2}$$

where ${\sigma_i}^2 := \frac{1}{N_i}\int_{\mathbb{R}}(z-\overline{z_i})^2\,n_i(t,z)\,dz$ and ${\psi_i}^3 := \int_{\mathbb{R}}\frac{1}{N_i}\int(z-\overline{z_i})^3\,n_i(t,z)\,dz$ are respectively the variance and the third central moment of the trait distribution of each subpopulation (see Appendix 2.A for details about the derivation). At this point, a common key assumption used to close the system that arises in quantitative genetics models is the normality of such a trait distribution, with a constant variance (Hendry, Day, and Taylor 2001; Ronce and Kirkpatrick 2001). In Ronce and Kirkpatrick 2001, such an assumption results in the following system (with their original notations for the parameters):

$$\begin{cases} \frac{dN_i}{dt} = \left[r_0(1 - \frac{N_i}{K}) - \frac{\gamma}{2}{\sigma_p}^2 - \frac{\gamma}{2}(\overline{z_i} - \theta_i)^2\right] N_i + m(N_j - N_i), \\ \frac{d\overline{z_i}}{dt} = {\sigma_g}^2\gamma(\theta_i - \overline{z_i}) + m\frac{N_j}{N_i}(\overline{z_j} - \overline{z_i}). \end{cases}$$

where ${\sigma_p}^2$ and ${\sigma_g}^2$ are respectively the constant phenotypic and genotypic variance, differing additively by a constant variance due to environmental effects ${\sigma_e}^2$ (${\sigma_p}^2 = {\sigma_g}^2 + {\sigma_e}^2$). With this method, the authors of Ronce and Kirkpatrick 2001 analyse the equilibria of the system above, by distinguishing two types of equilibrium:

- symmetrical equilibrium, where both local populations have equal size and are equally maladapted to their local habitat. The species survives in both habitats, and is therefore characterized as a generalist species. The authors derived this equilibrium analytically.
- asymmetrical equilibria, where the species mainly inhabits one habitat to which it is adapted. It acts as a source for the other habitat that is almost deserted, if it were not for a few unsuccessful migrants, sent from the first habitat, and therefore poorly adapted to the second one (the sink). This type of equilibrium characterizes a specialist species, that can only live in a restricted set of environments . The authors numerically explored this type of equilibrium and derived approximations for low migration rates.

However, this approach disregards the effect of higher moments of the trait distribution (like the skewness), that may become significant due to the presence of gene flow, as pointed out in Yeaman and Guillaume 2009 and Débarre, Yeaman, and Guillaume 2015.

The infinitesimal model of sexual reproduction. To account for the influence of higher moments calls for models bypassing any prior assumption on the trait distribution, both to assess the validity of the Gaussian approximation or examine the departure from it. Therefore, it is necessary to make explicit the interplay between sexual reproduction and phenotypic inheritance. The infinitesimal model of sexual reproduction, first introduced by R.Fisher in 1919 (Fisher 1919) offers a simple way to tackle this issue for complex traits. Consequently, it has been used both in several biological studies (under truncation selection in Turelli and Barton 1994, or in a continent-island model in Tufto 2000) and mathematical ones (Mirrahimi and Raoul 2013; Bourgeron et al. 2017; Raoul 2017). Aligning with these, we choose it in our study to model trait inheritance due to sexual reproduction. The classical version of this model translates the stochasticity of the segregation process by the fact that the offspring trait variable $\boldsymbol{\mathcal{Z}}$ (conditioned to the parental traits $\boldsymbol{\mathcal{Z}_1} = \boldsymbol{z_1}$ and $\boldsymbol{\mathcal{Z}_2} = \boldsymbol{z_2}$) follows a Gaussian law centered in the mean parental trait and with a segregational variance of $\frac{\boldsymbol{\sigma}^2}{2}$:

$$\boldsymbol{\mathcal{Z}} | \{ \boldsymbol{\mathcal{Z}_1} = \boldsymbol{z_1}, \boldsymbol{\mathcal{Z}_2} = \boldsymbol{z_2} \} \sim \frac{\boldsymbol{z_1} + \boldsymbol{z_2}}{2} + \mathcal{N}\left(0, \frac{\boldsymbol{\sigma}^2}{2}\right). \tag{2.3}$$

Consequently, this model makes a normal assumption, not on the distribution of trait in the population, but on the distribution of offspring within each family, with a fixed and constant segregational variance (Turelli 2017). A common Mendelian interpretation of this mixing model is that the trait results from the expression of a large number of alleles with small additive effects (Fisher 1919; Bulmer 1971; Lange 1978). Recently, a rigorous framework of the use of that model in various biological contexts has been derived in Barton, Etheridge, and Véber 2017.

The regime of small variance: $\boldsymbol{\sigma^2 \ll \theta^2}$. There also has been increasing mathematical interest in developing integro-differential equations for the whole trait distribution to study qualitatively quantitative genetics models (Diekmann, Jabin, et al. 2005; Desvillettes et al. 2008). A framework introduced by Diekmann, Jabin, et al. 2005 to study asexual models in the regime of small mutations led to first rigorous results in Perthame and Barles 2008 in the context of homogeneous environment. Next, it has been extended to study spatially heterogeneous environment where asexual species evolve, like in Mirrahimi 2017 that successfully characterizes the equilibrium states by using a Hamilton-Jacobi approach in the limit of small mutations. For sexually reproducing populations, using the infinitesimal model in an asymptotic regime allowed Mirrahimi and Raoul 2013 to study invasions by phenotypically structured populations. More recently, using the infinitesimal model in a small variance regime led Garnier et al. 2022 to formally derive features of the underlying trait distribution of a population under a changing environment. Their formal derivations have next been justified in a homogeneous space framework in Calvez, Garnier, and Patout 2019. Our work aligns with these studies: our main analysis lies in the small variance regime: $\boldsymbol{\sigma^2 \ll \theta^2}$, namely when the diversity introduced by sexual reproduction is small compared to the heterogeneity of the environment (recall that $\boldsymbol{\theta} = \frac{|\boldsymbol{\theta_2} - \boldsymbol{\theta_1}|}{2}$).

Contributions. We use the infinitesimal model operator and the formalism of small segregational variance to study evolutionary dynamics of a sexually reproducing population under

stabilizing selection in a heterogeneous and symmetrical environment in an integrated model (Section 2.2). From the PDE system on the local trait distributions, we derive a system of ODE on their moments. In the particular asymptotic regime considered: $\boldsymbol{\sigma^2 \ll \theta^2}$, our ODE system approximates the one of Ronce and Kirkpatrick 2001 (Section 2.2):

$$\begin{cases} \frac{d\boldsymbol{N_i}}{dt} = \left[\boldsymbol{r} - \boldsymbol{\kappa N_i(t)} - \boldsymbol{g}(\overline{\boldsymbol{z}}_{\boldsymbol{i}}(\boldsymbol{t}) - \boldsymbol{\theta_i})^2 - \boldsymbol{g\sigma}^2\right] \boldsymbol{N_i(t)} + \boldsymbol{m}(\boldsymbol{N_j(t)} - \boldsymbol{N_i(t)}) + \mathcal{O}\left(\frac{\sigma^4}{\theta^4}\right), \\ \\ \frac{d\overline{\boldsymbol{z}}_{\boldsymbol{i}}}{dt} = 2\boldsymbol{\sigma}^2\boldsymbol{g}(\boldsymbol{\theta_i} - \overline{\boldsymbol{z}}_{\boldsymbol{i}}(\boldsymbol{t})) + \boldsymbol{m}\frac{\boldsymbol{N_j(t)}}{\boldsymbol{N_i(t)}}(\overline{\boldsymbol{z}}_{\boldsymbol{j}}(\boldsymbol{t}) - \overline{\boldsymbol{z}}_{\boldsymbol{i}}(\boldsymbol{t})) + \mathcal{O}\left(\frac{\sigma^4}{\theta^4}\right). \end{cases} \tag{2.4}$$

To support that, we provide a numerical comparison between the two models, showing their equivalence in the small variance regime, and their discrepancy when this variance becomes large (Section 2.3). By doing so, we are justifying the validity of the Gaussian assumption on local trait distributions in this small variance regime. Next, we show that, in the regime of small variance, our system of moments can be reformulated as a slow-fast system (Section 2.4), which highlights the blending force of our sexual reproduction operator that strains monomorphism to quickly emerge at the metapopulation level. The study of the corresponding unperturbed problem, with a reduced complexity, leads to the complete analytical description of the equilibria in the asymptotic regime of small variance. In particular, it gives the conditions of existence of bistable asymmetrical equilibria numerically observed by Ronce and Kirkpatrick 2001 (Section 2.5).

To put this study in a broader context, let us first recall some findings of Ronce and Kirkpatrick 2001, our reference moment-based model in the quantitative genetics field. It makes a Gaussian assumption on the local trait distributions, without specifying any particular mode of reproduction. The authors numerically found that bistable mirrored asymmetrical equilibria can exist, allowing source-sink dynamics to completely reverse after a demographical loss event. Based on their study, however, it remains unclear which hypotheses on the inheritance process allow for such dynamics to arise. More recently, two studies interested in the equilibria states of asexual populations highlight the need for precise hypotheses with regard to such conclusions. If the authors of Débarre, Ronce, and Gandon 2013 indicate that asymmetrical equilibria can be locally stable in a restrained range of mutational parameters, Mirrahimi 2017 and Mirrahimi and Gandon 2020 show through using a continuum-of-alleles model that, under broader mutational parameters, only a single stable symmetrical equilibrium can arise in a symmetrical setting. Here, we claim that we can explain the dynamics of the analysis done in Ronce and Kirkpatrick 2001 via a model on phenotypic densities dynamics, analogous to Mirrahimi 2017 and Mirrahimi and Gandon 2020 but with a sexual reproduction operator derived from the infinitesimal model and in a small segregational variance regime. We thereby make explicit the details of another mechanism that can provide with those locally bistable asymmetrical equilibria, which relies on the blending effect of the infinitesimal model in a regime of small segregational variance.

2.2 The infinitesimal model and the regime of small variance

In this section, we present the specific framework in which we choose to perform our analysis. We first present some properties of the infinitesimal model operator in general, then its relationship with the specific regime of small variance. Then, we will show that the asymptotic approximation allows us to formally derive a closed system for the dynamics of the moments.

Let us define the following rescaled variables and parameters to get a dimensionless system:

$$z := \frac{\boldsymbol{z}}{\boldsymbol{\theta}}, \quad g := \frac{\boldsymbol{g\theta^2}}{\boldsymbol{r}}, \quad m := \frac{\boldsymbol{m}}{\boldsymbol{r}}, \quad \varepsilon := \frac{\boldsymbol{\sigma}}{\boldsymbol{\theta}}, \quad t := \varepsilon^2 \boldsymbol{rt},$$

$$n_{\varepsilon,i}(t,z) := \frac{\boldsymbol{\kappa}}{\boldsymbol{r}}\, \boldsymbol{n_i(t,z)}, \quad N_{\varepsilon,i}(t) = \frac{\boldsymbol{\kappa}}{\boldsymbol{r}}\, \boldsymbol{N_i(t)},$$

and the reproduction operator $\mathcal{B}_\varepsilon(n_{\varepsilon,i})(t,z) = \boldsymbol{\mathcal{B}_\sigma(n_i)(t,z)}$. Then, (2.1) gives the rescaled system:

$$\begin{cases} \varepsilon^2 \frac{\partial n_{\varepsilon,1}}{\partial t}(t,z) = \mathcal{B}_\varepsilon(n_{\varepsilon,1})(t,z) - g(z+1)^2 n_{\varepsilon,1}(t,z) - N_{\varepsilon,1}(t) n_{\varepsilon,1}(t,z) + m\left(n_{\varepsilon,2}(t,z) - n_{\varepsilon_1}(t,z)\right), \\ \varepsilon^2 \frac{\partial n_{\varepsilon,2}}{\partial t}(t,z) = \mathcal{B}_\varepsilon(n_{\varepsilon,2})(t,z) - g(z-1)^2 n_{\varepsilon,2}(t,z) - N_{\varepsilon,2}(t) n_{\varepsilon,2}(t,z) + m\left(n_{\varepsilon,1}(t,z) - n_{\varepsilon,2}(t,z)\right). \end{cases} \tag{2.5}$$

From the remaining of this section and unless specified otherwise, we will refer to that system for all analysis purposes.

2.2.1 The sexual reproduction operator

Presentation. For modelling the segregation process resulting from sexual reproduction, we use the infinitesimal model, first introduced in Fisher 1919. It is inspired originally from the observation that the phenotypic variance among families does not seem to depend on their breeding values (Galton 1877). Although this can be formulated solely from a phenotypic perspective, Fisher 1919 gives a Mendelian interpretation by proposing to consider that the quantitative trait z results from the infinitesimally small additive effects of a large number of alleles. That interpretation, in the spirit of a central limit theorem, has been followed on (Bulmer 1971; Lange 1978; Bulmer 1980; Barton, Etheridge, and Véber 2017). It leads to (2.3). With our notations, we can express the number of individuals born at time t with trait z in habitat i by:

$$\mathcal{B}_\varepsilon(n_\varepsilon)(t,z) = \frac{1}{\sqrt{\pi}\varepsilon} \int_{\mathbb{R}^2} \exp\left[\frac{-(z - \frac{z_1+z_2}{2})^2}{\varepsilon^2}\right] n_\varepsilon(t,z_1) \frac{n_\varepsilon(t,z_2)}{N_\varepsilon(t)} dz_1 dz_2. \tag{2.6}$$

The scaled segregational variance $\frac{\varepsilon^2}{2}$ is assumed to be constant with regard to time and independent of the parental traits. These are strong biological assumptions. Their relevance in the context of a spatially structured population will be the subject of a forthcoming work.

Equilibria under random mating only. To study the behaviour of the reproduction operator (2.6), it is informative to consider the conservative case where a sexually reproducing population only experiences random mating, without any structure due to space or mating preferences:

$$\varepsilon^2 \frac{\partial n_\varepsilon}{\partial t}(t,z) = \frac{1}{\sqrt{\pi}\varepsilon} \int_{\mathbb{R}^2} \exp\left[\frac{-(z - \frac{z_1+z_2}{2})^2}{\varepsilon^2}\right] n_\varepsilon(t,z_1) \frac{n_\varepsilon(t,z_2)}{N_\varepsilon(t)} dz_1 dz_2 - n_\varepsilon(t,z), \tag{2.7}$$

(the term $-n_\varepsilon(t,z)$ is meant to keep the size of the population constant by balancing birth and death). Then, every Gaussian distribution of variance ε^2 (arbitrarily centered) is a stable distribution under (2.7) (see Appendix 2.B). Furthermore, it is shown in Raoul 2017 that

there are no other equilibrium and that the convergence toward such a Gaussian distribution is exponential in quadratic Wasserstein distance. Therefore, with this operator of sexual reproduction, a fixed and finite variance in trait at equilibrium arises under random mating only and without selection.

2.2.2 The regime of small variance: $\varepsilon^2 \ll 1$.

The framework presented in this section is inspired by a methodology developed in Diekmann, Jabin, et al. 2005 and Perthame and Barles 2008 that uses asymptotic regime in partial differential equations in order to derive analytical features of quantitative genetics models. In a regime where few diversity is introduced by reproduction at each generation, the continuous trait distributions are expected to converge toward Dirac masses concentrated on some specific traits. Performing a suitable transformation on the trait distribution allows to unfold the singularities of these Dirac masses and define more regular objects to study and calculate, in order to follow trait densities. That methodology has already been successfully applied for asexual populations, in homogeneous (Perthame and Barles 2008) and heterogeneous space (Mirrahimi 2017), then in other frameworks such as the study of adaptation to a changing environment (Garnier et al. 2022), and lately for sexual populations in homogeneous space (Calvez, Garnier, and Patout 2019). Applying a similar approach as described above, we will show that, within a regime of small variance yet to be defined, we can reduce the complexity of the system while rigorously justify that reduction.

In our context, a relative measure of diversity introduced by reproduction comes from comparing the variance of the segregation process to a measure of habitats' difference (recall that $\boldsymbol{\theta} = \frac{|\boldsymbol{\theta_2} - \boldsymbol{\theta_1}|}{2}$):

$$\frac{\boldsymbol{\sigma}^2}{\boldsymbol{\theta}^2} = \varepsilon^2.$$

One can thus define the small variance regime by $\boldsymbol{\sigma}^2 \ll \boldsymbol{\theta}^2$, or equivalently $\varepsilon^2 \ll 1$. Moreover, we perform the unfolding of singularities by shaping the traits distributions according to:

$$n_{\varepsilon,i} = \frac{1}{\sqrt{2\pi}\varepsilon} e^{-\frac{U_{\varepsilon,i}}{\varepsilon^2}}. \tag{2.8}$$

The exponential form, known as the Hopf-Cole transform in scalar conservation laws, presumes that $U_{\varepsilon,i}$ will be a more regular object to analyze when $\varepsilon^2 \ll 1$ than $n_{\varepsilon,i}$, which we expect to converge toward a sum of Dirac distributions centered at the minima of $U_{\varepsilon,i}$. In fact, Garnier et al. 2022 performed a formal analysis on the behaviour of the reproduction term in the regime of small variance under such a formalism. They found that, for the various contributions to be well-balanced in the equation (reproduction and mortality) when $\varepsilon^2 \ll 1$, $U_{\varepsilon,i}$ is formally constrained to have the following expansion with regard to successive powers of ε^2 (see Appendix 2.C):

$$U_{\varepsilon,i}(z) = \frac{(z - z_i^*)^2}{2} + \varepsilon^2 u_{\varepsilon,i}, \tag{2.9}$$

where z_i^* is a byproduct of the formal analysis and $u_{\varepsilon,i}$ is the following order term in the expansion. It leads to:

$$n_{\varepsilon,i} = \frac{1}{\sqrt{2\pi}\varepsilon} e^{-\frac{(z-z_i^*)^2}{2\varepsilon^2}} e^{-u_{\varepsilon,i}(z)}. \tag{2.10}$$

Let us interpret this formalism. For $\varepsilon^2 \ll 1$, the leading term in the expansion (2.10) is precisely the Gaussian distribution of (yet unknown) mean z_i^* and variance ε^2, namely a

distribution we know to be at equilibrium under random mating only. Only considering this term would be to assume that the trait distribution is Gaussian. As we want to capture the departure from normality, we introduce the term $u_{\varepsilon,i}$, which we can see as the next order term in the expansion of $\log(n_{\varepsilon,i})$ with regard to successive powers of ε. It embodies the correction to the Gaussian distribution due to the effect of selection, competition and migration. The study of its analytical properties is beyond the scope of this paper and will be the project of a forthcoming paper. For now, we will assume that such a limit exist and we will use it in our analysis without rigorously justifying it.

2.2.3 Derivation of the dynamics of the moments in the regime of small variance

Although our method describes directly the trait distribution, we propose to formally derive the equations describing the dynamics of the first three moments of the trait distribution from its dynamics under the small variance of segregation ($\varepsilon^2 \ll 1$) to compare our framework to other quantitative genetic studies. Toward that purpose, we define (assuming persistence of each subpopulation):

$$\begin{aligned} N_{\varepsilon,i}(t) &= \int_{\mathbb{R}} n_{\varepsilon,i}(t,z)\,dz, & \overline{z}_{\varepsilon,i}(t) &= \frac{1}{N_{\varepsilon,i}}\int_{\mathbb{R}} z\, n_{\varepsilon,i}(t,z)\,dz, \\ \sigma^2_{\varepsilon,i}(t) &= \frac{1}{N_{\varepsilon,i}}\int_{\mathbb{R}} (\overline{z}_{\varepsilon,i}-z)^2\, n_{\varepsilon,i}(t,z)\,dz, & \psi^3_{\varepsilon} &= \frac{1}{N_{\varepsilon}}\int_{\mathbb{R}} (z-\overline{z}_{\varepsilon,i})^3 n_{\varepsilon}(z)dz. \end{aligned} \tag{2.11}$$

Let us omit for a moment the time dependency. Using the expression (2.10) and under the formal assumption that $u := \lim_{\varepsilon\to 0} u_\varepsilon$ is sufficiently regular, we get the following expansions (where $v_{i,\varepsilon}$ is the expansion term of order ε^4 of $U_{\varepsilon,i}$ - see Appendix 2.D):

$$\begin{cases} N_{\varepsilon,i} = e^{-u_i(z_i^*)}\left[1+\varepsilon^2\left(\frac{\left(\partial_z u_i(z_i^*)\right)^2}{2} - \frac{\partial_{zz}u_i(z_i^*)}{2} - v_{i,\varepsilon}(z_i^*)\right)\right] + \mathcal{O}(\varepsilon^4), \\ \overline{z}_{\varepsilon,i} = z_i^* - \varepsilon^2 \partial_z u_i(z_i^*) + \mathcal{O}(\varepsilon^4), \\ \sigma^2_{\varepsilon,i} = \varepsilon^2 + \mathcal{O}(\varepsilon^4), \\ \psi^3_{\varepsilon,i} = \mathcal{O}(\varepsilon^4). \end{cases} \tag{2.12}$$

These expansions are informative, particularly the one describing the rescaled variance of the trait distribution. We can observe that it is equivalent to twice the rescaled segregational variance (which is given as a parameter of the model) when the latter is small. The local rescaled variance in trait are thereby asymptotically constant and independent of the local environment.

Now, from scaling (2.2), we obtain:

$$\begin{cases} \varepsilon^2 \frac{dN_{\varepsilon,i}}{dt} = \left[1 - N_{\varepsilon,i}(t) - g(\overline{z}_{\varepsilon,i}(t) - (-1)^i)^2 - g\,\sigma_i(t)^2\right] N_{\varepsilon,i}(t) + m\big(N_{\varepsilon,j}(t) - N_{\varepsilon,i}(t)\big), \\ \varepsilon^2 \frac{d\overline{z}_{\varepsilon,i}}{dt} = 2g\,\sigma_i(t)^2((-1)^i - \overline{z}_{\varepsilon,i}(t)) - g\,\psi_i^3(t) + m\frac{N_{\varepsilon,j}(t)}{N_{\varepsilon,i}(t)}(\overline{z}_{\varepsilon,j}(t) - \overline{z}_{\varepsilon,i}(t)). \end{cases}$$

Next, using the formal expansions of the variances and skews given by (2.12) when $\varepsilon^2 \ll 1$ yields:

$$\begin{cases} \varepsilon^2 \frac{dN_{\varepsilon,i}}{dt} = \left[1 - N_{\varepsilon,i}(t) - g(\overline{z}_{\varepsilon,i}(t) - (-1)^i)^2 - g\varepsilon^2\right] N_{\varepsilon,i}(t) + m\big(N_{\varepsilon,j}(t) - N_{\varepsilon,i}(t)\big) + \mathcal{O}(\varepsilon^4), \\ \varepsilon^2 \frac{d\overline{z}_{\varepsilon,i}}{dt} = 2\varepsilon^2 g((-1)^i - \overline{z}_{\varepsilon,i}(t)) + m\frac{N_{\varepsilon,j}(t)}{N_{\varepsilon,i}(t)}(\overline{z}_{\varepsilon,j}(t) - \overline{z}_{\varepsilon,i}(t)) + \mathcal{O}(\varepsilon^4), \end{cases} \tag{2.13}$$

which is equivalent to (2.4).

Remark 1 (Relationship between the rescaling of time and small variance regime $\varepsilon^2 \ll 1$.)**.** *The small variance regime $\boldsymbol{\sigma^2 \ll \theta^2}$ (or equivalently $\varepsilon^2 \ll 1$) considers the case where the variance introduced by reproduction is very small compared to the phenotypic gap between the two habitats (recall that $\boldsymbol{\theta} = \frac{|\boldsymbol{\theta_2} - \boldsymbol{\theta_2}|}{2}$). Therefore, it takes a very long ecological time to bridge the gap. An interpretation of that intuition can be seen in the rescaled system (2.13). The effects of the ecology (migration, population growth, death by competition and selection) are of order 1. The evolutionary effects (how selection shifts the mean traits of both subpopulations toward the local optima) are represented by the terms $2\varepsilon^2 g((-1)^i - \overline{z}_{\varepsilon,i}(t))$, and are therefore comparatively very small (of order ε^2). This discrepancy is the motivation of the change in time scales $t = \varepsilon^2 \boldsymbol{T}$ to capture the slow dynamics of the local mean traits. It is also behind the motivation for the slow-fast analysis (see Section 2.4).*

Remark 2 (Relationship between the small variance regime and the weak selection approximation.)**.** *A widespread regime studied in quantitative genetics models using the Gaussian assumption of trait distributions is the weak selection approximation. As we showed formally that the local trait distributions are well approximated by Gaussian distributions in the small variance regime (see (2.10)), it is natural to examine if the regime of small variance $\boldsymbol{\sigma^2 \ll \theta^2}$ and the weak selection approximation are equivalent.*

However, the small variance regime $\boldsymbol{\sigma^2 \ll \theta^2}$ presents an alternative that seems to differ from the weak selection approximation:

1. *Either the segregational variance $\boldsymbol{\sigma}^2$ is of order 1, and therefore $\boldsymbol{\theta}^2$ must be large, ie. the local optimal traits are far apart. However, this has an indirect consequence on the strength of selection $\boldsymbol{g}$, which must be small, since $g = \frac{\boldsymbol{g\theta}^2}{r}$ must be of order 1 to be relevant in the rescaled system (13). Nevertheless, this framework is distinct from the weak selection approximation, in the sense that the effective selection felt by an individual adapted to one patch and migrating to the other is of order $\boldsymbol{g\theta^2}$, hence of order 1.*

2. *Either the segregational variance $\boldsymbol{\sigma}^2$ is small compared to $\boldsymbol{\theta}^2$, the latter being of order 1, as well as the other parameters of the system. Therefore, in that case, the selection does not need to be weak. A way to get such a small segregational variance can be illustrated by the following with haploid individuals: suppose that we consider $\boldsymbol{L}$ loci that contribute to the focal quantitative trait additively, and that, at each locus, two alleles segregate, having opposite effects of $\pm\frac{\boldsymbol{a}}{2\sqrt{\boldsymbol{L}}}$, where $\boldsymbol{a}$ is a parameter that scales the magnitude of the effect. An estimation of the variance in the offsprings of two mates is $\hat{\boldsymbol{\sigma}}^2 = \frac{\boldsymbol{a}^2\boldsymbol{D}}{\boldsymbol{L}}$, where $\boldsymbol{D} < \boldsymbol{L}$ is the number of differences between their respective genetic backgrounds. So $\hat{\boldsymbol{\sigma}}^2 = \mathcal{O}(\boldsymbol{a}^2)$ can be uniformly small provided that the allelic effect size parameter $\boldsymbol{a}$ is small.*

2.3 Equivalence with a moment based model

2.3.1 Presentation of the moment based model

In Ronce and Kirkpatrick 2001, the authors present a quantitative genetic model to tackle the same problem: the evolutionary dynamics of a species under the effects of stabilizing selection and migration between two symmetric patches. Let us first recall the model and indicate the parameters. Stabilizing selection toward a local phenotypic optima $\boldsymbol{\theta_i} \in \mathbb{R}$ is added to competition for resources within each patch to build the fitness of an individual of phenotype $\boldsymbol{z}$ in patch i:

$$\boldsymbol{r_i}(\boldsymbol{z}) = \boldsymbol{r_0}\left(1 - \frac{\boldsymbol{N_i}}{\boldsymbol{K}}\right) - \frac{\boldsymbol{\gamma}}{2}(\boldsymbol{z} - \boldsymbol{\theta_i})^2,$$

where $\boldsymbol{r_0} > 0$ is the maximal fitness at low density, $\boldsymbol{K} > 0$ the carrying capacity of each environment (assumed to be the same in both of them), and $\boldsymbol{\gamma} > 0$ the intensity of the selection. Migration occurs symmetrically between the two patches at a rate $\boldsymbol{m} > 0$. The mode of reproduction is left unspecified, but phenotypes and breeding values are assumed to follow a Gaussian distribution within each population, of constant genetic ($\boldsymbol{\sigma_g}^2 > 0$) and phenotypic ($\boldsymbol{\sigma_p}^2 > 0$) variances, independent of the patch with:

$$\boldsymbol{\sigma_p}^2 = \boldsymbol{\sigma_g}^2 + \boldsymbol{\sigma_e}^2,$$

where $\boldsymbol{\sigma_e}^2 > 0$ is the environmental variance. The analysis is focused on the ordinary differential equation system of the first two moments of the local trait distributions (assuming persistence of each subpopulation). Namely, the sizes of the subpopulations ($\boldsymbol{N_1}, \boldsymbol{N_2}$) and the mean phenotypic traits ($\overline{\boldsymbol{z_1}}, \overline{\boldsymbol{z_2}}$):

$$\begin{cases} \frac{d\boldsymbol{N_i}}{dt} = \left[\boldsymbol{r_0}(1 - \frac{\boldsymbol{N_i}}{\boldsymbol{K}}) - \frac{\boldsymbol{\gamma}}{2}\boldsymbol{\sigma_p}^2 - \frac{\boldsymbol{\gamma}}{2}(\overline{\boldsymbol{z_i}} - \boldsymbol{\theta_i})^2\right]\boldsymbol{N_i} + \boldsymbol{m}(\boldsymbol{N_j} - \boldsymbol{N_i}), \\ \frac{d\overline{\boldsymbol{z_i}}}{dt} = \boldsymbol{\sigma_g}^2\boldsymbol{\gamma}(\boldsymbol{\theta_i} - \overline{\boldsymbol{z_i}}) + \boldsymbol{m}\frac{\boldsymbol{N_j}}{\boldsymbol{N_i}}(\overline{\boldsymbol{z_j}} - \overline{\boldsymbol{z_i}}). \end{cases} \tag{2.14}$$

2.3.2 Formal comparison

Let us consider (2.14) in the case where we neglect the additional variance due to the environment, so that all the variation in trait results from the genetic variance. We will denote this variance by $\boldsymbol{\varsigma}^2$, so that: $\boldsymbol{\sigma_p}^2 = \boldsymbol{\sigma_g}^2 := \boldsymbol{\varsigma}^2$. Then, let us also consider the equations of the trait distribution moments derived from our model (2.4), when disregarding the errors of $\mathcal{O}\left(\frac{\sigma^4}{\theta^4}\right)$. Then, the dynamics of the moments and their stationary states are equivalent under the change of parameters:

$$\boldsymbol{r} = \boldsymbol{r_0}, \quad \boldsymbol{g} = \frac{\boldsymbol{\gamma}}{2}, \quad \boldsymbol{\kappa} = \frac{\boldsymbol{r_0}}{\boldsymbol{K}}, \quad \boldsymbol{\sigma}^2 = \boldsymbol{\varsigma}^2, \quad \boldsymbol{\sigma_e} = 0. \tag{2.15}$$

This change of parameters is only possible because, in both models, the variance in trait in the subpopulations is derived from a single parameter encoding the genetic stochasticity ($\boldsymbol{\sigma_g}^2$ in Ronce and Kirkpatrick 2001 and $\boldsymbol{\sigma}^2$ in our model). Particularly, the variance is independent from the other biological parameters, which is a structural difference with asexual models (see Mirrahimi 2017).

2.3.3 Numerical comparison

In this subsection, we provide results from numerical simulations performed to confirm this formal equivalence between the stationary states of the two models under the regime of small variance in which we expect this link to hold. In these simulations, we follow two systems:

- the first one is a discretization of (2.1), where we follow the evolution of the local trait distributions $\boldsymbol{n}_i(\boldsymbol{t}, \cdot)$. We then compute at each time the sizes, mean traits and variances in trait of the subpopulations $\boldsymbol{N}_i(\boldsymbol{t})$, $\overline{\boldsymbol{z}}_i(\boldsymbol{t})$ and $\boldsymbol{\sigma}_i$. We emphasize the fact that we do not deduce $\boldsymbol{N}_i(\boldsymbol{t})$ and $\overline{\boldsymbol{z}}_i(\boldsymbol{t})$ from the system of moments (2.4).
- the second one is the system of moments (2.14) provided in the article Ronce and Kirkpatrick 2001, initialized by integration of $\boldsymbol{n}_i(0, \cdot)$. We denote the respective quantitites $\boldsymbol{N}_{i,RK}(\boldsymbol{t})$ and $\overline{\boldsymbol{z}}_{i,RK}(\boldsymbol{t})$.

We then compare the evolution of the sizes and the mean traits of the subpopulations given by both systems. We also provide the evolution of the variance and the skewness in trait in both subpopulations compared to the value of the fixed and constant variance $\boldsymbol{\sigma_g}$ and the skew null of the Gaussian approximation, for it can shed some lights on the divergence of the two systems. The results are displayed in Fig. 2.2. Details about numerical domains and schemes can be consulted in Section 2.H.

Parameters of the simulations. The value of the parameters were taken from Ronce and Kirkpatrick 2001 (the optimal phenotypes are translated without loss of generality to reduce the numbers of parameters):

$$\boldsymbol{m} = 0.1, \quad \boldsymbol{\gamma} = 0.1, \quad \boldsymbol{r_0} = 1 + \frac{\boldsymbol{\gamma}}{2}{\boldsymbol{\sigma_p}}^2, \quad \boldsymbol{K} = 2.5\,\boldsymbol{r_0}, \quad \boldsymbol{\theta} = |\frac{\boldsymbol{\theta_2} - \boldsymbol{\theta_1}}{2}| = 3.5,$$

where the value of ${\boldsymbol{\sigma_g}}^2 = {\boldsymbol{\sigma_p}}^2 = \boldsymbol{\sigma}^2$ determines completely the parameters. Two values are chosen for $\boldsymbol{\sigma}^2 = {\boldsymbol{\sigma_g}}^2 = {\boldsymbol{\sigma_p}}^2$: the first, $\boldsymbol{\sigma}^2 = 0.0025$, is set to assess the regime of small variance ($\boldsymbol{\sigma}^2 \ll \boldsymbol{\theta^2}$) in which our formal link of equivalence should hold. The second, $\boldsymbol{\sigma}^2 = 1$, comes from the value set in Ronce and Kirkpatrick 2001 and illustrates the discrepancy between the two models when not in the small variance regime.

Initial conditions. In both simulations, the initial conditions are the same, conditioned to the value of $\boldsymbol{\sigma}$, for we want to be close to the equilibrium when under random mating only and selection only, as if the two habitats were disconnected at first. We consider two populations locally adapted to their habitats, but one is a little smaller in size than the other. To do so, we set:

$$\begin{cases} \boldsymbol{n}_1(0, \boldsymbol{z}) = \frac{9}{10\boldsymbol{\kappa}} \frac{e^{-\frac{(\boldsymbol{z}+\boldsymbol{\theta})^2}{2\boldsymbol{\sigma^2}}}}{\sqrt{2\pi}\boldsymbol{\sigma}} \\ \boldsymbol{n}_2(0, \boldsymbol{z}) = \frac{1}{\boldsymbol{\kappa}} \frac{e^{-\frac{(\boldsymbol{z}-\boldsymbol{\theta})^2}{2\boldsymbol{\sigma^2}}}}{\sqrt{2\pi}\boldsymbol{\sigma}} \end{cases}$$

Results of the numerical comparison. As Fig. 2.2a and Fig. 2.2c display the dynamics of the mean traits and population size in both subpopulations in the regime of small variance ($\boldsymbol{\sigma}^2 = 0.0025$), it confirms numerically that both the model used in Ronce and Kirkpatrick 2001 and ours share similar dynamics (except maybe at initial times when the migratory

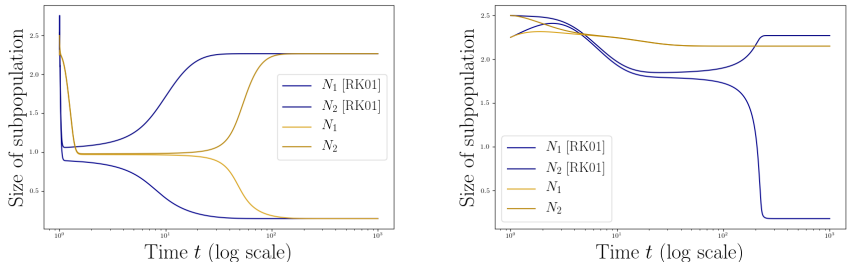

(a) Small variance $\boldsymbol{\sigma}^2 = 0.0025$ (b) $\boldsymbol{\sigma}^2 = 1$

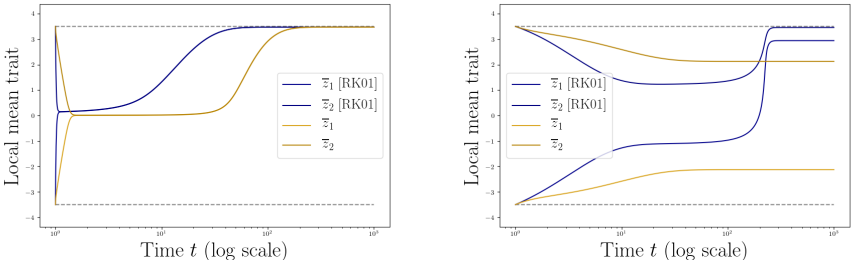

(c) Small variance $\boldsymbol{\sigma}^2 = 0.0025$ (d) $\boldsymbol{\sigma}^2 = 1$

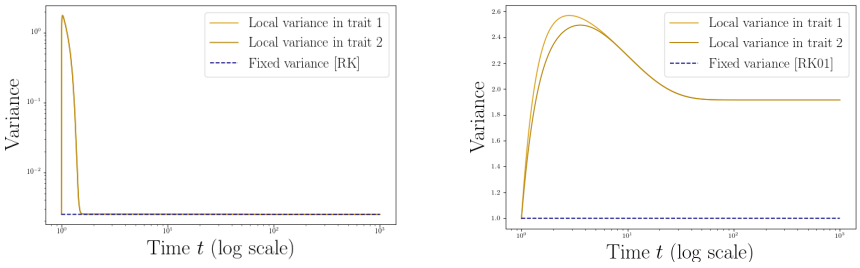

(e) Small variance $\boldsymbol{\sigma}^2 = 0.0025$ (f) $\boldsymbol{\sigma}^2 = 1$

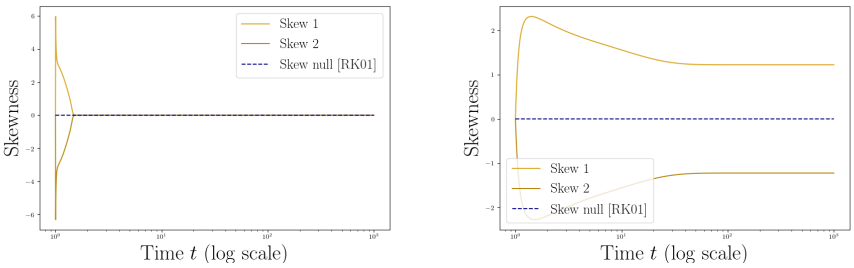

(g) Small variance $\boldsymbol{\sigma}^2 = 0.0025$ (h) $\boldsymbol{\sigma}^2 = 1$

Figure 2.2: **Numerial comparison of our model (yellow lines) with Ronce and Kirkpatrick 2001's model (blue line) in small (left panel) and large (right panel) variance regime.** All parameters are the same or given by (2.15) and initial conditions are the same for both models. The left panel shows the results in the small variance regime ($\boldsymbol{\sigma}^2 = 2.5 \times 10^{-3}$). Both models converge quickly to an asymmetrical equilibrium where both subpopulations are adapted to the second habitat ($\overline{z_1} = \overline{z_2} \approx \theta_2$). The right panel shows the results when not in the small variance regime ($\boldsymbol{\sigma}^2 = 1$): the same link of equivalence does not hold. The discrepancy can be explained by looking at the local variances and skews in trait. They are asymptotically supporting a Gaussian assumption with fixed variance on the trait distributions in the small variance regime (note the logarithmic scale for the y-axis of Fig. 2.2e), but not when the segregational variance is larger. Note the logarithmic time scale for the sake of clarity.

fluxes are transiently high). When not in this regime ($\boldsymbol{\sigma}^2 = 1$), Fig. 2.2b and Fig. 2.2d show that it does not need to be the case: the model used in Ronce and Kirkpatrick 2001 converges toward a monomorphic asymmetrical equilibrium whereas ours converges toward a dimorphic symmetrical equilibrium. The four bottom plots give an intuition of the source of this discrepancy. In the regime of small variance, we can see with Fig. 2.2e the variances in trait of the subpopulations in our model match the fixed genetical variance assumed by the gaussian approximation made in Ronce and Kirkpatrick 2001 (note the logarithmic scale for the y-axis on this figure). Moreover, Fig. 2.2g shows that the skew in both distributions are very small, as expected by our formal expansions, which makes the Gaussian approximation consistent. On the contrary, when not in the regime of small variance, Fig. 2.2f shows that the stationary variances in trait in both subpopulations derived from our model are significantly greater than the prescribed fixed variance ${\boldsymbol{\sigma_g}}^2$ of Ronce and Kirkpatrick 2001. It is also important to note that with our model, even if the variance of segregation within families is held constant, the local variances in trait (byproducts of our numerical analysis) vary over time. The presence of respectively negative and positive skews (Fig. 2.2h) for the subpopulations confirms that the gaussian approximation breaks down in this regime in our model, hence the discrepancy in the outcomes with Ronce and Kirkpatrick 2001.

The two models have their own limit. Ronce and Kirkpatrick 2001 assumes that the variance in traits is the same in both subpopulations and constant through time and disregards any skewness in the local trait distributions. Our model assumption acts on the segregation: variance in each family is constant and independent of parental traits or habitat. As a result of that discrepancy between the models, their results differ on some ranges of parameters, as the previous figures show (Fig. 2.2b, Fig. 2.2d), while they match on others (Fig. 2.2a, Fig. 2.2c). To determine the range of parameters on which each model is closer to an explicit genetic model that includes drift, individual-based simulations are to be carried. That is the prospect of future work.

For now, since we have shown that our model was equivalent to Ronce and Kirkpatrick 2001's one in the regime of small variance, we will next develop a slow-fast analysis that will reduce the complexity of the system (Section 2.4) in the limit of vanishing variance in order to complete the equilbrium analysis done in Ronce and Kirkpatrick 2001 (Section 2.5).

2.4 Slow-fast system in small variance regime

In this section, we will see that the small variance regime allows for a separation of time scales to arise, as (2.13) can be seen as a slow-fast system when $\varepsilon^2 \ll 1$. Using a singular perturbation approach similar to the one described in Levin and Levinson 1954, we will show that it converges in the limit of small variance to the following system, constrained in having $N_1^* > 0, N_2^* > 0$:

$$\begin{cases} \left[1 - N_1^* - g(z^*+1)^2 - m\right] N_1^* + mN_2^* = 0, \\ \left[1 - N_2^* - g(z^*-1)^2 - m\right] N_2^* + mN_1^* = 0, \\ \frac{dz^*}{dt} = 2g \left(\frac{\frac{N_2^*}{N_1^*} - \frac{N_1^*}{N_2^*}}{\frac{N_2^*}{N_1^*} + \frac{N_1^*}{N_2^*}} - z^* \right). \end{cases} \tag{2.16}$$

Until further notice, let us consider ourselves in the regime of small variance: $\varepsilon^2 \ll 1$.

Monomorphism in the regime of small variance. The slow-fast system reduces the complexity of the system (2.13) from four equations to three (see (2.16)), as the local

mean traits $\bar{z}_{\varepsilon,1}$ and $\bar{z}_{\varepsilon,2}$ both relax rapidly toward the same value $z^*(t)$. Since asymptotically, the mean traits in both subpopulations are the same and the local variances in trait are infinitesimally small, the metapopulation can be considered as *monomorphic* in $z^*(t)$, which we call the dominant trait.

Biological interpretation of the slow-fast analysis in terms of separation between ecological and evolutionary time scales. The limit system (2.16) highlights the separation of ecological and evolutionary time scales in the limit of small variance, seen from the evolutionary perspective. Indeed, the two first equations of (2.16) are algebraic and therefore describe an instantaneous equilibrium reached by the local population sizes N_1^* and N_2^*. This equilibrium can be seen as an ecological one, as it results from the balanced actions of birth, death and migration. It depends on the value of the trait z^*, which changes according to the last differential equation. As explained in the previous paragraph, this differential equation results from the changes in local mean traits driven by local selection (attested here by the prefactor g), weighted by the discrepancy between local population sizes. Consequently, the dynamics of z^* can be seen as evolutionary dynamics, constrained to occur on the manifold of ecological equilibrium defined by the first two equations (considered as instantaneously reached on the evolutionary time scale considered).

2.4.1 Slow-fast system formulation.

As we expect monomorphism to occur rapidly in the regime of small variance, let us operate the following change in variables:

$$\delta_\varepsilon = \frac{\bar{z}_{\varepsilon,2} - \bar{z}_{\varepsilon,1}}{2\varepsilon^2}, \quad z_\varepsilon^* = \frac{\bar{z}_{\varepsilon,2} + \bar{z}_{\varepsilon,1}}{2}.$$

Then (2.13) is equivalent to:

$$\begin{cases} \varepsilon^2 \frac{dN_{\varepsilon,1}}{dt} = \left[1 - N_{\varepsilon,1}(t) - g(z_\varepsilon^*(t) + 1 - \varepsilon^2\delta_\varepsilon(t))^2 - g\varepsilon^2\right] N_{\varepsilon,1}(t) + m\big(N_{\varepsilon,2}(t) - N_{\varepsilon,1}(t)\big) + \mathcal{O}(\varepsilon^4), \\ \varepsilon^2 \frac{dN_{\varepsilon,2}}{dt} = \left[1 - N_{\varepsilon,2}(t) - g(z_\varepsilon^*(t) - 1 + \varepsilon^2\delta_\varepsilon(t))^2 - g\varepsilon^2\right] N_{\varepsilon,2}(t) + m\big(N_{\varepsilon,1}(t) - N_{\varepsilon,2}(t)\big) + \mathcal{O}(\varepsilon^4), \\ \varepsilon^2 \frac{d\,\delta_\varepsilon(t)}{dt} = 2g - m\left(\frac{N_{\varepsilon,2}(t)}{N_{\varepsilon,1}(t)} + \frac{N_{\varepsilon,1}(t)}{N_{\varepsilon,2}(t)}\right)\delta_\varepsilon(t) + \mathcal{O}(\varepsilon^2), \\ \frac{dz_\varepsilon^*}{dt} = -2gz_\varepsilon^*(t) + m\left(\frac{N_{\varepsilon,2}(t)}{N_{\varepsilon,1}(t)} - \frac{N_{\varepsilon,1}(t)}{N_{\varepsilon,2}(t)}\right)\delta_\varepsilon(t) + \mathcal{O}(\varepsilon^2). \end{cases} \tag{2.17}$$

Let us denote $\Omega = (\mathbb{R}_+^*)^2 \times \mathbb{R}$ and $\bar{Y} = (N_1, N_2, \delta)$ the elements of Ω. Let us define $F : \Omega \to \mathbb{R}$ and $G : \mathbb{R} \times \Omega \to \mathbb{R}^3$ by :

$$\begin{gathered} \forall (z, (N_1, N_2, \delta)) \in \mathbb{R} \times \Omega, \\ F(N_1, N_2, \delta) = m\left(\frac{N_2}{N_1} - \frac{N_1}{N_2}\right)\delta, \\ G(z, N_1, N_2, \delta) = \begin{pmatrix} \left[1 - N_1 - g(z+1)^2 - m\right] N_1 + mN_2 \\ \left[1 - N_2 - g(z-1)^2 - m\right] N_2 + mN_1 \\ 2g - m\left(\frac{N_2}{N_1} + \frac{N_1}{N_2}\right)\delta \end{pmatrix}, \end{gathered} \tag{2.18}$$

where F and G are respectively in $C^\infty(\Omega, \mathbb{R})$ and $C^\infty(\mathbb{R} \times \Omega, \mathbb{R}^3)$.

Let the following be called the perturbed system (P_ε), where $\varepsilon > 0$ is a vanishing parameter and $\nu_{N,\varepsilon}$ and $\nu_{z,\varepsilon}$ are uniformly bounded as $\varepsilon \to 0$:

$$(P_\varepsilon) \quad \begin{cases} \varepsilon^2 \frac{d\bar{Y}_\varepsilon}{dt} = G(z_\varepsilon, \bar{Y}_\varepsilon) + \varepsilon^2 \nu_{N,\varepsilon}(t), \\ \frac{dz_\varepsilon}{dt} = -2gz_\varepsilon + F(\bar{Y}_\varepsilon) + \varepsilon^2 \nu_{z,\varepsilon}(t), \\ (z_\varepsilon(0), \bar{Y}_\varepsilon(0)) = (z_0^\varepsilon, \bar{Y}_0^\varepsilon). \end{cases} \tag{2.19}$$

One can verify that any solution of (2.17) also solves (P_ε). The framework is concordant with fast/slow system studies, like in Levin and Levinson 1954. We seek to establish the convergence over a finite time interval of the solutions of (P_ε) towards the solution of the unperturbed system (P_0), when $(z_0^\varepsilon, \bar{Y}_0^\varepsilon)$ is close enough to $(z_0^*, \bar{Y}_0^*)$ which verifies $G(z_0^*, \bar{Y}_0^*) = 0$:

$$(P_0) \quad \begin{cases} G(z^*(t), \bar{Y}^*(t)) = 0, \\ \frac{dz^*}{dt} = -2gz^* + F(\bar{Y}^*) \\ (z^*(0), \bar{Y}^*(0)) = (z_0^*, \bar{Y}_0^*), \end{cases} \tag{2.20}$$

The first line $G(z^*(t), \bar{Y}^*(t)) = 0$ in (2.20) defines the slow manifold, parametrized by the slow variable $z^*(t)$, whereas the equation $\frac{dz^*}{dt} = -2gz^* + F(\bar{Y}^*)$ (second line) encodes the slow dynamic on that manifold. The slow manifold can be interpreted as the set of fast equilibria $\bar{Y}^*(t)$ corresponding to the levels given by slow variables $z^*(t)$. We will first assess the number of coexisting fast equilibria for any given parameter set $(g, m) \in {\mathbb{R}_+^*}^2$ and value of the slow variable z^*. We will show that there exists either one or none of those, which constrains our proof of convergence to apply when $(z_0^\varepsilon, \bar{Y}_0^\varepsilon)$ is close enough to $(z_0^*, \bar{Y}_0^*)$ (the latter being on the slow manifold). Then, we will show that those fast equilibria are locally stable in Lemma 6. This lemma represents the essential condition for the convergence to apply on the finite time interval $[0, t^*]$, where t^* will be subsequently defined (see Levin and Levinson 1954 and Appendix 2.E for the detailed proof). We state the following theorem:

Theorem 2.4.1. *Let $(\bar{Y}^*, z^*)$ be solution of (2.20) on $[0, t^*]$ with initial conditions $(z_0^*, \bar{Y}_0^*)$, located on the slow manifold (ie. such that $G\left(z^*(t), \bar{Y}^*(t)\right) = 0$ for $t \in [0, t^*]$). For $0 < \varepsilon < 1$, let $(\bar{Y}_\varepsilon, z_\varepsilon)$ be solution of (2.19) on $[0, t^*]$ with initial conditions $(z_0^\varepsilon, \bar{Y}_0^\varepsilon)$. Then, as $\max(\varepsilon, |z_0^\varepsilon - z_0^*|, |\bar{Y}_0^\varepsilon - \bar{Y}_0^*|) \to 0$, $(\bar{Y}_\varepsilon, z_\varepsilon)$ converges toward $(\bar{Y}^*, z^*)$ uniformly on $[0, t^*]$.*

2.4.2 Number of coexisting fast equilibria.

Let us explicit that fast equilibria corresponding to $z^* \in \mathbb{R}$ are $\bar{Y}^* = (N_1^*, N_2^*, \delta^*) \in \Omega = (\mathbb{R}_+^*)^2 \times \mathbb{R}$ verifying: $G(z^*, \bar{Y}^*) = 0$, ie. the system:

$$\begin{cases} \left[1 - N_1^* - g(z^* + 1)^2 - m\right] N_1^* + mN_2^* = 0, \\ \left[1 - N_2^* - g(z^* - 1)^2 - m\right] N_2^* + mN_1^* = 0, \\ 2g - m\left(\frac{N_2^*}{N_1^*} + \frac{N_1^*}{N_2^*}\right)\delta^* = 0. \end{cases} \tag{2.21}$$

We stress that this definition of fast equilibria requires both sizes of the subpopulations to be positive (we can notice that the two first equations of (2.21) do not allow for one population to go extinct while the other one persists). The objective is to identify how many coexisting fast equilibria there are for each set of parameter $(g, m, z^*) \in (\mathbb{R}_+^*)^2 \times \mathbb{R}$. To that purpose, let us first notice that the fast equilibria can be defined only using their demographic ratio $\frac{N_2^*}{N_1^*}$.

Lemma 1. *For $z^* \in \mathbb{R}$, let us define:*

$$P_{z^*}(X) = X^3 - f_1(z^*)X^2 + f_2(z^*)X - 1,$$

where

$$f_1(z^*) = 1 + \frac{g}{m}(z^*+1)^2 - \frac{1}{m}, \quad f_2(z^*) = 1 + \frac{g}{m}(z^*-1)^2 - \frac{1}{m}.$$

If (N_1^*, N_2^*, δ^*) is a fast equilibrium, then: $\rho^* = \frac{N_2^*}{N_1^*}$ is a positive root of P_{z^*} greater than $f_1(z^*)$. Conversely, if ρ^* is a positive root of P_{z^*} greater than $f_1(z^*)$, then:

$$(N_1^*, N_2^*, \delta^*) = \left(m[\rho^* - f_1(z^*)],\, m\,\rho^*\,[\rho^* - f_1(z^*)],\, \frac{2g}{m\left(\rho^* + \frac{1}{\rho^*}\right)} \right) \in \Omega,$$

is a fast equilibrium corresponding to z^* and $\rho^* = \frac{N_2^*}{N_1^*}$.

Consequently, the number of fast equilibria corresponding to z^* is the number of positive roots of $P_{z^*}(X)$ greater than $f_1(z^*)$.

Proof of Lemma 1. For $z^* \in \mathbb{R}$, since $\bar{Y}^* \in \Omega = \mathbb{R}_+^* \times \mathbb{R}_+^* \times \mathbb{R}$, one can notice that (2.21) is equivalent to:

$$\begin{cases} \frac{N_2^*}{N_1^*} = \frac{g(z^*-1)^2+m-1-m\frac{N_1^*}{N_2^*}}{g(z^*+1)^2+m-1-m\frac{N_2^*}{N_1^*}}, \\ N_1^* = m\frac{N_2^*}{N_1^*} + 1 - g(z^*+1)^2 - m, \\ \delta^* = \frac{2g}{m\left(\frac{N_2^*}{N_1^*}+\frac{N_1^*}{N_2^*}\right)}. \end{cases}$$

$$\iff \begin{cases} \left[\frac{N_2^*}{N_1^*}\right]^3 - \left[\frac{N_2^*}{N_1^*}\right]^2 \left[1 + \frac{g}{m}(z^*+1)^2 - \frac{1}{m}\right] + \left[\frac{N_2^*}{N_1^*}\right] \left[1 + \frac{g}{m}(z^*-1)^2 - \frac{1}{m}\right] - 1 = 0, \\ N_1^* = m\left[\frac{N_2^*}{N_1^*} - \left(1 + \frac{g}{m}(z^*+1)^2 - \frac{1}{m}\right)\right], \\ \delta^* = \frac{2g}{m\left(\frac{N_2^*}{N_1^*}+\frac{N_1^*}{N_2^*}\right)}. \end{cases}$$

Hence the result. □

Remark 3. *Thanks to the symmetrical setting of the habitats, one can notice that, for all $z^* \in \mathbb{R}$, $P_{-z^*}(X) = X^3 P_{z^*}(1/X)$ and $f_1(-z^*) = f_2(z^*)$. Hence, the number of positive roots of P_{z^*} that are greater than $f_1(z^*)$ is the number of positive roots of P_{-z^*} that are greater than $f_2(z^*)$. Therefore, from now on, we will consider that $z^* \geq 0$ without loss of generality.*

The Lemma 2 shows that multiple fast equilibria cannot coexist and fast equilibria do not need to exist for any given set of parameters $(g, m, z^*) \in {\mathbb{R}_+^*}^2 \times \mathbb{R}_+$.

Lemma 2. *Let $z^* \geq 0$. Then:*

(i) If P_{z^*} has more than a single positive root, then they are all lower than $f_1(z^*)$. Hence, no fast equilibrium can exist in this configuration.

(ii) If P_{z^*} has a single positive root ρ^*, then:

$$[\rho^* > f_1(z^*)] \quad \iff \quad [f_1(z^*) \leq 0] \vee [P_{z^*}(f_1(z^*)) < 0]\,.$$

Proof of Lemma 2. Let $z^* \geq 0$. As $P_{z^*}(0) = -1$, and the leading coefficient is 1, P_{z^*} has at least one positive root and has either 1 or 3 positive roots.

(i) Let us assume that P_{z^*} has three positive roots x_1, x_2, x_3. Then $f_1(z^*) = x_1 + x_2 + x_3 > \max\{x_1, x_2, x_3\}$, since the three roots are positive.

(ii) Let us assume now that P_{z^*} has a single positive root ρ^*. As $P_{z^*}(0) = -1 < 0$ and the leading coefficient of P_{z^*} is 1, we deduce that, for $y > 0$: $y < \rho^* \iff P_{z^*}(y) < 0$. Hence the result. □

The second point of the Lemma 2 allows us to precise in the next proposition the conditions on z^* such that a fast equilibrium exists, depending on $(g, m) \in {\mathbb{R}_+^*}^2$ (see also Fig. 2.3):

Proposition 2.4.1. *For $(g, m, z^*) \in \mathbb{R}_+^* \times \mathbb{R}_+^* \times \mathbb{R}_+$ such that P_{z^*} has a single positive root, let us define:*

$$\Delta = \frac{4}{g^2}\left[m^2 - 4g\,(m-1)\right], \quad z_1 = \frac{1}{2}\left[\frac{2\,(g+1-m)}{g} - \sqrt{\Delta}\right], \quad z_2 = \frac{1}{2}\left[\frac{2\,(g+1-m)}{g} + \sqrt{\Delta}\right].$$

The following holds:

- *If $g \geq 1$ and:*
  - *$m < 2g\left(1 - \sqrt{1 - \frac{1}{g}}\right)$, then for all $z^* \in]\sqrt{z_1}, \sqrt{z_2}[$, there exists a single fast equilibrium, and none otherwise.*
  - *$m \geq 2g\left(1 - \sqrt{1 - \frac{1}{g}}\right)$ (ie. $\Delta \leq 0$), then for all $z^* \geq 0$, there exists no fast equilibria.*
- *If $g < 1$, then :*
  - *If $m \leq \frac{1-g}{2}$, then, for $z^* \in [0, \sqrt{\frac{1-m}{g}} - 1[\cup]\sqrt{z_1}, \sqrt{z_2}[$, there exists a single fast equilibrium associated to z^*, and none otherwise.*
  - *If $\frac{1-g}{2} < m < 1 - g$, then, for $z^* \in [0, \max\left(\sqrt{\frac{1-m}{g}} - 1, \sqrt{z_2}\right)[$, there exists a single fast equilibrium associated to z^*, and none otherwise.*
  - *If $1 - g \leq m$, then, for $0 \leq z^* < \sqrt{z_2}$, there exists a single fast equilibrium associated to z^*, and none otherwise.*

The proof of Proposition 2.4.1 is located in Section 2.F.

Finally, we examine the conditions upon which P_{z^*} has three positive roots. Due to the high degrees of the polynomials involved, an analytical condition on $(g, m) \in {\mathbb{R}_+^*}^2$ has only been found when $z^* \in [-1, 1]$:

Proposition 2.4.2. *If $1 + 2m \geq g$, for all $z^* \in [-1, 1]$, P_{z^*} has a single positive root.*

If $1 + 2m < g$, there exists an interval $I \neq \emptyset$ centered in 0 such that for all $z^* \in I$, P_{z^*} has three distinct positive roots.

Proof. The proof will require three lemma. The first one states conditions upon which P_{z^*} has three distinct positive roots for $z^* \in \mathbb{R}$. The second one gives an explicit condition determining if $P_0 = P_{z^*=0}$ has one $(1 + 2m \geq g)$ or three distinct positive roots $(1 + 2m < g)$. The third one shows that if there exists a $z^* \in [-1, 1] \backslash \{0\}$ such that P_{z^*} has three distinct positive roots, then P_0 also has three distinct positive roots.

Lemma 3. *Let $z^* \in \mathbb{R}$. $P_{z^*}(X) = X^3 - f_1(z^*)X^2 + f_2(z^*)X - 1$ has three distinct positive roots if and only if the three following conditions hold simultaneously:*

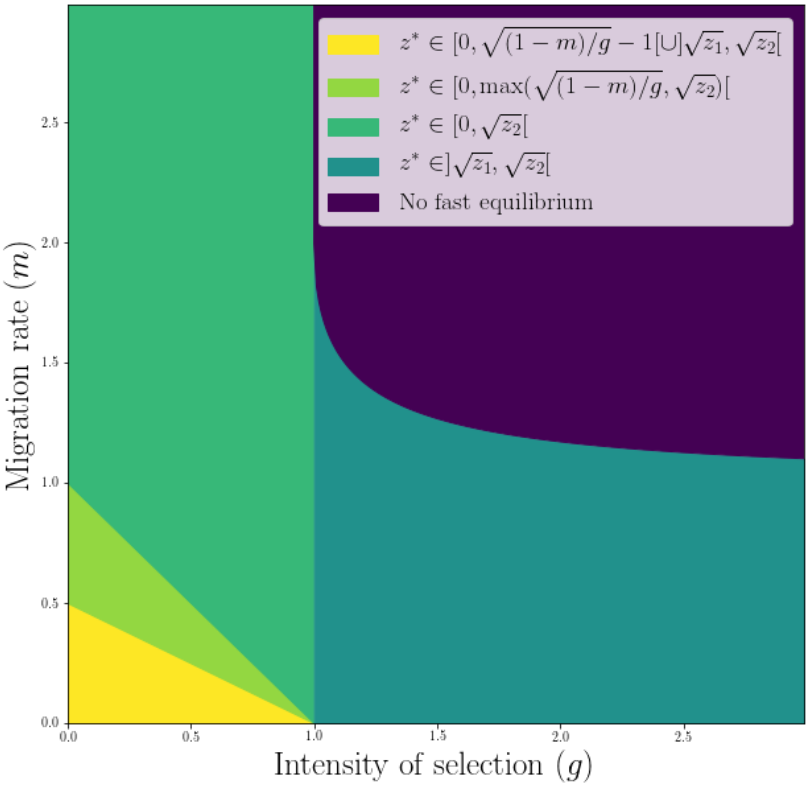

Figure 2.3: **Description of the conditions imposed on $z^* \geq 0$ to get a fast equilibrium depending on the pair (g, m) under the preliminary assumption that P_{z^*} has a single positive root, according to the results of Proposition 2.4.1.** When selection is smaller than 1, symmetrical fast equilibria exist ($z^* = 0$), and do not when selection is larger than 1. When both migration and selection are both too strong, no fast equilibrium can exist.

(i) $f_1(z^*) > 0$,

(ii) $f_2(z^*) > 0$,

(iii) $\Delta(z^*) := f_1(z^*)^2 f_2(z^*)^2 - 4(f_1(z^*)^3 + f_2(z^*)^3) + 18 f_1(z^*) f_2(z^*) - 27 > 0$.

Proof of Lemma 3. Let $(x_1, x_2, x_3) \in \mathbb{C}^{*3}$ be the roots of P_{z^*}. Since $x_1 x_2 x_3 = 1$, we have:

$$f_1(z^*) = x_1 + x_2 + x_3, \quad f_2(z^*) = \frac{x_1 x_2 + x_2 x_3 + x_3 x_1}{x_1 x_2 x_3} = \frac{1}{x_1} + \frac{1}{x_2} + \frac{1}{x_3}.$$

Let us assume first that x_1, x_2, x_3 are positive and distinct. Then they are real and from the latter, $f_1(z^*) > 0$ and $f_2(z^*) > 0$. Moreover, they are real and distinct if and only if the discriminant of P_{z^*} is positive, hence condition (iii).

Conversely, let us assume $(i), (ii)$ and (iii). Then x_1, x_2, x_3 are real and distinct. Since $P_{z^*}(0) < 0$, two of them (for example x_2 and x_3) share the same sign. Suppose that they are negative (they cannot be 0 since $P_{z^*}(0) = -1$) . Then (i) yields:

$$x_1 > |x_2| + |x_3|.$$

Hence :

$$f_2(z^*) = \frac{1}{x_1} + \frac{1}{x_2} + \frac{1}{x_3} = \frac{1}{x_1} - \frac{1}{|x_2|} - \frac{1}{|x_3|} < \frac{1}{|x_2| + |x_3|} - \frac{1}{|x_2|} - \frac{1}{|x_3|} < 0,$$

which contradicts (ii). Hence x_1, x_2, x_3 are positive and distinct. □

Lemma 4. *$P_0 = P_{z^*=0}$ has three distinct positive roots if and only if $g > 1 + 2m$ and one positive root otherwise.*

Proof of Lemma 4. One can notice that $f_1(0) = f_2(0) = 1 + \frac{g}{m} - \frac{1}{m}$ and:

$$\Delta(0) = f_1(0)^4 - 8 f_1(0)^3 + 18 f_1(0)^2 - 27 = (f_1(0) + 1)(f_1(0) - 3)^3.$$

Hence, the precedent lemma ensures that P_0 has three distinct positives roots only in the region where $f_1(0) = f_2(0) = 1 + \frac{g}{m} - \frac{1}{m} > 0$ and $\Delta(0) > 0$. That occurs if and only if $f_1(0) > 3$, which yields $g > 1 + 2m$. □

Lemma 5. *If there exists $z^* \in [-1, 1]$ such that P_{z^*} has three distinct positive roots, then P_0 has three distinct positive roots.*

Proof of Lemma 5. We recall that we study the case $z^* > 0$ without loss of generality. Let us consider $z^* \in]0, 1]$ such that P_{z^*} has three distinct positive roots. From Remark 3, P_{-z^*} has also three distinct positive roots. Thereby, Lemma 3 implies that $f_i(\pm z^*) > 0$, $i = 1, 2$ and $\delta(\pm z^*) > 0$.

It is clear that f_1 is strictly increasing on $]-1, 1[$ and f_2 is strictly decreasing on $]-1, 1[$. As $f_i(\pm z^*) > 0$, $i = 1, 2$, we get that $f_1 > 0$ and $f_2 > 0$ on $[-z^*, z^*]$, in particular $f_1(0) > 0$ and $f_2(0) > 0$.

Moreover, let us introduce the function $g : z \mapsto f_1(z)^2 - 3 f_2(z)$. For $z \in]-1, 1[$, $g'(z) = 2 f_1'(z) f_1(z) - 3 f_2'(z) > 0$, because $f_1(z) > 0$, $f_1'(z) > 0$ and $f_2'(z) < 0$. Therefore, g is increasing on $]-1, 1[$. One can also notice that $g(z)$ is the quarter of the discriminant of $P_z'(X)$. As P_{z^*} and P_{-z^*} have three distinct positive roots, by Rolle's theorem, P'_{z^*} and P'_{-z^*} have two distinct positive roots. Therefore, $g(-z^*)$ and $g(z^*)$ are positive. As g is increasing on $[-z^*, z^*]$, we get: $0 < g(0) = f_1(0)(f_1(0) - 3)$. Since $f_1(0) > 0$ and $g(0) > 0$, we have $3 < f_1(0) = 1 + \frac{g}{m} - \frac{1}{m}$. By the Lemma 4, P_0 has then three distinct positive roots.

□

The successive applications of Lemma 4 and Lemma 5 are sufficient to conclude. □

2.4.3 Fast relaxation towards the slow manifold.

We hereby prove the following lemma on the stability of the slow manifold:

Lemma 6. *For $(z,\bar{Y}) \in \mathbb{R}\times\Omega$ such that $G(z,\bar{Y},0)=0$, $J_G(z,\bar{Y}) := \partial_{\bar{Y}} G(z,\bar{Y},0)$ is invertible. Furthermore, its eigenvalues are real and negative.*

Proof. For $(z,\bar{Y}) \in \mathbb{R}\times\Omega$ such that $G(z,\bar{Y},0)=0$, we have:

$$J_G(z,\bar{Y}) = \begin{pmatrix} -2N_1 + [1-g(z+1)^2 - m] & m & 0 \\ m & -2N_2 + [1-g(z-1)^2 - m] & 0 \\ \frac{m\,\delta}{N_1}\left(\frac{N_2}{N_1} - \frac{N_1}{N_2}\right) & -\frac{m\,\delta}{N_2}\left(\frac{N_2}{N_1} - \frac{N_1}{N_2}\right) & -m\left(\frac{N_2}{N_1} + \frac{N_1}{N_2}\right) \end{pmatrix}.$$

Since $G(z,\bar{Y},0)=0$, (2.18) leads to:

$$J_G(z,\bar{Y}) = \begin{pmatrix} -m\frac{N_2}{N_1} - N_1 & m & 0 \\ m & -m\frac{N_1}{N_2} - N_2 & 0 \\ \frac{m\,\delta}{N_1}\left(\frac{N_2}{N_1} - \frac{N_1}{N_2}\right) & -\frac{m\,\delta}{N_2}\left(\frac{N_2}{N_1} - \frac{N_1}{N_2}\right) & -m\left(\frac{N_2}{N_1} + \frac{N_1}{N_2}\right) \end{pmatrix}$$

$$= \begin{pmatrix} & J & \\ & & \\ \frac{m\,\delta}{N_1}\left(\frac{N_2}{N_1} - \frac{N_1}{N_2}\right) & -\frac{m\,\delta}{N_2}\left(\frac{N_2}{N_1} - \frac{N_1}{N_2}\right) & -m\left(\frac{N_2}{N_1} + \frac{N_1}{N_2}\right) \end{pmatrix} \begin{matrix} 0 \\ 0 \\ \end{matrix}$$

so that we can compute :

$$\det J_G(z,\bar{Y}) = -m\left(\frac{N_2}{N_1} + \frac{N_1}{N_2}\right)\left[m\frac{N_2^2}{N_1} + m\frac{N_1^2}{N_2} + N_1N_2\right] < 0.$$

Hence $J_G(z,\bar{Y})$ is invertible. A first eigenvalue is $-m\left(\frac{N_2}{N_1} + \frac{N_2}{N_1}\right) < -2m$. The last two eigenvalues are those of the upper left block J. We have:

$$\mathrm{tr}(J) < -2m < 0, \quad \det(J) = m\frac{N_1^2}{N_2} + m\frac{N_1^2}{N_2} + N_1N_2 > 0,$$

and:

$$\mathrm{tr}(J)^2 - 4\det(J) = 4m^2 + \left(m\frac{N_2}{N_1} - m\frac{N_1}{N_2} + N_1 - N_2\right)^2 > 4m^2 > 0.$$

Hence J has two real negative eigenvalues and consequently, $J_G(z,\bar{Y})$ has three real negative eigenvalues. □

2.5 Analytical description of the equilibria in the limit of vanishing variance

In this section, we will perform an equilibrium analysis for the stationary problem in the limit of vanishing variance. As numerically illustrated in Section 2.3, under this regime, our

model (2.1) leads to the same dynamics of the moments as in Ronce and Kirkpatrick 2001. Consequently, this equilibrium analysis corresponds to the one made in Ronce and Kirkpatrick 2001 (in the limit of vanishing variance where their system of four equations converges to the system (2.16)). Recall from the introduction that the study done in Ronce and Kirkpatrick 2001 reveals two types of equilibrium:

- symmetrical equilibrium, where both populations are of the same size and equally maladapted to their local habitat (corresponding to a generalist species). Such an equilibrium is derived analytically by the authors. It is worthy to note that in the small variance regime, this equilibrium becomes monomorphic.
- asymmetrical equilibria, where one larger population of locally adapted individuals acts as a source for the other more poorly adapted smaller population (corresponding to a specialist species). The authors numerically explored this type of equilibrium and derived approximations for low migration rates. One aim of this section is to characterize such equilibria analytically.

The fast/slow analysis done in Section 2.4 gives us the opportunity to go further in the equilibrium analysis in the small variance regime, as the asymptotic system (2.16) presents a reduced complexity (three equations instead of four). Moreover, adopting the notation $\rho^* = \frac{N_2^*}{N_1^*} > 0$ and using the polynomial previously defined:

$$P_{z^*}(X) = X^3 - X^2\left[1 + \frac{g}{m}(z^*+1)^2 - \frac{1}{m}\right] + X\left[1 + \frac{g}{m}(z^*-1)^2 - \frac{1}{m}\right] - 1,$$

the Lemma 1 implies that (2.16) is equivalent to:

$$\begin{cases} P_{z^*}(\rho^*) = 0, \\ \frac{dz^*}{dt} = 2g\left(\frac{\rho^{*2}-1}{\rho^{*2}+1} - z^*\right), \end{cases} \tag{2.22}$$

with the constraint $\rho^* > \max\left(1 + \frac{g}{m}(z^*+1)^2 - \frac{1}{m}, 0\right)$ (ie. $N_1^* > 0$). This reduction in the regime of small variance allows us in a second time to derive analytical expressions of every possible equilibrium $(z^*, N_1^*, N_2^*) \in \mathbb{R} \times {\mathbb{R}_+^*}^2$ from solving:

$$\left[P_{\frac{\rho^{*2}-1}{\rho^{*2}+1}}(\rho^*) = 0\right] \wedge \left[\rho^* > \max\left(1 + \frac{g}{m}\frac{4\rho^{*4}}{(\rho^*+1)^2} - \frac{1}{m}, 0\right)\right], \tag{2.23}$$

and next setting:

$$\begin{cases} z^* = \frac{\rho^{*2}-1}{\rho^{*2}+1}, \\ N_1^* = m\left[\rho^* - \left[1 + \frac{g}{m}(z^*+1)^2 - \frac{1}{m}\right]\right], \\ N_2^* = m\left[\frac{1}{\rho^*} - \left[1 + \frac{g}{m}(z^*-1)^2 - \frac{1}{m}\right]\right]. \end{cases} \tag{2.24}$$

We will show that there exists a unique symmetrical equilibrium, which correspond to the monomorphic one analytically found by Ronce and Kirkpatrick 2001 (in the regime of small variance). We will then show that there can additionally exist a mirrored pair of asymmetrical equilibria uniquely defined, corresponding to the ones found numerically by Ronce and Kirkpatrick 2001.

2.5.1 Equilibrium analysis

The objective of this section is to find the steady states (z^*, N_1^*, N_2^*) of the system (2.16) that lie in $\mathbb{R} \times {\mathbb{R}_+^*}^2$ (or equivalently, solve (2.23) and set (2.24)). Henceforth, we will call these (z^*, N_1^*, N_2^*) **equilibria**. The systems (2.23) and (2.24) imply that $(z^*, N_1^*, N_2^*) \in \mathbb{R} \times {\mathbb{R}_+^*}^2$ is an equilibrium if and only if $\bar{Y}^* = \left(N_1^*, N_2^*, \frac{2g}{m\left[\rho^* + \frac{1}{\rho^*}\right]}\right)$ is a fast equilibrium corresponding to $z^* = \frac{\rho^{*2}-1}{\rho^{*2}+1}$. As a corollary of the Proposition 2.4.1, we get that the following region of parameters does not allow for any equilibria to exist:

Corollary 1. *If* $\left[\,[g \geq 1] \wedge \left[m \geq 2g\left(1 - \sqrt{1 - \frac{1}{g}}\right)\right]\right]$, *then there can exist no equilibria as defined by* (2.23) *and* (2.24), *i.e. that leads to* $N_1^* > 0$ *and* $N_2^* > 0$.

Remark 4. *Although our analysis is not meant to describe extinction, we observe numerically that the system goes to extinction in the region defined in the previous corollary (see Fig. 2.6).*

From now on and until further notice, we will thus consider $(m, g) \in {\mathbb{R}_+^*}^2$ such that:

$$[g < 1] \vee \left[m < 2g\left(1 - \sqrt{1 - \frac{1}{g}}\right)\right].$$

2.5.1.1 Symmetric equilibrium: fixation of a generalist species

Definition 1. *We call symmetric equilibrium the* $(z^*, N_1^*, N_2^*) \in \mathbb{R} \times {\mathbb{R}_+^*}^2$ *solutions of* (2.23) *and* (2.24) *where both subpopulations have the same size:* $N_1^* = N_2^* = N^* > 0$.

We first state that there can only exist one viable symmetrical equilibrium:

Proposition 2.5.1. *There exists a single symmetric equilibrium when* $g < 1$, *given by* $(0, 1-g, 1-g)$ *and none when* $g \geq 1$.

Proof. Regarding (2.23): we have $\rho^* = 1$ is a positive root of:

$$P_{z^*=0}(X) = X^3 - (1 + \frac{g-1}{m})X^2 + (1 + \frac{g-1}{m})X - 1,$$

that additionally satisfies:

$$\rho^* > 1 + \frac{g-1}{m} \iff 1 > g.$$

Hence the symmetrical equilibrium is uniquely defined by $(0, 1-g, 1-g)$ (from considering (2.24)). □

In this case, as 0 is the middle point between the local optimal phenotypes -1 in habitat 1 and 1 in habitat 2, each subpopulation is equally maladapted.

Remark 5. *The existence of this equilibrium (or the associated extinction when it is not viable) was expected, for we consider symmetrical habitats and thus symmetrical dynamics. Therefore, under symmetrical initial conditions, the outcome is necessarily symmetrical.*

2.5.1.2 Asymmetric equilibrium: specialist species

We define as asymmetric equilibrium any solution of (2.24) in $\mathbb{R}\times{\mathbb{R}_+^*}^2$ that is not a symmetric equilibrium.

Remark 6. *One can notice that the system (2.23) is invariant under the transformation $\rho^* \mapsto \frac{1}{\rho^*}$ or equivalently (2.24) under $(z^*, N_1^*, N_2^*) \mapsto (-z^*, N_2^*, N_1^*)$. Thus, we do not lose in generality if we look for equilibria with $N_1^* < N_2^*$ instead of $N_1^* \neq N_2^*$: to each asymmetrical equilibrium with $N_1^* < N_2^*$, we can associate its mirrored version.*

This section is dedicated to confirm the numerical intuition of Ronce and Kirkpatrick 2001 and show that there exists a range of parameters such that a unique mirrored couple of asymmetrical equilibria exists.

Proposition 2.5.2. *Let $(m, g) \in {\mathbb{R}_+^*}^2$ be such that:*

$$[1 + 2m < 5g] \wedge \left[m^2 > 4g\,(m-1)\right]. \tag{2.25}$$

Then there exists a single asymmetrical equilibrium (z^*, N_1^*, N_2^*) with $N_1^* < N_2^*$, given by:

$$\begin{cases} N_1^* = (1-m) + m\rho - 4g\frac{\rho^{*4}}{(\rho^{*2}+1)^2}, \\ N_2^* = (1-m) + \frac{m}{\rho^*} - 4g\frac{1}{(\rho^{*2}+1)^2}, \\ z^* = \frac{\rho^{*2}-1}{\rho^{*2}+1} \neq 0, \end{cases} \tag{2.26}$$

where $\rho^* = \frac{y^*+\sqrt{y^{*2}-4}}{2}$ and $y^*\left(= \rho^* + \frac{1}{\rho^*}\right)$ is the only root greater than 2 of the polynomial:

$$S(Y) = Y^3 + \frac{(1-4g)}{m}Y^2 - \frac{4g}{m}Y + \frac{4g}{m}.$$

Conversely, if the condition (2.25) is not verified, there can be no asymmetrical equilibria.

Remark 7. *For $g > 1, m > 0$, we have the equivalence:*

$$[1 + 2m < 5g] \wedge \left[m^2 > 4g\,(m-1)\right] \iff \left[m < 2g\left(1 - \sqrt{1 - \frac{1}{g}}\right)\right].$$

Fig. 2.4 summarizes the conditions obtained with Proposition 2.5.1 and Proposition 2.5.2. It illustrates the analytical range of parameters where the different types of equilibrium exist when the strength of selection g and the migration rate m vary. In the region where none of the conditions are met, we observe numerically that the system leads to extinction (upper right region). In the intermediate green triangle, the two asymmetrical equilibria coexist with the symmetrical equilibrium.

Proof of Proposition 2.5.2. The first part of the proof is directed to solve the equation given in (2.23) and consists in two lemmas. The second part of the proof examines the conditions under which such solutions verify the inequality constraint given by (2.23). It consists in a lemma that involves tedious computations. Consequently, the second part of the proof is left to be consulted in Section 2.G.

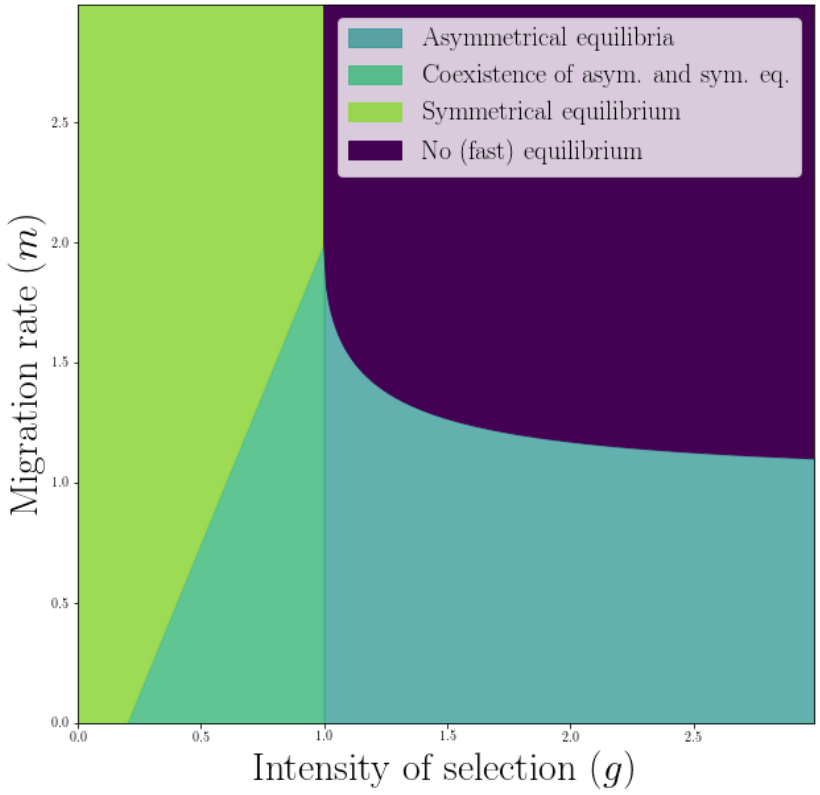

Figure 2.4: **Regions of existence of the equilibria, according to Proposition 2.5.1 and Proposition 2.5.2**. The symmetrical equilibrium is only determined by the intensity of selection, regardless of the migration rate. The asymmetrical equilibria cannot exist for large migration rate ($m > 2$) or small intensity of selection. The limit of the blue region is given by $m = 1$ when g goes to ∞. Interestingly enough, at intermediate migration: $m \in [1, 2]$, asymmetrical equilibria only exist for a bounded range of positive g: selection cannot be too strong nor too weak. Moreover, see Section 2.5.2 for stability results about these equilibria to determine which equilibria prevail when both symmetrical and asymmetrical coexist (turquoise triangular region).

First part of the proof. (2.23) provides us with a close equation: $P_{\frac{\rho^{*2}-1}{\rho^{*2}+1}}(\rho^*) = 0$. Solving it seems necessary, however, the direct search for solutions of this equation leads to consider a seventh degree polynomial. The first part of the proof consists in two lemmas. We first rely on the symmetry of the system noticed by Remark 6 ((z^*, ρ^*) is solution if and only if $\left(-z^*, \frac{1}{\rho^*}\right)$ is too) to reduce the complexity from a seventh degree polynomial to a third degree polynomial S:

Lemma 7. *Let us define:*

$$S(Y) = Y^3 + \frac{(1-4g)}{m}Y^2 - \frac{4g}{m}Y + \frac{4g}{m}.$$

Then, we have the following relation for $\rho^* \in \mathbb{R}_+^* \backslash \{1\}$:

$$S\left(\rho^* + \frac{1}{\rho^*}\right) = \frac{(1+\rho^{*2})^2}{(\rho^*-1)\rho^{*3}} P_{\frac{\rho^{*2}-1}{\rho^{*2}+1}}(\rho^*).$$

As for $\rho^* \in \mathbb{R}_+^* \backslash \{1\}$, $\rho^* + \frac{1}{\rho^*} > 2$, we next look for the number of roots of S greater than 2:

Lemma 8. *Let $a > 0, b \in \mathbb{R}$. Let us define $b(a) := \frac{5a}{4} - 2$. Then: if $b \geq b(a)$, $S(Y) = Y^3 + (b-a)Y^2 - aY + a$, has no root greater than 2. If $b < b(a)$, S has a single root greater than 2.*

The successive application of the Lemma 7 and Lemma 8 with:

$$\begin{cases} b = \frac{1}{m}, \\ a = \frac{4g}{m} > 0, \end{cases}$$

yields that there exists a unique solution to (2.23) if and only if $1 + 2m < 5g$, and therefore to (2.24) in $\mathbb{R} \times {\mathbb{R}_+^*}^2$ which is exactly (2.26). Proving the two lemmas concludes the first part of the proof.

Proof of Lemma 7. Let us consider $\rho^* \in \mathbb{R}^* \backslash \{1\}$. Then we have:

$$\begin{aligned} \frac{(1+\rho^{*2})^2}{(\rho^*-1)\rho^{*3}} P_{\frac{\rho^{*2}-1}{\rho^{*2}+1}}(\rho^*) &= \frac{2-4g}{m} + \frac{(3m-4g)}{m}\left(\rho^* + \frac{1}{\rho^*}\right) + \frac{(1-4g)}{m}\left(\rho^{*2} + \frac{1}{\rho^{*2}}\right) + \rho^{*3} + \frac{1}{\rho^{*3}} \\ &= \frac{2-4g}{m} + \frac{(3m-4g)}{m}\left(\rho^* + \frac{1}{\rho^*}\right) + \frac{(1-4g)}{m}\left(\rho^{*2} + \frac{1}{\rho^{*2}}\right) + \rho^{*3} + \frac{1}{\rho^{*3}}. \end{aligned}$$

Since:

$$\begin{aligned} \rho^{*2} + \frac{1}{\rho^{*2}} &= \left(\rho^* + \frac{1}{\rho^*}\right)^2 - 2, \\ \rho^{*3} + \frac{1}{\rho^{*3}} &= \left(\rho^* + \frac{1}{\rho^*}\right)^3 - 3\left(\rho^* + \frac{1}{\rho^*}\right), \end{aligned}$$

we have:

$$\begin{aligned} \frac{(1+\rho^{*2})^2}{(\rho^*-1)\rho^{*3}} P_{\frac{\rho^{*2}-1}{\rho^{*2}+1}}(\rho^*) &= \left(\rho^* + \frac{1}{\rho^*}\right)^3 + \frac{1-4g}{m}\left(\rho^* + \frac{1}{\rho^*}\right)^2 - \frac{4g}{m}\left(\rho^* + \frac{1}{\rho^*}\right) + \frac{4g}{m} \\ &= S\left(\rho^* + \frac{1}{\rho^*}\right). \end{aligned}$$

□

Proof of Lemma 8. As $S(0) = a > 0$ and since S goes to $-\infty$ in $-\infty$, S has always a negative root.

Thereby, the case that we take interest in is included within the case where all three roots Z_1, Z_2, Z_3 of S are real. Furthermore, we have the following relations:

$$\begin{cases} Z_1 Z_2 Z_3 = -a < 0, \\ Z_1 Z_2 + Z_2 Z_3 + Z_3 Z_1 = -a < 0. \end{cases}$$

From the first relation, we deduce that S has an even number of positive roots, so either 0 or 2. The second relation leads to a contradiction if all roots are negative. Thus S has necessarily two positive roots and one negative.

Moreover, we have:

$$\frac{1}{Z_1} + \frac{1}{Z_2} + \frac{1}{Z_3} = \frac{Z_1 Z_2 + Z_2 Z_3 + Z_3 Z_1}{Z_1 Z_2 Z_3} = 1.$$

Without loss of generality, let us assume that $Z_3 < 0$. If the remaining two positive roots were greater than 2, then we would get:

$$1 < \frac{1}{Z_1} + \frac{1}{Z_2} \leq \frac{1}{2} + \frac{1}{2} = 1$$

which is a contradiction. Hence at most one is greater than or equal to 2.

The only fact that is left to prove is that such a root exists. Let $S_a(X) = X^3 + (b(a) - a)X^2 - aX + a$. Under the choice of $b(a)$, we can verify that $S_a(2) = 0$. Consequently, the following holds:

$$b < b(a) \iff S(2) < S_a(2) = 0.$$

Therefore, because S goes to $+\infty$ in $+\infty$, if $b > b(a)$, S has an even number of roots greater than 2. Thereby, from the previous part of the proof, in that case, S do not have any roots greater than 2. If $b = b(a)$, 2 is the only root of S greater than or equal to 2. If $b < b(a)$, S has at least one root strictly greater than 2. This root is unique by the argument above (which was independent of b).

□

Second part of the proof. The second part of the proof is dedicated to show that for all $(m, g) \in {\mathbb{R}_+^*}^2$ verifying (2.25), the solution $\rho^* > 0$ that we found in the first part of the proof verifies the constraint given in (2.23). It consists in the following lemma, that is obtained after tedious calculations done in part with the help of the software Mathematica, so the proof is left to be consulted in Appendix 2.G.

Lemma 9. *Let $(m, g) \in {\mathbb{R}_+^*}^2$ verifying (2.25), and $\rho^* > 0$ be the unique solution of the equation $\left[P_{\frac{\rho^{*2}-1}{\rho^{*2}+1}}(\rho^*) = 0\right]$. Then:*

$$\rho^* > 1 + \frac{g}{m}\frac{4\rho^{*4}}{(\rho^* + 1)^2} - \frac{1}{m}.$$

Consequently: for $(g, m) \in {\mathbb{R}_+^*}^2$ such that $1 + 2m < 5g$ and $m^2 > 4g\,(m - 1)$, ρ^* defined in Proposition 2.5.2 defines an equilibrium with positive subpopulation sizes.

Conversely: if (2.25) is not met, either $1 + 2m > 5g$, in which case no asymmetrical equilibrium can exist from Lemma 7 and Lemma 8, or $m^2 < 4g\,(m - 1)$ (which implies that $g > 1$), in which case Remark 7 and Corollary implies that no equilibrium can exist. □

2.5.2 Stability analysis

In this subsection, we examine the stability of the equilibria of the system (2.22) that we described previously.

Proposition 2.5.3. *Let $(z^*, N_1^*, N_2^*) \in \mathbb{R} \times {\mathbb{R}_+^*}^2$ be an equilibrium and $\rho^* = \frac{N_2^*}{N_1^*}$. Then the equilibrium is locally stable (respectively unstable) if:*

$$\frac{4\rho^*}{({\rho^*}^2+1)^2} \times \frac{1}{P'_{z^*}(\rho^*)} \times \frac{2g}{m}\left[z^*\left(\rho^* - {\rho^*}^2\right) - \left(\rho^* + {\rho^*}^2\right)\right] + 1 > 0 \quad (resp. < 0).$$

Proof. If $(z^*, N_1^*, N_2^*) \in \mathbb{R} \times {\mathbb{R}_+^*}^2$ is an equilibrium and $\rho^* = \frac{N_2^*}{N_1^*}$, then (N_1^*, N_2^*) is a fast equilibrium associated to z^* (Lemma 1), which implies that P_{z^*} has a single positive root (without multiplicity) that is ρ^* (Lemma 2). Hence ρ^* cannot be a double root of P_{z^*}, which yields: $P'_{z^*}(\rho^*) \neq 0$.

(2.22) implies that the local stability of the equilibria can be examined by the following system:

$$\begin{cases} \mathcal{G}(z^*, \rho^*) := P_{z^*}(\rho^*) = 0, \\ \rho^* > \left[1 + \frac{g}{m}(z^*+1)^2 - \frac{1}{m}\right], \\ \frac{dz^*}{dt} = \mathcal{F}(z^*, \rho^*) := 2g\left(\frac{{\rho^*}^2-1}{{\rho^*}^2+1} - z^*\right). \end{cases}$$

As $\partial_\rho \mathcal{G}(z^*, \rho^*) = P'_{z^*}(\rho^*) \neq 0$, we apply the implicit function theorem to get U a open neighbourhood of z^* and a smooth function $\rho : U \to \mathbb{R}_+^*$ such that:

$$\forall z \in U, \mathcal{G}(z, \rho(z)) = 0.$$

For $z \in U$, we define $f : U \to \mathbb{R}$, $z \mapsto \mathcal{F}(z, \rho(z))$. Hence, (z^*, N_1^*, N_2^*) is locally stable (resp. unstable) if :

$$f'(z^*) = \nabla \mathcal{F}(z^*, \rho^*) \cdot \begin{pmatrix} 1 \\ \frac{d\rho}{dz}(z^*) \end{pmatrix} = \partial_\rho \mathcal{F}(z^*, \rho^*)\left[-\left(\partial_\rho \mathcal{G}(z^*, \rho^*)\right)^{-1} \partial_z \mathcal{G}(z^*, \rho^*)\right] - 2g < 0 \quad (\text{resp. } > 0).$$

Since we have:

$$\partial_\rho \mathcal{F}(z^*, \rho^*) = 2g\frac{4{\rho^*}^2}{(\rho^*+1)^2}, \quad \left(\partial_\rho \mathcal{G}(z^*, \rho^*)\right)^{-1} = \frac{1}{P'_{z^*}(\rho^*)},$$

and

$$\partial_z \mathcal{G}(z^*, \rho^*) = -2\frac{g}{m}(z^*+1){\rho^*}^2 + 2\frac{g}{m}(z^*-1)\rho^*,$$

the considered equilibrium is locally stable (reps. unstable) if:

$$\frac{4\rho^*}{({\rho^*}^2+1)^2} \times \frac{1}{P'_{z^*}(\rho^*)} \times \frac{2g}{m}\left[z^*\left(\rho^* - {\rho^*}^2\right) - \left(\rho^* + {\rho^*}^2\right)\right] + 1 > 0 \quad (\text{resp. } < 0).$$

□

Corollary 2. *The symmetrical equilibrium $z^* = 0, \rho^* = 1$ is locally stable (resp. unstable) if $5g < 1 + 2m$ (resp. $5g > 1 + 2m$) (ie, when it is alone).*

Proof. If $z^* = 0$ and $\rho^* = 1$, we have:

$$\frac{4\rho^*}{(\rho^{*2}+1)^2} \times \frac{1}{P'_{z^*}(\rho^*)} \times \frac{2g}{m}\left[z^*\left(\rho^* - \rho^{*2}\right) - \left(\rho^* + \rho^{*2}\right)\right] + 1$$
$$= \frac{1}{3 - 2\left(1 + \frac{g}{m} - \frac{1}{m}\right) + \left(1 + \frac{g}{m} - \frac{1}{m}\right)} \times \frac{-4g}{m} + 1 = \frac{1 + 2m - 5g}{1 + 2m - g}.$$

We recall that for the symmetrical equilibrium to exist, we need: $g < 1$, which imply: $g < 1 + 2m$. Hence the result. □

Analytical derivations are more tedious for asymmetrical equilibria. However, when $1 + 2m > g$, we showed that P_{z^*} has a single (without multiplicity) positive root $\rho(z^*)$ for all $z^* \in [-1, 1]$ (Proposition 2.4.2). The function $\rho : [-1, 1] \to \mathbb{R}_+^*, z \mapsto \rho(z)$ is therefore smooth (where $\rho(z)$ designates the single positive root of P_z). Thus, we can globally define the smooth function f similarly as in Proposition 2.5.3 on $]-1, 1[$:

$$f : \begin{cases}]-1, 1[\to \mathbb{R} \\ z \mapsto 2g\left(\frac{\rho(z)^2 - 1}{\rho(z)^2 + 1} - z\right), \end{cases} .$$

That leads to the following result:

Corollary 3. *Let $5g > 1 + 2m > g$. Then the asymmetrical equilibria are locally stable.*

Proof. Let (z^*, N_1^*, N_2^*) be an asymmetrical equilibrium. We recall that $z^* = \frac{\rho^{*2}-1}{\rho^{*2}+1} \in]-1, 1[$. From the previous corollary, the symmetric equilibrium is locally unstable, i.e.:

$$f'(0) > 0.$$

Moreover, from Proposition 2.4.2, $P_{z^*=1}$ has a single positive root, and we can extend f in 1 by continuity and calculate :

$$f(1) = 2g\left(\frac{\rho^2(1) - 1}{\rho^2(1) + 1} - 1\right) = -\frac{4g}{\rho^2(1) + 1} < 0.$$

Since 0 and z^* are the only zeros of f on $[0, 1]$ (from the uniqueness of the mirrored couple of asymmetric equilibria) and $f'(0) > 0$, f is positive on $]0, z^*[$ ane negative on $]z^*, 1]$. Hence, the asymmetrical equilibria are locally stable. □

To illustrate the diversity of cases in both the number of equilibria and their stability, we display in Fig. 2.5 the graph of the function f defined above as a function of the dominant trait z when $g = 1.5$ and m takes the following values :

1. $m = 0.02$. There are multiple branches near the origin (yellow curve), as the function f is multi-valued. Indeed, we are in the case where: $1 + 2m < g$. Therefore, for z^* near 0, there is three distinct positive roots for P_{z^*} (from Proposition 2.4.2), which leads to non-viable fast equilibria (from Lemma 2). Therefore, if the initial dominant trait is near 0, the system will go to extinction.

2. $m = 0.25$, so that the equality $1 + 2m = g$ holds, which is the limit case of the folding near the origin.

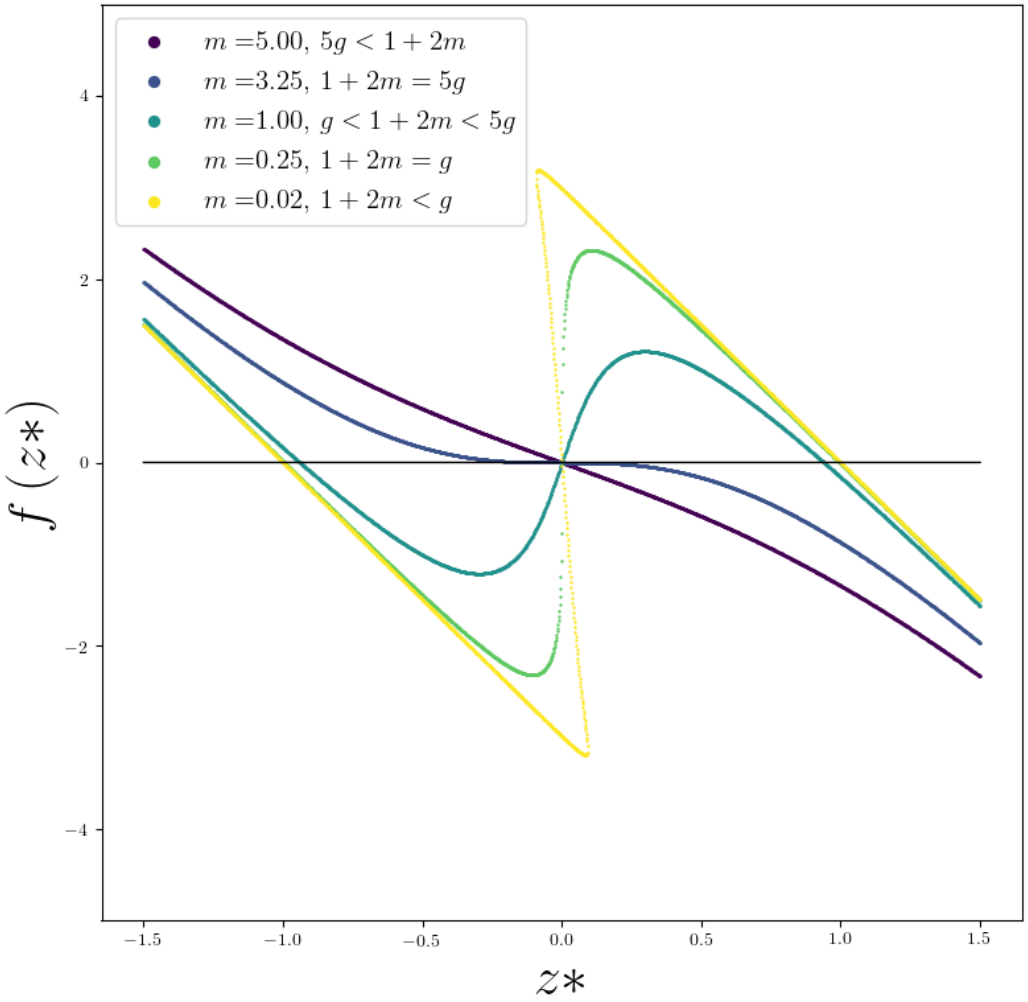

Figure 2.5: **Graph of the function f for $g = 1.5$ and $m \in \{0.02, 0.25, 1, 3.25, 5\}$**. The dominant traits z^* of the different equilibria are located where the curve crosses the horizontal line ($f(z^*) = 0$). An equilibrium is locally stable if the slope of f at the point of equilibrium is negative. For decreasing values of m (dark to light colors), at first, only the symmetric equilibrium exists and is stable (see also Corollary). Then, the asymmetrical equilibria emerge (in the parameter region indicated in Proposition 2.5.2) and are bistable (see also Corollary), while the symmetric equilibrium becomes unstable. For small values of m, the curve folds near the origin, as for z^* near 0, P_{z^*} has three distinct positive roots (Proposition 2.4.2). For those z^*, the fast equilibria are all non viable (Lemma 2): numerically, the system goes to extinction if the initial dominant trait is near 0.

3. $m = 1$. For each value of the dominant trait z^*, there is only one root to P_{z^*}. There are three equilibria, an unstable symmetric and two stable asymmetric equilibria ($1 + 2m < 5g$).

4. $m = 3.25$, so that the equality $1 + 2m = 5g$ holds. This displays the limit of existence of the asymmetrical equilibria (see Proposition 2.5.2). The three equilibria are merging and exchanging stability.

5. $m = 5$. As m grows further, the asymmetric equilibria do not exist anymore. Therefore, only the symmetric one is left and is stable.

2.6 Discussion

Contributions In this Chapter, we have studied the evolutionary dynamics of a complex trait under stabilizing selection in a heterogeneous environment in a sexually reproducing population. To model the process of inheritance of this trait, we have used a mixing sexual reproduction operator according to the infinitesimal model (Fisher 1919; Bulmer 1971; Barton, Etheridge, and Véber 2017), assuming that the segregational variance is constant and independent of the families. We have set our analysis in a regime of small variance of segregation, aligning with a framework developed by Diekmann, Jabin, et al. 2005; Perthame and Barles 2008 and recurrently used with the infinitesimal model Garnier et al. 2022; Calvez, Garnier, and Patout 2019. By doing so, we showed two types of results. First, we compared the system of moments derived from our model in the limit of small variance with a seminal work in quantitative genetics (Ronce and Kirkpatrick 2001), showing their equivalence in that limit, while bypassing any prior normality assumption on the trait distributions. Next, we showed that this small variance regime discriminates two time scales, allowing to perform a slow-fast analysis, which reduces the complexity of our system in the asymptotic limit. Thus, we were able to fully derive analytically its equilibria thanks to algebraic arguments of symmetry reflecting the symmetrical habitats. The theoretical outcomes of our model are shown in the upper panel of Fig. 2.6. They are to be compared to numerical outcomes shown in the lower panel, where the same colours indicate the same types of equilibria. For the numerical analysis, for each couple of parameters (m, g), the initial state is the same: both local distributions are normal of same mean (0.2) and same variance $\varepsilon^2 = 2.5 \times 10^{-3}$. The initial state is taken as monomorphic so that it falls within the scope of the slow-fast analysis. Moreover, the color yellow is attributed to simulations whose final state does not meet the small segregational variance regime analysis prediction, which in particular states that the distribution of trait in the metapopulation has a variance of order ε^2 (see (2.12) and recall that the population is monomorphic (Section 2.4)). In the two simulations that present the color yellow, the variance in trait in the metapopulation is of approximately $3\,\varepsilon^2$, which exceeds the chosen threshold ($2\,\varepsilon^2$). The detailed setting and scoring of the simulations involved in the lower panel of Fig. 2.6 are available in Section 2.I.

One can notice that the justification of the validity of the Gaussian approximation of local trait distributions in the regime of small variance (see Section 2.2 and Garnier et al. 2022) and most of the slow-fast analysis (Section 2.4) are robust when introducing asymmetries in our model, or changing the selection functions. However, we stress that our analytical derivation of the equilibria in the asymptotic limit uses specific arguments that rely crucially on the symmetries between habitats in our model (see Remark 6 and Proposition 2.5.2).

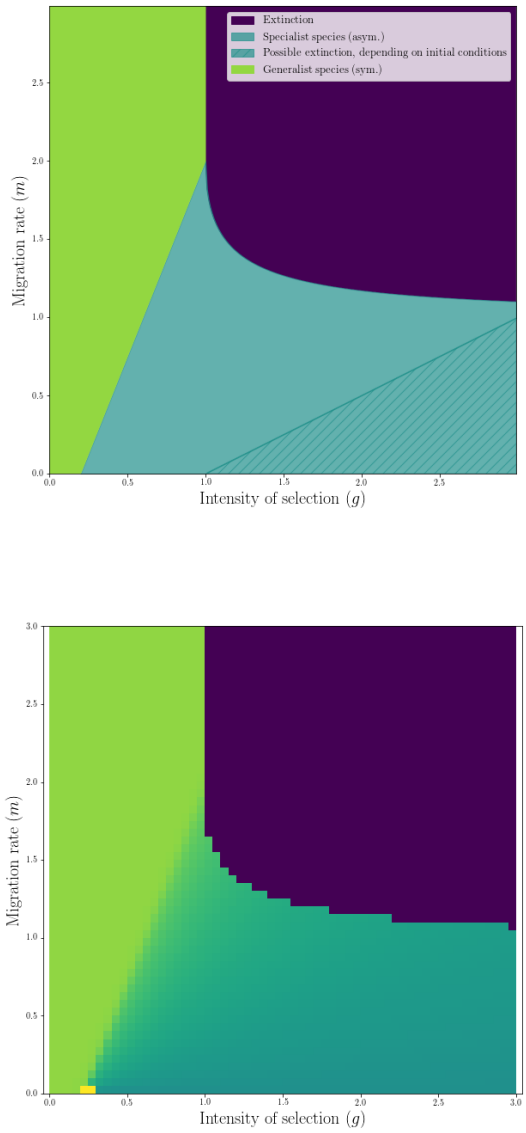

Figure 2.6: **Summary of the different theoretical (upper panel, in the limit of vanishing segregational variance) and numerical (lower panel, $\varepsilon^2 = 2.5 \times 10^{-3}$) outcomes of our model when selection (g) and migration (m) are varying**. The same colors represents the same outcomes in both figures. Fig. 2.4 complemented by the stability analysis (see Section 2.5.2) gives the upper figure. In the dashed region, the system goes to one of the asymmetrical equilibrium, except if the initial conditions are too symmetrical (the system goes then numerically to extinction, typically due to the folding near $z^* = 0$ of the yellow curve in Fig. 2.5). For the lower figure, all simulations share the same initial state: the metapopulation is monomorphic and asymmetrical as local distributions are both normal with same mean (0.2) and same variance ($2\varepsilon^2$). Hence, the potential extinction in the dashed region does not occur and the numerical analyis falls within the scope of the slow-fast analysis (Section 2.4). The color yellow is attributed to simulations whose final state does not meet the small segregational variance regime analysis prediction, which, in particular, states that the distribution of trait in the metapopulation has a variance of order ε^2 (see (2.12) and recall that the population is monomorphic (Section 2.4)). For more details on the simulations and their scoring resulting in the lower panel figure, see Section 2.I.

Robustness with regard to dimorphic initial state. The theoretical outcomes given in Fig. 2.6 are in particular a consequence of the reduction of system due to the slow-fast theorem, which applies provided that the initial state is close enough from a fast equilibrium from the slow manifold (see Theorem 2.4.1). Those fast equilibria are monomorphic. A natural question would be to ask to what extent those results apply for an initial state that is dimorphic. This would model for example two initially isolated subpopulations, locally adapted, that are suddenly being connected. Here we give a numerical taste of what a more complete answer could look like. We display Fig. 2.7 using the same methodology and scoring than for the lower panel of Fig. 2.6, the only difference being the initial state, now constituted by two locally adapted subpopulations, slightly asymmetrical in size (see Section 2.I for details). To get a sense of what could occur in the regime of vanishing variance, we choose to display the results for two values of ε^2: $\varepsilon^2 = 2.5 \times 10^{-3}$ (upper panel) and $\varepsilon^2 = 6.25 \times 10^{-4}$ (lower panel). Both panels of Fig. 2.7 and the lower panel of Fig. 2.6 are globally quite similar, except for the yellow region that is much wider in both panels of Fig. 2.7. Particularly, there is a net trend for strong selection and small migration. That is expected, because the initial state of the simulations involved in both panels of Fig. 2.7 is presumably far from the conditions asked by Theorem 2.4.1. These simulations suggest that, in this particular range of parameters, the fast relaxation to a monomorphic state, that is central in Theorem 2.4.1, breaks down and dimorphism is maintained. However, we can note that this yellow region decreases for decreasing values of ε^2 (difference between upper and lower panel of Fig. 2.7). That suggests that our analysis remains quite robust to dimorphic initial states in the limit of vanishing variance.

Comparison with asexual studies. In Section 2.5, we found that bistable asymmetrical equilibria can exist in our system (Proposition 2.5.2, Corollary). That is a strong difference with the findings of Mirrahimi 2017 and Mirrahimi and Gandon 2020: with a similar mesoscopic model but using an asexual reproduction operator with frequent mutations of small effects, they find that symmetrical habitats lead to a single stable symmetrical equilibrium, either monomorphic or dimorphic. In particular, if migration is small enough compared to selection, each subpopulation adapts to their habitats and dimorphism occurs at the metapopulation scale. In our case, the mixing effect of the infinitesimal operator of sexual reproduction does not allow for such a local adaptation to occur in the limit of small variance. In Section 2.4, we showed that it forces monomorphism quickly and the only option to adapt to strong forces of selection is an asymmetrical equilibrium (Proposition 2.5.2, Fig. 2.6) that describes a source sink scenario. One population is adapted to its habitat, and the other is essentially composed by poorly adapted migrants ; the choice of which depends on the initial conditions.

Our findings share notable similarities with some in Débarre, Ronce, and Gandon 2013, which conducts a hybrid analysis on asexual populations with tools of adaptive dynamics applied to quantitative genetics equations. Particularly, under gradual evolution (when mutations are rare and of small effects), they state that asymmetrical equilibria can be reached if the population is initially monomorphic, under a similar range of migration and selection parameters as indicated by our analysis. They identified these equilibria as locally stable singular strategies, which are defined as critical points of the invasion fitness. It can be shown that the equations obtained when looking for these critical points in their case are the same as the ones defining the equilibria in the present study. Consequently, we suggest that the asymmetrical equilibria found in Débarre, Ronce, and Gandon 2013 should have the same coordinates as the ones found in our analysis. However, there is a substantial difference in the dynamics leading to those equilibria. Even with an initially dimorphic metapopulation, our hypotheses

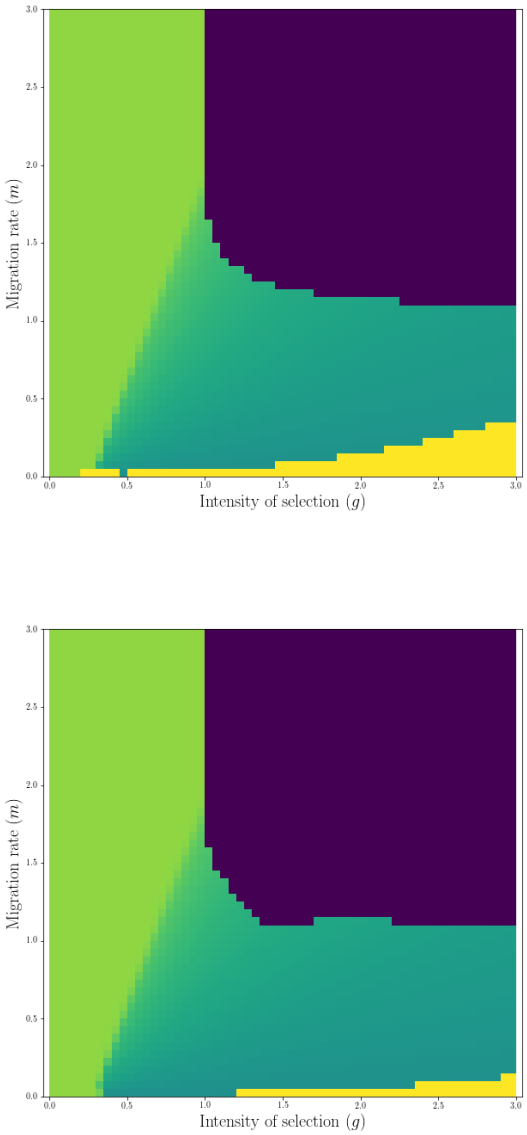

Figure 2.7: **Numerical outcomes with initial dimorphic state (locally adapted subpopulations), for $\varepsilon^2 = 2.5 \times 10^{-3}$ (upper panel) and $\varepsilon^2 = 6.25 \times 10^{-4}$ (lower panel).** The colors for both figures results from the same scoring scheme as for Fig. 2.6 (see Section 2.I for details). The results are quite similar as Fig. 2.6, except for the yellow region. In the upper panel ($\varepsilon^2 = 2.5 \times 10^{-3}$), the yellow region is wider than when the initial state is monomorphic (Fig. 2.6), increasingly so for stronger selection. That highlights the numerical cases where the population ends up dimorphic as the species adapts locally to each deme's optimum, for strong selection and small migration. This is expected as the fast convergence toward a monomorphism state induced by Theorem 2.4.1 in the limit of vanishing variance of segregation is likeky to break down, as the initial state is far from the slow manifold and the segregational variance is small but not zero. However, this yellow region decreases as the value of ε^2 decreases, as indicated by the lower panel ($\varepsilon^2 = 6.25 \times 10^{-4}$). That suggests that our analysis remains quite robust to dimorphic initial states in the limit of vanishing variance.

on sexual reproduction typically strains toward monomorphism. With the same initial state, Débarre, Ronce, and Gandon 2013 indicate that dimorphism is typically maintained in the range of parameters where asymmetrical equilibria exist.

Gaussian assumption. In our study, we consider a regime where the segregational variance is small compared to how far apart the local optimal traits are. While this small variance regime is more general than the standard weak selection approximation widely used in quantitative genetics model using the Gaussian assumption (see Remark 2), we formally show that the local trait distributions can still be well approximated by normal distributions within this regime (Section 2.2). Hence, asymptotically, in the regime of small variance, the findings of our model are equivalent to Ronce and Kirkpatrick 2001, which relies on a Gaussian assumption of local trait distributions. This link of equivalence relies on the hypothesis that the genetic (and phenotypic) variance is constant, which we interpreted in our model to be twice the segregational variance in the limit of vanishing variance. Furthermore, together with the last paragraph, our study gives some elements of explanation to why the findings of Ronce and Kirkpatrick 2001 are structurally different from Mirrahimi 2017 and Mirrahimi and Gandon 2020, and closer to Débarre, Ronce, and Gandon 2013.

Constant segregational variance in a heterogeneous environment Our model relies on using the infinitesimal model with a constant segregational variance, independent of the mates deme. That is a strong assumption. However, in the perspective of linking the present study to population genetics approaches, one can question the limits of such a modelling assumption with regard to a Mendelian interpretation of this model. A future work is planned to examine it through conducting individual based simulations.

Acknowledgements

The author thanks Vincent Calvez and Sepideh Mirrahimi for supervising this project and Sarah P. Otto for precise and helpful comments. The author also thanks Ophélie Ronce, Florence Débarre, Amandine Véber, Alison Etheridge and Florian Patout for insightful conversations. This project has received funding from the European Research Council (ERC) under the European Union's Horizon 2020 research and innovation programm (grant agreement No 639638).

2.A System of moments derived from our model

Here, we derive the system of moments (2.2) from (2.1). In the preliminary computations, we will omit the time and deme dependency for the sake of clarity. We will then denote $\boldsymbol{n}$ the trait distribution density, $\boldsymbol{N}$ the size of the population, $\overline{\boldsymbol{z}}$ the mean trait, $\boldsymbol{\sigma}^2$ the mean variance, $\boldsymbol{\psi}^3$ the third central moment and $\boldsymbol{\theta}$ the optimal phenotype.

Preliminary integration of the selection term. We have:

$$\begin{aligned}\int_{\mathbb{R}}(z-\theta)^2 n(z)dz &= \int_{\mathbb{R}}\left[(z-\overline{z})^2+(\overline{z}-\theta)^2+2(z-\overline{z})(\overline{z}-\theta)\right]n(z)\,dz\\ &= \sigma^2 N+(\overline{z}-\theta)^2 N,\end{aligned}$$

and:

$$\begin{aligned}\int_{\mathbb{R}}(z-\overline{z})(z-\theta)^2 n dz &= \int_{\mathbb{R}}\left[(z-\overline{z})^3+(z-\overline{z})(\overline{z}-\theta)^2+2(z-\overline{z})^2(\overline{z}-\theta)\right]n(z)\,dz\\ &= 2\sigma^2(\overline{z}-\theta)N+\psi N.\end{aligned}$$

Size of the subpopulations. Recalling that $N_i(t)=\int_{\mathbb{R}} n_i(t,z)\,dz$, we get from the preliminary computations by integrating (2.1):

$$\begin{aligned}\frac{dN_i}{dt} &= \int_{\mathbb{R}}\frac{\partial n_i}{\partial t}(t,z)dz\\ &= \int_{\mathbb{R}} r\mathcal{B}_\sigma(n_i)(t,z)-g(z-\theta_i)^2 n_i(t,z)-\kappa N_i(t)n_i(t,z)+m\left(n(t,z)-n(t,z)\right)\,dz\\ &= \left[r-\kappa N_i(t)-g(\overline{z}_i(t)-\theta_i)^2-g{\sigma_i}^2\right]N_i(t)+m(N_j(t)-N_i(t)).\end{aligned}$$

Local mean trait. Recalling that $\overline{z}_i(t)=\frac{1}{N_i(t)}\int_{\mathbb{R}} z\,n_i(t,z)\,dz$, we have, thanks to the preliminary computations:

$$\begin{aligned}\frac{dz_i}{dt} &= \frac{1}{N_i}\int_{\mathbb{R}} z\frac{\partial n_i}{\partial t}(t,z)dz-\frac{1}{{N_i}^2}\frac{dN_i}{dt}\int_{\mathbb{R}} z n_i(t,z)dz\\ &= \frac{1}{N_i}\int_{\mathbb{R}}(z-\overline{z}_i)\frac{\partial n_i}{\partial t}(t,z)dz\\ &= \frac{1}{N_i}\int_{\mathbb{R}}(z-\overline{z}_i)\left[-g(z-\theta_i)^2 n_i(t,z)+m\left(n_j(t,z)-n_i(t,z)\right)\right]dz\\ &= 2g{\sigma_i}^2(\theta_i-\overline{z}_i)-g{\psi_i}^3+m\frac{N_j}{N_i}(\overline{z}_j-\overline{z}_i).\end{aligned}$$

2.B Equilibria of a dynamical system under the infinitesimal model of reproduction with random mating only

In this subsection, we show that (2.7) admits any Gaussian of variance ε^2 as equilibrium. That is equivalent to state that:

Proposition 2.B.1. *For $\mu\in\mathbb{R}$, the Gaussian distribution G_{μ,ε^2} of mean μ and variance ε^2 is a fixed point of the operator $\mathcal{B}_\varepsilon$, namely:*

$$\mathcal{B}_\varepsilon(G_{\mu,\varepsilon^2})=G_{\mu,\varepsilon^2}.$$

Proof. We can first notice that $\mathcal{B}_\varepsilon$ can be written using a double convolution product:

Lemma 10. *For $f \in \mathcal{L}_1(\mathbb{R})$, $\int_{\mathbb{R}} f \neq 0$, we have:*

$$\mathcal{B}_\varepsilon(f) = \frac{4}{\int_{\mathbb{R}} f(z')\,dz'} G_{0,\frac{\varepsilon^2}{2}} * F * F,$$

where $F : z \mapsto f(2z)$.

Proof of Lemma 10. For $f \in \mathcal{L}_1(\mathbb{R})$, $\int_{\mathbb{R}} f \neq 0$, a straight-forward computation yields:

$$\begin{aligned}
\mathcal{B}_\varepsilon(f)(z) &= \frac{1}{\sqrt{\pi}\varepsilon} \iint_{\mathbb{R}^2} \exp\left[\frac{-(z-\frac{z_1+z_2}{2})^2}{\varepsilon^2}\right] \frac{f(z_1)f(z_2)}{\int_{\mathbb{R}} f(z')\,dz'} dz_1 dz_2 \\
&= \frac{1}{\int_{\mathbb{R}} f(z')\,dz'} \int_{\mathbb{R}} \int_{\mathbb{R}} G_{0,\frac{\varepsilon^2}{2}}\left((z-\frac{z_1}{2}) - \frac{z_2}{2}\right) F(\frac{z_2}{2})\,dz_2\, F(\frac{z_1}{2})\,dz_1 \\
&= \frac{2}{\int_{\mathbb{R}} f(z')\,dz'} \int_{\mathbb{R}} G_{0,\frac{\varepsilon^2}{2}} * F(z-\frac{z_1}{2}) F(\frac{z_1}{2})\,dz_1 \\
&= \frac{4}{\int_{\mathbb{R}} f(z')\,dz'} G_{0,\frac{\varepsilon^2}{2}} * F * F(z).
\end{aligned}$$

□

If $f = G_{\mu,\varepsilon^2}$, then we find $F = \frac{1}{2} \times G_{\frac{\mu}{2},\frac{\varepsilon^2}{4}}$. Besides, as the convolution product of two Gaussian kernels G_{μ_1,σ_1^2} and G_{μ_2,σ_2^2} is the Gaussian kernel $G_{\mu_1+\mu_2,\sigma_1^2+\sigma_2^2}$, Proposition 2.B.1 is a corollary of the previous lemma. □

2.C Formal expansion within the exponential formalism for n_ε

In this subsection, we will remove the deme dependency for the sake of clarity. To formally derive (2.9), let us consider the following formal expansion of U_ε with regard to successive orders of ε^2:

$$U_\varepsilon = u_0 + \varepsilon^2 u_\varepsilon.$$

The aim is to characterize u_0 thanks to the behaviour of the reproduction term when $\varepsilon \ll 1$, which we expect neither to diverge nor to vanish:

$$\frac{\mathcal{B}_\varepsilon(n_\varepsilon)}{n_\varepsilon}(z) = \frac{1}{\sqrt{\pi}\varepsilon} \iint_{\mathbb{R}^2} \frac{\exp\left[\frac{1}{\varepsilon^2}\left[-\left[z-\frac{z_1+z_2}{2}\right]^2 + u_0(z) - u_0(z_1) - u_0(z_2)\right]\right] \exp\left[u_\varepsilon(z) - u_\varepsilon(z_1) - u_\varepsilon(z_2)\right] dz_1 dz_2}{\int_{\mathbb{R}} \exp\left[-\frac{u_0(z')}{\varepsilon^2} - u(z')\right] dz'}$$

Then, we have several considerations to make. First, if we assume that u_0 reaches its minimum at a non degenerate point z^*, then the following modified expression of the denominator:

$$\frac{1}{\sqrt{\pi}\varepsilon}\int_{\mathbb{R}}\exp\left[-\frac{1}{\varepsilon^2}\left[u_0(z')-\min u_0\right]-u(z')\right]dz',$$

will have its integrand concentrate around the minimum of u_0 and will converge as $\varepsilon \ll 1$. Therefore it is relevant to introduce this minimum both at the numerator and the denominator.

Then, since we expect the numerator not to diverge nor to vanish uniformly as $\varepsilon \ll 1$, we need that:

$$\forall z\in\mathbb{R},\ \max_{(z_1,z_2)}\left[-\left(z-\frac{z_1+z_2}{2}\right)^2+u_0(z)-u_0(z_1)-u_0(z_2)+\min u_0\right]=0. \tag{2.27}$$

As shown in Garnier et al. 2022, thanks to some convexity arguments, this leads necessarily to choose u_0 as a quadratic function in z, hence its decomposition:

$$u_0(z)=u(z^*)+\frac{(z-z^*)^2}{2}, \tag{2.28}$$

where z^* is realizing the minimum of u_0. Note that $u(z^*)=0$, due to the Laplace method of integration, since:

$$N_\varepsilon=\frac{1}{\sqrt{2\pi\varepsilon}}\int_{\mathbb{R}}\exp\left[-\frac{U_\varepsilon(z)}{\varepsilon^2}\right]dz\underset{\varepsilon\to 0}{\approx}\frac{\exp\left[-\frac{u(z^*)}{\varepsilon^2}\right]}{\sqrt{U_\varepsilon''(z^*)}}.$$

So either $u(z^*)=0$, either there is extinction or explosion of the population size. That yields (2.9).

Convexity arguments from Garnier et al. 2022. Let us recall the arguments of convexity involved in Garnier et al. 2022 to show that functional constraint (2.27) leads in our case to u_0 being quadratic:

1. first, they show that u_0 has some regularities (continuous and has left and right derivative everywhere), for (2.27) implies that $z\mapsto u_0(z)-z^2$ is concave as minimum of affine functions:

$$\forall z\in\mathbb{R},\quad u_0(z)-z^2=\min_{(z_1,z_2)}\left[-z(z_1+z_2)+\frac{(z_1+z_2)^2}{4}+u_0(z_1)+u_0(z_2)\right].$$

2. next, they introduce the Legendre convex conjugate

$$\hat{u_0}:p\mapsto\sup_{z\in\mathbb{R}}\left[(z-z^*)p-u(z)\right],$$

and show that it satisfies the following functional equality, by commuting the different sup operators while computing $\hat{u}_0(p)$ using (2.27):

$$\forall p\in\mathbb{R},\quad \hat{u_0}(p)=\frac{p^2}{4}+2\,\hat{u_0}\left(\frac{p}{2}\right). \tag{2.29}$$

3. As $\hat{u_0}$ is convex by definition, it is continuous and admits left and right derivative everywhere. Moreover, $\hat{u_0}$ has a minimum in 0 and $\hat{u_0}(0)=-u(z^*)=0$. Therefore (2.29) implies by recursion:

$$\forall p>0\quad(\text{resp. }<0),\quad \hat{u}_0(p)=\frac{p^2}{2}+\hat{u_0}'(0^+)\,p\quad(\text{resp. }\hat{u_0}'(0^-)\,p). \tag{2.30}$$

Note that 0 being a minimum of $\hat{u}_0$ implies that: $\hat{u_0}'(0^-)\le 0\le\hat{u_0}'(0^+)$.

4. The next step aims at showing that u_0 is equal to its convex bi-conjugate

$$\hat{\hat{u_0}} : z \mapsto \sup_{p \in \mathbb{R}} \left[p\,(z - z^*) - \hat{u_0}(p) \right],$$

which is computable from (2.30):

$$\hat{\hat{u_0}} : z \mapsto \begin{cases} \frac{(z - z^* - \hat{u}_0(0^-))^2}{2} & \text{if } z < z^* + \hat{u}_0(0^-) \\ 0 & \text{if } z^* + \hat{u}_0(0^-) \leq z \leq z^* + \hat{u}_0(0^+) \\ \frac{(z - z^* - \hat{u}_0(0^+))^2}{2} & \text{if } z > z^* + \hat{u}_0(0^+). \end{cases} \tag{2.31}$$

Standard convexity analysis shows also that $\hat{\hat{u_0}}$ is the lower convex envelope of u_0.

The first implication is that u_0 and $\hat{\hat{u_0}}$ coincide on $\mathbb{R} \backslash [z^* + \hat{u}_0(0^-), z^* + \hat{u}_0(0^+)]$, because $\hat{\hat{u_0}}$ is strictly convex there.

The second implication is that $u_0\left(z^* + \hat{u}_0(0^+)\right) = \hat{\hat{u}}_0\left(z^* + \hat{u}_0(0^+)\right) = 0$ (resp. $z^* + \hat{u}_0(0^-)$), since $z^* + \hat{u}_0(0^+)$ (resp. $z^* + \hat{u}_0(0^-)$) is an extremal point of the graph of $\hat{\hat{u}}_0$. One can show using (2.27) that the midpoint between any zeros of u_0 is still a zero of u_0 (recall that $u_0 \geq 0$). Hence, by density and continuity of u_0, u_0 vanishes on $[z^* + \hat{u}_0(0^-), z^* + \hat{u}_0(0^+)]$.

5. Finally, since u_0 satisfies (2.31) and we need N_ε not to explode when ε vanishes, we necessarily obtain that $\hat{u}_0(0^-) = \hat{u}_0(0^+)$. Hence u_0 quadratic.

2.D Formal approximations of the trait distributions moments in the regime of small variance $\varepsilon^2 \ll 1$

This appendix is dedicated to formally explain (2.12). We remove the time and the deme dependency for the sake of clarity. We denote n_ε the trait distribution density, N_ε the size of the population, $\overline{z}_\varepsilon$ the mean trait, σ_ε^2 the variance and ψ_ε the third central moment. Let us also recall that the computations are performed using the exponential formalism introduced in (2.10) while considering the following formal expansion of u_ε in the regime of small variance:

$$u_\varepsilon = u + \varepsilon^2\, v + \mathcal{O}(\varepsilon^4).$$

Size of population. We have:

$$\begin{aligned}
N_\varepsilon &= \int_{\mathbb{R}} n_\varepsilon(z)\,dz \\
&= \int_{\mathbb{R}} \frac{1}{\sqrt{2\pi}\varepsilon} e^{-\frac{(z-z^*)^2}{2\varepsilon^2}} e^{-u(z)-\varepsilon^2\, v(z)+\mathcal{O}(\varepsilon^4)} dz \\
&= \int_{\mathbb{R}} \frac{e^{-\frac{y^2}{2}}}{\sqrt{2\pi}} e^{-u(z^*+\varepsilon y)-\varepsilon^2 v(z^*+\varepsilon y)+\mathcal{O}(\varepsilon^4)} dy \qquad \left(y := \frac{z-z^*}{\varepsilon}\right) \\
&= \int_{\mathbb{R}} \frac{e^{-\frac{y^2}{2}}}{\sqrt{2\pi}} e^{-[u(z^*)+\varepsilon y u'(z^*)+\frac{\varepsilon^2 y^2}{2}u''(z^*)+\frac{\varepsilon^3 y^3}{6}u'''(z^*)+\mathcal{O}(\varepsilon^4)]-\varepsilon^2 v(z^*)-\varepsilon^3 y v'(z^*)+\mathcal{O}(\varepsilon^4)} dy \\
&= \int_{\mathbb{R}} \frac{e^{-\frac{y^2}{2}}}{\sqrt{2\pi}} e^{-u(z^*)} e^{-\left[\varepsilon y u'(z^*)+\varepsilon^2\left[\frac{y^2 u''(z^*)}{2}+v(z^*)\right]+\varepsilon^3\left[\frac{y^3}{6}u'''(z^*)+yv'\right]+\mathcal{O}(\varepsilon^4)\right]} dy \\
&= \int_{\mathbb{R}} \frac{e^{-\frac{y^2}{2}}}{\sqrt{2\pi}} e^{-u(z^*)} \left[1-\varepsilon y u'(z^*)-\varepsilon^2\left[\frac{y^2 u''(z^*)}{2}+v(z^*)\right]-\varepsilon^3\left[\frac{y^3}{6}u'''(z^*)-yv'(z^*)\right]\right. \\
&\qquad \left. +\frac{1}{2}\left[\varepsilon^2 y^2 u'(z^*)^2+\varepsilon^3\left[y^3 u'(z^*)u''(z^*)+2yu'(z^*)v(z^*)\right]\right]-\frac{\varepsilon^3 y^3 u'(z^*)^3}{6}+\mathcal{O}(\varepsilon^4)\right] \\
&= e^{-u(z^*)}\left[1+\varepsilon^2\left[\frac{u'^2(z^*)}{2}-\frac{u''(z^*)}{2}-v(z^*)\right]\right]+\mathcal{O}(\varepsilon^4),
\end{aligned}$$

from the computations of the moments of a Gaussian.

Mean trait. Similarly as above, we have:

$$\begin{aligned}
\overline{z}_\varepsilon &= \int_{\mathbb{R}} z\frac{n_\varepsilon}{N_\varepsilon}dz \\
&= \frac{1}{N_\varepsilon}\int_{\mathbb{R}} z\frac{1}{\sqrt{2\pi}\varepsilon} e^{-\frac{(z-z^*)^2}{2\varepsilon^2}} e^{-u(z)-\varepsilon^2\, v(z)+\mathcal{O}(\varepsilon^4)} dz \\
&= \frac{1}{N_\varepsilon}\int_{\mathbb{R}} (z^*+\varepsilon y)\frac{e^{-\frac{y^2}{2}}}{\sqrt{2\pi}} e^{-u(z^*+\varepsilon y)-\varepsilon^2 v(z^*+\varepsilon y)+\mathcal{O}(\varepsilon^4)} dy, \qquad \left(y := \frac{z-z^*}{\varepsilon}\right) \\
&= \frac{1}{N_\varepsilon}\int_{\mathbb{R}} (z^*+\varepsilon y)\frac{e^{-\frac{y^2}{2}}}{\sqrt{2\pi}} e^{-u(z^*)}\left[1-\varepsilon y u'(z^*)+\varepsilon^2\left[\frac{y^2 u'(z^*)^2}{2}-\frac{y^2 u''(z^*)}{2}-v(z^*)\right]\right. \\
&\qquad \left. +\varepsilon^3\left[-\frac{y^3}{6}u'''(z^*)-yv'(z^*)+\frac{y^3 u'(z^*)u''(z^*)}{2}+yu'(z^*)v(z^*)-\frac{3y^3 u'(z^*)^3}{6}\right]+\mathcal{O}(\varepsilon^4)\right] \\
&= \frac{e^{-u(z^*)}\left[z^*\left(1+\varepsilon^2\left[\frac{u'^2(z^*)}{2}-\frac{u''(z^*)}{2}-v(z^*)\right]\right)-\varepsilon^2 u'(z^*)\right]+\mathcal{O}(\varepsilon^4)}{e^{-u(z^*)}\left(1+\varepsilon^2\left[\frac{u'^2(z^*)}{2}-\frac{u''(z^*)}{2}-v(z^*)\right]\right)+\mathcal{O}(\varepsilon^4)} \\
&= z^*-\varepsilon^2 u'(z^*)+\mathcal{O}(\varepsilon^4).
\end{aligned}$$

Variance. Using the previous formal computations and methodology, we get:

$$\begin{aligned}
\sigma_\varepsilon^2 &= \frac{1}{N_\varepsilon}\int_{\mathbb{R}}(z-\overline{z}_\varepsilon)^2 n_\varepsilon(z)dz \\
&= \frac{1}{N_\varepsilon}\int_{\mathbb{R}}\left[(z-z^*)^2+(z^*-\overline{z}_\varepsilon)^2+2(z-z^*)(z^*-\overline{z}_\varepsilon)\right]n_\varepsilon(z)dz \\
&= \frac{1}{N_\varepsilon}\int_{\mathbb{R}}\left[\varepsilon^2y^2+2\varepsilon^3yu'(z^*)+\mathcal{O}(\varepsilon^4)\right]\left[1-\varepsilon yu'+\mathcal{O}(\varepsilon^2)\right]e^{-u(z^*)}\frac{e^{-\frac{y^2}{2}}}{\sqrt{2\pi}}dy \\
&= \frac{\varepsilon^2 e^{-u(z^*)}}{e^{-u(z^*)}\left[1+\mathcal{O}(\varepsilon^2)\right]} \\
&= \varepsilon^2+\mathcal{O}(\varepsilon^4).
\end{aligned}$$

Third central moment. We compute, using the same change in variable $y := \frac{z-z^*}{\varepsilon}$:

$$\begin{aligned}
\psi_\varepsilon^3 &= \frac{1}{N_\varepsilon}\int_{\mathbb{R}}(z-\overline{z}_\varepsilon)^3 n_\varepsilon(z)dz \\
&= \frac{1}{N_\varepsilon}\int_{\mathbb{R}}\left[(z-z^*)^3+(z^*-\overline{z}_\varepsilon)^3+3(z-z^*)^2(z^*-\overline{z}_\varepsilon)+3(z-z^*)(z^*-\overline{z}_\varepsilon)^2\right]n_\varepsilon(z)dz \\
&= \frac{1}{N_\varepsilon}\int_{\mathbb{R}}\left[\varepsilon^3y^3+\mathcal{O}(\varepsilon^4)\right]\left[e^{-u(z^*)}+\mathcal{O}(\varepsilon)\right]dz \\
&= \mathcal{O}(\varepsilon^4).
\end{aligned}$$

2.E Fast/slow system: proof of Theorem 2.4.1

This appendix is dedicated to prove Theorem 2.4.1.

Let $(z_0^*, \bar{Y}_0^*) \in \mathbb{R}\times\Omega$ (we recall that $\Omega = (\mathbb{R}_+^*)^2\times\mathbb{R}$) be on the slow manifold, ie. such that $G(z_0^*, \bar{Y}_0^*) = 0$. From Lemma 6 of fast relaxation towards the slow manifold, the jacobian matrix $J_G(z_0^*, \bar{Y}_0^*)$ is invertible. Consequently, the implicit function theorem gives us U open neighbourhood of z_0^* in $\mathbb{R}$, V open neighbourhood of $(z_0^*, \bar{Y}_0^*)$ in $\mathbb{R}\times\Omega$ and $\phi \in C^\infty(U, V)$ such that :

$$\forall (z^*, \bar{Y}^*) \in V,\ G(z^*, \bar{Y}^*, 0) = 0 \implies \bar{Y}^* = \phi(z^*).$$

Hence, we can define a notation that we shall use henceforth:

$$\forall z \in U, J_z := J_G(z, \phi(z)).$$

If K is a compact subset of U such that $z_0^* \in \mathring{K}$, we can define the Cauchy problem (E_0) by the following :

$$(E_0)\quad \begin{cases} \frac{dz^*}{dt} = -2gz^*(t) + F\left(\phi(z^*(t))\right), \\ z^*(0) = z_0^*, \end{cases} \tag{2.32}$$

for $t \le t^*$, that we define as the following:

$$t^* := \inf\{t > 0, z^*(t) \notin K\}.$$

It is similar to (2.20) with the initial conditions $(z^*(0), \bar{Y}_0^*) = (z_0^*, \phi(z_0^*))$. A essential part of the proof relies in the fact that we can define the following uniform positive constant, thanks to Lemma 6 of fast relaxation:

$$\lambda_K = -\frac{1}{2}\max_{z\in K}\{\lambda \in \mathbf{Sp}(J_z)\} > 0.$$

As the first step, we state the following lemma whose proof will be provided at the end of this appendix. It defines a uniform control constant $\gamma > 0$:

Lemma 11. *There exists $\gamma > 0$ such that:*

$$\max_{z\in K,\, s\geq 0}\left|\!\left|\!\left| e^{\lambda_K s} e^{J_z s} \right|\!\right|\!\right| \leq \gamma.$$

($|\!|\!|\cdot|\!|\!|_{\mathcal{M}_3(\mathbb{R})}$ is noted $|\!|\!|\cdot|\!|\!|$)

The next step is to show the convergence of solutions of (P_ε) (2.19) towards those of (P_0) (2.20) on a time interval, yet to be defined, that will be shown to be uniform with regard to ε and the initial conditions, provided that they are small enough. For that purpose, it is more convenient to consider the system (R_ε) verified by the residuals $r_z^\varepsilon(t) = z_\varepsilon(t) - z^*(t)$ and $r_Y^\varepsilon(t) = \bar{Y}_\varepsilon(t) - \bar{Y}^*(t)$:

$$(R_\varepsilon)\quad \begin{cases} \varepsilon^2 \frac{dr_Y^\varepsilon}{dt} = G(z^*(t) + r_z^\varepsilon(t), \bar{Y}^*(t) + r_Y^\varepsilon(t)) - G(z^*(t), \bar{Y}^*(t)) - \varepsilon^2 \frac{d\bar{Y}^*}{dt} + \varepsilon^2 \nu_{N,\varepsilon}(t), \\ \frac{dr_z^\varepsilon}{dt} = -2g r_z^\varepsilon(t) + F(\bar{Y}^*(t) + r_Y^\varepsilon) - F(\bar{Y}^*(t)) + \varepsilon^2 \nu_{z,\varepsilon}(t), \\ (r_z^\varepsilon(0), r_Y^\varepsilon(0)) = (z_0^\varepsilon - z_0^*, \bar{Y}_0^\varepsilon - \bar{Y}_0^*), \end{cases} \tag{2.33}$$

and introduce some further definitions.

Because K is a compact set, there exists $\delta_K > 0$ such that the following set is a compact subset of V:

$$\bar{K}_{\delta_K} = \left\{(z, \bar{Y}) \in \mathbb{R}\times\Omega \,|\, \exists z^* \in K,\ \left|(z,\bar{Y}) - (z^*, \phi(z^*))\right| \leq \delta_K\right\} \subset V.$$

Let us consider from now $(z_0^\varepsilon, N_0^\varepsilon) \in \bar{K}_{\delta_K}$. Then we define $\Delta = \min\left(\frac{\lambda_K}{4C\gamma}, \delta_K\right)$ and $T = \min(t^*, \frac{\lambda_K}{4C'\gamma})$, where:

$$C = \max\left(\|\partial_{\bar{Y}}^2 G\|_{\infty,\bar{K}_{\delta_K}}, \|\partial_z G\|_{\infty,\bar{K}_{\delta_K}}, \|\partial_{\bar{Y}} F\|_{\infty,\Pi_\Omega(\bar{K}_{\delta_K})}\right))$$

and :

$$C' = \max_{t\leq t^*}\left|\!\left|\!\left| \partial_t J_{z^*(t)} \right|\!\right|\!\right|,$$

where Π_Ω is the projection from $\mathbb{R}\times\Omega$ on Ω. One can notice from these definitions and from Lemma 11, that $\gamma, \Delta, T, \lambda_K, C, C'$ do not depend on ε and are uniform on $[0, t^*]$. Specifically taking $\Delta \leq \frac{\lambda_K}{4C\gamma}$ and $T \leq \frac{\lambda_K}{4C'\gamma}$ will turn out to be important in the proof.

On the time region $[0, T]$, we will show that we can control explicitly the various perturbed terms that arise. We can now state the following proposition, whose proof constitutes the core of the resolution of the problem:

Proposition 2.E.1. *As $\max(\varepsilon, |r_z^\varepsilon(0)|, |r_Y^\varepsilon(0)|) \to 0$, $(\bar{Y}_\varepsilon, z_\varepsilon)$ converges toward $(\bar{Y}^*, z^*)$ uniformly on $[0, T]$.*

For the final step, we will show that we can reiterate the process on each interval of time $[jT, \min\{(j+1)T, t^*\}]$ with $\forall j \leq \lfloor \frac{t^*}{T} \rfloor, jT \leq t^*_\varepsilon$. Thus, for sufficiently small ε and initial conditions, the control remains valid until t^*, hence Theorem 1.

For convenience, we will denote by $f * g\,(t)$ the convolution product of f and g at time $t > 0$:

$$f * g\,(t) = \int_0^t f(\tau) g(t-\tau) d\tau.$$

Proof of Proposition 2.E.1. Let $\varepsilon \in]0, 1]$. Let us define an auxiliary time t^*_ε:

$$t^*_\varepsilon = \min\left(t^*, \inf\{t > 0, |r^\varepsilon_z| + |r^\varepsilon_Y| > \Delta\}\right).$$

It ensures that the perturbed trajectory stays inside of $\bar{K}_{\delta_K}$ when $t \leq t^*_\varepsilon$.

Let us highlight the main steps of the proof:

1. preliminary controls on r^ε_Y by $|r^\varepsilon_Y(0)|$ and $\frac{1}{\varepsilon^2}|r^\varepsilon_z| * e^{-\frac{\lambda_K}{2\varepsilon^2}\cdot}$ thanks to the regularity of G, the fast relaxation properties (Lemma 6 and Lemma 11) and Gronwall's lemma.
2. control $|r^\varepsilon_z|$ by $|r^\varepsilon_z(0)|$ and $|r^\varepsilon_Y|$.
3. finish the control on r^ε_Y by using the latter and Gronwall's lemma.

1. For $t \leq \min(T, t^*_\varepsilon)$, we can introduce new terms in the equation from (2.33) on r^ε_Y :

$$\begin{aligned}
\frac{dr^\varepsilon_Y}{dt} &= \frac{J_{z^*(0)}}{\varepsilon^2} r^\varepsilon_Y + \frac{1}{\varepsilon^2}\left[G(z^*(t), \bar{Y}^*(t) + r^\varepsilon_Y(t)) - G(z^*(t), \bar{Y}^*(t)) - J_{z^*(0)} r^\varepsilon_Y\right] \\
&\quad + \frac{1}{\varepsilon^2}\left[G(z^*(t) + r^\varepsilon_z(t), \bar{Y}^*(t) + r^\varepsilon_Y(t)) - G(z^*(t), \bar{Y}^*(t) + r^\varepsilon_Y(t))\right] \\
&\quad - \phi'(z^*(t))(-2gz^*(t) + F(\phi(z^*(t)))) + \nu_{N,\varepsilon}(t) \\
&= \frac{J_{z^*(0)}}{\varepsilon^2} r^\varepsilon_Y + A_1(t) + A_2(t) + A_3(t).
\end{aligned}$$

Since $t \leq \min(T, t^*_\varepsilon)$ and G is C^∞ on $\bar{K}_{\delta_K} \times [0, 1]$, we can control A_1:

$$\begin{aligned}
|A_1(t)| &\leq \frac{1}{\varepsilon^2}\left[|G(z^*(t), \bar{Y}^*(t) + r^\varepsilon_Y(t)) - G(z^*(t), \bar{Y}^*(t) - J_{z^*(t)} r^\varepsilon_Y|\right] \\
&\qquad + \frac{1}{\varepsilon^2}\left[\left|\left|\left|J_{z^*(t)} - J_{z^*(0)}\right|\right|\right| |r^\varepsilon_Y(t)|\right] \\
&\leq \frac{1}{\varepsilon^2}\left[\|\partial^2_{\bar{Y}} G\|_{\infty, \bar{K}_{\delta_K}} |r^\varepsilon_Y(t)|^2 + T \max_{t \leq t^*}\left|\left|\left|\partial_t J_{z^*(t)}\right|\right|\right| |r^\varepsilon_Y(t)|\right] \\
&\leq \frac{1}{\varepsilon^2}(C\Delta + C'T)|r^\varepsilon_Y(t)|,
\end{aligned}$$

and A_2:

$$\begin{aligned}
|A_2(t)| &= \frac{1}{\varepsilon^2}|G(z^*(t) + r^\varepsilon_z(t), \bar{Y}^*(t) + r^\varepsilon_Y(t)) - G(z^*(t), \bar{Y}^*(t) + r^\varepsilon_Y(t))| \\
&\leq \frac{1}{\varepsilon^2}\|\partial_z G\|_{\infty, \bar{K}_{\delta_K}} |r^\varepsilon_z(t)| \leq \frac{C}{\varepsilon^2}|r^\varepsilon_z(t)|,
\end{aligned}$$

and A_3:

$$|A_3(t)| = |-\phi'(z^*(t))(-2gz^*(t) + F(\phi(z^*(t)))) + \nu_{N,\varepsilon}(t)| \leq C'',$$

for some constant C'' independent of ε and $z^*(0) \in K$. Using Duhamel formulas, we get, for $t \leq \min(T, t^*_\varepsilon)$:

$$r^\varepsilon_Y(t) = e^{\frac{J_{z^*(0)}t}{\varepsilon^2}} r^\varepsilon_Y(0) + \left[e^{\frac{J_{z^*(0)}\cdot}{\varepsilon^2}} * (A_1 + A_2 + A_3)\right](t). \tag{2.34}$$

Hence, applying Lemma 11 yields:

$$\begin{aligned}|r^\varepsilon_Y(t)| &\leq \gamma |r^\varepsilon_Y(0)| e^{-\frac{\lambda_K t}{\varepsilon^2}} + \frac{\gamma}{\varepsilon^2}\left[(C|r^\varepsilon_z| + (C\Delta + C'T)|r^\varepsilon_Y|) * e^{-\frac{\lambda_K}{\varepsilon^2}\cdot}\right](t) + \varepsilon^2\gamma\frac{C''}{\lambda_K} \\ &\leq A^{r^\varepsilon_z}(t) + \frac{\gamma(C\Delta + C'T)}{\varepsilon^2}\int_0^t |r^\varepsilon_Y(\tau)|\, e^{\frac{\lambda_K}{\varepsilon^2}(\tau - t)} d\tau,\end{aligned}$$

where $A^{r^\varepsilon_z}(t) := \gamma |r^\varepsilon_Y(0)| e^{-\frac{\lambda_K t}{\varepsilon^2}} + \frac{\gamma C}{\varepsilon^2}\left(|r^\varepsilon_z| * e^{-\frac{\lambda_K}{\varepsilon^2}\cdot}\right)(t) + \varepsilon^2\gamma\frac{C''}{\lambda_K}$.

Applying Gronwall inequality to $r^\varepsilon_Y(t) e^{\frac{\lambda_K t}{\varepsilon^2}}$ yields:

$$|r^\varepsilon_Y(t)| \leq A^{r^\varepsilon_z}(t) + \frac{\gamma(C\Delta + C'T)}{\varepsilon^2}\left[A^{r^\varepsilon_z} * e^{\left(\frac{-\lambda_K}{\varepsilon^2} + \frac{\gamma(C\Delta + C'T)}{\varepsilon^2}\right)\cdot}\right](t). \tag{2.35}$$

Having fixed $\Delta \leq \frac{\lambda_K}{4C\gamma}$ and $T \leq \frac{\lambda_K}{4C'\gamma}$ in the preliminaries ensures that $e^{\left(\frac{-\lambda_K}{\varepsilon^2} + \frac{\gamma(C\Delta + C'T)}{\varepsilon^2}\right)\cdot}$ defines a negative exponential term, that we can dominate by $e^{-\frac{\lambda_K}{2\varepsilon^2}\cdot}$. Hence:

$$|r^\varepsilon_Y(t)| \leq A^{r^\varepsilon_z}(t) + \left[A^{r^\varepsilon_z} * \frac{\lambda_K}{2\varepsilon^2} e^{-\frac{\lambda_K}{2\varepsilon^2}\cdot}\right](t). \tag{2.36}$$

Making $A^{r^\varepsilon_z}$ explicit gives:

$$\begin{aligned}|r^\varepsilon_Y(t)| &\leq \gamma |r^\varepsilon_Y(0)| e^{-\frac{\lambda_K t}{\varepsilon^2}} + \frac{\gamma C}{\varepsilon^2}|r^\varepsilon_z| * e^{-\frac{\lambda_K}{\varepsilon^2}\cdot}(t) + \varepsilon^2\gamma\frac{C''}{\lambda_K} \\ &\quad + \left[\left(\gamma |r^\varepsilon_Y(0)| e^{-\frac{\lambda_K}{\varepsilon^2}\cdot} + \frac{\gamma C}{\varepsilon^2}\left[|r^\varepsilon_z| * e^{-\frac{\lambda_K}{\varepsilon^2}\cdot}\right] + \varepsilon^2\gamma\frac{C''}{\lambda_K}\right) * \left(\frac{\lambda_K}{2\varepsilon^2} e^{-\frac{\lambda_K}{2\varepsilon^2}\cdot}\right)\right](t) \\ &\leq \gamma |r^\varepsilon_Y(0)| \left[e^{-\frac{\lambda_K t}{\varepsilon^2}} + e^{-\frac{\lambda_K}{\varepsilon^2}\cdot} * \left(\frac{\lambda_K}{2\varepsilon^2} e^{-\frac{\lambda_K}{2\varepsilon^2}\cdot}\right)(t)\right] + \varepsilon^2\gamma\frac{C''}{\lambda_K}\left(\left(1 + \int_0^t \frac{\lambda_K}{2\varepsilon^2} e^{-\frac{\lambda_K}{2\varepsilon^2}(\tau - t)} dt\right)\right. \\ &\quad \left. + \frac{\gamma C}{\varepsilon^2}|r^\varepsilon_z| * \left(e^{-\frac{\lambda_K}{\varepsilon^2}\cdot} + e^{-\frac{\lambda_K}{\varepsilon^2}\cdot} * \frac{\lambda_K}{2\varepsilon^2} e^{-\frac{\lambda_K}{2\varepsilon^2}\cdot}\right)(t), \right. \end{aligned} \tag{2.37}$$

thanks to the associativity of the convolution product. One can compute that, for $t \geq 0$:

$$\begin{aligned}e^{-\frac{\lambda_K t}{\varepsilon^2}} + e^{-\frac{\lambda_K}{\varepsilon^2}\cdot} * \left(\frac{\lambda_K}{2\varepsilon^2} e^{-\frac{\lambda_K}{2\varepsilon^2}\cdot}\right)(t) &= e^{-\frac{\lambda_K t}{\varepsilon^2}} + \frac{\lambda_K}{2\varepsilon^2}\int_0^t e^{-\frac{\lambda_K}{\varepsilon^2}\tau} e^{-\frac{\lambda_K}{2\varepsilon^2}(t-\tau)} d\tau \\ &= e^{-\frac{\lambda_K t}{\varepsilon^2}} + \frac{\lambda_K}{2\varepsilon^2}\int_0^t e^{-\frac{\lambda_K}{2\varepsilon^2}(t+\tau)} d\tau = e^{-\frac{\lambda_K}{2\varepsilon^2}t}.\end{aligned}$$

Hence, replacing those terms in (2.37) yields:

$$|r^\varepsilon_Y(t)| \leq \gamma |r^\varepsilon_Y(0)| e^{-\frac{\lambda_K}{2\varepsilon^2}t} + 2\varepsilon^2\gamma\frac{C''}{\lambda_K} + \frac{C\gamma}{\varepsilon^2}|r^\varepsilon_z| * e^{-\frac{\lambda_K}{2\varepsilon^2}\cdot}(t). \tag{2.38}$$

2. The next step is to gain similarly some control on $|r_z^\varepsilon|$. Using Duhamel formula on the equation from (2.33) on r_z^ε gives, for $t \leq \min(T, t_\varepsilon^*)$:

$$r_z^\varepsilon(t) = r_z^\varepsilon(0)e^{-2gt} + \left(\left[F(N^* + r_Y^\varepsilon) - F(N^*) + \varepsilon^2 \nu_{z,\varepsilon} \right] * e^{-2g\cdot} \right)(t),$$

which yields:

$$|r_z^\varepsilon(t)| \leq |r_z^\varepsilon(0)|e^{-2gt} + \varepsilon^2 \frac{\|\nu_{z,\varepsilon}\|_\infty}{2g} + \|\partial_{\bar{Y}} F\|_{\infty, \Pi_\Omega(\bar{K}_{\delta_K})} \left(|r_Y^\varepsilon| * e^{-2g\cdot} \right)(t).$$

Hence:

$$|r_z^\varepsilon(t)| \leq |r_z^\varepsilon(0)|e^{-2gt} + \varepsilon^2 \frac{\|\nu_{z,\varepsilon}\|_\infty}{2g} + C \left(|r_Y^\varepsilon| * e^{-2g\cdot} \right)(t). \tag{2.39}$$

At that point, it is clear that it is sufficient to control $|r_Y^\varepsilon|$ and $|r_z^\varepsilon(0)|$ in order to control $|r_z^\varepsilon(t)|$ for sufficiently small ε.

3. Plugging the latter in (2.38) gives:

$$|r_Y^\varepsilon(t)| \leq \gamma |r_Y^\varepsilon(0)| e^{-\frac{\lambda_K}{2\varepsilon^2}t} + \frac{C\gamma}{\varepsilon^2} |r_z^\varepsilon(0)| \left(e^{-2g\cdot} * e^{-\frac{\lambda_K}{2\varepsilon^2}\cdot} \right)(t) + \varepsilon^2 \frac{C\gamma \|\nu_{z,\varepsilon}\|_\infty}{\lambda_K g} + 2\varepsilon^2 \gamma \frac{C''}{\lambda_K} + \frac{\gamma C^2}{\varepsilon^2} \left[|r_Y^\varepsilon| * \left(e^{-2g\cdot} * e^{-\frac{\lambda_K}{2\varepsilon^2}\cdot} \right) \right](t). \tag{2.40}$$

Similarly as the computation above, we have, for $\varepsilon^2 < \min(\frac{\lambda_K}{8g}, 1)$ and $t \geq 0$:

$$e^{-2g\cdot} * e^{-\frac{\lambda_K}{2\varepsilon^2}\cdot}(t) = \frac{1}{\frac{\lambda_K}{2\varepsilon^2} - 2g} \left(e^{-2gt} - e^{-\frac{\lambda_K}{2\varepsilon^2}t} \right) \leq \frac{4\varepsilon^2}{\lambda_K} e^{-2gt}.$$

Hence, for $\varepsilon^2 < \min(\frac{\lambda_K}{8g}, 1)$, we get from (2.40):

$$\begin{aligned} |r_Y^\varepsilon(t)| &\leq \gamma |r_Y^\varepsilon(0)| e^{-\frac{\lambda_K}{2\varepsilon^2}t} + \frac{2\gamma C}{\lambda_K} |r_z^\varepsilon(0)| e^{-2gt} + \varepsilon^2 \frac{C\gamma \|\nu_{z,\varepsilon}\|_\infty}{\lambda_K g} + 2\varepsilon^2 \gamma \frac{C''}{\lambda_K} \\ &\quad + \frac{2\gamma C^2}{\lambda_K} \left(|r_Y^\varepsilon| * e^{-2g\cdot} \right)(t) \\ &\leq C_0^\varepsilon(t) + \frac{2\gamma C^2}{\lambda_K} \left(|r_Y^\varepsilon| * e^{-2g\cdot} \right)(t), \end{aligned}$$

where we define: $C_0^\varepsilon(t) := \gamma |r_Y^\varepsilon(0)| e^{-\frac{\lambda_K}{2\varepsilon^2}t} + \frac{2\gamma C}{\lambda_K} |r_z^\varepsilon(0)| e^{-2gt} + \varepsilon^2 \frac{C\gamma \|\nu_{z,\varepsilon}\|_\infty}{\lambda_K g} + 2\varepsilon^2 \gamma \frac{C''}{\lambda_K}$.
Using once again Gronwall inequality on $|r_Y^\varepsilon| e^{2g\cdot}$ yields:

$$|r_Y^\varepsilon(t)| \leq C_0^\varepsilon(t) + \frac{2\gamma C^2}{\lambda_K} \left(C_0^\varepsilon * e^{\left(-2g + \frac{2\gamma C^2}{\lambda_K}\right)\cdot} \right)(t). \tag{2.41}$$

Recalling that:

$$C_0^\varepsilon(t) = \gamma |r_Y^\varepsilon(0)| e^{-\frac{\lambda_K}{2\varepsilon^2}t} + \frac{2\gamma C}{\lambda_K} |r_z^\varepsilon(0)| e^{-2gt} + \varepsilon^2 \frac{C\gamma \|\nu_{z,\varepsilon}\|_\infty}{\lambda_K g} + 2\varepsilon^2 \gamma \frac{C''}{\lambda_K},$$

we get that, thanks to (2.41) and (2.39), for a given $0 < \delta < \Delta$, there exists $\eta_\delta > 0$ depending only on $\delta, g, m, K, t^*, F, G, \|\nu_{z,\varepsilon}\|_\infty$ such that :

$$\forall (\varepsilon, |r_Y^\varepsilon(0)|, |r_z^\varepsilon(0)|) \in [0, \eta_\delta]^3, \max_{t \leq \min(T, t_\varepsilon^*)} |r_Y^\varepsilon(t)| + |r_z^\varepsilon(t)| \leq \delta.$$

Recalling that $t_\varepsilon^* = \min\left(t^*, \inf\{t > 0, |r_z^\varepsilon| + |r_Y^\varepsilon| > \Delta\}\right)$, we get that $T \leq t_\varepsilon^*$, for $\delta < \Delta$ and $(\varepsilon, |r_Y^\varepsilon(0)|, |r_z^\varepsilon(0)|) \in [0, \eta_\delta]^3$. Consequently, the convergence is uniform on $[0, T]$. □

Proof of Theorem 1. One can notice that the control obtained in the proof of Proposition 1 can be applied on any time interval $[a, a+T]$ with $a \in [0, t^* - T]$, provided that $(\varepsilon, |r_Y^\varepsilon(a)|, |r_z^\varepsilon(a)|)$ are small enough. Therefore, we can reiterate the control a finite number of times on the intervals $[jT, \min\{(j+1)T, t^*\}]$ with $\forall j \leq \lfloor \frac{t^*}{T} \rfloor$. Hence, the uniform convergence on $[0, t^*]$. □

Proof of Lemma 11. Recall that for all $z \in K$, J_z has real negative eigenvalues, uniformly bounded over K by $-2\lambda_K < -\lambda_K$. Let us define, for $z \in K$:

$$f_{\lambda_K,z} : \mathbb{R}_+ \to \mathbb{R}_+, \quad s \mapsto \left|\!\left|\!\left| e^{J_z s} e^{\lambda_K s} \right|\!\right|\!\right|.$$

For all $z \in \mathbb{K}$, $f_{\lambda_K,z}$ is continuous. Moreover, Theorem 2.34 of Chicone 1999 ensures that $f_{l,z}$ is bounded for all $l < 2\lambda_K$.

We can thus define :

$$\Gamma_{\lambda_K} : K \to \mathbb{R}_+^*, \quad z \mapsto \max_{s \geq 0} f_{\lambda_K,z}(s).$$

Let us show that Γ_{λ_K} is a continuous function. Let $z_0 \in K$ and $\varepsilon > 0$.

One can first notice that, for $s \geq 0$:

$$f_{\lambda_K,z}(s) = f_{\frac{3\lambda_K}{2},z}(s) e^{-\frac{\lambda_K}{2}s} < \Gamma_{\frac{3\lambda_K}{2},z} e^{-\frac{\lambda_K}{2}s}.$$

Thus, $f_{\lambda_K,z}$ vanishes when s goes to infinity. As a consequence, there exists $s_0 \geq 0$ such that:

$$\Gamma_{\lambda_K}(z_0) = \left|\!\left|\!\left| e^{J_{z_0} s_0} e^{\lambda_K s_0} \right|\!\right|\!\right|.$$

Furthermore, for $l \in]\lambda_K, 2\lambda_K[$, we have:

$$\Gamma_l(z_0) = \left|\!\left|\!\left| e^{J_{z_0} s_0} e^{l s_0} \right|\!\right|\!\right| = \Gamma_{\lambda_K}(z_0) e^{(l-\lambda_K)s_0}.$$

We can therefore choose $l \in]\lambda_K, 2\lambda_K[$ such that $\Gamma_{\lambda_K}(z_0) \leq \Gamma_l(z_0) \leq \Gamma_{\lambda_K}(z_0) + \varepsilon$.

As $z \mapsto J_z$ is a continuous function, there exists $\delta > 0$ that ensures that for if $z \in K$ and $|z - z_0| \leq \delta$, then:

$$|||J_z - J_{z_0}||| < \frac{l - \lambda_K}{2\Gamma_l(z_0)}.$$

Let us consider such a z.

As $e^{J_z s}$ is solution of the ODE : $y' = J_{z_0} y + (J_z - J_{z_0})y$, we obtain, for $s \geq 0$:

$$e^{J_z s} = e^{J_{z_0} s} + e^{J_{z_0} \cdot} * (J_z - J_{z_0}) e^{J_z \cdot}(s).$$

Hence :

$$\left|\!\left|\!\left| e^{J_z t} \right|\!\right|\!\right| \leq \Gamma_l(z_0) e^{-ls} + \frac{l - \lambda_K}{2} \left|\!\left|\!\left| e^{J_z \cdot} \right|\!\right|\!\right| * e^{-l \cdot}$$

From applying Gronwall's inequality to $t \mapsto \left|\!\left|\!\left| e^{J_z s} \right|\!\right|\!\right| e^{ls}$, it comes that, for $s \geq 0$:

$$\begin{aligned} \left|\!\left|\!\left| e^{J_z s} \right|\!\right|\!\right| &\leq \Gamma_l(z_0) e^{-\left(l - \frac{l-\lambda_K}{2}\right)t} \leq \Gamma_l(z_0) e^{-\left(\frac{l+\lambda_K}{2}\right)s} \\ &\leq \left[\Gamma_{\lambda_K}(z_0) + \varepsilon\right] e^{-\lambda_K s}. \end{aligned}$$

Hence:

$$\Gamma_{\lambda_K}(z) \leq \Gamma_{\lambda_K}(z_0) + \varepsilon.$$

Moreover, recall that t_0 was defined so that :

$$\Gamma_{\lambda_K}(z_0) = \left|\!\left|\!\left| e^{J_{z_0} s_0} e^{\lambda_K s_0} \right|\!\right|\!\right|.$$

Then, by continuity of $z \mapsto e^{J_z s_0}$, there exists $\delta' > 0$ that ensures that for $|z - z_0| \leq \delta'$, we have:

$$\left|\!\left|\!\left| e^{J_z s_0} e^{\lambda_K s_0} \right|\!\right|\!\right| \geq \left|\!\left|\!\left| e^{J_{z_0} s_0} e^{\lambda_K s_0} \right|\!\right|\!\right| - \varepsilon.$$

Hence:

$$\Gamma_{\lambda_K}(z) \geq \Gamma_{\lambda_K}(z_0) - \varepsilon.$$

In conclusion, if $|z - z_0| \leq \min(\delta, \delta')$, then $|\Gamma_{\lambda_K}(z) - \Gamma_{\lambda_K}(z_0)| \leq \varepsilon$. Hence Γ_{λ_K} is continuous over K. Furthermore, as K is a compact set, Γ_{λ_K} is bounded, by γ. □

2.F Proof of Proposition 2.4.1

This appendix is dedicated to the proof of Proposition 2.4.1.

Proof. Let $(g, m, z^*) \in \mathbb{R}_+^* \times \mathbb{R}_+^* \times \mathbb{R}_+$ be such that P_{z^*} has a single positive root. From Lemma 1, this root defines a fast equilibrium if it is greater than $f_1(z^*)$. From Lemma 2, that is the case if and only if $f_1(z^*)$ is negative or $P_{z^*}(f_1(z^*))$ is negative.

First, regarding the sign of $f_1(z^*)$, we have:

$$f_1(z^*) < 0 \iff (z^* + 1)^2 < \frac{1 - m}{g},$$

which requires that $m < 1$. If $m < 1$ then:

$$f_1(z^*) < 0 \iff 0 \leq z^* < \sqrt{\frac{1 - m}{g}} - 1,$$

which requires that $m + g < 1$. Hence:

$$f_1(z^*) < 0 \iff [m + g < 1] \wedge [z^* < \sqrt{\frac{1 - m}{g}} - 1].$$

Next, regarding the sign of $P_{z^*}(f_1(z^*))$, we compute:

$$\begin{aligned} P_{z^*}(f_1(z^*)) &= f_1(z^*) f_2(z^*) - 1 \\ &= \left(1 + \frac{g}{m}(z^* + 1)^2 - \frac{1}{m}\right)\left(1 + \frac{g}{m}(z^* - 1)^2 - \frac{1}{m}\right) - 1 \\ &= \frac{g^2}{m^2}\left[z^{*4} + z^{*2}\,\frac{2(m - g - 1)}{g} + \frac{(g - 1)(2m + g - 1)}{g^2}\right] \end{aligned}$$

Let us define:

$$Q(X) = X^2 + X\,\frac{2(m - g - 1)}{g} + \frac{(g - 1)(2m + g - 1)}{g^2},$$

z_1, z_2 its two roots and $\Delta = \frac{4}{g^2}\left[m^2 - 4g\,(m - 1)\right]$ its discriminant. From the computation above,

$$P_{z^*}(f_1(z^*)) < 0 \iff [\,\Delta > 0\,] \wedge \left[\, z^{*2} \in]z_1, z_2[\,\right].$$

We have:

$$\Delta > 0 = \iff m^2 - 4\,g\,m + 4\,g > 0$$
$$\iff [g < 1] \vee \left[[g \geq 1] \wedge \left[\left[0 < m < 2g\left(1 - \sqrt{1 - \frac{1}{g}}\right)\right] \vee \left[m > 2g\left(1 + \sqrt{1 - \frac{1}{g}}\right)\right]\right]\right]$$

and:

$$z_1 z_2 = \frac{(g-1)(2m+g-1)}{g^2}, \quad z_1 + z_2 = \frac{2(g+1-m)}{g}.$$

Consequently:

- ◇ if $g \geq 1$, then $2m + g - 1 > 0$ and then $z_1 z_2 \geq 0$. If, additionally, $m < 2g\left(1 - \sqrt{1 - \frac{1}{g}}\right)$, then $m < 2 \leq g + 1$ ($g \mapsto 2g - 2\sqrt{g^2 - g}$ is decreasing on $[1, +\infty[$). Therefore, we get: $z_1 + z_2 > 0$ and thus, $z_2 > 0$ and $z_1 \geq 0$. At last, if $m > 2g\left(1 + \sqrt{1 - \frac{1}{g}}\right)$, then $m > 2\,g \geq g + 1$, which implies $z_1 + z_2 < 0$ and thus $z_1 < 0, z_2 \leq 0$.
- ◇ if $g < 1$, then $z_1 + z_2 \geq 0$ if and only if $m \leq g + 1$ and $z_1 z_2 \geq 0$ if and only if $m \leq \frac{1-g}{2}$ (which is lower than $g + 1$).

Hence the result. □

2.G Proof of Lemma 9

This section is dedicated to proving Lemma 9, which concludes the proof of Proposition 2.5.2.

Proof of Lemma 9. Let $(m, g) \in {\mathbb{R}_+^*}^2$ verify (2.25). Then, from the first part of the proof of Proposition 2.5.2, there exists a unique $\rho^* > 0$ that is solution of the equation in (2.23). Let us define N_1^* and N_2^* such as in (2.26). Then we have: $0 < \rho^* = \frac{N_2^*}{N_1^*}$. Thus:

$$N_1^* > 0 \iff N_2^* > 0 \iff \frac{1}{m}(N_1^* + N_2^*) > 0.$$

Borrowing once again the notations: $a = \frac{4g}{m}$, $b = \frac{1}{m}$ and $y^* = \rho^* + \frac{1}{\rho^*}$ (unique root of S larger than 2), (2.26) leads to:

$$\frac{1}{m}(N_1^* + N_2^*) = 2\left(\frac{1}{m} - 1\right) + y^* - \frac{4g}{m}\frac{{y^*}^2 - 2}{{y^*}^2}$$
$$= \frac{1}{{y^*}^2}\left[{y^*}^3 + \left[\frac{1-2m}{m} + \frac{1}{m} - \frac{4g}{m}\right]{y^*}^2 + 2 \times \frac{4g}{m}\right]$$
$$= \frac{1}{{y^*}^2}\left[S(y^*) + (\frac{1-2m}{m}){y^*}^2 + \frac{4g}{m}y^* + \frac{4g}{m}\right].$$

As $S(y^*) = 0$, we get:

$$N_1^* > 0 \iff N_2^* > 0 \iff (1-2m){y^*}^2 + 4gy^* + 4g > 0.$$

This is always true whenever $m \leq \frac{1}{2}$. Otherwise, let us suppose henceforth that $2m > 1$. The condition above is equivalent to:

$$y^* < c + \sqrt{c^2 + 2c}, \quad \text{where: } c = \frac{2g}{2m-1} > 0.$$

Let us show that: $c+\sqrt{c^2+2c} \geq 2$. It is sufficient to show that: $c \geq \frac{2}{3}$, which is equivalent to having: $3g+1 \geq 2m$. In this proof, we are considering $(m,g) \in {\mathbb{R}_+^*}^2$ such that $1+2m < 5g$ and $4g\,(m-1) < m^2$. Let us show that such pairs verify $3g+1 \geq 2m$:

- $\diamond$ if $g \leq 1$, then $m < \frac{5g-1}{2} \leq \frac{3g+1}{2}$.
- $\diamond$ if $g \geq 1$, then $m < 2g - 2\sqrt{g^2-g}$ which is a decreasing function on $[1,+\infty[$, which takes the value 2 when $g=1$. Hence it is always dominated by $g \mapsto \frac{3g+1}{2}$ on this interval.

Hence $c+\sqrt{c^2+2c} \geq \frac{2}{3}+\sqrt{\frac{4}{9}+\frac{4}{3}} = 2$. Therefore, as y^* is the only root of S greater than 2, we get the following equivalence:

$$y^* < c+\sqrt{c^2+c} \iff S\left(c+\sqrt{c^2+2c}\right) > 0.$$

The rest of the proof is dedicated to examine the conditions on (m,g) under which:

$$S\left(c+\sqrt{c^2+2c}\right) > 0.$$

Let us set $Q := \sqrt{c^2+2c} = \sqrt{4g\,\frac{g+2m-1}{(2m-1)^2}}$. Tedious computations done with the help of Mathematica show that: $S(c) = Q^2\left[\frac{g(4-6m)+(2m-1)^2}{m\,(2m-1)}\right]$, and we next compute:

$$S(c+Q) = S(c) + Q^2\left[3c+\frac{1-4g}{m}\right] + Q\left[Q^2+3c^2+2c\,\frac{(1-4g)}{m} - \frac{4g}{m}\right]$$

$$= Q^2\left[\frac{g(4-6m)+(2m-1)^2}{m\,(2m-1)} + \frac{6g}{2m-1} + \frac{1-4g}{m}\right] + Q\left[4c^2+2c\,\frac{(m+1-4g)}{m} - \frac{4g}{m}\right]$$

$$= Q\left[2Q\frac{\left(2m^2-m-4g\,(m-1)\right)}{m(2m-1)} - \frac{4g\,\left(4g\,(m-1)+2m^2-5m+2\right)}{m(2m-1)^2}\right].$$

Hence:

$$\begin{aligned} & S(c+Q) > 0 \\ \iff & Q\left(2m^2-m-4g\,(m-1)\right) > 2g\frac{\left(4g\,(m-1)+2m^2-5m+2\right)}{(2m-1)} \\ \iff & \sqrt{g+2m-1}\left(2m^2-m-4g\,(m-1)\right) > 2\sqrt{g}\left(4g\,(m-1)+2m^2-5m+2\right). \end{aligned}$$

Let us study different cases corresponding to different ranges of value of $m > \frac{1}{2}$.

If $\underline{m=1}$, then the last line is equivalent to :

$$\sqrt{1+g} > -2\sqrt{g},$$

which is true for all $g > 0$.

If $\underline{\frac{1}{2} < m < 1}$, then:

$$4g\,(m-1)+2m^2-5m+2 = 4g\,(m-1)+2(m-2)\left(m-\frac{1}{2}\right) < 0,$$

and:

$$2m^2-m-4g\,(m-1) = 2m\left(m-\frac{1}{2}\right)+4g(1-m) > 0.$$

Hence, for all g such that $1+2m<5g$ and $m^2>4g\,(m-1)$:

$$\sqrt{g+2m-1}\left(2m^2-m-4g\,(m-1)\right)>2\sqrt{g}\left(4g\,(m-1)+2m^2-5m+2\right).$$

If $\underline{m>1}$, then:

$$2m^2-m>m^2>4g\,(m-1).$$

Hence, if: $4g\,(m-1)+2m^2-5m+2<0$, then, for all g such that $1+2m<5g$ and $m^2>4g\,(m-1)$:

$$\sqrt{g+2m-1}\left(2m^2-m-4g\,(m-1)\right)>2\sqrt{g}\left(4g\,(m-1)+2m^2-5m+2\right).$$

Otherwise, if $4g\,(m-1)+2m^2-5m+2\geq 0$, then:

$$\begin{aligned}
&S(c+Q)>0\\
\iff\ &\sqrt{g+2m-1}\left(2m^2-m-4g\,(m-1)\right)>2\sqrt{g}\left(4g\,(m-1)+2m^2-5m+2\right)\\
\iff\ &\left(1+\frac{2m-1}{g}\right)\left(2m^2-2-4g\,(m-1)\right)^2>4\left(4g\,(m-1)+2m^2-5m+2\right)^2.
\end{aligned}$$

Let us note $x:=\frac{2m-1}{g}$. Then, the latter is equivalent to:

$$\begin{aligned}
&(1+x)\left[(m-1)x+(x-4(m-1))\right]^2-\left[(m-1)x-(x-4(m-1))\right]^2 &&>0\\
\iff\ &4(m-1)x(x-4(m-1))+x\left(mx-4(m-1)\right)^2 &&>0\\
\iff\ &4(m-1)x-16(m-1)^2+m^2x^2-8mx(m-1)+16(m-1)^2 &&>0\\
\iff\ &m^2x^2+4x(m-1)(1-2m) &&>0\\
\iff\ &m^2x^2-4x^2g\,(m-1) &&>0\\
\iff\ &m^2>4g\,(m-1).
\end{aligned}$$

□

2.H Details of the numerical analysis carried out in Section 2.3.

Domains. We consider a bounded trait domain $[-\boldsymbol{z_{\max}},\boldsymbol{z_{\max}}]$, discretised in a mesh $(\boldsymbol{z}_k)_{0\leq k<K}$ (K odd) with regard to the step length $\delta z>0$, and a time domain $[0,\boldsymbol{T_{\max}}]$, discretised in a mesh $\left(\boldsymbol{t}^l\right)_{0\leq l<L}$ with regard to the step length $\delta t>0$. In the the simulations involved in Fig. 2.2, we use the following values for the parameters:

$$\boldsymbol{z_{\max}}=7,\quad \boldsymbol{T_{\max}}=1000,\quad \delta z=1.6\times 10^{-2},\quad \delta t=5\times 10^{-3}.$$

Scheme. For $i\in\{1,2\}, 0\leq l<L$, we approximate the trait distributions $\boldsymbol{n_i}(\boldsymbol{t}^l,\cdot)$ by $\left(\boldsymbol{n}_{i,k}^l\right)_{0\leq k<K}$ with the following semi-implicit scheme:

$$\frac{\boldsymbol{\sigma}^2}{\delta t}\left(\boldsymbol{n}_{i,k}^{l+1}-\boldsymbol{n}_{i,k}^l\right)=\boldsymbol{r}\,\boldsymbol{B}_{i,k}^l-\left(\boldsymbol{g}\,(\boldsymbol{z_k}-\boldsymbol{\theta_i})^2+\boldsymbol{\kappa}\,\boldsymbol{N}_i^l+\boldsymbol{m}\right)\boldsymbol{n}_{i,k}^{l+1}+\boldsymbol{m}\,\boldsymbol{n}_{j,k}^{l+1},$$

where $\boldsymbol{N}_i^l = \sum_{k=0}^{K-2} \boldsymbol{n}_{i,k}^l \, \delta z$ and $\boldsymbol{B}_{i,k}^l$ is a discretisation of the reproduction operator $\boldsymbol{\mathcal{B}_\sigma}(\boldsymbol{n_i}(t^l, z_k)$. In the next paragraph, we detail how we compute $\left(\boldsymbol{B}_{i,k}^l\right)_{0\leq k<K}$.

We approximate the system of moments of Ronce and Kirkpatrick 2001 following a similar semi-implicit scheme.

Discretization of the reproduction operator. The discretization of the reproduction operator is in accordance with the double convolution form shown in Lemma 10, as it increases greatly the computational speed in comparison to a double loop. However, the half-arguments involved in Lemma 10 calls for a special attention to the meshes involved.

Let us define two auxiliary trait meshes

1. $(\tilde{\boldsymbol{z}}_{k'})_{0\leq k'<2K-1}$ on $[-\boldsymbol{z_{\max}}, \boldsymbol{z_{\max}}]$, with step length $\frac{\delta z}{2}$,
2. $(\hat{\boldsymbol{z}}_{k''})_{0\leq k''<4K-3}$ on $[-2\boldsymbol{z_{\max}}, 2\boldsymbol{z_{\max}}]$, with step length $\frac{\delta z}{2}$.

We define the vector $(G_{k'})_{0\leq k'<2K-1}$ discretising the Gaussian kernel involved in our reproduction operator on the trait grid $(\tilde{\boldsymbol{z}}_{k'})_{0\leq k'<2K-1}$:

$$G_{k'} = \frac{1}{\sqrt{\pi}\boldsymbol{\sigma}} \exp\left[-\frac{\tilde{\boldsymbol{z}}_{k'}^2}{\boldsymbol{\sigma^2}}\right].$$

We next define the vector $\left(\hat{B}_{i,k''}^l\right)_{0\leq k''<4K-3}$ resulting from the following double discrete convolution (denoted $*$):

$$\left(\hat{B}_{i,k''}^l\right)_{0\leq k''<4K-3} = \frac{1}{\boldsymbol{N}_i^l}\left(\boldsymbol{n}_{i,k}^l\right)_{0\leq k<K} * \left(\boldsymbol{n}_{i,k}^l\right)_{0\leq k<K} * (G_{k'})_{0\leq k'<2K-1}$$

We use a convolution algorithm with default settings: the size of the output is the sum of entry vector sizes minus one, and out of bounds index entries are extrapolated as 0. A straightforward computation shows that $\left(\hat{B}_{i,k''}^l\right)_{0\leq k''<4K-3}$ is the approximation of the reproduction operator on the mesh $(\hat{\boldsymbol{z}}_{k''})_{0\leq k''<4K-3}$:

$$\begin{aligned}
\hat{B}_{i,k''}^l &= \frac{\delta z^2}{\boldsymbol{N}_i^l} \sum_{k_1=0}^{4K-4} \boldsymbol{n}_{i,k_1}^l \sum_{k_2=0}^{3K-2} \boldsymbol{n}_{i,k_2}^l \, G_{k''-k_1-k_2} \\
&= \frac{\delta z^2}{\boldsymbol{N}_i^l} \sum_{k_1=0}^{4K-4} \boldsymbol{n}_{i,k_1}^l \sum_{k_2=0}^{3K-2} \boldsymbol{n}_{i,k_2}^l \frac{1}{\sqrt{\pi}\boldsymbol{\sigma}} \exp\left[-\frac{\tilde{\boldsymbol{z}}_{k''-k_1-k_2}^2}{\boldsymbol{\sigma^2}}\right] \\
&= \frac{\delta z^2}{\boldsymbol{N}_i^l} \sum_{k_1=0}^{4K-4} \boldsymbol{n}_{i,k_1}^l \sum_{k_2=0}^{3K-2} \boldsymbol{n}_{i,k_2}^l \frac{1}{\sqrt{\pi}\boldsymbol{\sigma}} \exp\left[-\frac{\left(-\boldsymbol{z}_{\max} + \frac{\delta z}{2}(k'' - k_1 - k_2)\right)^2}{\boldsymbol{\sigma^2}}\right] \\
&= \frac{\delta z^2}{\boldsymbol{N}_i^l} \sum_{k_1=0}^{4K-4} \boldsymbol{n}_{i,k_1}^l \sum_{k_2=0}^{3K-2} \boldsymbol{n}_{i,k_2}^l \frac{1}{\sqrt{\pi}\boldsymbol{\sigma}} \exp\left[-\frac{\left(-2\boldsymbol{z}_{\max} + \frac{k''\delta z}{2} - \frac{(-\boldsymbol{z}_{\max}+k_1\delta z)+(-\boldsymbol{z}_{\max}+k_2\delta z)}{2}\right)^2}{\boldsymbol{\sigma^2}}\right] \\
&= \frac{\delta z^2}{\boldsymbol{N}_i^l} \sum_{k_1=0}^{4K-4} \boldsymbol{n}_{i,k_1}^l \sum_{k_2=0}^{3K-2} \boldsymbol{n}_{i,k_2}^l \frac{1}{\sqrt{\pi}\boldsymbol{\sigma}} \exp\left[-\frac{\left(\hat{\boldsymbol{z}}_{k''} - \frac{z_{k_1}+z_{k_2}}{2}\right)^2}{\boldsymbol{\sigma^2}}\right].
\end{aligned}$$

Thus, we interpolate $\left(\hat{B}^l_{i,k''}\right)_{0\leq k''<4K-3}$ at the entries corresponding to $(\boldsymbol{z}_k)_{0\leq k<K}$ to obtain $\left(\boldsymbol{B}^l_{i,k}\right)_{0\leq k<K}$.

2.I Numerical outcomes details: Fig. 2.6 and Fig. 2.7.

Numerical setting. The lower panel of Fig. 2.6 has been produced by running 3600 simulations, one for each couple of migration rate $m \in [0.01,\, 3]$ and intensity of selection $g \in [0.01,\, 3]$, for $t \leq T_{max} \in \left[\frac{300}{\varepsilon^2}, \frac{600}{\varepsilon^2}\right]$, with a criteria to cut the simulation short at a time greater than $\frac{300}{\varepsilon^2}$ if the difference between two consecutive steps is small enough. The value of the other parameters are the same for each simulation: $r = 1, \theta = 1, \kappa = 1, \varepsilon = 0.05$, as well as the initial state:

$$\begin{cases} n_1^0(z) = 0.99 \times \frac{e^{-\frac{(z-0.2)^2}{2\varepsilon^2}}}{\sqrt{2\pi}\varepsilon}, \\ n_2^0(z) = \frac{e^{-\frac{(z-0.2)^2}{2\varepsilon^2}}}{\sqrt{2\pi}\varepsilon}. \end{cases}$$

The initial state is taken as monomorphic, as the aim of this figure is to be compared to the theoretical outcomes that are predicted within the scope of the slow-fast analysis as stated in Theorem 2.4.1 (so when the initial state is close enough from the slow manifold).

Scoring. Each simulation final state (n_1^f, n_2^f) is attributed a score between 0 and 1 according to the following scheme:

1. if $\max\left(N_1^f, N_2^f\right) < 0.01$, then the score is 0 (for extinction) and is corresponding to the deep purple color. Else, the score is a positive number (lower than 1) according to what follows.

2. if the variance in trait of the metapopulation is greater than $2\,\varepsilon^2$, the score is 1 (corresponding to the color yellow). This would be the case if the final state is dimorphic, but more generally, this is to highlight the simulations whose final state does not fall in the small segregational variance regime analysis prediction (which in particular predicts that the distribution of trait in the metapopulation is monomorphic (see Section 2.4), with a variance of order ε^2 (see (2.12)).

3. if both conditions above are not met, then the score S is given according to the following formula:
$$S = \frac{5}{6} - \frac{1}{3}\frac{\left|N_2^f - N_1^f\right|}{N_1^f + N_2^f}.$$
This formula discriminates between symmetrical equilibria (which are characterized by equal population sizes, see Proposition 2.5.1), which typically have a score of $\frac{5}{6}$ (corresponding to the color light green), and asymmetrical equilibria, which have a discrepancy in local population sizes and therefore have a typically much lower score (in the blue tones).

Adjustments for Fig. 2.7. The methodology is the same for the lower panel of Fig. 2.6 and both panels of Fig. 2.7, at the exception of the initial state, set as:

$$\begin{cases} n_1^0(z) = 0.9 \times \frac{e^{-\frac{(z+1)^2}{2\varepsilon^2}}}{\sqrt{2\pi}\varepsilon}, \\ n_2^0(z) = \frac{e^{-\frac{(z-1)^2}{2\varepsilon^2}}}{\sqrt{2\pi}\varepsilon}. \end{cases} .$$

and of the time step for the lower panel of Fig. 2.7, which is refined to keep up with the smaller value of ε^2.

Chapter 3

Adaptation of a sexually reproducing population to a heterogeneous environment: numerical comparison with individual-based simulations

3.1 Introduction

This short numerical project uses multi-loci individual-based simulations (IBS) in order to assess to what extent the hypotheses underlying the classical version of infinitesimal model for large populations (Fisher 1919; Bulmer 1971; Lange 1978; Bulmer 1980; Barton, Etheridge, and Véber 2017), i.e. a constant segregational variance across time, space and families, are reasonably valid in a two-patch environment for large sexual populations, with respect to the number of loci involved and the ancestral variance at linkage equilibrium. A particular focus is put on the case where the latter is small, as this corresponds to the asymptotic regime according to which the analysis in [Dekens 2022] was conducted.

The relationship between multi-loci IBS and discrete-time deterministic models has been studied in a context of *one-way migration*, where a source population sends migrants in a sink population under stabilizing selection around a optimum that differs from the source' mean trait, without migration in the other direction. In [Tufto 2000], the author compares (among others) a discrete-time deterministic model where the reproduction stage involves the infinitesimal model, with multi-loci models, with relatively few loci (1, 2 or 5). He found that the two are in good agreement when selection and migration are not too strong, or if the immigrants can compensate their initial maladaptation with a large enough variance at linkage equilibrium σ^2_{LE}. He also performed numerical simulations comparing the infinitesimal model based recursions with a model assuming normality of the population trait distribution with fixed variance, and had a similar conclusions. Moreover, he considered, among other values, a small variance at linkage equilibrium $\sigma_{LE} = 0.01$, and shows (fig. 2 of the article) that the trait variance in the population at equilibrium with the infinitesimal model can be very different for σ^2_{LE}, when migration is small, and selection very strong ($g \in \{4, 20, 100\}$. Finally, one notable difference between our studies is the life cycle order (migration followed by selection in his case) and the generations' time length (1 in his case). In [Huisman and Tufto 2012], the IBS also include unequal effects between loci (5 or 20). Their results highlight that the dynamics

of the mean traits are well approximated between the IBS and the deterministic model where segregation is modelled with the infinitesimal model. However, they indicate that the variance in trait might be overestimated, but less so as the number of loci increases (with fixed σ^2_{LE}).

In [Sachdeva and Barton 2017], the authors study the eco-evolutionary dynamics of a haploid sexual population in a two-patch environment connected by back-and-forth migration, characterized by a polygenic "magic trait" both conditioning local adaptation and mates' assortments. The polygenic trait results from a large number L of additive diallelic loci with equal effects $\pm\gamma$. The analysis relies an approximation according to the hypergeometric model, which assumes that, for a given trait value within the phenotypic range $[-\gamma L, \gamma L]$, all the combinations with the same number of + alleles that result in this trait are equiprobable in the population. Furthermore, they use individual-based simulations to assess how well the hypergeometric model perform, mentioning that the infinitesimal model is recovered in the limit $L \to \infty$. To my knowledge, there has not been any other study comparing deterministic recursions with the infinitesimal model with multi-loci IBS in the context of two patchs connected by back-and-forth migration.

Infinitesimal reproduction operator. Let us define the action of the infinitesimal reproduction operator on a trait density n by

$$\mathcal{B}_\sigma(n)(t,z) = \iint_{\mathbb{R}^2} G_{0,\sigma^2}\left(z - \frac{z_1+z_2}{2}\right) n(z_1)\, n(z_2)\, dz_1\, dz_2. \tag{3.1}$$

This operator encodes the inheritance of a complex continuous trait z, classically thought to result from a large number of small additive allelic contributions (see [Fisher 1919], [Bulmer 1971], [Turelli and Barton 1994] and [Barton, Etheridge, and Véber 2017]). As it is written here, it assumes that the variance with families σ^2, called the segregational variance, is constant with respect to time and across all mating events in the considered subpopulation. One objective of this work is to assess the validity of these assumption using IBS with an explicit genetic architecture (see Section 3.3) when modelling the adaptation of sexual diploid populations to heterogeneous environments.

3.2 Discrete-time deterministic model

Let us denote $q_i : z \mapsto g_i(z-\theta_i)^2$ the quadratic selection function in habitat i and consider the following system, for $z \in \mathbb{R}$ and $t_l := l\Delta t$, with $l \in \{0, 1, ..., N_{\text{gen}}\}$

$$\begin{cases} n_1(t_{l+1},z) &= (1-m_1\Delta t)\ \exp\left[-\Delta t\left(q_1(z)+\kappa(1+r\Delta t)N_1(t_l)\right)\right]\ \left(n_1(t_l,z)+r\Delta t\mathcal{B}_\sigma[n_1(t_l,\cdot)](z)\right) \\ &\quad +m_2\Delta t\ \exp\left[-\Delta t\left(q_2(z)+\kappa(1+r\Delta t)N_2(t_l)\right)\right]\ \left(n_2(t_l,z)+r\Delta t\mathcal{B}_\sigma[n_2(t_l,\cdot)](z)\right), \\ n_2(t_{l+1},z) &= (1-m_2\Delta t)\ \exp\left[-\Delta t\left(q_2(z)+\kappa(1+r\Delta t)N_2(t_l)\right)\right]\ \left(n_2(t_l,z)+r\Delta t\mathcal{B}_\sigma[n_2(t_l,\cdot)](z)\right) \\ &\quad +m_1\Delta t\ \exp\left[-\Delta t\left(q_1(z)+\kappa(1+r\Delta t)N_1(t_l)\right)\right]\ \left(n_1(t_l,z)+r\Delta t\mathcal{B}_\sigma[n_1(t_l,\cdot)](z)\right). \end{cases} \tag{3.2}$$

In (3.2), a splitting scheme is used to handle the migration. The last system reflects the following life cycle:

1. **reproduction**:

$$n_i(t_l,z) \rightsquigarrow n_i(t_l,z) + r\Delta t\mathcal{B}_\sigma[n_i](t_l,z) =: \tilde{n}_i(t_l,z).$$

2. **Selection-competition**:

$$\tilde{n}_i(t_l, z) \rightsquigarrow e^{-\Delta t\left(q_i(z)+\kappa \tilde{N}_i(t_l)\right)} \tilde{n}_i(t_l, z) := \bar{n}_i(t_l, z)$$

3. **migration**:

$$\bar{n}_i(t_l, z) \rightsquigarrow (1 - \Delta t m_i)\bar{n}_i(t_l, z) + \Delta t m_j \bar{n}_j(t_l, z) =: n_i(t_{l+1}, z).$$

Link with a continuous-time model. Here, I give some heuristics elements to hint that the discrete-time splitting scheme involved in (3.2) approximates reasonably the following continuous-time model, used in [Dekens 2022], when Δt is small

$$\begin{cases} \partial_t n_1(t, z) = r\mathcal{B}_\sigma[n_1](t, z) - \kappa N_1(t) n_1(t, z) - q_1(z) n_1(t, z) + m_2 n_2(t, z) - m_1 n_1(t, z), \\ \\ \partial_t n_2(t, z) = r\mathcal{B}_\sigma[n_2](t, z) - \kappa N_2(t) n_2(t, z) - q_2(z) n_2(t, z) + m_1 n_1(t, z) - m_2 n_2(t, z). \end{cases}$$

The case without migration is informative. Let us consider n a solution of the following equation

$$\partial_t n(t, z) = r\mathcal{B}_\sigma[n](t, z) - \kappa N(t) n(t, z) - q(z) n(t, z). \tag{3.3}$$

From applying Duhamel's formula on (3.3) between t_l and t_{l+1}, we obtain the following approximation:

$$\begin{aligned} n(t_{l+1}, z) &= e^{-\int_{t_l}^{t_{l+1}} \kappa N(\tau) d\tau - q(z)(t_{l+1}-t_l)} n(t_n, z) + r \int_{t_l}^{t_{l+1}} \mathcal{B}_\sigma[n](\tau, z) e^{-\int_\tau^{t_{l+1}} \kappa N(s) ds - q(z)(t_{l+1}-\tau)} d\tau \\ &\approx e^{-\Delta t\left(\kappa N\left(t_{n+\frac{1}{2}}\right)+q(z)\right)} n(t_n, z) + r\Delta t \mathcal{B}_\sigma[n](t_l, z) e^{-\Delta t\left(\kappa N\left(t_{n+\frac{1}{2}}\right)+q(z)\right)} \\ &\approx \exp\left[-\Delta t \left(\kappa N\left(t_{n+\frac{1}{2}}\right) + q(z)\right)\right] \left[n(t_n, z) + r\Delta t \mathcal{B}_\sigma[n](t_l, z)\right] \\ &\approx \exp\left[-\Delta t \left(\kappa(1 + r\Delta t) N\left(t_n\right) + q(z)\right)\right] \left[n(t_n, z) + r\Delta t \mathcal{B}_\sigma[n](t_l, z)\right]. \end{aligned}$$

3.3 Individual-based simulations

Populations and habitats. The species is split in two subpopulations living in two different habitats, with local carrying capacity $\boldsymbol{K} = 10^4$. In each habitat, individuals experience selection toward a local trait optimum $\boldsymbol{\theta_i} = (-1)^i$ (for habitat i).

Genetic architecture. We consider diploid individuals with $\boldsymbol{L} \in \{10, 100, 500\}$ unlinked loci (so $2\boldsymbol{L}$ alleles per individual). At each of these loci, two alleles segregate, having an additive effect on the trait of the individual of value $\frac{\boldsymbol{\sigma_{LE}}}{\boldsymbol{2\sqrt{L}}}$ or $-\frac{\boldsymbol{\sigma_{LE}}}{\boldsymbol{2\sqrt{L}}}$. No mutation occurs at those loci. The parameter $\boldsymbol{\sigma_{LE}}$ is the standard deviation at linkage equilibrium, which is taken to be either small ($\boldsymbol{\sigma_{LE}} = 0.1$) or large ($\boldsymbol{\sigma_{LE}} = 1$).

Life cycle. The life cycle involves overlapping generations of time length Δt (until further notice, the value of Δt will be fixed to 0.1) and proceeds as follows:

1. **reproduction**: each individual of the meta-population chooses at random one mate within their subpopulation, and their mating produces a viable offspring at a rate $r\Delta t$. All offspring are added at the end of this stage (so that they cannot be drawn to mate). This stage also provides an estimation of the average and variance of local segregational variance across all mating events, thanks to the following computation of within-family segregational variance for every mating event

$$\hat{\sigma}^2 = \frac{{\boldsymbol{\sigma_{LE}}}^2}{4\boldsymbol{L}} \left[\# \left(G_1^{(1)} \Delta G_2^{(1)} \right) + \# \left(G_1^{(2)} \Delta G_2^{(2)} \right) \right], \tag{3.4}$$

   where $G_j^{(i)}$ is the $j \in \{1,2\}$-th serie of autosomes of the $i \in \{1,2\}$-th parent, Δ represents here the symmetrical difference operator and $\#$ represents the number of elements of a considered set. Note that $\hat{\sigma}^2$ is of order ${\boldsymbol{\sigma_{LE}}}^2$. The justification for (3.4) is the following. An offspring receives its two series of autosomes independently from each of its parents' gametes. The variance in the offspring's trait is therefore the sum of the variances in each parent' gametes. According to Mendelian laws of segregation, each gamete produced by the i-th parent receives randomly one of the copies of this parent at each locus, following a Bernoulli law of parameter $\frac{1}{2}$, independently of segregation at other loci, since they are assumed unlinked. The segregation of the i-th parent's alleles during the gamete's formation only generates variance from the $\# \left(G_1^{(i)} \Delta G_2^{(i)} \right)$ heterozygotes loci, and this variance at each locus where two different alleles segregate is $\frac{1}{2} \left(\frac{\boldsymbol{\sigma_{LE}}}{\boldsymbol{2\sqrt{L}}} - 0 \right)^2 + \frac{1}{2} \left(-\frac{\boldsymbol{\sigma_{LE}}}{\boldsymbol{2\sqrt{L}}} - 0 \right)^2 = \frac{\boldsymbol{\sigma_{LE}^2}}{\boldsymbol{4L}}$.

2. **selection-competition**: each individual faces a selection-competition trial according to its trait z and habitat i in which they are currently living. They survive with probability $\exp\left(-\Delta t \boldsymbol{g}(z - \boldsymbol{\theta_i})^2\right)$ $\exp\left(-\Delta t \frac{\boldsymbol{N_i}}{\boldsymbol{K}}\right)$ and are removed otherwise. N_i denotes here the subpopulation size at the end of the reproduction stage in habitat i.

3. **migration**: at each migration event, within each subpopulation i, a number of migrants is drawn, according to a Poisson probability with parameter $\Delta t\, \boldsymbol{m}\, \boldsymbol{N_i}$ (with a hard cap of $\boldsymbol{N_i}$, that is the number of individuals currently in the subpopulation). Migrants are uniformly sampled accordingly within the subpopulation and are moved to the other deme.

Each simulation repeats this life cycle, first without migration for 100 generations of burn in and next for $\boldsymbol{N}_{\text{gen}} = 10^3$ generations with migration. The generation 0 is the one where migration starts. Additionally, before the start of generation 0, I simulate a catastrophic event affecting only the first habitat, to introduce an asymmetry in the initial state. Precisely, individuals in habitat 1 suffer from a decreased survival rate in the selection-competition stage (replacing punctually the carrying capacity $\boldsymbol{K}$ of the habitat 1 by $\frac{\boldsymbol{K}}{2}$).

Ancestral population (pre-migration). At the generation -100, the two subpopulations are at $\frac{4}{5}$ of the local carrying capacity. The genetic information of the individuals of the initial population is set as follows. In each subpopulation, at each locus ($\boldsymbol{L}$) of each genome (2) of each individual, an allelic effect is randomly drawn by

$$-\frac{\boldsymbol{\sigma_{LE}}}{2\sqrt{\boldsymbol{L}}}(1 - \mathcal{X}) + \frac{\boldsymbol{\sigma_{LE}}}{2\sqrt{\boldsymbol{L}}}\,\mathcal{X},$$

where $\mathcal{X}$ follows a Bernoulli law of parameter $p = \max\left(0, \min\left(1, \frac{1}{2} + (-1)^i \frac{1}{2\boldsymbol{\sigma_{LE}}\sqrt{\boldsymbol{L}}}\right)\right)$, so that the population is on average initial locally adapted (the mean trait of the subpopulation coincides with the local optimum).

3.4 Numerical results

Type of results:

1. **Final states**' comparison between the discrete-time deterministic model's (3.2) numerical resolution and the IBS with three different loci number (see Section 3.3), when the migration rate and the selection strength vary in $[0, 2]$.

2. **Transient trajectories**' comparison between the discrete-time deterministic model's numerical resolution and the IBS with three different number of loci (see Section 3.3)

3. **Consistence of small segregational variance hypotheses** as used in the discrete time deterministic model, which are that, throughout the simulation, the segregational variance can be considered as constant across time, space and families, while remaining small. The verification of these features thanks to the IBS with small standard deviation at linkage equilibrium $\boldsymbol{\sigma_{LE}} = 0.1$ and the collect of the segregational variances according to (3.4) is essential, as these hypotheses underly the validity of the reproduction operator in deterministic models (3.1).

3.4.1 Outcomes

In this subsection, we present the results about the qualitative comparison of the final states between the deterministic model (3.2) and the IBS (Section 3.3), for three different number of loci, when the migration rate $\boldsymbol{m}$ and the selection strength $\boldsymbol{g}$ vary both in $[0, 2]$. In particular, we focus on the case where the segregational variance in the deterministic model is small ($\sigma^2 = 0.01$), which corresponds to the case where the standard deviation at linkage equilibrium of the IBS is small ($\boldsymbol{\sigma_{LE}} = 0.1$), of the same order as σ (see (3.4)).

Deterministic model. For each couple of parameters $(\boldsymbol{m}, \boldsymbol{g}) \in [0, 2]^2$, 10^3 iterations of the deterministic model (3.2) are computed, with the other parameters set as follows: $r = 1, \kappa = 1, \Delta t = 0.1, \sigma^2 = 0.005$ (the latter being the segregational variance of the infinitesimal model operator (3.1)). The distributions are initially set to be asymmetrical in sizes (as in the IBS), each subpopulation being locally adapted according to the following (G_{m,s^2} denotes the Gaussian density of mean m and variance s^2):

$$\forall z \in \mathbb{R}, \quad n_1(t_0, z) = 0.2 \times G_{-1,2\sigma^2}(z), \quad n_2(t_0, z) = 0.8 \times G_{1,2\sigma^2}(z). \tag{3.5}$$

The numerical scheme is the same as in [Dekens 2022] (detailed in Appendix F of the latter). The state of the system after the last iteration is scored according to (3.6).

Individual-based simulations. For all loci number $L \in \{10, 100, 500\}$ and every couple of parameters $(\boldsymbol{m}, \boldsymbol{g}) \in [0, 2]^2$, 20 replicate simulations are ran following the framework indicated in Section 3.3, with a fixed small scaling allelic factor $\boldsymbol{\sigma_{LE}} = 0.1$. Scores are computed at the end of every replicate simulation according to (3.6), and then averaged to give the score for this set of parameter values.

Scoring scheme. For each simulations (either deterministic or individual-based), the final state is scored according to the following formula:

$$\text{Score} = \begin{cases} \frac{5}{6} - \frac{1}{3}\frac{\left|N_1^f - N_2^f\right|}{N_1^f + N_2^f} + \frac{1}{6}\left(1 - \exp(1 - 10\,V^f)\right) & \text{if } \max\left(N_1^f, N_2^f\right) > 0.01, \\ 0 \quad \text{otherwise,} \end{cases} \tag{3.6}$$

where N_1^f and N_2^f are the final subpopulations sizes, and V^f is the final trait variance in the meta-population (for IBS, N_i^f is the number of individuals of habitat i divided by the local carrying capacity $\boldsymbol{K}$). The scoring scheme (3.6) aims at discriminating between the different possible outcomes

- asymmetrical monomorphic equilibrium (V^f small and $\left|N_1^f - N_2^f\right| \approx \max\left(N_1^f, N_2^f\right)$), whose typical score is around $\frac{1}{2}$.
- symmetrical monomorphic equilibrium (V^f small and $N_1^f \approx N_2^f$), whose typical score is around $\frac{5}{6}$.
- symmetrical dimorphic equilibrium (V^f large and $N_1^f \approx N_2^f$), whose typical score is around 1.
- extinction, which is scored 0.

Results. The results are displayed in Figure 3.1. For each subfigure, the correspondence between the score computed for each simulation's final state given a parameter couple (m, g) and its colour is indicated in the legend of Fig. 3.1a and remains the same for all the subfigures. The upper left subfigure displays the outcomes of the numerical resolution of the discrete time deterministic model (3.2), while the other subfigures display the outcomes of the IBS for the three different number of alleles (500 in Fig. 3.1b, 100 in Fig. 3.1c, 10 in Fig. 3.1d), averaged across replicates. The outcomes of the discrete-time deterministic model and those of the continuous-time deterministic model, which are displayed in the Figure 6 of [Dekens 2022], indicate that the agreement between the two deterministic models is good, which is expected. Next, one can notice, by only looking at the outcomes of the IBS (Fig. 3.1b, Fig. 3.1c and Fig. 3.1d, that there is a substantial variation between the final states depending on the number of loci involved, especially at strong selection (bottom right corner of the subfigures), particularly between 10 loci and above 100. This results from the fact that all parameters of the IBS other that the number of loci are maintained the same between the subfigures, in particular the standard deviation at linkage equilibrium $\boldsymbol{\sigma_{LE}} = 0.1$, that determines the allelic effects at each locus together with the number of loci L: $\pm\frac{\sigma_{LE}}{\sqrt{L}}$. Consequently, for $L = 10$, the allelic effects at each locus are approximately ± 0.03. This implies that the extreme phenotypes that individuals can have ($-a\sqrt{L}$ and $a\sqrt{L}$) are approximately -0.3 and 0.3, which are quite far from the local phenoypic optima ($\theta_1 = -1$ and $\theta_2 = 1$). Therefore, at strong selection ($g \geq 1.5$), the selection is too strong for even individuals with these extreme phenotypes to be able to adapt. The same phenomenon is avoided for $L = 100$ and $L = 500$, where the extreme phenotypes are respectively $(-1, 1)$ and $(-2.2, 2.2)$ especially for the latter. This explains the qualitative agreement of the IBS with the final states of the deterministic model (Fig. 3.1a). It is quite poor for $L = 10$ loci (Figure 3.1d), quite good for $L = 100$ loci (Figure 3.1c) and even better for the largest number of loci $L = 500$ (Figure 3.1b).

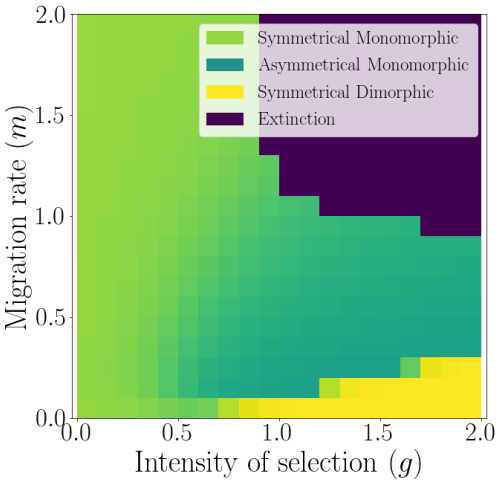

(a) **Numerical outcomes with the discrete deterministic model** (3.2)**.** Parameters: $r = 1, \kappa = 1, \Delta t = 0.1, \sigma^2 = 0.005$ (the latter is the segregational variance), with 10^3 iterations per simulation, with asymmetrical initial distributions (see (3.5)).

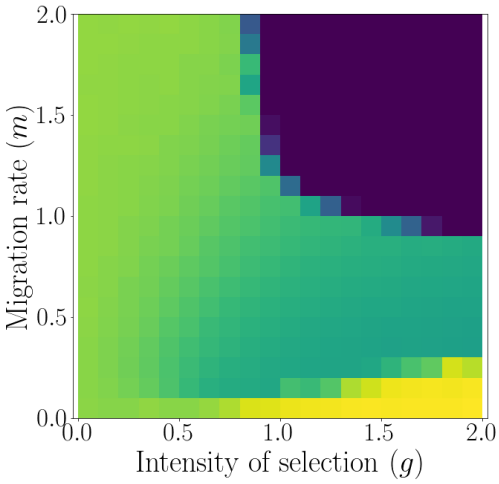

(b) **IBS outcomes - 500 loci.**

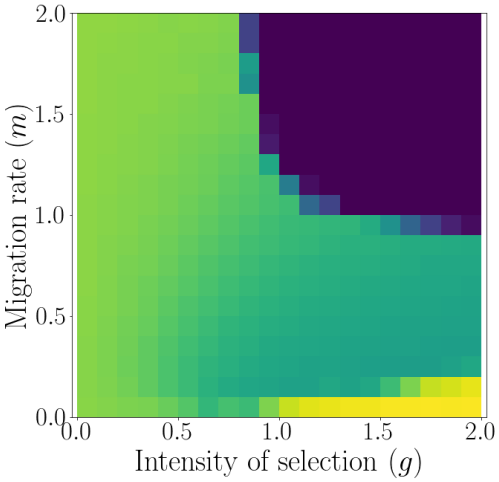

(c) **IBS outcomes - 100 loci.**

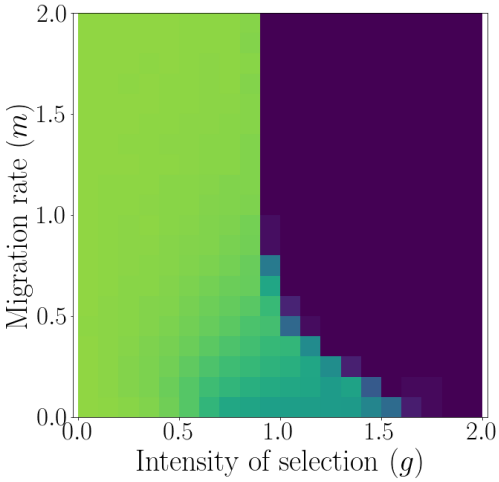

(d) **IBS outcomes - 10 loci.**

Figure 3.1: **Qualitative comparison between the outcomes of the deterministic model's** (3.2) **numerical resolution and the IBS for three different number of loci (10, 100, 500), when the migration rate ($m_1 = m_2 = m$) and intensity of selection ($g_1 = g_2 = g$) vary.** The IBS are designed according to Section 3.3, with generations of time length $\Delta t = 0.1$ and small standard deviation at linkage equilibrium $\boldsymbol{\sigma_{LE}} = 0.1$, and 20 replicates simulations for each point (m, g). The final state of each simulation (deterministic or stochastic) is attributed a score according to the same scheme (3.6). For the IBS, the score is averaged across replicates. The results indicate that there is a large variation in the outcomes among the IBS according to the number of loci involved, especially for strong selection levels (bottom right corner of each subfigures). The agreement with the deterministic model grows stronger as the number of loci involved grows (very similar for 500 loci).

3.4.2 Transient trajectories

In this section, we aim to quantify how close the numerical solutions of the deterministic model (3.2) is from the IBS throughout the whole time length of the simulations, depending on the number of loci involved (10, 100, 500), for small ($\boldsymbol{\sigma_{LE}} = 0.1$) and large ($\boldsymbol{\sigma_{LE}} = 1$) scaling allelic effects factors and for three migration rates $m \in \{0.05; 0.8; 1.4\}$ (henceforth qualified as low, intermediate and high migration) and three selection strengths $g \in \{0.1; 1.0; 2.0\}$ (henceforth qualified as weak, intermediate and strong selection).

Individual-based simulations. For each loci number, standard deviation at linkage equilibrium, migration rate and selection strengths, 20 replicate simulations are ran according to the framework described in Section 3.3. For each replicate k, all the system (meaning all the phenotypes in both habitats) is saved at each generation t, and the underlying trait densities $n_1^{\text{IBS},k}(t,z)$ and $n_2^{\text{IBS},k}(t,z)$ are estimated from it, with $z \in Z$, Z being the trait space's discritization grid for the deterministic model.

Deterministic model. For each loci number, standard deviation at linkage equilibrium, migration rate and selection strengths, 10^3 iterations of the deterministic model (3.2) are computed, with the other parameter set as follows: $r = 1, \kappa = 1, \delta t = 0.1$. The trait space's discritization grid Z is the same as indicated in Appendix F of [Dekens 2022] ($\Delta z \approx 1.6 \times 10^{-2}$). The parameter σ^2 (segregational variance of the infinitesimal model operator (3.1)) and the initial state are estimated from the IBS with corresponding parameter values. The parameter σ^2 takes the value of the average of all the segregational variances across mating events and habitats in the last generation of the IBS (with a lower cap at $\boldsymbol{\sigma_{LE}} \times 10^{-8}$ if the average is 0). The initial conditions are set as an average as follows:

$$n_i^{\text{deterministic}}(0,\cdot) = \frac{1}{20}\sum_{k=1}^{20} n_i^{\text{IBS},k}(0,\cdot). \tag{3.7}$$

(Generation 0 marks the start of the migration phenomenon).

Proximity of the trait distributions from the deterministic model and from the IBS The proximity of the trait distributions from the deterministic model and from the IBS obtained according to the framework previously described is computed at each generation t by

$$\overline{W_1\left(\frac{n_1^{\text{deterministic}}(t,\cdot) + n_2^{\text{deterministic}}(t,\cdot)}{N_1^{\text{deterministic}}(t) + N_2^{\text{deterministic}}(t)}, \frac{n_1^{\text{IBS},k}(t,\cdot) + n_2^{\text{IBS},k}(t,\cdot)}{N_1^{\text{IBS},k}(t) + N_2^{\text{IBS},k}(t)}\right)}. \tag{3.8}$$

In (3.8), W_1 denotes here the first Wasserstein distance defined on the space of probability measures on $\mathbb{R}$ with bounded first moment and the overline quantity represents the median across all replicates. We recall that for μ and ν two probability measures on $\mathbb{R}$ of bounded first moment, if we denote F_μ and F_ν their respective cumulative distribution function, then the W_1 distance between μ and ν is computed by

$$W_1(\mu,\nu) = \|F_\mu - F_\nu\|_{L_1}. \tag{3.9}$$

The W_1 distance is used here instead of the L_1 norm to quantify the proximity between distributions, because it handles better the distance between two distributions, one being a small perturbation of the other, but with disjoint support, which is expected to occur here when the variances are low.

Results In the case where the standard deviation at linkage equilibrium $\boldsymbol{\sigma_{LE}}$ is small, the agreement between IBS and the deterministic model on transient trajectories depends highly on the number of loci involved $\boldsymbol{L}$. When the number of loci is large enough for the phenotypic range $[-\boldsymbol{\sigma_{LE}}\sqrt{L}, \boldsymbol{\sigma_{LE}}\sqrt{L}]$ to encompass and extend well beyond the local trait optima $\boldsymbol{\theta}_1$ and $\boldsymbol{\theta}_2$ characterizing the heterogeneous environment, the IBS and the deterministic model are extremely close throughout the whole simulations. When the phenotypic range is just enough to include the local optima, the agreement between IBS and the deterministic model remains globally very good, but degrades slightly for intermediate migrations, which corresponds to the asymmetrical monomophic equilibria. When the number of loci is too small to include the local optima, the IBS and the deterministic model are only close when selection is weak, or intermediate with low migration. In the rest of the parameter space, in particular when selection increases, the phenotypic range limits too much the adaptation of the population which goes extinct, which is not the case of the deterministic model.

In the case where the standard deviation at linkage equilibrium $\boldsymbol{\sigma_{LE}}$ is large, the agreement between IBS and the deterministic model on transient trajectories does not depend too much on the number of loci involved $\boldsymbol{L}$ (at least, when it is above 10 loci), and the agreement between IBS and the deterministic model is globally excellent (though it degrades a bit for intermediate selection-migration).

3.4.3 Segregational variances

This section presents the numerical results from the data on segregational variances collected from the IBS. The aim is to assess whether, when the standard deviation at linkage equilibrium $\boldsymbol{\sigma_{LE}}$ is small (0.1), the central limit theorem assumption in the infinitesimal model (the segregational variance is constant across time, space and families) holds across the whole simulations time length and can produce a small segregational variance, depending on the number of alleles involved. The results are shown for 100 and 500 loci (since the outcomes with 10 loci Fig. 3.1d are very different from the deterministic model Fig. 3.1a, we do not include it in this section).

Segregational variance data collected from IBS and quantities of interests. There are two types of data about segregational variances that I collected from the IBS performed for the subsection Section 3.4.1 for each number of loci (100, 500 - 20 replicates for each):

1. $M_i^{t,k}$, which is the average segregational variance computed for all the mating events at generation t, for replicate k, in habitat i, according to (3.4).
2. $V_i^{t,k}$, which is the variance in the segregational variances computed for all the mating events at generation t, for replicate k, in habitat i.

Furthermore, I define the average data across replicates by

$$\bar{M}_i(t) := \frac{1}{\#\text{Replicates}} \sum_k M_i^{t,k}, \quad \bar{V}_i(t) := \frac{1}{\#\text{Replicates}} \sum_k V_i^{t,k}.$$

To quantify the extent of the validity of the four hypotheses on segregational variances (smallness, constancies across time, space and families), we compute four scores as follows.

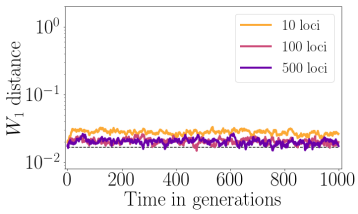

(a) Weak selection, low migration.

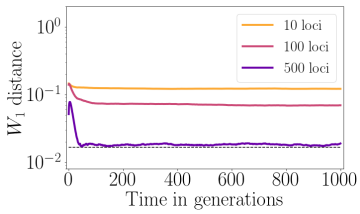

(b) Weak selection, intermediate migration.

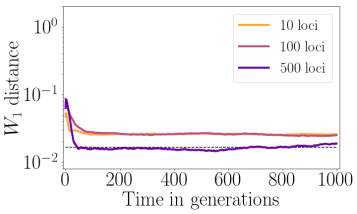

(c) Weak selection, high migration.

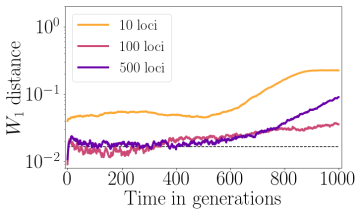

(d) Intermediate selection, low migration.

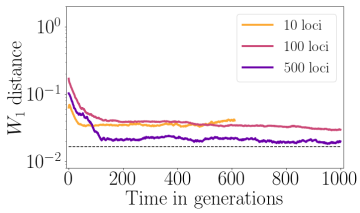

(e) Intermediate selection, intermediate migration.

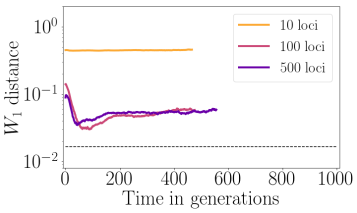

(f) Intermediate selection, high migration.

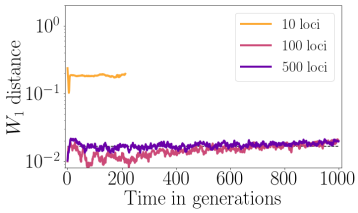

(g) Strong selection, low migration.

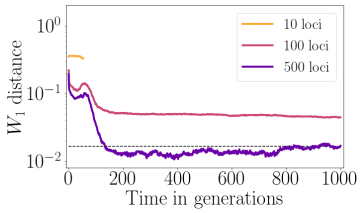

(h) Strong selection, intermediate migration.

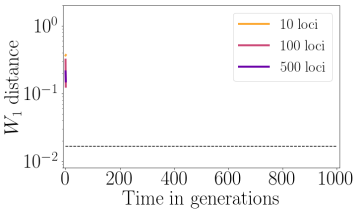

(i) Strong selection, high migration.

Figure 3.2: **Dynamics of the W_1 distance between the distributions of the IBS replicates according to (3.8) and the solutions of the deterministic discrete-time model (3.2), for 3 increasing levels of selection (rows, top to bottom 0.1, 1, 2) and 3 increasing levels of migration (columns, left to right 0.05, 0.8, 1.4), with a small standard deviation at linkage equilibrium $\sigma_{LE} = 0.1$ (small variance case).** For each figure, the three colors correspond to three different number of loci $\boldsymbol{L} = \{10, 100, 500\}$ (darker colors for larger number of alleles). The coloured lines represent the median distance across replicates (interrupted lines means that extinction occurred). The black dashed line represents the distance between two Dirac masses on consecutive points of the trait space's grid Z. Other parameter values for the deterministic models are: $r = 1, \kappa = 1, \Delta t = 0.1$ and those for the IBS as indicated in Section 3.3. Here, the number of loci matters substantially. With 500 loci, the distances between the IBS and deterministic trajectories (purple lines) are almost always equivalent to the minimum distance between two Dirac masses on the discretization grid (dashed horizontal line), with indicates excellent agreement, at the exception of extinction events (Fig. 3.2f, Fig. 3.2i). With 100 loci, which is the limit case where the phenotypic range matches the difference between local optima, the agreement with the deterministic model is similar than with 500 loci when migration is low (left column), but degrades when migration becomes higher (middle and right colum). With 10 loci, additional extinctions occur when selection is strong and migration is low (Fig. 3.2g) or intermediate (Fig. 3.2h), and at intermediate selection-migration (Fig. 3.2e), which is consistent with Fig. 3.1d. Notice that in Fig. 3.2d, the distance increases slightly after 600 generation for all number of loci. This comes from the fact that the outcomes at this particular migration-selection parameters are near the border of two qualitatively different phenomena (asymmetrical monomorphic or dimorphic - see Fig. 3.1a.)

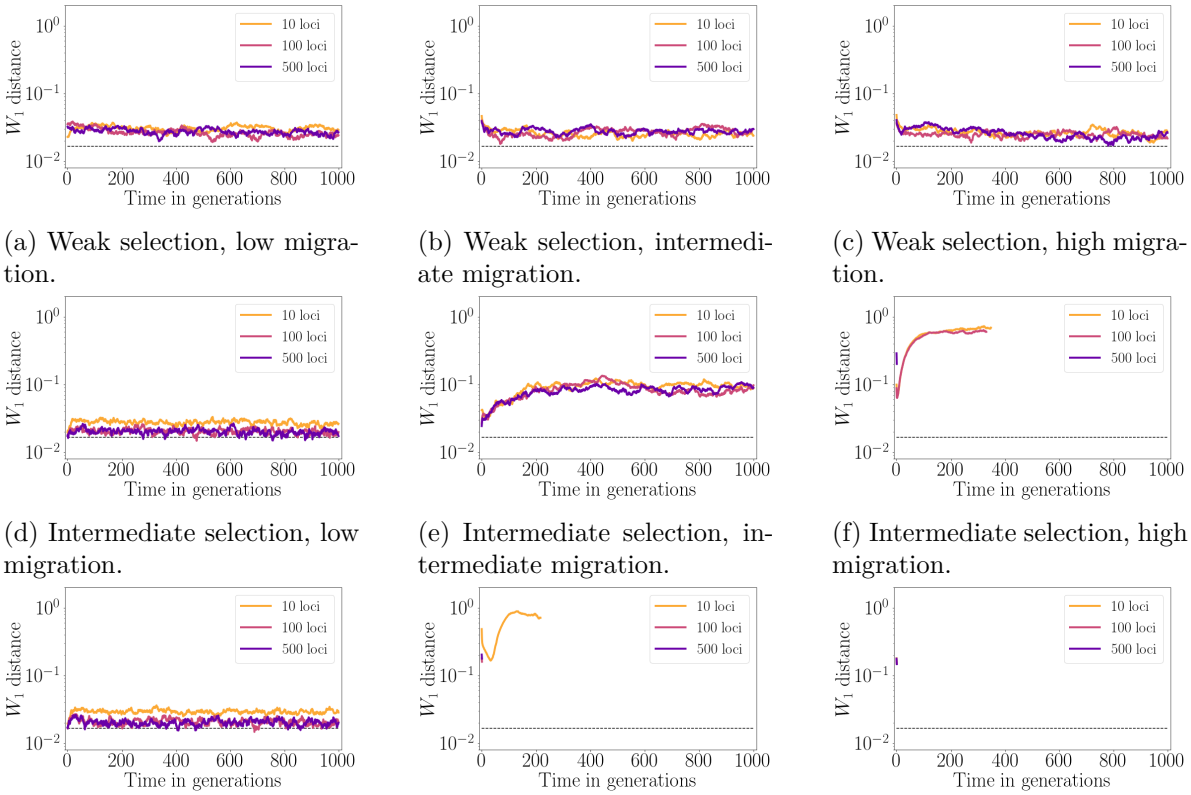

(a) Weak selection, low migration.

(b) Weak selection, intermediate migration.

(c) Weak selection, high migration.

(d) Intermediate selection, low migration.

(e) Intermediate selection, intermediate migration.

(f) Intermediate selection, high migration.

(g) Strong selection, low migration.

(h) Strong selection, intermediate migration.

(i) Strong selection, high migration.

Figure 3.3: **Dynamics of the W_1 distance between the distributions of the IBS replicates according to (3.8) and the solutions of the deterministic discrete-time model (3.2), for 3 increasing levels of selection (rows, top to bottom 0.1, 1, 2) and 3 increasing levels of migration (columns, left to right 0.05, 0.8, 1.4), with a large standard deviation at linkage equilibrium $\sigma_{LE} = 1$ (large variance case).** For each figure, the three colors correspond to three different number of loci $\boldsymbol{L} = \{10, 100, 500\}$ (darker colors for larger number of alleles). The coloured lines represent the median distance across replicates (interrupted lines means that extinction occurred). The black dashed line represents the distance between two Dirac masses on consecutive points of the trait space's grid Z. Other parameter values for the deterministic models are: $r = 1, \kappa = 1, \Delta t = 0.1$ and those for the IBS as indicated in Section 3.3. Here, the number of loci does not influence the proximity of the deterministic model with the IBS(at least above 10 loci). The agreement between the deterministic model and the IBS is strong (coloured lines at the level of the black dashed line, which is the minimum distance between two Dirac masses on the discritization grid) when either selection is weak (top row) or migration is low (left column), and a bit worse when both selection and migration are intermediate (Fig. 3.3e). Extinction occurs in all other cases, when migration and selection are both sufficiently high (Fig. 3.3f, Fig. 3.3h, Fig. 3.3i).

1. **Smallness**. The score is computed according to
$$\frac{\left\|\bar{M}_1\right\|_\infty + \left\|\bar{M}_2\right\|_\infty}{2}. \tag{3.10}$$

2. **Time constancy**. The score is computed according to
$$\frac{\max\left(\bar{M}_1 + \bar{M}_2\right) - \min\left(\bar{M}_1 + \bar{M}_2\right)}{\frac{1}{N_{\text{gen}}}\sum_{t\leq N_{\text{gen}}} \bar{M}_1(t) + \bar{M}_2(t)}. \tag{3.11}$$

3. **Space constancy**. The score is computed according to
$$\frac{\left\|\left[\bar{M}_1(t) - \bar{M}_2(t)\right]\right\|_\infty}{\frac{1}{2N_{\text{gen}}}\sum_{t\leq N_{\text{gen}}} \bar{M}_1(t) + \bar{M}_2(t)}. \tag{3.12}$$

4. **Constancy across families**. The score is computed according to
$$\frac{\left\|\left[\sqrt{\bar{V}_1(t)} + \sqrt{\bar{V}_2(t)}\right]\right\|_\infty}{\frac{1}{N_{\text{gen}}}\sum_{t\leq N_{\text{gen}}} \bar{M}_1(t) + \bar{M}_2(t)}. \tag{3.13}$$

On the contrary to the first score which is an absolute norm, the three last scores are relative norms, so scores significantly lower than 1 represent good agreement with the hypotheses.

Results. The results are displayed thanks to migration-selection heatmaps, for two different number of loci: 100 (Fig. 3.6) and 500 (Fig. 3.4). For each number of loci, four subfigures of the heatmaps of the four different scores described previously are shown, with a different colormap for each number of alleles, as to draw attention on the scale of the colorbar, which varies considerably from one plot to another. Additionally, to control for the influence of the first time steps, we display the same figures, but with the scores computed over the generations after the 30th (Fig. 3.5 and Fig. 3.7). Here is a short summary of the findings:

- ◇ **500 loci**: Figure 3.4 indicates that, when the standard deviation at linkage equilibrium $\boldsymbol{\sigma_{LE}}$ is small, and the number of loci $\boldsymbol{L}$ is large enough so that the phenotypic range $[-\boldsymbol{\sigma_{LE}}\sqrt{L}, \boldsymbol{\sigma_{LE}}\sqrt{L}]$ extends beyond the local optima (here, -1 and 1), segregational variances remain small (of order lower than $\boldsymbol{\sigma_{LE}}^2$) throughout the length of the IBS, constant across time, space and families. Additionally, Figure 3.5 indicates that most of the time variation of the segregational variance for parameters leading to monomorphic symmetrical equilibria (ie: bounded selection) happens during the first generations, following migration's start.

- ◇ **100 loci** : On the contrary to the previous case, Figure 3.6 tends to indicate that, even though segregational variances stay small, there is substantial variation across time, space and families in the parameter region which leads to the asymmetrical monomorphic equilibria (see Fig. 3.1c for the latter), especially at strong selection/intermediate migration. This might be linked to the fact that, with 100 loci, the phenotyipic range $[-\boldsymbol{\sigma_{LE}}\sqrt{L}, \boldsymbol{\sigma_{LE}}\sqrt{L}]$ match the local optimal traits, so they might be overrepresented in the subpopulations at strong selection. This would decrease the variances within families, and over time. Additionally, the segregational variance varies also greatly across time, at bounded selection. However, Figure 3.7 indicates that most of the variation in this parameter region occurs in the first generations, following migration's start.

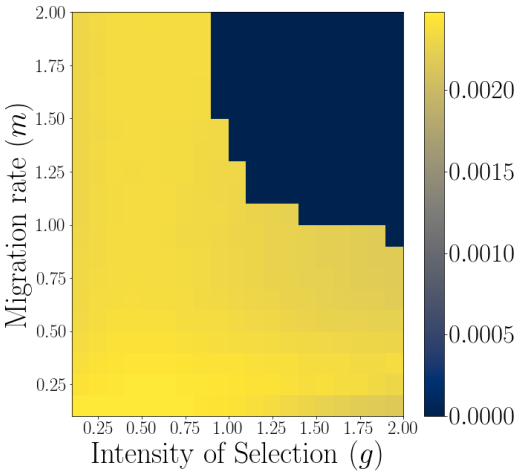

(a) **Smallness of the segregational variances throughout the IBS, for 500 loci**, according to (3.10).

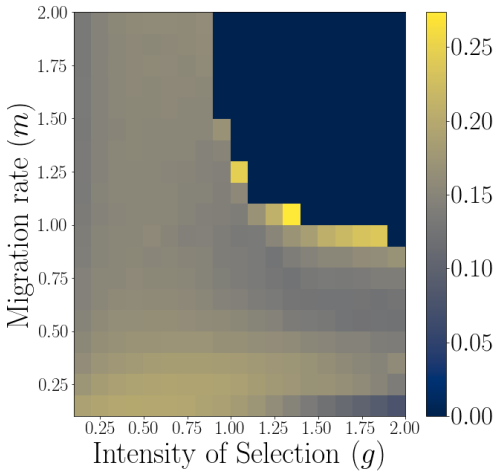

(b) **Time constancy of the segregational variance throughout the IBS, for 500 loci**, according to (3.11).

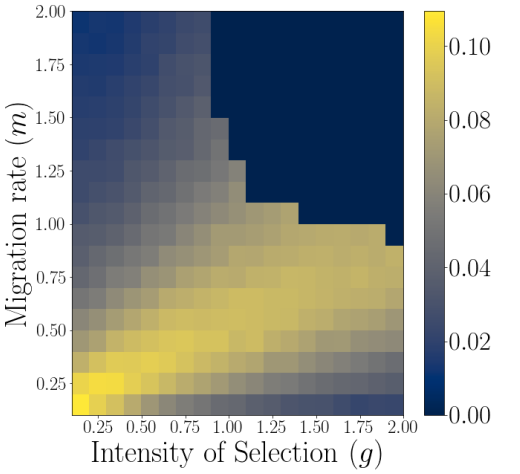

(c) **Spatial constancy of the segregational variances throughout the IBS, for 500 loci**, according to (3.12).

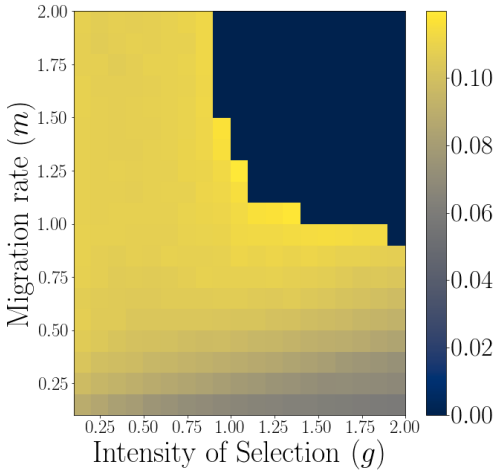

(d) **Constancy of the segregational variances across families throughout the IBS, for 500 loci**, according to (3.13).

Figure 3.4: **Quantification of the extent of the four hypotheses's validity regarding small segregational variance, throughout individual-based simulations, with 500 loci and small standard deviation at linkage equilibrium $\boldsymbol{\sigma_{LE} = 0.1}$.** Fig. 3.4a indicates that the segregational variances stay very small throughout the IBS (scores lower than 0.003), even compared to $\boldsymbol{\sigma_{LE}}^2$ (see (3.4)). Fig. 3.4b indicates that, except for IBS with migration-selection parameter values close to the extinction region (upper right corner), the segregational variances vary weakly across generations (scores lower than 0.25). Fig. 3.4c indicates that the differences between the average segregational variances across habitats are globally small (scores lower than 0.1), the highest scores occuring in the asymmetrical equilibria region (see Fig. 3.1b). Fig. 3.4d indicates that there is little variance in segregational variances across families (scores lower than 0.2). For each couple of parameters values $(\boldsymbol{m}, \boldsymbol{g})$, 20 replicate simulations have been conducted (see Section 3.3 for more details about the IBS).

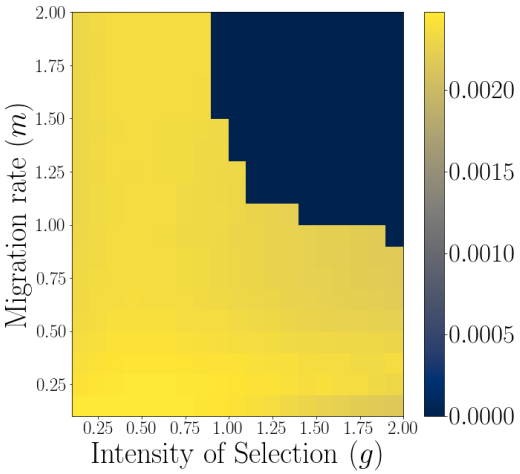

(a) **Smallness of the segregational variances throughout the IBS, for 500 loci**, according to (3.10).

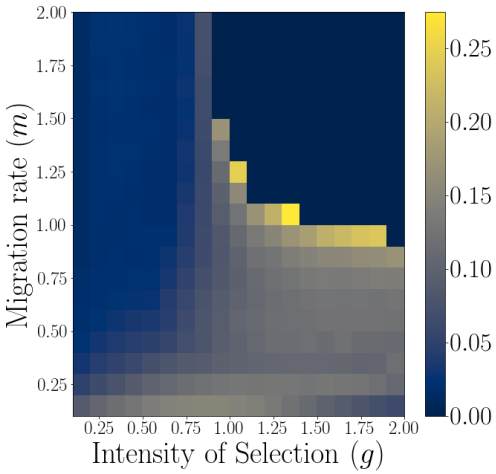

(b) **Time constancy of the segregational variance throughout the IBS, for 500 loci**, according to (3.11).

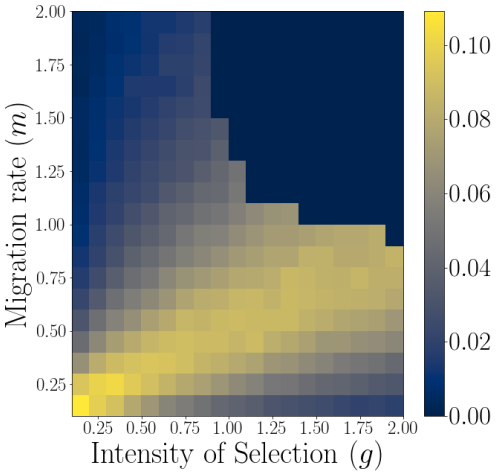

(c) **Spatial constancy of the segregational variances throughout the IBS, for 500 loci**, according to (3.12).

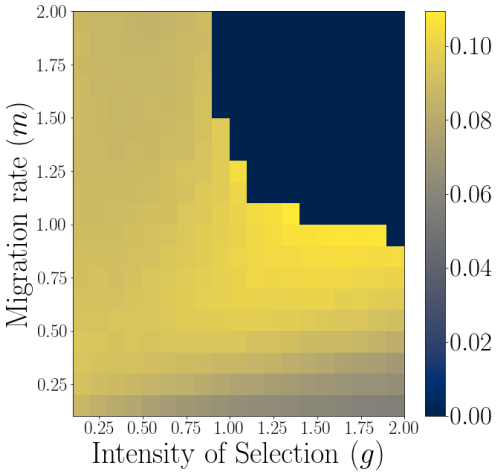

(d) **Constancy of the segregational variances across families throughout the IBS, for 500 loci**, according to (3.13).

Figure 3.5: **Control of the influence of first generations: Quantification of the extent of the four hypotheses's validity regarding small segregational variance, throughout individual-based simulations after 30 generations, with 500 loci and small standard deviation at linkage equilibrium $\sigma_{LE} = 0.1$.** The figure has been built exactly as Fig. 3.4, with the same IBS, but the four scores have been computed only over the generations after the 30th one, to control for the influence of the first generations on the scores. Of the four subfigures, only Fig. 3.5b quantifying the constancy across time changes, although moderately, in particular for intermediate to high migration and bounded selection (left side). This indicates that in the parameter region where the system tends to be monomorphic and symetrical (see Fig. 3.1b), the segregational variance varies moderately in the first generations, but is constant afterwards.

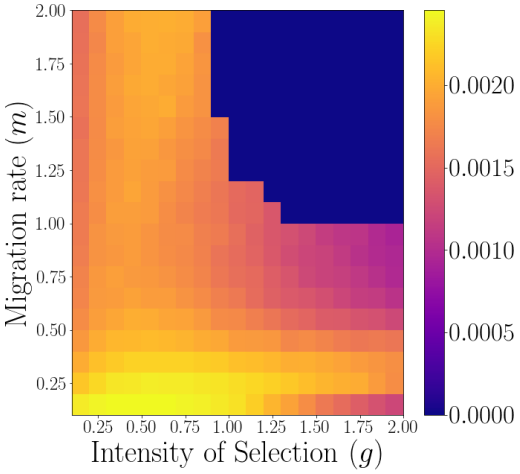

(a) **Smallness of the segregational variances throughout the IBS, for 100 loci**, according to (3.10).

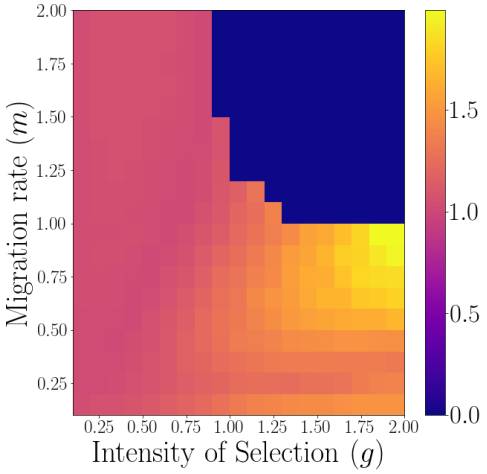

(b) **Time constancy of the segregational variance throughout the IBS, for 100 loci**, according to (3.11).

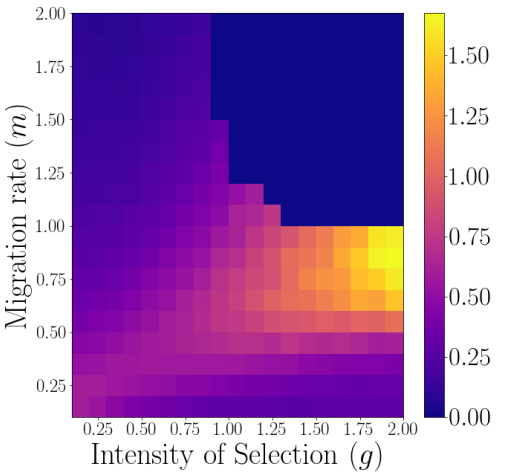

(c) **Spatial constancy of the segregational variances throughout the IBS, for 100 loci**, according to (3.12).

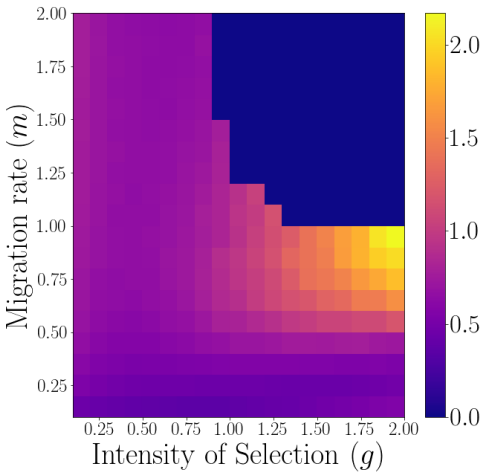

(d) **Constancy of the segregational variances across families throughout the IBS, for 100 loci**, according to (3.13).

Figure 3.6: **Quantification of the extent of the four hypotheses's validity regarding small segregational variance, throughout individual-based simulations, with 100 loci and small standard deviation at linkage equilibrium $\sigma_{LE} = 0.1$.** Fig. 3.6a indicates that the segregational variances stay very small throughout the IBS (scores lower than 0.003), even compared to ${\sigma_{LE}}^2$ (see (3.4)). However, Fig. 3.6b indicates that the segregational variances can vary substantially across time, at high migration (upper left corner, scores around 1) and even more at strong selection (lower right corner, score above 1). Fig. 3.6c indicates the differences between the average segregational variances across habitats are relatively small for high migration, weak selection or strong selection, low migration (scores around 0.25), but substantial in the parameter region corresponding to the asymmetrical equilibria (see Fig. 3.1c), especially at strong selection, intermediate migration (scores above 1). Fig. 3.6d indicates that there is moderate (score of 0.5) to high variance in segregational variances across families (scores above 1 at strong selection, intermediate migration). For each couple of parameters values (m, g), 20 replicate simulations have been conducted (see Section 3.3 for more details about the IBS).

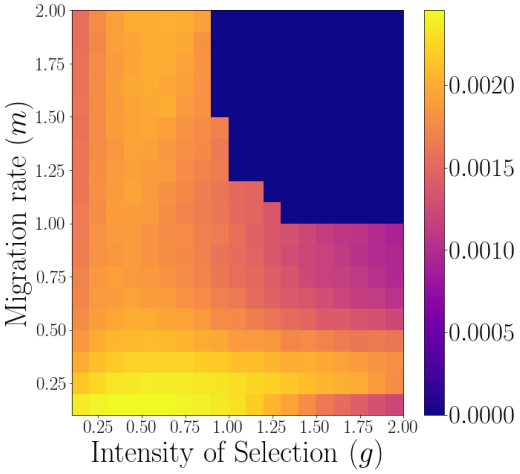

(a) **Smallness of the segregational variances throughout the IBS, for 100 loci**, according to (3.10).

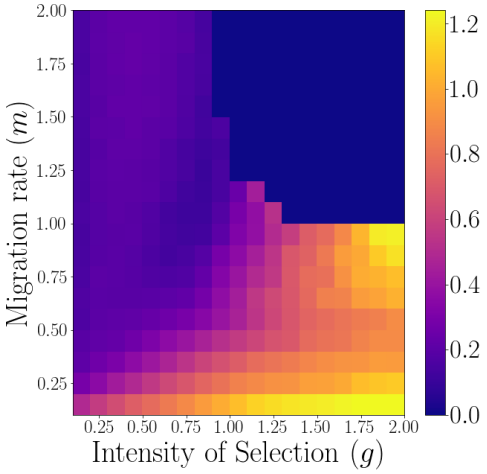

(b) **Time constancy of the segregational variance throughout the IBS, for 100 loci**, according to (3.11).

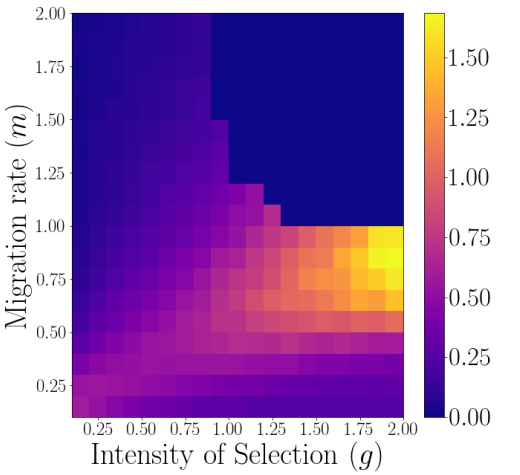

(c) **Spatial constancy of the segregational variances throughout the IBS, for 100 loci**, according to (3.12).

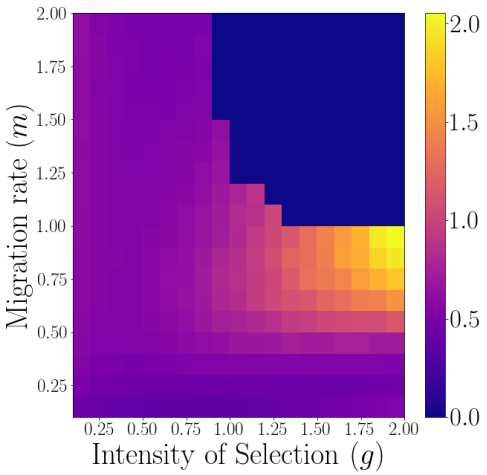

(d) **Constancy of the segregational variances across families throughout the IBS, for 100 loci**, according to (3.13).

Figure 3.7: **Control of the influence of first generations: Quantification of the extent of the four hypotheses's validity regarding small segregational variance, throughout individual-based simulations after 30 generations, with 100 loci and small standard deviation at linkage equilibrium $\sigma_{LE} = 0.1$.** The figure has been built exactly as Fig. 3.6, with the same IBS, but the four scores have been computed only over the generations after the 30th one, to control for the influence of the first generations on the scores. Of the four subfigures, only Fig. 3.7b quantifying the constancy across time changes substantially, in particular for intermediate to high migration and bounded selection (left side). This indicates that in the parameter region where the system tends to be monomorphic and symetrical (see Fig. 3.1c), the segregational variance varies greatly in the first generations, but is constant afterwards (scores close to 0). However, the rest of the subfigure remains the same, meaning that for intermediate to strong selections, time constancy is not respected, even after the 30 first generations (scores of order 1).

3.5 Conclusion

The infinitesimal model has been commonly thought to emerge in particular from discrete di-allelic genetic architecture involving a large number of loci $\boldsymbol{L}$ with small additive effects. The main motivation of this study is to clarify the relation between characteristics of this genetic architecture and the assumption behind the use of the infinitesimal model operator (3.1) in deterministic models, which is that the segregational variance is constant across time, space and families and is in fact a parameter of the model. This study focuses on doing so when modelling the adaptation of diploid sexual populations to heterogeneous environments, for example composed by two demes connected by migration. Furthermore, it aims at deriving a biological justification for the regime of small segregational variance, which has been shown to allow significant analytical derivations of quantitative features of the eco-evo equilibria (see Dekens 2022).

We decompose the di-allelic effects as $\pm\frac{\boldsymbol{\sigma_{LE}}}{2\sqrt{\boldsymbol{L}}}$, where $\boldsymbol{L}$ is the number of loci involved in the genetic architecture underlying the complex focal trait and the parameter $\boldsymbol{\sigma_{LE}}$ the standard deviation at linkage equilibrium. This decomposition is practical, as the segregational variances with families are lower than $\boldsymbol{\sigma_{LE}}^2$ (see (3.4)), and we first show that they remain indeed small throughout the IBS when the standard deviation at linkage equilibrium $\boldsymbol{\sigma_{LE}}$ is small. Furthermore, we show that the comparison between the phenotypic range $[-\boldsymbol{\sigma_{LE}}\sqrt{\boldsymbol{L}}, \boldsymbol{\sigma_{LE}}\sqrt{\boldsymbol{L}}]$ and the local phenotypic optima $\boldsymbol{\theta}_1$ and $\boldsymbol{\theta}_2$ characterizing the heterogeneous environment is essential for the evolutionary dynamics produced by a deterministic model using the infinitesimal model operator (3.1) in heterogeneous environments to be close to individual-based simulations with this explicit genetic architecture.

We find that when the number of loci $\boldsymbol{L}$ involved is large enough for the phenotypic range to extend well beyond the local trait optima, the segregational variances computed at each mating event occurring throughout the IBS present very little variation across time, space and families, which seems to justify summarizing it under a single parameter. Therefore, both the transient dynamics and the qualitative outcomes of the deterministic model are in excellent agreement with the IBS, on a time of order $\sqrt{\boldsymbol{L}}$. When the phenotypic range is just enough to include the local optima, segregational variances computed throughout the IBS can vary substantially across time, space and families in the parameter region which leads to the asymmetrical monomorphic equilibria, in particular for strong selection and intermediate migration. In this parameter region, the transient dynamics produced by the deterministic model are not as close to the IBS, but still good enough for the qualitative outcomes to be consistent. When the number of loci is too small for the phenotypic range to reach the local optima, the IBS lead to extinction on a wider region of parameter than for the deterministic model, as even the most extreme possible phenotypes are not viable under strong enough selections.

This criterion that the segregational variance is approximately constant across time, space and families if the phenotypic range extends well beyond the local optima is in agreement with the approximation derived in [Sachdeva and Barton 2017] according to the hypergeometric model. Under this assumption, they give an approximation of the segregational variance V conditional to the parental traits Y and Z in the limit of large number of loci L (equation (6), Appendix S1, Sachdeva and Barton 2017):

$$V \approx \frac{\gamma^2 L}{2} - \frac{YZ}{2L}.$$

The latter implies that V is approximately constant across families if the local optimal $\pm\theta$

satisfies $\theta \ll \gamma L$, which is consistent with our conclusion transposed from diploid to haploid organisms, that the constant segregational variance assumption holds if the phenotypic range $[-\gamma L, \gamma L]$ extends well beyond the local optima $\pm\theta$.

Despite the framework presented here being different from the ones in [Tufto 2000] and [Huisman and Tufto 2012], for it allows migration to go back-and-forth, the fact that the initial populations is asymmetrical and thus the metapopulation displays pseudo source-sink dynamics under strong selection (asymmetrical equilibria of [Ronce and Kirkpatrick 2001] and [Dekens 2022]) makes the comparison relevant. The results are overall relatively consistent with these studies, conditioned on the differences in terms of number of loci (here a lot higher) and the commutativity of the different stages as a consequence of small generation length $\boldsymbol{\Delta t} = 0.1$. In [Tufto 2000], the latter has a significant importance, because of the succession of the migration and selection stages, which at high selection culls automatically all the migrants before allowing them to mate with the local population. However, the conclusion that the infinitesimal model and the Gaussian approximation are consistent with multi-loci IBS when the immigrants can compensate their initial maladaptation with a large enough $\boldsymbol{\sigma_{LE}^2}$ (at fixed distance between the sink's optimum and the source' mean trait) goes in the same direction as my conclusion on the trait range $[-\boldsymbol{\sigma_{LE}}\sqrt{\boldsymbol{L}}, \boldsymbol{\sigma_{LE}}\sqrt{\boldsymbol{L}}]$ extending beyond the local optima. Besides, I would also like to address the findings of [Tufto 2000] that the variance in trait at equilibrium is largely over $\boldsymbol{\sigma_{LE}}^2$ when the latter is small (0.01), as it is not observed here. My explanation for the discrepancy is the very strong selection levels considered (4, 20, and 100) and the life cycle order, as described above. As for the observation that the recursions with the infinitesimal model in [Huisman and Tufto 2012] might overestimate the variance in trait when the difference between the subpopulations increases (fig. 5 of their article, with 5 loci), with this discrepancy in variance decreasing when the number of loci passes from 5 to 20 (fig. 6 of their article) aligns with our findings. Indeed, the first effect relates directly with the trait range including or not the local optima and the second relates to the fact that the trait range increases with the number of loci (at fixed $\boldsymbol{\sigma_{LE}}$).

3.A Example of a numerical comparison of transient moments' dynamics between deterministic recursions and IBS

In this appendix, I illustrate how the Wasserstein distance between the renormalized trait distributions of the IBS and the deterministic recursions (Fig. 3.2) translates macroscopically onto the visual difference of the first moments' dynamics. The example shown in Fig. 3.8 indicates in particular how the Wasserstein distance can capture subtle discrepancies which are unsuspected at macroscopic level.

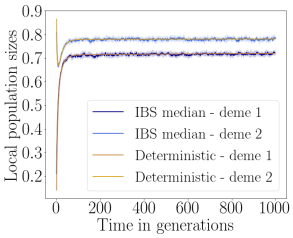

(a) Subpopulations sizes, 500 loci.

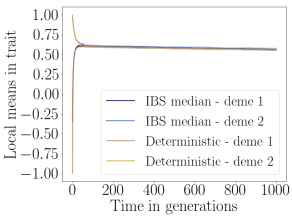

(b) Local mean traits, 500 loci.

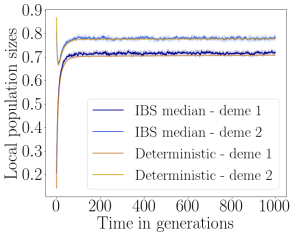

(c) Subpopulations sizes, 100 loci.

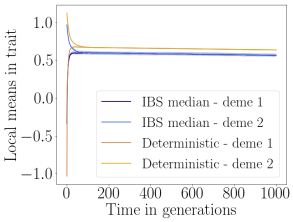

(d) Local mean traits, 100 loci.

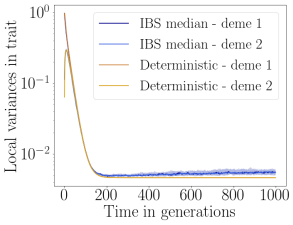

(e) Local variances in trait, 500 loci.

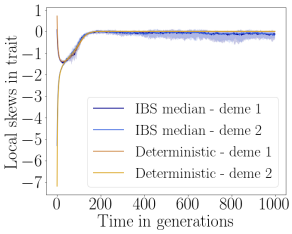

(f) Local skews, 500 loci.

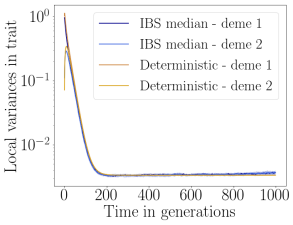

(g) Local variances in trait, 100 loci.

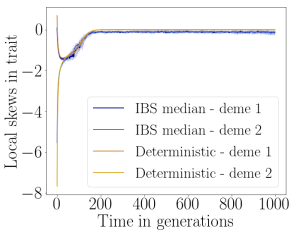

(h) Local skews, 100 loci.

Figure 3.8: **Comparison of the transient dynamics of the first moments of local trait distributions, obtained from IBS (blue lines) and deterministic recursions of (3.2) (yellow lines)**, for weak selection $g = 0.1$ and intermediate migration $m = 0.8$, with small standard deviation at linkage equilibrium $\sigma_{LE} = 0.1$. All the figures show that the IBS and the deterministic recursions are in excellent agreement. Moreover, the left half panel is with 500 loci, and the right panel with 100 loci. The most significant difference between the two (which is still quite small) is the slight discrepancy in the local mean traits with 100 loci (Fig. 3.8d) between IBS and deterministic trajectories, which does not appear with 500 loci (Fig. 3.8b).

Chapter 4

The best of both worlds: combining population genetic and quantitative genetic models

Traits under migration-selection balance are increasingly shown to exhibit complex patterns of genetic architecture, with allelic differences of varying magnitude. However, studying the influence of a large number of small allelic effects on the maintenance of spatial polymorphism is mathematically challenging, due to the high complexity of the systems that arise. Here we propose a new methodology that allows us to take into account the combined contributions of a major locus and of a quantitative background resulting from small effect loci, inherited according to the infinitesimal model. In a regime of small variance contributed by the quantitative loci, we found new arguments of convex analysis to justify that traits are concentrated around the major alleles effects according to a normal distribution, which leads to a slow-fast analysis approach. By applying it to a symmetrical two patch model, we predict an undocumented phenomenon of loss of polymorphism at the major locus despite strong selection for local adaptation under some conditions, where the infinitesimal quantitative background slowly disrupts the fast established symmetrical polymorphism at the major locus, which is confirmed by individual-based simulations. We also provide a comprehensive toolbox designed to describe how to apply our method to more complex population genetic models.

4.1 Introduction

Many species, if not most, evolve in heterogeneous habitats, where varying selection acts upon phenotypic traits in a manner that causes local adaptation. The genetic architecture that underlies those traits is known to present an array of possibilities, from major responses at one particular gene to diffuse polygenic reponses (Slate 2005; Walsh and Lynch 2018). The genetic basis of adaptation has been the subject of an ongoing debate since the early days of evolutionary biology. On the one hand, the field of population genetics explicitly describes and models the dynamics of a few major genes and alleles that have discrete effects, like eye color. On the other hand, the quantitative genetic field explores the evolution of quantitative and continuous traits, like limb size, which are thought to arise from the combined small effects of many genes. A first theoretical milestone in the relationship between the two fields was reached in 1919, when Fisher proposed the infinitesimal model to formalize how such a polygenic trait can be inherited, using the Mendelian framework, clarifying the connection between the two genetic approaches (Fisher 1919). His framework was subsequently made more precise (Bulmer 1971; Lange 1978) and recently justified in various situations using a multi-loci model and a central limit theorem approach (Barton, Etheridge, and Véber 2017).

In the last four decades, enormous progress in genome sequencing has allowed for more data to inform this debate on the genetic architecture underlying traits under selection. However, global conclusions on when a major allele or a polygenic response evolves are still yet to be drawn. For example, as reviewed in [Walsh and Lynch 2018], one notable paradox surrounding the study of the evolution of resistance to the insecticide BT toxin is the difference of results between field and lab experiments. Indeed, in the field, major effects are more often found to be the main drivers of evolution of resistance than in the lab, where a polygenic response is more common (McKenzie and Batterham 1994), even if intensity of selection might not differ (Groeters and Tabashnik 2000). Moreover, the length of the experiment seems to matter: the results of QTL mapping on long-term experiments involving crosses between lines subjected to opposing directional selection (like the Illinois corn experiment) often suggest that a polygenic response emerges over time, due to a large number of QTL of small additive effects (see Laurie et al. 2004; Dudley et al. 2007). Note that such a setting of opposing directional selection can arise in heterogeneous environments, where different phenotypic optima are selectively favoured in different patches.

In order to gain general insights on the likely genetic architecture underlying a trait experiencing heterogeneous selection, one should turn to models that analyse population dynamics of a trait resulting from multiple loci with different effect size on the trait, with spatial heterogeneity. In population genetics, one-locus or two-locus models in heterogeneous environments are well studied (Nagylaki and Lou 2001; Bürger and Akerman 2011), with a nuanced picture when including the effect of drift (Yeaman and Otto 2011). A two-deme two-locus model is analysed in [Geroldinger and Bürger 2014], which in particular shows that a concentrated genetic architecture (a major locus and a tightly linked minor one) maintains polymorphism (full or single-locus) even under high migration rates when selection acts in opposite directions in the two patches. Increasing the number of loci quickly leads to an analytical complexity too great for a general study. There also exist multi-loci models in heterogeneous environments (Lythgoe 1997; Szép, Sachdeva, and Barton 2021), but they focus on equal allelic effects. On the other end of the spectrum, quantitative genetic models do not typically account for additional discrete major allelic effects on the focal quantitative trait (for sexually reproducing populations in heterogeneous environment, see Ronce and Kirkpatrick 2001; Hendry, Day, and Taylor 2001; Dekens 2022 and for asexually reproducing populations, see Débarre, Ronce, and

Gandon 2013; Mirrahimi 2017; Mirrahimi and Gandon 2020; Hamel, Lavigne, and Roques 2021).

To our knowledge, the first model that bridges this gap is from [Lande 1983]. In this work, the author considers the dynamics of a major locus where two alleles segregate along with a polygenic background, in a diploid population subjected to a sudden change of environment. He models the influence of the polygenic background on the trait by assuming that the trait distribution for each genotype at the major effect locus is Gaussian, centered around the phenotype of each genotype at the major effect locus. This study opened the way for more recent work on the genetic architecture of adaptation in a suddenly changing environment, where the central question is whether this adaptation is due to major allelic sweeps or to subtle shifts in the frequency of many small effect alleles. In [Chevin and Hospital 2008], the authors extend the framework of [Lande 1983] to include less specific selection functions than exponential ones. Subsequent studies (Vladar and Barton 2014; Jain and Stephan 2017) explicitly model the short-term dynamics of a polygenic trait in a mutation-selection balance, following a sudden change of environment. They show that there exists a sharp threshold in allelic sizes under which polymorphism remains and over which fixation occurs. Lately, in a similar context, [Höllinger, Pennings, and Hermisson 2019] proposes an extension to take genetic drift into account on the dynamics of adaptation with a polygenic binary trait under mutation-selection balance. However, all those works from [Lande 1983] to [Höllinger, Pennings, and Hermisson 2019] study panmicitic populations, without spatial structure, even though spatial heterogeneities generate gene flow, which indirectly shapes genetic architecture through local adaptation (see [Yeaman and Whitlock 2011], or below for more details). Moreover, they focus solely on the dynamics of the allelic frequencies without considering their coupling with population size dynamics, assuming it to be constant.

The aim of this work is twofold. A first global aim is to propose a hybrid framework between population and quantitative genetics, which allows us to study analytically the long-term eco-evo dynamics of a sexually reproducing population characterized by a composite trait resulting from the interplay between a few major loci and a quantitative polygenic background, in spatially heterogeneous environments (migration-selection balance). We want to emphasize that, by "eco-evo dynamics", we mean that we study both the ecological and evolutionary dynamics of the local trait distributions and therefore do not assume that the sizes of the populations remain constant; rather, they are variables of the system. Furthermore, we aspire to step back from the Gaussian assumption made by [Lande 1983] and [Chevin and Hospital 2008] to model the background polygenic effect on the trait and propose a framework that does not make a priori assumptions on its shape. Instead, our model relies on an extension of the standard infinitesimal model (Fisher 1919), that encodes both the inheritance of the quantitative background and the major alleles. Analytical progress is possible, despite not specifying the shape of the trait distribution, in a regime of small segregational variance for the quantitative component of the trait. This approximation uses the fact that the variance introduced at each event of reproduction by the quantitative background is small compared to the discrete allelic effects at major loci. This modelling regime allows us to use a methodology developed by [Diekmann, Jabin, et al. 2005], inspired by perturbative tools of optic geometrics. This method has been used in several quantitative genetic studies, first for asexually reproducing populations (Perthame and Barles 2008; Barles, Mirrahimi, and Perthame 2009; Mirrahimi 2017; Mirrahimi and Gandon 2020) and more recently models using the infinitesimal model of sexual reproduction (Garnier et al. 2022; Calvez, Garnier, and Patout 2019; Patout 2020; Dekens 2022).

A second aim is to illustrate the insights given by our framework for local adaptation,

by applying it to the simplest case: a haploid population living in a two patch environment, where selection acts on a trait that results from the segregation of two major alleles at a single locus along with a quantitative polygenic background. This choice is partly inspired by the study of [Yeaman and Whitlock 2011], which looks at the emergence of patterns in the genetic architecture of local adaptation in a migration-selection balance setting through individual-based simulations. Our model also bridges the following population genetic and quantitative genetic models:

1. The one-locus haploid model in a two-patch environment, which considers two alleles A and a segregating at the same locus, each improving the survival chance in one of the habitats and being deleterious in the other. With symmetrical migration and selection, this model predicts that *polymorphism at the focal locus is always stable*, whenever the metapopulation persists (see Remark 11 and Proposition 4.4.3 for a proof of this fact). We aim at challenging the robustness of this conclusion by asking: *does this prediction hold when adding a small perturbation due to a quantitative polygenic component on the trait under local selection?*

2. The quantitative genetic model from [Dekens 2022], which studies the eco-evo dynamics of a quantitative trait in a heterogeneous environment, where the trait is inherited according to the standard version of the infinitesimal model. Our work can be seen as an extension of this model, to which we add the segregation of two major alleles at a single locus. Moreover, if one major allele fixes (loss of polymorphism), the two models are equivalent. Since [Dekens 2022] gives a complete analytical description of the outcomes of their system (in the small segregation variance regime), the outcomes for our present study are known given the fixation of a major allele. Therefore, *our study focuses on the description of polymorphism at the major locus and its stability.*

Contributions. We show that our hybrid model gives new analytical insights on the stability of polymorphism at a major locus underlying local adaptation in a symmetrical heterogeneous environment, which is not captured by the one-locus haploid population genetic model. Due to small perturbations induced by the quantitative component of the trait around the genotypic effects of the major alleles, polymorphism at the major locus is lost both at low and high levels of selection, below a certain level of migration. The first region of loss of polymorphism, at low selection intensities, is intuitively expected, as migration blends more strongly than selection differentiates. More surprising is the lost of polymorphism at high intensities of selection, where one would expect polymorphism at the major locus to be strongly favoured. Up to our knowledge, this phenomenon, where quantitative differences displace polymorphism at a major locus, has not yet been documented. We confirm that our analysis is qualitatively consistent with individual-based simulations.

This study-case suggests that the long-term influence of a quantitative polygenic background on a major loci polymorphic equilibrium can lead to unforeseen phenomena. In this work, we present an integrative framework that is meant to help analytically bridge population genetics and quantitative genetics that is meant to help analytically identifying them. Our method goes deeper than previous models (Lande 1983) by justifying in a certain regime of small variance that the traits are normally distributed around the major alleles effects, thanks to new arguments of convex analysis. It allows a slow-fast analysis, that ultimately leads to derive the conditions for when the infinitesimal quantitative background slowly disrupts the fast established symmetrical polymorphism at the major locus.

Furthermore, we provide a comprehensive toolbox that describes how to apply our methodology to more general cases in terms of number of major loci, number of patch, and form of

selection for haploid or diploid populations (see Appendices 4.A and 4.B).

Outline. In Section 4.2, we first present how we build our hybrid model. We detail how we incorporate the effects of selection acting on major alleles segregating at a single locus within a generic quantitative genetic model in a two-patch environment, and their inheritance, thanks an extension to the infinitesimal model. Next, in Section 4.3, we use a perturbative approach and present new arguments of convex analysis to derive a closed moment-based system in a regime where the segregational variance of the quantitative component of the trait is small compared to the major gene effect. This approach allows us to perform a separation between ecological and evolutionary time scales that leads to an asymptotic system with reduced complexity (Section 4.4). In Section 4.5, we analyse the stability of the polymorphism at the major locus (for analytical purposes, we restrict ourselves to the case where the environment is symmetrical in that section). Next in Section 4.6, we confirm the phenomena of loss of polymorphism at the major locus with individual-based simulations.

4.2 Model

4.2.1 From a generic quantitative genetic model to a hybrid model.

We consider a haploid population reproducing sexually and characterized by a quantitative trait $\boldsymbol{\zeta}$ in a heterogeneous environment with two habitats connected by constant migration at rate $\boldsymbol{m_1}$ (from habitat 1 to habitat 2) and $\boldsymbol{m_2}$ (from habitat 2 to habitat 1). Following classical models of quantitative genetics, we model each habitat i selecting toward a different optimum $\boldsymbol{\theta_i}$ with strength $\boldsymbol{g_i}$. Maladaptation and local uniform competition for resources (with intensity $\boldsymbol{\kappa_i}$ in deme i) are sources of mortality leading to a per capita decline at rate:

$$-\boldsymbol{g_i}(\boldsymbol{\zeta}-\boldsymbol{\theta_i})^2-\boldsymbol{\kappa_i}\,\boldsymbol{N_i},$$

for individuals of trait $\boldsymbol{\zeta}$ in habitat i ($\boldsymbol{N_i}$ denotes the local population size). At time $\boldsymbol{t}\geq 0$, let $\boldsymbol{n_1}(\boldsymbol{t},\boldsymbol{\zeta})$ and $\boldsymbol{n_2}(\boldsymbol{t},\boldsymbol{\zeta})$ be the local trait densities in patches 1 and 2, and $\boldsymbol{\mathcal{B}}[\boldsymbol{n_i}](\boldsymbol{t},\boldsymbol{\zeta})$ the number of individuals born with a trait $\boldsymbol{\zeta}$ in habitat i, with reproduction occuring at rate $\boldsymbol{\lambda_i}$. The dynamics of the local trait densities read:

$$\begin{cases}\frac{\partial \boldsymbol{n_1}}{\partial \boldsymbol{t}}(\boldsymbol{t},\boldsymbol{\zeta})=\boldsymbol{\lambda_1}\,\boldsymbol{\mathcal{B}}[\boldsymbol{n_1}](\boldsymbol{t},\boldsymbol{\zeta})-\boldsymbol{g_1}\,(\boldsymbol{\zeta}-\boldsymbol{\theta_1})^2\,\boldsymbol{n_1}(\boldsymbol{t},\boldsymbol{\zeta})-\boldsymbol{\kappa_1}\boldsymbol{N_1}(\boldsymbol{t})\,\boldsymbol{n_1}(\boldsymbol{t},\boldsymbol{\zeta})\\ \qquad\qquad\qquad\qquad\qquad\qquad\qquad\qquad\qquad\qquad+\boldsymbol{m_2}\,\boldsymbol{n_2}(\boldsymbol{t},\boldsymbol{\zeta})-\boldsymbol{m_1}\,\boldsymbol{n_1}(\boldsymbol{t},\boldsymbol{\zeta}),\\ \\ \frac{\partial \boldsymbol{n_2}}{\partial \boldsymbol{t}}(\boldsymbol{t},\boldsymbol{\zeta})=\boldsymbol{\lambda_2}\,\boldsymbol{\mathcal{B}}[\boldsymbol{n_2}](\boldsymbol{t},\boldsymbol{\zeta})-\boldsymbol{g_2}\,(\boldsymbol{\zeta}-\boldsymbol{\theta_2})^2\,\boldsymbol{n_2}(\boldsymbol{t},\boldsymbol{\zeta})-\boldsymbol{\kappa_2}\,\boldsymbol{N_2}(\boldsymbol{t})\,\boldsymbol{n_2}(\boldsymbol{t},\boldsymbol{\zeta})\\ \qquad\qquad\qquad\qquad\qquad\qquad\qquad\qquad\qquad\qquad+\boldsymbol{m_1}\,\boldsymbol{n_1}(\boldsymbol{t},\boldsymbol{\zeta})-\boldsymbol{m_2}\,\boldsymbol{n_2}(\boldsymbol{t},\boldsymbol{\zeta}).\end{cases}\tag{4.1}$$

We can define the trait axis such that: $\boldsymbol{\theta}:=\boldsymbol{\theta_2}=-\boldsymbol{\theta_1}>0$ without loss of generality. We next describe the novel aspect of this work, which allows the trait $\boldsymbol{\zeta}$ to be sum of two components, a major effect locus and an quantitative background $\boldsymbol{z}$. We furthermore describe the sexual reproduction operator used.

Major effect. The first component comes from a locus where two alleles A/a are segregating. They have a major effect on the trait: $\boldsymbol{\eta_A}$ and $\boldsymbol{\eta_a}$. Inheritance of this locus is Mendelian.

Quantitative background. The second component, denoted by $\boldsymbol{z} \in \mathbb{R}$, represents the quantitative background due to infinitesimally small additive contributions to the trait from a large number of unlinked alleles. Although it comes from infinitesimally small contributions, $\boldsymbol{z}$ should not be thought as being necessarily small, due to the large number of alleles contributing to it. We also assume that the major locus is effectively unlinked with the small-effect ones.

Inheritance of the trait: an extension of the infinitesimal model. Let us recall that the infinitesimal model, first introduced in [Fisher 1919], provides a way to encode efficiently the inheritance of complex traits coming from a large number of alleles, each with small effects. The classical version states that an offspring receives a trait $\mathcal{Z}$ from its parents with traits $\mathcal{Z}_1$ and $\mathcal{Z}_2$, where $\mathcal{Z}$ differs from the mean parental trait $\frac{\mathcal{Z}_1+\mathcal{Z}_2}{2}$ following a centered Gaussian law, with variance $\frac{\sigma^2}{2}$. The latter accounts for the stochasticity of segregation, and therefore the variance is called the segregational variance. Specifically:

$$\mathcal{Z}|\mathcal{Z}_1, \mathcal{Z}_2 \sim \frac{\mathcal{Z}_1 + \mathcal{Z}_2}{2} + \mathcal{Y}, \quad \mathcal{Y} \sim \mathcal{N}\left(0, \frac{\sigma^2}{2}\right), \ \mathcal{Y} \perp \mathcal{Z}_1, \mathcal{Z}_2.$$

The Mendelian view of the infinitesimal model has been discussed in [Fisher 1919; Bulmer 1971; Lange 1978]: the common interpretation is that the trait results from a large number of small additive contributions at unlinked loci. For a more in depth description, see [Barton, Etheridge, and Véber 2017].

Because the trait we are considering is a composite of a major effect locus inherited according to Mendelian laws and an infinitesimal background, it is natural to use an extension of the infinitesimal model for this hybrid case. Now, the offspring's trait $(\mathcal{A}, \mathcal{Z})$ given their parents $(\mathcal{A}_1, \mathcal{Z}_1)$ and $(\mathcal{A}_2, \mathcal{Z}_2)$ reads:

$$(\mathcal{A}, \mathcal{Z},) \mid (\mathcal{A}_1, \mathcal{Z}_1), (\mathcal{A}_2, \mathcal{Z}_2) \sim \left(X\mathcal{A}_1 + (1-X)\mathcal{A}_2, \ \frac{\mathcal{Z}_1 + \mathcal{Z}_2}{2} + \mathcal{Y}\right), \tag{4.2}$$

where $\mathcal{Y} \sim \mathcal{N}\left(0, \frac{\sigma^2}{2}\right)$ follows a centered Gaussian law of variance $\frac{\sigma^2}{2}$ and $X \sim B\left(\frac{1}{2}\right)$ follows a Bernoulli law with parameter $\frac{1}{2}$ (assuming fair meiosis). The latter are independent of each other and of $\mathcal{Z}_1, \mathcal{Z}_2, \mathcal{A}_1, \mathcal{A}_2$.

4.2.2 Modified reproduction operator.

Let us translate Eq. (4.2) into a continuous density model. Let $\boldsymbol{n_i^A(z)}$ (respectively $\boldsymbol{n_i^a(z)}$) denote the density of individuals of patch i carrying allele A (respectively a) along with an infinitesimal background $\boldsymbol{z}$, therefore having a trait $\boldsymbol{\zeta = \eta^A + z}$ (respectively, $\boldsymbol{\eta^a + z}$). In agreement with Eq. (4.2), the number of offspring born with the allele A and an infinitesimal contribution $\boldsymbol{z}$ in habitat i then reads:

$$\begin{aligned}
\boldsymbol{\mathcal{B}_\sigma^A[n_i^A, n_i^a](z)} &= \int_{\mathbb{R}^2} \frac{1}{\sqrt{\pi}\boldsymbol{\sigma}} \exp\left[-\frac{\left(\boldsymbol{z} - \frac{\boldsymbol{z_1}+\boldsymbol{z_2}}{2}\right)^2}{\boldsymbol{\sigma^2}}\right] \times \\
&\qquad \frac{1}{N_i}\left[\boldsymbol{n_i^A(z_1)\, n_i^A(z_2)} + \frac{1}{2}\left[\boldsymbol{n_i^A(z_1)\, n_i^a(z_2) + n_i^a(z_1) n_i^A(z_2)}\right]\right] d\boldsymbol{z_1}\, d\boldsymbol{z_2} \\
&= \int_{\mathbb{R}^2} \frac{1}{\sqrt{\pi}\boldsymbol{\sigma}} \exp\left[-\frac{\left(\boldsymbol{z} - \frac{\boldsymbol{z_1}+\boldsymbol{z_2}}{2}\right)^2}{\boldsymbol{\sigma^2}}\right] \boldsymbol{n_i^A(z_1)}\, \frac{\boldsymbol{n_i^A(z_2) + n_i^a(z_2)}}{\boldsymbol{N_i}}\, d\boldsymbol{z_1}\, d\boldsymbol{z_2}.
\end{aligned}$$

Similarly, the corresponding number of offspring born with the allele a and an infinitesimal part $\boldsymbol{z}$ reads:

$$\begin{aligned}\boldsymbol{\mathcal{B}}_{\boldsymbol{\sigma}}^{a}[\boldsymbol{n}_i^{\boldsymbol{A}}, \boldsymbol{n}_i^{a}](\boldsymbol{z}) &= \int_{\mathbb{R}^2} \frac{1}{\sqrt{\pi}\boldsymbol{\sigma}} \exp\left[-\frac{\left(\boldsymbol{z} - \frac{\boldsymbol{z_1}+\boldsymbol{z_2}}{2}\right)^2}{\boldsymbol{\sigma}^2}\right] \times \\ &\qquad \frac{1}{N_i}\left[\boldsymbol{n}_i^{a}(\boldsymbol{z_1})\,\boldsymbol{n}_i^{a}(\boldsymbol{z_2}) + \frac{1}{2}\left[\boldsymbol{n}_i^{\boldsymbol{A}}(\boldsymbol{z_1})\,\boldsymbol{n}_i^{a}(\boldsymbol{z_2}) + \boldsymbol{n}_i^{a}(\boldsymbol{z_1})\boldsymbol{n}_i^{\boldsymbol{A}}(\boldsymbol{z_2})\right]\right] d\boldsymbol{z_1}\, d\boldsymbol{z_2} \\ &= \int_{\mathbb{R}^2} \frac{1}{\sqrt{\pi}\boldsymbol{\sigma}} \exp\left[-\frac{\left(\boldsymbol{z} - \frac{\boldsymbol{z_1}+\boldsymbol{z_2}}{2}\right)^2}{\boldsymbol{\sigma}^2}\right] \boldsymbol{n}_i^{a}(\boldsymbol{z_1})\,\frac{\boldsymbol{n}_i^{a}(\boldsymbol{z_2}) + \boldsymbol{n}_i^{\boldsymbol{A}}(\boldsymbol{z_2})}{\boldsymbol{N_i}}\, d\boldsymbol{z_1}\, d\boldsymbol{z_2}.\end{aligned}$$

The operator reproduction $\boldsymbol{\mathcal{B}_\sigma}$ indicates that it is more relevant to model the dynamics of the two local allelic densities $\boldsymbol{n_i^a}, \boldsymbol{n_i^A}$, instead of $\boldsymbol{n_i}$ (which is their sum). From now on, we will therefore adopt this point of view.

4.2.3 Dimensionless system

Let us rescale Eq. (4.1) according to:

$$\eta^A := \frac{\boldsymbol{\eta^A}}{\boldsymbol{\theta}}, \quad z := \frac{\boldsymbol{z}}{\boldsymbol{\theta}}, \quad g_i := \frac{\boldsymbol{g_i\theta^2}}{\boldsymbol{\lambda_1}}, \quad m_i := \frac{\boldsymbol{m_i}}{\boldsymbol{\lambda_1}}, \quad \varepsilon := \frac{\boldsymbol{\sigma}}{\boldsymbol{\theta}}, \quad t := \varepsilon^2\boldsymbol{\lambda_1 t}, , \quad \alpha := \frac{\boldsymbol{\kappa_1}}{\boldsymbol{\kappa_2}}, \quad \lambda := \frac{\boldsymbol{\lambda_2}}{\boldsymbol{\lambda_1}},$$

and introduce the rescaled trait densities:

$$n_{\varepsilon,i}^{A}(t,z) := \frac{\boldsymbol{\kappa_i}}{\boldsymbol{\lambda_1}}\,\boldsymbol{n_i^A(t,z)}, \quad n_{\varepsilon,i}^{a}(t,z) := \frac{\boldsymbol{\kappa_i}}{\boldsymbol{\lambda_1}}\,\boldsymbol{n_i^a(t,z)}.$$

so that Eq. (4.1) reads:

$$\begin{cases} \varepsilon^2 \frac{\partial n_{\varepsilon,1}^{A}}{\partial t}(t,z) = \mathcal{B}_\varepsilon{}^{A}(n_{\varepsilon,1}^{A}, n_{\varepsilon,1}^{a})(t,z) - g_1(z+\eta^A+1)^2\, n_{\varepsilon,1}^{A}(t,z) - N_{\varepsilon,1}(t)\, n_{\varepsilon,1}^{A}(t,z) \\ \qquad\qquad +\alpha\, m_2\, n_{\varepsilon,2}^{A}(t,z) - m_1\, n_{\varepsilon_1}^{A}(t,z), \\ \varepsilon^2 \frac{\partial n_{\varepsilon,1}^{a}}{\partial t}(t,z) = \mathcal{B}_\varepsilon{}^{a}(n_{\varepsilon,1}^{a}, n_{\varepsilon,1}^{A})(t,z) - g_1(z+\eta^a+1)^2\, n_{\varepsilon,1}^{a}(t,z) - N_{\varepsilon,1}(t)\, n_{\varepsilon,1}^{a}(t,z) \\ \qquad\qquad +\alpha\, m_2\, n_{\varepsilon,2}^{a}(t,z) - m_1\, n_{\varepsilon_1}^{a}(t,z), \\ \varepsilon^2 \frac{\partial n_{\varepsilon,2}^{A}}{\partial t}(t,z) = \lambda\,\mathcal{B}_\varepsilon{}^{A}(n_{\varepsilon,2}^{A}, n_{\varepsilon,2}^{a})(t,z) - g_2(z+\eta^A-1)^2\, n_{\varepsilon,2}^{A}(t,z) - N_{\varepsilon,2}(t)\, n_{\varepsilon,2}^{A}(t,z) \\ \qquad\qquad +\frac{m_1}{\alpha}\, n_{\varepsilon,1}^{A}(t,z) - m_2\, n_{\varepsilon_2}^{A}(t,z), \\ \varepsilon^2 \frac{\partial n_{\varepsilon,2}^{a}}{\partial t}(t,z) = \lambda\,\mathcal{B}_\varepsilon{}^{a}(n_{\varepsilon,2}^{a}, n_{\varepsilon,2}^{A})(t,z) - g_2(z+\eta^a-1)^2\, n_{\varepsilon,2}^{a}(t,z) - N_{\varepsilon,2}(t)\, n_{\varepsilon,2}^{a}(t,z) \\ \qquad\qquad +\frac{m_1}{\alpha}\, n_{\varepsilon,1}^{a}(t,z) - m_2\, n_{\varepsilon_2}^{a}(t,z), \end{cases} \tag{4.3}$$

where the rescaled reproduction operator is given by:

$$\mathcal{B}_\varepsilon^{\mathcal{A}}(n_{\varepsilon,i}^{A}, n_{\varepsilon,i}^{a})(t,z) = \frac{1}{\sqrt{\pi}\varepsilon}\int_{\mathbb{R}^2} \exp\left[\frac{-(z-\frac{z_1+z_2}{2})^2}{\varepsilon^2}\right] n_{\varepsilon,i}^{A}(t,z_1)\frac{n_{\varepsilon,i}^{A}(t,z_2)+n_{\varepsilon,i}^{a}(t,z_2)}{N_{\varepsilon,i}(t)} dz_1\, dz_2. \tag{4.4}$$

Working assumption 1. *One can notice that if one allele, for instance A, has fixed and the other is lost ($\boldsymbol{n^a(z)} = 0$), then $\boldsymbol{\mathcal{B}_\sigma^A}$ coincides with the infinitesimal model reproduction operator used in [Dekens 2022]. Therefore, in that case, then (4.3) is the same*

system as the one fully analysed in [Dekens 2022], up to a translation: $z + \eta^A \to \tilde{z}$. Hence, in all that follows, we assume that both alleles are still present in the population and focus on the conditions of the persistence of this polymorphism.

4.3 Derivation of a moment-based system in the regime of small variance: $\varepsilon^2 \ll 1$

4.3.1 The regime of small variance: a formal analysis.

Presentation of the methodology. We choose to place our study in a regime where the amount of diversity introduced by the segregation of the infinitesimal background at each event of reproduction is small in comparison to the difference between the habitats' optima, which reads:

$$\frac{\boldsymbol{\sigma^2}}{\boldsymbol{\theta^2}} \ll 1 \implies \varepsilon^2 \ll 1.$$

In this regime of small variance, the trait distributions are expected in the limit to be Dirac masses centred at the major locus genotypes, where our focus is to determine the distribution near this limit. [Diekmann, Jabin, et al. 2005] introduced in 2005 a methodology to determine the dynamics of the trait values at which the distribution gets concentrated. This methodology has since been used successfully to study several evolutionary questions, initially for asexual models where the diversity generated by mutations is modelled by a linear operator translating the distribution of mutational effects (Perthame and Barles 2008; Barles, Mirrahimi, and Perthame 2009; Mirrahimi 2017; Mirrahimi and Gandon 2020), and recently adapted to study sexually reproducing populations with the infinitesimal model operator (Garnier et al. 2022; Calvez, Garnier, and Patout 2019; Patout 2020; Dekens 2022). The method consists in defining proxies U_ε from the trait densities n_ε through a suitable transformation so that such proxies are regular functions (by comparison to Dirac masses) and their asymptotic analysis is easier. Studying them often induces a reduction in the complexity of the system and retains fundamental quantitative information about the distributions, such as around which traits they are concentrated. Here, we follow quantitative genetic studies that use the infinitesimal model according to the same methodology (Garnier et al. 2022; Calvez, Garnier, and Patout 2019; Patout 2020; Dekens 2022) and define the proxies $U^A_{\varepsilon,i}$ (resp. $U^a_{\varepsilon,i}$):

$$n^A_{\varepsilon,i} = \frac{1}{\sqrt{2\pi}\varepsilon} e^{-\frac{U^A_{\varepsilon,i}}{\varepsilon^2}}, \quad n^a_{\varepsilon,i} = \frac{1}{\sqrt{2\pi}\varepsilon} e^{-\frac{U^a_{\varepsilon,i}}{\varepsilon^2}}. \tag{4.5}$$

Fig. 4.1 displays an example of this kind of exponential transformation (called Hopf-Cole transformation in scalar conservation laws). A key observation is that the trait density n_ε concentrates at the minima (zero) of U_ε. As the proxies U^A_ε and U^a_ε are expected to be more regular in the regime of small variance, they are thought to be the right object on which to perform a Taylor expansion series to gain information on the asymptotic distributions in the limit of small variance (see Calvez, Garnier, and Patout 2019). We therefore define $u^A_{0,i}$ (resp. $u^a_{0,i}$) as the leading term in the Taylor expansion of $U^A_{\varepsilon,i}$ (resp. $U^a_{\varepsilon,i}$) :

$$U^A_{\varepsilon,i} = u^A_{0,i} + \varepsilon^2 u^A_{1,i} + \varepsilon^4 v^A_{\varepsilon,i}, \qquad U^a_{\varepsilon,i} = u^a_{0,i} + \varepsilon^2 u^a_{1,i} + \varepsilon^4 v^a_{\varepsilon,i} \tag{4.6}$$

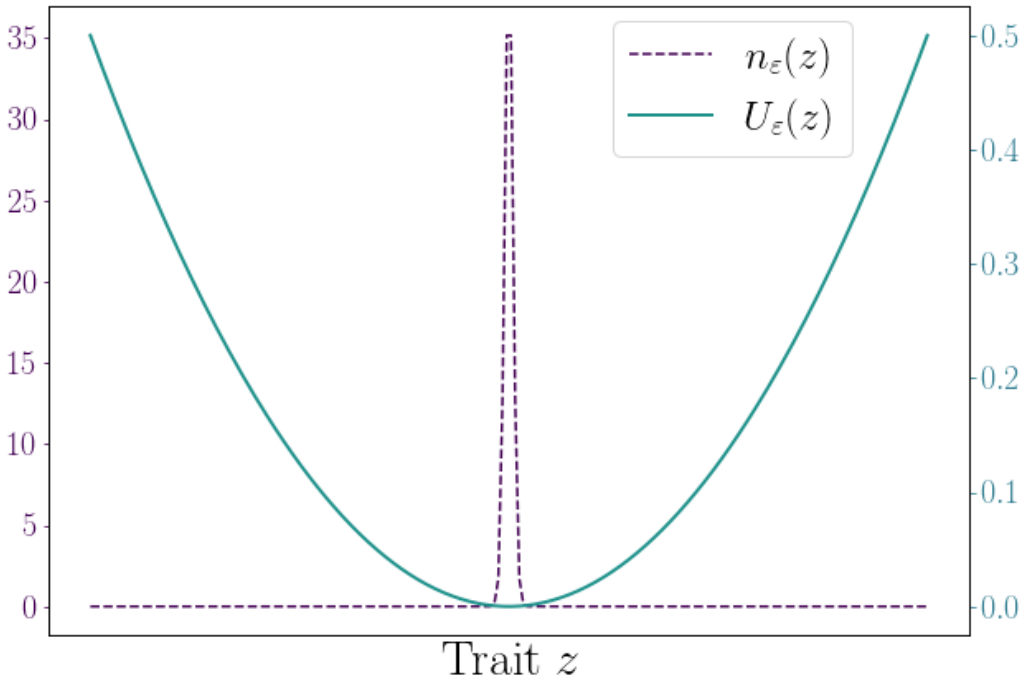

Figure 4.1: **Illustration of the Hopf-Cole transform to study concentration phenomena**. This transformation unfolds singular distributions n_ε close to a Dirac mass (in purple), by defining more regular proxies: U_ε (in green) such that $n_\varepsilon = \frac{1}{\sqrt{2\pi\varepsilon}} e^{-\frac{U_\varepsilon}{\varepsilon^2}}$. This figure suggests that, when ε vanishes, the limit U is regular and positive and cancels at the support of the limit measure n.

where $u^A_{1,i}$ and $u^a_{1,i}$ are the next term in the Taylor expansion, and $\varepsilon^4 v^A_{\varepsilon,i}$ and $\varepsilon^4 v^a_{\varepsilon,i}$ are the residues. [Calvez, Garnier, and Patout 2019] provides the tools to control these residues and thus rigorously justify that (4.6) is an admissible Taylor expansion; adapting them is left for future work.

Characterization of the main terms $u^A_{0,i}$ and $u^a_{0,i}$. The first step for the analysis in the regime of small variance is the characterization of the main terms $u^A_{0,i}$ and $u^a_{0,i}$. However, the arguments given in [Garnier et al. 2022] and used in [Dekens 2022] are not sufficient, due to the mixing of alleles and the discrete nature of Mendelian inheritance. However, we extend the convex analysis to circumvent this limitation (Proposition 4.3.1). Assuming (4.6) is an admissible Taylor expansion (which is suggested by the analysis of [Calvez, Garnier, and Patout 2019]), this step is crucial as it justifies the following formal approximations for $n^A_{\varepsilon,i}$ and $n^a_{\varepsilon,i}$ ($i \in \{1,2\}$):

$$n^A_{\varepsilon,i}(z) = \frac{e^{-\frac{-(z-z_i)^2}{2\varepsilon^2}}}{\sqrt{2\pi}\varepsilon} e^{-u^A_{1,i}(z)+\mathcal{O}(\varepsilon^2)}, \qquad n^a_{\varepsilon,i}(z) = \frac{e^{-\frac{-(z-z_i)^2}{2\varepsilon^2}}}{\sqrt{2\pi}\varepsilon} e^{-u^a_{1,i}(z)+\mathcal{O}(\varepsilon^2)}. \tag{4.7}$$

Hence, to the leading order, $n^A_{\varepsilon,i}$ and $n^a_{\varepsilon,i}$ are formally Gaussian, centered at the same infinitesimal contribution z_i, with the same variance ε^2, but they differ in their prefactors, which are related to the first corrector terms $u^A_{1,i}$ and $u^a_{1,i}$, which generates asymmetries in the distributions.

Remark 8. *The expressions for $n^A_{\varepsilon,i}$ and $n^a_{\varepsilon,i}$ imply that in the regime of small variance, when both alleles A and a are still present in the population, the trait divergence within a habitat is mainly due to the major-effect locus.*

To support (4.7), we first derive constraints (C) on the main terms $u^A_{0,i}$ and $u^a_{0,i}$. In order for the contribution of both reproduction operators $\mathcal{B}^A_\varepsilon$ and $\mathcal{B}^a_\varepsilon$ to remain well-balanced with the other biological phenomena in the regime of small variance in (4.3), $u^A_{0,i}$ and $u^a_{0,i}$ formally need to satisfy the following (see Appendix 4.C for the details):

$$\begin{cases} \forall z \in \mathbb{R}, \quad \max\Big[\sup\limits_{z_1,z_2} u^A_{0,i}(z) - \big(z - \frac{z_1+z_2}{2}\big)^2 - u^A_{0,i}(z_1) - u^A_{0,i}(z_2), \\ \qquad\qquad \sup\limits_{z_1,z_2} u^A_{0,i}(z) - \big(z - \frac{z_1+z_2}{2}\big)^2 - u^A_{0,i}(z_1) - u^a_{0,i}(z_2)\Big] = 0, \\ \forall z \in \mathbb{R}, \quad \max\Big[\sup\limits_{z_1,z_2} u^a_{0,i}(z) - \big(z - \frac{z_1+z_2}{2}\big)^2 - u^a_{0,i}(z_1) - u^a_{0,i}(z_2), \\ \qquad\qquad \sup\limits_{z_1,z_2} u^a_{0,i}(z) - \big(z - \frac{z_1+z_2}{2}\big)^2 - u^A_{0,i}(z_1) - u^a_{0,i}(z_2)\Big] = 0. \end{cases} \tag{C}$$

Proposition 4.3.1. *Let u^A_0 and u^a_0 satisfying Eq. (C), positive almost everywhere and cancelling somewhere. Then, there exists $z^* \in \mathbb{R}$ such that:*

$$\forall z \in \mathbb{R}, \quad u^A_0(z) = u^a_0(z) = \frac{(z-z^*)^2}{2}. \tag{4.8}$$

The conditions on $u^A_{0,i}$ and $u^a_{0,i}$ in Proposition 4.3.1 (positive everywhere and cancelling somewhere) are explained in Appendix 4.C.

Consequently, assuming that (4.6) is the correct ansatz so that we can control the residues in (4.7) (which the analysis of [Calvez, Garnier, and Patout 2019] suggests and provides a framework to show), using the result of Proposition 4.3.1 in (4.5) and (4.6) leads to (4.7).

Proof. The proof relies on the same kind of approach as in [Garnier et al. 2022], in which the authors derive the solutions to a constraint that is equivalent to (C) with the additional constraint of $u_0^A = u_0^a$. As we do not assume the latter, this proof presents a novel part located in the 4th and 5th points. We therefore shorten the presentation of the proof to mainly develop these new arguments. As Proposition 4.3.1 is actually a particular case of Proposition 4.B.1, stated and proven in Section 4.B, we invite the interested reader to refer to the proof of Proposition 4.B.1 for the complete arguments.

1) u_0^A and u_0^a are continuous and have right and left derivatives everywhere.

2) u_0^A and u_0^a both cancels only once, and their zeros are the same. We denote henceforth this zero z^*.

3) Convex Legendre conjugates $\hat{u_0}^A(y) = \sup_z (z-z^*)y - u_0^A(z)$ and $\hat{u_0}^a(y) = \sup_z (z-z^*)y - u_0^a(z)$. One can show that:

$$\begin{aligned} \hat{u_0}^A(y) &= \max\left[\frac{y^2}{4} + 2\,\hat{u_0}^A\left(\frac{y}{2}\right),\ \frac{y^2}{4} + \hat{u_0}^A\left(\frac{y}{2}\right) + \hat{u_0}^a\left(\frac{y}{2}\right),\right], \\ \hat{u_0}^a(y) &= \max\left[\frac{y^2}{4} + 2\,\hat{u_0}^a\left(\frac{y}{2}\right),\ \frac{y^2}{4} + \hat{u_0}^a\left(\frac{y}{2}\right) + \hat{u_0}^A\left(\frac{y}{2}\right),\right]. \end{aligned} \tag{4.9}$$

The fact that both u_0^A and u_0^a cancel at the same point z^* plays a crucial part for the crossed term.

4) Conservation of order with half arguments. Let us consider $y \in \mathbb{R}$ such that $\hat{u_0}^A(y) \geq \hat{u_0}^a(y)$. Then (4.9) implies:

$$\max\left[2\,\hat{u_0}^A\left(\frac{y}{2}\right), \hat{u_0}^A\left(\frac{y}{2}\right) + \hat{u_0}^a\left(\frac{y}{2}\right)\right] \geq \max\left[\hat{u_0}^A\left(\frac{y}{2}\right) + \hat{u_0}^a\left(\frac{y}{2}\right), 2\,\hat{u_0}^a\left(\frac{y}{2}\right)\right],$$

which in turn implies that

$$\hat{u_0}^A\left(\frac{y}{2}\right) \geq \hat{u_0}^a\left(\frac{y}{2}\right).$$

By recursion, for $k \in \mathbb{N}$, we deduce that

$$\hat{u_0}^A\left(\frac{y}{2^k}\right) \geq \hat{u_0}^a\left(\frac{y}{2^k}\right).$$

5) Showing that $\hat{u_0}^A = \hat{u_0}^a$. Let us still consider $y \in \mathbb{R}$ such that $\hat{u_0}^A(y) \geq \hat{u_0}^a(y)$. For $k \in \mathbb{N}$, using the latter in (4.9) leads to

$$\begin{aligned} \hat{u_0}^A\left(\frac{y}{2^k}\right) &= \frac{y^2}{2^{2k+2}} + 2\,\hat{u_0}^A\left(\frac{y}{2^{k+1}}\right), \\ \hat{u_0}^a\left(\frac{y}{2^k}\right) &= \frac{y^2}{2^{2k+2}} + \hat{u_0}^A\left(\frac{y}{2^{k+1}}\right) + \hat{u_0}^a\left(\frac{y}{2^{k+1}}\right). \end{aligned} \tag{4.10}$$

The second line implies that

$$\forall k \in \mathbb{N}, \quad \hat{u_0}^a\left(\frac{y}{2^k}\right) - \hat{u_0}^A\left(\frac{y}{2^k}\right) = \hat{u_0}^a\left(\frac{y}{2^{k+1}}\right) - \hat{u_0}^A\left(\frac{y}{2^{k+1}}\right).$$

By continuity of $\hat{u_0}^A$ and $\hat{u_0}^a$, we obtain

$$\hat{u_0}^A(y) - \hat{u_0}^a(y) = \hat{u_0}^A(z^*) - \hat{u_0}^a(z^*) = 0.$$

As the same can be applied to $y \in \mathbb{R}$ such that $\hat{u_0}^A(y) \leq \hat{u_0}^a(y)$, we obtain

$$\hat{u_0}^A = \hat{u_0}^a.$$

So from now on, we will only show the arguments for $\hat{u_0}^A$.

6) Computing $\hat{u_0}^A$. One can show that (4.9) implies by recursion (denoting $(\alpha, \beta) := \left(\hat{u_0}^{A'}(0^-), \hat{u_0}^{A'}(0^+)\right)$) that:

$$\forall y > 0 \quad (\text{resp.} < 0), \quad \hat{u_0}^A(y) = \frac{y^2}{2} + \beta\, y \quad (\text{resp. } \alpha\, y). \tag{4.11}$$

Note that 0 being a minimum of $\hat{u_0}^A$ implies that: $\alpha \leq 0 \leq \beta$.

7) Using the convex bi-conjugate to obtain: $u_0^A = \frac{z-z^*}{2}$. We can compute the bi-conjugate's expression from (4.11):

$$\hat{\hat{u_0^A}} : z \mapsto \begin{cases} \frac{(z-z^*-\alpha)^2}{2} & \text{if } z < z^* + \alpha \\ 0 & \text{if } z^* + \alpha \leq z \leq z^* + \beta \\ \frac{(z-z^*-\beta)^2}{2} & \text{if } z > z^* + \beta. \end{cases} \tag{4.12}$$

Standard convexity analysis states also that $\hat{\hat{u_0^A}}$ is the lower convex envelope of u_0^A. We actually show that they are equal

$$u_0^A = \hat{\hat{u_0^A}}.$$

Finally, u_0^A vanishes only at z^* (second point of the proof), so $\alpha = \beta = 0$ and we obtain the desired result. □

4.3.2 Moment-based system in the regime of small variance

First, let us derive a formal expansion of the first moments of $n^A_{\varepsilon,i}$ and $n^a_{\varepsilon,i}$ when $\varepsilon^2 \ll 1$ (similar to the derivation in Dekens 2022):

$$\begin{cases} N^A_{\varepsilon,i} := \displaystyle\int_{\mathbb{R}} n^A_{\varepsilon,i}(z)\, dz & = e^{-u^A_{1,i}(z_i)} \left[1 + \varepsilon^2 \left(\frac{\left(\partial_z u^A_{1,i}(z_i)\right)^2}{2} - \frac{\partial_{zz} u^A_{1,i}(z_i)}{2} - v^A_{i,\varepsilon}(z_i) \right)\right] + \mathcal{O}(\varepsilon^4), \\ \overline{z^A_{\varepsilon,i}} := \displaystyle\int_{\mathbb{R}} z\, \frac{n^A_{\varepsilon,i}(z)}{N^A_{\varepsilon,i}}\, dz & = z_i - \varepsilon^2 \partial_z u^A_{1,i}(z_i) + \mathcal{O}(\varepsilon^4), \\ \left(\sigma^A_{\varepsilon,i}\right)^2 := \displaystyle\int_{\mathbb{R}} (z - \overline{z^A_{\varepsilon,i}})^2\, \frac{n^A_{\varepsilon,i}(z)}{N^A_{\varepsilon,i}}\, dz & = \varepsilon^2 + \mathcal{O}(\varepsilon^4), \\ \left(\psi^A_{\varepsilon,i}\right)^3 := \displaystyle\int_{\mathbb{R}} (z - \overline{z^A_{\varepsilon,i}})^3\, \frac{n^A_{\varepsilon,i}(z)}{N^A_{\varepsilon,i}}\, dz & = \mathcal{O}(\varepsilon^4). \end{cases} \tag{4.13}$$

Hence, by integration in the regime of small variance, we can close the infinite system of moments derived from (4.3), producing a system of eight ODEs:

$$
\begin{cases}
\varepsilon^2 \frac{d\, N^a_{\varepsilon,1}}{dt} = N^a_{\varepsilon,} - \left(N^A_{\varepsilon,1} + N^a_{\varepsilon,1}\right) N^a_{\varepsilon,1} - g_1 \left[\overline{z^a_{\varepsilon,1}} + \eta^a + 1\right]^2 N^a_{\varepsilon,1} + \alpha\, m_2\, N^a_{\varepsilon,2} - m_1\, N^a_{\varepsilon,1}, \\
\qquad\qquad\qquad\qquad\qquad\qquad\qquad\qquad\qquad\qquad\qquad\qquad\qquad\qquad\qquad\qquad +\mathcal{O}(\varepsilon^2), \\
\varepsilon^2 \frac{d\, N^A_{\varepsilon,1}}{dt} = N^A_{\varepsilon,1} - \left(N^A_{\varepsilon,1} + N^a_{\varepsilon,1}\right) N^A_{\varepsilon,1} - g_1 \left[\overline{z^A_{\varepsilon,1}} + \eta^A + 1\right]^2 N^A_{\varepsilon,1} + \alpha\, m_2\, N^A_{\varepsilon,2} - m_1\, N^A_{\varepsilon,1} \\
\qquad\qquad\qquad\qquad\qquad\qquad\qquad\qquad\qquad\qquad\qquad\qquad\qquad\qquad\qquad\qquad +\mathcal{O}(\varepsilon^2), \\
\varepsilon^2 \frac{d\, N^a_{\varepsilon,2}}{dt} = \lambda\, N^a_{\varepsilon,2} - \left(N^A_{\varepsilon,2} + N^a_{\varepsilon,2}\right) N^a_{\varepsilon,2} - g_2 \left[\overline{z^a_{\varepsilon,2}} + \eta^a - 1\right]^2 N^a_{\varepsilon,2} + \frac{m_1}{\alpha}\, N^a_{\varepsilon,1} - m_2\, N^a_{\varepsilon,2} \\
\qquad\qquad\qquad\qquad\qquad\qquad\qquad\qquad\qquad\qquad\qquad\qquad\qquad\qquad\qquad\qquad +\mathcal{O}(\varepsilon^2), \\
\varepsilon^2 \frac{d\, N^A_{\varepsilon,2}}{dt} = \lambda\, N^A_{\varepsilon,2} - \left(N^A_{\varepsilon,2} + N^a_{\varepsilon,2}\right) N^A_{\varepsilon,2} - g_2 \left[\overline{z^A_{\varepsilon,2}} + \eta^A - 1\right]^2 N^A_{\varepsilon,2} + \frac{m_1}{\alpha}\, N^a_{\varepsilon,1} - m_2\, N^a_{\varepsilon,2} \\
\qquad\qquad\qquad\qquad\qquad\qquad\qquad\qquad\qquad\qquad\qquad\qquad\qquad\qquad\qquad\qquad +\mathcal{O}(\varepsilon^2), \\
\varepsilon^2 \frac{d\, \overline{z^a_{\varepsilon,1}}}{dt} = \varepsilon^2 2 g_1 \left[-1 - \eta^a - \overline{z^a_{\varepsilon,1}}\right] + \left(\frac{\overline{z^A_{\varepsilon,1}} - \overline{z^a_{\varepsilon,1}}}{2}\right) \frac{N^A_{\varepsilon,1}}{N_{\varepsilon,1}} + \alpha\, m_2 \frac{N^a_{\varepsilon,2}}{N^a_{\varepsilon,1}} \left(\overline{z^a_{\varepsilon,2}} - \overline{z^a_{\varepsilon,1}}\right) + \mathcal{O}(\varepsilon^4), \\
\varepsilon^2 \frac{d\, \overline{z^A_{\varepsilon,1}}}{dt} = \varepsilon^2 2 g_1 \left[-1 - \eta^A - \overline{z^A_{\varepsilon,1}}\right] + \left(\frac{\overline{z^a_{\varepsilon,1}} - \overline{z^A_{\varepsilon,1}}}{2}\right) \frac{N^a_{\varepsilon,1}}{N_{\varepsilon,1}} + \alpha\, m_2 \frac{N^A_{\varepsilon,2}}{N^A_{\varepsilon,1}} \left(\overline{z^A_{\varepsilon,2}} - \overline{z^A_{\varepsilon,1}}\right) + \mathcal{O}(\varepsilon^4), \\
\varepsilon^2 \frac{d\, \overline{z^a_{\varepsilon,2}}}{dt} = \varepsilon^2 2 g_2 \left[1 - \eta^a - \overline{z^a_{\varepsilon,2}}\right] + \left(\frac{\overline{z^A_{\varepsilon,2}} - \overline{z^a_{\varepsilon,2}}}{2}\right) \frac{N^A_{\varepsilon,2}}{N_{\varepsilon,2}} + \frac{m_1}{\alpha} \frac{N^a_{\varepsilon,1}}{N^a_{\varepsilon,2}} \left(\overline{z^a_{\varepsilon,1}} - \overline{z^a_{\varepsilon,2}}\right) + \mathcal{O}(\varepsilon^4), \\
\varepsilon^2 \frac{d\, \overline{z^A_{\varepsilon,2}}}{dt} = \varepsilon^2 2 g_2 \left[1 - \eta^A - \overline{z^A_{\varepsilon,2}}\right] + \left(\frac{\overline{z^a_{\varepsilon,2}} - \overline{z^A_{\varepsilon,2}}}{2}\right) \frac{N^a_{\varepsilon,2}}{N_{\varepsilon,2}} + \frac{m_1}{\alpha} \frac{N^A_{\varepsilon,1}}{N^A_{\varepsilon,2}} \left(\overline{z^A_{\varepsilon,1}} - \overline{z^A_{\varepsilon,2}}\right) + \mathcal{O}(\varepsilon^4).
\end{cases}
\tag{4.14}
$$

Remark 9. *As in the analogous ODE system obtained without the major effect locus [Dekens 2022], when $\varepsilon \ll 1$, migration induces a fast relaxation on the difference between the mean quantitative traits between the two demes given a major-effect allele: $\overline{z^A_{\varepsilon,j}} - \overline{z^A_{\varepsilon,i}}$ and $\overline{z^a_{\varepsilon,j}} - \overline{z^a_{\varepsilon,i}}$. However, in this study, there is an additional term in the dynamics of the quantitative mean trait $\overline{z^A_{\varepsilon,i}}$ (resp. $\overline{z^a_{\varepsilon,i}}$): $\left(\frac{\overline{z^a_{\varepsilon,i}} - \overline{z^A_{\varepsilon,i}}}{2}\right) \frac{N^a_{\varepsilon,i}}{N_{\varepsilon,i}}$, which describes how the difference between the mean quantitative trait for alleles A and a within a deme relaxes over time. That is consistent with the result provided by Proposition 4.3.1.*

Remark 10. *In the system (4.14), the difference in the system between the residues in the first four equations on the local sizes of population of order $\mathcal{O}(\varepsilon^2)$ and the ones in the last four equations on the mean quantitative components of order $\mathcal{O}(\varepsilon^4)$ is consistent with the analysis of [Patout 2020] (see in particular Theorem 1.4) for the homogeneous space time-marching problem.*

4.4 Separation of time scales: slow-fast analysis

The objective of this section is to show that (4.14) converges when $\varepsilon \to 0$ toward a simplified problem. Let us make the separation of time scales explicit by introducing the following change of variables, which is motivated by the formal analysis of Section 4.3.1, Proposition 4.3.1 and Remark 9:

$$\delta_\varepsilon^a = \frac{\overline{z_{\varepsilon,2}^a} - \overline{z_{\varepsilon,1}^a}}{2\varepsilon^2}, \quad \delta_\varepsilon^A = \frac{\overline{z_{\varepsilon,2}^A} - \overline{z_{\varepsilon,1}^A}}{2\varepsilon^2}, \quad \delta_\varepsilon = \frac{\overline{z_{\varepsilon,1}^A} + \overline{z_{\varepsilon,2}^A} - \overline{z_{\varepsilon,1}^a} - \overline{z_{\varepsilon,2}^a}}{4\varepsilon^2}, \quad Z_\varepsilon = \frac{\overline{z_{\varepsilon,1}^A} + \overline{z_{\varepsilon,2}^A} + \overline{z_{\varepsilon,1}^a} + \overline{z_{\varepsilon,2}^a}}{4}. \tag{4.15}$$

Z_ε can be interpreted as the mean infinitesimal part of the metapopulation, δ_ε the spatial average of the local difference between the two allelic mean infinitesimal parts, δ_ε^A and δ_ε^a the spatial discrepancies in the mean infinitesimal parts per allele (see an illustration of those new variables in Fig. 4.2).

Under this change of variable, the system (4.14) is equivalent to the following:

$$\begin{cases}
\varepsilon^2 \frac{d N_{\varepsilon,i}^a}{dt} = \lambda^{i-1} N_{\varepsilon,i}^a - \left[N_{\varepsilon,i}^A + N_{\varepsilon,i}^a\right] N_{\varepsilon,i}^a - g_i \left[Z_\varepsilon + \eta^a - (-1)^i\right]^2 N_{\varepsilon,i}^a \\
\qquad\qquad + \alpha^{(-1)^j} m_j N_{\varepsilon,j}^a - m_i N_{\varepsilon,i}^a + \mathcal{O}(\varepsilon^2), \\
\varepsilon^2 \frac{d N_{\varepsilon,i}^A}{dt} = \lambda^{i-1} N_{\varepsilon,i}^A - \left[N_{\varepsilon,i}^A + N_{\varepsilon,i}^a\right] N_{\varepsilon,i}^A - g_i \left[Z_\varepsilon + \eta^A - (-1)^i\right]^2 N_{\varepsilon,i}^A \\
\qquad\qquad + \alpha^{(-1)^j} m_j N_{\varepsilon,j}^A - m_i N_{\varepsilon,i}^A + \mathcal{O}(\varepsilon^2), \\
\varepsilon^2 \frac{d \delta_\varepsilon^a}{dt} = g_1 + g_2 + (g_1 - g_2)(Z_\varepsilon + \eta^a) + \frac{\delta_\varepsilon}{2}\left[\frac{N_{\varepsilon,2}^A}{N_{\varepsilon,2}^a + N_{\varepsilon,2}^A} - \frac{N_{\varepsilon,1}^A}{N_{\varepsilon,1}^a + N_{\varepsilon,1}^A}\right] \\
\qquad\qquad - \delta_\varepsilon^a \left[\frac{m_2 \alpha N_{\varepsilon,2}^a}{N_{\varepsilon,1}^a} + \frac{m_1 N_{\varepsilon,1}^a}{\alpha N_{\varepsilon,2}^a}\right] + \frac{\delta_\varepsilon^A - \delta_\varepsilon^a}{4}\left[\frac{N_{\varepsilon,2}^A}{N_{\varepsilon,2}^a + N_{\varepsilon,1}^A} + \frac{N_{\varepsilon,1}^A}{N_{\varepsilon,1}^a + N_{\varepsilon,1}^A}\right] + \mathcal{O}(\varepsilon^2), \\
\varepsilon^2 \frac{d \delta_\varepsilon^A}{dt} = g_1 + g_2 + (g_1 - g_2)(Z_\varepsilon + \eta^A) + \frac{\delta_\varepsilon}{2}\left[\frac{N_{\varepsilon,1}^a}{N_{\varepsilon,1}^a + N_{\varepsilon,1}^A} - \frac{N_{\varepsilon,2}^a}{N_{\varepsilon,2}^a + N_{\varepsilon,2}^A}\right] \\
\qquad\qquad - \delta_\varepsilon^A \left[\frac{m_2 \alpha N_{\varepsilon,2}^A}{N_{\varepsilon,1}^A} + \frac{m_1 N_{\varepsilon,1}^A}{\alpha N_{\varepsilon,2}^A}\right] + \frac{\delta_\varepsilon^a - \delta_\varepsilon^A}{4}\left[\frac{N_{\varepsilon,2}^a}{N_{\varepsilon,2}^a + N_{\varepsilon,2}^A} + \frac{N_{\varepsilon,1}^a}{N_{\varepsilon,1}^a + N_{\varepsilon,1}^A}\right] + \mathcal{O}(\varepsilon^2), \\
\varepsilon^2 \frac{d \delta_\varepsilon}{dt} = -\frac{\delta_\varepsilon}{2} - (g_1 + g_2)\frac{\eta^A - \eta^a}{2} + \left(\frac{\delta_\varepsilon^A}{2}\left[\frac{\alpha m_2 N_{\varepsilon,2}^A}{N_{\varepsilon,1}^A} - \frac{m_1 N_{\varepsilon,1}^A}{\alpha N_{\varepsilon,2}^A}\right] - \frac{\delta_\varepsilon^a}{2}\left[\frac{\alpha m_2 N_{\varepsilon,2}^a}{N_{\varepsilon,1}^a} - \frac{m_1 N_{\varepsilon,1}^a}{\alpha N_{\varepsilon,2}^a}\right]\right) \\
\qquad\qquad + \mathcal{O}(\varepsilon^2), \\
\frac{dZ_\varepsilon}{dt} = (g_2 - g_1) - (g_1 + g_2)\left(Z_\varepsilon + \frac{\eta^A + \eta^a}{2}\right) + \frac{\delta_\varepsilon}{2}\left[\frac{N_{1,\varepsilon}^A}{N_{1,\varepsilon}^A + N_{1,\varepsilon}^a} + \frac{N_{2,\varepsilon}^A}{N_{2,\varepsilon}^A + N_{2,\varepsilon}^a} - 1\right] \\
\qquad\qquad + \left(\frac{\delta_\varepsilon^a}{2}\left[\frac{\alpha m_2 N_{\varepsilon,2}^a}{N_{\varepsilon,1}^a} - \frac{m_1 N_{\varepsilon,1}^a}{\alpha N_{\varepsilon,2}^a}\right] + \frac{\delta_\varepsilon^A}{2}\left[\frac{\alpha m_2 N_{\varepsilon,2}^A}{N_{\varepsilon,1}^A} - \frac{m_1 N_{\varepsilon,1}^A}{\alpha N_{\varepsilon,2}^A}\right]\right) \\
\qquad\qquad + \frac{\delta_\varepsilon^A - \delta_\varepsilon^a}{4}\left[\frac{N_{2,\varepsilon}^A}{N_{2,\varepsilon}^A + N_{2,\varepsilon}^a} - \frac{N_{1,\varepsilon}^A}{N_{1,\varepsilon}^A + N_{1,\varepsilon}^a}\right] + \mathcal{O}(\varepsilon^2).
\end{cases} \tag{4.16}$$

The system (4.16) is in a suitable form for a slow-fast analysis when $\varepsilon \to 0$. Indeed, denoting $\Omega = \left(\mathbb{R}_+^*\right)^4 \times \mathbb{R}^3$, there exists $G \in C^\infty(\Omega \times \mathbb{R})$ and $F \in C^\infty(\Omega)$ such that (4.16) is equivalent to the more compactly written slow-fast system:

$$\begin{cases}
\varepsilon^2 \frac{d\bar{Y}_\varepsilon}{dt} = G(\bar{Y}_\varepsilon, Z_\varepsilon) + \varepsilon^2 \nu_\varepsilon^G(t), \\
\frac{dZ_\varepsilon}{dt} = -(g_1 + g_2) Z_\varepsilon + F(\bar{Y}_\varepsilon) + \varepsilon^2 \nu_\varepsilon^F(t),
\end{cases} \tag{P_ε}$$

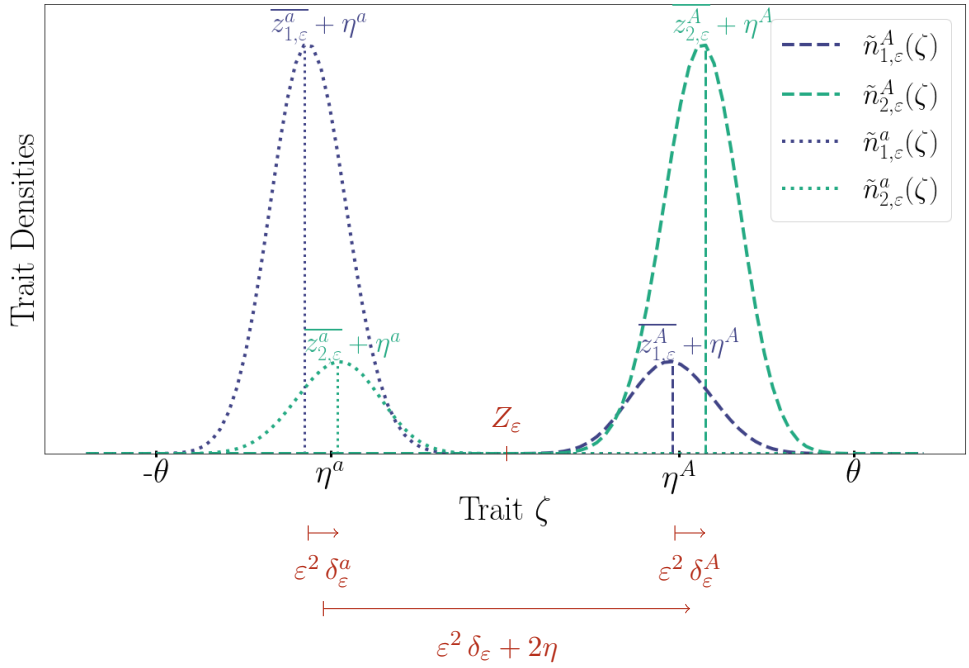

Figure 4.2: **Illustration of the slow-fast variables Z_ε, δ_ε, δ^A_ε and δ^a_ε (in red)**, introduced in (4.15). This figure displays a situation where both major alleles are segregating in both demes in a symmetrical fashion. The main graph represents the two local trait densities for each of the two alleles: $\tilde{n}^A_{1,\varepsilon}$, $\tilde{n}^A_{2,\varepsilon}$, $\tilde{n}^a_{1,\varepsilon}$, $\tilde{n}^a_{2,\varepsilon}$ (the same color is for the same deme, and the same linestyle is for the same major allele), as a function of the trait $\zeta = z + \eta^A$ (resp. $z + \eta^a$, where z is the infinitesimal contribution and η^A (resp η^a) is the effect of the major allele. In red, we indicate a visualization of the new variables introduced in (4.15). Z_ε is the mean infinitesimal part of the metapopulation, δ_ε the spatial average of the local difference between the two allelic mean infinitesimal parts, δ^A_ε and δ^a_ε the spatial discrepancies in the mean infinitesimal parts per allele. Note the difference in notation between the trait densities $\tilde{n}^A_{i,\varepsilon}$ and the infinitesimal contribution densities $n^A_{i,\varepsilon}$ (which are the ones used in the analysis), which are linked by $n^A_{i,\varepsilon}(z) = \tilde{n}^A_{i,\varepsilon}(z + \eta^A)$ (respectively $z + \eta^a$ for $\tilde{n}^a_{i,\varepsilon}$).

where $\bar{Y}_\varepsilon = \left(N^a_{1,\varepsilon}, N^a_{1,\varepsilon}, N^A_{1,\varepsilon}, N^A_{2,\varepsilon}, \delta^a_\varepsilon, \delta^A_\varepsilon, \delta_\varepsilon\right)$ denotes the elements of Ω, and ν^F_ε and ν^G_ε are residues, uniformly bounded with respect to ε when ε vanishes. The first equation of (P_ε) happens on a fast ecological timescale and drives the dynamics of the ecological part of the system, whereas the second equation acts on a slow evolutionary time scale, driving the dynamics of Z_ε.

This section is dedicated to show that the solutions of (P_ε) converge when ε goes to 0, toward the solutions of the limit system:

$$\begin{cases} G(\bar{Y}, Z) = 0, \\ \frac{dZ}{dt} = -(g_1 + g_2)\, Z + F(\bar{Y}). \end{cases} \tag{P_0}$$

We can interpret this limit system (P_0) as the dynamics of the slow variable Z that occurs on the slow manifold defined by the algebraic system $G(\bar{Y}, Z) = 0$. Its solutions are the instantaneous ecological equilibria $\bar{Y}$ given the slow variable Z. The convergence is stated by the following:

Theorem 4.4.1. *For $(\bar{Y}, Z)$ a solution of (P_0), there exists $T^* > 0$ such that, for $0 < \varepsilon < 1$, any solution $(\bar{Y}_\varepsilon, Z_\varepsilon)$ of (P_ε) on $[0, T^*]$ converges to $(\bar{Y}, Z)$ uniformly on $[0, T^*]$, as ε goes to 0 and $(\bar{Y}_\varepsilon(0), Z_\varepsilon(0))$ goes to $(\bar{Y}(0), Z(0))$.*

The arguments of the proof of Theorem 4.4.1 are similar to the analogous theorems proved in [Levin and Levinson 1954; Dekens 2022]. The proof requires some preliminaries results, particularly of stability, to which we dedicate the rest of this section. The structure of this section is represented in Fig. 4.3.

In the rest of this section, we first solve the slow manifold algebraic system $G(\bar{Y}, Z) = 0$, showing that there can only exist one instantaneous ecological equilibrium at a given $Z \in]-1, 1[$ (Proposition 4.4.1 and Proposition 4.4.2 of Section 4.4.1.1). Surprisingly, this resolution is easier than the analogous one in [Dekens 2022] (see Remark 12). Next, in Section 4.4.1.2, we show a stability criterion of the slow manifold (Proposition 4.4.3 and Proposition 4.4.4), which justifies the separation of time scales approach.

Remark 11 (One-locus haploid model's equilibrium is a fast equilibrium)**.** *One can notice that the one-locus haploid model is equivalent to the first four differential equations of (4.16) on the allelic sizes of each subpopulation, when $Z_\varepsilon = 0$ (no infinitesimal part) (we can obtain from these equations a system describing the allelic frequencies and local population sizes $(p_1, p_2, N_1, N_2) := \left(\frac{N_1^A}{N_1^A + N_1^a}, \frac{N_2^A}{N_2^A + N_2^a}, N_1^A + N_1^a, N_2^A + N_2^a\right)$, dropping the ε that is a parameter of the infinitesimal part). Applying Proposition 4.4.1 with $Z = 0$ gives a unique equilibrium satisfying the first four equations, which is the one found with the one-locus haploid model. One can thus interpret the symmetrical polymorphic equilibrium of the one-locus haploid model as a fast equilibrium in the model presented in this article. It is therefore stable (Proposition 4.4.3) whenever it entails positive population sizes (same condition as in Proposition 4.4.1).*

4.4.1 Analysis of the fast equilibria.

The fast equilibria, for $Z \in]-1, 1[$, are defined as the solutions $\bar{Y}$ to the algebraic system $G(\bar{Y}, Z) = 0$, or equivalently seven equations that we group in two subsystems $S_0(Z)$ and

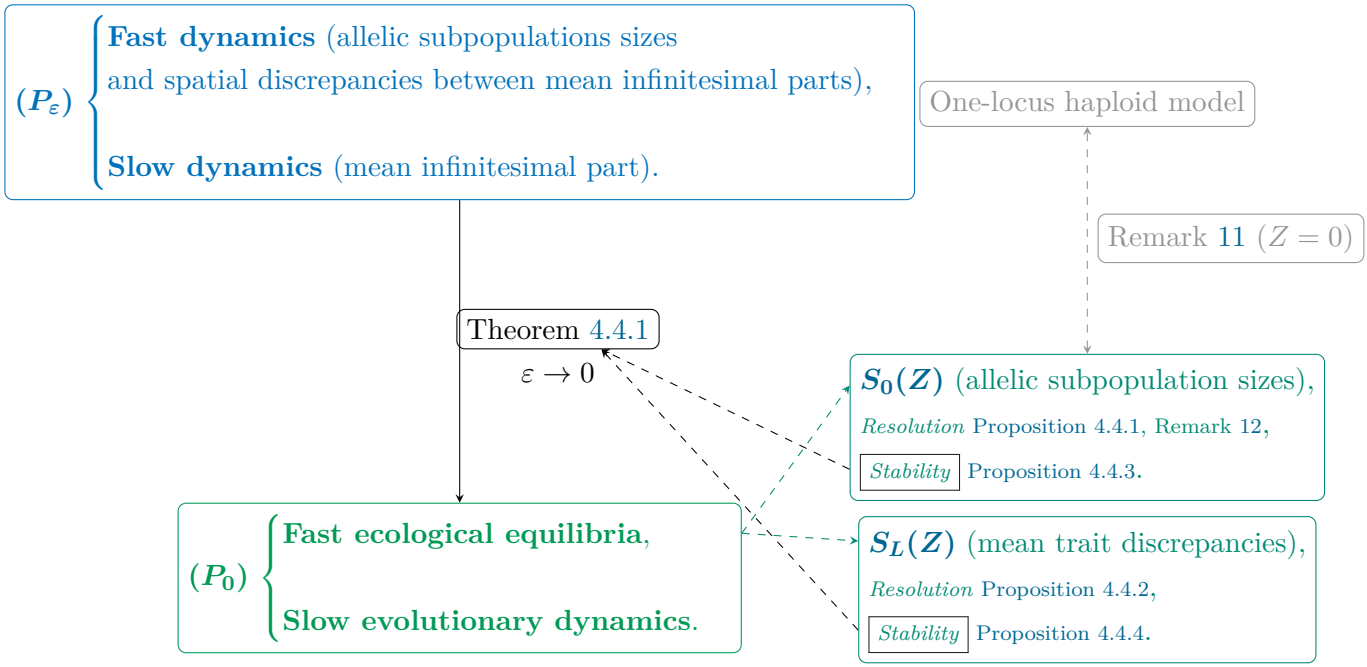

Figure 4.3: **Layout of the slow-fast analysis in Section 4.4**. This figure presents the key elements of the separation of time scales leading from P_ε to P_0. The stability of the fast equilibria (studied in the two subsystems $S_0(Z)$ and $S_L(Z)$) is the crucial argument underlying the convergence result stated in Theorem 4.4.1. The resolution of $S_0(Z)$ leads to a uniqueness result that is unexpected with regard to the analogous resolution in [Dekens 2022] (see Remark 12).

$S_L(Z)$:

$$\begin{cases} \alpha\, m_2\, N_2^a - m_1 N_1^a + N_1^a \left[1 - (N_1^a + N_1^A) - g_1\,(Z+\eta^a+1)^2\right] & = 0, \\ \alpha\, m_2\, N_2^A - m_1 N_1^A + N_1^A \left[1 - (N_1^a + N_1^A) - g_1\,(Z+\eta^A+1)^2\right] & = 0, \\ \frac{m_1}{\alpha}\, N_1^a - m_2\, N_2^a + N_2^a \left[\lambda - (N_2^a + N_2^A) - g_2\,(Z+\eta^a-1)^2\right] & = 0, \\ \frac{m_1}{\alpha}\, N_1^A - m_2\, N_2^A + N_2^A \left[\lambda - (N_2^a + N_2^A) - g_2\,(Z+\eta^A-1)^2\right] & = 0. \end{cases} \tag{$S_0(Z)$}$$

$$J_{S_L} \begin{pmatrix} \delta \\ \delta^A \\ \delta^a \end{pmatrix} = \begin{pmatrix} (g_1+g_2)\frac{\eta^A-\eta^a}{2} \\ -(g_1+g_2) + (g_2-g_1)(Z+\eta^A) \\ -(g_1+g_2) + (g_2-g_1)(Z+\eta^a) \end{pmatrix}, \tag{$S_L(Z)$}$$

where:

$$J_{S_L} := \begin{pmatrix} -\frac{1}{2} & \frac{1}{2}\left[\frac{\alpha\, m_2\, N_2^A}{N_1^A} - \frac{m_1\, N_1^A}{\alpha\, N_2^A}\right] & -\frac{1}{2}\left[\frac{\alpha\, m_2\, N_2^a}{N_1^a} - \frac{m_1\, N_1^a}{\alpha\, N_2^a}\right] \\ \frac{\frac{N_1^a}{N_1^A+N_1^a} - \frac{N_2^a}{N_2^A+N_2^a}}{2} & -\left[\frac{\alpha\, m_2\, N_2^A}{N_1^A} + \frac{m_1\, N_1^A}{\alpha\, N_2^A}\right] - \frac{\frac{N_1^a}{N_1^A+N_1^a} + \frac{N_2^a}{N_2^A+N_2^a}}{4} & \frac{\frac{N_1^a}{N_1^A+N_1^a} + \frac{N_2^a}{N_2^A+N_2^a}}{4} \\ \frac{\frac{N_2^A}{N_2^A+N_2^a} - \frac{N_1^A}{N_1^A+N_1^a}}{2} & \frac{\frac{N_1^A}{N_1^A+N_1^a} + \frac{N_2^A}{N_2^A+N_2^a}}{4} & -\left[\frac{\alpha\, m_2\, N_2^a}{N_1^a} + \frac{m_1\, N_1^a}{\alpha\, N_2^a}\right] - \frac{\frac{N_1^A}{N_1^A+N_1^a} + \frac{N_2^A}{N_2^A+N_2^a}}{4} \end{pmatrix}$$

4.4.1.1 Resolution.

Following Working assumption 1, we recall that we assume that no major allele has fixed. Here, we show that there is at most one instantaneous ecological equilibrium at each Z-level (for $Z \in]-1-\frac{\eta^A+\eta^a}{2}, 1-\frac{\eta^A+\eta^a}{2}[$), thanks to Proposition 4.4.1 and Proposition 4.4.2.

Proposition 4.4.1. *Suppose that no major allele has fixed. Then, for $Z \in]-1-\frac{\eta^A+\eta^a}{2}, 1-\frac{\eta^A+\eta^a}{2}[$, $S_0(Z)$ has exactly one solution $(N_1^a, N_1^A, N_2^a, N_2^A) \in (\mathbb{R}^*)^4$, given by:*

$$N_1^a = \frac{Y^A\, N_1 - N_2}{Y^A - Y^a}, \quad N_2^a = Y^a \frac{Y^A\, N_1 - N_2}{Y^A - Y^a}, \quad N_1^A = \frac{N_2 - Y^a\, N_1}{Y^A - Y^a}, \quad N_2^A = Y^A \frac{N_2 - Y^a\, N_1}{Y^A - Y^a},$$

where the quantities (Y^A, Y^a, N_1, N_2) are defined by (4.17):

$$\begin{cases} Y^A = \frac{g_1}{\alpha\, m_2}\left(\eta^A + \eta^a + 2\,(Z+1)\right)\frac{\eta^A-\eta^a}{2}\left[\sqrt{1 + \frac{m_1\, m_2}{4\, g_1\, g_2\left(\frac{\eta^A-\eta^a}{2}\right)^2\left(1-\left(\frac{\eta^A+\eta^a}{2}+Z\right)^2\right)}} + 1\right], \\ Y^a = \frac{g_1}{\alpha\, m_2}\left(\eta^A + \eta^a + 2\,(Z+1)\right)\frac{\eta^A-\eta^a}{2}\left[\sqrt{1 + \frac{m_1\, m_2}{4\, g_1\, g_2\left(\frac{\eta^A-\eta^a}{2}\right)^2\left(1-\left(\frac{\eta^A+\eta^a}{2}+Z\right)^2\right)}} - 1\right], \\ N_1 = 1 - g_1\,(Z+1+\eta^A)^2 - m_1 + \alpha\, m_2\, Y^A, \\ N_2 = \lambda - g_2\,(Z-1+\eta^A)^2 - m_2 + \frac{m_1}{\alpha\, Y^A}. \end{cases} \tag{4.17}$$

This solution $(N_1^a, N_1^A, N_2^a, N_2^A)$ defines viable numbers of each allele in each sub-populations if and only if:

$$[Y^A\, N_1 > N_2] \text{ and } [N_2 > Y^a\, N_1]. \tag{4.18}$$

Remark 12 (Degrees of freedom of $S_0(Z)$)**.** *Proposition 4.4.1 states that there are fewer degrees of freedom in $S_0(Z)$ than in the analogous system of two equations from the analysis done in [Dekens 2022], that can be obtained in the case where one allele has fixed (up to a translation). Indeed, [Dekens 2022] shows that the analogous system can have up to three algebraic solutions depending on the parameters. The result of Proposition 4.4.1 is thus unexpected, since $S_0(Z)$ has twice the number of equations and variables.*

Proof. Let us introduce the following change of variables, valid under the assumption that no major allele has fixed:

$$N_1 := N_1^A + N_1^a, \quad N_2 := N_2^A + N_2^a, \quad Y^A := \frac{N_2^A}{N_1^A}, \quad Y^a := \frac{N_2^a}{N_1^a}.$$

Then, under the assumptions made in Working assumption 1, the system ($S_0(Z)$) is equivalent to:

$$\begin{cases} \alpha\, m_2\, Y^a - m_1 + \left[1 - N_1 - g_1\,(Z + \eta^a + 1)^2\right] & = 0, \\ \alpha\, m_2\, Y^A - m_1 + \left[1 - N_1 - g_1\,(Z + \eta^A + 1)^2\right] & = 0, \\ \frac{m_1}{\alpha}\,\frac{1}{Y^a} - m_2 + \left[\lambda - N_2 - g_2\,(Z + \eta^a - 1)^2\right] & = 0, \\ \frac{m_1}{\alpha}\,\frac{1}{Y^A} - m_2 + \left[\lambda - N_2 - g_2\,(Z + \eta^A - 1)^2\right] & = 0. \end{cases} \tag{4.19}$$

This is equivalent to the following system:

$$\begin{cases} \alpha\, m_2\,(Y^a - Y^A) + g_1\,\left(\eta^A + \eta^a + 2\,(Z+1)\right)(\eta^A - \eta^a) & = 0, \\ \frac{m_1}{\alpha}\,(\frac{1}{Y^a} - \frac{1}{Y^A}) + g_2\,\left(\eta^A + \eta^a + 2\,(Z-1)\right)(\eta^A - \eta^a) & = 0, \\ N_1 - \left(1 - g_1\,(Z + 1 + \eta^A)^2 - m_1 + \alpha\, m_2\, Y^A\right) & = 0, \\ N_2 - \left(\lambda - g_2\,(Z - 1 + \eta^A)^2 - m_2 + \frac{m_1}{\alpha\, Y^A}\right) & = 0. \end{cases}$$

As $Z \neq 1 - \frac{\eta^A + \eta^a}{2}$, the closed subsystem on (Y^A, Y^a) is, in turn, equivalent to:

$$\begin{cases} Y^A - Y^a & = A_1(Z) := \frac{g_1}{\alpha\, m_2}\,\left(\eta^A + \eta^a + 2\,(Z+1)\right)(\eta^A - \eta^a), \\ -Y^A\, Y^a & = A_0(Z) := \frac{g_1\, m_1}{\alpha^2\, g_2\, m_2}\,\frac{\eta^A + \eta^a + 2\,(Z+1)}{\eta^A + \eta^a + 2\,(Z-1)}. \end{cases}$$

Y^A and $-Y^a$ are the roots of the polynomial:

$$P(X) = X^2 - A_1(Z)\,X + A_0(Z).$$

P has two real roots of opposite signs if and only if:

$$\left[A_0(Z) < 0\right],$$

which is equivalent to:

$$-1 - \frac{\eta^A + \eta^a}{2} < Z < 1 - \frac{\eta^A + \eta^a}{2}.$$

Under the last condition on Z, $A_1(Z)$ is positive, $A_0(Z)$ is negative and we get:

$$\begin{cases} Y^A = \frac{A_1(Z)}{2}\,\left[\sqrt{1 - \frac{A_0(Z)}{\left(\frac{A_1(Z)}{2}\right)^2}} + 1\right], \\ Y^a = \frac{A_1(Z)}{2}\,\left[\sqrt{1 - \frac{A_0(Z)}{\left(\frac{A_1(Z)}{2}\right)^2}} - 1\right], \end{cases} \tag{4.20}$$

which is equivalent to (4.17).

Inverting the initial change of variables leads to:

$$N_1^a = \frac{Y^A N_1 - N_2}{Y^A - Y^a}, \quad N_2^a = Y^a \frac{Y^A N_1 - N_2}{Y^A - Y^a}, \quad N_1^A = \frac{N_2 - Y^a N_1}{Y^A - Y^a}, \quad N_2^A = Y^A \frac{N_2 - Y^a N_1}{Y^A - Y^a},$$

hence (4.17). It defines a viable solution with positive entries if and only if $Y^A N_1 > N_2$ and $N_2 > Y^a N_1$. □

Proposition 4.4.2. *For all allelic sizes of subpopulations $(N_1^a, N_1^A, N_2^a, N_2^A) \in (\mathbb{R}_+^*)^4$, there exists a unique solution $(\delta, \delta^A, \delta^a)$ to the system $S_L(Z)$.*

Proof. Using the notation $N_1 := N_1^A + N_1^a$ and $N_2 := N_2^A + N_2^a$, we compute thanks to a symbolic computation tool (Mathematica©):

$$\begin{aligned}\det(J_{S_L}) = &-\frac{1}{4}\left[\frac{m_1}{\alpha}\frac{N_1}{N_2} + \alpha\, m_2 \frac{N_2}{N_1} + 2\frac{m_1^2}{\alpha^2}\frac{N_1^a N_1^A}{N_2^a N_2^A} + 2\alpha^2 m_2^2 \frac{N_2^a N_2^A}{N_1^a N_1^A}\right.\\ &\left. + 2m_1 m_2 \left(\frac{{N_1^A}^2 N_2^a}{N_1^a N_1 N_2} + \frac{{N_1^a}^2 N_2^A}{N_1^A N_1 N_2} + \frac{{N_2^A}^2 N_1^a}{N_2^a N_1 N_2} + \frac{{N_2^a}^2 N_1^A}{N_2^A N_1 N_2} + 2\frac{N_2^A N_1^a}{N_1\, N_2} + 2\frac{N_1^a N_2^a}{N_1 N_2}\right)\right]\\ &< 0.\end{aligned}$$

□

4.4.1.2 Stability.

Convergence toward a limit system locally in time in a slow-fast analysis relies essentially on a stability criterion of the fast equilibria which constitute the slow manifold (Levin and Levinson 1954; Dekens 2022). In this subsection, we show that all fast equilibria found in Proposition 4.4.1 and Proposition 4.4.2 for a level $Z \in]-1-\frac{\eta^A+\eta^a}{2}, 1-\frac{\eta^A+\eta^a}{2}[$, are stable. Due to the particular shape of the slow manifold, it is sufficient to study separately the Jacobian matrix associated to $S_0(Z)$ denoted J_{S_0} (Proposition 4.4.3) and the Jacobian matrix associated to the linear system $S_L(Z)$, which is exactly J_{S_L} (Proposition 4.4.4).

Proposition 4.4.3. *Let $Z \in]-1-\frac{\eta^A+\eta^a}{2}, 1-\frac{\eta^A+\eta^a}{2}[$ such that $(S_0(Z))$ has a unique solution $(N_1^a, N_1^A, N_2^a, N_2^A) \in (\mathbb{R}_+^*)^4$. Let us define the following matrix:*

$$J_{S_0} = \begin{pmatrix} -\frac{\alpha\, m_2\, N_2^a}{N_1^a} - N_1^a & \alpha\, m_2 & -N_1^a & 0 \\ \frac{m_1}{\alpha} & -\frac{m_1 N_1^a}{\alpha N_2^a} - N_2^a & 0 & -N_2^a \\ -N_1^A & 0 & -\frac{\alpha\, m_2 N_2^A}{N_1^A} - N_1^A & \alpha\, m_2 \\ 0 & -N_2^A & \frac{m_1}{\alpha} & -\frac{m_1 N_1^A}{\alpha N_2^A} - N_2^A \end{pmatrix}. \tag{4.21}$$

Then:

1. *J_{S_0} is the Jacobian of $S_0(Z)$ at $(N_1^a, N_1^A, N_2^a, N_2^A)$.*
2. *All the eigenvalues of J_{S_0} are located in the left open half plane.*

Proof. 1. Let $(N_1^a, N_1^A, N_2^a, N_2^A)$ be solution of $S_0(Z)$. One can verify that:

$$\frac{\partial\left[\alpha\, m_2\, N_2^a - m_1 N_1^a + N_1^a\,\left[1-(N_1^a+N_1^A) - g_1\,(Z+\eta^a+1)^2\right]\right]}{\partial N_1^a}$$
$$= \left[1-(N_1^a+N_1^A) - g_1\,(Z+\eta^a+1)^2 - m_1\right] - N_1^a = -\frac{\alpha\, m_2\, N_2^a}{N_1^a} - N_1^a,$$

for $(N_1^a, N_1^A, N_2^a, N_2^A)$ solves $S_0(Z)$. The same holds for the other diagonal entries.

2. Let:

$$\chi_{J_{S_0}}(X) = X^4 - \mathrm{tr}\,(J_{S_0})\,X^3 + b\,X^2 + c\,X + \det J_{S_0},$$

be the characteristic polynomial of J_{S_0}. Let us verify the Routh-Hurwitz criterion: all the eigenvalues of J_{S_0} are located in the left open half plane if and only if:

(i) $\det J_{S_0} > 0$,

(ii) $-\mathrm{tr}\,(J_{S_0}) > 0$,

(iii) $-\mathrm{tr}\,(J_{S_0})\; b - c > 0$,

(iv) $(-\mathrm{tr}\,(J_{S_0})\; b - c)\, c - \mathrm{tr}\,(J_{S_0})^2\; \det J_{S_0} > 0$.

We have:

$$\det J_{S_0} = m_1\, m_2 \left(N_1^a\, N_2^a - N_1^A\, N_2^A\right)^2 \left(\frac{1}{N_1^a\, N_2^A} + \frac{1}{N_1^A\, N_2^a}\right) > 0.$$

and:

$$-\mathrm{tr}\,(J_{S_0}) = N_1 + N_2 + \sqrt{m_1\, m_2}\left(\frac{\alpha\sqrt{m_2}N_2^a}{\sqrt{m_1}N_1^a} + \frac{\sqrt{m_1}N_1^a}{\alpha\sqrt{m_2}N_2^a} + \frac{\alpha\sqrt{m_2}N_2^A}{\sqrt{m_1}N_1^A} + \frac{\alpha\sqrt{m_2}N_2^A}{\sqrt{m_1}N_1^A}\right) > 0.$$

With the help of a symbolic computation tool (Mathematica©), we verify that the left hand side of the two last conditions are sums of positive terms, but are too long to be displayed here. □

The Jacobian matrix of the linear system $S_L(Z)$ is exactly J_{S_L} and we also show that J_{S_L} satisfies the Routh-Hurwitz criterion:

Proposition 4.4.4. *J_{S_L} has all its eigenvalues located in the left open half plane.*

Proof. Let the following be the characteristic polynomial of J_{S_L}:

$$\chi_{J_{S_L}}(X) = X^3 - \mathrm{tr}(J_{S_L})X^2 - \frac{1}{2}\left(\mathrm{tr}(J_{S_L}^2) - \mathrm{tr}(J_{S_L})^2\right)X - \det(J_{S_L}).$$

We show that J_{S_L} satisfies the Routh-Hurwitz criterion:

(i) $-\det(J_{S_L}) > 0$,

(ii) $-\mathrm{tr}(J_{S_L}) > 0$,

(iii) $\frac{1}{2}\left(\mathrm{tr}(J_{S_L}^2) - \mathrm{tr}(J_{S_L})^2\right)\mathrm{tr}(J_{S_L}) + \det(J_{S_L}) > 0$.

We have $-\det(J_{S_L}) > 0$ from the proof of Proposition 4.4.2 and:

$$-\mathrm{tr}(J_{S_L}) = 1 + \sqrt{m_1\, m_2}\left(\frac{\alpha\sqrt{m_2}N_2^a}{\sqrt{m_1}N_1^a} + \frac{\sqrt{m_1}N_1^a}{\alpha\sqrt{m_2}N_2^a} + \frac{\alpha\sqrt{m_2}N_2^A}{\sqrt{m_1}N_1^A} + \frac{\alpha\sqrt{m_2}N_2^A}{\sqrt{m_1}N_1^A}\right) > 1 + 4\sqrt{m_1 m_2}.$$

We verify that the l.h.s. of the last condition is a sum of positive terms. □

4.5 Stability of polymorphism in the limit system

This section follows naturally the result given by Theorem 4.4.1 by being dedicated to the study of the stability of polymorphism at the major effect locus. To be able to derive analytical conditions, we assume henceforth a symmetrical setting (in migration rates, selection strengths, carrying capacities, reproduction rates and major allelic effects):

$$m := m_1 = m_2, \quad g := g_1 = g_2, \quad \alpha = 1, \quad \lambda = 1, \quad \eta := \eta^A = -\eta^a > 0.$$

Under these symmetrical conditions, there can exist a symmetrical polymorphic equilibrium, that we henceforth denote $(Z_0, \bar{Y}_0)$, where $Z_0 = 0$. Recall that the first four coordinates of $\bar{Y}_0$, which are the allelic sizes of subpopulations, are shared with the one-locus haploid model (see Remark 11). The results of this section show that the unconditional stability of the polymorphism in the one-locus haploid model can be disturbed by the presence of an infinitesimal background, for a substantial range of parameters. The interpretation of Remark 11 offers the idea that the infinitesimal background slowly disrupts the fast established symmetrical polymorphism at the major locus.

We first show that a symmetrical polymorphic equilibrium can exist under a range of parameters specified in Proposition 4.5.1, as a stationary state of the limit system, hence a solution of (4.22):

$$\begin{cases} N_i^a - \left[N_i^A + N_i^a\right] N_i^a - g\left[Z - \eta - (-1)^i\right]^2 N_i^a + m(N_j^a - N_i^a) = 0, \\ N_i^A - \left[N_i^A + N_i^a\right] N_i^A - g\left[Z + \eta - (-1)^i\right]^2 N_i^A + m(N_j^A - N_i^A) = 0, \\ 2g - m\,\delta^a \left[\frac{N_2^a}{N_1^a} + \frac{N_1^a}{N_2^a}\right] + \frac{\delta^A - \delta^a}{4}\left[\frac{N_2^A}{N_2^a+N_2^A} + \frac{N_1^A}{N_1^a+N_1^A}\right] + \frac{\delta}{2}\left[\frac{N_2^A}{N_2^a+N_2^A} - \frac{N_1^A}{N_1^a+N_1^A}\right] = 0, \\ 2g - m\,\delta^A \left[\frac{N_2^A}{N_1^A} + \frac{N_1^A}{N_2^A}\right] + \frac{\delta^a - \delta^A}{4}\left[\frac{N_2^a}{N_2^a+N_2^A} + \frac{N_1^a}{N_1^a+N_1^A}\right] + \frac{\delta}{2}\left[\frac{N_1^A}{N_2^a+N_2^A} - \frac{N_2^a}{N_1^a+N_1^A}\right] = 0, \\ -\frac{\delta}{2} - 2\,g\,\eta + m\left(\frac{\delta^A}{2}\left[\frac{N_2^A}{N_1^A} - \frac{N_1^A}{N_2^A}\right] - \frac{\delta^a}{2}\left[\frac{N_2^a}{N_1^a} - \frac{N_1^a}{N_2^a}\right]\right) = 0, \\ -2\,g\,Z + m\left(\frac{\delta^a}{2}\left[\frac{N_2^a}{N_1^a} - \frac{N_1^a}{N_2^a}\right] + \frac{\delta^A}{2}\left[\frac{N_2^A}{N_1^A} - \frac{N_1^A}{N_2^A}\right]\right) + \frac{\delta^A - \delta^a}{4}\left[\frac{N_2^A}{N_2^A+N_2^a} - \frac{N_1^A}{N_1^A+N_1^a}\right] \\ \qquad\qquad + \frac{\delta}{2}\left[\frac{N_1^A}{N_1^A+N_1^a} + \frac{N_2^A}{N_2^A+N_2^a} - 1\right] = 0. \end{cases} \tag{4.22}$$

Next, we give the condition under which it is stable.

Resolution.

Proposition 4.5.1. *There exists a unique polymorphic equilibrium corresponding to the infinitesimal average $Z = 0$ under the condition:*

$$\left[g(\eta^2+1) < 1\right] \vee \left[m < \frac{2\,g^2\,\eta^2}{g(\eta^2+1) - 1} - g(\eta^2+1) + 1\right]. \tag{4.23}$$

The allelic local population sizes corresponding to this equilibrium satisfy the property:

$$N_{1,0}^a = N_{2,0}^A, \quad N_{2,0}^a = N_{1,0}^A,$$

and for both alleles, the spatial discrepancies between the mean infinitesimal parts of the two demes per allele are the same:

$$\delta_0^A = \delta_0^a.$$

Therefore, this polymorphic equilibrium at $Z = 0$ is called symmetrical.

Proof. Let us define the quantities:

$$\begin{cases} Y_0^A = \frac{2\,g\,\eta}{m}\left[\sqrt{1+\frac{m^2}{4\,g^2\,\eta^2}}+1\right], \\ Y_0^a = \frac{2\,g\,\eta}{m}\left[\sqrt{1+\frac{m^2}{4\,g^2\,\eta^2}}-1\right], \\ N_{1,0} = 1 - g\,\eta^2 - g - m + 2\,g\,\eta\sqrt{1+\frac{m^2}{4\,g^2\,\eta^2}}, \\ N_{2,0} = N_{1,0}. \end{cases} \tag{4.24}$$

Proposition 4.4.1 states that the latter defines a solution to $S_0(Z)$ given that $Z = 0$:

$$(N_{1,0}^a, N_{2,0}^a, N_{1,0}^A, N_{2,0}^A) = \left(N_{1,0}\frac{Y_0^A - 1}{Y_0^A - Y_0^a},\ N_{1,0}\frac{1 - Y_0^a}{Y_0^A - Y_0^a},\ N_{1,0}\frac{1 - Y_0^a}{Y_0^A - Y_0^a},\ N_{1,0}\frac{Y_0^A - 1}{Y_0^A - Y_0^a}\right).$$

Since $Y_0^A > 1$ and $Y_0^A\ Y_0^a = 1$, this solution is viable under the condition: $N_{1,0} > 0$, hence requiring :

$$1 + \sqrt{4\,g^2\,\eta^2 + m^2} > g\,\eta^2 + g + m,$$

which in turn is equivalent to (4.23).

Proposition 4.4.2 next states that $S_L(Z)$ has a unique solution $(\delta_0, \delta_0^A, \delta_0^a)$ for such allelic population sizes $(N_{1,0}^a, N_{2,0}^a, N_{1,0}^A, N_{2,0}^A)$. One can compute that:

$$\delta_0^A = \delta_0^a = \frac{g\left(1 + \eta + Y_0^A(1-\eta)\right)}{m(1+Y_0^A)}, \quad \delta_0 = -\frac{2g\left(1 + \eta - {Y_0^A}^2(1-\eta)\right)}{Y_0^A}.$$

Finally, one can verify that $(N_{1,0}^a, N_{2,0}^a, N_{1,0}^A, N_{2,0}^A, \delta_0, \delta_0^A, \delta_0^a)$ along with setting $Z = 0$ is a solution of the last equation of (4.22). □

Stability. Let us recall the limit system (P_0):

$$\begin{cases} G(\bar{Y}, Z) = 0, \\ \frac{dZ}{dt} = -2\,g\,Z + F(\bar{Y}). \end{cases} \tag{4.25}$$

Stability of the symmetrical polymorphic equilibrium (denoted $(0, \bar{Y}_0)$) described in Proposition 4.5.1 is studied in the same manner as in [Dekens 2022]. Thanks to the implicit function theorem used in the vicinity of the symmetrical polymorphic equilibrium, this equilibrium is asymptotically locally stable if and only if:

$$0 < 2g + \partial_{\bar{Y}} F \cdot \left([\partial_{\bar{Y}} G]^{-1}\,\partial_Z G\right)\Big|_{Z=0, \bar{Y}=\bar{Y}_0}.$$

Due to the large number of dimensions involved, the explicit formula is too long to be given here.

However, we provide numerical analysis results of the stability, displayed in Fig. 4.4. We show the stability region in yellow for four values of the effect of the major locus $\eta \in \{0.5, 0.7, 1, 1.3\}$, with selection strength (g, x-axis) and migration rate (m, y-axis) varying in $[0, 3]$. For each value of η, we can observe that the symmetrical polymorphic equilibrium is

not stable under weak selection. Moreover, at weak to strong migration, stability exhibits non-monotonic behaviour when selection is increasing. Stability is gained at an intermediate level of selection that depends on the migration rate and lost at a higher level of selection. It is worth recalling that the one-locus haploid model predicts that the equilibrium is stable, regardless of selection and migration in this symmetrical case as long as the population does not go extinct (under the dashed curve) (see Remark 11). Therefore, the instability observed in this model results from the small-effect loci.

Pushing further the numerical analysis of polymorphic equilibria. Here, we show a numerical analysis of all the equilibria of the limit system (P_0) in Fig. 4.5.

Suppose that the parameters allow for the symmetrical polymorphic equilibrium to exist, i.e. satisfy (4.23). From the explicit resolution of the fast ecological equilibrium given an evolutionary state $Z \in]-1,1[$ (Proposition 4.4.1 and Proposition 4.4.2), we deduce, thanks to the implicit function theorem, that there exists an open interval I centered in 0 and a smooth function $\bar{Y} : I \to {\mathbb{R}_+^*}^4 \times \mathbb{R}^3$, which links an evolutionary state Z to its corresponding ecological equilibrium $\bar{Y}(Z)$ (solving $G(\bar{Y}(Z), Z) = 0$). The system (P_0) can thus be represented by the following autonomous differential equation:

$$\frac{dZ}{dt} = \mathcal{F}(Z) := -2\,g\,Z + F\left(\bar{Y}(Z)\right). \tag{4.26}$$

Hence, a couple $(Z, \bar{Y}(Z))$ is a polymorphic equilibrium if $\mathcal{F}(Z) = 0$, and this equilibrium is locally stable if $\mathcal{F}'(Z) < 0$.

Even if the complexity of the limit system is still too great to be analytically solved (due to the implicit nature of the function $\bar{Y}$), we show in Fig. 4.5 phase lines corresponding to the autonomous limit equation (4.26), when the migration rate and the effect size of the major locus are held constant ($m = 0.1, \eta = \frac{1}{2}$) and the selection strength varies (the lighter the color, the stronger the selection). Solid lines indicate that the system is polymorphic, whereas dotted lines indicate that one major allele has fixed. Every intersection of the null horizontal line and a solid colored line with a negative slope indicates a locally stable polymorphic equilibrium (conversely, a positive slope indicates an unstable equilibrium).

This figure is consistent with the analysis of Section 4.5 and Fig. 4.4a: at $Z = 0$, all the curves return to 0 ($F(Z)$), confirming that a polymorphic equilibrium exists when the mean contribution of the small-effect loci is 0. Their local slope indicates the stability of this equilibrium (stable if negative, instable is positive). Furthermore, Fig. 4.5 gives insights on the existence of asymmetrical polymorphic equilibria. Particularly, it seems that such equilibria exist for a narrow window of intermediate selection strength: the green curve corresponding to $g = 0.86$ displays two mirrored stable asymmetrical polymorphic equilibria at $Z \approx \pm 0.5$ (indicated by the red arrows), which is hard to predict analytically due to the high orders of polynomials involved. Moreover, such equilibria are presumably quite subtle to catch in an individual-based simulations, because the window of selection and the basin of attraction are both narrow. However, this illustrates the new and unsuspected insights that can be obtained from this hybrid model.

4.6 Individual-based simulations

In this section, we explore some of the insights given by our analysis on the stability of the symmetrical polymorphic equilibrium, using individual-based simulations conducted with the

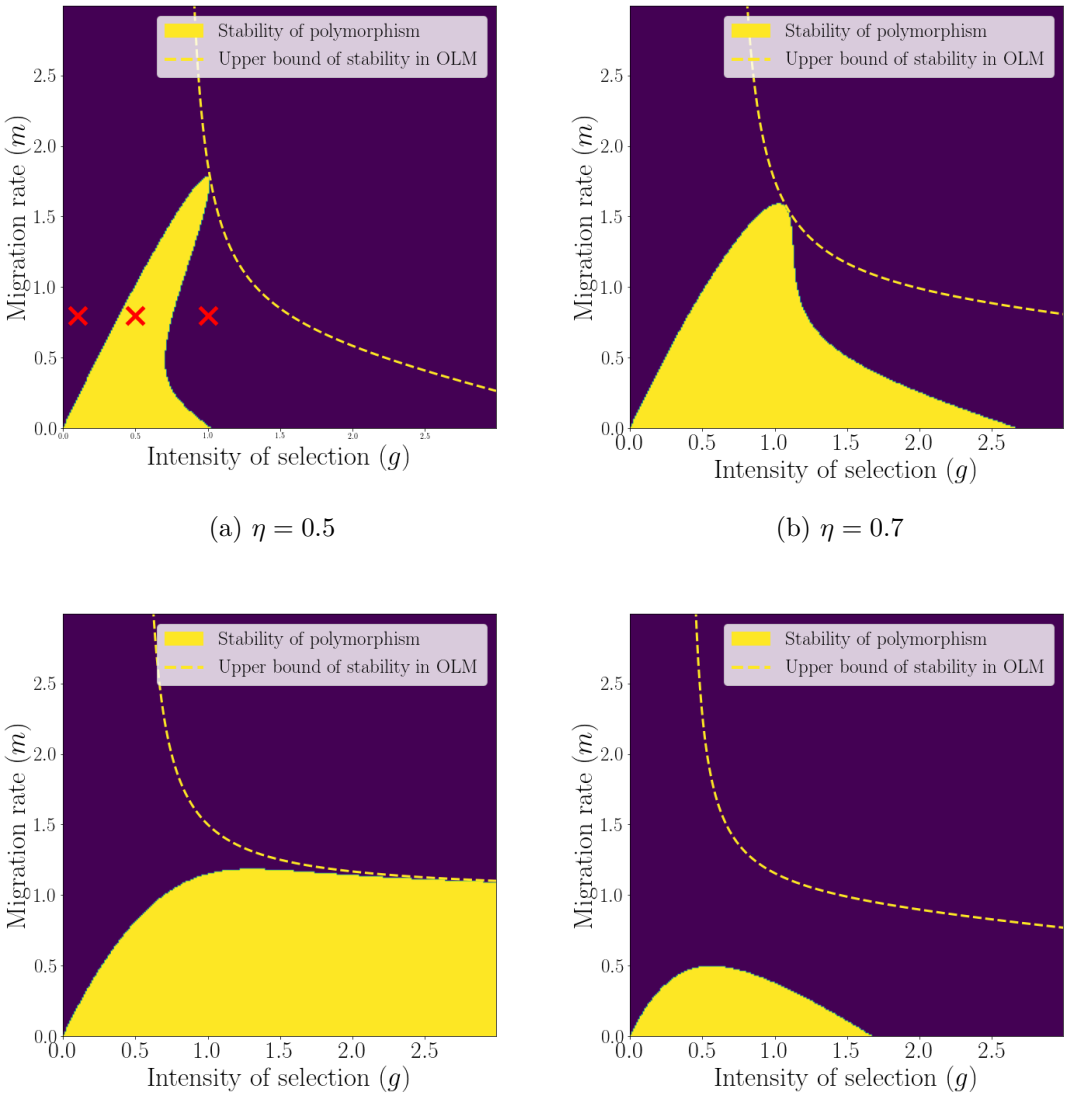

(a) $\eta = 0.5$ (b) $\eta = 0.7$

(c) $\eta = 1$ (d) $\eta = 1.3$

Figure 4.4: **Stability region of the symmetrical polymorphic equilibrium (in yellow), for four major locus effects $\eta \in \{0.5, 0.7, 1, 1.3\}$** (recalling that $\theta = 1$), when m (y-axis) and g (x-axis) vary in $[0, 3]$). This figure highlights the gain and loss of polymorphism with regard to increasing selection, which is not predicted by the one-locus model (abbreviated as OLM in the legend). The stable region (in yellow) becomes larger as η grows closer to 1, as the major allele effect can then fully explain the divergence between the two demes, then shrinks again. The red crosses in Fig. 4.4a indicate the parameters used for the individual-based simulations (see Section 4.6 and Fig. 4.6 and Fig. 4.7).

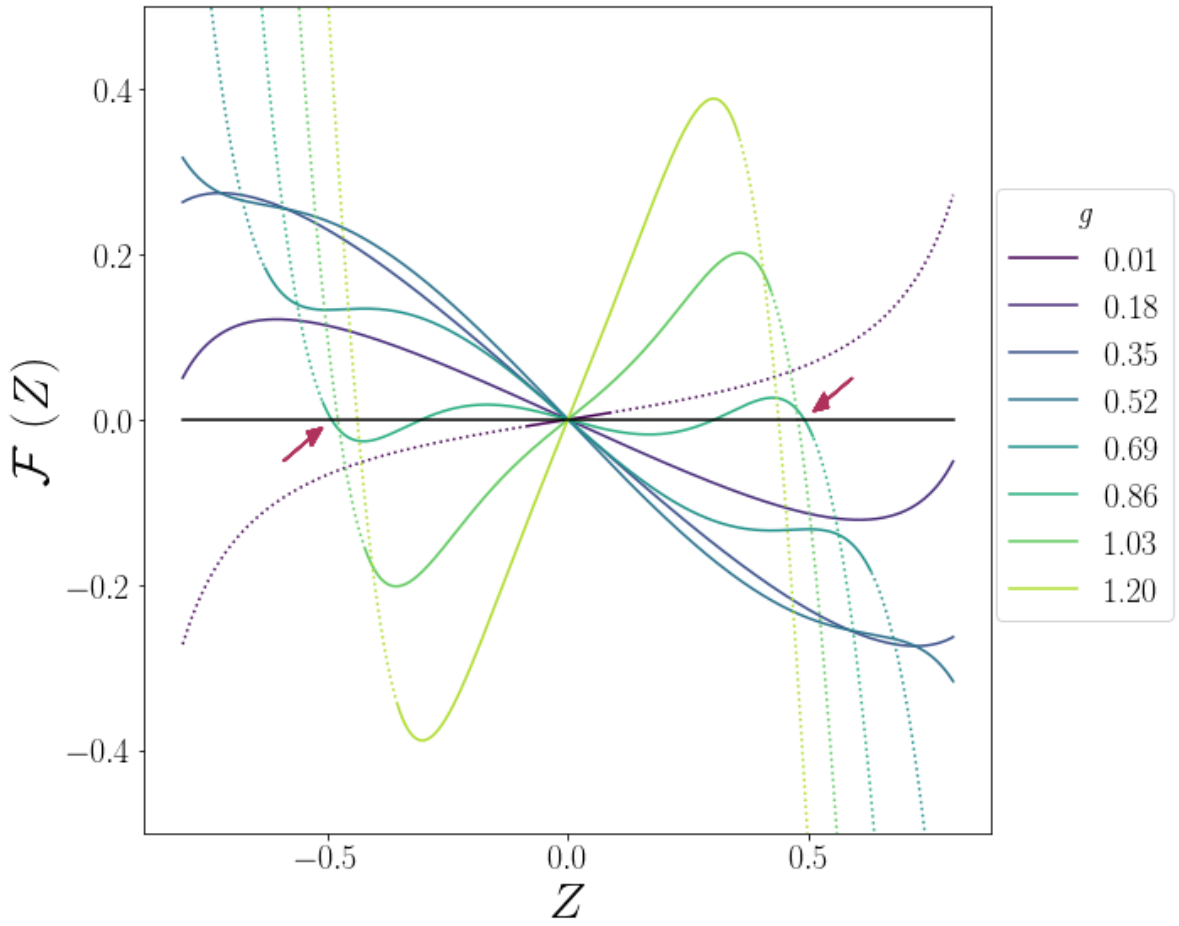

Figure 4.5: **Phases lines of the autonomous limit equation** (4.26)**, when the migration rate and the strong effect are held constant** ($m = 0.1, \eta = \frac{1}{2}$) **and the selection strength varies** (the lighter the color, the stronger the selection). Solid curves indicate that the system is polymorphic, whereas dashed curves indicate that one major allele has fixed. Every intersection of the horizontal black line and a solid colored curve with a negative (resp. positive) slope indicates a locally stable (resp. unstable) polymorphic equilibrium. The darker curve with weak selection $g = 0.01$ has a positive slope at $Z = 0$ (unstable), the following curves have a negative slope at $Z = 0$ (stable for selection between $g = 0.18$ and $g = 0.86$), and finally the lightest curves have a positive slope at $Z = 0$ (unstable for $g \geq 1.03$), which is consistent with Fig. 4.4a. Note that there exists additionally two mirrored asymmetrical polymorphic equilibria for $g = 0.86$, for $Z \approx \pm 0.5$ (indicated by the red arrows), which were unsuspected prior to this numerical analysis.

software SLiM (Haller and Messer 2019). We focus on the gain and loss of polymorphism with regard to increasing selection, when $\eta \neq 1$, for symmetrical and asymmetrical initial conditions. For each set of parameters, we ran 20 replicate simulations. The results on the major locus are displayed in Fig. 4.6 and Fig. 4.7, both with a quantitative background (left panel) and without (right panel). The simulations confirm that variation is maintained only for intermediate for intermediate levels of selection (as measured by $p(1-p)$, where p is the local frequency of allele A). The framework of the simulations is detailed as follows.

Populations and habitats. The species is split in two subpopulations living in two different habitats, with local carrying capacity $\boldsymbol{K} = 10^4$. In each habitat, individuals experience selection toward a local trait optimum $\boldsymbol{\theta_i} = (-1)^i$ (for habitat i). Initially, the two subpopulations are at $\frac{4}{5}$ of the local carrying capacity. The genetic information of the individuals of the initial population is set as follows. In each subpopulation, all the individuals have, at the major locus, the allele whose effect is the closest to the optimum of the habitat they are in ($\boldsymbol{\eta}$ in habitat 2 and $-\boldsymbol{\eta}$ in habitat 1). The infinitesimal background is then set randomly and uniformly.

Genetic architecture. We consider $\boldsymbol{L} = 200$ unlinked loci constituting the infinitesimal background. At each of these loci, two alleles segregate, having an additive effect on the trait of the individual of value $\frac{\boldsymbol{\sigma_{LE}}}{\sqrt{\boldsymbol{L}}}$ or $-\frac{\boldsymbol{\sigma_{LE}}}{\sqrt{\boldsymbol{L}}}$, where $\boldsymbol{\sigma^2_{LE}}$ is the variance at linkage equilibrum of the quantitative background. No mutation occurs at those loci. We set the variance at linkage equilibrium to $\boldsymbol{\sigma_{LE}} = 0.1$ small, so that our analysis in a small variance regime is a good approximation. (In Section 4.D, we consider the same framework with a smaller number of loci involved in the quantitative background $\boldsymbol{L} = 50$).

There is an additional locus of interest, which carries the major alleles $+\boldsymbol{\eta}$ or $-\boldsymbol{\eta}$. This locus is also unlinked to all the others and no mutation occurs at this site. Note also that the trait range, given by $[-\boldsymbol{\eta} - \boldsymbol{\sigma_{LE}}\sqrt{\boldsymbol{L}}, \boldsymbol{\eta} + \boldsymbol{\sigma_{LE}}\sqrt{\boldsymbol{L}}] = [-\boldsymbol{\eta} - \sqrt{2}, \boldsymbol{\eta} + \sqrt{2}]$ extends beyond the local optima (-1,1), even in the absence of major effects.

Life cycle. The life cycle involves overlapping generations of small time length $\boldsymbol{\Delta t} = 0.1$. The life cycle proceeds as follows:

1. *reproduction*: each individual of the metapopulation chooses at random one mate within its subpopulation, and their mating produces an offspring with probability $\boldsymbol{\Delta t}$.

2. *selection-competition*: each individual (including offsprings that are generated in the previous step) faces a selection-competition trial according to its trait $\boldsymbol{\zeta}$ and habitat i in which they are currently living. They survive with probability $\exp\left(-\boldsymbol{g\Delta t}(\boldsymbol{\zeta} - \boldsymbol{\theta}_i)^2 - \boldsymbol{\Delta t}\frac{\boldsymbol{N_i}}{\boldsymbol{K}}\right)$ and are removed otherwise (here $\boldsymbol{N_i}$ denotes the size of the subpopulation i after reproduction).

3. *migration*: at each migration event, within each subpopulation i, a number of migrants is drawn, according to a Poisson law with parameter $\boldsymbol{m\Delta t}\ \boldsymbol{N_i}$ (with a hard cap of $\boldsymbol{N_i}$, which is the number of individuals currently in the subpopulation after the selection-competition step). Migrants are uniformly sampled accordingly within the subpopulation and are moved to the other deme. We stress that a given value of the migration rate $\boldsymbol{m} = 0.8$ means that, on average, a fraction $\boldsymbol{m\Delta t} = 0.08$ of the population will change of deme at each generation.

Each simulation repeats this life cycle, first without migration for 100 generations of burn in (10 time units) and next with migration for $\boldsymbol{N}_{\text{gen}} = 10^4$ generations (10^3 time units). We model two types of initial events when migration starts: either nothing happens, and the initial state is symmetrical, or we model a sudden catastrophic loss of population in only one of the habitat during the first generation with migration, so that the initial state is asymmetrical. Precisely, we change the mortality of the uniform competition term only in the habitat 1, by replacing $\exp\left(-\boldsymbol{\Delta t}\frac{\boldsymbol{N_1}}{\boldsymbol{K}}\right)$ by $\exp\left(-\frac{\boldsymbol{N_1}}{\boldsymbol{K}}\right)$ (which is consistent with the interpretation that this catastrophic loss of population is very abrupt). This leads to asymmetrical initial subpopulation sizes.

Control case without infinitesimal background. To confirm that the loss of polymorphism at weak and strong selections is due to the infinitesimal background and not to genetic drift (although drift is unlikely to have an effect under this time range of 10^3 time units with a population of order 10^4), we additionally run an equal number of replicates for each set of parameters without any infinitesimal background ($\boldsymbol{L} = 0, \boldsymbol{\sigma_{LE}} = 0$). Only the major alleles segregates, and this corresponds to the one-locus haploid model. Results shown in the right panel of Fig. 4.6 and Fig. 4.7 are consistent with the one-locus haploid model analysis, that states that the polymorphism at this major locus is stable at all level of selection.

Consistency with the continuous-time deterministic model (4.1). We ran two series of deterministic numerical resolutions of (4.1), one for each type of initial conditions (symmetrical or asymmetrical initial subpopulations sizes), and in each series, for each replicate individual-based simulation and set of parameter. This choice was motivated by a discrepancy in the sensitivity of the deterministic numerical resolutions with regard to initial conditions. Indeed, since the environment is symmetrical, the symmetrical initial state is at an unstable edge between two symmetrical stable valleys for the interesting range of parameters. Therefore, we initialized the deterministic resolutions with the symmetrical initial state according to their respective IBS replicate states at 20% of the time before the median fixation time (140 times units for Fig. 4.6a and 40 time units for Fig. 4.6e). With the asymmetrical initial conditions (or more generally, any asymmetry in the environmental parameters), this sensitivity is greatly reduced, and the deterministic resolutions are initialized according to their respective IBS replicate states when migration starts (0 time units). Furthermore, the numerical scheme for the resolution of the deterministic model (4.1) uses a splitting scheme to handle successively migration and the ecological dynamics internal to each habitat. For the latter, we use a discretization of the Duhamel' integral formula on time step of lengths $\boldsymbol{\Delta t}$ for the asymmetrical initial state series and $\frac{\boldsymbol{\Delta t}}{4}$ (and on four times more time steps) for the symmetrical initial state series.

In the left panel of Fig. 4.6 and Fig. 4.7, we display the median deterministic trajectory for each set of parameter. The comparison of trajectories suggests that the continuous-time deterministic trajectories of (4.1) provide good approximations of the discrete-time individual based simulations, consistently with regard to the symmetry of the initial conditions (albeit with more precautions in the initialization of the deterministic resolutions with symmetrical initial states)..

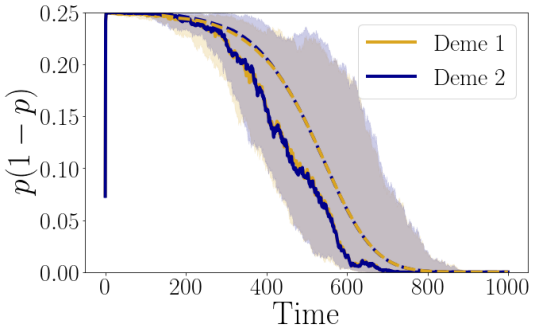

(a) Major locus with infinitesimal background: weak selection ($g = 0.1$). Polymorphism at the major locus is lost after around 800 time units.

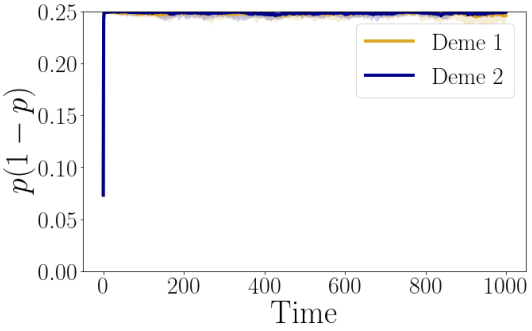

(b) Control case without infinitesimal background: weak selection ($g = 0.1$). Polymorphism at the major locus is maintained over the course of all simulations.

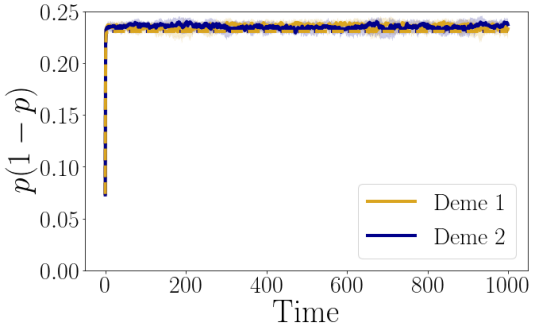

(c) Major locus with infinitesimal background: intermediate selection ($g = 0.5$). Polymorphism at the major locus is maintained over the course of all simulations.

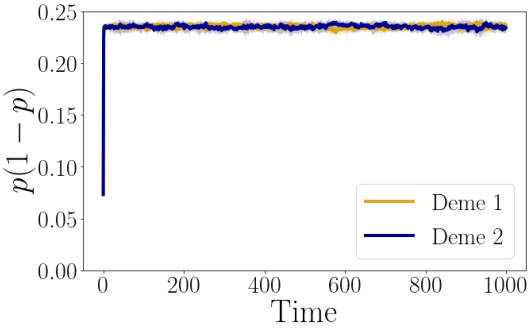

(d) Control case without infinitesimal background: intermediate selection ($g = 0.5$). Polymorphism at the major locus is maintained over the course of all simulations.

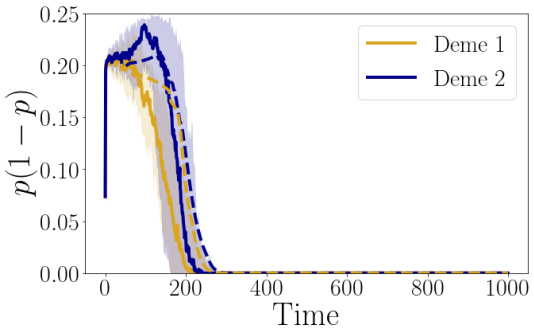

(e) Major locus with infinitesimal background: strong selection ($g = 1$). Polymorphism at the major locus is lost after around 200 time units.

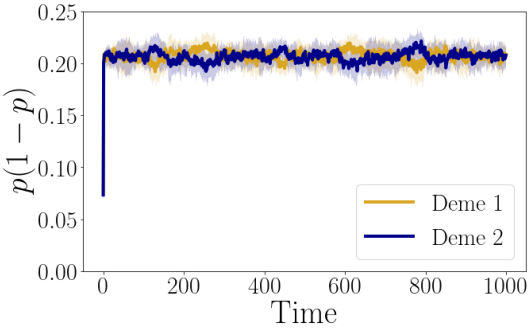

(f) Control case without infinitesimal background : strong selection ($g = 1$). Polymorphism at the major locus is maintained over the course of all simulations.

Figure 4.6: **Variance at the major locus across time for increasing selection (top to bottom: $g = 0.1,\ 0.5,\ 1$) at a fixed rate of migration ($m = 0.8$), with symmetrical initial subpopulation sizes**. p denotes the local frequency of the major allele A. The left panel is obtained with both a major locus ($\eta = 1/2$) and an infinitesimal background of 200 loci, whereas only the major locus is present in the right panel. For each subfigure, 20 replicates simulations were run per set of parameters, according to the setting explained in Section 4.6. In each subfigure, the solid line represents the median trajectory and the shaded area indicates the 0.2 and 0.8 quantiles. The dashed lines represents the median trajectories of the numerical resolutions of the deterministic model (4.1). This figure confirms that polymorphism of the major-effect locus is maintained only when selection is intermediate in strength in presence of a infinitesimal background.

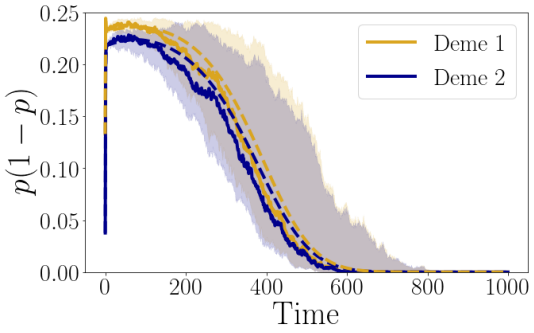

(a) Major locus with infinitesimal background: weak selection ($g = 0.1$). Polymorphism at the major locus is lost after around 600 time units.

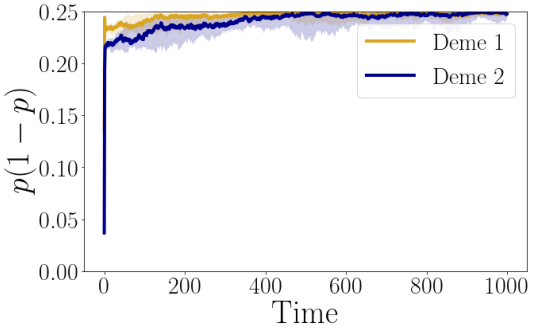

(b) Control case without infinitesimal background: weak selection ($g = 0.1$). Polymorphism at the major locus is maintained over the course of all simulations.

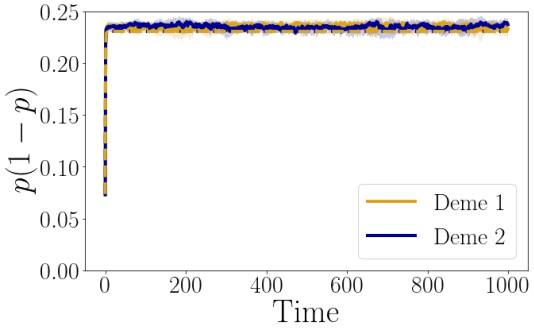

(c) Major locus with infinitesimal background: intermediate selection ($g = 0.5$). Polymorphism at the major locus is maintained over the course of all simulations.

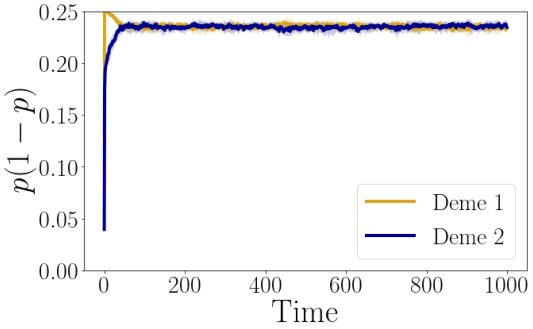

(d) Control case without infinitesimal background: intermediate selection ($g = 0.5$). Polymorphism at the major locus is maintained over the course of all simulations.

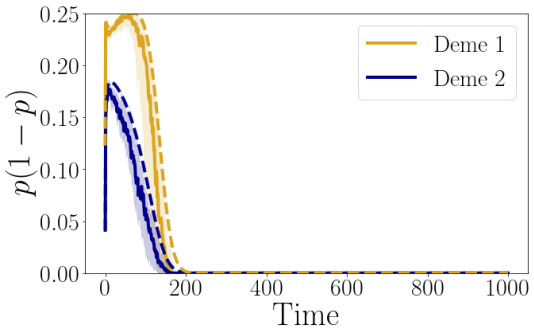

(e) Major locus with infinitesimal background: strong selection ($g = 1$). Polymorphism at the major locus is lost after around 200 time units.

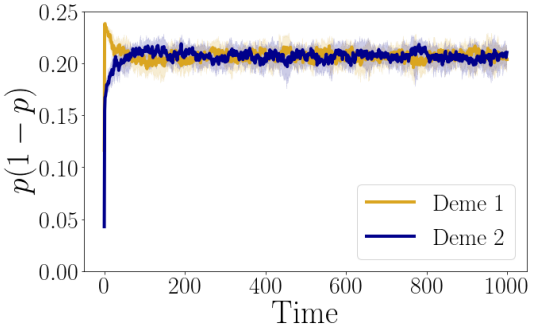

(f) Control case without infinitesimal background : strong selection ($g = 1$). Polymorphism at the major locus is maintained over the course of all simulations.

Figure 4.7: **Variance at the major locus across time, for increasing selection (top to bottom: $g = 0.1,\ 0.5,\ 1$) at a fixed rate of migration ($m = 0.8$), with asymmetrical initial subpopulation sizes**. p denotes the local frequency of the major allele A. The left panel is obtained with both a major locus ($\boldsymbol{\eta} = 1/2$) and an infinitesimal background of 200 loci, whereas only the major locus is present in the right panel. For each subfigure, 20 replicates simulations were run per set of parameters, according to the setting explained in Section 4.6. In each subfigure, the solid line represents the median trajectory and the shaded area indicates the 0.2 and 0.8 quantiles. The dashed lines represents the median trajectories of the numerical resolutions of the deterministic model (4.1). This figure confirms that polymorphism of the major-effect locus is maintained only when selection is intermediate in strength in presence of a infinitesimal background.

4.7 Discussion

Contributions. In this work, we present a new model for selection in a heterogeneous environment that combines a major-effect locus with a quantitative genetic background, without assuming that the latter are normally distributed. This model bridges a population genetic model (one-locus haploid model) with a quantitative genetic model recently studied in a heterogenous environement (Dekens 2022). To do so, it introduces a new reproduction operator, inspired by the infinitesimal model, that encodes the inheritance of a major effect and a quantitative background. The analysis goes deeper than previous studies (Lande 1983), by formally justifying, in a regime of small variance, that the polygenic component of the trait is normally distributed around the major allelic effects. To that effect, we find new convex analysis arguments that leads to a separation of time scales, which allows us to study the stability of the polymorphism at the major locus. We show that this polymorphism, which is maintained at intermediate selection, is subsequently lost when selection increases beyond a certain threshold, a phenomenon qualitatively confirmed by individual-based simulations. The separation of time scales' point of view offers the interpretation that the infinitesimal background slowly disrupts the fast established symmetrical polymorphism at the major locus. Therefore, this phenomenon cannot be predicted by the one-locus haploid model (without the quantitative background). To our knowledge, this phenomenon has not yet been documented.

Summary of complete analytical outcomes. The analysis performed in Section 4.5 is centered on the persistence of polymorphism at the major effect locus. As stated in Working assumption 1, the loss of polymorphism by fixation would lead to the dynamics of the quantitative background alone, as covered in [Dekens 2022]. Hence, Fig. 4.8 complements Fig. 4.4 (for $\eta = 0.5$ and varying migration and selection), by displaying both the region of parameters where the system would go to the symmetrical polymorphic equilibrium (in yellow, corresponding to the region where polymorphism is stable), and the region of parameters corresponding to the two types of monomorphic equilibria for a quantitative trait in the regime of small variance described in [Dekens 2022].

For bounded selection, there exists a critical threshold in the migration rate under which the polymorphism at the major locus is stable (yellow region) and above which it is lost due to the strong blending effect of migration. In that case, the population trait distribution is concentrated on the trait at the midpoint between the two habitats' optima, and occupies equally the two habitats. this corresponds to the symmetrical monomorphic equilibrium (see Ronce and Kirkpatrick 2001; Dekens 2022), where the population can be qualified as generalist (green region). One can notice that there exists an interval of selection strengths $g \in [0.7, 1]$ in which the major polymorphism might not be stable for all migration rates under the critical threshold. This phenomenon does not hold for greater major allelic effects (see Fig. 4.4b,Fig. 4.4c,Fig. 4.4d).

For bounded migration rates, and with weak selection, the major polymorphism is unstable, as the diverging selection is too weak compared to the blending migration to maintain differentiation at the major locus (green region). When selection strength increases, the polymorphism at the major locus is first stable (yellow region), but eventually lost above a certain selection strength. The population becomes adapted to one of the two habitats that it mostly inhabits (blue region). This asymmetrical equilibria, highlighted as a source-sink scenario in [Ronce and Kirkpatrick 2001], was analytically derived in [Dekens 2022].

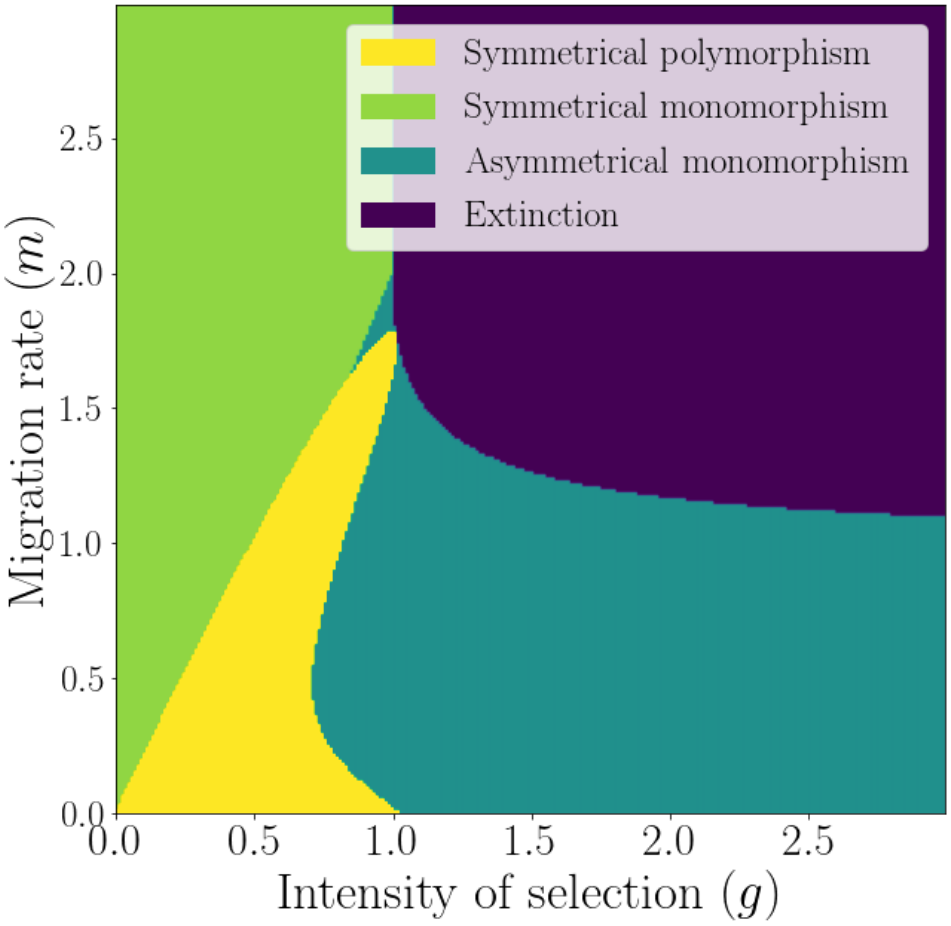

Figure 4.8: **Summary of the complete analytical outcomes of the model**, for $\eta = 0.5$ and varying migration (y-axis) and selection (x-axis). The figure combines the results obtained in Section 4.5 on the stability of the symmetrical polymorphic equilibrium with the results of the model of [Dekens 2022] (equivalent to this model upon loss of polymorphism). For bounded selection, when migration increases, there is a threshold over which the polymorphism at the major locus is lost due to the blending effect of migration (consistent with Yeaman and Whitlock 2011). The population becomes equally maladapted to both habitats (generalist - symmetrical monomorphism, in the green region). For this specific major allelic effect $\eta = 0.5$, there exists additionally an interval of selection strength ($\approx [0.7 - 1]$) for which the major polymorphism is not stable at migration rates below the critical threshold. This phenomenon does not seem to hold when the allelic effect is larger (see Fig. 4.4b). For bounded migration (below the threshold rate over which the strong migration blending hampers the major polymorphism), when selection strength increases, the polymorphism at the major allele (yellow region) is lost, and the population becomes adapted to one of the two habitats (specialist - asymmetrical monomorphism, in the blue region). As this figure is obtained in the small segregational variance regime (which should remain smaller than the other parameters of the system for the analysis to be valid), we warn that the outcomes displayed in the vicinity of the x-axis (very small migration rates) might not correspond to the limit when the migration rate is 0 (no migration).

Extensions to more complex population genetic models. We provide a comprehensive toolbox (Section 4.A) at the end of this document, to describe how to apply the method more broadly. In particular, the toolbox is meant to indicate how to extend the method to more complex population genetic models by adding a quantitative background. It relies on Proposition 4.B.1, and we detail the hypotheses that the population genetic models must satisfy in order to use it (see Section 4.B for details and examples).

Further prospects. The loss of the polymorphism at the major locus at strong selection levels in heterogeneous environment, where one might think that it is most favoured, illustrates the value of our method. However, a natural question would be: does this phenomenon hold if the major alleles are allowed to accumulate mutations? Fig. 4.4 for example suggests that polymorphism at the major-effect locus would persist over a wider range of parameters if the alleles at the major-effect locus evolve to match the difference in optima. This possibility was indicated by the numerical findings of [Yeaman and Whitlock 2011], who found the emergence of tightly linked clusters of major loci underlying local adaptation for intermediate migration rates. To study this phenomenon, a more complex model is required, which will be the prospect of a future work.

4.A Toolbox: How to study the interplay between a quantitative background and a finite number of major loci.

The aim is to study the interplay between a quantitative background and a finite number of major loci.

We start with a population genetic model. Let us consider I different genotypes $\mathcal{A}^{(i)}$ which have genotypic effects on the phenotype $a^{(i)}$ (we use the index i o indicate genotypes). For our method to be applied, the genotypes should verify two hypotheses H1 and H2 described in Appendix 4.B. The metapopulation lives in a heterogeneous environement of K patches (we use the index k to indicate location). We denote the population of patch k carrying genotype i by $N_k^{(i)}$. Let us denote the system of equations that describes the dynamics of the genotypic local population sizes: $\frac{d\bar{N}}{dT} = \tilde{G}_{\bar{a}}\left(\bar{N}(T)\right)$ and of a viable stable equilibrium $\bar{N}^*$. *We recall that $\bar{N}^*$ is an equilibrium of the system if $\tilde{G}_{\bar{a}}(\bar{N}^*)$. This equilibrium is viable if all the population sizes are non-negative, and at least one is positive. Its local stability is determined by standard linear analysis (sign of the real parts of the eigenvalues of the system's Jacobian).*

Let us modify the previous population genetic framework to include the effect of a quantitative background on the trait, generically denoted z. While previously, all individuals carrying the same genotype $\mathcal{A}^{(i)}$ shared the same phenotype, now their phenotypes can differ due to the quantitative background they present. Consequently, among individuals of the same patch k carrying the same major genotype $\mathcal{A}^{(i)}$, we distinguish those sharing the same quantitative background z, and denote their number $n_k^{(i)}(z)$:

$$\begin{aligned} \mathcal{A}^{(i)} &\rightsquigarrow (\mathcal{A}^{(i)}, z) \\ a^{(i)} &\rightsquigarrow a^{(i)} + z \\ N_k^{(i)} &\rightsquigarrow n_k^{(i)}(z). \end{aligned}$$

The PDE system that we obtain on the trait distributions $n_k^{(i)}$ is not easily analysed. That is why we provide a five steps plan in order to guide the analysis when the diversity introduced by the segregation of the quantitative component of the trait is small compared to the variance generated by the major loci (H6 - regime of small variance):

1. first, we operate a scaling of time according to the regime of small variance. It anticipates on the separation of time scales such that the major allelic frequencies change rapidly, followed by the slow changes of the quantitative components (see step 3).

2. in this regime of small variance, we can justify the Gaussian approximation of the local genotypic distributions $n_k^{(i)}$ centered at the same mean and the same variance ε^2, thanks to Proposition 4.B.1, as soon as the assumptions (H1) and (H2) are satisfied (see Appendix 4.B) and every genotypic population randomly mates with themselves and every other genotypic population (H3) (the latter excludes for example models that differentiate sexes). This guides the intuition toward which change of variables to perform in order to get a system separating time scales explicitly (see Step 3). We emphasize that Proposition 4.B.1 is crucial to be able to apply this method.

3. From the PDE system on the distributions $n_k^{(i)}$, we can deduce the ODE system of their moments. Since we have justified the Gaussian approximation for all local genotypic distributions $n_k^{(i)}$, the new system is closed in the regime of small variance $\varepsilon^2 \ll 1$, and only involves the dynamics of the genotypic local sizes of populations $N_k^{(i)}$ and the genotypic local mean quantitative components $z_k^{(i)}$.

4. This step aims at obtaining a system that explicitly separates time scales, in order to ultimately reduce the complexity of the analysis. It requires a technical change of variables, which is guided by the formal analysis of the step 1 (mean quantitative components roughly the same within patches), and the intuition that migration has a strong blending effect between patches in the small variance regime (which would result in the mean quantitative components roughly being equal between patches). These considerations bring the following new variables replacing the genotypic local mean quantitative component $z_k^{(i)}$:

   - ◇ for each genotype $1 \leq i \leq I$, $\delta_{k,\varepsilon}^{(i)}$ is the difference in the mean quantitative component of the genotypic population i between the patch $k+1$ and patch k '$1 \leq k \leq K-1$. Dividing by ε^2 comes from the intuition given above.
   - ◇ for each genotype $1 \leq i \leq I-1$, $\delta_{\varepsilon}^{(i)}$ is the difference between the mean quantitative component averaged across patches of genotypic population $i+1$ and i. Dividing by ε^2 comes from the intuition givenin Step 1.
   - ◇ Z_ε is the overall mean quantitative component across patches and major genotypes. It is the slow evolving variable.

   Rewriting the dynamics of the genotypic local population sizes $\bar{N}_\varepsilon$ along these new variables $\bar{\delta}_\varepsilon$ and $Z\varepsilon$ delivers a system in which all the differential equations are multiplied by ε^2 (fast dynamics of $\bar{N}_\varepsilon$ and $\bar{\delta}_\varepsilon$) except the one governing the dynamics of Z_ε (slow dynamics).

   To finally complete the separation of time scales and obtain the limit system by letting ε^2 vanish, it is sufficient to show that at each value Z of the slow variable, the fast time-

scale equilibria $\left(\bar{N}, \bar{\delta}\right)$ are stable, for example by using the Routh Hurwitz criterion for linear analysis on the Jacobian $\text{Jac}_{\mathcal{G}_{\bar{a}}}\left(\bar{N}, \bar{\delta}\right)$.

5. The last step to determine the stability of the global equilibria of the full system of the genotypic population with the influence of the quantitative background $\left(\bar{N}^*, \bar{\delta}^*, Z^*\right)$, consists in applying the formula given in the last box (see the next page).

Toolbox: How to study the interplay between a quantitative background and a finite number of major loci dynamics.

Population genetic model

The stadium:
K patches P_k $(1 \leq k \leq K)$

The teams:
I different genotypes $\mathcal{A}^{(i)}$ $(1 \leq i \leq I)$
Vector of genotypic effects on phenotype: $\bar{a} = (a^{(1)}, ..., a^{(I)})$
Matrix of local genotypic population sizes: $\bar{N} = \left(N_k^{(i)}\right)$

Pop. gen. model:
$\frac{d\bar{N}}{dT} = \tilde{G}_{\bar{a}}\left(\bar{N}(T)\right)$

Pop gen. analysis:

(i) Viable equilibria: $G_{\bar{a}}\left(\bar{N}^*\right) = 0$ and $\bar{N}^* > \bar{0}$.

(ii) Stability: eigenvalues of $\mathrm{Jac}_{G_{\bar{a}}}\left(\bar{N}^*\right)$ in open left plane.

Hybrid model combining population and quantitative genetics

The new players:

(i) Quantitative background z

(ii) Individuals carrying genotype i and a quantitative background z have a phenotype $z + a^{(i)}$.

(iii) Distribution in patch k : $n_k^{(i)}(z)$

Work hypotheses:

H1 - H2 (reflexivity and irreducible graph - see App.4.B)

H3 every genotypic population reproduces randomly with themselves and every other in the same patch

H4 inheritance of the quantitative background in accordance with the infinitesimal model with segregational variance σ^2.

H5 the quantitative background is unlinked to $\mathcal{A}^{(i)}$

H6 $\sigma^2 \ll \min\left|a^{(i)}\right|^2$: small variance regime.

Steps to apply the hybrid analysis

0) Scaling of time $t := \varepsilon^2 T$
($\varepsilon^2 := \frac{\sigma^2}{\min\left|a^{(i)}\right|^2} \ll 1 \rightsquigarrow$ few diversity via inf. model of reproduction)

1) Formal analysis (justify Gaussian distributions - Proposition 4.B.1):

(i) $n_{k,\varepsilon}^{(i)}(z) \approx N_{k,\varepsilon}^{(i)} \times \mathrm{Gauss}\left(z_{k,\varepsilon}^{(i)}, \varepsilon^2\right)$

(ii) $z_{k,\varepsilon}^{(i)} \approx z_{k,\varepsilon}^{(j)}$

2) ODE system of moments ($\bar{z}_\varepsilon := (z_{k,\varepsilon}^{(i)})$):

$$\begin{cases} \varepsilon^2 \frac{d\bar{N}_\varepsilon}{dt} = G_{\bar{a}}\left(\bar{N}_\varepsilon(t), \bar{z}_\varepsilon(t)\right), \\ \varepsilon^2 \frac{d\bar{z}_\varepsilon}{dt} = F_{\bar{a}}\left(\bar{N}_\varepsilon(t), \bar{z}_\varepsilon(t)\right). \end{cases}$$

3) Slow-fast analysis:

(i) Change in variables: $\delta_{k,\varepsilon}^{(i)} = \frac{z_{k+1,\varepsilon}^{(i)} - z_{k,\varepsilon}^{(i)}}{2\varepsilon^2}$ $[I(K-1)]$;
$\delta_\varepsilon^{(i)} = \frac{\sum_k z_{k,\varepsilon}^{(i+1)} - z_{k,\varepsilon}^{(i)}}{2K\varepsilon^2}$ $[(I-1)]$; $Z_\varepsilon = \frac{\sum_{k,i} z_{k,\varepsilon}^{(i)}}{K \times I}$

(ii) Slow-fast system:

$$\begin{cases} \varepsilon^2 \frac{d\left[\bar{N}_\varepsilon, \bar{\delta}_\varepsilon\right]}{dt} = \mathcal{G}_{\bar{a}}\left(\bar{N}_\varepsilon(t), \bar{\delta}_\varepsilon(t), Z_\varepsilon\right), \\ \frac{dZ_\varepsilon}{dt} = \mathcal{F}_{\bar{a}}\left(Z_\varepsilon, \bar{N}_\varepsilon, \bar{\delta}_\varepsilon\right). \end{cases}$$

(iii) Separation of time scales (via stability of zeros of $\mathcal{G}_{\bar{a}}$ by Routh-Hurwitz criterion on $\mathrm{Jac}_{\mathcal{G}_{\bar{a}}}(\bar{N}, \bar{\delta})$)

$$\begin{cases} 0 = \mathcal{G}_{\bar{a}}\left(\bar{N}, \bar{\delta}, Z\right), \\ \frac{dZ}{dt} = \mathcal{F}_{\bar{a}}\left(Z, \bar{N}, \bar{\delta}\right). \end{cases}$$

4) Analysis of the limit system:

(i) Viable equilibria: $\mathcal{G}_{\bar{a}}\left(\bar{N}^*, \bar{\delta}^*, Z^*\right) = \mathcal{F}_{\bar{a}}\left(Z^*, \bar{N}^*, \bar{\delta}^*\right) = 0$, $\bar{N}^* > 0$

(ii) Stability: $\nabla_{\bar{N},\bar{\delta}} \mathcal{F}_{\bar{a}} \cdot \left(\left[\mathrm{Jac}_{\mathcal{G}_{\bar{a}}}\left(\bar{N}, \bar{\delta}\right)\right]^{-1} \partial_Z \mathcal{G}_{\bar{a}}\right)\Big|_{Z^*, \bar{N}^*, \bar{\delta}^*} > 0.$

4.B Generalization of Proposition 4.3.1 for more complex genotypes.

To state a generalization of Proposition 4.3.1, we first need to specify the targeted scope of population genetic models. Let us consider I different genotypes $\mathcal{A}^{(i)}$ that satisfies the following hypotheses relating to how they interact with each other regarding the genotypes of their offspring:

H1 **Reflexivity**: For all $i \in (1, I)$, the offspring of two parents with the same genotype $\mathcal{A}^{(i)}$ has a positive probability to be of genotype $\mathcal{A}^{(i)}$.

H1 is a natural hypothesis when considering either haploid or diploid populations, even with non-Mendelian processes (genetic linkage/recombination, gene drives), provided that they are not too extreme (lowering the probability of inheriting a certain genotype is fine as long as it does not cancel it). The second hypothesis is more conveniently apprehendable by considering the graph $\mathcal{G}$ whose nodes are the genotypes $\mathcal{A}^{(i)}$. A vertex links two nodes $\mathcal{A}^{(i)}$ and $\mathcal{A}^{(j)}$ if and only if there exists a positive probability that their offspring has genotype $\mathcal{A}^{(i)}$ or $\mathcal{A}^{(j)}$.

H2 **Irreducible graph**: For all $(i, j) \in (1, I)^2$, there exists a path of vertices of $\mathcal{G}$ connecting $\mathcal{A}^{(i)}$ and $\mathcal{A}^{(j)}$.

This last hypothesis is satisfied by any haploid models, regardless of how many loci are considered, because an offspring can inherit all their alleles from only one parent. Consequently, in that case, every node of the graph is connected to every other. In diploid models, where an offspring can have a different genotype from both its parents, which vertices of the graph $\mathcal{G}$ exist is not clear. However, for example, we can show that the graph corresponding to a diploid model, with L loci and two alleles at each loci, is connected according to **H2**. Indeed, each genotype is directly connected to any other that differs from it from just one allele at one locus. Nevertheless, the interest of **H2** is that it is very easy to verify whether it is satisfied given any particular model.

To state the proposition that generalizes (Proposition 4.3.1), we first need to define the index set of couples that can yield an offspring with a particular genotype. For $i \leq I$, we denote it by $C^{(i)}$, where $(j, k) \in C^{(i)}$ if and only if parents with genotypes $\mathcal{A}^{(j)}$ and $\mathcal{A}^{(k)}$ can produce an offspring with genotype $\mathcal{A}^{(i)}$. The following proposition characterizes the genotypic functions $u^{\mathcal{A}^{(i)}}$ that respect the following constraints analogous to C

$$\forall i \leq I, \quad \forall z \in \mathbb{R}, \quad \max_{(j,k)\in C^{(i)}} \left[\sup_{z_1, z_2} u^{\mathcal{A}^{(i)}}(z) - \left(z - \frac{z_1 + z_2}{2} \right)^2 - u^{\mathcal{A}^{(j)}}(z_1) - u^{\mathcal{A}^{(k)}}(z_2) \right] = 0. \tag{C'}$$

Proposition 4.B.1. *Suppose that **H1** and **H2** are satisfied. For $i \in I$, we consider $u^{\mathcal{A}^{(i)}}$ a real valued non-negative function whose zero set is non-empty and of measure 0 (for example, is finite). If $\{u^{\mathcal{A}^{(i)}}, i \leq I\}$ respects (C'), then there exists $z^* \in \mathbb{R}$ such that for all $i \leq I$:*

$$\forall z \in \mathbb{R}, \quad u^{\mathcal{A}^{(i)}}(z) = \frac{(z - z^*)^2}{2}.$$

Proof.

0) $u^{\mathcal{A}^{(i)}}$ is continuous and has right and left derivatives everywhere. For $i \leq I$ and $z \in \mathbb{R}$, we have:

$$u^{\mathcal{A}^{(i)}}(z) - z^2 = \min_{(j,k)\in C^{(i)}} \inf_{z_1,z_2} \left[-z(z_1+z_2) + \left(\frac{z_1+z_2}{2}\right)^2 + u^{\mathcal{A}^{(j)}}(z_1) + u^{\mathcal{A}^{(k)}}(z_2) \right]. \quad (4.27)$$

Therefore, $u^{\mathcal{A}^{(i)}}(z) - z^2$ is concave as infimum of affine functions, and thus continuous and has right and left derivatives.

1) $u^{\mathcal{A}^{(i)}}$ cancels only once. Let us fix $i \leq I$. Let us suppose that $u^{\mathcal{A}^{(i)}}$ has two zeros $z_1^* \neq z_2^*$. **H1** implies that $(i,i) \in C^{(i)}$. Then, we deduce from (C') that:

$$u^{\mathcal{A}^{(i)}}(z) \leq \inf_{z_1,z_2} \left(z - \frac{z_1+z_2}{2}\right)^2 + u^{\mathcal{A}^{(i)}}(z_1) + u^{\mathcal{A}^{(i)}}(z_2).$$

In particular, for $z = \frac{z_1^*+z_2^*}{2}, z_1 = z_1^*, z_2 = z_2^*$, we obtain

$$u^{\mathcal{A}^{(i)}}(\frac{z_1^*+z_2^*}{2}) \leq 0. \quad (4.28)$$

As $u^{\mathcal{A}^{(i)}}$ is non-negative, the midpoint between two zeros of $u^{\mathcal{A}^{(i)}}$ is also a zero of $u^{\mathcal{A}^{(i)}}$. $u^{\mathcal{A}^{(i)}}$ is also continuous from the previous point, therefore, we deduce that $u^{\mathcal{A}^{(i)}}$ cancels on $[z_1^*, z_2^*]$. The latter violates the assumption that $u^{\mathcal{A}^{(i)}}$ has a zero set of measure 0. Because it is also not empty, we get that $u^{\mathcal{A}^{(i)}}$ cancels exactly once, in a point that we denote z_i^*.

2) The zero of $u^{\mathcal{A}^{(i)}}$ coincides with the zero of $u^{\mathcal{A}^{(j)}}$: $z_i^* = z_j^*$. First, let us consider the case where $(i,j) \in (1,I)^2$ is such that $\mathcal{A}^{(i)}$ and $u^{\mathcal{A}^{(j)}}$ are linked by a vertex in the graph $\mathcal{G}$. Then, we deduce that $(i,j) \in C^{(i)}$ or $(i,j) \in C^{(j)}$. We can assume the first without loss of generality. Similarly as the first part of the proof, we deduce that

$$u^{\mathcal{A}^{(i)}}(z) \leq \inf_{z_1,z_2} \left(z - \frac{z_1+z_2}{2}\right)^2 + u^{\mathcal{A}^{(i)}}(z_1) + u^{\mathcal{A}^{(j)}}(z_2).$$

Consequently, the midpoint between z_i^* and z_j^* is a zero of $u^{\mathcal{A}^{(i)}}$, which is necessarily z_i^*, which implies that $z_i^* = z_j^*$.

Let us now show the same for every couple (i,j) not necessarily linked by a vertex in $\mathcal{G}$. **H2** implies that there exists a path of vertices between $u^{\mathcal{A}^{(i)}}$ and $u^{\mathcal{A}^{(j)}}$. As we showed that for every pair of nodes connected by a vertex, the zeros of their function is the same point, that property also holds for the extremities of the path of vertices, hence $z_i^* = z_j^*$. We denote z^* the common zero.

3) Convex Legendre conjugates $u^{\hat{\mathcal{A}}^{(i)}}(y) = \sup_z (z - z^*)y - u^{\mathcal{A}^{(i)}}(z)$. Let us show that (C') implies that the convex Legendre conjugate satisfies

$$\forall y \in \mathbb{R}, \quad u^{\hat{\mathcal{A}}^{(i)}}(y) = \frac{y^2}{4} + \max_{(j,k)\in C^{(i)}} \left[u^{\hat{\mathcal{A}}^{(j)}}\left(\frac{y}{2}\right) + u^{\hat{\mathcal{A}}^{(k)}}\left(\frac{y}{2}\right) \right]. \quad (4.29)$$

Using (4.27) and commuting the sup, we obtain, for $y \in \mathbb{R}$,

$$u^{\hat{\mathcal{A}}^{(i)}}(y) = \sup_z \left[(z-z^*)y - \min_{(j,k)\in C^{(i)}} \inf_{z_1,z_2} \left(\left(z - \frac{z_1+z_2}{2} \right)^2 + u^{\mathcal{A}^{(j)}}(z_1) + u^{\mathcal{A}^{(k)}}(z_2) \right) \right]$$
$$= \max_{(j,k)\in C^{(i)}} \left[\sup_{z_1,z_2} \left(-u^{\mathcal{A}^{(j)}}(z_1) - u^{\mathcal{A}^{(k)}}(z_2) + \sup_z (z-z^*)y - \left(z - \frac{z_1+z_2}{2} \right)^2 \right) \right]. \tag{4.30}$$

Moreover, a straight-forward calculus shows that the $\sup_z$ is reached at $z = \frac{y+z_1+z_2}{2}$, which leads to

$$\begin{aligned} \sup_z (z-z^*)y - \left(z - \frac{z_1+z_2}{2} \right)^2 &= \left(\frac{y+z_1+z_2}{2} - z^* \right) y - \frac{y^2}{4} \\ &= \frac{y^2}{4} + (z_1 - z^*)\frac{y}{2} + (z_2 - z^*)\frac{y}{2}. \end{aligned} \tag{4.31}$$

Combining (4.31) and (4.30) (the fact that $z^A = z^a = z^*$ plays a crucial part for the crossed term) leads to (4.29).

Moreover, we obtain classically that:

$$u^{\hat{\mathcal{A}}^{(i)}}(y) \geq (z^* - z^*)y - u^{\mathcal{A}^{(i)}}(z^*) = 0 = u^{\hat{\mathcal{A}}^{(i)}}(0) \tag{4.32}$$

.

4) $\max_{i\leq I} u^{\hat{\mathcal{A}}^{(i)}} : y \mapsto \frac{y^2}{2}$**.** We obtain from (4.29) that:

$$\forall y \in \mathbb{R}, \quad \max_{i\leq I} u^{\hat{\mathcal{A}}^{(i)}}(y) = \frac{y^2}{4} + \max_{i\leq I} \max_{(j,k)\in C^{(i)}} \left[u^{\hat{\mathcal{A}}^{(j)}}\left(\frac{y}{2}\right) + u^{\hat{\mathcal{A}}^{(k)}}\left(\frac{y}{2}\right) \right]. \tag{4.33}$$

For $y \in \mathbb{R}$, let $i_0 \leq I$ be such that $\max_{i\leq I} u^{\hat{\mathcal{A}}^{(i)}}\left(\frac{y}{2}\right) = u^{\hat{\mathcal{A}}_{i_0}}\left(\frac{y}{2}\right)$. **H1** implies in particular $(i_0, i_0) \in C^{(i_0)}$ and therefore, the maximum of the r.h.s of (4.33) is reached in $2u^{\hat{\mathcal{A}}_{i_0}}\left(\frac{y}{2}\right)$. Consequently, we deduce that

$$\forall y \in \mathbb{R}, \quad \max_{i\leq I} u^{\hat{\mathcal{A}}^{(i)}}(y) = \frac{y^2}{4} + 2\max_{i\leq I} u^{\hat{\mathcal{A}}^{(i)}}\left(\frac{y}{2}\right). \tag{4.34}$$

Moreover, one can notice that

$$\begin{aligned} \forall y \in \mathbb{R}, \quad \max_{i\leq I} u^{\hat{\mathcal{A}}^{(i)}}(y) &= \max_{i\leq I} \max_{z\in\mathbb{R}} (z-z^*)y - u^{\mathcal{A}^{(i)}}(z) \\ &= \max_{z\in\mathbb{R}} (z-z^*)y - \min_{i\leq I} u^{\mathcal{A}^{(i)}}(z) \\ &= \left(\min_{i\leq I} u^{\hat{\mathcal{A}}^{(i)}} \right)(y). \end{aligned}$$

Therefore, $\max_{i\leq I} u^{\hat{\mathcal{A}}^{(i)}}$ is a convex continuous function that has left and right derivative everywhere, in particular in 0. Hence, iterating (4.34) implies first that:

$$\forall y > 0 \quad (\text{resp.} < 0), \quad \max_{i\leq I} u^{\hat{\mathcal{A}}^{(i)}}(y) = \frac{y^2}{2} + \beta\, y \quad (\text{resp. } \alpha\, y), \tag{4.35}$$

where $(\alpha, \beta) = \left(\max_{i \leq I} u^{\hat{\mathcal{A}}^{(i)}}{}'(0^-), \max_{i \leq I} u^{\hat{\mathcal{A}}^{(i)}}{}'(0^+) \right)$. From (4.32), we deduce that the $\alpha \leq 0 \leq \beta$. Since $\max_{i \leq I} u^{\hat{\mathcal{A}}^{(i)}}$ is the convex conjugate of $\min_{i \leq I} u^{\mathcal{A}^{(i)}}$, we compute that the convex bi-conjugate of $\min_{i \leq I} u^{\mathcal{A}^{(i)}}$ is

$$z \mapsto \begin{cases} \frac{(z-z^*-\alpha)^2}{2} & \text{if } z < z^* + \alpha \\ 0 & \text{if } z^* + \alpha \leq z \leq z^* + \beta \\ \frac{(z-z^*-\beta)^2}{2} & \text{if } z > z^* + \beta. \end{cases} \tag{4.36}$$

As the convex bi-conjugate of $\min_{i \leq I} u^{\mathcal{A}^{(i)}}$ is the lower convex envelope of $\min_{i \leq I} u^{\mathcal{A}^{(i)}}$, the two of them are equal at the extremal points of its graph, namely for $z = z^* + \alpha$ and $z = z^* + \beta$. We deduce from (4.36) that

$$\min_{i \leq I} u^{\mathcal{A}^{(i)}}(z^* + \alpha) = \min_{i \leq I} u^{\mathcal{A}^{(i)}}(z^* + \beta) = 0.$$

Since all the $u^{\mathcal{A}^{(i)}}, i \leq I$ only cancels for $z = z^*$, we obtain that $\alpha = \beta = 0$ and (4.35) yields that $\max_{i \leq I} u^{\hat{\mathcal{A}}^{(i)}} : y \mapsto \frac{y^2}{2}$.

5) $\max_{i \leq I} u^{\hat{\mathcal{A}}^{(i)}} = \min_{i \leq I} u^{\hat{\mathcal{A}}^{(i)}}$**.** First let us state that $\min_{i \leq I} u^{\hat{\mathcal{A}}^{(i)}}$ is continuous as minimum of a finite number of continuous functions and that it is non-negative and reaches its minimum in 0, with $\min_{i \leq I} u^{\hat{\mathcal{A}}^{(i)}}(0) = 0$ (from (4.32)). Moreover, (4.29) implies that

$$\forall y \in \mathbb{R}, \quad \min_{i \leq I} u^{\hat{\mathcal{A}}^{(i)}}(y) \leq \frac{y^2}{4} + 2 \max_{i \leq I} u^{\hat{\mathcal{A}}^{(i)}}\left(\frac{y}{2}\right) = \frac{y^2}{2}. \tag{4.37}$$

Therefore $\min_{i \leq I} u^{\hat{\mathcal{A}}^{(i)}}$ has left and right derivatives in 0, and $\min_{i \leq I} u^{\hat{\mathcal{A}}^{(i)}}{}'(0^+) = \min_{i \leq I} u^{\hat{\mathcal{A}}^{(i)}}{}'(0^-) = 0$. Furthermore, (4.29) also implies that

$$\forall y \in \mathbb{R}, \quad \min_{i \leq I} u^{\hat{\mathcal{A}}^{(i)}}(y) \geq \frac{y^2}{4} + 2 \min_{i \leq I} u^{\hat{\mathcal{A}}^{(i)}}\left(\frac{y}{2}\right).$$

Iterating the last inequality, and knowing that

$$\min_{i \leq I} u^{\hat{\mathcal{A}}^{(i)}}(0) = \min_{i \leq I} u^{\hat{\mathcal{A}}^{(i)}}{}'\left(0^+\right) = \min_{i \leq I} u^{\hat{\mathcal{A}}^{(i)}}{}'(0^-) = 0,$$

leads to

$$\forall y \in \mathbb{R}, \quad \min_{i \leq I} u^{\hat{\mathcal{A}}^{(i)}}(y) \geq \frac{y^2}{2} = \max_{i \leq I} u^{\hat{\mathcal{A}}^{(i)}}(y).$$

Consequently, we deduce that $\min_{i \leq I} u^{\hat{\mathcal{A}}^{(i)}} = \max_{i \leq I} u^{\hat{\mathcal{A}}^{(i)}}$.

End of proof. The last result implies that

$$\forall i \leq I, \quad \forall y \in \mathbb{R}, \quad u^{\hat{\mathcal{A}}^{(i)}}(y) = \max_{i \leq I} u^{\hat{\mathcal{A}}^{(i)}}(y) = \frac{y^2}{2}.$$

From the latter we compute the bi-conjugates $u^{\hat{\hat{\mathcal{A}}}^{(i)}} : z \mapsto \frac{(z-z^*)^2}{2}$. Since $z \mapsto \frac{z-z^*}{2}$ is strictly convex and it is the lower convex envelope of $u^{\mathcal{A}^{(i)}}$, we obtain that

$$\forall i \leq I, \quad \forall z \in \mathbb{R}, \quad u^{\mathcal{A}^{(i)}}(z) = \frac{(z-z^*)^2}{2}.$$

□

4.C Formal justification of the constraints (C) on the main terms u_0^A and u_0^a

We drop the index i indicating the habitat and the time dependence t for this appendix for the sake of simpler notations.

Let us first formally justify that U_0^A and U_0^a are positive almost everywhere and cancelling somewhere. As we are interested in the maintenance of the polymorphism at the major locus, we consider that no major allele has yet fixed. Hence, N_ε^A and N_ε^a need to remain positive and bounded when ε vanishes. Using the Hopf-Cole transforms on n_ε^A and n_ε^a (4.5) along with the formal Taylor expansions (4.6) on U_ε^A and U_ε^a leads to

$$N_\varepsilon^A = \int_{\mathbb{R}} n_\varepsilon^A(z')\,dz' = \int_{\mathbb{R}} \frac{1}{\sqrt{2\pi}\varepsilon} e^{-\frac{U_\varepsilon^A(z')}{\varepsilon^2}}\,dz' = \int_{\mathbb{R}} \frac{1}{\sqrt{2\pi}\varepsilon} e^{-\frac{u_0^A(z')}{\varepsilon^2}} e^{-u_1^A+\varepsilon^2 v_\varepsilon^A}\,dz'. \tag{4.38}$$

If we assume that the residues u_1^A and v_ε^A stay bounded when ε vanishes (as [Calvez, Garnier, and Patout 2019] suggests it), then (4.38) implies that u_0^A must be non-negative for N_ε^A to remain bounded when ε vanishes. For N_ε^A not to vanish asymptotically, u_0^A must cancel. Moreover, for any interval $I \subset \mathbb{R}$, u_0^A cannot cancel on I, or we would have:

$$N_\varepsilon^A > \int_I \frac{1}{\sqrt{2\pi}\varepsilon} e^{\frac{1}{\varepsilon^2}} e^{-u_1^A+\varepsilon^2 v_\varepsilon^A}\,dz' \to +\infty.$$

So u_0^A is positive almost everywhere, and cancelling somewhere. The same holds for u_0^a.

Now, for determining the constraints (C), let us notice that if we divide the r.h.s of the first equality of (4.3) by $n_\varepsilon^A(z)$, the reproduction term $\frac{\mathcal{B}_\varepsilon^A(n_\varepsilon^A,n_\varepsilon^a)(z)}{n_\varepsilon^A(z)}$ has to remain positive and bounded for all $z \in \mathbb{R}$ when ε vanishes for the effect of reproduction to remain well-balanced with selection, migration and competition. We assume henceforth that (4.6) is the correct ansatz (as suggested by Calvez, Garnier, and Patout 2019). Using the Hopf-Cole transforms on n_ε^A and n_ε^a (4.5) along with the formal Taylor expansions (4.6) on U_ε^A and U_ε^a in (4.4) leads to

$$\frac{\mathcal{B}_\varepsilon^A(n_\varepsilon^A,n_\varepsilon^a)(t,z)}{n_\varepsilon^A(z)} = \frac{\mathcal{B}_\varepsilon^A(n_\varepsilon^A,n_\varepsilon^a)(z)}{\frac{1}{\sqrt{2\pi}\varepsilon} e^{-\frac{u_0^A(z)}{\varepsilon^2}} e^{-u_1^A(z)+\mathcal{O}(\varepsilon^2)}}$$

$$= \frac{\sqrt{2}}{N_\varepsilon^A} \times$$

$$\left[\int_{\mathbb{R}^2} \exp\left(\frac{1}{\varepsilon^2}\left[u_0^A(z) - \left(z - \frac{z_1+z_2}{2}\right)^2 - u_0^A(z_1) - u_0^A(z_2)\right]\right) \exp\left(u_1^A(z) - u_1^A(z_1) - u_1^A(z_2) + \mathcal{O}(\varepsilon^2)\right) dz_1 dz_2\right.$$

$$\left. + \int_{\mathbb{R}^2} \exp\left(\frac{1}{\varepsilon^2}\left[u_0^A(z) - \left(z - \frac{z_1+z_2}{2}\right)^2 - u_0^A(z_1) - u_0^a(z_2)\right]\right) \exp\left(u_1^A(z) - u_1^A(z_1) - u_1^a(z_2) + \mathcal{O}(\varepsilon^2)\right) dz_1 dz_2\right].$$

As N_ε^A remains bounded and does not vanish asymptotically, we need the maximum of the two integrals nor to vanish, nor to diverge to infinity when ε vanishes, for all $z \in \mathbb{R}$. Therefore the maximum of the terms into brackets that are multiplied by $\frac{1}{\varepsilon^2}$ needs to be null for all $z \in \mathbb{R}$:

$$\forall z \in \mathbb{R}, \quad \max\Big[\sup_{z_1,z_2} u_0^A(z) - \left(z - \frac{z_1+z_2}{2}\right)^2 - u_0^A(z_1) - u_0^A(z_2), \\ \sup_{z_1,z_2} u_0^A(z) - \left(z - \frac{z_1+z_2}{2}\right)^2 - u_0^A(z_1) - u_0^a(z_2)\Big] = 0,$$

which is the first constraint of (C). The same holds for $\frac{\mathcal{B}_\varepsilon^{\dashv}(n_\varepsilon^a, n_\varepsilon^A)(z)}{n_\varepsilon^a(z)}$, which gives the second constraint of (C).

4.D Individual-based simulations with $L = 50$ loci and $\sigma_{LE} = 0.2$

In this appendix, we show that our findings hold when considering a smaller number of loci involved in the quantitative background ($L = 50$ instead of 200), with increased relative effect ($\sigma_{LE} = 0.2$ instead of 0.1), so that the trait range $[-\eta - \sigma_{LE}\sqrt{L}, \eta + \sigma_{LE}\sqrt{L}] \approx [-\eta - 1.4, \eta + 1.4]$ extends beyond the local optima (-1 and 1) even in the absence of major locus effects. We display the results of the IBS with symmetrical initial subpopulation sizes in Fig. 4.9 and with asymmetrical initial subpopulation sizes in Fig. 4.10. Note that the right panel of each figure does not change from Fig. 4.6 and Fig. 4.7, because the control case does not depend on the number of loci, but we choose to display it anyway for consistency of comparison. One can notice that the time to fixation at the major effect locus in presence of quantitative background at weak (Fig. 4.9e, Fig. 4.10a) and strong selection (Fig. 4.9e, Fig. 4.10e) is reduced compared to when the quantitative background comes from a larger number of loci (Fig. 4.6, Fig. 4.7). Moreover, the sensitivity of the numerical resolutions of (4.1) with regard to symmetrical initial states is more pronounced here.

Acknowledgements

L.D thanks Sepideh Mirrahimi for valuable discussions and comments, and Florence Débarre and Barbara Neto-Bradley for insightful conversations. L.D has received partial funding from the ANR project DEEV ANR-20-CE40-0011-01 and a Mitacs Globalink Research Award. S.P.O. has received funding from the NSERC Discovery Grant: RGPIN-2016-03711. This project has received funding from the European Research Council (ERC) under the European Union's Horizon 2020 research and innovation programm (grant agreement No 865711).

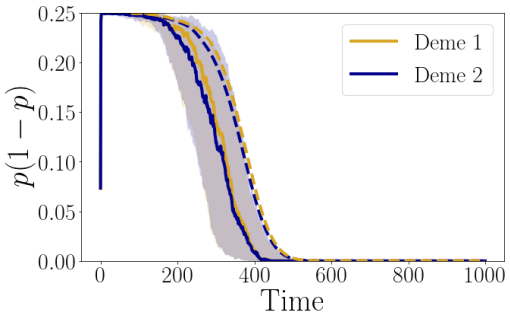

(a) Major locus with infinitesimal background: weak selection ($g = 0.1$). Polymorphism at the major locus is lost after around 400 time units.

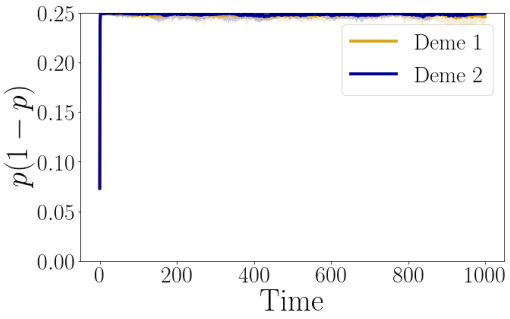

(b) Control case without infinitesimal background: weak selection ($g = 0.1$). Polymorphism at the major locus is maintained over the course of all simulations.

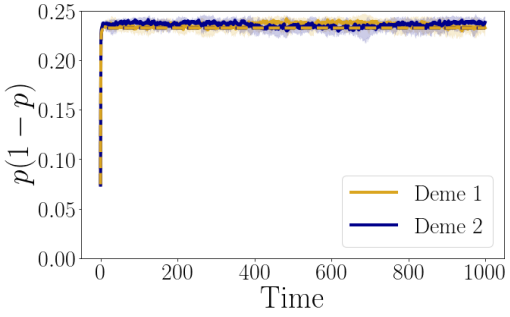

(c) Major locus with infinitesimal background: intermediate selection ($g = 0.5$). Polymorphism at the major locus is maintained over the course of all simulations.

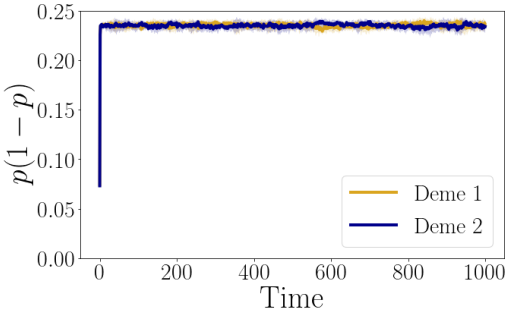

(d) Control case without infinitesimal background: intermediate selection ($g = 0.5$). Polymorphism at the major locus is maintained over the course of all simulations.

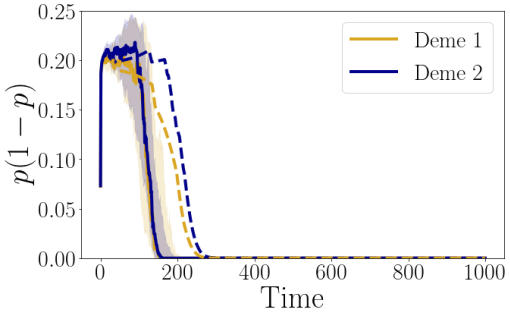

(e) Major locus with infinitesimal background: strong selection ($g = 1$). Polymorphism at the major locus is lost after around 160 time units.

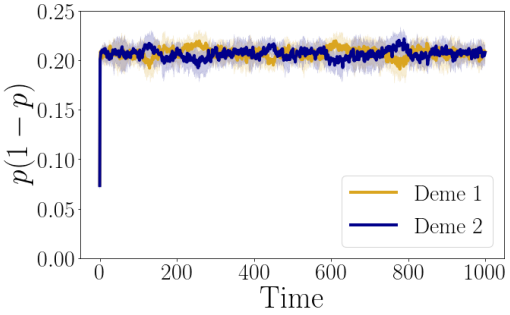

(f) Control case without infinitesimal background : strong selection ($g = 1$). Polymorphism at the major locus is maintained over the course of all simulations.

Figure 4.9: **Variance at the major locus across time with a quantitative background of $L = 50$ loci (left panel), for increasing selection (top to bottom: $g = 0.1,\ 0.5,\ 1$) at a fixed rate of migration ($m = 0.8$), and symmetrical initial subpopulation sizes**. p denotes the local frequency of the major allele A. The left panel is obtained with both a major locus ($\eta = 1/2$) and an infinitesimal background of 50 loci, whereas only the major locus is present in the right panel. For each subfigure, 20 replicates simulations were run per set of parameters, according to the setting explained in Section 4.6. In each subfigure, the solid line represents the median trajectory and the shaded area indicates the 0.2 and 0.8 quantiles. The dashed lines represents the median trajectories of the numerical resolutions of the deterministic model (4.1). This figure confirms that polymorphism of the major-effect locus is maintained only when selection is intermediate in strength in presence of a infinitesimal background.

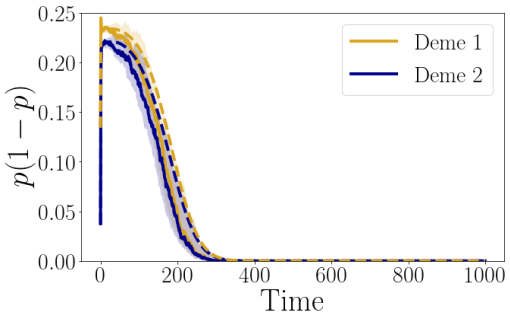

(a) Major locus with infinitesimal background: weak selection ($g = 0.1$). Polymorphism at the major locus is lost after around 300 time units.

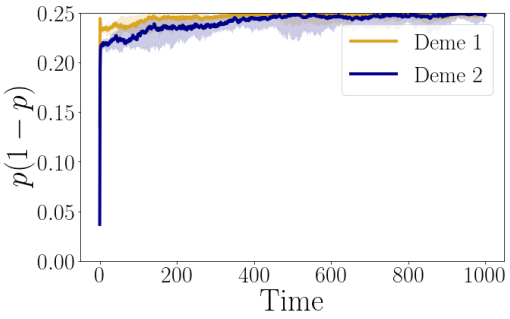

(b) Control case without infinitesimal background: weak selection ($g = 0.1$). Polymorphism at the major locus is maintained over the course of all simulations.

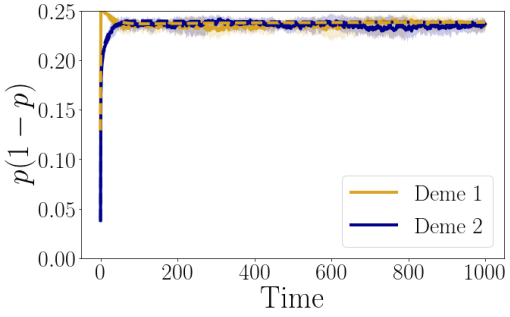

(c) Major locus with infinitesimal background: intermediate selection ($g = 0.5$). Polymorphism at the major locus is maintained over the course of all simulations.

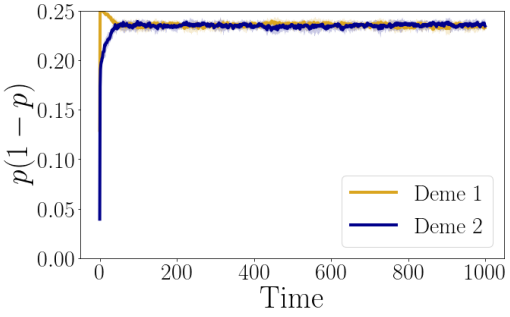

(d) Control case without infinitesimal background: intermediate selection ($g = 0.5$). Polymorphism at the major locus is maintained over the course of all simulations.

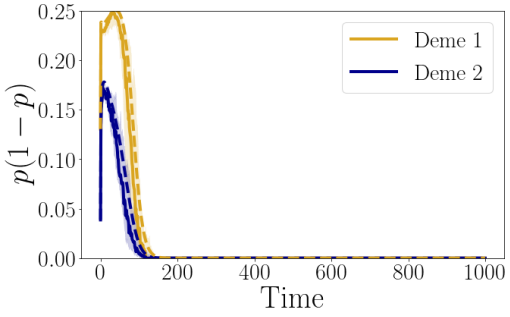

(e) Major locus with infinitesimal background: strong selection ($g = 1$). Polymorphism at the major locus is lost after around 100 time units.

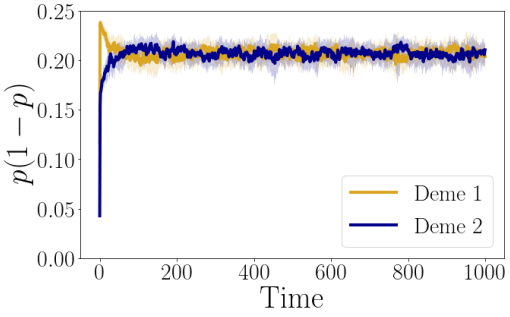

(f) Control case without infinitesimal background : strong selection ($g = 1$). Polymorphism at the major locus is maintained over the course of all simulations.

Figure 4.10: **Variance at the major locus across time with a quantitative background of $L = 50$ loci (left panel), for increasing selection (top to bottom: $g = 0.1,\ 0.5,\ 1$) at a fixed rate of migration ($m = 0.8$), with asymmetrical initial subpopulation sizes**. p denotes the local frequency of the major allele A. The left panel is obtained with both a major locus ($\eta = 1/2$) and an infinitesimal background of 50 loci, whereas only the major locus is present in the right panel. For each subfigure, 20 replicates simulations were run per set of parameters, according to the setting explained in Section 4.6. In each subfigure, the solid line represents the median trajectory and the shaded area indicates the 0.2 and 0.8 quantiles. The dashed lines represents the median trajectories of the numerical resolutions of the deterministic model (4.1). This figure confirms that polymorphism of the major-effect locus is maintained only when selection is intermediate in strength in presence of a infinitesimal background.

Chapter 5

Front propagation of a sexual population with evolution of dispersion: a formal analysis

The adaptation of biological species to their environment depends on their traits. When various biological processes occur (survival, reproduction, migration, *etc.*), the trait distribution may change with respect to time and space. In the context of invasions, when considering the evolution of a heritable trait that encodes the dispersive ability of individuals, the trait distribution develops a particular spatial structure that leads to the acceleration of the front propagation. That phenomenon is known as spatial sorting. Many biological examples can be cited like the bush cricket in Britain, the cane toad invasion in Australia or the common myna one in South Africa.

Adopting this framework, recent mathematical studies have led to highlight the influence of the reproductive mode on the front propagation. Asexual populations have been shown to spread with an asymptotic rate of $t^{3/2}$ in a minimal reaction-diffusion model, whereas the analogous rate for sexual populations is of $t^{5/4}$ (where t denotes the time). However, the precise description of the behaviour of the front propagation in the sexual case is still an open question.

The aim of this paper is to give precise approximations for large times of its position, as well as some features of the local trait distribution at the front. To do so, we solve explicitly the asymptotic problem derived formally. Numerical simulations are shown to confirm these calculations.

5.1 Introduction

Individuals can be more or less adapted to their environment, depending on their traits. Various processes shape the trait distributions: some of them intervene locally, like survival and reproduction, and others highly depend on the spatial structure of the environment, like migration. Biological invasions are an example of a process where the role of space is structuring. As the combination of locally limited amount of resources and large available inhabited space tends to drive individuals further away, the ability to explore can be selected upon. Morphological features can therefore evolve to increase dispersion: closer to the front of the invasion, cane toads in Australia tends to develop longer legs Phillips, Brown, Webb, et al. 2006, common myna birds in South Africa and *conocephalus discolor* bush cricket in Britain, larger wings Berthouly-Salazar et al. 2012; Thomas et al. 2001.

However, that process is not homogeneous in space: individuals with higher dispersal ability are typically located at the range expansion front. This phenomenon is called *spatial sorting*. Its relationship with the evolution of dispersion has been studied by biologists for the past two decades Birzu, Hallatschek, and Korolev 2018; Shine, Brown, and Phillips 2011; Thomas et al. 2001; Travis and Dytham 2002; Travis, Mustin, et al. 2009. More recently, mathematical studies have been quantifying its influence on the asymptotic speed of the invasion. Our model equation describes the effects of evolution of a trait $\boldsymbol{\theta} > 1$, which determines the dispersion rate, in space ($\boldsymbol{x} \in \mathbb{R}$) and through time ($\boldsymbol{t} \geq 0$) in a population subject to sexual reproduction and competition. The trait density $f(\boldsymbol{t}, \boldsymbol{x}, \boldsymbol{\theta})$ evolves according to:

$$\partial_{\boldsymbol{t}} \boldsymbol{f}(\boldsymbol{t}, \boldsymbol{x}, \boldsymbol{\theta}) = \boldsymbol{r}\,[\underbrace{\boldsymbol{B}[\boldsymbol{f}](\boldsymbol{t}, \boldsymbol{x}, \boldsymbol{\theta})}_{\text{reproduction}} - \underbrace{\boldsymbol{K}^{-1}\boldsymbol{\varrho}(\boldsymbol{t}, \boldsymbol{x})\boldsymbol{f}(\boldsymbol{t}, \boldsymbol{x}, \boldsymbol{\theta})}_{\text{competition}}] + \underbrace{\boldsymbol{\theta}\Delta_{\boldsymbol{x}}\boldsymbol{f}(\boldsymbol{t}, \boldsymbol{x}, \boldsymbol{\theta})}_{\text{dispersion}}, \tag{5.1}$$

for $\boldsymbol{\Delta_x}$ the Laplace operator with respect to $\boldsymbol{x}$.

When the dispersal rate is possibly unbounded, the relationship between the front propagation and sustained spatial sorting leads to an acceleration of front propagation Berestycki, Mouhot, and Raoul n.d.; Bouin, Calvez, et al. 2012; Bouin, Henderson, and Ryzhik 2017a; Calvez, Henderson, et al. 2022, contrary to the case of constant dispersion for which it is well established that the front expands asymptotically at constant speed Aronson and Weinberger 1978; Berestycki, Hamel, and Nadin 2008; Fang and Zhao 2011; Genieys, Volpert, and Auger 2006; Gourley 2000; Hamel and Ryzhik 2014; Mirrahimi and Raoul 2013.

To our knowledge, analytical results describing the asymptotic accelerating rate of propagation exist only for asexual (clonal) populations (*e.g.*, see Berestycki, Mouhot, and Raoul n.d.; Bouin, Henderson, and Ryzhik 2017a; Calvez, Henderson, et al. 2022), for which the reproduction operator in (5.1) is :

$$\boldsymbol{B}[\boldsymbol{f}] = \boldsymbol{f} + \boldsymbol{\sigma^2}\boldsymbol{\Delta_\theta}\,\boldsymbol{f},$$

for some constant $\boldsymbol{\sigma^2} \geq 0$ depending on the mutation variance and mutation rate and for $\boldsymbol{\Delta_\theta}$ the Laplace operator with respect to $\boldsymbol{\theta}$. In this case, the position of the population range asymptotically expands as $t^{3/2}$ (see Bouin, Calvez, et al. 2012; Berestycki, Mouhot, and Raoul n.d.; Bouin, Henderson, and Ryzhik 2017a; Calvez, Henderson, et al. 2022 for more details). Furthermore, the precise asymptotic position of the front obtained from (5.1) has been derived in Calvez, Henderson, et al. 2022, by specifying the prefactor term. The value of this prefactor is sensitive to how the competition is modelled : when it is local in trait, it has been shown to be equal to a larger value (Berestycki, Mouhot, and Raoul n.d.; Bouin, Henderson, and Ryzhik 2017a).

However, as reproductive mode is thought to potentially significantly influence the rate of propagation Williams, Hufbauer, and Miller 2019, we take interest into invasions of sexually reproducing populations. An analogous model as for asexual populations can be built using Fisher's infinitesimal model, a model of allelic segregation that has been studied and used for a century in quantitative genetics, a branch of evolutionary biology Barton, Etheridge, and Véber 2017; Bulmer 1971; Fisher 1919; Lange 1978; Tufto 2000; Turelli 2017; Turelli and Barton 1994. This model has also been used to model sexually reproducing populations in several integro-differential studies Calvez, Garnier, and Patout 2019; Mirrahimi and Raoul 2013; Raoul 2017, with the following reproduction operator in (5.1):

$$\boldsymbol{B}[\boldsymbol{f}](\boldsymbol{t},\boldsymbol{x},\boldsymbol{\theta}) = \iint_{(\boldsymbol{\theta_{\min}},\infty)^2} \mathcal{G}_{\boldsymbol{\lambda}}\left[\boldsymbol{\theta} - \frac{\boldsymbol{\theta}_1+\boldsymbol{\theta}_2}{2}\right] \frac{\boldsymbol{f}(\boldsymbol{t},\boldsymbol{x},\boldsymbol{\theta}_1)\,\boldsymbol{f}(\boldsymbol{t},\boldsymbol{x},\boldsymbol{\theta}_2)}{\boldsymbol{\varrho}(\boldsymbol{t},\boldsymbol{x})}\mathrm{d}\boldsymbol{\theta}_1\,\mathrm{d}\boldsymbol{\theta}_2.$$

It assumes that the trait of the offspring is given by the mean parental trait up to a random normal deviation given by $\mathcal{G}_{\boldsymbol{\lambda}}$ with constant segregational variance $\boldsymbol{\lambda^2}$. Using this model, the authors of the report Calvez, Crevat, et al. 2020 predicted and numerically confirmed an asymptotic invasion rate of $t^{5/4}$ for sexually reproducing populations.

However, to understand the complexity of the interplay between ecology and evolution in the dynamics of an invasion, the relationship between the propagation and the trait distribution has to be untangled. That requires to describe precisely the trait distribution and the effect of spatial sorting at the front of the invasion, which is the goal of this paper. First, we present our model and the explicit formula that we derive to approximate the position of the front propagation and its local trait distribution at large times (Section 5.2). Next, we present numerical simulations that confirm this formula (Section 5.3). Finally, we derive formally the limit problem for large times and find an explicit solution to it (Section 5.4).

5.2 Deterministic model

In this section, we present the integro - differential model that we use and state our formal result as an approximation of the solutions of the resulting equation. The population is described according to its location $\boldsymbol{x} \in \mathbb{R}$ and its dispersive trait $\boldsymbol{\theta} \in (\boldsymbol{\theta_{\min}}, +\infty)$, with $\boldsymbol{\theta_{\min}} > 0$. Here we are interested by the evolution of the density $\boldsymbol{f}(\boldsymbol{t},\boldsymbol{x},\boldsymbol{\theta})$ of individuals being at time $\boldsymbol{t} \geq 0$ at the location $\boldsymbol{x} \in \mathbb{R}$, presenting the trait $\boldsymbol{\theta}$. We also assume that, initially, the density is compactly supported.

Our model. The evolution of the density $\boldsymbol{f}(\boldsymbol{t},\boldsymbol{x},\boldsymbol{\theta})$ can be modeled with the following reaction - diffusion equation for all $\boldsymbol{t} > 0$, $\boldsymbol{x} \in \mathbb{R}$ and $\boldsymbol{\theta} > \boldsymbol{\theta_{\min}}$:

$$\partial_{\boldsymbol{t}}\boldsymbol{f}(\boldsymbol{t},\boldsymbol{x},\boldsymbol{\theta}) = \boldsymbol{r}\left[\boldsymbol{B}[\boldsymbol{f}](\boldsymbol{t},\boldsymbol{x},\boldsymbol{\theta}) - \boldsymbol{K}^{-1}\boldsymbol{\varrho}(\boldsymbol{t},\boldsymbol{x})\boldsymbol{f}(\boldsymbol{t},\boldsymbol{x},\boldsymbol{\theta})\right] + \boldsymbol{\theta}\Delta_{\boldsymbol{x}}\boldsymbol{f}(\boldsymbol{t},\boldsymbol{x},\boldsymbol{\theta}), \tag{5.2}$$

where $\boldsymbol{r} > 0$ and $\boldsymbol{K} > 0$ are fixed constants, and $\boldsymbol{\varrho}(\boldsymbol{t},\boldsymbol{x}) := \int_{\boldsymbol{\theta_{\min}}}^{\infty} \boldsymbol{f}(\boldsymbol{t},\boldsymbol{x},\boldsymbol{\theta})\,\mathrm{d}\boldsymbol{\theta}$ is the population size at $\boldsymbol{x} \in \mathbb{R}$ and time $\boldsymbol{t} > 0$. We will detail the reaction term $\boldsymbol{B}[\boldsymbol{f}]$ later. At first, let us discuss the modelling motivation of each term.

First, the term $\boldsymbol{r}\left[\boldsymbol{B}[\boldsymbol{f}](\boldsymbol{t},\boldsymbol{x},\boldsymbol{\theta}) - \boldsymbol{K}^{-1}\boldsymbol{\varrho}(\boldsymbol{t},\boldsymbol{x})\boldsymbol{f}(\boldsymbol{t},\boldsymbol{x},\boldsymbol{\theta})\right]$ is analogous to a logistic growth term that models *reproduction* and *competition*. More precisely, the reproduction term $\boldsymbol{B}[\boldsymbol{f}](\boldsymbol{t},\boldsymbol{x},\boldsymbol{\theta})$ represents the number of new individuals that are born with the trait $\boldsymbol{\theta}$ at time $\boldsymbol{t} \geq 0$ and position $\boldsymbol{x} \in \mathbb{R}$ and we will detail the modelling of the segregational process later. Moreover, at point $\boldsymbol{x} \in \mathbb{R}$ and at time $\boldsymbol{t} \geq 0$, there is a competition between individuals for resources, related to the parameter $\boldsymbol{K}$ which is a measure of the *carrying capacity* of the

environment. When the local population size at $\boldsymbol{x}$ is relatively small – $\boldsymbol{\varrho(t,x)} \ll \boldsymbol{K}$ – the local population disposes of enough resources to allow an exponential - like growth, while, if $\boldsymbol{\varrho(t,x)} \gg \boldsymbol{K}$, then competition between individuals is strong, and consequently the local population size decreases. The constant $\boldsymbol{r} > 0$ is therefore called *growth rate at low density.*

Then, the diffusion term $\boldsymbol{\theta\, \Delta_x f}$ models the *dispersion* phenomenon. Individuals are assumed to diffuse through space at each time t, at a rate given by the dispersive trait $\boldsymbol{\theta \geq \theta_{\min}}$. When $\boldsymbol{\theta}$ gets larger, it models situations like having longer legs or bigger wings, which potentially give an advantage to explore a new environment faster.

Finally, let us come back to the reproduction operator $\boldsymbol{B[f]}$. We consider a monoecious population in which the individuals breed randomly and only with those at the same location $\boldsymbol{x} \in \mathbb{R}$. At time $\boldsymbol{t}$, an individual with trait $\boldsymbol{\theta_1}$ finds a mate with trait $\boldsymbol{\theta_2}$ with the probability density equal to the trait frequency at position $\boldsymbol{x}$: $\boldsymbol{f(t,x,\theta_2)/\varrho(t,x)}$. To model the segregation, we use Fisher's infinitesimal model, which classically states that the offspring trait differs from the mean parental trait $(\boldsymbol{\theta_1} + \boldsymbol{\theta_2})/2$ according to a normal distribution with a segregrational variance $\boldsymbol{\lambda^2} > 0$ assumed to be constant and independent of the parental trait values. These assumptions imply the following formulation of the reproduction term:

$$\boldsymbol{B[f](t,x,\theta)} = \iint_{(\boldsymbol{\theta_{\min}},\infty)^2} \mathcal{G}_{\boldsymbol{\lambda}} \left[\boldsymbol{\theta} - \frac{\boldsymbol{\theta_1} + \boldsymbol{\theta_2}}{2}\right] \frac{\boldsymbol{f(t,x,\theta_1)\, f(t,x,\theta_2)}}{\boldsymbol{\varrho(t,x)}} \mathrm{d}\boldsymbol{\theta_1}\, \mathrm{d}\boldsymbol{\theta_2}.$$

The term $\mathcal{G}_{\boldsymbol{\lambda}}[\boldsymbol{\theta} - (\boldsymbol{\theta_1} + \boldsymbol{\theta_2})/2]$, symbolizing the stochasticity of the segregation process, is defined as a normalized Gaussian density with variance $\boldsymbol{\lambda^2} > 0$, that is:

$$\mathcal{G}_{\boldsymbol{\lambda}}(\boldsymbol{\theta}) := \frac{1}{\sqrt{2\pi\boldsymbol{\lambda}^2}} \exp\left[-\frac{\boldsymbol{\theta}^2}{2\boldsymbol{\lambda}^2}\right]. \tag{5.3}$$

Let us rescale the equation by setting :

$$t = \boldsymbol{r}\boldsymbol{t}, \qquad x = \sqrt{\frac{\boldsymbol{r}}{\boldsymbol{\theta_{\min}}}}\,\boldsymbol{x}, \qquad \theta = \frac{\boldsymbol{\theta}}{\boldsymbol{\theta_{\min}}}, \quad \text{and} \quad f(t,x,\theta) = \frac{\boldsymbol{\theta_{\min}}}{\boldsymbol{K}} \boldsymbol{f(t,x,\theta)}.$$

Then, we can simplify the previous PDE into:

$$\partial_t f(t,x,\theta) = B[f](t,x,\theta) - \varrho(t,x) f(t,x,\theta) + \theta \Delta_x f(t,x,\theta), \tag{5.4}$$

with the rescaled population size:

$$\varrho(t,x) = \int_1^\infty f(t,x,\theta)\, \mathrm{d}\theta.$$

By this simplification, the reproduction term is:

$$B[f](t,x,\theta) = \iint_{(1,\infty)^2} \mathcal{G}_\lambda \left[\theta - \frac{\theta_1 + \theta_2}{2}\right] f(t,x,\theta_1)\, \frac{f(t,x,\theta_2)}{\varrho(t,x)}\, \mathrm{d}\theta_1\, \mathrm{d}\theta_2, \tag{5.5}$$

where $\mathcal{G}_\lambda$ is given by (5.3), and $\lambda = \boldsymbol{\lambda}/\boldsymbol{\theta_{\min}}$. One can notice the truncation at the bottom level $\theta_{\min} = 1$, chosen for the sake of simplicity (note that $\theta_{\min}$ can only take positive values), which does not influence the long time asymptotics in the subsequent analysis as θ is expected to take large values at the front.

Main result. In this paper, we denote the interval $[xa, xb]$ by $x \cdot [a,b]$, for some $x \in \mathbb{R}$ and compact interval $[a,b]$.Moreover, as some computations are only formal, we state our main result as a conjecture:

Conjecture 1. *Define the constant*

$$y_c = 4\left(\frac{\lambda}{3}\right)^{1/2}. \tag{5.6}$$

There exists an interval of trait values $\delta_0 \leq 1$ such that, for all $0 < \delta \leq \delta_0$, the density f at large time $t \geq 0$ can be approximated by:

$$f(t,x,\theta) = \begin{cases} \frac{1}{2\sqrt{\pi}\lambda} \exp\left[-\frac{1}{4\lambda^2}\left[\theta - \bar{\theta}^{behind}(x)\right]^2 + \underset{\delta\to 0}{\mathcal{O}}(\delta) + \underset{t\to\infty}{\mathcal{O}}(\frac{1}{t}) \right], \\ \qquad\qquad \text{for } x \leq y_c\, t^{5/4},\ \theta \in \bar{\theta}^{behind} \cdot [1-\delta, 1+\delta], \\ \exp\left[\left(1 - \left(\frac{x}{y_c\, t^{5/4}} \right)^{4/3} \right) t \right] \\ \qquad \times \frac{1}{2\sqrt{\pi}\lambda} \exp\left[-\frac{1}{4\lambda^2}\left[\theta - \bar{\theta}^{ahead}(t,x)\right]^2 + \underset{\delta\to 0}{\mathcal{O}}\left(\delta + \delta^2 \left[\frac{x}{t^{5/4}}\right]^{8/3} \right) + \underset{t\to\infty}{\mathcal{O}}(\frac{1}{t}) \right], \\ \qquad\qquad \text{for } x \geq y_c\, t^{5/4},\ \theta \in \bar{\theta}^{ahead} \cdot [1-\delta, 1+\delta]. \end{cases}$$

The approximated mean dispersal trait behind and ahead of the front are given by:

$$\begin{cases} \bar{\theta}^{behind}(x) = \lambda^{4/5}(6x^2)^{1/5}, & x \leq y_c t^{5/4}, \\ \bar{\theta}^{ahead}(t,x) = \left(3\lambda^2 \frac{x^2}{2t}\right)^{1/3}, & x \geq y_c t^{5/4}. \end{cases} \tag{5.7}$$

For $x \geq y_c\, t^{5/4}$, we call the coefficient $\exp\left[\left(1 - \left(\frac{x}{y_c\, t^{5/4}} \right)^{1/3} \right) t \right]$ *the prefactor of the trait distribution, which is of the form* $\exp\left[-c\left(\frac{x}{y_c\, t^{5/4}} \right) t \right]$*, where the function c is positive and increasing on $]1, +\infty[$.*

The justification of this conjecture is postponed to Section 5.4.

Conjecture 1 yields that at each time $t \geq 0$ large enough, the propagating front is at the position:

$$X(t) \approx y_c\, t^{5/4} = 4\left(\frac{\lambda}{3}\right)^{1/2} t^{5/4}. \tag{5.8}$$

Additionally, at large time t and all space position $x \in \mathbb{R}$, the dispersive trait is normally distributed, with variance $2\lambda^2$. Behind the front, *i.e.*, at all position $x \ll X(t)$, the mean of the dispersive trait can be approximated by the value of $\bar{\theta}^{behind}$ indicated at the first line of (5.7) while ahead of the front, *i.e.*, at all position $x \gg X(t)$, it can be approximated by the value of $\bar{\theta}^{ahead}$ indicated at the second line of (5.7).

Moreover, the prefactor of the distribution trait, $\exp\left[-c\left(\frac{y}{y_c} \right) t \right]$, with $c > 0$ increasing on $]1, +\infty[$ and $y = t^{-5/4}x$, indicates that, ahead of the front, the population size presumably decreases with regard to the rescaled space variable y at a given time $t > 0$.

5.3 Simulations and validation

In this section, we display numerical simulations, in order to validate the approximation of the solution of the Eq. (5.4) provided by Conjecture 1. The initial distribution used for simulation is assumed to be a truncated Gaussian distribution:

$$f(0,x,\theta) = \sqrt{\frac{2}{\pi}} \exp\left[-\frac{x^2 + (1-\theta)^2}{2} \right] \mathbf{1}_{\theta \geq 1}, \tag{5.9}$$

with $\mathbf{1}_{\theta\geq 1}$ the characteristic function of $\{\theta \geq 1\}$. The segregational variance λ^2 is taken equal to $1/2$. The discretization of the sexual reproduction term $B[f]$ represents the biggest challenge for the simulations, in comparison to the asexual case (see Calvez, Crevat, et al. 2020).

5.3.1 Scheme

We consider $x_{\max} \geq 0$ and $\theta_{\max} \geq 1$ so that we work with tuples (x, θ) in the bounded domain $[0, x_{\max}] \times [1, \theta_{\max}]$, discretized with the meshes $(x_i)_{1\leq i\leq N_x}$ and $(\theta_j)_{1\leq j\leq N_\theta}$, respectively of step length $\delta x > 0$ and $\delta\theta > 0$. As for the time discretization, let $\delta t > 0$ be a time step length, and let us define for all $n \in \mathbb{N}$, $t_n := n\,\delta t$. We denote by A_x^N the matrix of the discrete Laplace operator in x of size N_x with Neumann boundary condition at $x = 0$ and Dirichlet boundary condition at $x = x_{\max}$:

$$A_x^N = \frac{1}{\delta x^2} \begin{pmatrix} -1 & 1 & & & (0) \\ 1 & -2 & 1 & & \\ & \ddots & \ddots & \ddots & \\ & & 1 & -2 & 1 \\ (0) & & & 1 & -2 \end{pmatrix} \in \mathcal{M}_{N_x}(\mathbb{R}),$$

and the diagonal matrix:

$$D_\theta = \begin{pmatrix} \theta_1 & & (0) \\ & \ddots & \\ (0) & & \theta_{N_\theta} \end{pmatrix} \in \mathcal{M}_{N_\theta}(\mathbb{R}).$$

Futhermore, we introduce a 3D hypermatrix $G_\theta \in M_{N_\theta,N_\theta,N_\theta}(\mathbb{R})$ such that:

$$\forall i, j, k,\ G_\theta(i, j, k) = \mathcal{G}_\lambda \left[\theta_k - \frac{\theta_i + \theta_j}{2}\right],$$

representing the discretization of the segregation kernel ($\mathcal{G}_\lambda$ given by (5.3)).

For all $n \in \mathbb{N}$, we approximate $(f(t_n, x_i, \theta_j))_{1\leq i\leq N_x,1\leq j\leq N_\theta}$ by a matrix:

$$F^n = \left(F_{ij}^n\right)_{1\leq i\leq N_x,1\leq j\leq N_\theta} \in \mathcal{M}_{N_x,N_\theta}(\mathbb{R}),$$

and the population size $(\varrho(t_n, x_i))_{1\leq i\leq N_x}$ by the vector:

$$\widetilde{\varrho}_i^n := \sum_{k=1}^{N_\theta} F_{i,k}^n\,\delta\theta \approx \varrho(t_n, x_i),$$

using the following scheme. At each time iteration n,

1. For every index $1 \leq k \leq N_\theta$, we compute the vector $V_{k,l}^n$ defined by:

$$\forall l,\ V_{k,l}^n := \delta\theta^2 \left[F^n\, G_\theta(\cdot, \cdot, k)\, (F^n)^T\right]_{ll}.$$

We can check that $V^n_{k,l}$ is the discretization of the reproduction integral term:

$$\begin{aligned} V^n_{k,l} &= \delta\theta^2 \sum_{i,j=1}^{N_\theta} F^n_{l,i} G_\theta(i,j,k) F^n_{l,j}, \\ &\approx \delta\theta^2 \sum_{i,j=1}^{N_\theta} f(t_n, x_l, \theta_i) \mathcal{G}_\lambda \left[\theta_k - \frac{\theta_i + \theta_j}{2}\right] f(t_n, x_l, \theta_j), \\ &\approx \iint_{(1,\infty)^2} f(t_n, x_l, \theta_1) \mathcal{G}_\lambda \left[\theta_k - \frac{\theta_1 + \theta_2}{2}\right] f(t_n, x_l, \theta_2)\, \mathrm{d}\theta_1 \mathrm{d}\theta_2. \end{aligned}$$

Now to compute the reproduction matrix $\mathrm{Mat}_{\mathrm{Reprod}} \in \mathcal{M}_{N_x, N_\theta}(\mathbb{R})$, we need to divide the previous quantities by the corresponding $\widetilde{\varrho}^n_i$. To be consistent, we set:

$$\forall i,k,\ \mathrm{Mat}^n_{\mathrm{Reprod}}(i,k) = \begin{cases} V^n_{k,i}/\widetilde{\varrho}^n_i, & \text{if } \widetilde{\varrho}^n_i > 0, \\ 0, & \text{else.} \end{cases}$$

2. We define the diagonal matrix $D^n_\varrho := \mathrm{diag}\left((\widetilde{\varrho}^n_i)_{1\le i\le N_x}\right) \in \mathcal{M}_{N_x}(\mathbb{R})$.

3. We approximate in time using an explicit Euler scheme that is for all $n \in \mathbb{N}$:

$$F^{n+1} := F^n + \delta t \left[A^N_x \times F^n \times D_\theta + r\left(\mathrm{Mat}^n_{\mathrm{Reprod}} - K^{-1} \times D^n_\varrho \times F^n\right)\right]. \tag{5.10}$$

In this section, the parameters r and K are equal to 1. The general scheme 5.10 is used in supplementary materials, to show the effects of differents parameters on the invasion.

To be sure that this scheme gives a good approximation of the solution of the PDE (5.4), the spatial step δx is taken large enough.

5.3.2 Numerical results

We show our results of simulations of the solution of the Eq. (5.4) in two figures Fig. 5.1 and Fig. 5.2. In the first one, we display different features of the front, whereas in the second one, we compare the numerical trait distribution behind the front with the approximation formally obtained in Conjecture 1.

In the top subfigure Fig. 5.1 (a), the population size $\varrho(t,x)$ is displayed at multiple time regularly spaced between $t = 20$ and $t = 200$ for different scaled position x. As expected, thanks to Fig. 5.1 (a), we can see that this front accelerates: there exists a constant y_c^{num} such that the front at time t is at position:

$$X^{num}(t) = y_c^{num}\, t^{5/4},$$

where the numerical front position $X^{num}(t)$ at time $t \ge 0$ is defined by:

$$X^{num}(t_n) = x_{i^{num}(t_n)}, \quad \text{with} \quad i^{num}(t_n) := \underset{1\le i\le N_x}{\mathrm{argmin}} \left|\widetilde{\varrho}^n_i - 0.01\right|. \tag{5.11}$$

More precisely, thanks to a linear regression, the constant y_c^{num} can be approximated by 2.1, and the exponent of t by 1.22 (with $R^2 = 1$ and p-value $< 10^{-4}$). These numerical results are consistent with (5.8), which numerically gives:

$$X(t) = 4\left(\frac{1}{2\times 9}\right)^{1/4} t^{5/4} \approx 1.94\, t^{5/4}.$$

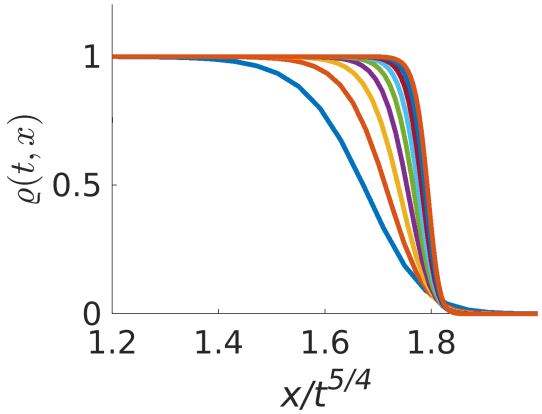

(a)

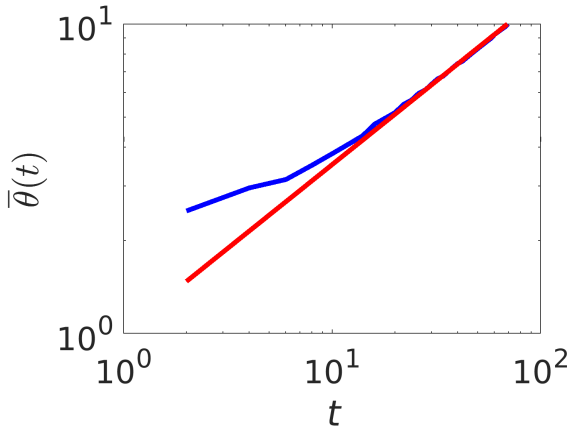

(b)

Figure 5.1: **Simulations of the invasion of a sexual population**, associated to the Eq.(5.4) with parameters $\delta t = 0.02$, $\delta x = 4$, $\delta\theta = 2/3$, $x_{\max} = 3000$ and $\theta_{\max} = 201$. (a) Plot of the population size $\varrho(t,\cdot)$ for successive fixed times at regular intervals from $t = 20$ to $t = 200$, with respect to the self - similar variable $xt^{-5/4}$. (b) Plot of the mean of the dispersive trait $\overline{\theta}^{num}(t)$ (see (5.12)) at the front position with respect to time (blue curve) and of the function $t \to 1.02t^{0.54}$ (red curve), in $\log - \log$ scale.

With Fig. 5.1 (b), we confirm that the mean of the dispersive trait at the front that we get from the numerical simulations is quite consistent with the approximation given by Conjecture 1. Precisely, let us define the mean of the dispersive trait $\bar{\theta}^{num}(t)$ at the front position $X^{num}(t)$, given by:

$$\bar{\theta}^{num}(t) := \frac{\int_{\mathbb{R}} \theta\, f(t, X^{num}(t), \theta)\, \mathrm{d}\theta}{\varrho(t, X^{num}(t))}. \tag{5.12}$$

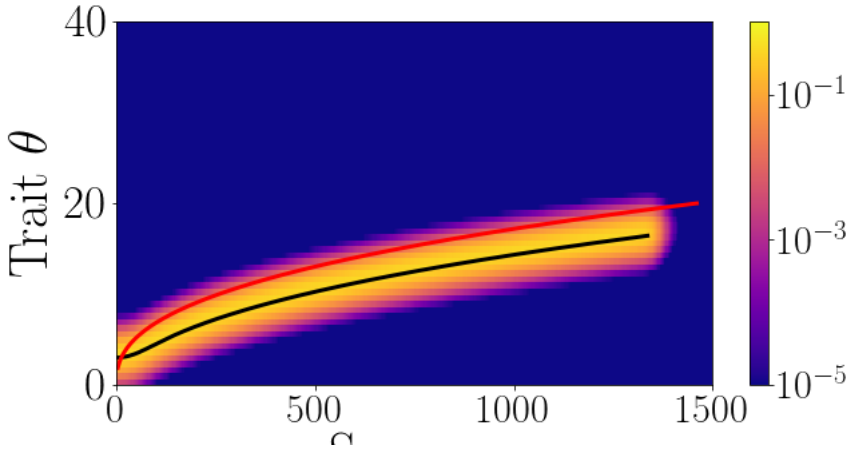

(a)

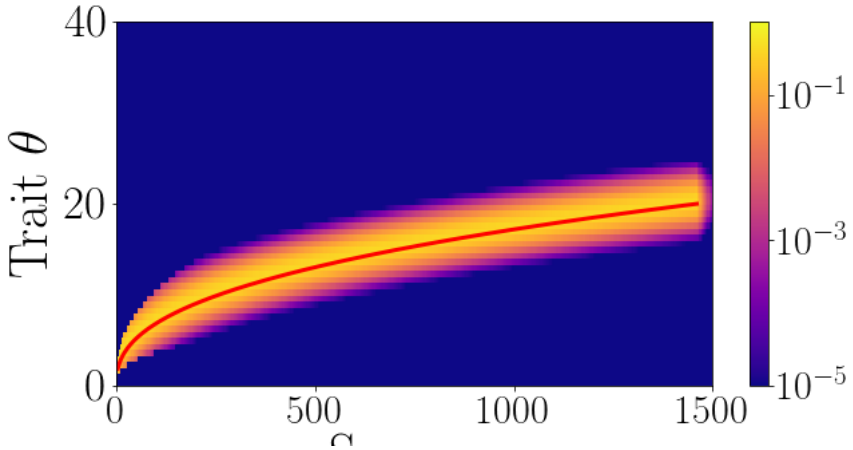

(b)

Figure 5.2: **Heatmap of the trait distribution of a sexual population**, associated to the Eq. (5.4) with parameters $\delta t = 0.02$, $\delta x = 4$, $\delta\theta = 2/3$, $x_{\max} = 3000$ and $\theta_{\max} = 201$. (a) Trait distribution given by the numerical simulations, at $t = 200$. The red line represents the approximation of the mean trait behind the propagating front given by (5.7), and is common to both subfigures, while the black line is the mean trait behind the propagating front given by the simulations. (b) Trait distribution behind the propagating front given by Conjecture 1, at $t = 200$.

Using a linear regression on the values for $t \in [60, 200]$ (illustrated in Fig. 5.1 (b)), the mean of the dispersive trait $\bar{\theta}^{num}$ can be approximated by:

$$\bar{\theta}^{num}(t) \approx 1.02\, t^{0.54}, \quad (R^2 = 1,\ p\text{-value} < 10^{-14}).$$

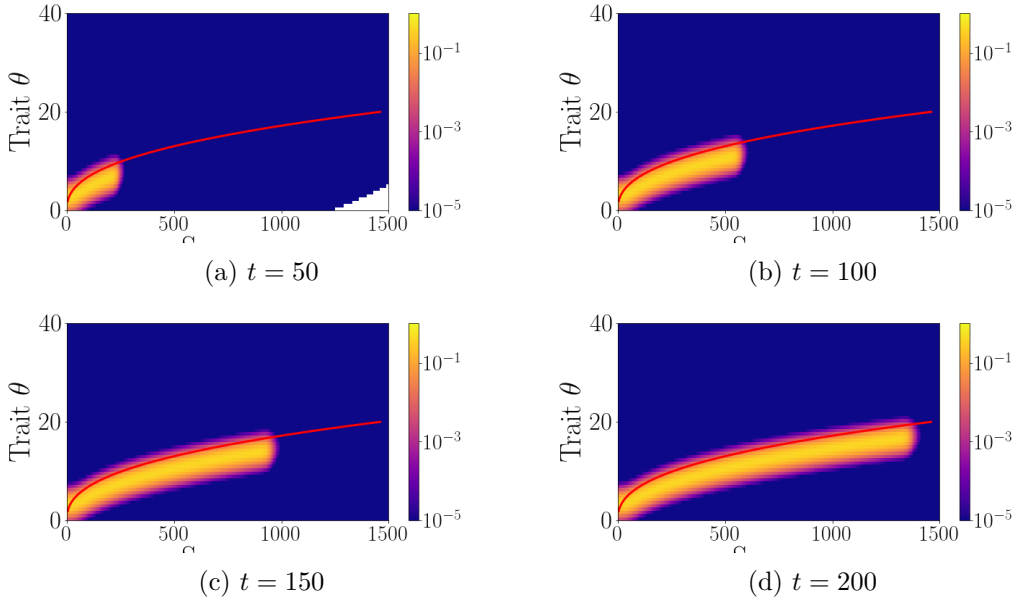

(a) $t = 50$ (b) $t = 100$

(c) $t = 150$ (d) $t = 200$

Figure 5.3: **Contour lines of the trait distribution during the invasion of a sexual population**, given by simulations, at (a) $t = 50$ (b) $t = 100$ (c) $t = 150$ (d) $t = 200$. The red line represents the approximation of the mean trait behind the propagating front given by (5.7), at time $t = 200$. The parameters are $\delta t = 0.02$, $\delta x = 4$, $\delta\theta = 2/3$, $x_{\max} = 3000$ and $\theta_{\max} = 201$.

We can compare this relationship with the mean of the dispersive trait $\bar{\theta}(t)$ at the front $X(t)$, given respectively by (5.7) and (5.8):

$$\bar{\theta}(t) = \lambda^{4/5}(6X(t)^2)^{1/5} = 2\lambda\sqrt{t} = \sqrt{2t}.$$

We notice a non trivial difference between $\bar{\theta}(t)$ and $\bar{\theta}^{num}$, mainly in their prefactors ($\sqrt{2}$ and 1.02), but also in their exponents (0.5 and 0.54) (see also the gap between the red and black lines in Fig. 5.2). This seems partly due to numerical inaccuracies resulting from having a bounded trait space (thus disregarding the largest traits) and from numerical scheme errors. One can also note that the asymptotic distribution indicated by Conjecture 1 might not yet be reached at time 200 (upper time bound in our numerical simulations).

Let us turn to the description of the trait distribution behind the front. In Fig. 5.2, we display the contour lines of the trait distribution at time $t = 200$: subfigure (a) is the trait distribution given by the simulations, while (b) is the formal trait distribution (behind the front only) given by Conjecture 1. Our approximation appears to fit the numerical results. More precisely, the red curve, representing the mean of the dispersive trait at each position behind the front given by (5.7), yields a good approximation of the numerical mean of the dispersive trait. Moreover, if we represent the numerical trait distribution behind the front at multiple times (see Fig. 5.3), we can see that it seems to remain stationary, which is consistent with the fact that the expression of the approximation behind the front given by Conjecture 1 is independent of the time.

Fig. 5.4 shows the evolution of the amplitude of the trait distribution $f(t, x, \cdot)$ ahead of the front, in blue curve (log scale). We can see that it can be approximated by the red curve, which displays the prefactor of the trait distribution ahead of the front given by Conjecture 1, and that this approximation holds even at very low density. The difference is due to the other

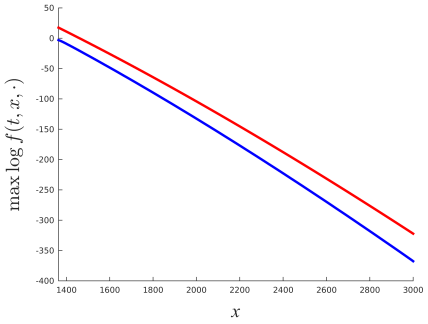

Figure 5.4: **Plot of logarithm of the amplitude of the distribution ahead of the front at time $t = 200$.** The blue curve represents the log of the maximum of the distribution $f(t, x, \cdot)$ of the numerical approximation given by the scheme, for different positions x located beyond the numerical value of the front position ($X^{\text{num}}(200) \approx 1400$). The red curve represents the prefactor of the trait distribution ahead of the front given by Conjecture 1. The parameters are $\delta t = 0.02$, $\delta x = 4$, $\delta\theta = 2/3$, $x_{\max} = 3000$ and $\theta_{\max} = 201$.

terms of higher power, which are neglected.

5.4 Formal proof of the results

This section is devoted to the formal proof of Conjecture 1. In Section 5.4.1, we set the self-similar variables framework suitable to capture the asymptotic invasion acceleration process. Then in Section 5.4.2, we formally derive an asymptotic equation that will allow us in Section 5.4.3 to determine the position of the front and to derive an approximation of the trait distribution $f(t, x, \theta)$ by finding a solution to the limit problem.

5.4.1 Preliminaries

According to the same methodology used in previous studies that model the evolution of dispersion (see for instance Bouin, Henderson, and Ryzhik 2017a; Calvez, Henderson, et al. 2022; Calvez, Crevat, et al. 2020), we define the function u such that:

$$f(t, x, \theta) = \exp\left[-t\, u\left(s(t), t^{-5/4}x, t^{-1/2}\theta\right)\right], \tag{5.13}$$

where $s(t) = \log(t)$ is a time parametrization (chosen so that $ts'(t) = 1$). According to the formal arguments of Calvez, Crevat, et al. 2020, we also scale the spatial variable ($y = t^{-5/4}x$) and trait variable ($\eta = t^{-1/2}\theta$), which leads to the spatial invasion rate accelerating proportionally to $t^{5/4}$ (see Calvez, Crevat, et al. 2020 for details). Like in the latter, we recall that the power exponents are chosen so that the all biological forces (particularly, migration and reproduction) contribute in a balanced way in the following PDE on u, satisfied for all $t \geq 0$, for all $y \in \mathbb{R}$ and for all $\eta \geq e^{-s/2}$:

$$\begin{aligned} -u(s,y,\eta) - \partial_s u(s,y,\eta) + \frac{5}{4} y \partial_y u(s,y,\eta) + \frac{\eta}{2}\partial_\eta u(s,y,\eta) \\ = \eta\left[(\partial_y u(s,y,\eta))^2 - e^{-s}\Delta_y u(s,y,\eta)\right] \\ + \left(I[u](s,y,\eta) - \varrho_u(s,y)\right), \end{aligned} \tag{5.14}$$

where:

$$\varrho_u(s,y) = e^{s/2}\int_{e^{-s/2}}^{\infty} \exp\left[-e^s u(s,y,\eta)\right] \mathrm{d}\eta, \tag{5.15}$$

and:

$$I[u](s,y,\eta) = \frac{e^s}{\sqrt{2\pi\lambda^2}\varrho_u(s,y)} \iint_{(e^{-s/2},\infty)^2} \exp\left[e^s\left(-\frac{\left(\eta-\frac{\eta_1+\eta_2}{2}\right)^2}{2\lambda^2} + \left[u(s,y,\eta)-u(s,y,\eta_1)-u(s,y,\eta_2)\right]\right)\right] \mathrm{d}\eta_1\,\mathrm{d}\eta_2. \tag{5.16}$$

Henceforth, we note for the sake of clarity: $\alpha = 5/4$ and $\beta = 1/2$. We generalise also the notation $o_{\epsilon\to 0}(\epsilon^p)$ for a sequence of functions $r_\epsilon(y,\eta)$ by :

$$r_\epsilon(y,\eta) = o_{\epsilon\to 0}(\epsilon^p) \text{ if } \sup_{(y,\eta)} |\epsilon^{-p} r_\epsilon(y,\eta)| \text{ goes to } 0, \text{ as } \epsilon \text{ vanishes.}$$

Our formal aim is to determine the large time behaviour of the solution of (5.14), as $s \to \infty$ (which is equivalent to take $t \to \infty$).

5.4.2 Formal asymptotic equation

In this subsection, we will derive from (5.14) an asymptotic equation in the limit $s \to \infty$ that will explicit the interplay between spatial sorting and trait distribution at the front of the solution. The main idea is to perform a Taylor expansion of u. For that purpose, let us define the variation $\epsilon = e^{-s/2}$. In the line of Calvez, Garnier, and Patout 2019, we make the following ansatz:

$$u(s,y,\eta) = u_0(y,\eta) + \epsilon^2 u_1(y,\eta) + o_{\epsilon\to 0}(\epsilon^2). \tag{5.17}$$

In the next paragraph, we justify the following separation of trait and space variable in u_0, where:

$$u_0(y,\eta) = b(y) + \frac{(\eta - a(y))^2}{4\lambda^2}. \tag{5.18}$$

where a and b are continuous and piecewise differentiable functions of the space variable. Let us interpret them.

Using the ansatz (5.17) and (5.18) in (5.13) yields (we recall that $\epsilon = e^{-s/2}$):

$$f(s,y,\eta) = \exp\left[-\frac{b(y)}{\epsilon^2}\right]\exp\left[-\frac{(\eta-a(y))^2}{4\lambda^2\epsilon^2}\right]\exp\left[-u_1(y,\eta) + \underset{\epsilon\to 0}{\mathcal{O}}(\epsilon^2)\right]. \tag{5.19}$$

Hence, when $s \to \infty$, the leading term of the trait distribution $\eta \mapsto f(s,y,\cdot)$ is Gaussian, and the correction is brought by a term determined by u_1. The space dependent functions a and b crystallize the main effect of spatial sorting on the trait distribution:

- $\diamond$ $a(y)$ gives the mean rescaled dispersal trait $\eta > 0$ at position y. It is therefore positive and satisfies the relation:

$$u_0(y,a(y))) = \min\{u_0(y,\eta), \text{ with } \eta \in (0,\infty)\};$$

- $\diamond$ $b(y)$ determines the prefactor of this distribution: formally, we will see that if $b(y) > 0$, $\varrho_u(s, \cdot)$ vanishes when s tends to ∞. On the contrary, the set $\{b(y) = 0\}$ is associated to that area where ϱ_u is asymptotically non-zero. In the context of a spatial invasion, it corresponds to the spatial area that has already been invaded. Hence, we are searching b such that there exists a constant y_c such that $\{b(y) = 0\} = \{y \leq y_c\}$. We can interpret y_c as the rescaled position of the front.

Finally, the space dependent functions a and b are linked to the corrector term u_1 by an asymptotic equation that we deduce from (5.14) (see below for the details). For y where a and b are differentiable (recall that $\alpha = 5/4$ and $\beta = 1/2$ are known):

$$-b(y) - \frac{(\eta - a(y))^2}{4\lambda^2} + \alpha y \left[b'(y) - a'(y) \frac{\eta - a(y)}{2\lambda^2} \right] + \beta\eta \frac{\eta - a(y)}{2\lambda^2} - \eta \left[b'(y) - a'(y) \frac{\eta - a(y)}{2\lambda^2} \right]^2 = \exp\left[u_1(y, \eta) + u_1(y, a(y)) - 2u_1\left(y, \frac{\eta + a(y)}{2} \right) \right] - \mathbf{1}_{\{y \leq y_c\}}. \quad (5.20)$$

In the next section, we find an explicit solution to (5.20), which encodes the intertwined relationship between spatial sorting and trait distribution.

Explanation for the decomposition of u_0 (5.18). We will recall the fundamental steps, more extensively detailed formally in Garnier et al. 2022 and rigorously in Calvez, Garnier, and Patout 2019 (for a model without any spatial structure). From the Taylor expansion of u given in (5.17), we get the following expression for $I[u]$:

$$I[u](s, \eta, y) = \frac{1}{\epsilon\sqrt{2\pi\lambda^2}} \iint_{(\epsilon,\infty)^2} \frac{\exp\left[\frac{1}{\epsilon^2} A^0_{y,\eta}(\eta_1, \eta_2)\right] \exp\left[A^1_{y,\eta}(\eta_1, \eta_2)\right] \exp\left[\underset{\epsilon\to 0}{o}(1)\right] \mathrm{d}\eta_1 \mathrm{d}\eta_2}{\int_\epsilon^\infty \exp\left[-\frac{u_0(y,\eta')}{\epsilon^2} - u_1(y, \eta')\right] \mathrm{d}\eta'},$$

where:

$$\begin{cases} A^0_{y,\eta}(\eta_1, \eta_2) = -\frac{1}{2\lambda^2} \left[\eta - \frac{\eta_1 + \eta_2}{2}\right]^2 + u_0(y, \eta) - u_0(y, \eta_1) - u_0(y, \eta_2), \\ A^1_{y,\eta}(\eta_1, \eta_2) = u_1(y, \eta) - u_1(y, \eta_1) - u_1(y, \eta_2). \end{cases}$$

Then, we have several considerations to make. First, if we assume that u_0 reaches its minimum at a non degenerated-point, then the following modified expression of the denominator:

$$\int_\epsilon^\infty \exp\left[-\frac{1}{\epsilon^2} \left[u_0(y, \eta') - \min u_0(y, .) \right] - u_1(y, \eta') \right] \mathrm{d}\eta',$$

will concentrate, as ϵ goes to 0, around the minimum of $u_0(y, \cdot)$ and have a finite limit. Therefore it is relevant to introduce it both at the numerator and the denominator:

$$\frac{1}{\left[\epsilon\sqrt{2\pi\lambda^2}\right]^2} \frac{\iint_{(\epsilon,\infty)^2} \exp\left[\frac{1}{\epsilon^2}\left(A^0_{y,\eta}(\eta_1, \eta_2) + \min u_0(y, .)\right)\right] \exp\left[A^1_{y,\eta}(\eta_1, \eta_2) + \underset{\epsilon\to 0}{o}(1)\right] d\eta_1 d\eta_2}{\frac{1}{\epsilon\sqrt{2\pi\lambda^2}} \int_\epsilon^\infty \exp\left[-\frac{1}{\epsilon^2}\left[u_0(y, \eta') - \min u_0(y, .)\right] - u_1(y, \eta')\right] d\eta'}.$$

As we want consequently the numerator not to diverge as $\epsilon \to 0$, we need that:

$$\forall \eta \in \mathbb{R}, \max_{(\eta_1,\eta_2)} \left[-\frac{1}{2\lambda^2} \left(\eta - \frac{\eta_1 + \eta_2}{2} \right)^2 + u_0(y, \eta) - u_0(y, \eta_1) - u_0(y, \eta_2) + \min u_0(y, .) \right] = 0. \quad (5.21)$$

As shown in Garnier et al. 2022, thanks to some convexity arguments, this leads necessarily to choose $u_0(y, \cdot)$ as a quadratic function in η with variance λ^2, hence (5.18).

Derivation of the asymptotic Eq. (5.20) verified by y_c, $a(y)$, $b(y)$ and $u_1(y, \eta)$. To get an asymptotic equation from (5.14), we still need to establish (formally) the limit of

$I[u](s,y,\eta)$ as $s=-2\log(\epsilon)$ goes to ∞, by incorporating the quadratic expression (5.18) of u_0 in $I[u]$. We will separate the cases of the numerator and the denominator for the sake of clarity.

According to Laplace's method, as we expect the denominator to concentrate around the minimum of u_0, namely at $a(y)$, one can perform the change of variable $z := \frac{\eta' - a(y)}{\epsilon}$:

$$\frac{1}{\epsilon\sqrt{2\pi\lambda^2}}\int_\epsilon^\infty \exp\left[-\frac{1}{\epsilon^2}\left[u_0(y,\eta') - \min u_0(y,.)\right] - u_1(y,\eta')\right] d\eta'$$
$$= \frac{1}{\sqrt{2\pi\lambda^2}}\int_{1-a(y)/\epsilon}^\infty \exp\left[-\frac{z^2}{4\lambda^2}\right]\exp\left[-u_1\left[y, a(y)+\epsilon z\right]\right] dz \underset{\epsilon\to 0}{\to} \sqrt{2}\exp\left[-u_1\left[y,a(y)\right]\right].$$

Similarly, following the analysis of the authors of Garnier et al. 2022 and Calvez, Garnier, and Patout 2019 on (5.21), we get that the numerator concentrates around the point $(\overline{\eta},\overline{\eta})$, with $\overline{\eta} = \frac{\eta + a(y)}{2} > 0$, realizing its minimum. One can thus perform the change of variables $(\eta_1,\eta_2) = (\overline{\eta}+\epsilon z_1, \overline{\eta}+\epsilon z_2)$, so that a straightforward computation following the quadratic expression (5.18) of u_0 leads to:

$$-\frac{1}{\epsilon^2}\left[-\frac{1}{2\lambda^2}\left[\eta - \frac{\eta_1+\eta_2}{2}\right]^2 + u_0(y,\eta) - u_0(y,\eta_1) - u_0(y,\eta_2) + \min u_0(y,.)\right]$$
$$= \frac{1}{4\lambda^2}z_1 z_2 + \frac{3}{8\lambda^2}(z_1^2+z_2^2), \quad (5.22)$$

and therefore:

$$\frac{1}{\left[\epsilon\sqrt{2\pi\lambda^2}\right]^2}\iint_{(\epsilon,\infty)^2}\exp\left[\frac{1}{\epsilon^2}\left(A^0_{y,\eta}(\eta_1,\eta_2) + \min u_0(y,.)\right)\right]\exp\left[A^1_{y,\eta}(\eta_1,\eta_2) + o_{\epsilon\to 0}(1)\right] d\eta_1 d\eta_2,$$
$$= \iint_{(1-\overline{\eta}/\epsilon,\infty)^2}\frac{\exp\left[-\frac{z_1 z_2}{4\lambda^2} - \frac{3}{8\lambda^2}(z_1^2+z_2^2)\right]}{[\sqrt{2\pi\lambda^2}]^2}\exp\left[u_1(y,\eta) - u_1(y,\overline{\eta}+\epsilon z_1) - u_1(y,\overline{\eta}+\epsilon z_2)\right] dz_1 dz_2,$$
$$\underset{\epsilon\to 0}{\to} \sqrt{2}\exp\left[u_1(y,\eta) - 2u_1(y,\overline{\eta})\right].$$

We can thereby obtain the formal limit of $I[u]$:

$$I[u](s,y,\eta) \underset{s\to\infty}{\to} \exp\left[u_1(y,\eta) + u_1(y,a(y)) - 2u_1\left(y, \frac{\eta+a(y)}{2}\right)\right].$$

Moreover, we need the formal limit of $\varrho_u(s,y)$ as $s=-2\log(\epsilon)$ tends to ∞:

$$\varrho_u(-2\log(\epsilon),y) = \frac{1}{\epsilon}\int_\epsilon^\infty \exp\left[-\frac{u(-2\log(\varepsilon,y,\eta)}{\epsilon^2}\right] d\eta,$$
$$= \exp\left[-\frac{b(y)}{\epsilon^2}\right]\frac{1}{\epsilon}\int_\epsilon^\infty \exp\left[-\frac{(\eta-a(y))^2}{4\lambda^2\epsilon^2}\right]\exp\left[-u_1(y,\eta) + \underset{\varepsilon\to 0}{o}(1)\right] d\eta,$$
$$= \exp\left[-\frac{b(y)}{\epsilon^2}\right]\int_{1-\frac{a(y)}{\varepsilon}}^\infty \exp\left[-\frac{z^2}{4\lambda^2}\right]\exp\left[-u_1(y,a(y)+\epsilon z) + \underset{\varepsilon\to 0}{o}(1)\right] dz.$$

Hence, formally, we get:

$$\varrho_u(-2\log(\epsilon),y) \underset{\epsilon\to 0}{\longrightarrow} \mathbf{1}_{\{b(y)=0\}} 2\sqrt{\pi}\lambda\exp\left[-u_1(y,a(y))\right].$$

By integrating all these formal computations in (5.14), we formally obtain an asymptotic equation satisfied by a, b and u_1, where a and b are differentiable:

$$-b(y) - \frac{(\eta-a(y))^2}{4\lambda^2} + \alpha y\left[b'(y) - a'(y)\frac{\eta-a(y)}{2\lambda^2}\right] + \beta\eta\frac{\eta-a(y)}{2\lambda^2} - \eta\left[b'(y) - a'(y)\frac{\eta-a(y)}{2\lambda^2}\right]^2$$
$$= \exp\left[u_1(y,\eta) + u_1(y,a(y)) - 2u_1\left(y,\frac{\eta+a(y)}{2}\right)\right]$$
$$- \mathbf{1}_{\{b(y)=0\}} 2\sqrt{\pi}\lambda\exp\left[-u_1(y,a(y))\right].$$

As we are describing a front propagation, we are looking for a and b continuous on $\mathbb{R}$ and differentiable everywhere but not necessarily at the front position (to be determined):

$$y_c = \sup\{y,\ b(y) = 0\}.$$

For such functions a and b, we have by evaluating the latter at $\eta = a(y)$ for $y < y_c$:

$$2\sqrt{\pi}\lambda \exp\left[-u_1(y, a(y))\right] = 1., \tag{5.23}$$

which set the constant part of $u(y,\cdot)$ for $y < y_c$. Hence, for $y \neq y_c$ and $\eta \in J_y$ (subset of $\mathbb{R}_+^*$ to be determined), we need to solve the asymptotic Eq. (5.20), i.e. finding y_c, a, b, u_1 such that $u_1(y, a(y)) = -\log(2\sqrt{\pi}\lambda)$ and :

$$\begin{aligned} -b(y) - \frac{(\eta - a(y))^2}{4\lambda^2} + \alpha y \left[b'(y) - a'(y)\,\frac{\eta - a(y)}{2\lambda^2}\right] + \beta\eta\frac{\eta - a(y)}{2\lambda^2} - \eta\left[b'(y) - a'(y)\,\frac{\eta - a(y)}{2\lambda^2}\right]^2 \\ = \exp\left[u_1(y,\eta) + u_1(y, a(y)) - 2u_1\left(y, \frac{\eta + a(y)}{2}\right)\right] - \mathbf{1}_{\{y<y_c\}}. \end{aligned}$$

5.4.3 Resolution of the asymptotic Eq. (5.20)

Heuristics. Let us define for $y \neq y_c$, $\eta > 0$ (recall that $\alpha = 5/4$ and $\beta = 1/2$ are known):

$$\begin{aligned} g(y,\eta) := &-b(y) - \frac{(\eta - a(y))^2}{4\lambda^2} + \alpha y\left[b'(y) - a'(y)\,\frac{\eta - a(y)}{2\lambda^2}\right] \\ &+ \beta\eta\frac{\eta - a(y)}{2\lambda^2} - \eta\left[b'(y) - a'(y)\,\frac{\eta - a(y)}{2\lambda^2}\right]^2 + \mathbf{1}_{\{y<y_c\}}. \end{aligned} \tag{5.24}$$

Let us fix $y \neq y_c$. For $\eta > 0$ such that $g(y,\eta) > 0$, we can reformulate (5.20) as:

$$T_y(\eta) = L_y(u_1)(\eta), \tag{5.25}$$

where:

$$T_y(\eta) := \log\left[g(y,\eta)\right],$$

and:

$$L_y(u_1) : \eta \mapsto u_1(y,\eta) + u_1(y, a(y)) - 2u_1\left(y, \frac{\eta + a(y)}{2}\right). \tag{5.26}$$

Eq. (5.25) suggests that a, b and y_c are to be chosen so that T_y lies in the image of the linear operator L_y. One can notice that the kernel of L_y is composed of the affine functions, hence:

$$\dim\ker\left(L_y\right) = 2.$$

Heuristically, the image of L_y is orthogonal to a two dimensional space, which is generated by $\delta_{a(y)}$ and $\delta'_{a(y)}$. More precisely, following Calvez, Garnier, and Patout 2019, one can show that if T_y verifies:

$$\begin{cases} T_y\left(a(y)\right) = 0, \\ T_y'\left(a(y)\right) = 0, \end{cases} \tag{5.27}$$

then the following sum converges:

$$u_y : \eta \mapsto \sum_{k=0}^{\infty} 2^k T_y\left[a(y) + (\eta - a(y))\ 2^{-k}\right], \tag{5.28}$$

and $L_y(u_y) = T_y$. The infinite serie (5.28) determines $u_1(y,\cdot)$ up to its affine part, which lies in the kernel of L_y. We already know its constant part from (5.23): $u_1(y, a(y)) = -\log(2\sqrt{\pi}\lambda)$ for $y < y_c$. We conjecture that the same holds for $y > y_c$. The linear part will be identified in a second time.

Determination of $y_c, a(y), b(y)$. Hence, we first need to solve (5.27), that is to find $y_c > 0$, $(a, b) \in C^0(\mathbb{R}_+) \cap C^1(\mathbb{R}_+ \backslash \{y_c\})$, such that:

$$\forall y \neq y_c, \quad \begin{cases} -b(y) + \alpha y b'(y) - a(y)(b'(y))^2 + \mathbf{1}_{\{y<y_c\}} = 1, \\ -\alpha y a'(y) + \beta a(y) - 2\lambda^2 (b'(y))^2 + 2a(y)b'(y)a'(y) = 0. \end{cases} \tag{5.29}$$

Here, we present an explicit solution to (5.29):

Proposition. *Let us define:*

$$y_c = 4\sqrt{\frac{\lambda}{3}}, \qquad a : y \mapsto \begin{cases} \lambda^{4/5}\, 6^{1/5}\, y^{2/5}, & \text{if } y \leq y_c, \\ \left(\frac{3\lambda^2}{2}\right)^{1/3} y^{2/3}, & \text{if } y > y_c, \end{cases}$$

and:

$$b : y \mapsto \begin{cases} 0, & \text{if } y \leq y_c, \\ \left(\frac{3}{\lambda 2^4}\right)^{2/3} y^{4/3} - 1, & \text{if } y > y_c. \end{cases}$$

Then $a, b \in C^0(\mathbb{R}_+) \cap C^1(\mathbb{R}_+ \backslash \{y_c\})$ and y_c, a and b are solutions of (5.29).

Remark 13. *The functions a, b and y_c given in the previous proposition are the only solutions of (5.29) of the form : $a(y) = Cy^m$, $b(y) = Ky^n - 1$ that are positive for $y > y_c$ and continuous in y_c.*

Identification of $u_1(y, \cdot)$ up to its linear part. To derive a solution for (5.20) from Proposition 5.4.3, one still has to determine $u_1(y, \cdot)$ for all y. The first step is doing so up to its linear part which will be specified later (the constant part $u_1(y, a(y))$ is known from (5.23)). According to the heuristics paragraph at the beginning of this section and to the analysis done in [Calvez, Garnier, and Patout 2019], the latter should be equal to the infinite series u_y introduced by (5.28). It involves therefore $T_y(\cdot) = \log[g(y, \cdot)]$, which requires $g(y, \cdot) > 0$ (g is defined by (5.24)). As the latter is a three order polynomial in η with a negative leading coefficient, it is negative as η becomes large so we cannot define T_y on the whole $\mathbb{R}_+^*$ space. However, because a, b and y_c are solutions of (5.29), the following holds and ensures that $g(y\cdot)$ is positive in the vicinity of $a(y)$:

$$g(y, a(y)) = 1, \quad \partial_\eta g(y, a(y)) = 0.$$

We aim therefore at solving (5.20) locally in η around $a(y)$.

Proposition. *Control of the infinite series (5.28) Let a, b and y_c be as in Proposition 5.4.3. Then, there exists $0 < \delta_0 \leq 1$ such that, for all $y \neq y_c$, $\eta > 0$ such that $\frac{\eta}{a(y)} \in [1-\delta_0, 1+\delta_0]$, we have $g(y, \eta) > 0$. Moreover, for $y \neq y_c$, $T_y = \log(g(y, \cdot))$ is well defined on $a(y) \cdot [1 - \delta_0, 1 + \delta_0]$ and for all $0 < \delta \leq \delta_0$:*

- ◇ *for $y < y_c$ and $\eta \in a(y) \cdot [1 - \delta, 1 + \delta]$, the series defined in (5.28) converges and is bounded uniformly with regard to η and y and the bound is of the form $A\,|\delta|^2$.*
- ◇ *for $y > y_c$ and $\eta \in a(y) \cdot [1 - \delta, 1 + \delta]$, the series defined in (5.28) converges and is bounded uniformly with regard to η, and the bound is of the form: $B|\delta|^2 y^{8/3}$.*

Proof. Since $g(y, \cdot)$ is a polynomial of order three in η such that:

$$g(y, a(y)) = 1, \qquad \partial_\eta g(y, a(y)) = 0,$$

we can define P_y polynomial of order three such that:

$$\forall \eta > 0, \quad g(y,\eta) = 1 - P_y\left(\frac{\eta}{a(y)}\right).$$

As $P_y(1) = P_y'(1) = 0$, we get:

$$P_y(X) = (X-1)^2\left[\gamma X + P_y(0)\right],$$

where $\gamma > 0$ is the leading coefficient of P_y.

We next compute, for $y \neq y_c$ (by continuity for $P_y(0)$):

$$\gamma = \frac{a'(y)^2 a(y)^3}{4\lambda^4}, \quad P_y(0) = b(y) + \frac{a(y)^2}{4\lambda^2} - \alpha y\left[b'(y) + a'(y)\,\frac{a(y)}{2\lambda^2}\right] + \mathbf{1}_{\{y>y_c\}}.$$

Hence (adopting the notations K_{a^-},K_{a^+} and K_b such that for $y < y_c$, $a(y) = K_{a^-}y^{2/5}$ and for $y > y_c$, $a(y) = K_{a^+}y^{2/3}$, $b(y) = K_b y^{4/3} - 1$ – see the previous proposition):

- ⋄ for $y < y_c$, $\gamma = \frac{a(y)^5}{25y^2\lambda^4} = \frac{K_{a^-}{}^5}{25\lambda^4}$ and:

$$P_y(0) = \frac{a^2}{4\lambda^2} - \frac{\alpha a'(y) y a(y)}{2\lambda^2} = \frac{a^2}{4\lambda^2} - \frac{5}{4}\cdot\frac{2a^2}{10\lambda^2} = 0.$$

  So, in that case, $P_y = \frac{K_{a^-}{}^5}{25\lambda^4}(X-1)^2X := P(X)$ does not depend on y. As $P(1) = 0$, there exists $\delta \in (0,1)$ such that for all $y < y_c$ and $\eta \in]a(y)(1-\delta), a(y)(1+\delta)[$, $P\left(\frac{\eta}{a(y)}\right) < 1$, hence $g(y,\eta) > 0$.

- ⋄ for $y > y_c$, $\gamma = \frac{4}{9}\frac{a(y)^5}{4y^2\lambda^4} = \frac{K_{a^+}^5}{9\lambda^4}y^{4/3} := \tilde{\gamma}y^{4/3}$ and:

$$\begin{aligned} P_y(0) &= (b(y)+1) - \frac{5}{3}(1+b(y)) + \frac{a(y)^2}{4\lambda^2} - \frac{5a(y)^2}{12\lambda^2}, \\ &= -y^{4/3}\left[\frac{K_{a^+}^2}{6\lambda^2} + \frac{2K_b}{3}\right] = -\tilde{\gamma}y^{4/3}\left[\frac{3\lambda^2}{2K_{a^+}^3} + \frac{6K_b\lambda^4}{K_{a^+}^5}\right], \\ &= -\tilde{\gamma}y^{4/3}\left[1 + 6\times\frac{3^{2/3}\lambda^4 2^{5/3}}{2^{8/3}\lambda^{12/3}3^{5/3}}\right] = -2\tilde{\gamma}y^{4/3}. \end{aligned}$$

  Hence: $P_y(X) = \tilde{\gamma}y^{4/3}(X-1)^2(X-2)$, thus: $\forall y > y_c, \forall \eta \in]0, 2a(y)[, g(y,\eta) > 1 > 0$.

This proves the first part of the proposition. Let us consider $0 < \delta_0 \leq 1$ such that, for all $y \neq y_c$, $g(y,.)$ is positive on $[1-\delta_0, 1+\delta_0]$, and on which interval T_y is therefore well-defined.

Let us now consider $0 < \delta \leq \delta_0$. For $y \neq y_c$, $\eta \in a(y)\cdot[1-\delta, 1+\delta]$, let us define, for $k \in \mathbb{N}$:

$$\eta_k := a(y) + \frac{\eta - a(y)}{2^k}.$$

Next, as $T_y(a(y)) = T'(a(y)) = 0$, we get the following:

$$2^k T_y(\eta_k) = 2^k \int_{a(y)}^{\eta_k} T_y''(t)\frac{\eta_k - t}{2}\mathrm{d}t.$$

With the change of variables $s = 2^k\,(t - a(y))$, we get:

$$2^k T_y(\eta_k) = \int_0^{\eta - a(y)} T_y''\left(a(y) + s2^{-k}\right) \frac{\eta - a(y) - s}{2^k} \mathrm{d}s. \tag{5.30}$$

T_y'' is continuous on $a(y) \cdot [1-\delta, 1+\delta]$, so the latter ensures that $\sum_{k\geq 0} 2^k T\left(\eta_k\right)$ converges for all $\eta \in a(y) \cdot [1-\delta, 1+\delta]$.

Finally, for $y \neq y_c$, we need to uniformly bound $\sum_{k\geq 0} 2^k T\left(\eta_k\right)$ with regard to $\eta \in a(y) \cdot [1-\delta, 1+\delta]$. For $y < y_c$, from the first part of the proof, we have:

$$\forall \eta \in a(y) \cdot [1-\delta, 1+\delta], \quad T_y(\eta) = \log\left(1 - P\left(\frac{\eta}{a(y)}\right)\right),$$

with $P(X) = \gamma X(X-1)^2$ and γ independent of y and η. Setting:

$$\begin{array}{rccl} F & : & [1-\delta, 1+\delta] & \to & \mathbb{R}, \\ & & x & \mapsto & \log\left(1 - P(x)\right), \end{array}$$

we dispose of a smooth function, independent from y and η, such that:

$$\forall \eta \in a(y) \cdot [1-\delta, 1+\delta], \quad T_y(\eta) = F\left(\frac{\eta}{a(y)}\right),$$

and therefore $T_y''(\eta) = F''\left(\eta/a(y)\right)/a(y)^2$. Following (5.30), we obtain:

$$\begin{aligned} \forall y < y_c, \eta \in a(y) \cdot [1-\delta, 1+\delta], \quad \sum_{k\geq 0} |2^k T_y(\eta_k)| &\leq \sum_{k\geq 0} 2^{-(k+1)} \|F''\|_{\infty,[1-\delta,1+\delta]} \frac{(\eta - a(y))^2}{a(y)^2} \\ &\leq |\delta|^2 \|F''\|_{\infty,[1-\delta_0,1+\delta_0]}. \end{aligned}$$

For $y > y_c$, we have from above:

$$\forall \eta \in a(y) \cdot [1-\delta, 1+\delta], \quad T_y(\eta) = \log\left(1 - y^{4/3} Q\left(\frac{\eta}{a(y)}\right)\right),$$

with $Q(X) = \gamma_Q (X-1)^2 (X-2)$ (γ_Q a constant independent of y and η). A straight-forward calculus leads to:

$$T_y''(\eta) = -\frac{y^{4/3}}{a(y)^2} \left[\frac{Q''\left(\frac{\eta}{a(y)}\right)}{1 - y^{4/3} Q\left(\frac{\eta}{a(y)}\right)} + y^{4/3} \frac{Q'\left(\frac{\eta}{a(y)}\right)^2}{\left(1 - y^{4/3} Q\left(\frac{\eta}{a(y)}\right)\right)^2} \right].$$

We recall that, additionally, for $y > y_c$ and $\eta \in a(y) \cdot [1-\delta, 1+\delta]$, we have: $1 - y^{4/3} Q\left(\frac{\eta}{a(y)}\right) > 1$. Hence, from (5.30), we obtain:

$$\begin{aligned} \forall y > y_c, \forall \eta \in a(y) \cdot [1-\delta, 1+\delta], \quad \sum_{k\geq 0} |2^k T_y(\eta_k)| &\leq y^{4/3} |\delta|^2 \left[\|Q''\|_{\infty,[1-\delta,1+\delta]} + y^{4/3} \|Q'^2\|_{\infty,[1-\delta,1+\delta]} \right] \\ &\leq y^{8/3} |\delta|^2 \left[\frac{\|Q''\|_{\infty,[1-\delta_0,1+\delta_0]}}{{y_c}^{4/3}} + \|Q'^2\|_{\infty,[1-\delta_0,1+\delta_0]} \right]. \end{aligned}$$

□

Linear part of u_1. The last proposition allows to determine the function u_1 for $y \neq y_c$ and $\eta \in a(y) \cdot [1-\delta, 1+\delta]$ for $0 < \delta \leq \delta_0$, up to its affine part $u_1(y, a(y)) + \gamma(y)(\eta - a(y))$, which cannot be seen in (5.20) (recasted as $L_y(u_1) = T_y$), because it lies in the kernel of the finite-difference operator L_y defined by (5.26) (see also Calvez, Garnier, and Patout 2019). Since the constant part is known from (5.23), we still need to determine the linear coefficient $\gamma(y)$ to complete the determination of u_1 according to the following

$$u_1 : (y, \eta) \mapsto \sum_{k \geq 0} 2^k T_y \left(a(y) + (\eta - a(y))\ 2^{-k} \right) - \log\left(2\sqrt{\pi}\lambda\right) + \gamma(y)(\eta - a(y)). \tag{5.31}$$

Following formally the computations made in [Calvez, Garnier, and Patout 2019] (see equations (1.10) and (3.2) of the latter) and thanks to the computations on $g(y, \cdot)$ performed in the proof of Section 5.4.3, we obtain that:

$$\gamma(y) = \frac{3}{4} \frac{\partial_\eta^3 u_1(y, a(y))}{\partial_\eta^2 u_1(y, a(y))} = \frac{1}{2} \frac{\partial_\eta^3 g(y, a(y))}{\partial_\eta^2 g(y, a(y))} = \begin{cases} \frac{3}{2a(y)} & \text{for } y < y_c, \\ \frac{-3}{2a(y)} & \text{for } y > y_c. \end{cases} \tag{5.32}$$

The fact that γ presents a discontinuity at the front position y_c reflects that g also presents a discontinuity in y_c because of the limit term of the local (in space) population size $\mathbf{1}_{y<y_c}$ (see (5.24)).

The description of $\gamma(y)$ by (5.32) together with Section 5.4.3 completes the identification of u_1. Furthermore, for $y \neq y_c$ and $\eta \in a(y) \cdot [1-\delta, 1+\delta]$, we dispose of the following control of the linear term:

$$|\gamma(y)\,(\eta - a(y))| = \frac{3}{2} \left| \frac{\eta}{a(y)} - 1 \right| \leq \frac{3}{2}\delta. \tag{5.33}$$

Conclusion of the resolution of Eq (5.20) Section 5.4.3 identifies the rescaled front position y_c, local mean trait $a(y)$ and prefactor coefficient $b(y)$ defining the main term of the spatial distribution according to the formal expansion (5.19). The equations (5.31), (5.32) and (5.33) together with Section 5.4.3 complete the identification and the control of u_1, the first corrector term indicated in (5.19). All this considerations allow us to propose the large-time approximation and the magnitude of the error terms indicated in Conjecture 1.

5.5 Discussion

Contributions In this paper, we have developed a different framework than the one used for the study of asexual populations (Berestycki, Mouhot, and Raoul n.d.; Bouin, Henderson, and Ryzhik 2017a; Calvez, Henderson, et al. 2022) by using a mixing operator to analyze the behaviour of the propagation front for sexual population. We have formally found an explicit approximation of the trait distribution during the invasion by finding a solution to the limit problem at large times. These formal computations have been numerically compared to the solution of (5.4) and thus confirmed. All the computations have been made after having rescaled the PDE (5.2). By a variable change, we have that, for all growth rate at low density $\boldsymbol{r} > 0$, carrying capacity $\boldsymbol{K} > 0$ and segregational variance $\boldsymbol{\lambda}^2 > 0$, for a population with

dispersive traits $\boldsymbol{\theta} \geq \boldsymbol{\theta_{\min}} > 0$, the density $\boldsymbol{f}$ can be approximated at large time $\boldsymbol{t} > 0$ by:

$$\boldsymbol{f}(\boldsymbol{t}, \boldsymbol{x}, \boldsymbol{\theta}) \approx \frac{\boldsymbol{K}}{\boldsymbol{\theta_{\min}}} \begin{cases} \exp\left[-\frac{1}{4\boldsymbol{\lambda}^2} \left[\boldsymbol{\theta} - \boldsymbol{\lambda}^{4/5} \left(6\boldsymbol{r}\boldsymbol{x}^2\right)^{1/5} \right]^2 \right], \text{ for } \boldsymbol{x} \leq \boldsymbol{y_c}\, \boldsymbol{t}^{5/4}, \\ \exp\left[\boldsymbol{r}\boldsymbol{t} - \left(\frac{9\boldsymbol{x}^4}{256\,\boldsymbol{\lambda}^2 \boldsymbol{t}^2} \right)^{1/3} \right] \exp\left[-\frac{1}{4\boldsymbol{\lambda}^2} \left[\boldsymbol{\theta} - \left(\frac{3\boldsymbol{\lambda}^2 \boldsymbol{x}^2}{2\boldsymbol{t}} \right)^{1/3} \right]^2 \right], \\ \qquad\qquad\qquad\qquad\qquad\qquad \text{for } \boldsymbol{x} \geq \boldsymbol{y_c}\, \boldsymbol{t}^{5/4}. \end{cases}$$

with:

$$\boldsymbol{y_c} = y_c \sqrt{\frac{\boldsymbol{\theta_{\min}}}{\boldsymbol{r}}}\, \boldsymbol{r}^{5/4} = 4 \left[\frac{\lambda}{3} \right]^{1/2} \sqrt{\boldsymbol{\theta_{\min}}}\, \boldsymbol{r}^{3/4} = 4 \left[\frac{\boldsymbol{\lambda}}{3} \right]^{1/2} \boldsymbol{r}^{3/4}.$$

Difference in acceleration rate between asexual and sexual invasive populations Our study shows that the effect of spatial sorting only, through the evolution of dispersion, accelerates the speed at which a sexual population invades. The rate of this acceleration, of $t^{5/4}$, is lower than when considering the influence of the same phenomenon on asexual populations ($t^{3/2}$, see Berestycki, Mouhot, and Raoul n.d.; Bouin, Henderson, and Ryzhik 2017a; Calvez, Henderson, et al. 2022). Mathematically, the blending inheritance property of the infinitesimal model operator reduces the effect of the spatial sorting by crossing extremely dispersive individuals with less dispersive ones, which does not happen for individuals reproducing clonally.

Extension: Shape of the front However, there are still structural questions to answer on the asymptotic behaviour of the front that we can observe numerically. For instance, the additional Fig. 5.5 allows us to study the deformation of the front propagation, more precisely the shape of the transition front. In Fig. 5.5 (a), the spatial distribution ϱ is displayed with respect to a re-centered scale in:

$$X_{1/2}(t) = \sup\{x \in \mathbb{R}, \varrho(t,x) \,=\, 1/2\}. \tag{5.34}$$

We can observe a flattening of the front shape, as $t \to +\infty$. More precisely, Fig 5.5 (b), displaying ϱ with respect to the re-scaled variable $\left(x - X_{1/2}(t)\right) t^{-1/4}$, shows that the shape of the front seems to flatten at order $t^{1/4}$, as the different curves overlap.

Expansion load Here, we consider only a trait linked to the dispersive ability, thus isolating the sole effect of spatial sorting in range expansions, for which there existed no previous precise results. By doing so, our model does not account for any process of selection by adaptation to the local environment. However, in cases of fast range expansion, a phenomenon called the *expansion load* can occur Peischl, Dupanloup, et al. 2013. As the density of individuals at the front is low, the effective strength of natural selection is reduced allowing deleterious mutations to accumulate at the front. That would eventually undermine the invasion process by reducing the fitness of leading individuals (see Burton, Phillips, and Travis 2010), with the potential effect of slowing down the speed of the front in comparison to the asymptotic formal result of our study. Nevertheless, the clear relationship between the effect of spatial sorting and expansion load is yet to be explored, as a recent analysis using a discrete space framework seems to indicate that the evolution of dispersal rate can prevent expansion load in certain cases (see Peischl and Gilbert 2018). By isolating the effect of spatial sorting, our

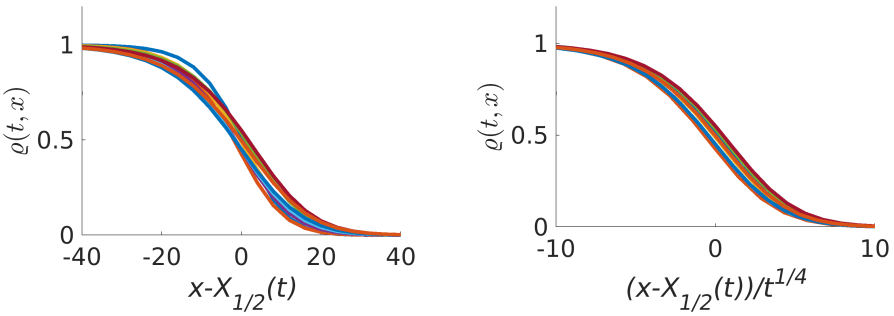

(a) (b)

Figure 5.5: **Plots of the density $\varrho(t,\cdot)$ of a sexual population, with respect to re-centered variables.** The two plots show the evolution of the population density, associated to (5.4), for successive times at regular intervals from $t = 20$ to $t = 200$, with respect to (a) the re-centered variable $x - X_{1/2}(t)$, and (b) to the re-scaled variable $(x - X_{1/2}(t))t^{-1/4}$, with $X_{1/2}(t)$ defined in (5.34). The parameters are $\delta t = 0.02$, $\delta x = 4$, $\delta\theta = 2/3$, $x_{\max} = 3000$ and $\theta_{\max} = 201$. Note that the x-axis are different between the two plots, for the sake of clarity.

study can therefore constitute a first step in understanding the intricate relationship between the evolution of dispersion and of life history traits, ultimately providing tools to analyse the source of variability in range expansions (see Williams, Hufbauer, and Miller 2019).

Because the formal computations ignore competition ahead of the front, even though the simulations seems to validate our results, this paper has to be seen as a premise for a consistent and rigorous proof for this problem.

Aknowledgement

This project has received funding from the European Research Council (ERC) under the European Union's Horizon 2020 research and innovation program (grant agreement No 639638) and from the ANR projects NONLOCAL (ANR-14-CE25-0013) and RESISTE (ANR-18-CE45-0019).

Special thanks to Vincent Calvez and Gaël Raoul for the supervision of this CEMRACS project, and to Joachim Crevat for his central role in the genesis of this work. Thanks also to Vincent Calvez, Sepideh Mirrahimi, Lionel Roques, Joachim Crevat, Barbara Neto-Bradley, Linnéa Sandell, Gil Henriques, Sarah Otto and Ailene Macpherson for helpful comments.

Chapter 6

Dynamics of dirac concentrations in the evolution of quantitative alleles with sexual reproduction

A proper understanding of the links between varying gene expression levels and complex trait adaptation is still lacking, despite recent advances in sequencing techniques leading to new insights on their importance in some evolutionary processes. This calls for extensions of the continuum-of-alleles framework first introduced by [Kimura 1965] that bypass the classical Gaussian approximation. Here, we propose a novel mathematical framework to study the evolutionary dynamics of quantitative alleles for sexually reproducing populations under natural selection and competition through an integro-differential equation. It involves a new reproduction operator which allows to use techniques based on the maximum principle, unlike the infinitesimal model operator used in other studies with sexual reproduction. In an asymptotic regime where initially the population has a small phenotypic variance, we analyse the long-term dynamics of the phenotypic distributions according to the methodology of small variance (Diekmann, Jabin, et al. 2005). Under some assumptions on the limit equation, we show that the population remains monomorphic, that is the phenotypic distribution remains concentrated as a moving Dirac mass. Moreover, in the case of a monomorphic distribution we derive a canonical equation describing the dynamics of the dominant alleles.

6.1 Introduction

6.1.1 Model and biological motivations.

The development and popularization of sequencing techniques of the last twenty years has been leading to a greater understanding of regulatory mechanisms of gene expression levels and to new insights on their importance in evolutionary trajectories of complex traits (see the recent theory of degeneration of the Y chromosome [Lenormand, Fyon, et al. 2020]). However, a complete picture of the relationship between varying gene expression levels and phenotypic adaptation is yet to be drawn (Romero, Ruvinsky, and Gilad 2012). To model varying gene expression levels on a trait under selection, one has to think of the effects of a gene as quantitative rather than discrete. One class of models that was motivated by a similar perspective stems from the reference study [Kimura 1965]: the continuum-of-alleles models in quantitative genetics, that assume that mutations produce always slightly new allelic effects, so that the allelic effect space is considered as continuous. The method indicated by [Kimura 1965] is adapted for asexual populations, or haploid sexual populations with only one locus contributing to the trait under quadratic stabilizing selection. Under these specific assumptions, [Kimura 1965] shows that the allelic effects are normally distributed under mutation-selection balance. Several studies (Latter 1972; Lande 1975) extended the model to account for finite number of loci with additive effects on the trait for sexual reproducing populations, still relying on the essential link between quadratic stabilizing selection and multivariate normal allelic distributions to derive quantitative information from their non-linear model. The aim of this paper is therefore to first study a quantitative genetics model that can account for polygenic traits under general selection functions (not restricted to quadratic and considering situations where the alleles do not necessarily have additive effects), in a sexually reproducing population regulated by competition for resources. More precisely, we are interested in the following integro-differential equation, where $\boldsymbol{t} \geq 0$ denotes the time:

$$\begin{cases} \partial_{\boldsymbol{t}} \boldsymbol{n}(\boldsymbol{t},x,y) = \frac{r}{2}\left[\frac{\boldsymbol{\rho^Y}(\boldsymbol{t},x)\,\boldsymbol{\rho^X}(\boldsymbol{t},y)}{\boldsymbol{\rho}(\boldsymbol{t})} + \boldsymbol{n}(\boldsymbol{t},x,y)\right] - (m(x,y) + \kappa\,\boldsymbol{\rho}(\boldsymbol{t}))\;\boldsymbol{n}(\boldsymbol{t},x,y), \\ \boldsymbol{\rho^X}(\boldsymbol{t},y) = \displaystyle\int_I \boldsymbol{n}(\boldsymbol{t},x',y)\,dx', \quad \boldsymbol{\rho^Y}(\boldsymbol{t},x) = \int_J \boldsymbol{n}(\boldsymbol{t},x,y')\,dy', \quad \boldsymbol{\rho}(t) = \int_{I\times J} \boldsymbol{n}(\boldsymbol{t},x',y')\,dx'\,dy', \\ \boldsymbol{n}(0,x,y) = \boldsymbol{n^0}(x,y). \end{cases} \tag{$P(\boldsymbol{n})$}$$

Here, $\boldsymbol{n}(t,x,y)$ denotes the allelic density of individuals of a haploid sexually reproducing population carrying the quantitative alleles x and y at two unlinked loci of interest. The alleles x and y are taken in compact allelic spaces I and J. Individuals experience mortality by natural selection at a rate $m(x,y) \in C^1(I\times J)$ depending on their genotype $(x,y) \in I\times J$ and regulated by a uniform competition for resources with intensity κ. The first term in the r.h.s of $P(\boldsymbol{n})$ is the reproduction term, which translates how alleles are transmitted across generations under random mating. According to Mendel's laws, the alleles x and y can be inherited either each from a different parent or both from the same.

Remark 14. *One can notice that up to setting $\tilde{m} := m - \frac{r}{2}$, $\tilde{r} = \frac{r}{2}$, $P(\boldsymbol{n})$ also describes the dynamics of a population of diploid individuals (each individual has two copies of each gene) whose adaptation are determined by the quantitative alleles (x,y) carried at a single*

focal locus. The following equation was derived as deterministic limit of an individual-based model in [Collet, Méléard, and Metz 2013]

$$\begin{cases} \partial_t \boldsymbol{n}(\boldsymbol{t},x,y) = \tilde{r}\frac{\boldsymbol{\rho^Y}(\boldsymbol{t},x)\,\boldsymbol{\rho^X}(\boldsymbol{t},y)}{\boldsymbol{\rho}(\boldsymbol{t})} - (\tilde{m}(x,y) + \kappa\,\boldsymbol{\rho}(\boldsymbol{t}))\ \boldsymbol{n}(\boldsymbol{t},x,y), \\ \boldsymbol{\rho^X}(\boldsymbol{t},y) = \displaystyle\int_I \boldsymbol{n}(\boldsymbol{t},x',y)\,dx', \quad \boldsymbol{\rho^Y}(\boldsymbol{t},x) = \int_J \boldsymbol{n}(\boldsymbol{t},x,y')\,dy', \quad \boldsymbol{\rho}(t) = \int_{I\times J} \boldsymbol{n}(\boldsymbol{t},x',y')\,dx'\,dy', \\ \boldsymbol{n}(0,x,y) = \boldsymbol{n^0}(x,y). \end{cases} \tag{$P_{\text{diploid}}\,(\boldsymbol{n})$}$$

According to Mendel's laws, the copies x and y must be inherited each from a different parent. In that case, $\tilde{r}$ is the reproduction rate and both the selection function $\tilde{m}$ and the initial genotypic density $\boldsymbol{n_0}$ are assumed symmetrical (requiring $I = J$) (one can verify that the genotypic density $\boldsymbol{n}$ remains symmetrical at all times).

We place our analysis in an asymptotic regime where we consider that the initial distribution is concentrated, with a small variance ε so that it is convenient to introduce the following transformation:

$$\boldsymbol{n}_{0,\varepsilon} = \frac{e^{\frac{\boldsymbol{u}_{0,\varepsilon}}{\varepsilon}}}{\varepsilon}. \tag{6.1}$$

The motivation behind (6.1) comes from a future project that will include mutations on the alleles with a small mutational variance of order ε^2. Here, we expect that starting with such an initial condition (6.1), the population density $\boldsymbol{n}_\varepsilon$ solution of $P\,(\boldsymbol{n})$ would keep the same exponential form and would remain asymptotically concentrated with a small variance. Consequently, the dynamics of its mean, driven by natural selection with an intensity correlated to its variance, cannot be observed at shallow time scales, and ($P\,(\boldsymbol{n})$) needs to be adequately rescaled in order to explore long-term dynamics. To that effect, let us define the following rescaling in time:

$$t = \varepsilon\,\boldsymbol{t}, \quad n_\varepsilon(t,\cdot,\cdot) = \boldsymbol{n}_\varepsilon(\boldsymbol{t},\cdot,\cdot), \quad \rho^X_\varepsilon(t,\cdot) = \boldsymbol{\rho^X}_\varepsilon(\boldsymbol{t},\cdot), \quad \rho^Y_\varepsilon(t,\cdot) = \boldsymbol{\rho^Y}_\varepsilon(\boldsymbol{t},\cdot),, \quad \rho_\varepsilon(t) = \boldsymbol{\rho}_\varepsilon(\boldsymbol{t}).$$

Under the latter, the problem ($P\,(\boldsymbol{n})$) becomes, for $t \geq 0$, $(x,y) \in I \times J$:

$$\begin{cases} \varepsilon\,\partial_t n_\varepsilon(t,x,y) = \frac{r}{2}\left[\frac{\rho^Y_\varepsilon(x)\,\rho^X_\varepsilon(y)}{\rho_\varepsilon} + n_\varepsilon(t,x,y)\right] - (m(x,y) + \kappa\,\rho_\varepsilon)\ n_\varepsilon, \\ \rho^X_\varepsilon(y) = \displaystyle\int_I n_\varepsilon(x',y)\,dx', \quad \rho^Y_\varepsilon(x) = \int_J n_\varepsilon(x,y')\,dy', \quad \rho_\varepsilon(t) = \int_{I\times J} n_\varepsilon(x',y')\,dx'\,dy', \\ n_\varepsilon(0,x,y) = n^0_\varepsilon(x,y). \end{cases} \tag{$P\,(n_\varepsilon)$}$$

As we expect the density n_ε to remain concentrated in our regime, the objective is to analytically describe the dynamics of the Dirac masses (ie. of the dominant alleles in the population), for various selection functions.

6.1.2 State of the art.

Integro-differential models for quantitative genetics modelling the evolutionary dynamics of large sexually reproducing populations with selection have been on the rise recently, especially

those that model the phenotypic trait inheritance according to the non-linear infinitesimal model introduced by [Fisher 1919] (Mirrahimi and Raoul 2013; Raoul 2017; Bourgeron et al. 2017; Calvez, Garnier, and Patout 2019; Patout 2020; Dekens and Lavigne 2021; Dekens 2022; Raoul 2021; Dekens, Otto, and Calvez 2021). According to the latter, the offspring's trait deviates from the mean parental trait according to a Gaussian kernel of fixed segregational variance. The classical interpretation is that the trait under consideration results from the combination of a large number of loci with small additive allelic effects (Lange 1978; Bulmer 1980; Turelli and Barton 1994; Tufto 2000; Turelli 2017), a framework rigorously justified in [Barton, Etheridge, and Véber 2017]. In another study [Perthame, Strugarek, and Taing 2021], asymmetrical kernels are considered to model the effect of asymmetrical trait inheritance or fecundity on the asymptotic behaviour of the trait distribution. The present work also studies sexually reproducing populations, but the genetical framework is different from the ones aforementioned: here, we consider that the allelic effects at the two loci are continuous and not necessarily small nor additive.

Small variance methodology and long term-dynamics. We choose to place our study in the small variance methodology, introduced for quantitative genetics studies in [Diekmann, Jabin, et al. 2005] from a high-frequency method used in geometric optics. When the variance introduced by events of reproduction (by mutations, segregation...) is small compared to the reduction of diversity following natural selection, they propose to unfold Dirac singularities that are expected to arise using the so-called Hopf-Cole transform:

$$\boldsymbol{n}_\varepsilon = \frac{e^{\frac{\boldsymbol{u}_\varepsilon}{\varepsilon}}}{\varepsilon}.$$

The idea behind considering u_ε instead of n_ε stems from the fact that, when ε vanishes, the limit u (to be characterized) is expected to have more regularity than the (measure) limit n, making it more suitable for analysis. Moreover, u would retain important quantitative information on the support of n.

The small variance methodology has first been applied successfully to several quantitative genetics settings for asexual reproducing populations in the regime of small variance of mutations: adaptation to homogeneous environments [Perthame and Barles 2008; Barles, Mirrahimi, and Perthame 2009], to spatially heterogeneous environments [Mirrahimi 2017; Mirrahimi and Gandon 2020], in a time-periodic environment [Figueroa Iglesias and Mirrahimi 2018]. Recently, it has been extended to quantitative genetics models for sexually reproducing populations characterized by complex traits inherited according to the aforementioned infinitesimal model (Calvez, Garnier, and Patout 2019; Patout 2020; Dekens and Lavigne 2021; Dekens 2022; Dekens, Otto, and Calvez 2021). However, the asymptotic analysis of this non-local, non-monotone, non-linear operator of reproduction presents great analytical challenges, and it has only been rigorously derived in a model for homogeneous environments (Calvez, Garnier, and Patout 2019; Patout 2020). The same methodology is used in [Perthame, Strugarek, and Taing 2021] to study the asymptotic behaviour of the trait distribution under asymmetrical reproduction kernels. Here, as described above, our genetical framework differs significantly from the infinitesimal model's one. Therefore, it yields a different reproduction operator (see Eq. ($P(n_\varepsilon)$)), which is in fact more similar to the ones used for asexual populations (Perthame and Barles 2008; Barles, Mirrahimi, and Perthame 2009). However, the nonlinear nonlocal term describing the reproduction operator still leads to new difficulties to be overcomed.

Let us then consider $(\boldsymbol{u}_{0,\varepsilon})_{\varepsilon>0}$ a sequence in $C^1(I \times J)$, uniformly bounded when ε vanishes. It defines subsequently a sequence of concentrated initial genotypic densities with de-

creasingly small variance $\boldsymbol{n}_{0,\varepsilon}$ through the Hopf-Cole transform (6.1). Let us define $\boldsymbol{n}_\varepsilon$ solution of ($P(\boldsymbol{n})$) with initial distribution $\boldsymbol{n}_{0,\varepsilon}$, and $\boldsymbol{u}_\varepsilon$ similarly as above:

$$\boldsymbol{n}_\varepsilon = \frac{e^{\frac{\boldsymbol{u}_\varepsilon}{\varepsilon}}}{\varepsilon}.$$

We expect indeed that starting with such an initial condition (6.1), the population density $\boldsymbol{n}_\varepsilon$ would keep the same exponential form and would remain asymptotically concentrated with a small variance. Consequently, the dynamics of its mean, driven by natural selection with an intensity correlated to its variance, cannot be observed at shallow time scales, and ($P(\boldsymbol{n})$) needs to be adequately rescaled in order to explore long term dynamics.

Moreover, in order to study the asymptotic properties of n_ε, we align with [Perthame and Barles 2008; Barles, Mirrahimi, and Perthame 2009; Mirrahimi 2017; Mirrahimi and Gandon 2020], and introduce the derived problem on $u_\varepsilon := \varepsilon \log(\varepsilon\, n_\varepsilon)$:

$$\begin{cases} \partial_t\, u_\varepsilon = -\left(m(x,y) + \kappa\, \rho_\varepsilon - \frac{r}{2}\right) + \frac{r}{2\rho_\varepsilon} \iint_{I\times J} \frac{1}{\varepsilon} \exp\left[\dfrac{u_\varepsilon(x,y') + u_\varepsilon(x',y) - u_\varepsilon(x,y)}{\varepsilon}\right] dx'\, dy', \\ u_\varepsilon(0,\cdot,\cdot) = u^0_\varepsilon, \\ \rho_\varepsilon = \iint_{I\times J} \dfrac{1}{\varepsilon} \exp\left[\dfrac{u_\varepsilon(x',y')}{\varepsilon}\right] dx'\, dy'. \end{cases} \tag{P_{u_ε}}$$

6.1.3 Assumptions

We assume that the selection term m satisfies the following:

$$m \in C^1(I\times J, \mathbb{R}_+), \quad 4\,\|m\|_\infty < r. \tag{H1}$$

For $\varepsilon > 0$, let $u_{0,\varepsilon} \in C^1(I\times J)$ be such that:

$$\exists M > 0, \quad \forall \varepsilon \le 1, \quad \|u_{0,\varepsilon}\|_{W^{1,\infty}(I\times J)} \le M. \tag{H2}$$

Then we define the initial state by

$$n_{0,\varepsilon} = \frac{e^{\frac{u_{0,\varepsilon}}{\varepsilon}}}{\varepsilon}.$$

Let us define the following uniform bounds:

$$\rho_0^- := \frac{r - \|m\|_\infty}{\kappa}, \quad \rho_0^+ := \frac{r}{\kappa}.$$

We assume that the initial size of population is bounded uniformly by ρ_0^- and ρ_0^+:

$$\forall \varepsilon > 0, \quad \rho^0_\varepsilon := \iint_{I\times J} n^0_\varepsilon(x,y)\, dx\, dy \ \in \left]\rho_0^-, \rho_0^+\right[. \tag{H3}$$

Next, to prepare Proposition 6.1.1, we assume that there exists $0 < \nu_m \le 1 - 4\frac{\|m\|_\infty}{r} < 1 + 4\frac{\|m\|_\infty}{r} \le \nu_M$ such that:

$$\forall \varepsilon,\ \forall (x,y) \in I\times J, \quad \nu_m \le \nu^0_\varepsilon(x,y) := \frac{\rho^{X,0}_\varepsilon(y)\, \rho^{Y,0}_\varepsilon(x)}{n^0_\varepsilon(x,y)\, \rho^0_\varepsilon} \le \nu_M. \tag{H4}$$

6.1.4 Presentation of the results and outline.

First, we show some preliminary results of well-posedness of $P(n_\varepsilon)$:

Theorem 6.1.1. *Under the assumption H3, $(P(n_\varepsilon))$ has a unique solution with positive values n_ε in $C^1(\mathbb{R}_+ \times I \times J) \cap C^1(\mathbb{R}_+, L^1(I \times J))$. More precisely, we have for all ε:*

$$\rho_0^- \leq \rho_\varepsilon \leq \rho_0^+.$$

Hence, for all $T > 0$, (n_ε) converges along subsequences in $L^\infty(w^* - [0,T], M^1(I \times J))$ toward a measure n when ε vanishes.

We recall that we expect n_ε to concentrate as ε vanishes. As such, we expect the weak limit n to be a sum of Dirac masses. The aim of this paper is to determine where n is supported, that is to determine which alleles become dominant in the population. To study the asymptotic properties of n, it is more convenient to shift the asymptotic analysis from n_ε on $u_\varepsilon = \varepsilon \log(\varepsilon\, n_\varepsilon)$. Consequently, the main result of this paper focuses on the asymptotic behaviour of u_ε:

Theorem 6.1.2. *Under the assumptions H2-H4, for all $T > 0$, $u_\varepsilon \underset{\varepsilon \to 0}{\longrightarrow} u$ in $C^0([0,T] \times I \times J)$ (along subsequences). Additionally, u satisfies the following properties:*

(i) *u is Lipschitz continuous,*

(ii) *u is non-positive and satisfies an additive separation of variables property:*

$$\forall (t,x,y) \in [0,T] \times I \times J, \quad u(t,x,y) = u^Y(t,x) + u^X(t,y) := \max u(t,x,\cdot) + \max u(t,\cdot,y). \tag{6.2}$$

Furthermore, we have at all time t: $\max u^Y(t,\cdot) = \max u^X(t,\cdot) = 0$.

(iii) *$n(t,\cdot,\cdot)$ is supported at the zeros of $u(t,\cdot,\cdot)$ for a.e. t:*

$$\begin{aligned} \operatorname{supp}(n(t,\cdot,\cdot)) &\subset \{(x,y) \,|\, u(t,x,y) = 0\} \\ &= \{x \,|\, u^Y(t,x) = 0\} \times \{y \,|\, u^X(t,y) = 0\}. \end{aligned}$$

(iv) *u^X (resp. u^Y) satisfies the following limit equation for a.e. y:*

$$\forall t \in [0,T] \quad u^X(t,y) = u^X(0,y) + r\,t - \kappa \int_0^t \rho(s)\, ds - \int_0^t \left\langle \phi^X(t,\cdot,y), m(\cdot,y) \right\rangle ds, \tag{6.3}$$

where ϕ^X is the limit of $\frac{n_\varepsilon}{\rho_\varepsilon^X}$ in $L^\infty\left(w^* - [0,T] \times I, M^1(I)\right)$. Moreover, for a.e. (t,y)

$$\operatorname{supp}\left(\phi^X(t,\cdot,y)\right) = \{x \,|\, u^Y(t,x) = 0\}.$$

The second and third point of the results in Theorem 6.1.2 highlight the originality of this problem: the limit u separates the variables additively and therefore, the limit measure n is a product measure. This asymptotic decorrelation of the effects of the two loci relies on the following proposition, that is key to establish the convergence stated in Theorem 6.1.2:

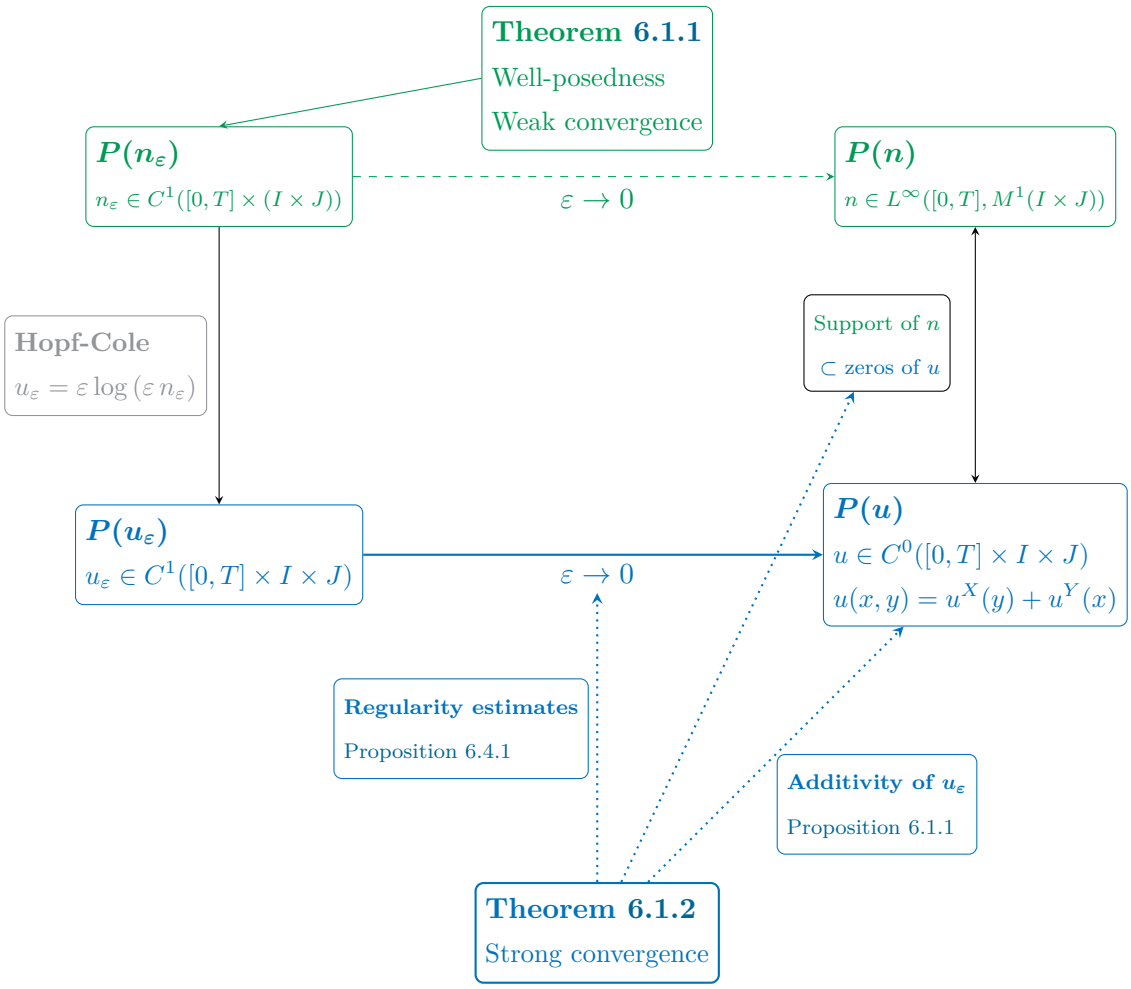

Figure 6.1: Flowchart of the analytical results of Section 6.3, Section 6.4 and Section 6.5.

Proposition 6.1.1. *Let us assume H4. Let n_ε be the positive solution of $(P(n_\varepsilon))$ on $[0,T]$. Define $\nu_\varepsilon = \frac{\rho_\varepsilon^X \rho_\varepsilon^Y}{n_\varepsilon \rho_\varepsilon}$. Then:*

$$0 < \nu_m \leq \nu_\varepsilon \leq \nu_M.$$

Indeed, the compactness result of Proposition 6.1.1 together with some a priori estimates relying on a maximum principle yield the convergence of Theorem 6.1.2 thanks to the Arzela-Ascoli theorem (see 6.1 for a flowchart that exposes the layout of the different results).

Moreover, although P_{u_ε} involves an equation on u_ε, one can notice that Theorem 6.1.2 states limit equations on u^X and u^Y (6.3). Instead of passing to the limit in the equation of u in P_{u_ε} once the convergence is established (as it is done in most asexual studies in the regime of small variance), the separation of variables $u(x,y) = u^X(y) + u^Y(x)$ allows us to take an alternative approach. In the proof Theorem 6.1.2, we will show indeed that $u^X = \lim_{\varepsilon\to 0} \varepsilon \log\left(\rho_\varepsilon^X\right)$ and $u^Y = \lim_{\varepsilon\to 0} \varepsilon \log\left(\rho_\varepsilon^Y\right)$. The idea is then to focus on the equations satisfied by ρ_ε^X and ρ_ε^Y instead of the equation satisfied by n_ε:

$$\begin{cases} \varepsilon\, \partial_t \rho_\varepsilon^X = (r - \kappa\, \rho_\varepsilon)\, \rho_\varepsilon^X - \int_I m(x,y)\, n_\varepsilon(t,x,y)\, dx, \\ \varepsilon\, \partial_t \rho_\varepsilon^Y = (r - \kappa\, \rho_\varepsilon)\, \rho_\varepsilon^Y - \int_J m(x,y)\, n_\varepsilon(t,x,y)\, dy. \end{cases} \tag{6.4}$$

The advantage of considering (6.4) over (P_{u_ε}) is that the reproduction terms involved are linear, much simpler than the integral operator involved in the equation on u_ε. However, the difficulties are transferred on the selections terms $\int_I m(x,y)\, n_\varepsilon(t,x,y)\, dx$ and $\int_I m(x,y)\, n_\varepsilon(t,x,y)\, dx$ that asymptotically lead to involve ϕ^X and ϕ^Y in (6.3). These terms are new compared to the typical asexual studies, which only present two unknown variables in their constrained limit equation: u and ρ. Consequently, here, regularity in time, which would allow us to write the limit equation (6.3) under a differential form, is harder to get for ρ and ϕ^X (resp. ϕ^Y).

Nevertheless, under an additional hypothesis on the selection term m being additive, we show that the limit size of population ρ is BV. This result aligns with the typical analogous regularity obtained on the asymptotic size of population in aforementioned asexual studies.

Theorem 6.1.3. *Suppose that there exists $m^X : I \to \mathbb{R}$ and $m^Y : I \to \mathbb{R}$ such that:*

$$m(x,y) = m^X(x) + m^Y(y). \tag{$\mathrm{H}_{m,\mathrm{add}}$}$$

Let n_ε be the solution to Eq. ($P\,(n_\varepsilon)$). Then, ρ_ε is locally uniformly bounded in $W^{1,1}(\mathbb{R}_+)$. Consequently, after extraction of a subsequence, ρ_ε converges to a BV-function ρ as ε vanishes. The limit ρ is non-decreasing as soon as there exists a constant $C > 0$ such that:

$$(r - \kappa\, \rho_\varepsilon^0)\, \rho_\varepsilon^0 - \iint_{\mathbb{R}^2} m(x,y)\, n_\varepsilon^0(x,y)\, dx\, dy \geq -C\, e^{\frac{o(1)}{\varepsilon}}. \tag{6.5}$$

The paper is organized as follows. In Section 6.2, we present qualitative results and numerical analysis that stem from the analysis of the subsequent sections, and demonstrate the interest of the model by exploring some biologically relevant situations. Next, in Section 6.3, we prove the well-posedness of $P\,(n_\varepsilon)$. Section 6.4 is dedicated to show Proposition 6.1.1 and derive uniform L^∞ and Lipschitz bounds for u_ε, which prepares the proof of the main result in Section 6.5. The interplay between the different results until that point is displayed in Fig. 6.1. Finally, in Section 6.6, we show that ρ is a BV-function, under the additional hypothesis ($\mathrm{H}_{m,\mathrm{add}}$).

6.2 Qualitative results and numerical analysis.

In this section, we explore the insights on the dynamics of the allelic distribution in a population following the main result of the paper (Theorem 6.1.2), assuming that $(t,y) \mapsto \phi^X(t,\cdot,y)$, $(t,x) \mapsto \phi^Y(t,x,\cdot)$ and $t \mapsto n(t,\cdot,\cdot)$ (and by extension $t \mapsto \rho^X(t,\cdot)$, $t \mapsto \rho^Y(t,\cdot)$ and ρ) are continuous so that we can formally write:

$$\begin{cases} \forall (t,y) \in [0,T] \times I, \quad \partial_t u^X(t,y) = r - \kappa\, \rho(t) - \left\langle \phi^X(t,\cdot,y), m(\cdot,y) \right\rangle, \\ \forall (t,x) \in [0,T] \times I, \quad \partial_t u^Y(t,x) = r - \kappa\, \rho(t) - \left\langle \phi^Y(t,x,\cdot), m(x,\cdot) \right\rangle. \end{cases} \tag{6.6}$$

We first show that under a hypothesis of strict monotony $\mathrm{H}_{\mathrm{increasing}}$ on the selection, the population is strained to be monomorphic, i.e. all individuals share the same alleles $(\bar{x}(t), \bar{y}(t))$ at all times. Then, we derive canonical equations describing the dynamics of $(\bar{x}(t), \bar{y}(t))$ under monomorphism.

6.2.1 Monotonic selection yields monomorphism.

We first show that a condition of monotony on m (in both variables) yields the limit allelic distribution to be monomorphic at all times:

Proposition 6.2.1. *For $T > 0$, assume that (6.6) holds and that m satisfies:*

$$\forall (x,y) \in I \times J, m(x,\cdot) \text{ and } m(\cdot,y) \text{ are increasing (resp. decreasing).} \qquad (\mathrm{H}_{\mathrm{increasing}})$$

Then: $\forall t \in [0,T],\ \exists!\, (\bar{x}(t), \bar{y}(t))$,

$$Supp\left(\rho^X\right) = \left[u^X\right]^{-1}(\{0\}) = \{\bar{y}(t)\}, \quad Supp\left(\rho^Y\right) = \left[u^Y\right]^{-1}(\{0\}) = \{\bar{x}(t)\}.$$

Proof of Proposition 6.2.1. For $t \in [0,T]$, since $n(t,\cdot,\cdot)$ is supported at the zeros of $u(t,\cdot,\cdot)$ (see Theorem 6.1.2), $\rho^X(t,\cdot)$ is supported on the set of the zeros of $u^X(t,\cdot)$, that we denote by $F_X(t)$, and $\rho^Y(t,\cdot)$ is supported on the set of the zeros of $u^Y(t,\cdot)$, that we denote by $F_Y(t)$. It is therefore sufficient to prove that $F_X(t)$ and $F_Y(t)$ are both singletons for all $t \in [0,T]$.

Since $u^X(t,\cdot)$ and $u^Y(t,\cdot)$ are continuous, $F_X(t)$ and $F_Y(t)$ are closed subsets of I and J, and are therefore compact sets. In particular, the extreme points of $F_X(t)$ (resp. $F_Y(t)$) denoted by $y_{\inf}(t)$ and $y_{\sup}(t)$ (respectively, $x_{\inf}(t)$ and $x_{\sup}(t)$) lie in $F_X(t)$ (respectively, $F_Y(t)$). As $(t, y_{\inf}(t))$ and $(t, y_{\sup}(t))$ maximise u^X and $(t, x_{\inf}(t))$ and $(t, x_{\sup}(t))$ maximise u^Y (since u^X are u^Y are non-positive, from Theorem 6.1.2), we obtain that

$$0 = \partial_t u^X(t, y_{\inf}(t)) = \partial_t u^X(t, y_{\sup}(t)) = \partial_t u^Y(t, x_{\inf}(t)) = \partial_t u^Y(t, x_{\sup}(t)).$$

The equations Eq. (6.6) next implies that

$$\begin{aligned}\forall t \in [0,t], \left\langle \phi^X(t,\cdot,y_{\inf}(t)), m(\cdot,y_{\inf}(t))\right\rangle &= \left\langle \phi^X(t,\cdot,y_{\sup}(t)), m(\cdot,y_{\sup}(t))\right\rangle \\ = \left\langle \phi^Y(t,x_{\inf}(t),\cdot), m(x_{\inf}(t),\cdot)\right\rangle &= \left\langle \phi^Y(t,x_{\sup}(t),\cdot), m(x_{\sup}(t),\cdot)\right\rangle.\end{aligned}$$

Recall that, for $(t,x,y) \in [0,T] \times I \times J$, $\phi^X(t,\cdot,y)$ and $\phi^X(t,x,\cdot)$ are probability distributions supported respectively on a subset of $F_X(t)$ and $F_Y(t)$ (from Theorem 6.1.2). Then, we deduce from $\mathrm{H}_{\mathrm{increasing}}$ that:

$$\begin{aligned} m\left(x_{\inf}(t), y_{\sup}(t)\right) &\leq \left\langle \phi^X(t,\cdot,y_{\sup}(t)), m(\cdot,y_{\sup}(t))\right\rangle \\ &= \left\langle \phi^Y(t,x_{\inf}(t),\cdot), m(x_{\inf}(t),\cdot)\right\rangle \\ &\leq m\left(x_{\inf}(t), y_{\sup}(t)\right).\end{aligned}$$

Similarly, we obtain

$$\begin{aligned} m\left(x_{\sup}(t), y_{\inf}(t)\right) &\leq \left\langle \phi^Y(t,x_{\sup}(t),\cdot), m(x_{\sup}(t),\cdot)\right\rangle \\ &= \left\langle \phi^X(t,\cdot,y_{\inf}(t)), m(\cdot,y_{\inf}(t))\right\rangle \\ &\leq m\left(x_{\sup}(t), y_{\inf}(t)\right).\end{aligned}$$

All the inequalities above must be equalities, which implies

$$\begin{aligned} \phi^X(t,x,y_{\sup}(t)) &= \delta_{x=x_{\inf}(t)}, \quad \phi^X(t,x,y_{\inf}(t)) = \delta_{x=x_{\sup}(t)}, \\ \phi^Y(t,x_{\sup}(t),y) &= \delta_{y=y_{\inf}(t)}, \quad \phi^Y(t,x_{\inf}(t),y) = \delta_{y=y_{\sup}(t)}. \end{aligned} \tag{6.7}$$

Since the support of $\phi^X(t,\cdot,y)$ (resp. $\phi^Y(t,x,\cdot)$) does not depend on y (resp. x) (see (iv) of Theorem 6.1.2), we obtain from (6.7) that $x_{\inf}(t) = x_{\sup}(t)$ and $y_{\inf}(t) = y_{\sup}(t)$. The latter yields the result. □

Numerical simulations: robustness of monomorphism with regard to $\mathrm{H}_{\text{increasing}}$ of Proposition 6.2.2 with dimorphic initial densities. We show in Fig. 6.2 the result of numerical simulations solving a discretized version of $(P(n_\varepsilon))$ with initial dimophic states to test the robustness of monomorphic trajectories with regard to $\mathrm{H}_{\text{increasing}}$. We consider three different selection functions $m(x,y) = x^2 + y^2$, $m(x,y) = (x+y)^2$, $m(x,y) = (1-xy)^2$. Fig. 6.2 seems to indicate that monomorphic trajectories occur under a wider scope than the what is required by Proposition 6.2.1. Fig. 6.2 also gives some insights on the diversity of trajectories that can arise under different selections functions (see the next subsection for a more complete view).

6.2.2 Canonical equations under monomorphism.

In all this section, let us fix $T > 0$ and let us assume that for all time $t \in [0,T]$, there exists unique points $\bar{x}(t)$ and $\bar{y}(t)$ such that:

$$\forall t \in [0,T] \quad u(t,\cdot,\cdot)^{-1}(\{0\}) = \{(\bar{x}(t),\bar{y}(t))\}. \tag{6.8}$$

In that case, for all $(t,x,y) \in [0,T] \times I \times J$, we deduced from Theorem 6.1.2 that:

$$\phi^X(t,\cdot,y) = \delta_{\bar{x}(t)}, \quad \phi^Y(t,x,\cdot) = \delta_{\bar{y}(t)}.$$

Hence, (6.6) reads:

$$\begin{cases} \forall (t,y) \in [0,T] \times I, & \partial_t u^X(t,y) = r - \kappa\,\rho(t) - m(\bar{x}(t)),y), \\ \forall (t,x) \in [0,T] \times I, & \partial_t u^Y(t,x) = r - \kappa\,\rho(t) - m(x,\bar{y}(t)). \end{cases} \tag{6.9}$$

Proposition 6.2.2. *For $T > 0$, assume that $m, u_0 \in C^2(I \times J)$ and that (6.9) holds. Then: $u \in C^0([0,T], C^2(I \times J))$ and the dynamics of the dominant alleles $(\bar{x}(t),\bar{y}(t))$ read:*

$$\begin{cases} \partial_{xx} u^Y(\bar{x}(t))\,\frac{d\bar{x}}{dt} = \partial_x m(\bar{x}(t),\bar{y}(t)), \\ \partial_{yy} u^X(\bar{y}(t))\,\frac{d\bar{y}}{dt} = \partial_x m(\bar{x}(t),\bar{y}(t)). \end{cases} \tag{6.10}$$

Proof. Let us show how to obtain the first equation of (6.10) on $\bar{x}(t)$. The equation on $\bar{y}(t)$ can be obtained similarly.

As $0 = \partial_x u^Y(t,\bar{x}(t)) = u^Y(t,\bar{x}(t)) = \max u^Y(t,\cdot)$ for all $t \in [0,T]$, we get:

$$0 = \frac{d\,\partial_x u^Y(t,\bar{x}(t))}{dt} = \partial_t \partial_x u^Y(t,\bar{x}(t)) + \partial_{xx} u^Y(t,\bar{x}(t))\,\frac{d\bar{x}}{dt}.$$

Differentiating (6.9) with regard to x reads:

$$\forall (t,x) \in [0,T] \times I, \quad \partial_x \partial_t u^Y(t,x) = -\partial_x m(x,\bar{y}(t)).$$

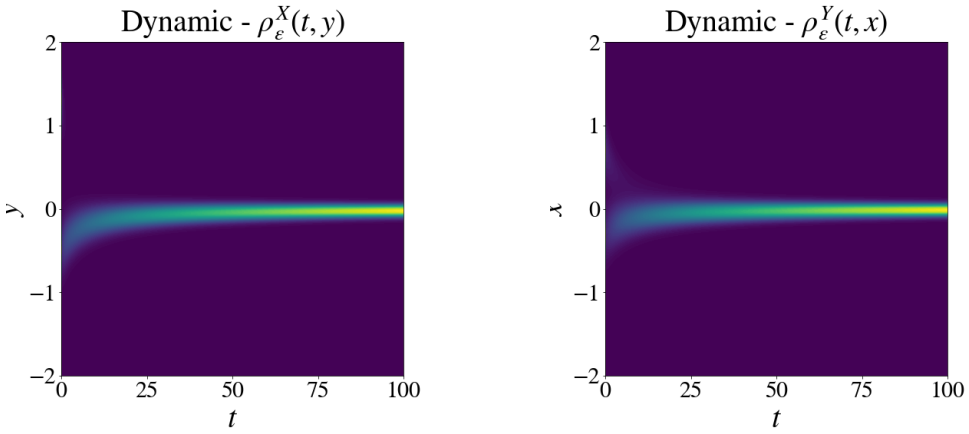

(a) $m(x,y) = x^2 + y^2$ (b) $m(x,y) = x^2 + y^2$.

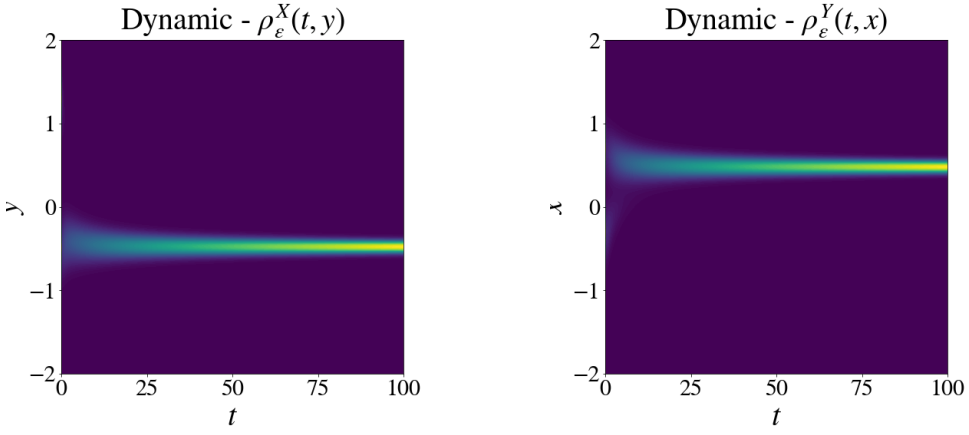

(c) $m(x,y) = (x+y)^2$. (d) $m(x,y) = (x+y)^2$.

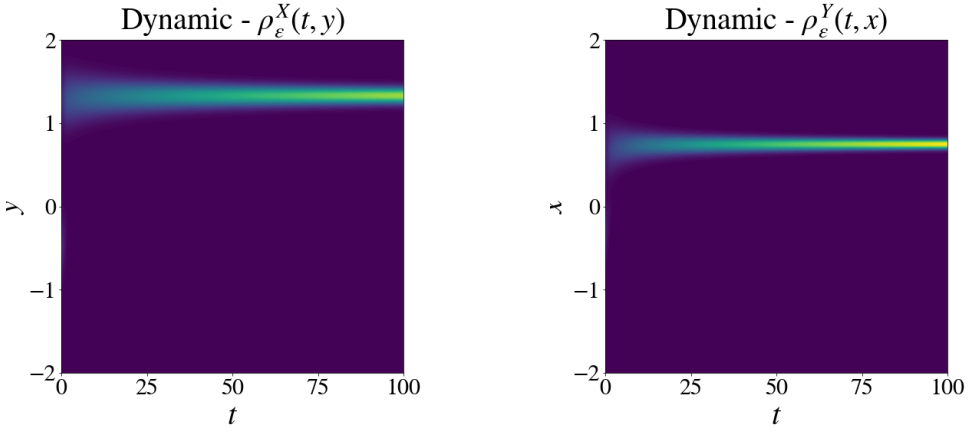

(e) $m(x,y) = (1 - x\,y)^2$. (f) $m(x,y) = (1 - x\,y)^2$.

Figure 6.2: **Robustness of monomorphism with regard to assumption $\mathrm{H}_{\text{increasing}}$ of Proposition 6.2.2 with dimorphic initial densities.** For each selection function (by row), we display the numerically solved dynamics of $\rho^X(t,y)$ (left panel) and $\rho^Y(t,x)$ (right panel) ($(x,y) \in [-2,2]$). The initial state is sum of two Gaussians centered in $(x_1,y_1) = (-0.3, 1.3)$ and $(x_2,y_2) = (0.7,-0.5)$ and of variance $\varepsilon = 0.05$. Lighter colors indicate stronger densities. The figures seem to indicate that the trajectories become monomorphic almost instantaneously and that this phenomenon actually occur under weaker conditions than $\mathrm{H}_{\text{increasing}}$ of Proposition 6.2.2. One can also notice that the stationary dominant alleles that arise vary greatly from one selection function to another.

By substitution, we obtain:

$$\frac{d\bar{x}}{dt}\,\partial_{xx}u^Y(t,\bar{x}(t)) = \partial_x m(\bar{x}(t),\bar{y}(t)).$$

□

Remark 15. *As $\bar{x}(t)$ maximizes u^Y, we have $\partial_{xx}u^Y(t,\bar{x}(t)) \leq 0$ for all $t \in [0,T]$. If $\partial_{xx}u^Y(t,\bar{x}(t)) < 0$ for all $t \in [0,T]$, then we obtain:*

$$\forall t \in [0,T], \quad \frac{d\bar{x}}{dt} = \frac{\partial_x m(\bar{x}(t),\bar{y}(t))}{\partial_{xx}u^Y(t,\bar{x}(t))}.$$

As $\partial_t\partial_{xx}u^Y(t,x) = -\partial_{xx}m(x,\bar{y}(t))$, we obtain

$$\partial_{xx}u^Y(t,x) = \partial_{xx}u^Y(0,x) - \int_0^t \partial_{xx}m(x,\bar{y}(s))\,ds.$$

Consequently, the strict inequality is ensured if u_0 is strictly concave and m is convex.

Three examples. In this paragraph, we illustrate the insights provided by Proposition 6.2.2 through the study of the system for three given selection functions m. In all examples, we consider that $I = J = [-2,2]$ and the initial state u_0 is given by $(\bar{x}_0,\bar{y}_0) \in [-2,2]^2$ and:

$$u_0(x,y) = -((x-\bar{x}_0)^2 + (y-\bar{y}_0)^2).$$

1) $m(x,y) = x^2+y^2$, $\partial_x m(x,y) = 2x$, $\partial_y m(x,y) = 2y$, $\partial_{xx}m(x,y) = \partial_{yy}m(x,y) = 2$.

This selection function separates additively the variables. The canonical equation Eq. (6.10) then reads:

$$\begin{cases} \frac{d\bar{x}(t)}{dt} = -\frac{\bar{x}(t)}{t+1}, \\ \frac{d\bar{y}(t)}{dt} = -\frac{\bar{y}(t)}{t+1}. \end{cases}$$

We obtain that, for $t \geq 0$

$$\bar{x}(t) = \frac{\bar{x}_0}{t+1}, \quad \bar{y}(t) = \frac{\bar{y}_0}{t+1}.$$

Consequently, the system remains monomorphic and the dominant alleles evolve and converge towards $(0,0)$.

2) $m(x,y) = (x+y)^2$, $\partial_x m(x,y) = \partial_y m(x,y) = 2(x+y)$, $\partial_{xx}m(x,y) = \partial_{yy}m(x,y) = 2$.

The canonical equation Eq. (6.10) then reads:

$$\frac{d\bar{x}(t)}{dt} = \frac{d\bar{y}(t)}{dt} = -\frac{\bar{x}(t)+\bar{y}(t)}{t+1}.$$

We deduce that, for $t \geq 0$

$$\bar{x}(t)+\bar{y}(t) = \frac{\bar{x}_0+\bar{y}_0}{(t+1)^2}, \quad \bar{x}(t)-\bar{y}(t) = \bar{x}_0-\bar{y}_0,$$

which leads to:

$$\bar{x}(t) = \frac{\bar{x}_0-\bar{y}_0}{2} + \frac{\bar{x}_0+\bar{y}_0}{2(t+1)^2}, \quad \bar{y}(t) = \frac{\bar{y}_0-\bar{x}_0}{2} + \frac{\bar{x}_0+\bar{y}_0}{2(t+1)^2}.$$

On the contrary to the previous example, the dominant alleles of the monomorphic system evolve to converge towards a state that is dependent on the initial state of the system. Geometrically, it is the orthogonal projection of the initial point $(\bar{x}_0, \bar{y}_0)$ on the diagonal defined by $x + y = 0$.

3) $m(x,y) = (1-xy)^2$, $\partial_x m(x,y) = -2\,y\,(1-xy)$, $\partial_y m(x,y) = -2\,x\,(1-xy)$, $\partial_{xx} m(x,y) = 2\,y^2$, $\partial_{yy} m(x,y) = 2\,x^2$.

In this case, the canonical equation (6.10) reads:

$$\frac{d\bar{x}(t)}{dt} = \frac{\bar{y}(t)\,(1-\bar{x}(t)\bar{y}(t))}{1+\int_0^t \bar{y}(s)^2\,ds} \qquad \frac{d\bar{y}(t)}{dt} = \frac{\bar{x}(t)\,(1-\bar{x}(t)\bar{y}(t))}{1+\int_0^t \bar{x}(s)^2\,ds}. \tag{6.11}$$

Without lack of generality, we can assume that $\bar{x}_0 \leq \bar{y}_0$.

Proposition 6.2.3. *Let $0 < \bar{x}_0 \leq \bar{y}_0 \leq 2$. Then the dominant alleles of the monomorphic system converge towards the stationary state $(x_F, y_F) \in \left(\mathbb{R}_+^*\right)^2$ that solves:*

$$\begin{cases} x_F\, y_F = 1, \\ y_F^2 - x_F^2 = \bar{y}_0^2 - \bar{x}_0^2. \end{cases} \tag{6.12}$$

Proof. First, we treat the case where $x_0\, y_0 = 1$. Then, the function $t \mapsto (x_0, y_0)$ defines a solution of (6.11). By uniqueness, it is the only solution and (x_0, y_0) satisfies (6.12).

Let us now suppose that $x_0\, y_0 < 1$ (the case where $x_0\, y_0 > 1$ can be treated following similar arguments). We define, for $A > 0$ yet to be specified:

$$t_A = \min\left\{\inf\{t \geq 0, (\bar{x}(t), \bar{y}(t)) \notin]0, A[^2\}, \inf\{t \geq 0, \bar{x}(t)\bar{y}(t) \notin]0,1[\}\right\}.$$

For $t \leq t_A$, we have the following inequalities

$$\frac{\bar{y}\,(1-\bar{x}\bar{y})}{1+A^2\,t} \leq \frac{d\bar{x}}{dt} \leq \bar{y}\,(1-\bar{x}\bar{y}), \qquad \frac{\bar{x}\,(1-\bar{x}\bar{y})}{1+A^2\,t} \leq \frac{d\bar{y}}{dt} \leq \bar{x}\,(1-\bar{x}\bar{y}). \tag{6.13}$$

Let us define (x^-, y^-) and (x^+, y^+) solutions of the following equations:

$$\begin{cases} \frac{dx^-(t)}{dt} = \frac{y^-(t)\left(1-x^-(t)y^-(t)\right)}{1+A^2\,t}, & \frac{dx^+(t)}{dt} = y^+(t)\,(1-x^+(t)y^+(t)), \\ \frac{dy^-(t)}{dt} = \frac{x^-(t)\left(1-x^-(t)y^-(t)\right)}{1+A^2\,t}, & \frac{dy^+(t)}{dt} = x^+(t)\,(1-x^+(t)y^+(t)), \\ (x^-(0), y^-(0)) = (\bar{x}_0, \bar{y}_0), & (x^+(0), y^+(0)) = (\bar{x}_0, \bar{y}_0). \end{cases} \tag{6.14}$$

By comparison, we deduce that (x^-, y^-) and (x^+, y^+) are respectively subsolution and supersolution of $(\bar{x}, \bar{y})$:

$$\forall t \leq t_A, \quad x^-(t) \leq \bar{x}(t) \leq x^+(t), \quad y^-(t) \leq \bar{y}(t) \leq y^+(t). \tag{6.15}$$

We define t_A^+ by

$$t_A^+ = \min\left\{\inf\{t \geq 0, (x^+(t), y^+(t)) \notin]0, A[^2\}, \inf\{t \geq 0, x^+(t)y^+(t) \notin]0,1[\}\right\}.$$

We will show that x^+y^+ converges increasingly toward 1. First one can compute that

$$\frac{d\left(x^+y^+\right)}{dt} = \left(1 - x^+y^+\right)\left(x^{+2} + y^{+2}\right).$$

Next, one can notice from (6.14) that x^+ and y^+ both increase on $[0, t_A^+]$. We thus obtain that for $t \in [0, t_A^+]$

$$\left(1 - x^+ y^+\right)\left(x_0^2 + y_0^2\right) \leq \frac{d(x^+ y^+)}{dt} \leq 2A^2\left(1 - x^+ y^+\right).$$

Hence, by comparison, $x^+ y^+$ converges increasingly toward 1.

We next notice thanks to (6.14) that:

$$\frac{1}{2}\frac{dx^{+2}(t)}{dt} = x^+(t)y^+(t)\left(1 - x^+(t)y^+(t)\right) = \frac{1}{2}\frac{dy^{+2}(t)}{dt},$$

and hence:

$$\forall t \leq t_A^+, \quad x^{+2}(t) - y^{+2}(t) = \bar{x}_0^2 - \bar{y}_0^2.$$

Therefore, since $(\bar{x}_0, \bar{y}_0) \in [0,2]^2$, and $0 < x^+(t)\, y^+(t) < 1$ for $t \leq t_A^+$, the latter implies that, if we choose A large enough, x^+ and y^+ remain uniformly bounded above away from A. Therefore, we can consider t_A^+ arbitrarily large. We deduce that x^+ and y^+ converge increasingly to $x_F > 0$ and $y_F > 0$, satisfying (6.12).

We next show that (x^-, y^-) converges toward the same couple (x_F, y_F). Notice that for $t \leq t_A^+$, we have

$$(x^-(t), y^-(t)) \in]0, A[^2, \quad x^-(t), y^-(t) \leq 1.$$

Similarly as previously, we show by comparison that $x^- y^-$ converges increasingly toward 1, since

$$\left(1 - x^- y^-\right)\left(\frac{x_0^2 + y_0^2}{1 + A^2 t_A^+}\right) \leq \frac{d(x^- y^-)}{dt} \leq 2A^2\left(1 - x^- y^-\right).$$

Next, we notice that we still have:

$$\frac{dx^{-2}(t)}{dt} = \frac{dy^{-2}(t)}{dt} \implies \forall t \leq t_A^+, \quad x^{-2}(t) - y^{-2}(t) = \bar{x}_0^2 - \bar{y}_0^2.$$

We deduce that x^- and y^- converge also increasingly to a solution of (6.12). As (6.12) has a unique solution in $\left(\mathbb{R}_+^*\right)^2$, it must be (x_F, y_F).

Finally, we obtain the announced result using (6.15). □

Numerical analysis. Note that Proposition 6.2.2 relies on the fact that equation (6.9) holds. Due to lack of regularity estimates, in this paper we have proved this property only in a weaker integral form (6.3). However, we conjecture that this property would hold in a rather general framework. In Fig. 6.3 using numerical simulations, we investigate whether the qualitative results obtained above are consistent in the case of the three examples considered in Fig. 6.2. For each selection function above, we display the trajectories of the dominant allelic effects $\bar{x}$ and $\bar{y}$, for 20 numerical resolution of Eq. ($P(n_\varepsilon)$) with $\varepsilon = 0.01$ (plain lines), with initial conditions uniformly randomized over the square $[-2, 2]^2$ (each color corresponds to an initial condition). We confront them to the canonical equations given in Proposition 6.2.2, for the same set of 20 initial conditions (dashed lines). The corresponding trajectories as well as the final states (full circle for the model and cross for the canonical equations) are quite in agreement.

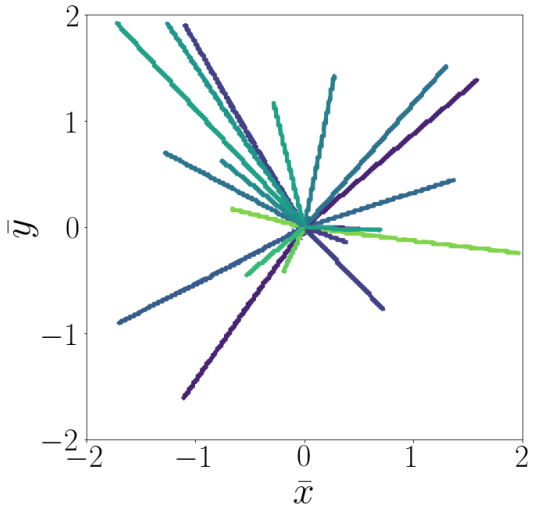

(a) $m(x, y) = x^2 + y^2$.

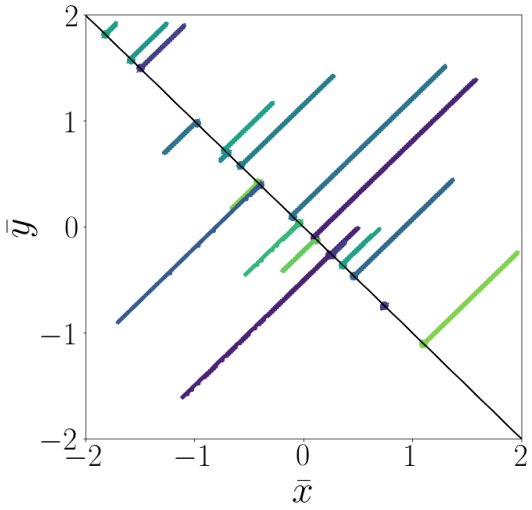

(b) $m(x, y) = (x + y)^2$. (the black line represents the line $x + y = 0$).

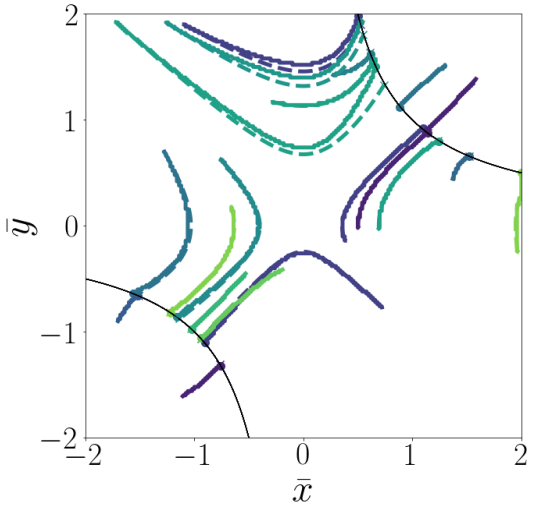

(c) $m(x, y) = (1 - x\,y)^2$. (the black line represents the hyperbola $x\,y = 1$).

Figure 6.3: **Simulated trajectories of the dominant alleles $\bar{x}$ and $\bar{y}$.** The plain lines correspond to the numerical resolution of ($P\,(n_\varepsilon)$), with $\varepsilon = 0.01$. The dashed lines correspond to the numerical resolution of the canonical equations given in Proposition 6.2.2. Each color corresponds to one trajectory starting at an initial monomorphic state chosen randomly and uniformly in $[-2, 2]^2$. The final states of the trajectories obtained from the discretization of ($P\,(n_\varepsilon)$) are indicated by full circles. This figure shows that the qualitative derivation of the section are numerically consistent with the model.

6.3 Preliminary results on the well-posedness of $P(n_\varepsilon)$: proof of Theorem 6.1.1.

Well-posedness of $P(n_\varepsilon)$. In this section, we prove Theorem 6.1.1. The proof relies on two lemmas. We fix $T_M > 0$. The first lemma gives a priori estimates for a solution of $(P(n_\varepsilon))$ on $[0,T_M]\times I\times J$. The second one relies on a contraction mapping argument for $T>0$ small, chosen uniformly with regard to the initial state, so that the reiteration of the process ensures the existence and uniqueness of a solution on $[0,T_M]\times I\times J$.

Lemma 12. *Let $T_M>0$ and $n_\varepsilon\in C^1([0,T_M]\times I\times J)$ be a solution of $(P(n_\varepsilon))$. Then, under the assumptions H1 and H3, we have the following a priori bounds for $t\in[0,T_M]$*

$$\rho_0^- \le \rho_\varepsilon(t)\le \rho_0^+,\quad \|\rho_\varepsilon^X(t,\cdot)\|_\infty \le \|\rho_\varepsilon^{X,0}\|_\infty e^{\frac{r\,t}{\varepsilon}},\quad \|\rho_\varepsilon^Y(t,\cdot)\|_\infty \le \|\rho_\varepsilon^{Y,0}\|_\infty e^{\frac{r\,t}{\varepsilon}}, \tag{6.16}$$

$$\begin{aligned}\|n_\varepsilon(t,\cdot,\cdot)\|_\infty &\le e^{\frac{rt}{2\varepsilon}}\|n_\varepsilon(0,\cdot,\cdot)\|_\infty + e^{\frac{2rt}{\varepsilon}}\frac{\|\rho_\varepsilon^{X,0}\|_\infty\|\rho_\varepsilon^{Y,0}\|_\infty}{\rho_0^-}(e^{\frac{rt}{2\varepsilon}}-1)\\ &\le \mathrm{e}^{\frac{rT_M}{2\varepsilon}}\|n_\varepsilon(0,\cdot,\cdot)\|_\infty + e^{\frac{2rT_M}{\varepsilon}}\frac{\|\rho_\varepsilon^{X,0}\|_\infty\|\rho_\varepsilon^{Y,0}\|_\infty}{\rho_0^-}(e^{\frac{rT_M}{2\varepsilon}}-1) =: N_{T_M},\end{aligned} \tag{6.17}$$

$$\begin{aligned}\|\partial_x n_\varepsilon(t,\cdot,\cdot)\|_\infty &\le \left(\|\partial_x n_\varepsilon^0\|_\infty + N_{T_M}\frac{t}{\varepsilon}\|\partial_x m\|_\infty\right) e^{\frac{\|\rho_\varepsilon^{X,0}\|_\infty |J|}{2\rho_0^-}e^{\frac{r\,t}{\varepsilon}}+\frac{rt}{2\varepsilon}}\\ &\le \left(\|\partial_x n_\varepsilon^0\|_\infty + N_{T_M}\frac{T_M}{\varepsilon}\|\partial_x m\|_\infty\right) e^{\frac{\|\rho_\varepsilon^{X,0}\|_\infty |J|}{2\rho_0^-}e^{\frac{r\,T_M}{\varepsilon}}+\frac{rT_M}{2\varepsilon}} =: N^x_{T_M}.\end{aligned} \tag{6.18}$$

The proof of Lemma 12 relies on classical computations and is left to be consulted in 6.A.

Before stating the next lemma, let us define, for $n\in C^1([0,T]\times I\times J,\mathbb{R}_+)$

$$\rho(n) := \iint_{I\times J} n(\cdot,x,y)\,dx\,dy,\quad \rho^X(n)(t,y) := \int_I n(t,x,y)\,dx,\quad \rho^Y(n)(t,x) := \int_J n(t,x,y)\,dy.$$

We also define, for $T\le T_M$

$$\begin{aligned}\mathcal{A}_\varepsilon^0 = \Big\{ & n\in C^1([0,T]\times I\times J,\mathbb{R}_+)\,|\,n(0,\cdot,\cdot)=n_\varepsilon^0,\quad \rho(n)\in[\rho_0^-,\rho_0^+],\\ & \rho^X(n)(t,y)\le \left\|\rho_\varepsilon^{X,0}\right\|_\infty e^{r\frac{t}{\varepsilon}},\quad \rho^Y(n)(t,x)\le \left\|\rho_\varepsilon^{Y,0}\right\|_\infty e^{r\frac{t}{\varepsilon}},\\ & \|n(t,\cdot,\cdot)\|_\infty \le \left\|n_\varepsilon^0\right\|_\infty e^{\frac{rt}{2\varepsilon}} + e^{\frac{2rt}{\varepsilon}}\frac{\left\|\rho_\varepsilon^{Y,0}\right\|_\infty\left\|\rho_\varepsilon^{Y,0}\right\|_\infty}{\rho_0^-}(e^{\frac{rt}{2\varepsilon}}-1),\\ & \|\partial_x n_\varepsilon(t,\cdot,\cdot)\|_\infty \le \left(\|\partial_x n_\varepsilon^0\|_\infty + N_{T_M}\frac{T_M}{\varepsilon}\|\partial_x m\|_\infty\right) e^{\frac{\|\rho_\varepsilon^{X,0}\|_\infty |J|}{2\rho_0^-}e^{\frac{r\,t}{\varepsilon}}+\frac{rt}{2\varepsilon}}\\ & \|\partial_y n_\varepsilon(t,\cdot,\cdot)\|_\infty \le \left(\|\partial_y n_\varepsilon^0\|_\infty + N_{T_M}\frac{T_M}{\varepsilon}\|\partial_y m\|_\infty\right) e^{\frac{\|\rho_\varepsilon^{Y,0}\|_\infty |I|}{2\rho_0^-}e^{\frac{r\,t}{\varepsilon}}+\frac{rt}{2\varepsilon}}\Big\},\end{aligned}$$

which is a closed subspace of $X := C^1([0,T]\times I\times J,\mathbb{R}_+)$ and has a Banach space structure with the norm $\|.\|_X := \|.\|_\infty + \|\partial_x\cdot\|_\infty + \|\partial_y\cdot\|_\infty$. Let us also define

$$\Phi : \begin{cases}\mathcal{A}_\varepsilon^0\to X\\ n\mapsto \Phi(n) : (t,x,y)\mapsto n_\varepsilon^0(x,y)e^{-\frac{1}{\varepsilon}\int_0^t A[n](s,x,y)ds} + \dfrac{1}{\varepsilon}\displaystyle\int_0^t B[n](\tau,x,y)e^{-\frac{1}{\varepsilon}\int_\tau^t A[n](s,x,y)ds}\,d\tau,\end{cases} \tag{6.19}$$

where

$$A[n](s,x,y) = m(x,y) + \kappa\,\rho(n)(s), \quad B[n](\tau,x,y) = \frac{r}{2}\left(\frac{\rho^X(n)(\tau,y)\,\rho^Y(n)(\tau,x)}{\rho(n)(\tau)} + n(\tau,x,y)\right).$$

.

Lemma 13. *Let $T \leq T_M$. Then, under the assumptions H1 and H3, we have:*

1. $\Phi\left(\mathcal{A}_\varepsilon^0\right) \subset \mathcal{A}_\varepsilon^0$.
2. *For T small enough, Φ is a contraction mapping. Such a T can be chosen uniformly with regard to the intial state.*

The proof of this lemma can be found in Section 6.B.

From Lemma 12, any solution of $P\left(n_\varepsilon\right)$ in $C^1\left([0,T]\times I\times J,\mathbb{R}_+\right)$, for all $T \leq T_M$, lies in $\mathcal{A}_\varepsilon^0$. Next, Lemma 13 allows us to use the Banach-Picard fixed point theorem in $\mathcal{A}_\varepsilon^0$ to prove existence and uniqueness of a solution to $P\left(n_\varepsilon\right)$ in $\mathcal{A}_\varepsilon^0$, hence in $C^1\left([0,T]\times I\times J,\mathbb{R}_+\right)$. Since T does not depend on the initial state, we can iterate this process to extend the well-posedness to $C^1\left([0,T_M]\times I\times J,\mathbb{R}_+\right)$. Finally, since T_M can be arbitrarily large, there exists a unique solution to $P\left(n_\varepsilon\right)$ is $C^1\left(\mathbb{R}_+\times I\times J,\mathbb{R}_+\right)$

Weak convergence of (n_ε). From Lemma 12, for $\varepsilon > 0$ and $t \in [0,T]$, we have:

$$\|n_\varepsilon(t,\cdot,\cdot)\|_{L^1(I\times J)} \leq \rho_0^+.$$

Consequently, (n_ε) is bounded in $L^\infty\left([0,T],L^1(I\times J)\right)$. Hence, there exists a subsequence that converges in $L^\infty\left(w^* - [0,T],M^1(I\times J)\right)$ to a measure n (this fact comes from Lemma 15, stated and proven in Section 6.C).

6.4 Proof of Proposition 6.1.1 and regularity estimates on u_ε.

In this section, we provide the proofs of the regularity estimates that will be used in the proof of Theorem 6.1.2.

6.4.1 Proof of Proposition 6.1.1.

In this subsection, we prove the Proposition 6.1.1, which is a key step to prove the additive separation of variables for u (see Theorem 6.1.2).

Let $t \in [0,T]$, $(x,y) \in I \times J$. We differentiate ν_ε with regard to t to find:

$$\begin{aligned}
\varepsilon\,\partial_t \nu_\varepsilon(t,x,y) &= \frac{\rho_\varepsilon^X\,\varepsilon\,\partial_t\rho_\varepsilon^Y + \rho_\varepsilon^Y\,\varepsilon\,\partial_t\rho_\varepsilon^X}{n_\varepsilon\,\rho_\varepsilon} - \left(\frac{\varepsilon\,\partial_t n_\varepsilon}{n_\varepsilon} + \frac{\varepsilon\,\partial_t\rho_\varepsilon}{\rho_\varepsilon}\right)\nu_\varepsilon \\
&= 2\,(r-\kappa\,\rho_\varepsilon)\,\nu_\varepsilon - \int_I m(x',y)\,\frac{n_\varepsilon(x',y)\,\rho_\varepsilon^Y(x)}{n_\varepsilon(x,y)\rho_\varepsilon}\,dx' - \int_J m(x,y')\,\frac{n_\varepsilon(x,y'),\rho_\varepsilon^X(y)}{n_\varepsilon(x,y)\rho_\varepsilon}\,dy' \\
&\quad - \nu_\varepsilon\left(\frac{r}{2}\nu_\varepsilon + \frac{r}{2} - m(x,y) - \kappa\,\rho_\varepsilon + r - \kappa\,\rho_\varepsilon - \iint_{I\times J} m(x,y)\,\frac{n_\varepsilon(x,y)}{\rho_\varepsilon}dx\,dy\right) \\
&= \frac{r}{2}\nu_\varepsilon(1-\nu_\varepsilon) + \nu_\varepsilon\left(m(x,y) + \iint_{I\times J} m(x,y)\,\frac{n_\varepsilon(x,y)}{\rho_\varepsilon}dx\,dy\right) \\
&\quad - \iint_{I\times J}\left(m(x',y) + m(x,y')\right)\frac{n_\varepsilon(x',y)\,n_\varepsilon(x,y')}{n_\varepsilon(x,y)\,\rho_\varepsilon}\,dx'\,dy'.
\end{aligned} \tag{6.20}$$

Since $m \geq 0$ and $n_\varepsilon, \rho_\varepsilon^X, \rho_\varepsilon^Y, \rho_\varepsilon > 0$, we get:

$$\varepsilon\,\partial_t\nu_\varepsilon(t,x,y) \leq \left(\frac{r}{2} + 2\,\|m\|_\infty\right)\nu_\varepsilon - \frac{r}{2}\,\nu_\varepsilon^2.$$

Hence:

$$\begin{aligned}
\nu_\varepsilon(t,x,y) &\leq \frac{1}{\frac{1}{\nu_\varepsilon^0(x,y)}\,e^{-\left(\frac{r}{2}+2\|m\|_\infty\right)\frac{t}{\varepsilon}} + \frac{r}{(r+4\|m\|_\infty)}\left(1 - e^{-\left(\frac{r}{2}+2\|m\|_\infty\right)\frac{t}{\varepsilon}}\right)} \\
&\leq \frac{1}{\min\left(\frac{1}{\nu_\varepsilon^0(x,y)}, \frac{r}{(r+4\|m\|_\infty)}\right)} \leq \max\left(\|\nu_\varepsilon^0\|_\infty, \left(1 + \frac{4\|m\|_\infty}{r}\right)\right) \leq \nu_M.
\end{aligned}$$

Similarly, from (6.20), we have:

$$\varepsilon\,\partial_t\nu_\varepsilon(t,x,y) \geq \left(\frac{r}{2} - 2\|m\|_\infty\right)\nu_\varepsilon - \frac{r}{2}\nu_\varepsilon^2.$$

Recall from H1 that: $r > 2\|m\|_\infty$. Hence:

$$\begin{aligned}
\nu_\varepsilon(t,x,y) &\geq \frac{1}{\frac{1}{\nu_\varepsilon^0(x,y)}\,e^{-\left(\frac{r}{2}-2\,\|m\|_\infty\right)\frac{t}{\varepsilon}} + \frac{r}{r-4\,\|m\|_\infty}\left(1 - e^{-\left(\frac{r}{2}-2\,\|m\|_\infty\right)\frac{t}{\varepsilon}}\right)} \\
&\geq \frac{1}{\max\left(\frac{1}{\nu_\varepsilon^0(x,y)}, \frac{r}{r-4\|m\|_\infty}\right)} \geq \min\left(\|\nu_\varepsilon^0\|_\infty, \left(1 - \frac{4\|m\|_\infty}{r}\right)\right) = \nu_m.
\end{aligned}$$

6.4.2 Regularity estimates on u_ε.

In this subsection, we prove the regularity estimates that underlie the convergence of u_ε based on the Arzela-Ascoli theorem.

Proposition 6.4.1. *Assume that H1, H2 and H3 hold. Let $\varepsilon > 0$, and $u_\varepsilon \in C^1([0,T]\times I\times J)$ be the solution of P_{u_ε}. Then, u_ε is Lipschitz continuous in time and in space, and is bounded in $C([0,T]\times I\times J)$, all the bounds being uniform with regard to ε.*

Proof of Proposition 6.4.1.

Lipshitz bounds in time. The existence of the upper bound for ν_ε in Proposition 6.1.1 along with H1 and Theorem 6.1.1 imply directly the following uniform Lipschitz bound in time on u_ε:

$$\|\partial_t u_\varepsilon\|_\infty \leq \|m\|_\infty + \kappa\, \rho_0^+ + \frac{r}{2}\,(1+\nu_M).$$

Lipschitz bounds in space. In this paragraph, we rely on a maximum principle to show the following inequalities for all $(t,x,y) \in [0,T]\times I\times J$:

$$|\partial_x u_\varepsilon(t,x,y)| < 2\|\partial_x m\|_\infty T + \|\partial_x u_\varepsilon^0\|_\infty + 1, \quad |\partial_y u_\varepsilon(t,x,y)| < 2\|\partial_y m\|_\infty T + \|\partial_y u_\varepsilon^0\|_\infty + 1. \tag{6.21}$$

The latter together with H2 implies that (u_ε) is uniformly Lipschitz continuous in space.

Let us show (6.21). For $t\in[0,T], (x,y,x',y') \in \mathring{I}^4$, define $\Delta_\varepsilon(x',y',x,y,t) = u_\varepsilon(t,x',y) + u_\varepsilon(t,x,y') - u_\varepsilon(t,x,y)$. Differentiating the equation on u_ε from P_{u_ε} with regard to x, we obtain:

$$\partial_t\,\partial_x u_\varepsilon = -\partial_x m + \frac{r}{2\rho_\varepsilon}\iint_{I\times J}\frac{1}{\varepsilon}\left[\partial_x u_\varepsilon(x,y') - \partial_x u_\varepsilon(x,y)\right] e^{\Delta_\varepsilon(x',y',x,y,t)}dx'\,dy'.$$

Let us define for $(x,y)\in I\times J$:

$$w_\varepsilon(t,x,y) = \partial_x u_\varepsilon(t,x,y) - 2\|\partial_x m\|_\infty\, t - \|\partial_x u_\varepsilon^0\|_\infty - 1.$$

First, we have that for all $(x,y)\in I\times J$: $w_\varepsilon(0,x,y) < 0$. Next, let us assume that there exists $t>0$ such that $\max\limits_{I\times J} w_\varepsilon(t,\cdot) \geq 0$. Then we can define:

$$t_0 = \inf\{t>0, \max_{I\times J} w_\varepsilon(t,\cdot)\geq 0\}.$$

By continuity of $\partial_x u_\varepsilon$ at $t=0$ and compactness of I, we have: $t_0>0$. Let $(x_0,y_0)\in I\times J$ be such that: $w_\varepsilon(t_0,x_0,y_0) = \max\limits_{I\times J} w_\varepsilon(t_0,\cdot)$. Then, we have:

$$\begin{aligned}
&0 \leq \partial_t\, w_\varepsilon(t_0,x_0,y_0)\\
&= -\partial_x m(x_0,y_0) + \frac{r}{2\rho_\varepsilon(t_0)}\iint_{I\times J}\frac{1}{\varepsilon}\left[w_\varepsilon(x_0,y') - w_\varepsilon(x_0,y_0)\right] e^{\Delta_\varepsilon(x',y',x,y,t)}dx'\,dy - 2\|\partial_x m\|_\infty\\
&\leq -\|\partial_x m\|_\infty < 0.
\end{aligned}$$

which is a contradiction. Therefore:

$$\forall t\in[0,t],\ (x,y)\in I\times J, w_\varepsilon(t,x,y) < 0,$$

which yields:

$$\partial_x u_\varepsilon(t,x,y) < 2\|\partial_x m\|_\infty t + \|\partial_x u_\varepsilon^0\|_\infty + 1.$$

Next, let us consider, for $(t,x,y)\in[0,T]\times I\times J$:

$$v_\varepsilon(t,x,y) = \partial_x u_\varepsilon(t,x,y) + 2\|\partial_x m\|_\infty\, t + \|\partial_x u_\varepsilon^0\| + 1.$$

We can repeat the argument above switching maximum to minimum. First, we have that $v_\varepsilon(0,\cdot,\cdot) > 0$. If we assume that there exists $t>0$ such that $\min v_\varepsilon(t,\cdot,\cdot)\leq 0$ and define:

$$t_0 = \inf\{t>0, \min v_\varepsilon(t,\cdot,\cdot)\leq 0\} > 0,$$

and (x_0, y_0) realising that minimum, we would have:

$$\begin{aligned}
0 &\geq \partial_t v_\varepsilon(t_0, x_0, y_0) \\
&= -\partial_x m(x_0, y_0) + \frac{r}{2\rho_\varepsilon(t_0)} \iint_{I\times J} \frac{1}{\varepsilon} \left[w_\varepsilon(x_0, y') - w_\varepsilon(x_0, y_0)\right] e^{\Delta_\varepsilon(x', y', x, y, t)} dx'\, dy + 2\|\partial_x m\|_\infty \\
&\geq \|\partial_x m\|_\infty > 0.
\end{aligned}$$

Which is a contradiction. Thus $v_\varepsilon > 0$ and for all $(t, x, y) \in [0, T] \times I \times J$:

$$\partial_x u_\varepsilon > -2\|\partial_x m\|_\infty\, t - \|\partial_x u_\varepsilon^0\| - 1.$$

The bound on $\partial_y u_\varepsilon$ can be obtained using similar arguments.

Uniform L^∞ bounds on u_ε. Let us show the following lemma:

Lemma 14. *For any $\delta > 0$, there exists $\varepsilon_0 > 0$ such that for all $0 < \varepsilon \leq \varepsilon_0$:*

$$-\delta < \max u_\varepsilon < \delta, \qquad \min u_\varepsilon > -\delta - |I|\, \left(\|\partial_x u_\varepsilon\|_\infty + \|\partial_y u_\varepsilon\|_\infty\right).$$

Hence, (u_ε) is uniformly bounded for ε small.

Proof.

1. Bounds on $\max u_\varepsilon$. Let $\delta > 0$. On the one hand, we have:

$$\rho_0^- \leq \iint_{I\times J} \frac{\exp\left(\frac{u_\varepsilon(x,y)}{\varepsilon}\right)}{\varepsilon}\, dx\, dy \leq |I|^2\, \frac{\exp\left(\frac{\max u_\varepsilon}{\varepsilon}\right)}{\varepsilon},$$

which leads to:

$$\max u_\varepsilon \geq \varepsilon\, \log\left(\frac{\varepsilon\, \rho_0^-}{|I|^2}\right) \underset{\varepsilon\to 0}{\longrightarrow} 0.$$

That implies that there exists $\varepsilon_0 > 0$, such that:

$$\forall\, 0 < \varepsilon \leq \varepsilon_0, \quad -\delta < \max u_\varepsilon.$$

On the other hand, if $\max u_\varepsilon = u_\varepsilon(x_m, y_m) > 0$, then, for all $(x, y) \in I \times J$, we have:

$$u_\varepsilon(x, y) \geq u_\varepsilon(x_m, y_m) - \|\partial_x u_\varepsilon\|_\infty\, |x - x_m| - \|\partial_y u_\varepsilon\|_\infty\, |y - y_m|. \tag{6.22}$$

Therefore, using the fact that u_ε is Lipschitz continuous in space, we obtain, for $(x, y) \in I \times J$ such that $|x - x_m| \leq \frac{u_\varepsilon(x_m,y_m)}{4\|\partial_x u_\varepsilon\|_\infty}$, $|y - y_m| \leq \frac{u_\varepsilon(x_m,y_m)}{4\|\partial_y u_\varepsilon\|_\infty}$:

$$u_\varepsilon(x, y) \geq \frac{u_\varepsilon(x_m, y_m)}{2}.$$

We deduce that:

$$\begin{aligned}
\rho_0^+ \geq \iint_{I\times J} \frac{\exp\left(\frac{u_\varepsilon(x,y)}{\varepsilon}\right)}{\varepsilon}\, dx\, dy &\geq \iint_{|x-x_m|\leq \frac{u_\varepsilon(x_m,y_m)}{4\|\partial_x u_\varepsilon\|_\infty},\ |y-y_m|\leq \frac{u_\varepsilon(x_m,y_m)}{4\|\partial_y u_\varepsilon\|_\infty}} \frac{\exp\left(\frac{u_\varepsilon(x,y)}{\varepsilon}\right)}{\varepsilon}\, dx\, dy \\
&\geq \frac{u_\varepsilon(x_m, y_m)^2}{4\, \|\partial_x u_\varepsilon\|_\infty\, \|\partial_y u_\varepsilon\|_\infty}\, \frac{\exp\left(\frac{u_\varepsilon(x_m,y_m)}{2\varepsilon}\right)}{\varepsilon}.
\end{aligned}$$

The latter yields that if $u_\varepsilon(x_m, y_m) \geq \delta$, then:

$$\rho_0^+ \geq \frac{\delta^2}{4 \left\|\partial_x u_\varepsilon\right\|_\infty \left\|\partial_y u_\varepsilon\right\|_\infty} \frac{\exp\left(\frac{\delta}{2\varepsilon}\right)}{\varepsilon} \underset{\varepsilon \to 0}{\longrightarrow} +\infty.$$

Therefore, there exists $\varepsilon_0 > 0$ such that:

$$\forall\, 0 < \varepsilon \leq \varepsilon_0, \quad -\delta < \max u_\varepsilon < \delta.$$

2. Bound on $\min u_\varepsilon$**.** From (6.22), for all $(x, y) \in I \times J$, we have:

$$u_\varepsilon(x, y) > \max u_\varepsilon - |I| \left(\left\|\partial_x u_\varepsilon\right\|_\infty + \left\|\partial_y u_\varepsilon\right\|_\infty\right) > -\delta - |I| \left(\left\|\partial_x u_\varepsilon\right\|_\infty + \left\|\partial_y u_\varepsilon\right\|_\infty\right).$$

Thanks to (6.21), the r.h.s is uniformly bounded. □

□

6.5 Proof of Theorem 6.1.2.

In this section, we provide the proof for the main result of this paper, which is the convergence of u_ε towards a non-positive limit u that separates additively the variables. We also link the support of n to the zeros of u and derive a limit equation.

Limit $\boldsymbol{u}$**.** From Proposition 6.4.1, there exists $\varepsilon_0 > 0$ such that $(u_\varepsilon)_{\varepsilon \leq \varepsilon_0}$ is uniformly bounded in $C^0([0, T] \times I \times J)$, and uniformly Lipschitz continuous in space and time. Hence, from the theorem of Arzela-Ascoli, after extraction of a subsequence, (u_ε) converges uniformly toward a limit $u \in C^0([0, T] \times I \times J)$, that is also Lipschitz continuous.

$\boldsymbol{u(t, x, y) \leq \max u(t, x, \cdot) + \max u(t, \cdot, y)}$**.** From H4 and Proposition 6.1.1, there exists $\nu_m > 0$ such that:

$$\begin{aligned}
\forall (t, x, y) \in [0, T] \times I \times J, \quad \nu_m &\leq \nu_\varepsilon(t, x, y) \\
&= \iint_{I \times J} \frac{1}{\varepsilon\, \rho_\varepsilon} \exp\left[\frac{u_\varepsilon(t, x, y') + u_\varepsilon(t, x', y) - u_\varepsilon(t, x, y)}{\varepsilon}\right] dx\, dy \\
&\leq \frac{|I|^2}{\rho_0^-} \frac{1}{\varepsilon} \exp\left[\frac{\max(u_\varepsilon(t, x, \cdot)) + \max u_\varepsilon(t, \cdot, y)) - u_\varepsilon(t, x, y)}{\varepsilon}\right].
\end{aligned}$$

Moreover, for all $(t, x, y) \in [0, T] \times I \times J$, and $\delta > 0$, there exists $\varepsilon_0 > 0$ such that for $0 < \varepsilon \leq \varepsilon_0$,

$$\max(u_\varepsilon(t, x, \cdot)) \leq \max(u(t, x, \cdot)) + \delta, \quad \max(u_\varepsilon(t, \cdot, y)) \leq \max(u(t, \cdot, y)) + \delta.$$

We deduce that, for $0 < \varepsilon < \varepsilon_0$:

$$u_\varepsilon(t, x, y) - u(t, x, y) + \varepsilon \log\left(\varepsilon \frac{\rho_0^-\, \nu_m}{|I|^2}\right) - 2\delta \leq \max(u(t, x, \cdot)) + \max(u(t, \cdot, y)) - u(t, x, y).$$

Letting δ and ε vanish yields:

$$u(t, x, y) \leq \max(u(t, x, \cdot)) + \max(u(t, \cdot, y)).$$

$u(t,x,y) \geq \max u(t,x,\cdot) + \max u(t,\cdot,y)$. For $\delta > 0$, there exists $\varepsilon_0 > 0$ such that for $0 < \varepsilon \leq \varepsilon_0$, for $(t,x,y) \in [0,T] \times I \times J$,

$$\max(u_\varepsilon(t,x,\cdot)) \geq \max(u(t,x,\cdot)) - \delta, \quad \max(u_\varepsilon(t,\cdot,y)) \geq \max(u(t,\cdot,y)) - \delta.$$

Let $\varepsilon \leq \varepsilon_0$ and $y_\varepsilon(x)$ be such that: $u_\varepsilon(t,x,y_\varepsilon(x)) = \max(u_\varepsilon(t,x,\cdot))$. Since u_ε is uniformly Lipschitz in space (Proposition 6.4.1), we can choose $M > 0$ such that:

$$\forall (y,y') \in I \times J,\ |u_\varepsilon(t,x,y) - u_\varepsilon(t,x,y')| \leq M|y-y'|.$$

Combining the last two estimations leads to:

$$|y - y_\varepsilon(x)| \leq \frac{\delta}{M} \implies u_\varepsilon(t,x,y') > \max u(t,x,\cdot) - 2\delta.$$

The same holds for $\max(u(t,\cdot,y))$. Hence, from Proposition 6.1.1, there exists ν_M such that:

$$\begin{aligned}\rho_0^+ \nu_M &\geq \iint_{I\times J} \frac{1}{\varepsilon} \exp\left[\frac{u_\varepsilon(t,x,y') + u_\varepsilon(t,x',y) - u_\varepsilon(t,x,y)}{\varepsilon}\right] dx\, dy \\ &\geq \left(\frac{\delta}{M}\right)^2 \frac{1}{\varepsilon} \exp\left[\frac{\max(u(t,x,\cdot)) + \max(u(t,\cdot,y)) - 4\delta - u_\varepsilon(t,x,y)}{\varepsilon}\right].\end{aligned}$$

We next obtain:

$$\varepsilon \log\left(\varepsilon \frac{\rho_0^+ \nu_M\, M^2}{\delta^2}\right) + 4\delta + u_\varepsilon(t,x,y) - u(t,x,y) \geq \max(u(t,x,\cdot)) + \max(u(t,\cdot,y)) - u(t,x,y).$$

Letting δ and ε vanish yields:

$$u(t,x,y) \geq \max(u(t,x,\cdot)) + \max(u(t,\cdot,y)).$$

This concludes the proof of (6.2).

u is non-positive. This property follows directly from the uniform convergence of u_ε towards u and the uniform estimates on the $\max(u_\varepsilon)$ from Lemma 14.

Support of n and zeros of u. Let $t \in [0,T]$. Let: $(x_0,y_0) \notin \{(x,y)\,|\,u(t,x,y) = 0\}$. Since $u(t,\cdot,\cdot)$ is uniformly continuous, there exists $\delta > 0$ such that: $\max(|x'-x_0|, |y'-y_0|) \leq \delta \implies u(t,x',y') \leq \frac{u(t,x_0,y_0)}{2}$. Also, from Theorem 6.1.2, there exists $\varepsilon_0 > 0$ such that, for all $\varepsilon < \varepsilon_0$, we have: $\|u_\varepsilon - u\|_\infty \leq \frac{|u(t,x_0,y_0)|}{4}$. Then, for $\varepsilon < \varepsilon_0$, we have:

$$\begin{aligned}\int_{[x_0-\delta,x_0+\delta]\times[y_0-\delta,y_0+\delta]} n_\varepsilon(t,x',y')\, dx'\, dy' &= \int_{[x-\delta,x+\delta]\times[y_0-\delta,y_0+\delta]} \frac{e^{\frac{u_\varepsilon(t,x',y')}{\varepsilon}}}{\varepsilon} dx'\, dy' \\ &\leq 4\delta^2\, \frac{e^{\frac{u(t,x_0,y_0)}{4\varepsilon}}}{\varepsilon} \\ &\underset{\varepsilon\to 0}{\longrightarrow} 0.\end{aligned}$$

From the weak convergence result of Theorem 6.1.1, $(x_0,y_0) \notin \mathrm{supp}(n(t,\cdot,\cdot))$.

Limit equation on u^X. Let $\varepsilon > 0$. From the equation (6.4) verified by ρ_ε^X, we get, by integration:

$$\forall (t,y) \in [0,T] \times J, \quad \varepsilon \log\left(\frac{\rho_\varepsilon^X(t,y)}{\rho_\varepsilon^X(0,y)}\right) = rt - \kappa \int_0^t \rho_\varepsilon(s) ds - \int_0^t \int_I m(x,y) \frac{n_\varepsilon(s,x,y)}{\rho_\varepsilon^X(s,y)} dx\, ds. \tag{6.23}$$

Let us define $\phi_\varepsilon^X \in C\left([0,T] \times I \times J\right)$ by:

$$\phi_\varepsilon^X(t,x,y) = \frac{n_\varepsilon(t,x,y)}{\rho_\varepsilon^X(t,y)}.$$

1. Convergence of ϕ_ε^X to ϕ^X. For $(t,y) \in [0,T] \times J$, we have:

$$\int_I \phi_\varepsilon^X(t,x',y)\, dx' = 1.$$

Hence, $\left(\phi_\varepsilon^X\right)_{\varepsilon>0}$ is bounded in $L^\infty([0,T] \times J, L^1(I))$. Thus, from Lemma 15, there exists a subsequence still denoted $\left(\phi_\varepsilon^X\right)_{\varepsilon>0}$ that converges in $L^\infty(w^* - [0,T] \times J, M^1(I))$ toward a measure ϕ^X.

Support of $\phi^X(t,\cdot,y)$. Proposition 6.1.1 implies that, for $f \in C_c(I, \mathbb{R}_+)$, for a.e. (t,y)

$$\frac{1}{\nu_M\, \rho_0^-} \int_I \rho^Y(t,x)\, f(x)\, dx \le \left\langle \phi^X(t,\cdot,y),\, f \right\rangle \le \frac{1}{\nu_m\, \rho_0^+} \int_I \rho^Y(t,x)\, f(x)\, dx.$$

Hence, for a.e. (t,y), $\phi^X(t,\cdot,y)$ and $\rho^Y(t,\cdot)$ share the same support. As $n(t,\cdot,\cdot)$ is supported at $u(t,\cdot,\cdot)^{-1}\left(\{(0,0)\}\right) = u^X(t,\cdot)^{-1}\left(\{0\}\right) \times u^Y(t,\cdot)^{-1}\left(\{0\}\right)$ for a.e. t, we obtain that $\rho^Y(t,\cdot)$ (and therefore $\phi^X(t,\cdot,y)$) is supported at the zeros of $u^Y(t,\cdot)$.

2. $\varepsilon \log\left(\rho_\varepsilon^X\right) \underset{\varepsilon\to 0}{\longrightarrow} u^X \in C^0([0,T] \times I)$. We fix $\delta > 0$ and let $\varepsilon_0 > 0$ be such that: $\forall \varepsilon < \varepsilon_0$, $\|u_\varepsilon - u\|_\infty \le \delta$. Next, we compute:

$$\begin{aligned}
\varepsilon \log\left(\rho_\varepsilon^X(t,y)\right) &= \varepsilon \log\left(\int_I \frac{e^{\frac{u_\varepsilon(t,x,y)}{\varepsilon}}}{\varepsilon} dx\right) \\
&\le \varepsilon \log\left(\int_I \frac{e^{\frac{u(t,x,y)+\delta}{\varepsilon}}}{\varepsilon} dx\right) \\
&= \varepsilon \log\left(\int_I \frac{e^{\frac{u^X(t,y)+\delta}{\varepsilon}}}{\varepsilon} e^{\frac{u^Y(t,x)}{\varepsilon}} dx\right) \\
&\le u^X(t,y) + \delta - \varepsilon \log(\varepsilon) + \varepsilon \log\left(\int_I e^{\frac{u^Y(t,x)}{\varepsilon}} dx\right) \\
&\le u^X(t,y) + \delta - \varepsilon \log(\varepsilon) + \varepsilon \log\left(|I|\right).
\end{aligned} \tag{6.24}$$

Similarly, we have:

$$\varepsilon \log\left(\rho_\varepsilon^X(t,y)\right) \ge u^X(t,y) - \delta - \varepsilon \log(\varepsilon) + \varepsilon \log\left(\int_I e^{\frac{u^Y(t,x)}{\varepsilon}} dx\right). \tag{6.25}$$

For all $t \in [0,T]$, we have shown at the step (ii) that there exists $x_0(t) \in I$ such that $u^Y(x_0(t)) = 0$. We have therefore the following lower bound:

$$\begin{aligned}\varepsilon \log\left(\int_I e^{\frac{u^Y(t,x)}{\varepsilon}}\,dx\right) &\geq \varepsilon \log\left(\int_{x_0(t)-\varepsilon}^{x_0(t)+\varepsilon} e^{\frac{u^Y(t,x)}{\varepsilon}}\,dx\right)\\ &\geq \varepsilon \log\left(\int_{x_0(t)-\varepsilon}^{x_0(t)+\varepsilon} e^{\frac{-M|x-x_0(t)|}{\varepsilon}}\,dx\right)\\ &\geq -\varepsilon\, M + \varepsilon \log(2\,\varepsilon)\end{aligned}$$

where the intermediate inequality is obtained due to the fact that there exists $M > 0$ such that $u(t,\cdot,\cdot)$ is M-lipschitz in space, and thus, so is $u^Y(t,\cdot)$.

The two inequalities (6.24) and (6.25) above ensure the convergence of $\varepsilon \log\left(\rho_\varepsilon^X\right)$ toward u^X uniformly in $[0,T]\times J$.

3. Limit equation. For all $(t,y) \in [0,T]\times J$:

$$\int_0^t \int_I m(x,y)\phi_\varepsilon^X(s,x,y)\,dx\,ds = \varepsilon \log\left(\frac{\rho_\varepsilon^X(t,y)}{\rho_\varepsilon^X(0,y)}\right) - rt + \kappa\int_0^t \rho_\varepsilon(s)ds.$$

From the strong convergence $\varepsilon \log\left(\rho_\varepsilon^X\right) \underset{\varepsilon\to 0}{\longrightarrow} u^X \in C^0([0,T]\times J)$ shown previously, the r.h.s of the equality above converges toward a function in $C^0([0,T]\times J)$ as ε vanishes. Hence, $G_\varepsilon := (t,y) \mapsto \int_0^t \int_I m(x,y)\phi_\varepsilon^X(t,x,y)\,dx\,ds$ converges uniformly toward a function denoted $G(t,y)$ in $C^0([0,T]\times J)$.

We aim to show that for all $t \in [0,T]$:

$$G(t,\cdot) = y \mapsto \int_0^t \left\langle \phi^X(t,\cdot,y), m(\cdot,y)\right\rangle\,ds \in L^\infty(J),$$

which would yield (6.3). Let $f \in L^1(J)$. We have, for $t \in [0,T]$:

$$\begin{aligned}&\left|\int_J \left(G(t,y) - \int_0^t \left\langle \phi^X(t,\cdot,y), m(\cdot,y)\right\rangle\,ds\right) f(y)\,dy\right|\\ &\leq \|G - G_\varepsilon\|_\infty \|f\|_1 + \left|\int_0^T \int_J \left\langle \phi_\varepsilon^X(s,\cdot,y) - \phi^X(s,\cdot,y),\, m(\cdot,y)\right\rangle \mathbf{1}_{[0,t]}(s)\, f(y)ds\,dy\right|.\end{aligned}$$

The first term vanishes because of the uniform convergence of G_ε to G. The second term does the same because of the weak convergence of ϕ_ε^X to ϕ^X in $L^\infty(w^* - [0,T]\times J, M^1(I))$ applied to $(s,x,y) \mapsto \mathbf{1}_{[0,t]}(s)f(y)m(x,y) \in L^1([0,T]\times J, C^0(I))$, since $f \in L^1(J)$ and $m \in C^1(I\times J)$. We obtain that for all $t \in [0,T]$, $f \in L^1(J)$:

$$\int_J \left(G(t,y) - \int_0^t \left\langle \phi^X(t,\cdot,y), m(\cdot,y)\right\rangle\,ds\right) f(y)\,dy = 0.$$

Therefore, we deduce that for all $t \in [0,T]$, for a.e y, $G(t,y) = \int_0^t \left\langle \phi^X(t,\cdot,y), m(\cdot,y)\right\rangle\,ds$.

6.6 Convergence of (ρ_ε) toward a BV limit: proof of Theorem 6.1.3.

In this section, we provide the proof of Theorem 6.1.3 under the additional hypothesis that the selection function m is additive ($H_{m,\text{add}}$).

Let $\varepsilon > 0$. First, we have, for all $t \in [0,T]$:

$$\begin{aligned}\int_0^t \left|\frac{d\rho_\varepsilon}{dt}(s)\right| ds &= \int_0^t \frac{d\rho_\varepsilon}{dt}(s)\, ds + 2\int_0^t \left(\frac{d\rho_\varepsilon}{dt}\right)_-(s)\, ds \\ &= \rho_\varepsilon(t) - \rho_\varepsilon(0) + 2\int_0^t \left(\frac{d\rho_\varepsilon}{dt}\right)_-(s)\, ds \\ &\le \rho_0^+ + 2\int_0^t \left(\frac{d\rho_\varepsilon}{dt}\right)_-(s)\, ds,\end{aligned}$$

using the estimates of Lemma 12. Let us define:

$$\mathcal{I}_\varepsilon(t) := \frac{d\rho_\varepsilon}{dt}(t) = \frac{r - \kappa\,\rho_\varepsilon(t)}{\varepsilon}\,\rho_\varepsilon(t) - \iint_{I\times J} m(x,y)\,\frac{n_\varepsilon(t,x,y)}{\varepsilon}\,dx\,dy.$$

To prove that ρ_ε is locally uniformly bounded in $W^{1,1}([0,T])$, it is sufficient to give an upper bound on $\int_0^t (\mathcal{I}_\varepsilon)_-\, ds$. To this end, let us notice that for a.e.t:

$$\frac{d\,(\mathcal{I}_\varepsilon)_-}{dt}(t) = -\mathbf{1}_{\mathcal{I}_\varepsilon \le 0}\,\frac{d\mathcal{I}_\varepsilon}{dt}.$$

We deduce that, for a.e.t

$$\begin{aligned}\frac{d\,(\mathcal{I}_\varepsilon)_-}{dt}(t) &= -\frac{d\mathcal{I}_\varepsilon}{dt}(t)\,\mathbf{1}_{\{\mathcal{I}_\varepsilon(t)\le 0\}} \\ &= -\left[\frac{r - 2\,\kappa\,\rho_\varepsilon}{\varepsilon}\,\mathcal{I}_\varepsilon(t) - \iint_{I\times J} m(x,y)\,\frac{\partial_t n_\varepsilon(t,x,y)}{\varepsilon}\,dx\,dy\right]\mathbf{1}_{\{\mathcal{I}_\varepsilon(t)\le 0\}} \\ &= \left[\frac{r - 2\,\kappa\,\rho_\varepsilon}{\varepsilon}\,(\mathcal{I}_\varepsilon)_-(t)\right. \\ &\quad \left. + \iint_{I\times J} m(x,y)\,\frac{1}{\varepsilon^2}\left(\frac{r}{2}\left[\frac{\rho_\varepsilon^X\,\rho_\varepsilon^Y}{\rho_\varepsilon} + n_\varepsilon\right] - \kappa\,\rho_\varepsilon\,n_\varepsilon - m(x,y)\,n_\varepsilon\right)dx\,dy\right]\mathbf{1}_{\{\mathcal{I}_\varepsilon(t)\le 0\}}.\end{aligned} \tag{6.26}$$

Let us show that the following term is non positive:

$$\begin{aligned}&\mathbf{1}_{\{\mathcal{I}_\varepsilon(t)\le 0\}} \iint_{I\times J} m(x,y)\left(\frac{r}{2}\left[\frac{\rho_\varepsilon^X\,\rho_\varepsilon^Y}{\rho_\varepsilon} + n_\varepsilon\right] - \kappa\,\rho_\varepsilon\,n_\varepsilon - m(x,y)\,n_\varepsilon\right)dx\,dy \\ &= \mathbf{1}_{\{\mathcal{I}_\varepsilon(t)\le 0\}}\left[\frac{r}{2}\iint_{I\times J} m(x,y)\frac{\rho_\varepsilon^X\,\rho_\varepsilon^Y}{\rho_\varepsilon}dx\,dy + \left(\frac{r}{2} - \kappa\rho_\varepsilon\right)\iint_{I\times J} m(x,y)\,n_\varepsilon dx dy - \iint_{I\times J} m^2(x,y)\,n_\varepsilon\,dx\,dy\right].\end{aligned}$$

On the one hand, from the Cauchy-Schwartz inequality, we get:

$$-\rho_\varepsilon \iint_{I\times J} m^2(x,y)\,n_\varepsilon\,dx\,dy = -\iint_{I\times J}\sqrt{n_\varepsilon}^2 \iint_{I\times J}(m(x,y)\sqrt{n_\varepsilon})^2\,dx\,dy \le -\left(\iint_{I\times J} m(x,y)\,n_\varepsilon\,dx\,dy\right)^2.$$

On the other hand, thanks to the additional hypothesis on m ($\mathrm{H}_{m,\mathrm{add}}$), we have

$$\begin{aligned}\iint_{I\times J} m(x,y)\frac{\rho_\varepsilon^X\,\rho_\varepsilon^Y}{\rho_\varepsilon}dx\,dy &= \iint_{I\times J}\left[m^X(x)+m^Y(y)\right]\frac{\rho_\varepsilon^X(y)\,\rho_\varepsilon^Y(x)}{\rho_\varepsilon}dx\,dy\\ &= \int_I m^X(x)\rho_\varepsilon^Y(x)\,dx+\int_I m^Y(y)\rho_\varepsilon^X(y)\,dy\\ &= \iint_{I\times J} m^X(x)\,n_\varepsilon(x,y)\,dx\,dy+\iint_{I\times J} m^Y(y)\,n_\varepsilon(x,y)\,dx\,dy\\ &= \iint_{I\times J} m(x,y)\,n_\varepsilon(x,y)\,dx\,dy.\end{aligned}$$

We deduce that

$$\begin{aligned}&\mathbf{1}_{\{\mathcal{I}_\varepsilon(t)\le 0\}}\iint_{I\times J} m(x,y)\left(\frac{r}{2}\left[\frac{\rho_\varepsilon^X\,\rho_\varepsilon^Y}{\rho_\varepsilon}+n_\varepsilon\right]-\kappa\,\rho_\varepsilon\,n_\varepsilon-m(x,y)\,n_\varepsilon\right)dx\,dy\\ &\le \mathbf{1}_{\{\mathcal{I}_\varepsilon(t)\le 0\}}\left[r\iint_{I\times J} m\,n_\varepsilon-\kappa\,\rho_\varepsilon\iint_{I\times J} m\,n_\varepsilon-\frac{1}{\rho_\varepsilon}\left(\iint_{I\times J} m(x,y)\,n_\varepsilon\,dx\,dy\right)^2\right]\\ &\le \mathbf{1}_{\{\mathcal{I}_\varepsilon(t)\le 0\}}\frac{\iint_{I\times J} m\,n_\varepsilon\,dx\,dy}{\rho_\varepsilon}\left[(r-\kappa\,\rho_\varepsilon)\,\rho_\varepsilon-\iint_{I\times J} m\,n_\varepsilon\,dx\,dy\right]\\ &\le \mathbf{1}_{\{\mathcal{I}_\varepsilon(t)\le 0\}}\frac{\iint_{I\times J} m\,n_\varepsilon\,dx\,dy}{\rho_\varepsilon}\,\varepsilon\,\mathcal{I}_\varepsilon(t)\le 0.\end{aligned}$$

Consequently, (6.26) implies the following inequality

$$\begin{aligned}\frac{d\,(\mathcal{I}_\varepsilon)_-}{dt}(t) &\le \frac{r-2\,\kappa\,\rho_\varepsilon}{\varepsilon}\,(\mathcal{I}_\varepsilon)_-(t)\\ &\le \frac{r-2\,\kappa\,\rho_0^-}{\varepsilon}\,(\mathcal{I}_\varepsilon)_-(t)\\ &= \frac{2\|m\|_\infty-r}{\varepsilon}\,(\mathcal{I}_\varepsilon)_-(t).\end{aligned}$$

Let us define $\delta := r-2\|m\|_\infty > 0$ from H1. From the last differential inequality, we deduce that

$$(\mathcal{I}_\varepsilon)_-(t)\le(\mathcal{I}_\varepsilon)_-(0)\,e^{-\frac{\delta}{\varepsilon}t}, \tag{6.27}$$

which concludes the first part of the proof.

For the last part of the theorem, recall that $I_\varepsilon(t)=\frac{d\rho_\varepsilon}{dt}(t)$. Then, the inequality (6.5) implies that there exists $C>0$ such that

$$(\mathcal{I}_\varepsilon(0))_-\le C\,\frac{e^{\frac{o(1)}{\varepsilon}}}{\varepsilon}.$$

As a corollary of (6.27), we obtain that for all $t\in[0,T]$

$$(\mathcal{I}_\varepsilon)_-(t)\le C\,\frac{e^{\frac{o(1)-\delta t}{\varepsilon}}}{\varepsilon}.$$

We deduce that the limit ρ is non decreasing.

6.A Proof of Lemma 12.

Proof of Lemma 12.

1. Bounds on ρ_ε. Integrating $(P(n_\varepsilon))$ leads to ρ_ε being solution of:

$$\begin{cases} \varepsilon\,\partial_t\rho_\varepsilon = (r-\kappa\,\rho_\varepsilon)\,\rho_\varepsilon - \iint_{I\times J} m(x,y)\,n_\varepsilon(t,x,y)\,dx\,dy. \\ \rho(0) = \rho_\varepsilon^0. \end{cases} \tag{6.28}$$

Since $m, n_\varepsilon \geq 0$, we get that ρ_ε is a subsolution of the Cauchy problem:

$$\begin{cases} \varepsilon\,d_t f_\varepsilon = (r-\kappa\,f_\varepsilon)\;f_\varepsilon, \\ f_\varepsilon(0) = \rho_\varepsilon^0. \end{cases}$$

whose solution is:

$$\forall t\geq 0, \quad f_\varepsilon(t) = \frac{1}{\frac{e^{-\frac{rt}{\varepsilon}}}{\rho_\varepsilon^0} + \frac{\kappa}{r}\left(1-e^{-\frac{rt}{\varepsilon}}\right)} \leq \max\left(\rho_\varepsilon^0,\,\frac{r}{\kappa}\right),$$

since $\rho_\varepsilon^0 \geq 0$ from assumptions. Using the comparison principle, we obtain

$$\forall t\geq 0, \quad \rho_\varepsilon(t) \leq f_\varepsilon(t) \leq \rho_0^+.$$

Similarly, we get:

$$\forall t\geq 0, \quad \rho_0^- =\leq \min\left(\rho_\varepsilon^0,\,\frac{r-\|m\|_\infty}{\kappa}\right) \leq \rho_\varepsilon(t).$$

2. Bounds on $\rho_\varepsilon^X, \rho_\varepsilon^Y$. Integrating $(P(n_\varepsilon))$ with regard to x leads to:

$$\begin{cases} \varepsilon\,\partial_t\rho_\varepsilon^X = (r-\kappa\,\rho_\varepsilon)\,\rho_\varepsilon^X - \int_I m(x,y)\,n_\varepsilon(t,x,y)\,dx \leq r\rho_\varepsilon^X, \\ \rho^X(0) = \rho_\varepsilon^{X,0}. \end{cases}$$

The upper bound on ρ_ε^X is then obtained by comparison with $\rho_\varepsilon^{X,0}\,e^{\frac{r\,t}{\varepsilon}}$. The upper bound on ρ_ε^Y can be proved using similar arguments.

3. Bound on n_ε. From Duhamel's formula, we obtain, for all $t\geq 0, (x,y)\in I\times J$:

$$n_\varepsilon(t,x,y) = n_\varepsilon^0(x,y)e^{-\int_0^t \frac{m+\kappa\,\rho_\varepsilon(s)-\frac{r}{2}}{\varepsilon}ds} + \frac{r}{2\varepsilon}\int_0^t \frac{\rho_\varepsilon^X(y,\tau)\rho_\varepsilon^Y(x,\tau)}{\rho_\varepsilon(\tau)}e^{-\int_\tau^t \frac{m+\kappa\,\rho_\varepsilon(s)-\frac{r}{2}}{\varepsilon}ds}d\tau.$$

Hence, using the bounds on ρ_ε^X and ρ_ε^Y from (6.16), we deduce that:

$$\begin{aligned} \|n_\varepsilon(t,\cdot,\cdot)\|_\infty &\leq e^{\frac{rt}{2\varepsilon}}\left\|n_\varepsilon^0\right\|_\infty + \frac{\|\rho_\varepsilon^{X,0}\|_\infty\,\|\rho_\varepsilon^{Y,0}\|_\infty}{\rho_0^-}\int_0^t \frac{r}{2\varepsilon}e^{\frac{2r\tau}{\varepsilon}}e^{\frac{r(t-\tau)}{2\varepsilon}}d\tau \\ &\leq e^{\frac{rt}{2\varepsilon}}\left\|n_\varepsilon^0\right\|_\infty + \frac{\|\rho_\varepsilon^{X,0}\|_\infty\,\|\rho_\varepsilon^{Y,0}\|_\infty}{\rho_0^-}e^{\frac{2rt}{\varepsilon}}\left(e^{\frac{rt}{2\varepsilon}}-1\right). \end{aligned}$$

4. Bound on $\partial_x n_\varepsilon$. We differentiate $P(n_\varepsilon)$ with respect to x to obtain:

$$\begin{cases} \varepsilon\,\partial_t\partial_x n_\varepsilon = \frac{r}{2}\left[\frac{\partial_x\rho_\varepsilon^Y(x)\,\rho_\varepsilon^X(y)}{\rho_\varepsilon} + \partial_x n_\varepsilon(x,y)\right] - \partial_x m(x,y)\,n_\varepsilon - (m+\kappa\,\rho_\varepsilon)\,\partial_x n_\varepsilon, \\ \partial_x n_\varepsilon(0) = \partial_x n_\varepsilon^0. \end{cases}$$

Putting the latter under integral form yields:

$$\partial_x n_\varepsilon = \partial_x n_\varepsilon^0\, e^{-\int_0^t \frac{m+\kappa\,\rho_\varepsilon(s)}{\varepsilon}ds} + \frac{1}{\varepsilon}\int_0^t \left(\frac{r}{2}\left[\frac{\partial_x\rho_\varepsilon^Y(x)\,\rho_\varepsilon^X(y)}{\rho_\varepsilon} + \partial_x n_\varepsilon(x,y)\right] - n_\varepsilon\,\partial_x m\right) e^{-\int_\tau^t \frac{m+\kappa\,\rho_\varepsilon(s)}{\varepsilon}ds} d\tau.$$

Hence, by first using the previous bounds (6.16) and (6.17) and next using the Gronwall's inequality on $t \mapsto \|\partial_x n_\varepsilon(t,\cdot,\cdot)\|_\infty$ (second line), we obtain that:

$$\begin{aligned} \|\partial_x n_\varepsilon(t,\cdot,\cdot)\|_\infty &\le \left\|\partial_x n_\varepsilon^0\right\|_\infty + N_{T_M}\frac{t}{\varepsilon}\|\partial_x m\|_\infty + \int_0^t \frac{r}{2\varepsilon}\left[\frac{\left\|\rho_\varepsilon^{X,0}\right\|_\infty |J|}{\rho_0^-}e^{\frac{r\,\tau}{\varepsilon}} + 1\right]\|\partial_x n_\varepsilon(\tau,\cdot,\cdot)\|_\infty\, d\tau \\ &\le \left(\|\partial_x n_\varepsilon^0\|_\infty + N_{T_M}\frac{t}{\varepsilon}\|\partial_x m\|_\infty\right) e^{\frac{\left\|\rho_\varepsilon^{X,0}\right\|_\infty |J|}{2\rho_0^-}e^{\frac{r\,t}{\varepsilon}} + \frac{rt}{2\varepsilon}}. \end{aligned}$$

□

6.B Proof of Lemma 13.

Proof of Lemma 13.

1. $\Phi(\mathcal{A}_\varepsilon^0) \subset \mathcal{A}_\varepsilon^0$. Let us recall the definition of $\mathcal{A}_\varepsilon^0$:

$$\begin{aligned} \mathcal{A}_\varepsilon^0 = \Big\{ & n \in C^1([0,T]\times I\times J,\mathbb{R}_+)\,|\,n(0,\cdot,\cdot) = n_\varepsilon^0, \quad \rho(n)\in[\rho_0^-,\rho_0^+], \\ & \rho^X(n)(t,y) \le \left\|\rho_\varepsilon^{X,0}\right\|_\infty e^{r\frac{t}{\varepsilon}}, \quad \rho^Y(n)(t,x) \le \left\|\rho_\varepsilon^{Y,0}\right\|_\infty e^{r\frac{t}{\varepsilon}}, \\ & \|n(t,\cdot,\cdot)\|_\infty \le \left\|n_\varepsilon^0\right\|_\infty e^{\frac{rt}{2\varepsilon}} + e^{\frac{2rt}{\varepsilon}}\frac{\left\|\rho_\varepsilon^{Y,0}\right\|_\infty\left\|\rho_\varepsilon^{Y,0}\right\|_\infty}{\rho_0^-}(e^{\frac{rt}{2\varepsilon}}-1), \\ & \|\partial_x n_\varepsilon(t,\cdot,\cdot)\|_\infty \le \left(\|\partial_x n_\varepsilon^0\|_\infty + N_{T_M}\frac{T_M}{\varepsilon}\|\partial_x m\|_\infty\right) e^{\frac{\left\|\rho_\varepsilon^{X,0}\right\|_\infty |J|}{2\rho_0^-}e^{\frac{r\,t}{\varepsilon}} + \frac{rt}{2\varepsilon}} \\ & \|\partial_y n_\varepsilon(t,\cdot,\cdot)\|_\infty \le \left(\|\partial_y n_\varepsilon^0\|_\infty + N_{T_M}\frac{T_M}{\varepsilon}\|\partial_y m\|_\infty\right) e^{\frac{\left\|\rho_\varepsilon^{Y,0}\right\|_\infty |I|}{2\rho_0^-}e^{\frac{r\,t}{\varepsilon}} + \frac{rt}{2\varepsilon}} \Big\}. \end{aligned}$$

We consider $n \in \mathcal{A}_\varepsilon^0$. Let us show that $\Phi(n)$ satisfies all the conditions defining $\mathcal{A}_\varepsilon^0$. From H1, H2 and (6.19), $\Phi(n)$ is in $C^1([0,T]\times I\times J,\mathbb{R}_+)$ and $\Phi(n)(0,\cdot,\cdot) = n_\varepsilon^0$. Next, for $t\in[0,T]$, since $n\in\mathcal{A}_\varepsilon^0$, we use the bounds on $\rho(n),\rho^X(n),\rho^Y(n)$ and we obtain the same bound for

$\Phi(n)$:

$$
\begin{aligned}
|\Phi(n)(t,\cdot,\cdot)| &\le \left\|n_\varepsilon^0\right\|_\infty + \frac{r}{2\varepsilon}\int_0^t \left(\frac{\left\|\rho_\varepsilon^{Y,0}\right\|_\infty \left\|\rho_\varepsilon^{Y,0}\right\|_\infty}{\rho_0^-} e^{\frac{2\,r\,\tau}{\varepsilon}} + \|n_\varepsilon(\tau,\cdot,\cdot)\|_\infty \right) d\tau \\
&\le \left\|n_\varepsilon^0\right\|_\infty + \frac{r}{2\varepsilon}\int_0^t \left(\frac{\left\|\rho_\varepsilon^{Y,0}\right\|_\infty \left\|\rho_\varepsilon^{Y,0}\right\|_\infty}{\rho_0^-} e^{\frac{2\,r\,\tau}{\varepsilon}} \right. \\
&\qquad \left. + e^{\frac{r\tau}{2\varepsilon}} \left\|n_\varepsilon^0\right\|_\infty + e^{\frac{2r\tau}{\varepsilon}} \frac{\left\|\rho_\varepsilon^{X,0}\right\|_\infty \left\|\rho_\varepsilon^{Y,0}\right\|_\infty}{\rho_0^-} (e^{\frac{r\tau}{2\varepsilon}} - 1) \right) d\tau \qquad (6.29) \\
&\le \left\|n_\varepsilon^0\right\|_\infty \left(1 + e^{\frac{rt}{2\varepsilon}} - 1\right) + e^{\frac{2rt}{\varepsilon}} \frac{\left\|\rho_\varepsilon^{Y,0}\right\|_\infty \left\|\rho_\varepsilon^{Y,0}\right\|_\infty}{\rho_0^-} \int_0^t \frac{r}{2\varepsilon} e^{\frac{r\tau}{2\varepsilon}} d\tau \\
&= \left\|n_\varepsilon^0\right\|_\infty e^{\frac{rt}{2\varepsilon}} + e^{\frac{2rt}{\varepsilon}} \frac{\left\|\rho_\varepsilon^{Y,0}\right\|_\infty \left\|\rho_\varepsilon^{Y,0}\right\|_\infty}{\rho_0^-} (e^{\frac{rt}{2\varepsilon}} - 1).
\end{aligned}
$$

Next, for $t \in [0,T]$, integrating twice (6.19) reads:

$$
\begin{aligned}
&\iint_{I\times J} \Phi(n)(t,x,y)\,dx\,dy = \iint_{I\times J} n_\varepsilon^0\, e^{-\frac{1}{\varepsilon}\int_0^t m(x,y)+\kappa\,\rho(n)(s)\,ds}\,dx\,dy \\
&\quad + \frac{r}{\varepsilon}\iint_{I\times J}\int_0^t \frac{1}{2}\left[\frac{\rho^X(n)(\tau,y)\,\rho^Y(\tau,x)}{\rho(n)(\tau)} + n(\tau,x,y)\right] e^{-\frac{1}{\varepsilon}\int_\tau^t m(x,y)+\kappa\,\rho(n)(s)\,ds}\,d\tau\,dx\,dy \\
&\le \rho_\varepsilon^0\, e^{-\frac{1}{\varepsilon}\int_0^t \kappa\,\rho(n)(s)\,ds} + \frac{r}{\kappa}\int_0^t \frac{\kappa\,\rho(n)(\tau)}{\varepsilon}\, e^{-\frac{1}{\varepsilon}\int_\tau^t \kappa\,\rho(n)(s)\,ds}\,d\tau \\
&\le \rho_\varepsilon^0\, e^{-\frac{1}{\varepsilon}\int_0^t \kappa\,\rho(n)(s)\,ds} + \frac{r}{\kappa}\left(1 - e^{-\frac{1}{\varepsilon}\int_0^t \kappa\,\rho(n)(s)\,ds}\right) \le \rho_0^+.
\end{aligned}
$$

Similarly, using that $n \in \mathcal{A}_\varepsilon^0$ and thus $\rho(n) \ge \rho_0^-$, we obtain that:

$$
\begin{aligned}
&\iint_{I\times J} \Phi(n)(t,x,y)\,dx\,dy \ge \rho_\varepsilon^0\, e^{-\frac{1}{\varepsilon}\int_0^t \|m\|_\infty+\kappa\,\rho(n)(s)\,ds} + \frac{r}{\varepsilon}\int_0^t \rho(n)(\tau)\, e^{-\frac{1}{\varepsilon}\int_\tau^t \|m\|_\infty+\kappa\,\rho(n)(s)\,ds}\,d\tau \\
&\ge \rho_\varepsilon^0\, e^{-\frac{1}{\varepsilon}\int_0^t \left[\frac{\|m\|_\infty}{\rho_0^-}+\kappa\right]\rho(n)(s)\,ds} + \frac{r}{\frac{\|m\|_\infty}{\rho_0^-}+\kappa}\int_0^t \left[\frac{\|m\|_\infty}{\rho_0^-}+\kappa\right] \frac{\rho(n)(\tau)}{\varepsilon}\, e^{-\frac{1}{\varepsilon}\int_\tau^t \left[\frac{\|m\|_\infty}{\rho_0^-}+\kappa\right]\rho(n)(s)\,ds}\,d\tau \\
&\ge \rho_\varepsilon^0\, e^{-\frac{1}{\varepsilon}\int_0^t \left[\frac{\|m\|_\infty}{\rho_0^-}+\kappa\right]\rho(n)(s)\,ds} + \frac{r}{\frac{\|m\|_\infty}{\rho_0^-}+\kappa}\left(1 - e^{-\frac{1}{\varepsilon}\int_0^t \left[\frac{\|m\|_\infty}{\rho_0^-}+\kappa\right]\rho(n)(s)\,ds}\right) \\
&\ge \min\left(\rho_\varepsilon^0, \frac{r}{\frac{\|m\|_\infty}{\rho_0^-}+\kappa}\right) = \min\left(\rho_\varepsilon^0, \frac{r}{\frac{\|m\|_\infty}{\frac{r-\|m\|_\infty}{\kappa}}+\kappa}\right) = \min\left(\rho_\varepsilon^0, \frac{r-\|m\|_\infty}{\kappa}\right) = \rho_0^-.
\end{aligned}
$$

Next, for $y \in J$ and $t \in [0,T]$, we get from (6.19):

$$
\begin{aligned}
&\rho^X\left(\Phi(n)\right)(t,y) = \int_I \Phi(n)(t,x,y)\,dx = \int_I n_\varepsilon^0(x,y)\, e^{-\frac{1}{\varepsilon}\int_0^t m(x,y)+\kappa\,\rho(n)(s)\,ds}\,dx \\
&\quad + \frac{r}{\varepsilon}\int_I\int_0^t \frac{1}{2}\left[\frac{\rho^X(n)(\tau,y)\,\rho^Y(\tau,x)}{\rho(n)(\tau)} + n(\tau,x,y)\right] e^{-\frac{1}{\varepsilon}\int_\tau^t m(x,y)+\kappa\,\rho(n)(s)\,ds}\,d\tau\,dx \\
&\le \rho_\varepsilon^{X,0}(y) + \frac{r}{\varepsilon}\int_0^t \left\|\rho^X(n)(\tau,\cdot)\right\|_\infty d\tau \le \left\|\rho_\varepsilon^{X,0}\right\|_\infty + \frac{r}{\varepsilon}\int_0^t \left\|\rho^{X,0}\right\|_\infty e^{\frac{r\,\tau}{\varepsilon}}\,d\tau \le \left\|\rho_\varepsilon^{X,0}\right\|_\infty e^{\frac{r\,t}{\varepsilon}},
\end{aligned}
$$

since $n \in \mathcal{A}_\varepsilon^0$. The same holds for $\rho^Y\left(\Phi(n)\right)(t,x) := \int_J \Phi(n)(t,x,y)\,dy$.

Finally, we compute:

$$\begin{aligned}
\partial_x\Phi(n) &= \left(\partial_x n_\varepsilon^0 - n_\varepsilon^0\,\frac{1}{\varepsilon}\int_0^t \partial_x A\,ds\right) e^{-\frac{1}{\varepsilon}\int_0^t A\,ds} + \frac{1}{\varepsilon}\int_0^t \left(\partial_x B - B\,\frac{1}{\varepsilon}\int_\tau^t \partial_x A\,ds\right) e^{-\frac{1}{\varepsilon}\int_\tau^t A\,ds}\,d\tau \\
&= \partial_x n_\varepsilon^0\, e^{-\frac{1}{\varepsilon}\int_0^t A\,ds} + \frac{1}{\varepsilon}\int_0^t \partial_x B\, e^{-\frac{1}{\varepsilon}\int_\tau^t A\,ds}\,d\tau \\
&\quad - \frac{1}{\varepsilon}\int_0^t \partial_x m \left(n_\varepsilon^0\, e^{-\frac{1}{\varepsilon}\int_0^\tau A\,ds} + B\,\frac{1}{\varepsilon}(t-\tau)\right) e^{-\frac{1}{\varepsilon}\int_\tau^t A\,ds} d\tau.
\end{aligned}$$

We next consider the following integration by parts:

$$\int_0^t (t-\tau)\,B(\tau)\,e^{-\frac{1}{\varepsilon}\int_\tau^t A(s)\,ds} d\tau = 0 + \int_0^t \int_0^\tau B(s)\,e^{-\frac{1}{\varepsilon}\int_s^t A(u)\,du} ds\,d\tau,$$

The latter leads to:

$$\begin{aligned}
\partial_x\Phi(n) &= \partial_x n_\varepsilon^0\, e^{-\frac{1}{\varepsilon}\int_0^t A\,ds} + \frac{1}{\varepsilon}\int_0^t \partial_x B\, e^{-\frac{1}{\varepsilon}\int_\tau^t A\,ds}\,d\tau \\
&\quad - \frac{\partial_x m}{\varepsilon}\int_0^t \left(n_\varepsilon^0\, e^{-\frac{1}{\varepsilon}\int_0^\tau A\,ds} + \frac{1}{\varepsilon}\int_0^\tau B(s)\,e^{-\frac{1}{\varepsilon}\int_s^\tau A(u)\,du}\right) e^{-\frac{1}{\varepsilon}\int_\tau^t A\,ds} d\tau \\
&= \partial_x n_\varepsilon^0\, e^{-\frac{1}{\varepsilon}\int_0^t A\,ds} + \frac{1}{\varepsilon}\int_0^t \partial_x B\, e^{-\frac{1}{\varepsilon}\int_\tau^t A\,ds}\,d\tau - \frac{\partial_x m}{\varepsilon}\int_0^t \Phi(n)(\tau)\,e^{-\frac{1}{\varepsilon}\int_\tau^t A\,ds} d\tau.
\end{aligned}$$

Hence, since $n \in \mathcal{A}_\varepsilon^0$, we obtain thanks to (6.29): $|\Phi(n)(t,\cdot,\cdot)| \le N_{T_M}$ for $t \in [0,T]$, which implies:

$$\begin{aligned}
&\|\partial_x\Phi(n)(t,\cdot,\cdot)\|_\infty \\
&\le \left\|\partial_x n_\varepsilon^0\right\|_\infty + \int_0^t \frac{r}{2\varepsilon}\left[\frac{\left\|\rho_\varepsilon^{X,0}\right\|_\infty |J|}{\rho_0^-}\,e^{\frac{r\,\tau}{\varepsilon}} + 1\right] \|\partial_x n_\varepsilon(\tau,\cdot,\cdot)\|_\infty\,d\tau + \frac{t\,\|\partial_x m\|_\infty}{\varepsilon}\,N_{T_M} \\
&\le \left\|\partial_x n_\varepsilon^0\right\|_\infty + \frac{T_M\,\|\partial_x m\|_\infty}{\varepsilon}\,N_{T_M} \\
&+ \int_0^t \frac{r}{2\varepsilon}\left[\frac{\left\|\rho_\varepsilon^{X,0}\right\|_\infty |J|}{\rho_0^-}\,e^{\frac{r\,\tau}{\varepsilon}} + 1\right] \left(\|\partial_x n_\varepsilon^0\|_\infty + N_{T_M}\,\frac{T_M}{\varepsilon}\,\|\partial_x m\|_\infty\right) e^{\frac{\left\|\rho_\varepsilon^{X,0}\right\|_\infty |J|}{2\rho_0^-}(e^{\frac{r\,\tau}{\varepsilon}}-1)+\frac{r\tau}{2\varepsilon}}\,d\tau \\
&= \left(\left\|\partial_x n_\varepsilon^0\right\|_\infty + \frac{T_M\,\|\partial_x m\|_\infty}{\varepsilon}\,N_{T_M}\right)\left[1 + \int_0^t \frac{r}{2\varepsilon}\left[\frac{\left\|\rho_\varepsilon^{X,0}\right\|_\infty |J|}{\rho_0^-}\,e^{\frac{r\,\tau}{\varepsilon}} + 1\right] e^{\frac{\left\|\rho_\varepsilon^{X,0}\right\|_\infty |J|}{\rho_0^-}\frac{e^{\frac{r\,\tau}{\varepsilon}}}{2}+\frac{r\tau}{2\varepsilon}}\,d\tau\right] \\
&= \left(\left\|\partial_x n_\varepsilon^0\right\|_\infty + \frac{T_M\,\|\partial_x m\|_\infty}{\varepsilon}\,N_{T_M}\right)\left[1 + \int_0^t \left(e^{\frac{\left\|\rho_\varepsilon^{X,0}\right\|_\infty |J|}{\rho_0^-}\frac{e^{\frac{r\,\tau}{\varepsilon}}}{2}+\frac{r\tau}{2\varepsilon}}\right)' d\tau\right] \\
&= \left(\left\|\partial_x n_\varepsilon^0\right\|_\infty + \frac{T_M\,\|\partial_x m\|_\infty}{\varepsilon}\,N_{T_M}\right) e^{\frac{\left\|\rho_\varepsilon^{X,0}\right\|_\infty |J|}{2\rho_0^-}e^{\frac{r\,t}{\varepsilon}}+\frac{rt}{2\varepsilon}}.
\end{aligned}$$

The same holds for $\|\partial_y\Phi(n)(t,\cdot,\cdot)\|_\infty$. Hence: $\Phi(n) \in \mathcal{A}_\varepsilon^0$.

2. Φ is a contraction mapping for T small. Let n and $\tilde{n}$ be in $\mathcal{A}^0_\varepsilon$. We have, for all $(t,x,y) \in [0,T] \times I \times J$:

$$\begin{aligned}
\Phi(n)(t,x,y) - \Phi(\tilde{n})(t,x,y) &= n^0_\varepsilon(x,y) \left[e^{-\frac{1}{\varepsilon}\int_0^t A(s,x,y)\,ds} - e^{-\frac{1}{\varepsilon}\int_0^t \tilde{A}(s,x,y)\,ds} \right] \\
&+ \frac{1}{\varepsilon}\left[\int_0^t \left(B(\tau,x,y) - \tilde{B}(\tau,x,y) \right) e^{-\frac{1}{\varepsilon}\int_\tau^t A(s,x,y) ds} \right. \\
&\left. + \tilde{B}(\tau,x,y) \left(e^{-\frac{1}{\varepsilon}\int_\tau^t A(s,x,y) ds} - e^{-\frac{1}{\varepsilon}\int_\tau^t \tilde{A}(s,x,y) ds} \right) d\tau \right] \\
&\leq N_{T_M} \left| e^{\frac{1}{\varepsilon}\int_0^t \kappa\,[\rho(s) - \tilde{\rho}(s)] ds} - 1 \right| \\
&+ \frac{r}{2\varepsilon} \int_0^t \left| \frac{\rho^X \rho^Y}{\rho} - \frac{\tilde{\rho}^X \tilde{\rho}^Y}{\tilde{\rho}} + n - \tilde{n} \right| d\tau \\
&+ \frac{r}{2\varepsilon} \left[\frac{N^2_{T_M} |I||J|}{\rho_0^-} + N_{T_M} \right] \int_0^t \left| e^{\frac{1}{\varepsilon}\int_\tau^t \kappa\,[\rho(s) - \tilde{\rho}(s)] ds} - 1 \right| d\tau.
\end{aligned}$$

Using that $|e^x - 1| \leq |x|\, e^{|x|}$, we get that:

$$\left| e^{\frac{1}{\varepsilon}\int_0^t \kappa\,[\rho(s) - \tilde{\rho}(s)] ds} - 1 \right| \leq \frac{T\,\kappa\,|I||J|}{\varepsilon}\, e^{\frac{2\,\kappa\,T_M\,\rho_0^+}{\varepsilon}} \|n - \tilde{n}\|_\infty. \tag{6.30}$$

Furthermore, we have:

$$\begin{aligned}
&\frac{r}{2\varepsilon} \int_0^t \left| \frac{\rho^X \rho^Y}{\rho} - \frac{\tilde{\rho}^X \tilde{\rho}^Y}{\tilde{\rho}} \right| d\tau \leq \frac{r}{2\varepsilon} \int_0^t \left| \rho^X - \tilde{\rho}^X \right| \frac{\rho^Y}{\rho} + \tilde{\rho}^X \left| \frac{\rho^Y}{\rho} - \frac{\tilde{\rho}^Y}{\tilde{\rho}} \right| d\tau \\
&\leq \frac{r\,T}{2\varepsilon}\,|I|\,\frac{N_{T_M}|J|}{\rho_0^-} \|n - \tilde{n}\|_\infty + \frac{r\,|I| N_{T_M}}{2\varepsilon} \int_0^t \frac{\rho^Y}{\rho_0^{-2}} |\rho - \tilde{\rho}| + \frac{1}{\rho_0^-} \left| \rho^Y - \tilde{\rho}^Y \right| d\tau \qquad (6.31) \\
&\leq T \frac{r\,|I||J| N_{T_M}}{2\varepsilon\,\rho_0^-} \left[2 + \frac{N_{T_M}|I||J|}{\rho_0^-} \right] \|n - \tilde{n}\|_\infty.
\end{aligned}$$

Hence, we have:

$$\|\Phi(n) - \Phi(\tilde{n})\|_\infty \leq T\, k^1_{T_M,\varepsilon}\, \|n - \tilde{n}\|_\infty, \tag{6.32}$$

where $k^1_{T_M,\varepsilon}$ is a constant that does not depend on T.

Moreover, we need to control the difference of the derivatives:

$$\begin{aligned}
\partial_x \Phi(n) - \partial_x \Phi(\tilde{n}) &= \partial_x n^0_\varepsilon(x,y) \left[e^{-\frac{1}{\varepsilon}\int_0^t A(s,x,y)} ds - e^{-\frac{1}{\varepsilon}\int_0^t \tilde{A}(s,x,y)} ds \right] \\
&+ \frac{1}{\varepsilon} \int_0^t \left(\partial_x B\, e^{-\frac{1}{\varepsilon}\int_\tau^t A\, ds} - \partial_x \tilde{B}\, e^{-\frac{1}{\varepsilon}\int_\tau^t \tilde{A}\, ds} \right) d\tau \\
&+ \frac{\partial_x m}{\varepsilon} \int_0^t \left(\Phi(\tilde{n}) e^{-\frac{1}{\varepsilon}\int_\tau^t \tilde{A}\, ds} - \Phi(n) e^{-\frac{1}{\varepsilon}\int_\tau^t A\, ds} \right) d\tau.
\end{aligned}$$

Similarly as above (6.30), the first term is controlled by:

$$\begin{aligned}
&\left| \partial_x n^0_\varepsilon(x,y) \left[e^{-\frac{1}{\varepsilon}\int_0^t A(s,x,y)} ds - e^{-\frac{1}{\varepsilon}\int_0^t \tilde{A}(s,x,y)} ds \right] \right| \leq \left\| \partial_x n^0_\varepsilon \right\|_\infty \left| e^{\frac{1}{\varepsilon}\int_0^t \kappa\,(\tilde{\rho}(s) - \rho(s))\, ds} - 1 \right| \\
&\leq T\, \frac{N^x_{T_M}\,\kappa\,|I||J|}{\varepsilon}\, e^{\frac{2\,\kappa\,T_M\,\rho_0^+}{\varepsilon}} \|n - \tilde{n}\|_\infty.
\end{aligned}$$

The second term is broken down in two:

$$\begin{aligned}
&\frac{1}{\varepsilon}\int_0^t \left(\partial_x B\, e^{-\frac{1}{\varepsilon}\int_\tau^t A\,ds} - \partial_x \tilde{B}\, e^{-\frac{1}{\varepsilon}\int_\tau^t \tilde{A}\,ds}\right) d\tau \\
&= \frac{1}{\varepsilon}\int_0^t \partial_x B \left(e^{-\frac{1}{\varepsilon}\int_\tau^t A\,ds} - e^{-\frac{1}{\varepsilon}\int_\tau^t \tilde{A}\,ds}\right) d\tau + \frac{1}{\varepsilon}\int_0^t \left(\partial_x B - \partial_x \tilde{B}\right) e^{-\frac{1}{\varepsilon}\int_\tau^t \tilde{A}\,ds} d\tau
\end{aligned}$$

The first part is controlled thanks to (6.30) and the estimates defining $\mathcal{A}_\varepsilon^0$:

$$\begin{aligned}
&\left|\frac{1}{\varepsilon}\int_0^t \partial_x B \left(e^{-\frac{1}{\varepsilon}\int_\tau^t A\,ds} - e^{-\frac{1}{\varepsilon}\int_\tau^t \tilde{A}\,ds}\right) d\tau\right| \leq \int_0^t \frac{r}{2\varepsilon}\left[\frac{\left|\partial_x \rho^Y(n)\right| \rho^X(n)}{\rho_0^-} + |\partial_x n|\right] \left|e^{\frac{1}{\varepsilon}\int_\tau^t \kappa\,(\tilde{\rho}(s)-\rho(s))\,ds} - 1\right| \\
&\leq \frac{r\,T\,N_{T_M}^x}{2\varepsilon\,\rho_0^-}\left[1 + \frac{N_{T_M}|I||J|}{\rho_0^-}\right] \frac{T_M\,\kappa\,|I||J|}{\varepsilon}\, e^{\frac{2\,\kappa\,T_M\,\rho_0^+}{\varepsilon}}\, \|n-\tilde{n}\|_\infty \\
&= T\frac{r\,T_M\,N_{T_M}^x}{2\varepsilon^2\,\rho_0^-}\left[1 + \frac{N_{T_M}|I||J|}{\rho_0^-}\right] \kappa\,|I||J|\, e^{\frac{2\,\kappa\,T_M\,\rho_0^+}{\varepsilon}}\, \|n-\tilde{n}\|_\infty.
\end{aligned}$$

The second part is controlled similarly as in (6.31):

$$\begin{aligned}
&\left|\frac{1}{\varepsilon}\int_0^t \left(\partial_x B - \partial_x \tilde{B}\right) e^{-\frac{1}{\varepsilon}\int_\tau^t \tilde{A}\,ds} d\tau\right| \leq \frac{1}{\varepsilon}\int_0^t \left|\partial_x B - \partial_x \tilde{B}\right| d\tau \\
&\leq \frac{r}{2\varepsilon}\int_0^t \left|\partial_x \rho^X - \partial_x \tilde{\rho}^X\right| \frac{\rho^Y}{\rho} + \left|\partial_x \tilde{\rho}^X\right| \left|\frac{\rho^Y}{\rho} - \frac{\tilde{\rho}^Y}{\tilde{\rho}}\right| d\tau \\
&\leq \frac{r}{2\varepsilon}\left[\frac{T|I||J|N_{T_M}}{\rho_0^-}\,\|\partial_x n - \partial_x \tilde{n}\|_\infty + |I|N_{T_M}^x \int_0^t \frac{\rho^Y}{{\rho_0^-}^2}\,|\rho-\tilde{\rho}| + \frac{1}{\rho_0^-}\left|\rho^Y - \tilde{\rho}^Y\right|\right] \\
&\leq \frac{r}{2\varepsilon}\left[\frac{T|I||J|N_{T_M}}{\rho_0^-}\,\|\partial_x n - \partial_x \tilde{n}\|_\infty + \frac{|I|N_{T_M}^x T|J|\left(1 + \frac{|I||J|N_{T_M}}{\rho_0^-}\right)}{\rho_0^-}\|n-\tilde{n}\|_\infty\right] \\
&= T\frac{r|I||J|}{2\varepsilon\rho_0^-}\left[\frac{N_{T_M}}{\rho_0^-}\,\|\partial_x n - \partial_x \tilde{n}\|_\infty + N_{T_M}^x\left(1 + \frac{|I||J|N_{T_M}}{\rho_0^-}\right)\|n-\tilde{n}\|_\infty\right].
\end{aligned}$$

The last term is controlled thanks to the first part of the proof on $\|\Phi(n) - \Phi(\tilde{n})\|_\infty$ (6.32) and that $\|\Phi(n)\|_\infty \leq N_{T_M}$, for $\Phi(n) \in \mathcal{A}_0^\varepsilon$:

$$\begin{aligned}
&\left|\frac{\partial_x m}{\varepsilon}\int_0^t \left(\Phi(\tilde{n})e^{-\frac{1}{\varepsilon}\int_\tau^t \tilde{A}\,ds} - \Phi(n)e^{-\frac{1}{\varepsilon}\int_\tau^t A\,ds}\right) d\tau\right| \\
&\leq \frac{\|\partial_x m\|_\infty}{\varepsilon}\int_0^t \|\Phi(n)(\tau,\cdot,\cdot) - \Phi(\tilde{n})(\tau,\cdot,\cdot)\|_\infty + \|\Phi(n)(\tau,\cdot,\cdot)\|_\infty \left|e^{\frac{1}{\varepsilon}\int_\tau^t \kappa\,(\tilde{\rho}(s)-\rho(s))\,ds} - 1\right| d\tau \\
&\leq T\frac{\|\partial_x m\|_\infty}{\varepsilon}\left(\|\Phi(n) - \Phi(\tilde{n})\|_\infty + N_{T_M}\,\frac{T_M\,\kappa\,|I||J|}{\varepsilon}\, e^{\frac{2\,\kappa\,T_M\,\rho_0^+}{\varepsilon}}\,\|n-\tilde{n}\|_\infty\right) \\
&\leq T\frac{\|\partial_x m\|_\infty}{\varepsilon}\left(T_M k^1_{T_M,\varepsilon} + N_{T_M}\,\frac{T_M\,\kappa\,|I||J|}{\varepsilon^2}\, e^{\frac{2\,\kappa\,T_M\,\rho_0^+}{\varepsilon^2}}\right)\|n-\tilde{n}\|_\infty
\end{aligned}$$

The same controls hold up for $\partial_y\Phi(n) - \partial_y\Phi(\tilde{n})$. Hence:

$$\|\Phi(n) - \Phi(\tilde{n})\|_X \leq T\,k_{T_M,\varepsilon}\,\|n-\tilde{n}\|_X\,,$$

where $k_{T_M,\varepsilon}$ is a constant that does not depend on T.

Hence, we can choose $T > 0$ small enough uniformly on $[0, T_M]$ so that Φ is a contraction mapping. □

Remark 16. *Thanks to (6.32), the uniqueness can be obtained in* $C^0([0,T_M],C^0(I\times J))$.

6.C Technical lemma

Lemma 15. *Let* K *and* K' *be two compact sets of* $\mathbb{R}$ *and* (f_n) *be a bounded sequence in* $L^\infty(K,L^1(K'))$. *Then, there exists* $f\in L^\infty(K,M^1(K'))$ *and a subsequence of* (f_n) *that converges toward* f *in the weak* $L^\infty(w^*-K,M^1(K'))$ *topoplogy.*

Proof of Lemma 15. Since K and K' are compact sets of $\mathbb{R}$, $L^\infty(K,L^1(K'))\subset L^1(K,L^1(K'))\subset M^1(K\times K')$. Since (f_n) is then a bounded sequence in $M^1(K\times K')$, from Banach-Alaoglu theorem, there exists $f\in M^1(K\times K')$ and a subsequence still noted (f_n) that converges weakly$-*$ toward $f\in M^1(K\times K')$. As, for all $n\in\mathbb{N}$, $f_n\geq 0$, we deduce that f is non-negative almost everywhere.

$f\in L^\infty(K,M^1(K'))$. Let us denote:

$$F_n:\left\{\begin{array}{l} K\to\mathbb{R}\\ x\mapsto\displaystyle\int_{K'}f_n(x,y)\,dy.\end{array}\right.$$

Since f_n is a bounded sequence in $L^\infty(K,L^1(K'))$, (F_n) is a bounded sequence in $L^\infty(K,\mathbb{R})$. As $L^\infty(K,\mathbb{R})=(L^1(K,R))^*$, and $L^1(K,R)$ is separable, the Banach-Alaoglu theorem implies that there exists a subsequence of (F_n), still noted (F_n), and $F\in L^\infty(K,\mathbb{R})$ such that:

$$F_n\overset{*}{\rightharpoonup}F.$$

Let $\phi\in C(K,\mathbb{R})$. From the previous convergence, we have:

$$\int_K\phi(x)\int_{K'}f_n(x,y)\,dy\,dx\to\int_K\phi(x)F(x)\,dx.$$

Also, since (f_n) converges weakly$-*$ toward $f\in M^1(K\times K')$, we have:

$$\int_{K\times K'}\phi(x)f_n(x,y)\,dx\,dy\to\int_{K\times K'}\phi(x)df(x,y).$$

The latter holds for all $\phi\in C(K,\mathbb{R})$. Hence:

$$x\mapsto\int_{K'}df(x,y)=F\in L^\infty(K,\mathbb{R}).$$

We thus obtain that: $f\in L^\infty(K,M^1(K'))$.

(f_n) converges weakly toward f in $L^\infty(K,M^1(K'))-*$. Let us consider $\varepsilon>0$, $\phi\in L^1(K,C(K'))$ and, by density, $(\phi_k)\in C(K\times K')^{\mathbb{N}}$ such that: $\phi_k\overset{L^1(K,C(K'))}{\longrightarrow}\phi$. Then

(denoting $\|\cdot\|_{M^1(K')}$ the dual norm on $M^1(K')$):

$$
\begin{aligned}
&\left|\int_{K\times K'} \phi(x,y)\,df(x,y) - \int_{K\times K'} f_n(x,y)\,\phi(x,y)\,dx\,dy\right| \\
&\leq \left|\int_{K\times K'} (\phi(x,y)-\phi_k(x,y))\;df(x,y)\right| + \left|\int_{K\times K'} f_n(x,y)\,(\phi(x,y)-\phi_k(x,y))\right| \\
&\qquad + \left|\int_{K\times K'} \phi_k(x,y)\,(f_n(x,y)\,dx\,dy - df(x,y))\right| \\
&\leq \int_K \|\phi(x,\cdot)-\phi_k(x,\cdot)\|_\infty \left(\|f(x,\cdot)\|_{M^1(K')} + \|f_n(x,\cdot)\|_{L^1(K')}\right) dx \\
&\qquad + \left|\int_{K\times K'} \phi_k(x,y)\,(f_n(x,y)\,dx\,dy - df(x,y))\right| \\
&\leq \left(\|f\|_{L^\infty(K,M^1(K'))} + \|f_n\|_{L^\infty(K,L^1(K'))}\right) \|\phi_k-\phi\|_{L^1(K,C(K'))} \\
&\qquad + \left|\int_{K\times K'} \phi_k(x,y)\,(f_n(x,y)\,dx\,dy - df(x,y))\right|
\end{aligned}
$$

Since $\phi_k \to \phi$ in $L^1(K,C(K'))$ and (f_n) is bounded in $L^\infty(K,L^1(K'))$, the first term is smaller than ε for k large enough. For such a $k\in\mathbb{N}$, the weak convergence of (f_n) toward f in $M^1(K\times K')$ ensures that for n large enough, the second term is smaller than ε, which concludes the proof. □

Acknowledgments

Both authors thank Vincent Calvez for the introduction of the model and fruitful discussions and Denis Roze for valuable discussions about the biological motivations. L.D. thanks also Sarah Otto for enlightening initial conversations. Both authors have received funding from the ANR project DEEV ANR-20-CE40-0011-01 and the chaire Modélisation Mathématique et Biodiversité of Véolia Environment - École Polytechnique - Museum National d'Histoire Naturelle - Fondation X. This project has received funding from the European Research Council (ERC) under the European Union's Horizon 2020 research and innovation programm (grant agreement No 639638).

Chapter 7

Annex: Volunteer modelling project of the Covid epidemic in Mayotte (first part: May 2020)

Context and description of the project. On the 11th of March 2020, the World Health Organization (WHO) assessed that the COVID-19 epidemic spreading around the globe had reached the pandemic stage. As public policies were considering extremely stringent measures to contain the first wave of the epidemic, modelling efforts sparked worldwide to try to provide some guiding elements. The academic platform of MODCOV19 was created to coordinate and support this effort in France. Through the intermediary of Amandine Véber (a member of MODCOV19), Vincent Calvez was put in contact with Julien Balicchi of the Regional Health Agency of Mayotte (ARS) in mid-April 2020.

The aim was to extend a first epidemiological model built in collaboration with a mathematician from the Centre Universitaire de Mayotte to account for the influence of the particular age structure of Mayotte's population on the trajectory of the COVID-19 epidemic wave that was unfolding there since mid-March 2020 (according to the reports at the time). Indeed, Mayotte is one of the French departments with the highest fecundity (over 4) and with over half of its total population under 20 (UN 2019 - per comparison, the same age class in the whole French population represents under 25 percent of the total French population). As studies were starting to be published showing large discrepancies of susceptibility to infection by COVID-19 with regard to age (Davies et al. 2020), it seemed relevant to include the demographic structure of Mayotte in the existing epidemiological model, in order to assess in particular how the reopening of school, forecasted to be on the 18th of May 2020, would impact the course of the epidemic and translate into severe cases, as requested by the ARS. The head of the ARS of Mayotte was forecasted to speak about the potential impact of this measure at the French Parliament during the week of the 11th of May 2020. Mete Demircigil and myself joined this short volunteer modelling project on the 5th of May 2020.

This document presents the part of this short project to which I dedicated myself from the 5th of May to the 11th of May 2020, under the supervision of V. Calvez and in collaboration with the ARS of Mayotte. My first task was to dive into the scientific literature on the COVID-19 epidemic to reduce the number of parameter values of the age-structured model to be estimated, and next to implement this model into a Python code in order to give some quantitative predictions about the effect of school's reopening on the incidence level. The complementary part of the project, conducted by M. Demircigil and V. Calvez, was to

analyse the hospitalizations and ICU data provided by the ARS of Mayotte and translate the dynamics of the age-specific incidence output of the Python code into age-specific dynamics of hospitalizations and ICU cases.

7.1 Epidemiological model

Compartments and age structure. As Mayotte presents a particular age structure (with more than half its inhabitants under 20 [UN 2019]), we consider an age-structured compartmental model with three age classes: 0-19, 20-59 and 60+. The different epidemiological compartments, whose densities vary in time, are therefore vectors in $\mathbb{R}_+^3$ denoted in bold $\boldsymbol{S}(t), \boldsymbol{E}(t), \boldsymbol{A}(t), \boldsymbol{I}(t), \boldsymbol{R}(t)$ (respectively: Susceptible, Exposed, Asymptomatic, Infected and Removed). The asymptomatic compartment represent individuals either exhibiting no symptoms or only mild ones.

Epidemiological parameters We define

- $C(t) \in M_3(\mathbb{R})$: time-dependent contact matrix per age. The coefficient $c_{i,j}(t)$ is the average estimated number of contact of a person from age class i with another from age class j at time t. Therefore, C does not need to be symmetrical. The temporal dependency of C allows to model the effects of public policies on contact levels.
- $\boldsymbol{u} \in \mathbb{R}_+^3$: vector of age-specific susceptibility per contact (the probability that a susceptible person meeting with an infected person becomes infected upon contact and transmission).
- $\boldsymbol{\gamma} \in \mathbb{R}_+^3$: the vector of age-specific latency rate (the inverse of the average time from being exposed to become infected).
- $\boldsymbol{a} \in [0,1]^3$: the vector of age-specific asymptomatic frequency.
- $\boldsymbol{\beta} \in \mathbb{R}_+$: the vector of age-specific transmissibility rate (the probability that an infected person transmits the virus upon contact to a susceptible person)
- $\boldsymbol{\beta_A}$: the age-specific transmissibility reduction factor from an asymptomatic person compared to an infected person.
- $\boldsymbol{\alpha} \in \mathbb{R}_+^3$: the vector of age-specific removal rates for infected.
- $\boldsymbol{\delta}$ the vector of age-specific removal rates for asymptomatic.

Summary sketch of the relationships between stages.

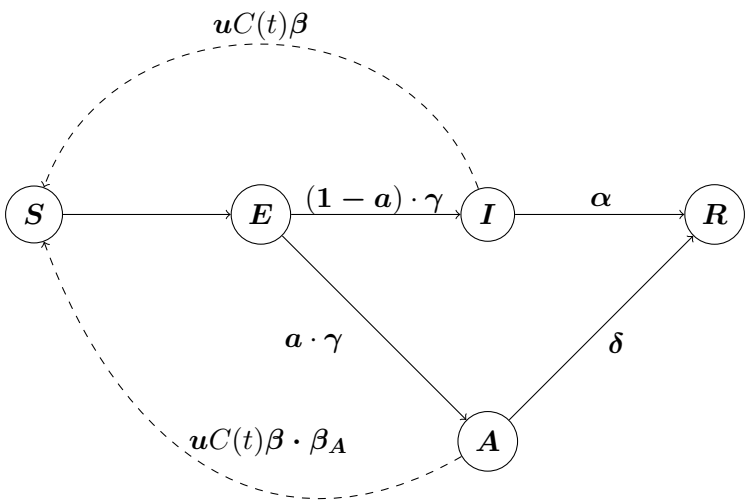

ODE system. Denoting $\boldsymbol{N}$ the vector of the total sizes of each age class, the following system is obtained according to the law of mass action:

$$\begin{cases} \dot{\boldsymbol{S}}(t) = -\boldsymbol{S}(t)\cdot\boldsymbol{u}\cdot C(t)\boldsymbol{\beta}\left[\boldsymbol{I}(t)+\boldsymbol{\beta_A}\boldsymbol{A}(t)\right]\cdot\boldsymbol{N}^{-1} \\ \dot{\boldsymbol{E}}(t) = \boldsymbol{S(t)}\cdot\boldsymbol{u}\cdot C(t)\boldsymbol{\beta}\left[\boldsymbol{I}(t)+\boldsymbol{\beta_A}\boldsymbol{A}(t)\right]\boldsymbol{N}^{-1} - \boldsymbol{\gamma}\cdot\boldsymbol{E}(t) \\ \dot{\boldsymbol{A}}(t) = \boldsymbol{a}\cdot\boldsymbol{\gamma}\cdot\boldsymbol{E}(t) - \boldsymbol{\delta}\cdot\boldsymbol{A}(t) \\ \dot{\boldsymbol{I}}(t) = \mathbf{1}-\boldsymbol{a}\cdot\boldsymbol{\gamma}\cdot\boldsymbol{E}(t) - \boldsymbol{\alpha}\cdot\boldsymbol{I}(t) \\ \dot{\boldsymbol{R}}(t) = \boldsymbol{\alpha}\cdot\boldsymbol{I}(t) + \boldsymbol{\delta}\cdot\boldsymbol{A}(t) \end{cases} \tag{7.1}$$

Basic reproduction number $\mathcal{R}_0(t)$. As the model that we consider involves an age structure, the computation of the basic reproduction number $\mathcal{R}_0(t)$ requires here more tools that in the analogous homogeneous compartmental model. More precisely, I used the Next-Generation Matrix framework for compartmental models (see Diekmann, Heesterbeek, and Britton 2013). This approach relies on two matrices F and V, where $F_{i,j}$ is the rate at which individuals of compartment j infect individuals of compartment i (here, we consider the compartments of Exposed, Infected and Asymptomatics) and $V_{i,j}$ relates to the average time that individuals in compartment j will spend (have spent) in compartment i

$$F(t) = \begin{pmatrix} 0 & \mathrm{Diag}\,(\boldsymbol{u})\,C(t)\boldsymbol{\beta} & \mathrm{Diag}\,(\cdot\boldsymbol{u})\,C(t)\,\mathrm{Diag}(\boldsymbol{\beta}\boldsymbol{\beta_A}) \\ 0 & 0 & 0 \\ 0 & 0 & 0 \end{pmatrix},$$

adn

$$V = \begin{pmatrix} \mathrm{Diag}(\boldsymbol{\gamma}) & 0 & 0 \\ -\mathrm{Diag}((1-\boldsymbol{a})\cdot\boldsymbol{\gamma}) & \mathrm{Diag}(\boldsymbol{\alpha}) & 0 \\ -\mathrm{Diag}(\boldsymbol{a}\cdot\boldsymbol{\gamma}) & 0 & \mathrm{Diag}(\boldsymbol{\delta}) \end{pmatrix}.$$

The next-generation matrix FV^{-1}, whose spectral radius is the basic reproduction number $\mathcal{R}_0t$), reads as follows

$$FV^{-1} = \begin{pmatrix} \mathrm{Diag}\,(\boldsymbol{u})\,C(t)\boldsymbol{\beta}\left[\mathrm{Diag}(\boldsymbol{\alpha}^{-1}\cdot(1-\boldsymbol{a})) + \mathrm{Diag}(\boldsymbol{\beta_A}\cdot\boldsymbol{\delta}^{-1}\cdot\boldsymbol{a})\right] & * & * \\ 0 & 0 & 0 \\ 0 & 0 & 0 \end{pmatrix}$$

We thus obtain the following formula for the basic reproduction number at time t (where $\rho(M)$ denotes the spectral radius of M)

$$\mathcal{R}_0(t) = \rho\left(\mathrm{Diag}\left(\boldsymbol{\beta u}\right) C(t) \left[\mathrm{Diag}(\boldsymbol{\alpha}^{-1} \cdot (1 - \boldsymbol{a})) + \mathrm{Diag}(\boldsymbol{\beta_A} \cdot \boldsymbol{\delta}^{-1} \cdot \boldsymbol{a})\right]\right).$$

Doubling time We define the doubling time the exponential growth phase at the start of the epidemic when $\boldsymbol{S} \approx \boldsymbol{N}$ as:

$$T_{1/2} = \frac{\log(2)}{r}, \quad \text{where} \quad r = \max(\mathrm{Re}(\mathrm{Sp}(F - V))),$$

where F and V are the matrices defined in the last paragraph.

Incidence At a time t, we compute the incidence $\boldsymbol{\lambda}(t)$ as :

$$\boldsymbol{\lambda}(t) = \boldsymbol{S}(t) \cdot \boldsymbol{u} \cdot C\boldsymbol{\beta}\left[\boldsymbol{I}(t) + \boldsymbol{\beta_A} \boldsymbol{A}(t)\right] \boldsymbol{N}^{-1}.$$

7.2 Python code implementation

The Python code implements a time-discretization of the system (7.1) using an explicit scheme.

7.2.1 Epidemiological parameter values

- age-specific susceptibility $\boldsymbol{u}$: gross values have been taken from the Extended Table 1 of [Davies et al. 2020] (back then still a preprint). The definitive values for the three age classes considered in this project have next been obtained as weighed average accounting for for Mayotte's age class sizes.

- age-specific frequency of asymptomatic cases $\boldsymbol{a}$: gross values have been taken from the ones indicated for the subclinical fraction ("those with very mild symptoms that may not be noticed or reported, even though they occur", 1 minus the clinical fraction) from the Extended Table 1 of [Davies et al. 2020] (back then still a preprint). The definitive values for the three age classes considered in this project have next been obtained as weighted average accounting for age class sizes.

- relative transmissibility of asymptomatics $\boldsymbol{\beta_A} = [0.55, 0.55, 0.55]$: this value was chosen from the study on "undocumented infections" in China by [Li et al. 2020] (95% confidence interval is [0.46-0.62]). It is homogeneous across age class as, up to my knowledge, there were not any data available at that time which indicated an age dependency on this parameter.

- the inverse of latency period between exposition to infection and from in infection to recovery $\boldsymbol{\gamma} = \boldsymbol{\delta} = \boldsymbol{\alpha} = [1/2.5, 1/2.5, 1/2.5]$: these values are estimated from the mean serial interval ("the time from illness onset in a primary case (infector) to illness onset in a secondary case (infectee)") indicated in [Nishiura, Linton, and Akhmetzhanov 2020], at 4.0 days (confidence interval of $[3.1, 4.9]$). Knowing that the mean serial interval is bounded from above by the sum of latency and recovery period $\alpha + \gamma$ or $\delta + \gamma$, I chose arbitrarily it to be 5.0 days, split evenly between latency and recovery period. Moreover, up to my knowledge, there were not any data available at that time which discriminated between asymptomatic and symptomatic serial interval, or any age-specific ones.

- the transmissibility rate $\beta = [1/6, 1/6, 1/6]$: this value is the only one that is not taken from the literature, and is calibrated so that the initial basic reproduction number $\mathcal{R}_0(t = 0)$ (on the 13th of March 2020) is of 3. The latter comes from the estimations of $\mathcal{R}_0(t)$ obtained with an epidemiological model without age structure done by V. Calvez prior to this work.

7.2.2 Age-structured contact matrix and demographic parameters

The age-structured contact matrix coefficients were estimated from the study building contact matrices from surveys in 152 countries [Prem, Cook, and Jit 2017]. In the latter, these contact matrices are stratified by locations: home, work, school and others. Mayotte is not one of the territories whose contact matrix were estimated in [Prem, Cook, and Jit 2017], so I decided to deduce its contact matrix from the corresponding one for the island of Sao Tomé. Aside from the insularity characteristic that these two African territories share (even though Sao Tomé is located westward from the continent), this choice was motivated by the fact that they present similar age structure patterns, fecundity and total population size (UN 2019 - although their population density is different, but remains of the same order).

The age-structured contact matrix for Mayotte was rebuilt from the one from Sao Tomé using age-structured demographic data for both Mayotte and Sao Tomé originating from [UN 2019]. The contact matrix C is the sum of four contact matrices by locations: C_{home}, C_{school}, C_{work} and C_{other}, weighted by time-dependent weights w_{home}, w_{school}, w_{work} and w_{other} which model the effects of different public policies on people's behaviours (confinement, closing/opening of schools, remote working). Setting a weight to 1 means that the corresponding contacts occur as before the pandemic, and setting it to a lower value represents the reduction of corresponding contacts following public policies. In this study, I explore different types of scenarii by choosing particular temporal dynamics for these four weights.

7.3 Numerical results from modelling specific scenarii of public policies

Preliminary calibration step for the period from the 13th of March to the 18th of May: first imported cases and reduction of contact levels due to public policies. First, the discussions with the ARS (which provided us with a local assessment of the compliance to public policies) indicated us that the first known (imported) case of COVID-19 in Mayotte (at the time) dated from the 13th of March 2020. Therefore, I set initially one person from the 20-59 age class as infected at $t = 0$ (corresponding to the 13th of March 2020) and the rest of the population as susceptible. From $t = 4$ to $t = 13$, the latter corresponding to the date where Mayotte closed its access from the mainland (26th of March 2020), 1/2 an imported infected individual is added to the 20-59 age class each day, in addition to the epidemic dynamics simulated according to (7.1). This choice was intending to match the incidence data reported by the ARS of Mayotte for the period between the 13th of March 2020 to early May 2020 with outputs from the simulations of (7.1) (see Fig. 7.1). As the project was conducted over a short amount of time (a week) and due to my limited knowledge of inference, I resorted to estimate roughly the correspondence between incidence data and initial simulated incidence increase.

Moreover, to simulate (7.1), one has to specify the contact weights corresponding to the different components of the age-structured contact matrix according to the compliance of the population to public policies. The ARS of Mayotte indicated that the confinement, school closing and mandatory remote-working from mid March 2020 were well respected for around three weeks, and but that social distancing behaviours got relaxed especially among the youth from early April to early May 2020. These observations were in agreement with the estimations of the dynamics of the $\mathcal{R}_0(t)$ done by V. Calvez with an epidemiological model without any age structure and the data of incidence provided by the ARS, prior to my involvement in the project (5th of May).

Therefore, I chose to set the temporal dynamics of the four contact weights between the 13th of March 2020 ($t = 0$) and the 18th of May 2020 ($t = 66$) to match the estimations for the dynamics of $\mathcal{R}_0$ provided by V. Calvez as follows:

- $w_{home} = 1$ for $0 < t \leq 66$ (we assumed that the contacts at home occur independently of public policies).
- $w_{school} = 0$ for $0 < t \leq 66$ (schools are closed during this first perdiod).
- $w_{work} = w_{other} = c(t)$ for $0 < t \leq 66$, where $c(t)$ is chosen so that the dynamics of the $\mathcal{R}_0(t)$ matches the estimations provided by V. Calvez

$$c(t) = \begin{cases} w_0 + (w_1 - w_0)\frac{t}{24} \text{ if } t < 24 \text{ (7th of April 2020)}, \\ w_1 + (w_2 - w_1)\frac{t-24}{40-24} \text{ if } 24 \leq t < 40 \text{ (23rd of April 2020)}, \\ w_2 \text{ if } 40 \leq t < 66 \text{ (18th of May 2020)}, \end{cases}$$

  where $w_0 = 1$, $w_1 = 1/20$ and $w_2 = 1/2.2$, corresponding respectively to $\mathcal{R}_0 \approx 2$, $\mathcal{R}_0 \approx 0.85$ and $\mathcal{R}_0 \approx 1.5$.

Moreover, at $t = 0$, all the weights are set at 1 (no reduction of contacts), corresponding to $\mathcal{R}_0 \approx 3$.

Comparison of three scenarii: stable, optimistic and pessimistic At the request of the ARS, we explored three scenarii which assume that the school stay closed ($w_{school} = 0$) for the period after the 18th of May 2020:

1. stable scenario: the levels of contact w_{work} and w_{other} are kept at the same value as on the 18th of May 2020, namely at $w_2 = 1/2.2$, corresponding to $\mathcal{R}_0 \approx 1.5$.
2. optimistic scenario: the levels of contact w_{work} and w_{other} are decreased to $w_1 = 1/20$, corresponding to $\mathcal{R}_0 \approx 0.8$ (modelling the highest level of compliance to public policies observed during the period from the 18th of March to the 7th of April).
3. pessimistic scenario: the levels of contact w_{work} and w_{other} are increased to $w_0 = 1$, corresponding to $\mathcal{R}_0 \approx 2$, modelling the corresponding contacts to come back at the level prior to confinement measures (but with schools closed).

The temporal dynamics of the basic reproduction number and the daily incidence across age classes for the three scenarii are displayed in Fig. 7.2. The simulations are consistent with classical relationships between the basic reproduction number and the spreading of the epidemics.

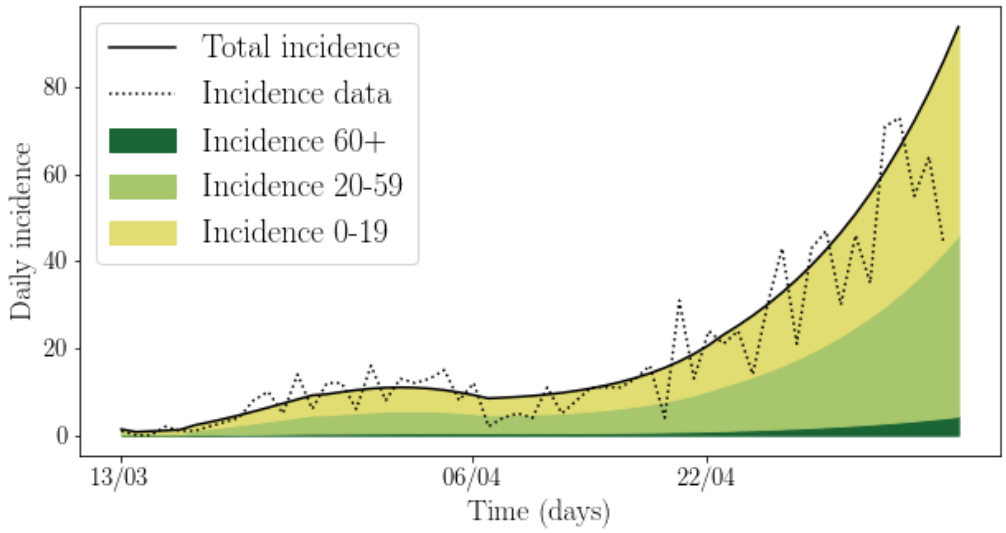

Figure 7.1: **Daily incidence obtained from numerical recursions of (7.1) for the calibration period, ranging from the date of the first known imported cases on the island (13th of March 2020) to the time of the project (5h of May 2020)**. Subsequent introduced cases before the access to the island got closed (on the 26th of March) and contact weights were chosen so that the total daily incidence obtained by simulation (full black line) matches approximately the daily incidence data provided by the ARS (dashed curve) and the estimations of the basic reproduction number done by V. Calvez from the same data.

Comparison between two scenarii of school reopening At the request of the ARS, we have simulated two scenarii of school reopening from the 18th of May ($t = 66$) onwards, as follows

1. sudden reopening: $w_{school}(t) = 1$ for $66 \leq t < 115$ (the latter corresponds to the end of the school year), and $w_{school}(t) = 0$ for $115 \leq t$.

2. progressive reopening of schools on 24 days : $w_{school}(t) = \frac{t-66}{90-66}$ pour $66 \leq t < 90$, and next $w_{school}(t) = 1$ for $90 \leq t < 115$ until the end of the school year. After the end of the school year, we set $w_{school}(t) = 0$ for $115 \leq t$.

Notice that we did not change simultaneously the weights affecting work, school and others, even though the school reopening might correlate with a decrease in remote-working. Moreover, we set the weight for school contact at 1, because the ARS informed us of structural difficulties regarding health measures, such as social distancing and hand-washing hygiene, to be implemented in schools.

The temporal dynamics of the basic reproduction number and the daily incidence under these different scenarii are displayed in Fig. 7.3 (the stable scenario is the same as defined in the previous paragraph). The simulations suggest that the impact of school reopening as modelled is likely to increase significantly the incidence rate around a narrower peak incidence, while not changing its date.

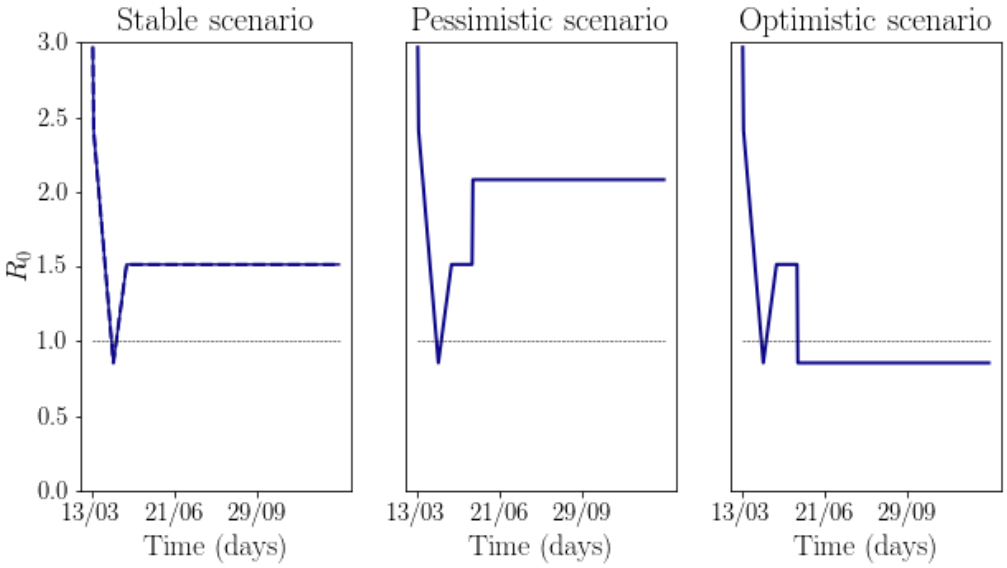

(a) Temporal dynamics of the basic reproduction number $\mathcal{R}_0(t)$.

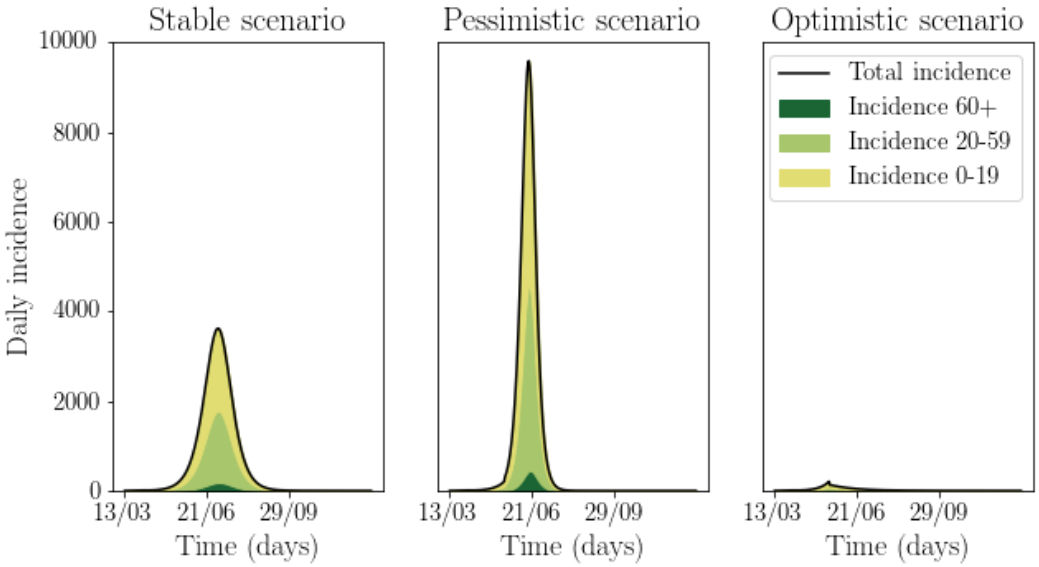

(b) Temporal dynamics of the daily incidence across age classes.

Figure 7.2: **Dynamics of the basic reproduction number (upper panel) and the daily incidence computed from numerical recursions on (7.1) (lower panel), according to three different scenarii of contact levels.**

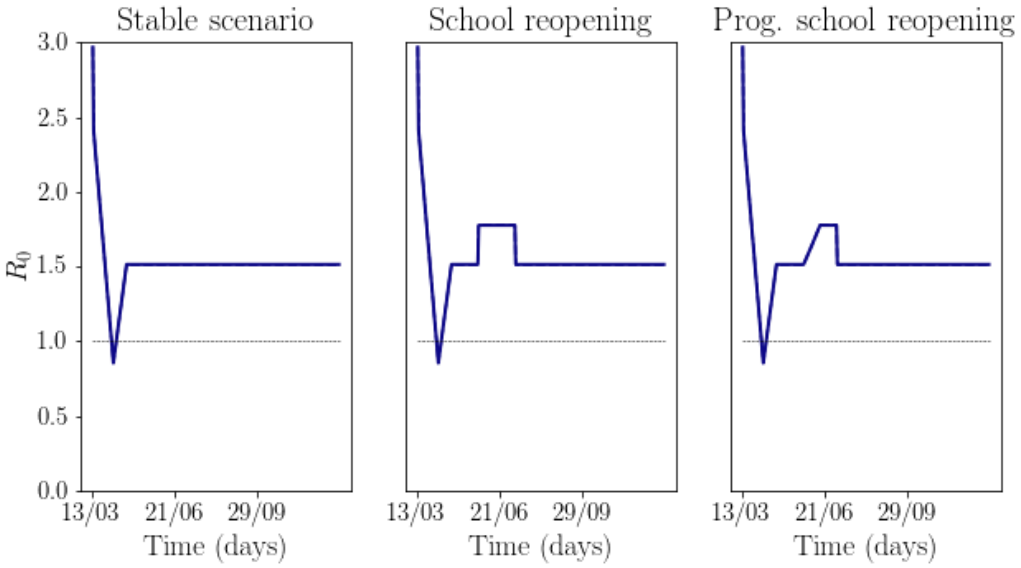

(a) Temporal dynamics of the basic reproduction number $\mathcal{R}_0(t)$.

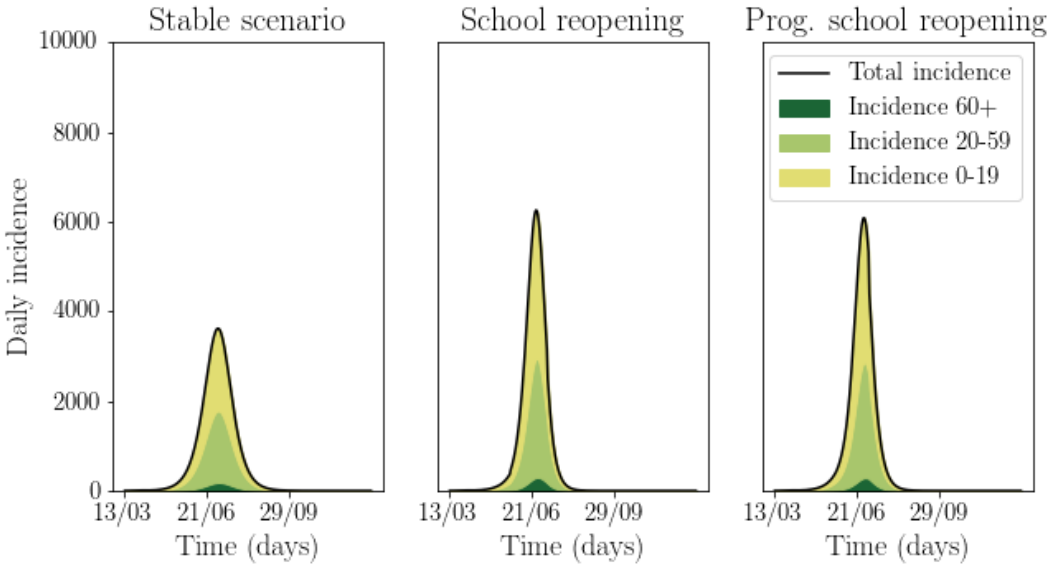

(b) Temporal dynamics of the daily incidence across age classes.

Figure 7.3: **Dynamics of the basic reproduction number (upper panel) and the daily incidence computed from numerical recursions on (7.1) (lower panel), according to three different scenarii of school reopening.**

7.4 Conclusion for my contribution - perspectives for the project

In this report, I present the numerical work that I did as part of a short modelling project simulating the effects of public policies on the first wave of the COVID-19 epidemic in Mayotte, in early May 2020, supervised by V. Calvez and in collaboration with the ARS of Mayotte. It is based on a classical age-structured epidemiological model (Diekmann, Heesterbeek, and Britton 2013) which takes into account the particular age structure of Mayotte's population (UN 2019), with age-specific epidemiological parameters taken from studies done in well-known epidemiological groups (Davies et al. 2020; Nishiura, Linton, and Akhmetzhanov 2020; Li et al. 2020) and an age-structured contact matrix specific to Mayotte inspired by [Prem, Cook, and Jit 2017], stratified into different locations (school, home, work, others) which allows to investigate the effects of different public policies (confinement, school closing/reopening, remote working). This report and the figures presented in it were provided to the ARS of Mayotte on the 11th of May 2020, as well as projections of hospitalizations and ICU cases estimated from the incidence output from the simulations described in this report. The head of the ARS of Mayotte communicated part of this report to the French Parliament and the presidential office. The school reopening in Mayotte got delayed by a week, to the 25th of May 2020.

I want to address a number of caveats surrounding this project, mainly due to the short time available (a week) to develop it from scratch to results and the relative inexperience of epidemiological models that I personally had at the start (I knew of age-structured epidemiological models without any real experience of working with them). Moreover, in May 2020, the epidemiological characteristics of the COVID-19 were not as well understood as nowadays (two years after) and were still under intense investigation, which produced a fast-growing vast literature that I had to navigate quickly, without prior knowledge of it. More in-depth sensitivity analyses and a better tuned statistical inference of some parameters w.r.t the incidence data were in particular lacking (although I investigated numerically a scenario assuming that the incidence data provided by the ARS were only reflecting a fraction of the total cases during the first month).

After this intense period in early May 2020, my involvement in the more global project decreased progressively as I focused on my main PhD projects, especially after I transferred the Python codes to Benoît Fabrèges (research engineer at the ICJ). B. Fabrèges joined the project in June 2020 and implemented a more robust statistical inference scheme of the initial parameters, in particular the date of the first imported case (the best estimation indicates that it occurred in February 2020, three weeks earlier compared to the date indicated to us by the ARS and used in this whole report). The global modelling project of the COVID-19 epidemic in Mayotte continued and was aiming at expand the model to explore among other features the effect of spatial heterogeneity, new variants and recontaminations in collaboration with the ARS of Mayotte. It motivated a serology study conducted by the ARS in Mayotte during the summer of 2021. I also punctually worked again for the global project of epidemic modelling in Mayotte in February 2021, to extend the age-structured model and the Python code to account for the variant Beta.

Bibliography

[AB14] Ada Akerman and Reinhard Bürger. "The consequences of gene flow for local adaptation and differentiation: a two-locus two-deme model". In: *Journal of Mathematical Biology* 68.5 (2014), pp. 1135–1198. ISSN: 0303-6812, 1432-1416. DOI: 10.1007/s00285-013-0660-z.

[ABR17] Matthieu Alfaro, Henri Berestycki, and Gaël Raoul. "The Effect of Climate Shift on a Species Submitted to Dispersion, Evolution, Growth, and Nonlocal Competition". In: *SIAM Journal on Mathematical Analysis* 49.1 (2017), pp. 562–596. ISSN: 0036-1410, 1095-7154. DOI: 10.1137/16M1075934.

[AC14] Matthieu Alfaro and Remi Carles. "EXPLICIT SOLUTIONS FOR REPLICATOR-MUTATOR EQUATIONS: EXTINCTION VS. ACCELERATION". In: *SIAM Journal on Applied Mathematics* 74.6 (2014), p. 15.

[ACR13] Matthieu Alfaro, Jérôme Coville, and Gaël Raoul. "Travelling Waves in a Nonlocal Reaction-Diffusion Equation as a Model for a Population Structured by a Space Variable and a Phenotypic Trait". In: *Communications in Partial Differential Equations* 38.12 (2013), pp. 2126–2154. ISSN: 0360-5302, 1532-4133. DOI: 10.1080/03605302.2013.828069.

[AD18] Matthieu Alfaro and Arnaud Ducrot. "Population invasion with bistable dynamics and adaptive evolution: The evolutionary rescue". In: *Proceedings of the American Mathematical Society* 146.11 (2018), pp. 4787–4799. ISSN: 0002-9939, 1088-6826. DOI: 10.1090/proc/14150.

[ADP12] Anton Arnold, Laurent Desvillettes, and Céline Prévost. "Existence of nontrivial steady states for populations structured with respect to space and a continuous trait". In: *Communications on Pure & Applied Analysis* 11.1 (2012), pp. 83–96. ISSN: 1553-5258. DOI: 10.3934/cpaa.2012.11.83.

[AGK21] Matthieu Alfaro, Pierre Gabriel, and Otared Kavian. "Confining integro-differential equations originating from evolutionary biology: ground states and long time dynamics". In: *arXiv:2110.07214 [math]* (2021). arXiv: 2110.07214. URL: http://arxiv.org/abs/2110.07214.

[Alf+21] Matthieu Alfaro, Léo Girardin, François Hamel, and Lionel Roques. "When the Allee threshold is an evolutionary trait: Persistence vs. extinction". In: *Journal de Mathématiques Pures et Appliquées* 155 (2021), pp. 155–191. ISSN: 00217824. DOI: 10.1016/j.matpur.2021.08.007.

[AV19] Matthieu Alfaro and Mario Veruete. “Evolutionary Branching via Replicator–Mutator Equations”. In: *Journal of Dynamics and Differential Equations* 31.4 (2019), pp. 2029–2052. ISSN: 1040-7294, 1572-9222. DOI: 10.1007/s10884-018-9692-9.

[AV20] Matthieu Alfaro and Mario Veruete. “Density dependent replicator-mutator models in directed evolution”. In: *Discrete & Continuous Dynamical Systems - B* 25.6 (2020), pp. 2203–2221. ISSN: 1553-524X. DOI: 10.3934/dcdsb.2019224.

[AVT20] Jordan A Anderson, Tauras P Vilgalys, and Jenny Tung. “Broadening primate genomics: new insights into the ecology and evolution of primate gene regulation”. In: *Current Opinion in Genetics & Development* 62 (2020), pp. 16–22. ISSN: 0959437X. DOI: 10.1016/j.gde.2020.05.009.

[AW78] D. G. Aronson and H. F. Weinberger. “Multidimensional nonlinear diffusion arising in population genetics”. In: *Advances in Mathematics* 30.1 (1978), pp. 33–76. ISSN: 0001-8708. DOI: https://doi.org/10.1016/0001-8708(78)90130-5.

[BA11] R. Bürger and A. Akerman. “The effects of linkage and gene flow on local adaptation: A two-locus continent-island model”. In: *Theor. Popul. Biol.* 80.4 (2011), pp. 272–288. ISSN: 00405809. DOI: 10.1016/j.tpb.2011.07.002.

[Bar01] Nick Barton. *Adaptation at the edge of a species’ range, In: Integrating Ecology and Evolution in a Spatial Context*. Cambridge University Press, 2001, pp. 365–392.

[Bar13] Guy Barles. “An Introduction to the Theory of Viscosity Solutions for First-Order Hamilton–Jacobi Equations and Applications”. In: Springer Berlin Heidelberg, 2013, pp. 49–109. ISBN: 978-3-642-36432-7. DOI: 10.1007/978-3-642-36433-4_2.

[BC14] Emeric Bouin and Vincent Calvez. “Travelling waves for the cane toads equation with bounded traits”. In: *Nonlinearity* 27.9 (2014), pp. 2233–2253. ISSN: 0951-7715, 1361-6544. DOI: 10.1088/0951-7715/27/9/2233.

[BE18] N.H. Barton and A.M. Etheridge. “Establishment in a new habitat by polygenic adaptation”. In: *Theoretical Population Biology* 122 (2018), pp. 110–127. ISSN: 00405809. DOI: 10.1016/j.tpb.2017.11.007.

[Ber+09] Henri Berestycki, Grégoire Nadin, Benoit Perthame, and Lenya Ryzhik. “The non-local Fisher–KPP equation: travelling waves and steady states”. In: *Nonlinearity* 22.12 (2009), pp. 2813–2844. ISSN: 0951-7715, 1361-6544. DOI: 10.1088/0951-7715/22/12/002.

[Ber+12] Cécile Berthouly-Salazar, Berndt J. van Rensburg, Johannes J. Le Roux, Bettine J. van Vuuren, and Cang Hui. “Spatial Sorting Drives Morphological Variation in the Invasive Bird, Acridotheris tristis”. In: *PLoS ONE* 7.5 (2012). Ed. by Martin Krkosek, e38145. ISSN: 1932-6203. DOI: 10.1371/journal.pone.0038145.

[Ber20] Rex Bernardo. “Reinventing quantitative genetics for plant breeding: something old, something new, something borrowed, something BLUE”. In: *Heredity* 125.6 (2020), pp. 375–385. ISSN: 0018-067X, 1365-2540. DOI: 10.1038/s41437-020-0312-1.

[BEV13] N H Barton, A M Etheridge, and A Véber. “Modelling evolution in a spatial continuum”. In: *Journal of Statistical Mechanics: Theory and Experiment* 2013.01 (2013), P01002. ISSN: 1742-5468. DOI: 10.1088/1742-5468/2013/01/P01002.

[BEV17] N.H. Barton, A.M. Etheridge, and A. Véber. "The infinitesimal model: Definition, derivation, and implications". In: *Theoretical Population Biology* 118 (2017), pp. 50–73. ISSN: 00405809. DOI: 10.1016/j.tpb.2017.06.001.

[BF73] Beverley J Balkau and Marcus W Feldman. "SELECTION FOR MIGRATION MODIFICATION". In: *Genetics* 74.1 (1973), pp. 171–174. ISSN: 1943-2631. DOI: 10.1093/genetics/74.1.171.

[BGG12] François Bolley, Ivan Gentil, and Arnaud Guillin. "Convergence to equilibrium in Wasserstein distance for Fokker–Planck equations". In: *Journal of Functional Analysis* 263.8 (2012), pp. 2430–2457. ISSN: 00221236. DOI: 10.1016/j.jfa.2012.07.007.

[BHK18] Gabriel Birzu, Oskar Hallatschek, and Kirill S. Korolev. "Neither pulled nor pushed: Genetic drift and front wandering uncover a new class of reaction-diffusion waves". In: *arXiv:1709.01601 [cond-mat, physics:physics, q-bio]* (2018). arXiv: 1709.01601. URL: http://arxiv.org/abs/1709.01601.

[BHN08] Henri Berestycki, François Hamel, and Grégoire Nadin. "Asymptotic spreading in heterogeneous diffusive excitable media". In: *Journal of Functional Analysis* 255.9 (2008), pp. 2146–2189. ISSN: 00221236. DOI: 10.1016/j.jfa.2008.06.030.

[BHR17a] Emeric Bouin, Christopher Henderson, and Lenya Ryzhik. "Super-linear spreading in local and non-local cane toads equations". In: *Journal de Mathématiques Pures et Appliquées* 108.5 (2017), pp. 724–750. ISSN: 00217824. DOI: 10.1016/j.matpur.2017.05.015.

[BHR17b] Emeric Bouin, Christopher Henderson, and Lenya Ryzhik. "The Bramson logarithmic delay in the cane toads equations". In: *Quarterly of Applied Mathematics* 75.4 (2017), pp. 599–634. ISSN: 0033-569X, 1552-4485. DOI: 10.1090/qam/1470.

[BM15] Emeric Bouin and Sepideh Mirrahimi. "A Hamilton–Jacobi approach for a model of population structured by space and trait". In: *Communications in Mathematical Sciences* 13.6 (2015), pp. 1431–1452. ISSN: 15396746, 19450796. DOI: 10.4310/CMS.2015.v13.n6.a4.

[BMP09] G. Barles, S. Mirrahimi, and B. Perthame. "Concentration in Lotka-Volterra Parabolic or Integral Equations: A General Convergence Result". In: *Methods and Applications of Analysis* 16.3 (2009), pp. 321–340. ISSN: 10732772, 19450001. DOI: 10.4310/MAA.2009.v16.n3.a4.

[BMR] N Berestycki, C Mouhot, and G Raoul. "EXISTENCE OF SELF-ACCELERATING FRONTS FOR A NON-LOCAL REACTION-DIFFUSION EQUATIONS". In: (), p. 36.

[Bod+21] Walter Bodmer, R. A. Bailey, Brian Charlesworth, Adam Eyre-Walker, Vernon Farewell, Andrew Mead, and Stephen Senn. "The outstanding scientist, R.A. Fisher: his views on eugenics and race". In: *Heredity* 126.4 (2021), pp. 565–576. ISSN: 0018-067X, 1365-2540. DOI: 10.1038/s41437-020-00394-6.

[Bou+12] Emeric Bouin, Vincent Calvez, Nicolas Meunier, Sepideh Mirrahimi, Benoît Perthame, Gaël Raoul, and Raphaël Voituriez. "Invasion fronts with variable motility: Phenotype selection, spatial sorting and wave acceleration". In: *Comptes Rendus Mathematique* 350.15–16 (2012), pp. 761–766. ISSN: 1631-073X. DOI: 10.1016/j.crma.2012.09.010.

[Bou+17] T. Bourgeron, V. Calvez, J. Garnier, and T. Lepoutre. “Existence of recombination-selection equilibria for sexual populations”. In: *arXiv:1703.09078 [math, q-bio]* (2017). arXiv: 1703.09078. URL: http://arxiv.org/abs/1703.09078.

[BPT10] Olivia J. Burton, Ben L. Phillips, and Justin M.J. Travis. “Trade-offs and the evolution of life-histories during range expansion: Evolution during range expansion”. In: *Ecology Letters* 13.10 (2010), pp. 1210–1220. ISSN: 1461023X. DOI: 10.1111/j.1461-0248.2010.01505.x.

[Bra+22] Haley Branch, Amanda Klingler, Kelsey Byers, Aaron Panofsky, and Danielle Peers. “Discussions of the “not-so-fit”: how ableism limits diverse thought and investigative potential in evolutionary biology”. In: *The American Naturalist* (2022).

[Bra78] Maury D. Bramson. “Maximal displacement of branching brownian motion”. In: *Communications on Pure and Applied Mathematics* 31.5 (1978), pp. 531–581. ISSN: 00103640, 10970312. DOI: 10.1002/cpa.3160310502.

[Bra83] Maury Bramson. “Convergence of solutions of the Kolmogorov equation to travelling waves”. In: *Mem. Amer. Math. Soc.* 44.285 (1983), pp. iv+190.

[Bul71] M. G. Bulmer. “The Effect of Selection on Genetic Variability”. In: *Am. Nat.* 105.943 (1971), pp. 201–211.

[Bul80] M. G. Bulmer. *The Mathematical Theory of Quantitative Genetics*. 1980.

[Bur00] Reinhard Burger. *The Mathematical Theory of Selection, Recombination, and Mutation*. 2000.

[Bür09a] Reinhard Bürger. “Multilocus selection in subdivided populations I. Convergence properties for weak or strong migration”. In: *Journal of Mathematical Biology* 58.6 (2009), pp. 939–978. ISSN: 0303-6812, 1432-1416. DOI: 10.1007/s00285-008-0236-5.

[Bür09b] Reinhard Bürger. “Multilocus selection in subdivided populations II. Maintenance of polymorphism under weak or strong migration”. In: *Journal of Mathematical Biology* 58.6 (2009), pp. 979–997. ISSN: 0303-6812, 1432-1416. DOI: 10.1007/s00285-008-0237-4.

[Bür20] Reinhard Bürger. “Multilocus population-genetic theory”. In: *Theoretical Population Biology* 133 (2020), pp. 40–48. ISSN: 00405809. DOI: 10.1016/j.tpb.2019.09.004.

[Cal+20] Vincent Calvez, Joachim Crevat, Léonard Dekens, Benoit Fabrèges, Frédéric Kuczma, Florian Lavigne, and Gaël Raoul. “Influence of the mode of reproduction on dispersal evolution during species invasion”. In: *ESAIM: Proceedings and Surveys* 67 (2020). Ed. by Vincent Calvez, Céline Grandmont, Eva Lochërbach, Clair Poignard, Magali Ribot, and Nicolas Vauchelet, pp. 120–134. ISSN: 2267-3059. DOI: 10.1051/proc/202067008.

[Cal+22] Vincent Calvez, Christopher Henderson, Sepideh Mirrahimi, and Olga Turanova. “NON-LOCAL COMPETITION SLOWS DOWN FRONT ACCELERATION DURING DISPERSAL EVOLUTION”. In: *Annales Henri Lebesgue* (2022).

[Can+20] Robert Stephen Cantrell, Chris Cosner, Mark A. Lewis, and Yuan Lou. “Evolution of dispersal in spatial population models with multiple timescales”. In: *Journal of Mathematical Biology* 80.1–2 (2020), pp. 3–37. ISSN: 0303-6812, 1432-1416. DOI: 10.1007/s00285-018-1302-2.

[CCL10] Robert Stephen Cantrell, Chris Cosner, and Yuan Lou. “Evolution of dispersal and the ideal free distribution”. In: *Mathematical Biosciences and Engineering* 7.1 (2010), pp. 17–36. ISSN: 1551-0018. DOI: 10.3934/mbe.2010.7.17.

[CF73] Luigi L Cavalli-Sforza and Marcus W Feldman. “Cultural versus Biological Inheritance: Phenotypic Transmission from Parents to Children (A Theory of the Effect of Parental Phenotypes on Children’s Phenotypes)”. In: *American Journal Of Human Genetics* 25.6 (1973), p. 20.

[CFB02] N. Champagnat, R Ferrière, and G. Ben Arous. “The Canonical Equation of Adaptive Dynamics: A Mathematical View”. In: *Selection* 2.1–2 (2002). Citation Key: champagnatCanonicalEquationAdaptive2002, pp. 73–83. ISSN: 1585-1931, 1588-287X. DOI: 10.1556/Select.2.2001.1-2.6.

[CFM06] Nicolas Champagnat, Régis Ferrière, and Sylvie Méléard. “Unifying evolutionary dynamics: From individual stochastic processes to macroscopic models”. In: *Theoretical Population Biology* 69.3 (2006), pp. 297–321. ISSN: 00405809. DOI: 10.1016/j.tpb.2005.10.004.

[CGP19] V. Calvez, J. Garnier, and F. Patout. “Asymptotic analysis of a quantitative genetics model with nonlinear integral operator”. In: *J. de l’École Polytechnique* 6 (2019), pp. 537–579. ISSN: 2270-518X. DOI: 10.5802/jep.100.

[CH08] Luis-Miguel Chevin and Frédéric Hospital. “Selective Sweep at a Quantitative Trait Locus in the Presence of Background Genetic Variation”. In: *Genetics* 180.3 (2008), pp. 1645–1660. ISSN: 1943-2631. DOI: 10.1534/genetics.108.093351.

[Chi99] C. Chicone. *Ordinary Differential Equations with Applications*. Springer, 1999.

[CL22] Vincent Calvez and King-Yeung Lam. “Uniqueness of the viscosity solution of a constrained Hamilton-Jacobi equation”. In: *Calculus of Variations and Partial Differential Equations* 59 (2022). arXiv: 1809.05317. URL: http://arxiv.org/abs/1809.05317.

[CLP22] Vincent Calvez, Thomas Lepoutre, and David Poyato. “ERGODICITY OF THE FISHER INFINITESIMAL MODEL WITH QUADRATIC SELECTION”. In: (2022), p. 44.

[CM07] Nicolas Champagnat and Sylvie Méléard. “Invasion and adaptive evolution for individual-based spatially structured populations”. In: *Journal of Mathematical Biology* 55.2 (2007), pp. 147–188. ISSN: 0303-6812, 1432-1416. DOI: 10.1007/s00285-007-0072-z.

[CMM13] Pierre Collet, Sylvie Méléard, and Johan A. J. Metz. “A rigorous model study of the adaptive dynamics of Mendelian diploids”. In: *Journal of Mathematical Biology* 67.3 (2013), pp. 569–607. ISSN: 0303-6812, 1432-1416. DOI: 10.1007/s00285-012-0562-5.

[CN20] Cécile Carrère and Grégoire Nadin. “Influence of mutations in phenotypically-structured populations in time periodic environment”. In: *Discrete & Continuous Dynamical Systems - B* 25.9 (2020), pp. 3609–3630. ISSN: 1553-524X. DOI: 10.3934/dcdsb.2020075.

[Cot+19] Olivier Cotto, Linnea Sandell, Luis-Miguel Chevin, and Ophélie Ronce. “Maladaptive Shifts in Life History in a Changing Environment”. In: *The American Naturalist* 194.4 (2019), pp. 558–573. ISSN: 0003-0147, 1537-5323. DOI: 10.1086/702716.

[Dav+20] Nicholas G. Davies et al. “Age-dependent effects in the transmission and control of COVID-19 epidemics”. In: *Nature Medicine* 26.8 (2020), pp. 1205–1211. ISSN: 1078-8956, 1546-170X. DOI: 10.1038/s41591-020-0962-9.

[Day00] Troy Day. “Competition and the Effect of Spatial Resource Heterogeneity on Evolutionary Diversification”. In: *The American Naturalist* 155.6 (2000), pp. 790–803. ISSN: 0003-0147, 1537-5323. DOI: 10.1086/303356.

[Déb10] Florence Débarre. “Persistance, compétition et évolution dans un environnement hétérogène”. 2010MON20067. PhD thesis. 2010. URL: http://www.theses.fr/2010MON20067/document.

[Dek22] Léonard Dekens. “Evolutionary dynamics of complex traits in sexual populations in a heterogeneous environment: how normal?” In: *Journal of Mathematical Biology* 84.3 (2022), p. 15. ISSN: 0303-6812, 1432-1416. DOI: 10.1007/s00285-021-01712-0.

[Des+08] L. Desvillettes, P. E. Jabin, S. Mischler, and G. Raoul. “On selection dynamics for continuous structured populations”. In: *Communications in Mathematical Sciences* 6.3 (2008), pp. 729–747. ISSN: 15396746, 19450796. DOI: 10.4310/CMS.2008.v6.n3.a10.

[DG10] F. Débarre and S. Gandon. “Evolution of specialization in a spatially continuous environment”. In: *Journal of Evolutionary Biology* 23.5 (2010), pp. 1090–1099. ISSN: 1010061X, 14209101. DOI: 10.1111/j.1420-9101.2010.01966.x.

[DG11] Florence Débarre and Sylvain Gandon. “Evolution in Heterogeneous Environments: Between Soft and Hard Selection”. In: *The American Naturalist* 177.3 (2011), E84–E97. ISSN: 0003-0147, 1537-5323. DOI: 10.1086/658178.

[DHB13] O. Diekmann, Hans Heesterbeek, and Tom Britton. *Mathematical tools for understanding infectious diseases dynamics*. Princeton series in theoretical and computational biology. Princeton University Press, 2013. ISBN: 978-0-691-15539-5.

[Die+05] O. Diekmann, P. E. Jabin, S. Mischler, and B. Perthame. “The dynamics of adaptation: An illuminating example and a Hamilton-Jacobi approach”. In: *Theor. Popul. Biol.* 67.4 (2005), pp. 257–271. ISSN: 0040-5809. DOI: 10.1016/j.tpb.2004.12.003.

[DL21] L. Dekens and F. Lavigne. “Front Propagation of a Sexual Population with Evolution of Dispersion: A Formal Analysis”. In: *SIAM Journal on Applied Mathematics* (2021).

[DL96] U. Dieckmann and R. Law. “The dynamical theory of coevolution: a derivation from stochastic ecological processes”. In: *J. Math. Biol.* 34 (1996), pp. 579–612.

[DM21] Dekens and Mirrahimi. “Dynamics of dirac concentrations in the evolution of quantitative alleles with sexual reproduction”. In: (2021). (submitted). arXiv: 2111.14814 [math.AP].

[DO16] Florence Débarre and Sarah P. Otto. “Evolutionary dynamics of a quantitative trait in a finite asexual population”. In: *Theoretical Population Biology* 108 (2016), pp. 75–88. ISSN: 00405809. DOI: 10.1016/j.tpb.2015.12.002.

[Doc+98] Jack Dockery, Vivian Hutson, Konstantin Mischaikow, and Mark Pernarowski. “The evolution of slow dispersal rates: a reaction diffusion model”. In: *Journal of Mathematical Biology* 37.1 (1998), pp. 61–83. ISSN: 0303-6812, 1432-1416. DOI: 10.1007/s002850050120.

[DOC21] Léonard Dekens, Sarah P. Otto, and Vincent Calvez. *The best of both worlds: combining population genetic and quantitative genetic models*. 2021. arXiv: 2111.11142 [q-bio.PE].

[Don+14] Michael J. Donoghue, Simon A. Levin, Trudy F. C. Mackay, Loren Rieseberg, Joseph Travis, and Gregory A. Wray. *The Princeton Guide to Evolution*. Princeton University Press, 2014. ISBN: 978-0-691-14977-6. URL: http://www.jstor.org/stable/j.ctt4cgc5m.

[DRG13] F. Débarre, O. Ronce, and S. Gandon. "Quantifying the effects of migration and mutation on adaptation and demography in spatially heterogeneous environments". In: *J. Evol. Biol.* 26.6 (2013), pp. 1185–1202. ISSN: 1010061X. DOI: 10.1111/jeb.12132.

[Dud+07] J. W. Dudley, Darryl Clark, Torbert R. Rocheford, and John R. LeDeaux. "Genetic Analysis of Corn Kernel Chemical Composition in the Random Mated 7 Generation of the Cross of Generations 70 of IHP × ILP". In: *Crop Science* 47.1 (2007), pp. 45–57. DOI: https://doi.org/10.2135/cropsci2006.03.0207. eprint: https://acsess.onlinelibrary.wiley.com/doi/pdf/10.2135/cropsci2006.03.0207. URL: https://acsess.onlinelibrary.wiley.com/doi/abs/10.2135/cropsci2006.03.0207.

[DW58] Charles Darwin and Alfred Wallace. "On the Tendency of Species to form Varieties; and on the Perpetuation of Varieties and Species by Natural Means of Selection." In: *Journal of the Proceedings of the Linnean Society of London. Zoology* 3.9 (1858), pp. 45–62. DOI: https://doi.org/10.1111/j.1096-3642.1858.tb02500.x. URL: https://onlinelibrary.wiley.com/doi/abs/10.1111/j.1096-3642.1858.tb02500.x.

[DYG15] F. Débarre, S. Yeaman, and F. Guillaume. "Evolution of Quantitative Traits under a Migration-Selection Balance: When Does Skew Matter?" In: *Am. Nat.* 186.S1 (2015), S37–S47. ISSN: 0003-0147, 1537-5323. DOI: 10.1086/681717.

[El +21] Athimed El Taher, Astrid Böhne, Nicolas Boileau, Fabrizia Ronco, Adrian Indermaur, Lukas Widmer, and Walter Salzburger. "Gene expression dynamics during rapid organismal diversification in African cichlid fishes". In: *Nature Ecology & Evolution* 5.2 (2021), pp. 243–250. ISSN: 2397-334X. DOI: 10.1038/s41559-020-01354-3.

[ES89] L C Evans and P E Souganidis. "A PDE Approach to Geometric Optics to Certain Semilinear Parabolic Equations". In: *Indiana University Mathematics Journal* 38 (1989).

[FE20] Félix Foutel-Rodier and Alison M. Etheridge. "The spatial Muller's ratchet: Surfing of deleterious mutations during range expansion". In: *Theoretical Population Biology* 135 (2020), pp. 19–31. ISSN: 00405809. DOI: 10.1016/j.tpb.2020.07.002.

[Fel72] Marcus W. Feldman. "Selection for linkage modification: I. Random mating populations". In: *Theoretical Population Biology* 3.3 (1972), pp. 324–346. ISSN: 00405809. DOI: 10.1016/0040-5809(72)90007-X.

[Fel74] Joseph Felsenstein. "THE EVOLUTIONARY ADVANTAGE OF RECOMBINATION". In: *Genetics* 78.2 (1974), pp. 737–756. ISSN: 1943-2631. DOI: 10.1093/genetics/78.2.737.

[Fel76] Joseph Felsenstein. “THE THEORETICAL POPULATION GENETICS OF VARIABLE SELECTION AND MIGRATION”. In: *Annual Review of Genetics* 10.1 (1976), pp. 253–280. ISSN: 0066-4197, 1545-2948. DOI: 10.1146/annurev.ge.10.120176.001345.

[Fis19] R. A. Fisher. “The Correlation between Relatives on the Supposition of Mendelian Inheritance.” In: *Transactions of the Royal Society of Edinburgh* 52.2 (1919), pp. 399–433. DOI: 10.1017/S0080456800012163.

[Fis37] R. A. Fisher. “The Wave of Advance of Advantageous Genes”. In: *Annals of Eugenics* 7.4 (1937), pp. 355–369. ISSN: 2050-1439. DOI: 10.1111/j.1469-1809.1937.tb02153.x.

[Fis50] R. A. Fisher. “Gene Frequencies in a Cline Determined by Selection and Diffusion”. In: *Biometrics* 6.4 (1950), p. 353. ISSN: 0006341X. DOI: 10.2307/3001780.

[FM18] Susely Figueroa Iglesias and Sepideh Mirrahimi. “Long Time Evolutionary Dynamics of Phenotypically Structured Populations in Time-Periodic Environments”. In: *SIAM Journal on Mathematical Analysis* 50.5 (2018), pp. 5537–5568. DOI: 10.1137/18M1175185. eprint: https://doi.org/10.1137/18M1175185. URL: https://doi.org/10.1137/18M1175185.

[Fre86] M. I. Freidlin. “Geometric Optics Approach to Reaction-Diffusion Equations”. In: *SIAM Journal on Applied Mathematics* 46.2 (1986), pp. 222–232. ISSN: 0036-1399, 1095-712X. DOI: 10.1137/0146016.

[FZ11] Jian Fang and Xiao-Qiang Zhao. “Monotone wavefronts of the nonlocal Fisher–KPP equation”. In: *Nonlinearity* 24.11 (2011), pp. 3043–3054. ISSN: 0951-7715, 1361-6544. DOI: 10.1088/0951-7715/24/11/002.

[Gal77] F. Galton. “Typical Laws of Heredity 1”. In: *Nature* 15 (1877), pp. 492–495.

[Gal83] Francis Galton. *Inquiries Into Human Faculty and Its Development*. Macmillan, 1883.

[Gar+22] J. Garnier, O. Cotto, T. Bourgeron, E. Bouin, T. Lepoutre, O. Ronce, and V. Calvez. “Adaptation to a changing environment: what me Normal?” In: *bioRxiv* (2022). DOI: 10.1101/2022.06.22.497192. eprint: https://www.biorxiv.org/content/early/2022/06/26/2022.06.22.497192.full.pdf. URL: https://www.biorxiv.org/content/early/2022/06/26/2022.06.22.497192.

[GB14] Ludwig Geroldinger and Reinhard Bürger. “A two-locus model of spatially varying stabilizing or directional selection on a quantitative trait”. In: *Theoretical Population Biology* 94 (2014), pp. 10–41. ISSN: 00405809. DOI: 10.1016/j.tpb.2014.03.002.

[GCD19] Léo Girardin, Vincent Calvez, and Florence Débarre. “Catch Me If You Can: A Spatial Model for a Brake-Driven Gene Drive Reversal”. In: *Bulletin of Mathematical Biology* 81.12 (2019), pp. 5054–5088. ISSN: 0092-8240, 1522-9602. DOI: 10.1007/s11538-019-00668-z.

[GD21] Léo Girardin and Florence Débarre. “Demographic feedbacks can hamper the spatial spread of a gene drive”. In: *Journal of Mathematical Biology* (2021), p. 31.

[Ger+97] Stefan A. H. Geritz, J. A. J. Metz, Éva Kisdi, and Géza Meszéna. “Dynamics of Adaptation and Evolutionary Branching”. In: *Physical Review Letters* 78.10 (1997), pp. 2024–2027. ISSN: 0031-9007, 1079-7114. DOI: 10.1103/PhysRevLett.78.2024.

[Gil+17] Marie-Eve Gil, Francois Hamel, Guillaume Martin, and Lionel Roques. “Mathematical Properties of a Class of Integro-differential Models from Population Genetics”. In: *SIAM Journal on Applied Mathematics* 77.4 (2017), pp. 1536–1561. ISSN: 0036-1399, 1095-712X. DOI: 10.1137/16M1108224.

[Gil+19] M-E Gil, F Hamel, G Martin, and L Roques. “Dynamics of fitness distributions in the presence of a phenotypic optimum: an integro-differential approach”. In: *Nonlinearity* 32.10 (2019), pp. 3485–3522. ISSN: 0951-7715, 1361-6544. DOI: 10.1088/1361-6544/ab1bbe.

[Gou00] S.A. Gourley. “Travelling front solutions of a nonlocal Fisher equation”. In: *Journal of Mathematical Biology* 41.3 (2000), pp. 272–284. ISSN: 0303-6812, 1432-1416. DOI: 10.1007/s002850000047.

[GRD21] Claire Godineau, Ophélie Ronce, and Céline Devaux. “Assortative mating can help adaptation of flowering time to a changing climate: Insights from a polygenic model”. In: *Journal of Evolutionary Biology* (2021), jeb.13786. ISSN: 1010-061X, 1420-9101. DOI: 10.1111/jeb.13786.

[GT00] Francis R. Groeters and Bruce E. Tabashnik. “Roles of Selection Intensity, Major Genes, and Minor Genes in Evolution of Insecticide Resistance”. In: *Journal of Economic Entomology* 93.6 (2000), pp. 1580–1587. ISSN: 00220493, 00220493. DOI: 10.1603/0022-0493-93.6.1580.

[GVA06] S. Genieys, V. Volpert, and P. Auger. “Pattern and Waves for a Model in Population Dynamics with Nonlocal Consumption of Resources”. In: *Mathematical Modelling of Natural Phenomena* 1.1 (2006), pp. 63–80. ISSN: 0973-5348. DOI: 10.1051/mmnp:2006004.

[Hal32] J. B. S. Haldane. “A mathematical theory of natural and artificial selection. Part IX. Rapid selection”. In: *Mathematical Proceedings of the Cambridge Philosophical Society* 28.2 (1932), pp. 244–248. ISSN: 0305-0041, 1469-8064. DOI: 10.1017/S0305004100010914.

[Hal48] J. B. S. Haldane. “The theory of a cline”. In: *Journal of Genetics* 48.3 (1948), pp. 277–284. ISSN: 0022-1333, 0973-7731. DOI: 10.1007/BF02986626.

[Ham+20] F. Hamel, F. Lavigne, G. Martin, and L. Roques. “Dynamics of adaptation in an anisotropic phenotype-fitness landscape”. In: *Nonlinear Analysis: Real World Applications* 54 (2020), p. 103107. ISSN: 14681218. DOI: 10.1016/j.nonrwa.2020.103107.

[Has83] Alan Hastings. “Can spatial variation alone lead to selection for dispersal?” In: *Theoretical Population Biology* 24.3 (1983), pp. 244–251. ISSN: 00405809. DOI: 10.1016/0040-5809(83)90027-8.

[HDT01] A. P. Hendry, T. Day, and E. B. Taylor. “POPULATION MIXING AND THE ADAPTIVE DIVERGENCE OF QUANTITATIVE TRAITS IN DISCRETE POPULATIONS: A THEORETICAL FRAMEWORK FOR EMPIRICAL TESTS”. In: *Evolution* 55.3 (2001), pp. 459–466. ISSN: 00143820. DOI: 10.1111/j.0014-3820.2001.tb00780.x.

[Her20] Evan Whitney Hersh. “A clone together: exploring the causes and consequences of range divergence between sexual and asexual Easter daisies”. PhD thesis. University of British Columbia, 2020. DOI: http://dx.doi.org/10.14288/1.0392003. URL: https://open.library.ubc.ca/collections/ubctheses/24/items/1.0392003.

[Hil14] William G Hill. “Applications of Population Genetics to Animal Breeding, from Wright, Fisher and Lush to Genomic Prediction”. In: *Genetics* 196.1 (2014), pp. 1–16. ISSN: 1943-2631. DOI: 10.1534/genetics.112.147850.

[HLL19] Wenrui Hao, King-Yeung Lam, and Yuan Lou. “Concentration phenomena in an integro-PDE model for evolution of conditional dispersal”. In: *Indiana University Mathematics Journal* 68.3 (2019), pp. 881–923. ISSN: 0022-2518. DOI: 10.1512/iumj.2019.68.7625.

[HLL21] Wenrui Hao, King-Yeung Lam, and Yuan Lou. “Ecological and evolutionary dynamics in advective environments: Critical domain size and boundary conditions”. In: *Discrete & Continuous Dynamical Systems - B* 26.1 (2021), pp. 367–400. ISSN: 1553-524X. DOI: 10.3934/dcdsb.2020283.

[HLR21] F. Hamel, F. Lavigne, and L. Roques. “Adaptation in a heterogeneous environment I: persistence versus extinction.” In: *Journal of Mathematical Biology* (2021). DOI: 10.1007/s00285-021-01637-8.

[HM19] Benjamin C Haller and Philipp W Messer. “SLiM 3: Forward Genetic Simulations Beyond the Wright–Fisher Model”. In: *Molecular Biology and Evolution* 36.3 (2019), pp. 632–637. ISSN: 0737-4038. DOI: 10.1093/molbev/msy228. eprint: https://academic.oup.com/mbe/article-pdf/36/3/632/27980602/msy228.pdf. URL: https://doi.org/10.1093/molbev/msy228.

[HM77] W. D. Hamilton and Robert M. May. “Dispersal in stable habitats”. In: *Nature* 269.5629 (1977), pp. 578–581. ISSN: 0028-0836, 1476-4687. DOI: 10.1038/269578a0.

[HPH19] Ilse Höllinger, Pleuni S. Pennings, and Joachim Hermisson. “Polygenic adaptation: From sweeps to subtle frequency shifts”. In: *PLOS Genetics* 15.3 (2019). Ed. by Justin C. Fay, e1008035. ISSN: 1553-7404. DOI: 10.1371/journal.pgen.1008035.

[HR14] F Hamel and L Ryzhik. “On the nonlocal Fisher–KPP equation: steady states, spreading speed and global bounds”. In: *Nonlinearity* 27.11 (2014), p. 2735.

[HR66] W. G. Hill and Alan Robertson. “The effect of linkage on limits to artificial selection”. In: *Genetical Research* 8.3 (1966), pp. 269–294. ISSN: 0016-6723, 1469-5073. DOI: 10.1017/S0016672300010156.

[HT12] Jisca Huisman and Jarle Tufto. “Comparison of Non-Gaussian Quantitative Genetic Models for Migration and Stabilizing Selection”. In: *Evolution* 66.11 (2012), pp. 3444–3461. ISSN: 1558-5646. DOI: 10.1111/j.1558-5646.2012.01707.x.

[JBK13] Yuexin Jiang, Daniel I. Bolnick, and Mark Kirkpatrick. “Assortative Mating in Animals”. In: *The American Naturalist* 181.6 (2013), E125–E138. ISSN: 0003-0147, 1537-5323. DOI: 10.1086/670160.

[JR11] Pierre-Emmanuel Jabin and Gaël Raoul. “On selection dynamics for competitive interactions”. In: *Journal of Mathematical Biology* 63.3 (2011), pp. 493–517. ISSN: 0303-6812, 1432-1416. DOI: 10.1007/s00285-010-0370-8.

[JS17] Kavita Jain and Wolfgang Stephan. “Rapid Adaptation of a Polygenic Trait After a Sudden Environmental Shift”. In: *Genetics* 206.1 (2017), pp. 389–406. ISSN: 1943-2631. DOI: 10.1534/genetics.116.196972.

[KB97] M. Kirkpatrick and N. H. Barton. “Evolution of a Species’ Range”. In: *Am. Nat.* 150.1 (1997). PMID: 18811273, pp. 1–23. DOI: 10.1086/286054. eprint: https://doi.org/10.1086/286054. URL: https://doi.org/10.1086/286054.

[Kim65] M. Kimura. “A stochastic model concerning the maintenance of genetic variability in quantitative characters”. In: *Proceedings of the National Academy of Sciences* 54.3 (1965), pp. 731–736. ISSN: 0027-8424. DOI: 10.1073/pnas.54.3.731. eprint: https://www.pnas.org/content/54/3/731.full.pdf. URL: https://www.pnas.org/content/54/3/731.

[KM72] Samuel Karlin and James McGregor. “Application of method of small parameters to multi-niche population genetic models”. In: *Theoretical Population Biology* 3.2 (1972), pp. 186–209. ISSN: 00405809. DOI: 10.1016/0040-5809(72)90026-3.

[KPP37] A.N. Kolmogorov, I.G. Petrovsky, and N.S. Piskunov. “Étude de l’équation de la diffusion avec croissance de la quantité de matière et son application à un problème biologique”. In: *Bulletin Université d’Etat à Moscou* (1937).

[Kru04] Loeske E. B. Kruuk. “Estimating genetic parameters in natural populations using the ‘animal model’”. In: *Philosophical Transactions of the Royal Society of London. Series B: Biological Sciences* 359.1446 (2004), pp. 873–890. ISSN: 0962-8436, 1471-2970. DOI: 10.1098/rstb.2003.1437.

[Lal+14] Kevin Laland, Tobias Uller, et al. “Does evolutionary theory need a rethink?” In: *Nature* 514.7521 (2014), pp. 161–164. ISSN: 0028-0836, 1476-4687. DOI: 10.1038/514161a.

[Lam19] King-Yeung Lam. “Dirac-concentrations in an integro-pde model from evolutionary game theory”. In: *Discrete & Continuous Dynamical Systems - B* 24.2 (2019), pp. 737–754. ISSN: 1553-524X. DOI: 10.3934/dcdsb.2018205.

[Lan75] Russell Lande. “The maintenance of genetic variability by mutation in a polygenic character with linked loci”. In: *Genetical Research* 26.3 (1975), pp. 221–235. ISSN: 0016-6723, 1469-5073. DOI: 10.1017/S0016672300016037.

[Lan78] K. Lange. “Central limit theorems of pedigrees”. In: *J. Math. Biol.* 6.1 (1978), pp. 59–66. ISSN: 0303-6812, 1432-1416. DOI: 10.1007/BF02478517.

[Lan83] Russell Lande. “The response to selection on major and minor mutations affecting a metrical trait”. In: *Heredity* 50.1 (1983), pp. 47–65. ISSN: 0018-067X, 1365-2540. DOI: 10.1038/hdy.1983.6.

[Lat72] B. Latter. “Selection in Finite Populations with Multiple Alleles. III. Genetic Divergence with Centripetal Selection and Mutation”. In: *Genetics* 70.3 (1972), pp. 475–490.

[Lau+04] Cathy C Laurie et al. “The Genetic Architecture of Response to Long-Term Artificial Selection for Oil Concentration in the Maize Kernel”. In: *Genetics* 168.4 (2004), pp. 2141–2155. ISSN: 1943-2631. DOI: 10.1534/genetics.104.029686.

[Lav+20] F. Lavigne, G. Martin, Y. Anciaux, J. Papaïx, and L. Roques. “When sinks become sources: Adaptive colonization in asexuals*”. In: *Evolution* 74.1 (2020), pp. 29–42. ISSN: 1558-5646. DOI: 10.1111/evo.13848.

[Len+20] Thomas Lenormand, Frederic Fyon, Eric Sun, and Denis Roze. “Sex Chromosome Degeneration by Regulatory Evolution”. In: *Current Biology* (2020).

[Li+20] Ruiyun Li, Sen Pei, Bin Chen, Yimeng Song, Tao Zhang, Wan Yang, and Jeffrey Shaman. “Substantial undocumented infection facilitates the rapid dissemination of novel coronavirus (SARS-CoV-2)”. In: *Science* 368.6490 (2020), pp. 489–493. ISSN: 0036-8075, 1095-9203. DOI: 10.1126/science.abb3221.

[Liu+20] Xuan Liu, Tim M. Blackburn, Tianjian Song, Xuyu Wang, Cong Huang, and Yiming Li. "Animal invaders threaten protected areas worldwide". In: *Nature Communications* 11.1 (2020), p. 2892. ISSN: 2041-1723. DOI: 10.1038/s41467-020-16719-2.

[LL14a] King-Yeung Lam and Yuan Lou. "Evolution of conditional dispersal: evolutionarily stable strategies in spatial models". In: *Journal of Mathematical Biology* 68.4 (2014), pp. 851–877. ISSN: 0303-6812, 1432-1416. DOI: 10.1007/s00285-013-0650-1.

[LL14b] King-Yeung Lam and Yuan Lou. "Evolutionarily Stable and Convergent Stable Strategies in Reaction–Diffusion Models for Conditional Dispersal". In: *Bulletin of Mathematical Biology* 76.2 (2014), pp. 261–291. ISSN: 0092-8240, 1522-9602. DOI: 10.1007/s11538-013-9901-y.

[LL14c] Yuan Lou and Frithjof Lutscher. "Evolution of dispersal in open advective environments". In: *Journal of Mathematical Biology* 69.6–7 (2014), pp. 1319–1342. ISSN: 0303-6812, 1432-1416. DOI: 10.1007/s00285-013-0730-2.

[LL17] King-Yeung Lam and Yuan Lou. "An integro-PDE model for evolution of random dispersal". In: *Journal of Functional Analysis* 272.5 (2017), pp. 1755–1790. ISSN: 00221236. DOI: 10.1016/j.jfa.2016.11.017.

[LL54] J. J. Levin and N. Levinson. "Singular Perturbations of Non-linear Systems of Differential Equations and an Associated Boundary Layer Equation". In: *J. of Rational Mechanics and Analysis* 3 (1954), pp. 247–270. ISSN: 19435282, 19435290. URL: http://www.jstor.org/stable/24900288.

[LLL15] King-Yeung Lam, Yuan Lou, and Frithjof Lutscher. "Evolution of dispersal in closed advective environments". In: *Journal of Biological Dynamics* 9.sup1 (2015), pp. 188–212. ISSN: 1751-3758, 1751-3766. DOI: 10.1080/17513758.2014.969336.

[LMP11] Alexander Lorz, Sepideh Mirrahimi, and Benoît Perthame. "Dirac Mass Dynamics in Multidimensional Nonlocal Parabolic Equations". In: *Communications in Partial Differential Equations* 36.6 (2011), pp. 1071–1098. ISSN: 0360-5302, 1532-4133. DOI: 10.1080/03605302.2010.538784.

[LO00] Thomas Lenormand and Sarah P Otto. "The Evolution of Recombination in a Heterogeneous Environment". In: *Genetics* 156.1 (2000), pp. 423–438. ISSN: 1943-2631. DOI: 10.1093/genetics/156.1.423.

[LOF03] Kevin Laland, John Odling-Smee, and Marc Feldman. *Niche Construction: The Neglected Process in Evolution*. Princeton University Press, 2003. ISBN: 9780691044378.

[Lyt97] Katrina A. Lythgoe. "Consequences of gene flow in spatially structured populations". In: *Genetical Research* 69.1 (1997), pp. 49–60. ISSN: 00166723. DOI: 10.1017/S0016672397002644.

[MB94] John A. McKenzie and Philip Batterham. "The genetic, molecular and phenotypic consequences of selection for insecticide resistance". In: *Trends in Ecology & Evolution* 9.5 (1994), pp. 166–169. ISSN: 0169-5347. DOI: https://doi.org/10.1016/0169-5347(94)90079-5. URL: https://www.sciencedirect.com/science/article/pii/0169534794900795.

[MCG97] G. Meszéna, I. Czibula, and S. Geritz. “Adaptive Dynamics in a 2−Patch Environment: A Toy Model for Allopatric and Parapatric Speciation”. In: *J. Biol. Syst.* 05.02 (1997), pp. 265–284. DOI: 10.1142/S0218339097000175.

[Met+96] J A J Metz, S A H Geritz, G Meszena, F J A Jacobs, and J S van Heerwaarden. “Adaptive Dynamics: A Geometrical Study of the Consequences of Nearly Faithful Reproduction”. In: *Stochastic and Spatial Structures of Dynamical Systems*. North-Holland, 1996, pp. 183–231.

[MG20] S. Mirrahimi and S. Gandon. “Evolution of Specialization in Heterogeneous Environments: Equilibrium Between Selection, Mutation and Migration”. In: *Genetics* 214.2 (2020), pp. 479–491. ISSN: 0016-6731. DOI: 10.1534/genetics.119.302868.

[Mir17] S. Mirrahimi. “A Hamilton-Jacobi approach to characterize the evolutionary equilibria in heterogeneous environments”. In: *Math. Models Methods Appl. Sci.* 27.13 (2017), pp. 2425–2460. ISSN: 0218-2025. DOI: 10.1142/s0218202517500488.

[MM10] Arnaud Monty and Grégory Mahy. “Evolution of dispersal traits along an invasion route in the wind-dispersed Senecio inaequidens (Asteraceae)”. In: *Oikos* 119.10 (2010), pp. 1563–1570. ISSN: 00301299. DOI: 10.1111/j.1600-0706.2010.17769.x.

[MOL06] Guillaume Martin, Sarah P Otto, and Thomas Lenormand. “Selection for Recombination in Structured Populations”. In: *Genetics* 172.1 (2006), pp. 593–609. ISSN: 1943-2631. DOI: 10.1534/genetics.104.039982.

[MPS15] Sepideh Mirrahimi, Benoît Perthame, and Panagiotis E. Souganidis. “Time fluctuations in a population model of adaptive dynamics”. In: *Annales de l’Institut Henri Poincaré C, Analyse non linéaire* 32.1 (2015), pp. 41–58. ISSN: 0294-1449, 1873-1430. DOI: 10.1016/j.anihpc.2013.10.001.

[MR13] Sepideh Mirrahimi and Gaël Raoul. “Dynamics of sexual populations structured by a space variable and a phenotypical trait”. In: *Theoretical Population Biology* 84 (2013), pp. 87–103. ISSN: 00405809. DOI: 10.1016/j.tpb.2012.12.003.

[MR15] Sepideh Mirrahimi and Jean-Michel Roquejoffre. “Uniqueness in a class of Hamilton–Jacobi equations with constraints”. In: *Comptes Rendus Mathematique* 353.6 (2015), pp. 489–494. ISSN: 1631073X. DOI: 10.1016/j.crma.2015.03.005.

[MR16a] Guillaume Martin and Lionel Roques. “The non-stationary dynamics of fitness distributions: asexual model with epistasis and standing variation”. In: *Genetics* 204 (2016), p. 85.

[MR16b] Sepideh Mirrahimi and Jean-Michel Roquejoffre. “A class of Hamilton–Jacobi equations with constraint: Uniqueness and constructive approach”. In: *Journal of Differential Equations* 260.5 (2016), pp. 4717–4738. ISSN: 00220396. DOI: 10.1016/j.jde.2015.11.027.

[MZ14] Judith R. Miller and Huihui Zeng. “Range limits in spatially explicit models of quantitative traits”. In: *Journal of Mathematical Biology* 68.1–2 (2014), pp. 207–234. ISSN: 0303-6812, 1432-1416. DOI: 10.1007/s00285-012-0628-4.

[Nag75] Thomas Nagylaki. “CONDITIONS FOR THE EXISTENCE OF CLINES”. In: *Genetics* 80.3 (1975), pp. 595–615. ISSN: 1943-2631. DOI: 10.1093/genetics/80.3.595.

[Nag78] Thomas Nagylaki. “CLINES WITH ASYMMETRIC MIGRATION”. In: *Genetics* 88.4 (1978), pp. 813–827. ISSN: 1943-2631. DOI: 10.1093/genetics/88.4.813.

[NL01] Thomas Nagylaki and Yuan Lou. “Patterns of Multiallelic Polymorphism Maintained by Migration and Selection”. In: *Theoretical Population Biology* 59.4 (2001), pp. 297–313. ISSN: 00405809. DOI: 10.1006/tpbi.2001.1526.

[NL07] Thomas Nagylaki and Yuan Lou. “Evolution under multiallelic migration–selection models”. In: *Theoretical Population Biology* 72.1 (2007), pp. 21–40. ISSN: 00405809. DOI: 10.1016/j.tpb.2007.02.005.

[NLA20] Hiroshi Nishiura, Natalie M. Linton, and Andrei R. Akhmetzhanov. “Serial interval of novel coronavirus (COVID-19) infections”. In: *International Journal of Infectious Diseases* 93 (2020), pp. 284–286. ISSN: 12019712. DOI: 10.1016/j.ijid.2020.02.060.

[OB01] Sarah P Otto and Nick H Barton. “SELECTION FOR RECOMBINATION IN SMALL POPULATIONS”. In: *Evolution* (2001), p. 11.

[OB97] Sarah Perin Otto and Nick H Barton. “The Evolution of Recombination: Removing the Limits to Natural Selection”. In: *Genetics* 147.2 (1997), pp. 879–906. ISSN: 1943-2631. DOI: 10.1093/genetics/147.2.879.

[OK17] Matthew M. Osmond and Christopher A. Klausmeier. “An evolutionary tipping point in a changing environment”. In: *Evolution* 71.12 (2017), pp. 2930–2941. ISSN: 1558-5646. DOI: 10.1111/evo.13374.

[OL02] S. P. Otto and T. Lenormand. “Resolving the paradox of sex and recombination”. In: *Nature Reviews Genetics* 3.4 (2002), pp. 252–261. ISSN: 1471-0056, 1471-0064. DOI: 10.1038/nrg761.

[OM17] Brad M. Ochocki and Tom E. X. Miller. “Rapid evolution of dispersal ability makes biological invasions faster and more variable”. In: *Nature Communications* 8.1 (2017), p. 14315. ISSN: 2041-1723. DOI: 10.1038/ncomms14315.

[Orr01] Allen Orr. “The genetics of species differences”. In: *Trends in Ecology & Evolution* 16.7 (2001), pp. 343–350. ISSN: 01695347. DOI: 10.1016/S0169-5347(01)02167-X.

[Ott09] Sarah P. Otto. “The Evolutionary Enigma of Sex”. In: *The American Naturalist* 174.S1 (2009), S1–S14. ISSN: 0003-0147, 1537-5323. DOI: 10.1086/599084.

[Pat20] Florian Patout. “The Cauchy problem for the infinitesimal model in the regime of small variance”. In: *arXiv:2001.04682 [math]* (2020). arXiv: 2001.04682. URL: http://arxiv.org/abs/2001.04682.

[PB08] Benoit Perthame and Guy Barles. “Dirac concentrations in Lotka-Volterra parabolic PDEs”. In: *Indiana University Mathematics Journal* 57.7 (2008), pp. 3275–3302. ISSN: 0022-2518. DOI: 10.1512/iumj.2008.57.3398.

[PBM09] Jitka Polechová, Nick Barton, and Glenn Marion. “Species’ Range: Adaptation in Space and Time”. In: *The American Naturalist* 174.5 (2009), E186–E204. ISSN: 0003-0147, 1537-5323. DOI: 10.1086/605958.

[PBS10] Benjamin L. Phillips, Gregory P. Brown, and Richard Shine. “Life-history evolution in range-shifting populations”. In: *Ecology* 91.6 (2010), pp. 1617–1627. ISSN: 0012-9658. DOI: 10.1890/09-0910.1.

[PCJ17] Kiesha Prem, Alex R. Cook, and Mark Jit. “Projecting social contact matrices in 152 countries using contact surveys and demographic data”. In: *PLOS Computational Biology* 13.9 (2017). Ed. by Betz Halloran, e1005697. ISSN: 1553-7358. DOI: 10.1371/journal.pcbi.1005697.

[Pei+13] S. Peischl, I. Dupanloup, M. Kirkpatrick, and L. Excoffier. “On the accumulation of deleterious mutations during range expansions”. In: *Molecular Ecology* 22.24 (2013), pp. 5972–5982. ISSN: 09621083. DOI: 10.1111/mec.12524.

[PG18] Stephan Peischl and Kimberly J. Gilbert. *Evolution of dispersal can rescue populations from expansion load*. 2018. DOI: 10.1101/483883. URL: http://biorxiv.org/lookup/doi/10.1101/483883.

[Phi+06] Benjamin L. Phillips, Gregory P. Brown, Jonathan K. Webb, and Richard Shine. “Invasion and the evolution of speed in toads”. In: *Nature* 439.7078 (2006), pp. 803–803. ISSN: 0028-0836, 1476-4687. DOI: 10.1038/439803a.

[PKE15] S. Peischl, M. Kirkpatrick, and L. Excoffier. “Expansion Load and the Evolutionary Dynamics of a Species Range”. In: *Am. Nat.* 185.4 (2015), E81–E93. ISSN: 0003-0147, 1537-5323. DOI: 10.1086/680220.

[Pre04] Céline Prevost. “Applications des équations aux dérivés partielles aux problèmes de dynamique des populations et traitement numérique”. 2004ORLE2072. PhD thesis. 2004, 1 vol. (142 p.) URL: http://www.theses.fr/2004ORLE2072.

[PS16] B. Perthame and P. E. Souganidis. “Rare Mutations Limit of a Steady State Dispersal Evolution Model”. In: *Mathematical Modelling of Natural Phenomena* 11.4 (2016). Ed. by A. Morozov and S. Petrovskii, pp. 154–166. ISSN: 1760-6101. DOI: 10.1051/mmnp/201611411.

[PST21] Benoît Perthame, Martin Strugarek, and Cécile Taing. “Selection-mutation dynamics with asymmetrical reproduction kernels”. In: (2021). arXiv: 2111.06648 [math.AP].

[PYW98] Joel R. Peck, Jonathan M. Yearsley, and David Waxman. “Explaining the geographic distributions of sexual and asexual populations”. In: *Nature* 391.6670 (1998), pp. 889–892. ISSN: 0028-0836, 1476-4687. DOI: 10.1038/36099.

[Rao17] Gaël Raoul. “Macroscopic limit from a structured population model to the Kirkpatrick-Barton model”. In: *arXiv:1706.04094 [math]* (2017). arXiv: 1706.04094. URL: http://arxiv.org/abs/1706.04094.

[Rao21] Gaël Raoul. “Exponential convergence to a steady-state for a population genetics model with sexual reproduction and selection”. In: *arXiv:2104.06089 [math]* (2021). arXiv: 2104.06089. URL: http://arxiv.org/abs/2104.06089.

[RB06] Denis Roze and Nick H Barton. “The Hill–Robertson Effect and the Evolution of Recombination”. In: *Genetics* 173.3 (2006), pp. 1793–1811. ISSN: 1943-2631. DOI: 10.1534/genetics.106.058586.

[Res18] Living with Resistance project. “Antibiotic and pesticide susceptibility and the Anthropocene operating space”. In: *Nature Sustainability* 1.11 (2018), pp. 632–641. ISSN: 2398-9629. DOI: 10.1038/s41893-018-0164-3.

[RK01] O. Ronce and M. Kirkpatrick. “WHEN SOURCES BECOME SINKS: MIGRATIONAL MELTDOWN IN HETEROGENEOUS HABITATS”. In: *Evolution* 55.8 (2001), pp. 1520–1531. ISSN: 0014-3820. DOI: 10.1111/j.0014-3820.2001.tb00672.x.

[Rod+19] Nicolas O. Rode, Arnaud Estoup, Denis Bourguet, Virginie Courtier-Orgogozo, and Florence Débarre. “Population management using gene drive: molecular design, models of spread dynamics and assessment of ecological risks”. In: *Conservation Genetics* 20.4 (2019), pp. 671–690. ISSN: 1566-0621, 1572-9737. DOI: 10.1007/s10592-019-01165-5.

[Ron07] Ophélie Ronce. “How Does It Feel to Be like a Rolling Stone? Ten Questions about Dispersal Evolution”. In: *Annual Review of Ecology, Evolution, and Systematics* 3 (2007), pp. 231–253.

[Roq+12] L. Roques, J. Garnier, F. Hamel, and E. K. Klein. “Allee effect promotes diversity in traveling waves of colonization”. In: *Proceedings of the National Academy of Sciences* 109.23 (2012), pp. 8828–8833. ISSN: 0027-8424, 1091-6490. DOI: 10.1073/pnas.1201695109.

[Rou72] Jonathan Roughgarden. “Evolution of Niche Width”. In: *The American Naturalist* (1972), p. 37.

[Roz09] Denis Roze. “Diploidy, Population Structure, and the Evolution of Recombination”. In: *The American Naturalist* 174.S1 (2009), S79–S94. ISSN: 0003-0147, 1537-5323. DOI: 10.1086/599083.

[RRG12] Irene Gallego Romero, Ilya Ruvinsky, and Yoav Gilad. “Comparative studies of gene expression and the evolution of gene regulation”. In: *Nature Reviews Genetics* 13.7 (2012), pp. 505–516. ISSN: 1471-0056, 1471-0064. DOI: 10.1038/nrg3229.

[Saa08] M Saastamoinen. “Heritability of dispersal rate and other life history traits in the Glanville fritillary butterfly”. In: *Heredity* 100.1 (2008), pp. 39–46. ISSN: 0018-067X, 1365-2540. DOI: 10.1038/sj.hdy.6801056.

[Sai19] Angela Saini. *Superior: The Return of Race Science*. 4th estate, 2019.

[SB17] Himani Sachdeva and Nicholas H. Barton. “Divergence and evolution of assortative mating in a polygenic trait model of speciation with gene flow: DIVERGENCE AND EVOLUTION OF ASSORTATIVE MATING”. In: *Evolution* 71.6 (2017), pp. 1478–1493. ISSN: 00143820. DOI: 10.1111/evo.13252.

[SBP11] Richard Shine, Gregory P. Brown, and Benjamin L. Phillips. “An evolutionary process that assembles phenotypes through space rather than through time”. In: *Proceedings of the National Academy of Sciences* 108.14 (2011), pp. 5708–5711. ISSN: 0027-8424, 1091-6490. DOI: 10.1073/pnas.1018989108.

[Shi+21] Richard Shine, Ross A. Alford, et al. “Increased rates of dispersal of free-ranging cane toads (Rhinella marina) during their global invasion”. In: *Scientific Reports* 11.1 (2021), p. 23574. ISSN: 2045-2322. DOI: 10.1038/s41598-021-02828-5.

[Sla05] Jon Slate. “INVITED REVIEW: Quantitative trait locus mapping in natural populations: progress, caveats and future directions”. In: *Molecular Ecology* 14.2 (2005), pp. 363–379. ISSN: 1365-294X. DOI: 10.1111/j.1365-294X.2004.02378.x.

[Sla70] M. Slatkin. “Selection and Polygenic Characters”. In: *Proceedings of the National Academy of Sciences* 66.1 (1970), pp. 87–93. ISSN: 0027-8424, 1091-6490. DOI: 10.1073/pnas.66.1.87.

[Sla73] Montgomery Slatkin. “GENE FLOW AND SELECTION IN A CLINE”. In: *Genetics* 75.4 (1973), pp. 733–756. ISSN: 1943-2631. DOI: 10.1093/genetics/75.4.733.

[SN18] Sarah A. Signor and Sergey V. Nuzhdin. “The Evolution of Gene Expression in cis and trans”. In: *Trends in Genetics* 34.7 (2018), pp. 532–544. ISSN: 01689525. DOI: 10.1016/j.tig.2018.03.007.

[Sol05] Rickie Solinger. *Pregnancy and Power: A Short History of Reproductive Politics in America*. New York University Press, 2005. ISBN: 9780814798270.

[SSB21] Enikő Szép, Himani Sachdeva, and Nicholas H. Barton. “Polygenic local adaptation in metapopulations: A stochastic eco-evolutionary model”. In: *Evolution* 75.5 (2021), pp. 1030–1045. ISSN: 1558-5646. DOI: 10.1111/evo.14210.

[TB90] Michael Turelli and N.H. Barton. “Dynamics of polygenic characters under selection”. In: *Theoretical Population Biology* 38.1 (1990), pp. 1–57. ISSN: 00405809. DOI: 10.1016/0040-5809(90)90002-D.

[TB94] M. Turelli and N. H. Barton. “Genetic and Statistical Analyses of Strong Selection on PolygenicTraits: What, Me Normal?” In: *Genetics* (1994), pp. 913–941.

[TD02] Justin M J Travis and Calvin Dytham. “Dispersal evolution during invasions”. In: *Evolutionary Ecology Research* (2002), p. 12.

[Tho+01] C. D. Thomas, E. J. Bodsworth, R. J. Wilson, A. D. Simmons, Z. G. Davies, M. Musche, and L. Conradt. “Ecological and evolutionary processes at expanding range margins”. In: *Nature* 411.6837 (2001), pp. 577–581. ISSN: 0028-0836, 1476-4687. DOI: 10.1038/35079066.

[TK16] Anaïs Tilquin and Hanna Kokko. “What does the geography of parthenogenesis teach us about sex?” In: *Philosophical Transactions of the Royal Society B: Biological Sciences* 371.1706 (2016), p. 20150538. ISSN: 0962-8436, 1471-2970. DOI: 10.1098/rstb.2015.0538.

[Tra+09] Justin M.J. Travis, Karen Mustin, Tim G. Benton, and Calvin Dytham. “Accelerating invasion rates result from the evolution of density-dependent dispersal”. In: *Journal of Theoretical Biology* 259.1 (2009), pp. 151–158. ISSN: 00225193. DOI: 10.1016/j.jtbi.2009.03.008.

[Tuf00] J. Tufto. “Quantitative genetic models for the balance between migration and stabilizing selection”. In: *Genetical Research* 76.3 (2000), pp. 285–293. ISSN: 0016-6723, 1469-5073. DOI: 10.1017/S0016672300004742.

[Tuf01] Jarle Tufto. “Effects of Releasing Maladapted Individuals: A Demographic-Evolutionary Model”. In: *The American Naturalist* 158.4 (2001), pp. 331–340. ISSN: 0003-0147, 1537-5323. DOI: 10.1086/321987.

[Tur15] Olga Turanova. “On a model of a population with variable motility”. In: *Mathematical Models and Methods in Applied Sciences* 25.10 (2015), pp. 1961–2014. ISSN: 0218-2025, 1793-6314. DOI: 10.1142/S0218202515500505.

[Tur17] M. Turelli. “Commentary: Fisher’s infinitesimal model: A story for the ages”. In: 118 (2017), pp. 46–49. ISSN: 00405809. DOI: 10.1016/j.tpb.2017.09.003.

[TW06] Stacey Lee Thompson and Jeannette Whitton. “Patterns of recurrent evolution and geographic parthenogenesis within apomictic polyploid Easter daises (Townsendia hookeri): GEOGRAPHIC PARTHENOGENESIS IN EASTER DAISIES”. In: *Molecular Ecology* 15.11 (2006), pp. 3389–3400. ISSN: 09621083, 1365294X. DOI: 10.1111/j.1365-294X.2006.03020.x.

[UN19] UN. *2019 Revision of World Population Prospects*. United Nations: Department of Economic and Social Affairs Population Dynamics, 2019. URL: https://population.un.org/wpp/.

[VB14] Harold de Vladar and Nick Barton. "Stability and Response of Polygenic Traits to Stabilizing Selection and Mutation". In: *Genetics* 197.2 (2014), pp. 749–767. ISSN: 1943-2631. DOI: 10.1534/genetics.113.159111.

[Vil08] Cédric Villani. *Topics in Optimal Transportation*. 2008.

[WHM19] Jennifer L. Williams, Ruth A. Hufbauer, and Tom E. X. Miller. "How Evolution Modifies the Variability of Range Expansion". In: *Trends in Ecology & Evolution* 34.10 (2019), pp. 903–913. ISSN: 0169-5347. DOI: https://doi.org/10.1016/j.tree.2019.05.012.

[WKL16] Jennifer L. Williams, Bruce E. Kendall, and Jonathan M. Levine. "Rapid evolution accelerates plant population spread in fragmented experimental landscapes". In: *Science* 353.6298 (2016), pp. 482–485. DOI: 10.1126/science.aaf6268. eprint: https://www.science.org/doi/pdf/10.1126/science.aaf6268. URL: https://www.science.org/doi/abs/10.1126/science.aaf6268.

[WL18] B. Walsh and M. Lynch. *Evolution and Selection of Quantitative Traits*. OUP Oxford, 2018. ISBN: 978-0-19-256664-5. URL: https://books.google.co.uk/books?id=L2liDwAAQBAJ.

[Wri31] Sewall Wright. "EVOLUTION IN MENDELIAN POPULATIONS". In: *Genetics* 16.2 (1931), pp. 97–159. ISSN: 1943-2631. DOI: 10.1093/genetics/16.2.97. eprint: https://academic.oup.com/genetics/article-pdf/16/2/97/35081059/genetics0097.pdf. URL: https://doi.org/10.1093/genetics/16.2.97.

[YG09] S. Yeaman and F. Guillaume. "Predicting Adaptation Under Migration Load: The Role of Genetic Skew". In: *Evolution* 63.11 (2009), pp. 2926–2938. ISSN: 1558-5646. DOI: 10.1111/j.1558-5646.2009.00773.x.

[YO11] S. Yeaman and S. P. Otto. "ESTABLISHMENT AND MAINTENANCE OF ADAPTIVE GENETIC DIVERGENCE UNDER MIGRATION, SELECTION, AND DRIFT". In: *Evolution* 65.7 (2011), pp. 2123–2129. ISSN: 00143820. DOI: 10.1111/j.1558-5646.2011.01277.x.

[YW11] S. Yeaman and M. C. Whitlock. "THE GENETIC ARCHITECTURE OF ADAPTATION UNDER MIGRATION-SELECTION BALANCE: THE GENETIC ARCHITECTURE OF LOCAL ADAPTATION". In: *Evolution* 65.7 (2011), pp. 1897–1911. ISSN: 00143820. DOI: 10.1111/j.1558-5646.2011.01269.x.

[Zub01] Tukufu Zuberi. *Thicker than Blood: How Racial Statistics Lie*. NED - New edition. University of Minnesota Press, 2001. ISBN: 9780816639083. URL: http://www.jstor.org/stable/10.5749/j.cttttcnc (visited on 04/06/2022).